Geophysical Atlas of Selected Oil and Gas Fields in Kansas

Neil L. Anderson and Dennis E. Hedke, editors

D. L. Baars, Michael L. Crouch, William A. Miller, Frank Mize, and Larry J. Richardson, assistant editors

Kansas Geological Survey and Kansas Geological Society,
co-publishers

Lawrence, Kansas
1995

Printed on recycled paper by the University of Kansas Printing Services

Contents

Preface

When Neil Anderson and Dennis Hedke approached the Survey and the Society for support of a *Geophysical Atlas of Selected Oil and Gas Fields in Kansas,* we were unsure as to the breadth and "depth" of the venture, but knew that the project would be in capable hands. The results of the four years of work to develop this volume are a comprehensive look at the potential for geophysical methods to influence exploration and development of petroleum plays in Kansas. Neil and Dennis have compiled background information and general geological settings, technology of geophysical methods, and applications of geophysical methods, mainly seismic, to the exploration and development of Kansas oil fields and stratigraphy. One of the unique aspects of this volume is the inclusion of case studies of potential fields for exploration and discussions of how geophysics "works."

Modern seismology has many uses beyond simple exploration and development of petroleum resources. Papers demonstrating use of reflection seismology to diagnose environmental impacts of both development and natural processes have been included in this book and should be useful to a large audience. These papers demonstrate both site-specific techniques and the use of shallow-reflection seismology to address environmental issues.

Cooperative ventures such as this are possible only by the commitment of individuals and organizations toward providing the tools, technology, and information necessary for the Kansas industry to better explore for and produce Kansas natural resources. It is noteworthy that of the 27 papers in this book, 12 are written by Survey authors, 10 by Society authors, and five are joint ventures. Compilation and editing of the papers and the final printing of this volume was under the direction of Rex Buchanan, Assistant Director for Publications and Public Affairs; Marla Adkins–Heljeson, Editor; and Jennifer Sims, Graphic Designer, at the Kansas Geological Survey. Past-Presidents of the Kansas Geological Society who have contributed to the project are Bill Shepherd, Jerry Langrehr, Alan DeGood, Brad Rine, and Paul Gunzelman.

The Kansas Geological Survey and the Kansas Geological Society are proud to present these results of our extensive joint venture to publish an assessment of the use of geophysics for Kansas petroleum exploration and development. We hope that operators and scientists alike will better understand how to increase efficiency and cost-benefits of use of geophysics in cratonic settings in a mature petroleum-producing region. As our industry moves further into 3D seismic and other advanced techniques, this volume should serve as a base from which to adapt more advanced geophysical methods to Kansas geology.

Lee C. Gerhard, State Geologist and Director, Kansas Geological Survey
Robert O'Dell, President, Kansas Geological Society

Introduction and Overview of the Atlas Papers

K. David Newell[1] and Neil L. Anderson[2]
[1]Kansas Geological Survey, The University of Kansas, Lawrence, KS 66047; and [2]Department of Geology and Geophysics, University of Missouri–Rolla, Rolla, MO 65401

The efficacy of geophysical methods in the search for petroleum in the midcontinent was summarized in two previous dedicated volumes published by the Kansas Geological Survey (Hambleton, 1959; Steeples, 1989). Hambleton (1959) presented several early case studies that utilized the reflection seismic method for petroleum exploration, in addition to presenting local and regional studies using electrical resistivity, magnetics, and gravimetry. Steeples (1989), in an update volume, summarized more recent advances in reflection seismology and data-processing techniques. The recent advances included the use of higher-frequency sources for shallow-depth seismic investigations, and the use of computer enhancement for aeromagnetic and gravity studies of the entire state.

The present atlas, a cooperative project by the Kansas Geological Survey and the Kansas Geological Society, emphasizes case studies in the application of reflection seismology in Kansas. Most of these studies relate to petroleum exploration, but also included are papers illustrating the wider use of reflection seismology in understanding salt dissolution (cf., two papers by Anderson et al.), hydrogeologic problems (Keiswetter et al.), and geomorphologic phenomena (Miller et al.). The application of high-resolution reflection-seismic profiles to stratigraphic investigations also is discussed in the context of recognition of depositional systems (Franseen et al., Knapp and Anderson, Knapp et al.) and detection of shallow fluvial-deltaic channel ("squirrel") sandstones (Miller and Weis). Stratigraphic investigations such as these are a component of this volume because the broader use of geophysical methods in areas other than the search for petroleum should be recognized.

The *Geophysical Atlas of Selected Oil and Gas Fields in Kansas* is composed of 28 papers. Notwithstanding this introduction, included are 10 exploration case histories, 10 test-site seismic studies, two potential-field case studies, two methodology papers, and three overview papers. These studies also encompass a broad range of geologic features that can be observed by reflection seismology, including sand bars, beaches, channel sandstones, deltas, carbonate banks, karsts, faults, folds, and salt-dissolution features. The papers are arranged so that the earlier articles set the stage for the later case studies. Articles 2 through 6 establish the Precambrian geologic framework for Kansas and illustrate that much hydrocarbon production can ultimately be correlated to structural and topographic relief on the Precambrian basement. These papers also illustrate that Precambrian tectonic zones may be extremely long-lived and that these zones influence many subsequent geologic events. The seventh and eighth papers are methodology-oriented and provide the reader with an appreciation of how seismic data tie to subsurface geology. Articles 9 through 17 are test-site seismic studies that illustrate the utility of the seismic technique, particularly recent development and application of high-resolution methods in various localities in Kansas (fig. 1). Papers 18 through 28 complete the atlas. These articles are case studies utilizing reflection-seismic lines over petroleum fields in Kansas, with each paper containing a geologic overview and at least one interpreted template seismic profile (fig. 1).

By documenting a selected group of petroleum fields and geologic features that are discernable by reflection seismology, this atlas aims to circulate knowledge of this geophysical tool to the energy industry, academia, and to other potential users of the seismic method. With continually improving technology, geoscientists need to access the accumulated technical experiences of their predecessors. A presentation of this knowledge will fulfill some of this need and stimulate new ideas on how reflection seismology may be used. The benefits of "scientific cross-pollination" can therefore be enjoyed by all.

In addition to disseminating information about geophysical methods to a wider audience, this atlas also serves as a "still photograph," as it were, to document how geophysics is presently being used in the midcontinent. Hopefully, others will reap the benefits of this knowledge and apply its methods and results toward their own research. In this way, the past and present state of the science of geophysics will partly influence its future.

Since the 1940's, petroleum-exploration activities have become increasingly dependent on the capabilities of the geophysical interpreter. Although interpretation of well data, guided by experience and creative geologic insight, is still the principal method for finding oil in Kansas, geophysical data are also incorporated in these studies. Correlation-point seismic data were the norm in the 1950's, but multi-fold reflection-seismic profiling, first with analog and then digitally processed data, became more common in the 1960's. Reflection seismology is probably now the most commonly used method to supplement subsurface geologic mapping, but in some plays it has been the principal impetus behind exploration efforts. For example, the drilling of the Texaco #1 Poersch well in Washington County, Kansas, in 1984—the first major petroleum-exploration test of the midcontinent rift (see Berendsen et al., 1988; Woelk and Hinze, this volume), was primarily based on data obtained from reflection-seismic lines. Furthermore, this exploration effort was originally prompted by geologic structures seen on a COCORP reflection-seismic line shot between 1979 and 1981 (Steeples, 1989). Seismic-reflection lines also are critical for defining depositional geometries for developmental drilling in channel sandstones in the Morrow Formation of southwestern Kansas and southeastern Colorado (see Rummerfield and Rummerfield, 1989; Richardson and Hedke, this volume; Miller et al., this volume).

Although geological methods will remain important both in finding new oil and efficiently recovering "old" oil in existing fields, an ever-increasing reliance on geophysics in energy exploration will probably occur. Similarly, a wider application of geophysics in hydrogeologic surveys and environmental remediation projects will be necessary. In the future, 3D seismic-data surveys may become more important for both the exploration and production of petroleum in Kansas (see Rutter, 1993). The economics of such complex surveys are still marginal; however, advances in computational and seismic hardware, together with progress in processing techniques, continually improve the feasibility of such enterprises so that even small petroleum plays and the small producers that chase them may eventually benefit from such advanced technology.

Knowing exactly where the future will send us is difficult, and even if we could know, the timetable of when we get there is mostly unclear. If achieving a perfect perspective on things to come were simple, and if precognition were common, years ago we would have easily foreseen that companies once making cash registers and adding machines would grow to be computer giants, and that obscure blue-print companies would rise to worldwide stature by producing photocopiers. Similarly, what type of geophysics will we be doing a generation from now in the midcontinent? Who will be doing it? What will we be finding? The organizers of this volume therefore make a plea to future geophysical researchers to document and save some of their more novel and interesting work . . . and even some of their "mundane" projects! Such studies may perhaps be published in a successor volume one day, which will serve as yet another building block for our future.

References

Berendsen, P., Doveton, J., Gerhard, L., Newell, K. D., Steeples, D., and Watney, W. L., 1988, Preliminary geologic report of the Texaco #1 Poersch borehole: Oil and Gas Journal, October 31, p. 48–52

Hambleton, W. W. (ed.), 1959, Symposium on geophysics in Kansas: Kansas Geological Survey, Bulletin 137, 375 p.

Rummerfield, B. F., and Rummerfield, L. J., 1989, Seismic exploration for the Morrow trend; *in* Geophysics in Kansas, D. W. Steeples, ed.: Kansas Geological Survey, Bulletin 226, p. 67-80

Rutter, A. W., III, 1993, 3D seismic applications and implementation; *in*, Reservoir Description Workshop—Application of Underused Technologies, W. L. Watney and R. S. Sawin, comp.: Energy Research Center, University of Kansas, Technology Transfer Series 93–1, p. 353–360

Steeples, D. W. (ed.), 1989, Geophysics in Kansas: Kansas Geological Survey, Bulletin 226, 312 p.

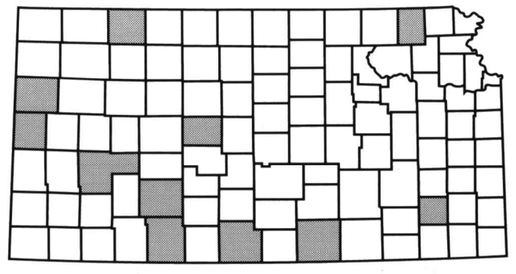

FIGURE 1—LOCATION OF CASE STUDIES PRESENTED IN THIS ATLAS.

Overview of Petroleum Geology and Production in Kansas

by K. David Newell
Kansas Geological Survey, The University of Kansas, Lawrence, KS 66047

Importance of Petroleum Production in Kansas

Booms and busts in the petroleum industry have occurred in Kansas since oil was first produced near Paola in the 1870's. Oil and gas prices are currently low, and as a result, the energy industry in Kansas is depressed, particularly compared to the boom times of the late 1970's. Although petroleum resources are slowly dwindling, approximately 8,500 jobs statewide are still directly involved with its extraction and conveyance (Gerhard, 1992). Over the last decade, annual cash receipts from Kansas oil and gas production equal that of the total annual statewide crop production (Carr, 1994). The energy industry therefore remains an impressive component of the economy of the state, and it will probably continue to be important well into the next century. Just how big the industry will be is difficult to predict because its prosperity largely hinges on mercurial world energy prices and politics. In any event, the future of the industry in Kansas will probably be dominated by small companies, at least with respect to the production of oil. Major companies and large independents still are involved with gas production in the state by virtue of extensive acreage holdings in southwestern Kansas.

The history of petroleum production in Kansas through this century has paralleled the evolution of the science of petroleum geology. At the turn of this century, finding energy resources was principally a process of guesswork, "witching," the knack of drilling wells near seeps, fast-talking promotion, and just plain luck. Although serendipity will always be a part of the process, energy exploration and development are now more systematic and less desultory, involving aspects of structural geology, stratigraphy, well-log interpretation, petrophysical analysis, geophysics, and petroleum engineering.

Various geologic methods have enjoyed their heyday. Structural mapping based on surface geology and topography was important around World War I, when El Dorado, the largest oil field in Kansas, was found along the Nemaha uplift in Butler County. In the following decades, as the more obvious surface structures were explored, subsurface mapping became increasingly important and led to the discovery of many major fields in Kansas. Some of these subsurface data were obtained by drilling grids of shallow core holes, but most data now are based on deeper exploratory well control.

Almost 6 billion barrels of oil have been produced in Kansas (Carr, 1994; fig. 1). Approximately 35% of this oil was from Pennsylvanian rock. Cambrian–Ordovician Arbuckle production, mostly from the Central Kansas uplift, accounts for another 32% of the total production of the state. Mississippian fields, primarily carbonates in the Hugoton and Sedgwick basins, have produced 19% of the oil (Carr, 1994). Cumulative gas production is 29.5 TCF, with the overwhelming percentage (86%) coming from Permian strata (fig. 1).

Kansas currently ranks eighth among states in terms of the amount of oil produced annually, and sixth among the states that produce gas (World Oil, 1994). Oil production peaked in 1956 at 124 million bbls/yr. Gas production peaked in 1970 at 920 BCF per year (Oros, 1979). Current oil production is approximately 50 million bbls/yr while gas production is approximately 650 BCF (Carr, 1994). As of 1990, estimated proved reserves for Kansas were 321 million BO and 9,614 BCFG (Gerhard, 1992). Potential future discoveries, however, may prove up to an additional 2.2 billion barrels of recoverable reserves (Gerhard et al., 1994).

General Petroleum Geology

Only a cursory outline of the geologic history of Kansas as it relates to petroleum production is provided in this article. More extensive and elaborate summaries are found in Jewett (1954), Merriam (1963), Zeller (1968), Adler et al. (1971), and Newell, Watney, Cheng, and Brownrigg (1987). Capsulated summaries in previous volumes on geophysics in Kansas (Jewett and Merriam, 1959; Newell et al., 1989) also are useful.

Nowhere in Kansas is the cover of sedimentary rocks more than about 9,500 ft (2,850 m) thick. Due to numerous unconformities, this veneer of sedimentary strata in Kansas cumulatively represents perhaps only 15–50% of post-Precambrian time (Merriam, 1963). Unconsolidated Quaternary sediments are confined mostly to present drainage systems and are relatively thin. Pleistocene glacial deposits cover much of northeastern Kansas but much of this unconsolidated strata has been lost to erosion. Nonmarine Pliocene rocks, the Ogallala Formation, blanket the western third of Kansas, effectively masking the underlying stratigraphy and structure.

A thick section of Mesozoic rock, composed predominantly of marine shales, limestones, chalks, and nonmarine deposits of sandstone and shale, covers the western half of Kansas (fig. 2). Most of these strata were deposited in a broad Cretaceous seaway that bisected North America. The eastern shores of this seaway were probably situated in eastern Kansas or western Missouri, but subsequent erosion has removed the Mesozoic strata from these areas.

The Pennsylvanian and Permian systems (fig. 2) are the thickest sequences of rock in the state, and they document in their stratigraphic record dozens of cyclothemic inundations of the sea. Thin but laterally persistent units can be traced over large areas of the midcontinent, but significant lateral facies changes can occur as depositional environments change from shallow shelf to deeper basin. Bedded rock salts occur at several levels in the Permian System (Anderson et al., this volume, p. 57).

Rocks representing all pre-Pennsylvanian systems are present in Kansas. These consist mainly of marine limestones and dolomites, alternating with shales and sandstones (fig. 2). The thickest sections of pre-Pennsylvanian rock are found near the centers of the broad intracratonic basins where they have been protected from extensive erosion.

The Precambrian basement in the state consists mainly of granite, quartzite, and schist. Aeromagnetic and gravity studies, combined with drill data and radiometric dating, help define Precambrian tectonic terranes (Lam and Yarger, 1989; Yarger, 1989). The Midcontinent Rift System, a major late Precambrian tectonic feature, transects the state and contains an assemblage of basaltic flows, intrusives, and arkosic sandstones (Baars, this volume, p. 7; Woelk and Hinze, this volume, p. 22; fig. 3).

Two major positive tectonic elements, the Central Kansas and Nemaha uplifts, are probably manifestations of the Ouachita orogeny on the margin of the craton in Late Mississippian–Early Pennsylvanian time (Merriam, 1963; Baars, this volume, p. 7). These two uplifts also serve to define five basins that partly underlie the state (fig. 3).

Only the southwestern part of the Forest City basin extends into Kansas. It is bounded on the west by the Nemaha uplift and on the south by the low, indistinct, northwest-southeast-trending Bourbon arch. The basin axis lies close to the Nemaha uplift, hence the basin is asymmetric with a steep, faulted western flank. A production trend paying from lower Paleozoic strata along the axis of the Forest City basin is related to a series of anticlines along the Humboldt fault zone (Merriam, 1963). The Forest City basin, and the Salina basin to the west, are formerly part of the older North Kansas basin (fig. 3). The North Kansas basin was split in Late Mississippian–Early Pennsylvanian time by the rise of the Nemaha uplift.

South of the Bourbon arch in southeastern Kansas is the Cherokee basin, which partly overlies the older pre-Devonian Chautauqua arch. Like the Forest City basin, the present structural axis of the Cherokee basin lies just east of the Nemaha uplift. Numerous stratigraphic traps characterize the venerable fields in the Cherokee basin and eastern flank of the Forest City basin, with production being principally from channel sandstones in the Pennsylvanian Cherokee Group.

The Nemaha uplift separates the Forest City and Cherokee basins from the Salina and Sedgwick basins. The Precambrian core of the Nemaha uplift is within 500 ft (150

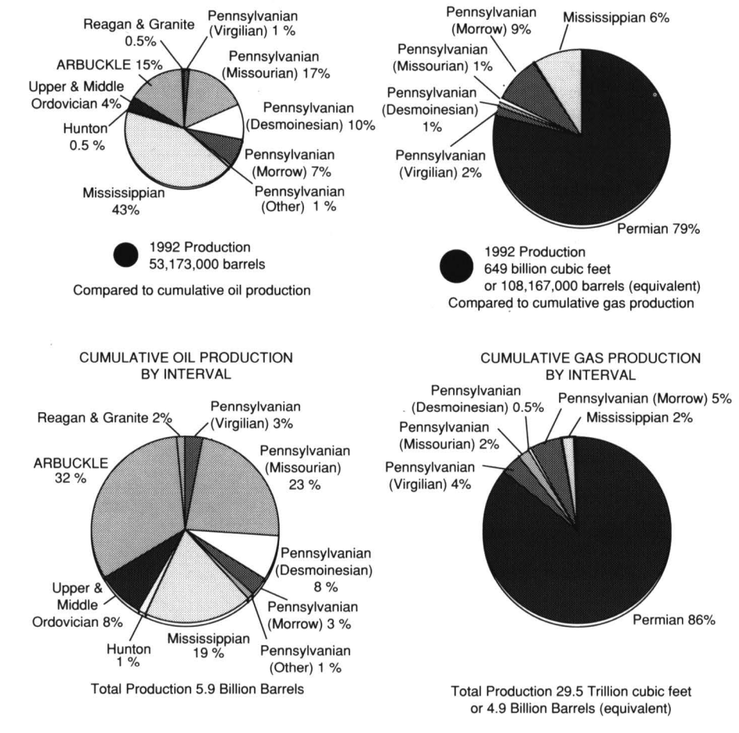

FIGURE 1—CUMULATIVE OIL AND GAS PRODUCTION (BY INTERVAL) COMPARED TO ANNUAL OIL AND GAS PRODUCTION (from Carr, 1994). Size of circle is proportional to volume of production.

m) of the surface near the Nebraska border but plunges to about 4,000 ft (1,200 m) at the Oklahoma border. Several structural culminations lie along its crest and one of these is the locus of the El Dorado field, the most prolific oil field in Kansas. Lower Paleozoic strata have been upturned and truncated by Pennsylvanian strata at several places on the crest of the Nemaha uplift. Faulting is particularly prevalent in the northeastern part of the state where the top of the Precambrian has approximately 2,000 ft (600 m) of vertical offset. In southern Kansas, structural relief is more subdued and in many places Paleozoic beds are folded over the crest. Small-magnitude earthquakes indicate that minor tectonic movement is continuing. The Nemaha uplift extends southward into Oklahoma and provides an element of structural closure for many petroleum fields in that state.

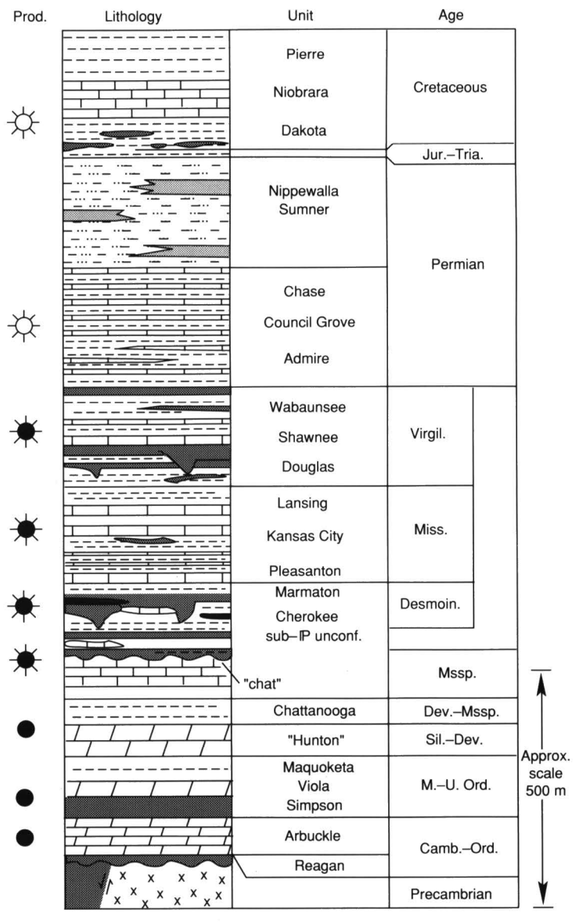

FIGURE 2—GENERALIZED PRE-TERTIARY STRATIGRAPHY OF KANSAS SHOWING APPROXIMATE THICKNESS OF MAJOR STRATIGRAPHIC UNITS (from Jenden et al., 1988). Cenozoic beds are not shown in this diagram.

The southern half of the Salina basin underlies much of north-central Kansas. The northern half underlies south-central Nebraska, where it is referred to as the Central Nebraska basin. The Salina basin is asymmetric like the Forest City basin, having a broad eastern flank and relatively steep western flank, but faulting is not evident along the western flank of the Salina basin. Although the axis of this basin is buried to a depth comparable to that in the Forest City basin, no oil production has been found to date along the axis of the Salina basin.

The Sedgwick basin, a shelflike extension of the Anadarko basin of Oklahoma, is roughly symmetrical and plunges southward. It extends across much of south-central Kansas and is separated from the Salina basin to the north by a low, unnamed east-west-trending arch. Oil production in the Sedgwick basin is from several stratigraphic horizons, but Mississippian pay zones dominate. The Pratt anticline, a southward-plunging nose off the Central Kansas uplift, defines the western flank of the Sedgwick basin.

The Central Kansas uplift is referred to as the structural backbone of Kansas. Along its crest, Precambrian rocks are overlain by rocks as young as Pennsylvanian; along its flanks, pre-Pennsylvanian units are upturned, truncated, and overstepped by younger Pennsylvanian strata. The Central Kansas uplift, the Cambridge arch to the northwest, and its northern extension in Nebraska, the Chadron arch, form an arcuate chain of uplifts that are convex to the southwest. The Central Kansas uplift is the most prolific oil province in Kansas, with principal pay zones being the Cambrian–Ordovician Arbuckle Group and the several stacked pays in the cyclothemic carbonates of the Pennsylvanian Lansing–Kansas City Group. This uplift is one of the most densely drilled petroleum provinces in the United States, and seven of the 10 largest fields in Kansas are located on it (Newell, Watney, Cheng, and Brownrigg, 1987). Outpost drilling has extended production of fields on the uplift where many of them have virtually merged. Although field boundaries are still maintained for accounting purposes, if these fields were considered as one entity, a large field having produced approximately a billion barrels of oil could be envisioned—a true giant on par with those in Texas and Oklahoma.

The Hugoton embayment, an extension of the Anadarko basin of Oklahoma, underlies the western third of Kansas. The axis of the embayment plunges generally southeastward, and strata within it thicken down-axis into the Anadarko basin. The greatest thickness of Phanerozoic strata in Kansas occurs in this basin where approximately 9,500 ft (2,850 m) of strata are preserved at the Oklahoma border. Permian strata in this basin account for the majority of gas production in the state, with most coming from carbonate reservoirs of the Chase Group in the giant Hugoton–Panhandle field and nearby smaller gas fields (Adler et al., 1971). Carbonate reservoirs of the Permian Council Grove Group in the Panoma gas field that underlies part of the Hugoton–Panhandle field are also important (Parham, 1993).

In the future, deeper targets in the Hugoton embayment may take the spotlight as the most important oil exploration area of the state, but venerable producing areas on the Central Kansas uplift also will remain important sources of production. Mississippian strata that now accounts for 43% of the production in the state (Carr, 1994) also will be an exploration target. Most of the larger Mississippian fields in the state are in the Sedgwick basin, but since the 1970's most big Mississippian discoveries have been in the Hugoton embayment. Pennsylvanian strata, principally the Morrow Formation, also hold promise for significant stratigraphic traps in the Hugoton embayment.

Distribution of Petroleum Production

Patterns of deformation in Kansas have changed throughout geologic time (fig. 3). Structurally positive areas can become downwarped areas, and visa versa. For example, the Nemaha uplift was once the location of the axis of the North Kansas basin. Earlier, the axis of the North Kansas basin was the locus of a broad uplift called the Southeast Nebraska arch. The Cherokee basin in southeastern Kansas overlies part of the earlier Chautauqua arch.

The erosion associated with these uplifts has produced a complex pattern of stratigraphic units that can be expressed by paleogeologic maps, also known as subcrop maps. Petroleum is often associated with traps and porosity developed along unconformities (see Schlee, 1984). For example, porosity can develop by weathering and karstification of rocks beneath unconformities. Porous sandstones can be deposited

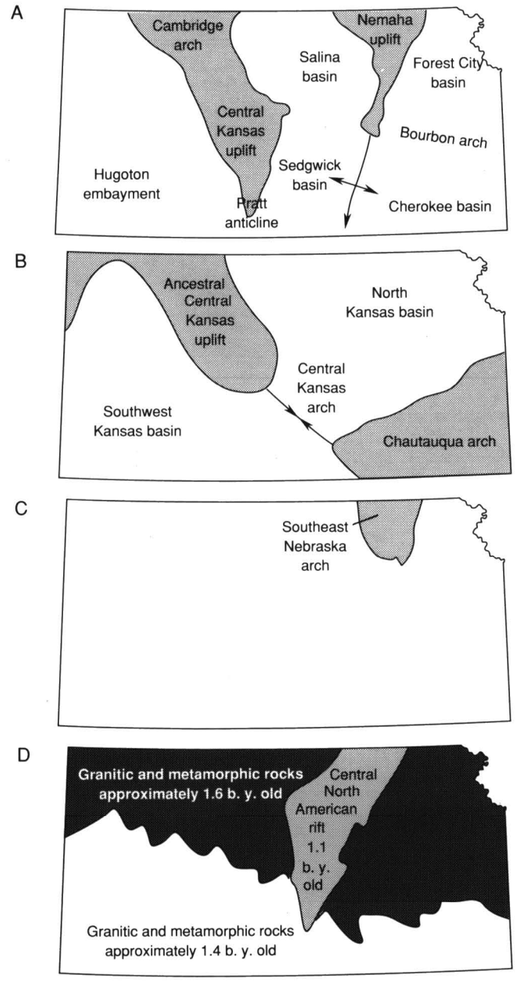

FIGURE 3—LARGE-SCALE STRUCTURAL FEATURES IN KANSAS (from Merriam, 1963; Bickford et al., 1981; Yarger, 1983): A—Pre-Desmoinesian–post-Mississippian features; B—Pre-Mississippian–post-Ordovician; C—Post-Cambrian–pre-Middle Ordovician; D—Precambrian.

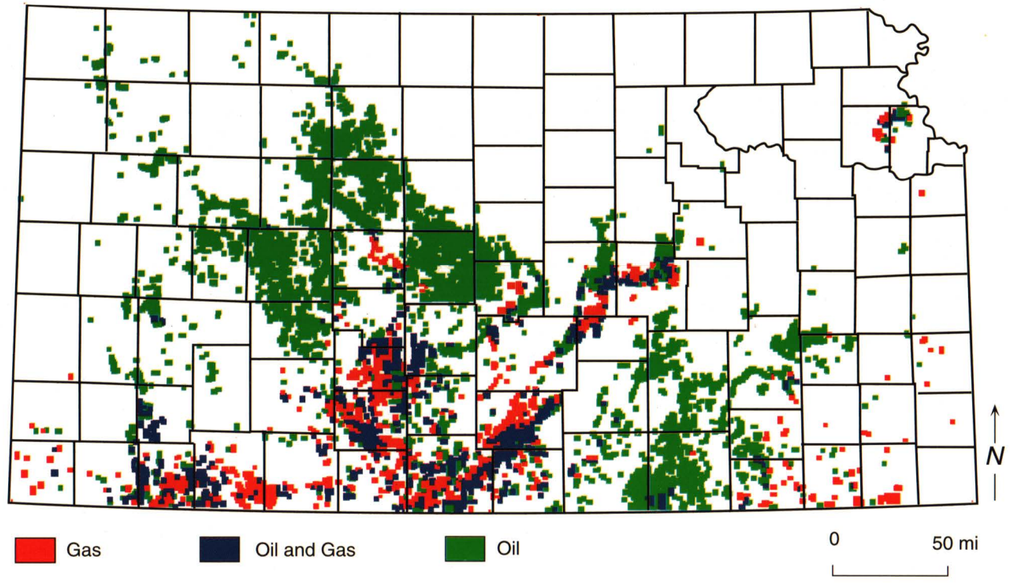

FIGURE 4—Distribution of petroleum production along the basal Pennsylvanian angular unconformity in Kansas (composited from data in Newell, Watney, Cheng, and Brownrigg, 1987).

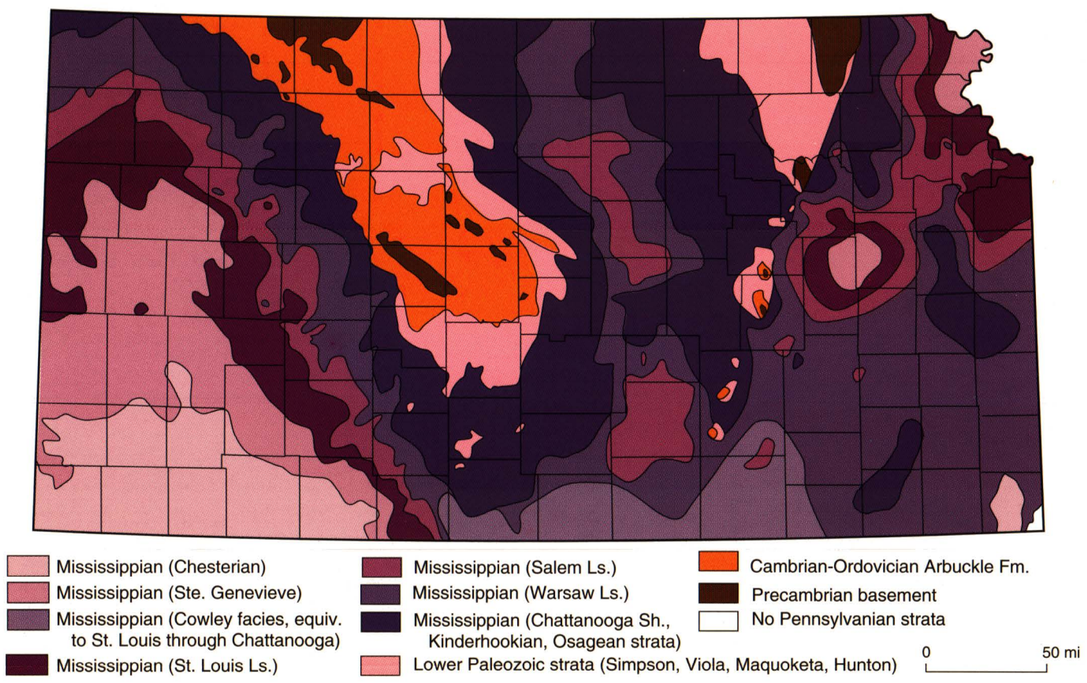

FIGURE 5—Paleogeologic map of units subcropping below the basal Pennsylvanian unconformity in Kansas (taken from Merriam, 1963; Newell, 1987a; Lambert, 1988).

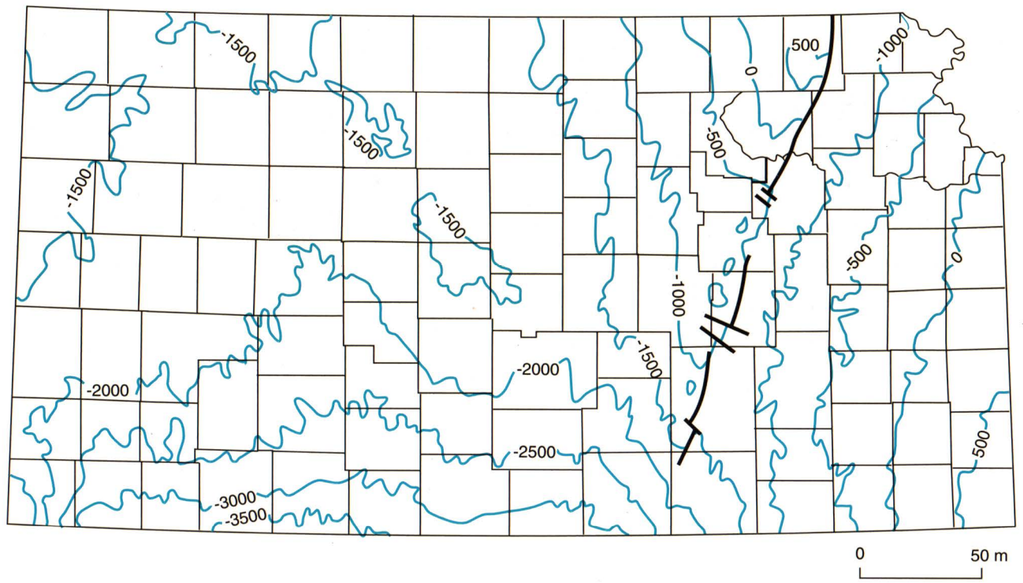

FIGURE 6—Subsea depth of basal Pennsylvanian unconformity in Kansas (from maps in Merriam, 1963).

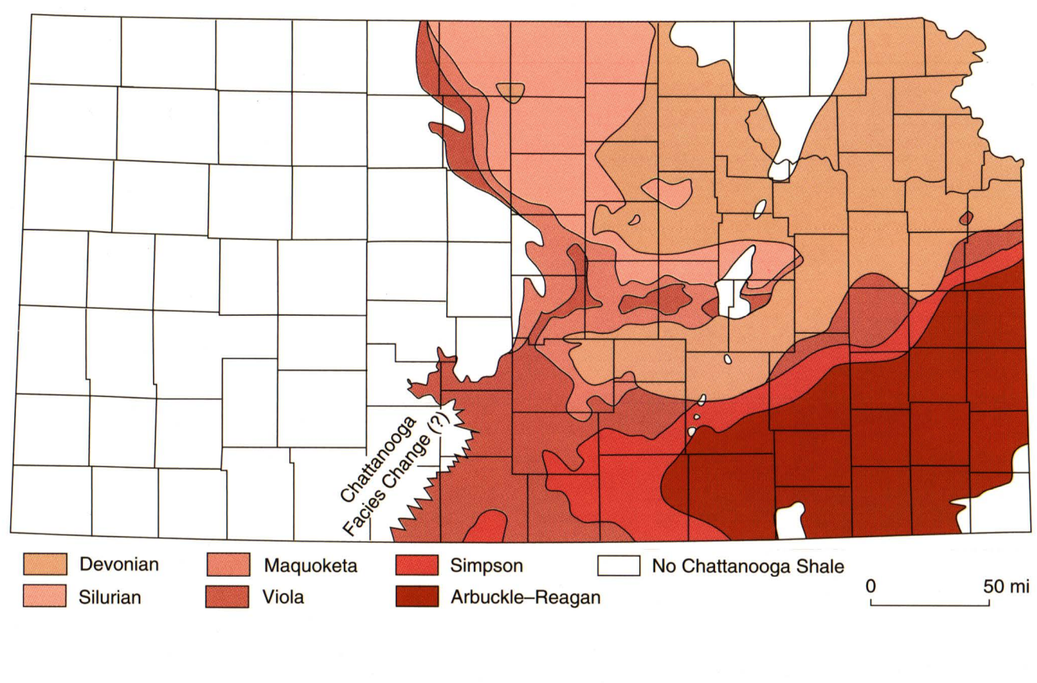

FIGURE 7—Paleogeologic map of units subcropping below the Chattanooga Shale in Kansas (taken from Merriam, 1963; Newell, 1987b).

upon an unconformity by a subsequent transgression of the sea. Unconformities can also act as regional "carrier beds" for petroleum.

Inasmuch as unconformities may influence both the migration and trapping of petroleum, it is perhaps informative to look at the distribution of petroleum along an unconformity, rather than conventionally noting the stratigraphic unit producing the petroleum (cf., Newell, Watney, Cheng, and Brownrigg, 1987; Carr et al., 1993). In this sense, the basal Pennsylvanian unconformity in Kansas has an enormous amount of petroleum distributed along it. The Cambrian–Ordovician Arbuckle Formation produces oil just below this unconformity at the crest of the prolific Central Kansas uplift, as do several lower Paleozoic formations on the flanks of the uplift (fig. 4). Mississippian "chat," together with "basal Pennsylvanian conglomerate," are also major pay zones along this unconformity, and both of these zones are components of many large stratigraphic traps in the Sedgwick basin and Hugoton embayment. Porosity associated with the basal Pennsylvanian unconformity may have functioned as a carrier bed for petroleum expelled from the deeper part of the Anadarko basin. Many of the traps downdip closer to the Anadarko basin produce gas (fig. 4), whereas updip traps produce oil—a pattern predicted by Gussow (1954) in his principle of differential petroleum migration. Curiously, the Central Kansas uplift appears quite imposing on a subcrop map (fig. 5), but a structure map of the basal Pennsylvanian unconformity (fig. 6) expresses it as only a subdued structural closure in the center of a broad structural low underlying much of the state.

Other major unconformities may also influence the migration and trapping of petroleum. The angular unconformity at the base of the Devonian–Mississippian Chattanooga Shale has much production associated with it, including several stratigraphic traps in central Kansas where the Silurian–Devonian "Hunton" carbonates pinch out beneath it (figs. 7 and 8). Misener sandstone, the erratically distributed transgressive sandstone present immediately above this unconformity, produces from several fields in Kansas and Oklahoma. In addition, the Chattanooga Shale is a major source rock in Oklahoma (Lambert, 1992), and hydrocarbons expulsed from it could migrate very efficiently into porous zones present along the unconformity at its base.

Although categorizing oil and gas by unconformity rather than by producing formation reduces the number of major producing horizons in the state, there is much production that is not associated with major unconformities. For example, Middle and Upper Ordovician oil (fig. 9), principally from Simpson Sandstone and Viola Limestone, is not associated with any major angular unconformity. The northeast-southwest production trend in these Ordovician units parallels the Transcontinetal arch, and its oil has a distinctive geochemical signature (Martin et al., 1963; Hatch et al., 1987). On the eastern flank of the Forest City basin, some of this oil has migrated vertically into Pennsylvanian reservoirs, and into Devonian "Hunton" carbonates along its axis (Newell,Watney, Stephens, and Hatch, 1987). Pennsylvanian production (fig. 10) and Permian production also are not consistently associated with any one major unconformity, although similarity in the spatial distribution of oil and gas production with that of the basal Pennsylvanian unconformity (fig. 4) indicates some of this production also may have leaked upwards through faults and stratigraphic connections.

If hydrocarbon production is considered by its distribution along unconformities, we then approach its occurrence as a "petroleum system." As defined by Magoon (1991), the "petroleum system" considers the relationships of all necessary conditions for the creation of a petroleum field, including source rock, overburden, reservoir, seal, and trap. Of course, only the locations of known traps are recorded by production maps; nevertheless, better inferences can be made as to migration and potential source beds of the petroleum. It is therefore proposed that most of the oil along the basal Pennsylvanian unconformity will be geochemically identical, regardless of whether it is found in Mississippian "chat" in the Sedgwick basin, or in Arbuckle carbonates on the crest of the Central Kansas uplift. Similarly, oil found at the base of the Chattanooga Shale may also be geochemically distinct regardless of whether the pay zone is in the Silurian–Devonian "Hunton Group" or the Middle Ordovician Viola Formation, just so long as these units are in the similar geologic position of being truncated by the unconformity at the base of the Chattanooga Shale. Although analyses (Hatch et al., 1987; Newell, Watney, Stephens, and Hatch, 1987) indicate that oil in Middle and Upper Ordovician strata (e.g., Simpson Group, Viola Formation, and Maquoketa Formation) is geochemically unique, this distinctive oil may be mixed with other oils where these units are truncated by major unconformities. A geochemical study of oil and gas along the major unconformities in Kansas could elucidate how the production migrated and accumulated, and the maps presented here may afford a more logical approach to such a study.

References

Adler, F. J., Caplan, W. M., Carlson, M. P., Goebel, E. D., Henslee, H. T., Hicks, I. C., Larson, T. G., McCracken, M. H., Parker, M. C., Rascoe, B., Schramm, M. W., and Wells, J. S., 1971, Future petroleum provinces of the midcontinent; *in,* Future Petroleum Provinces of the United States—Their Geology and Potential, I. H. Cram, ed.: American Association of Petroleum Geologists, Memoir 15, p. 985–1,120

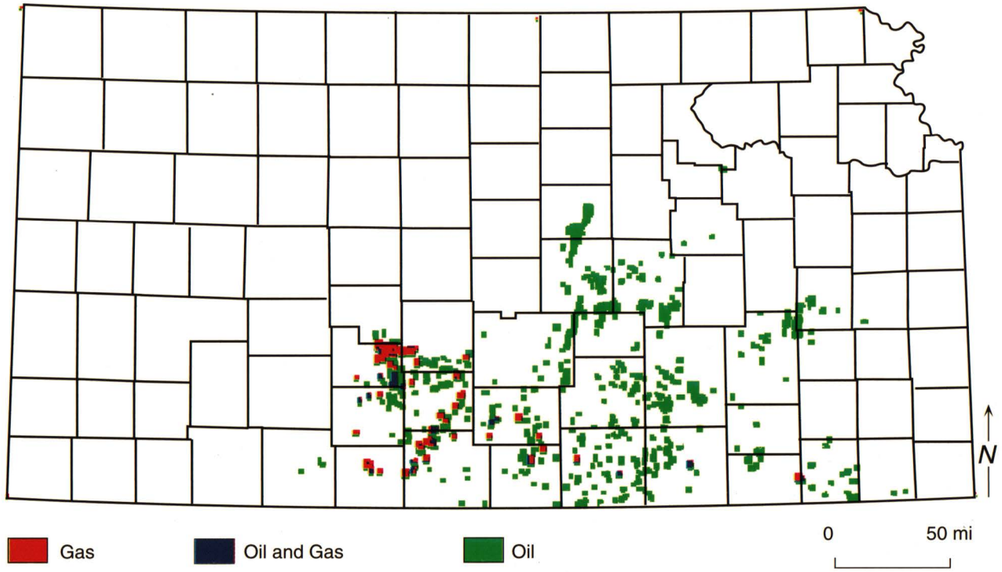

FIGURE 8—Distribution of petroleum production along the angular unconformity at the base of the Chattanooga Shale in Kansas (composited from data in Newell, Watney, Cheng, and Brownrigg, 1987).

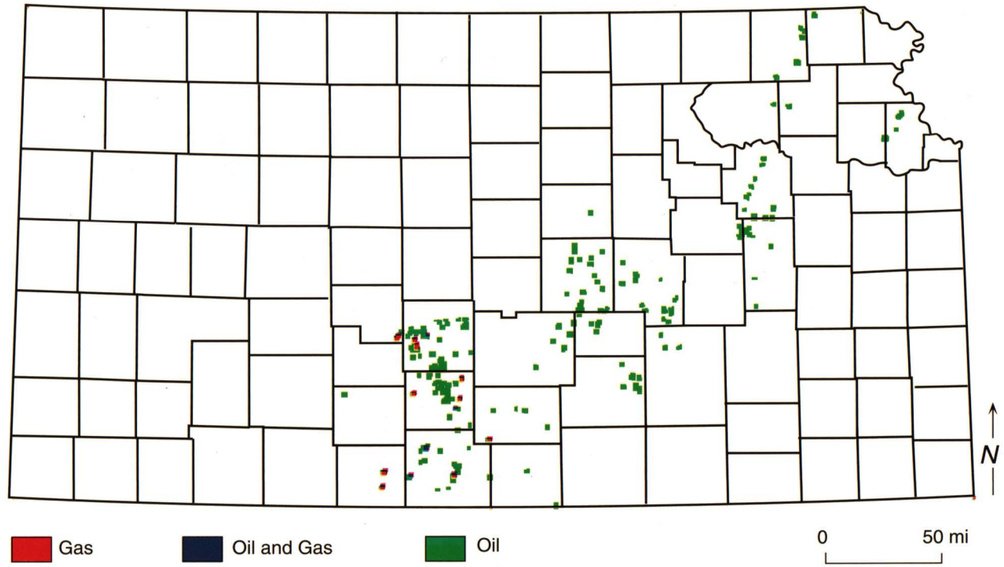

FIGURE 9—Distribution of petroleum production from Middle and Upper Ordovician strata in Kansas where these strata are not subcropping beneath either the angular unconformities at the base of the Chattanooga Shale, or the base of the Pennsylvanian System (composited from data in Newell, Watney, Cheng, and Brownrigg, 1987).

Bickford, M. E., Harrower, K. L., Nussbaum, R. L., Thomas, J. J., Nelson, B. K., and Hoppe, W. J., 1981, Rb-Sr and U-Pb geochronology and distribution of rock types in the Precambrian basement of Missouri and Kansas: Geological Society of America, Bulletin, v. 92, p. 323–341

Carr, T. R., 1994, Kansas oil and gas production trends: Kansas Geological Society, Bulletin, v. 69, no. 8, p. 12–14, 29–30

Carr, T. R., Ross, J. A., and Beene, D. L., 1993, Producing horizons of oil and gas fields: Kansas Geological Survey, Maps M35–1 to M35–12 (12 sheets, 1:250,000 scale)

Gerhard, L. C. (subcommittee chairman), 1992, Fossil energy strategy for Kansas; *in*, Kansas Energy Policy Committee Report submitted to Governor Joan Finney (February 1993), J. P. Jennings, chmn.: Energy Research Center, University of Kansas, Lawrence

Gerhard, L. C., Watney, W. L., Carr, T. R., Collins, D. R., and Newell, K. D., 1994, Potential for discovery and production from the Kansas crude oil resource base: Kansas Geological Survey, Open-file Report 94–30, 9 p.

Gussow, W. C., 1954, Differential entrapment of oil and gas: American Association of Petroleum Geologists, Bulletin, v. 39, p. 547–574

Hatch, J. R., Jacobson, S. R., Witzke, B. J., Risatti, J. B., Anders, D. E., Watney, W. L., Newell, K. D., and Vuletich, A. K., 1987, Possible late Middle Ordovician organic carbon isotope excursion; evidence from Ordovician oils and hydrocarbon source rocks, midcontinent and east-central United States: American Association of Petroleum Geologists, Bulletin, v. 71, p. 1,342–1,354

Jenden, P. D., Newell, K. D., Kaplan, I. R., and Watney, W. L., 1988, Composition and stable-isotope geochemistry of natural gases from Kansas, midcontinent, U.S.A.: Chemical Geology, v. 71, p. 117–147

Jewett, J. M., 1954, Oil and gas in eastern Kansas: Kansas Geological Survey, Bulletin 104 (reprinted 1979), 397 p.

Jewett, J. M., and Merriam, D. F., 1959, Geologic framework of Kansas—a review for geophysicists; *in,* Symposium on Geophysics in Kansas, W. W. Hambleton, ed.: Kansas Geological Survey, Bulletin 137, p. 9–52

Lam, C.-K., and Yarger, H. L., 1989, State gravity map of Kansas; *in,* Geophysics in Kansas, D. W. Steeples, ed.: Kansas Geological Survey, Bulletin 226, p. 185–196

Lambert, M. W., 1988, Sub-Pennsylvanian subcrop map of Mississippian units in the Salina basin: Kansas Geological Survey, Open-file Report 88–37 (1:500,000 scale map)

Lambert, M. W., 1992, Internal stratigraphy of the Chattanooga Shale in Kansas and Oklahoma; *in*, Source Rocks in the Southern Midcontinent, K. S. Johnson and B. Cardott, eds.: Oklahoma Geological Survey, Circular 93, p. 94–103

Magoon, L. B., 1991, The petroleum system—from source to trap: American Association of Petroleum Geologists, Bulletin, v. 75, p. 627

Martin, R., Winters, J. C., and Williams, J. A., 1963, Distributions of n-paraffins in crude oils and their implications to petroleum: Nature, v. 199, p. 110–113

Merriam, D. F., 1963, The geologic history of Kansas: Kansas Geological Survey, Bulletin 162, 317 p.

Newell, K. D., 1987a, Pre-Pennsylvanian subcrop map of Salina basin, Kansas: Kansas Geological Survey, Open-file Report 87–3 (1:500,000 scale map)

_____, 1987b, Pre-Chattanooga subcrop map of Salina basin, Kansas: Kansas Geological Survey, Open-file Report 87–4 (1:500,000 scale map)

Newell, K. D., Watney, W. L., Cheng, S. W. L., and Brownrigg, R. L., 1987, Stratigraphic and spatial distribution of oil and gas production in Kansas: Kansas Geological Survey, Subsurface Geology Series 9, 87 p.

Newell, K. D., Watney, W. L., Stephens, B. P., and Hatch, J. R., 1987, Hydrocarbon potential in Forest City basin: Oil and Gas Journal, v. 88 (October 19th), p. 58–62

Newell, K. D., Watney, W. L., Steeples, D. W., Knapp. R. W., and Cheng, S. W. L., 1989, Suitability of high-resolution seismic method to identifying petroleum reservoirs in Kansas—a geological perspective; *in*, Geophysics in Kansas, D. W. Steeples, ed.: Kansas Geological Survey, Bulletin 226, p. 9–29

Oros, M. O., 1979, Oil and gas in eastern Kansas, a 25-year update; in, Oil and Gas in Eastern Kansas: Kansas Geological Survey, Bulletin 104 (reprinted 1979), p. 3–30

Parham, K. D., 1993, Introduction to Permian plays; *in,* Atlas of Major Midcontinent Gas Reservoirs, D. G. Bebout, W. A. White, T. F. Hentz, and M. K. Grasmick, eds.: Bureau of Economic Geology, Austin, TX, p. 6–7

Rummerfield, B. F., and Rummerfield, L. J., 1989, Seismic exploration for the Morrow trend; *in,* Geophysics in Kansas, D. W. Steeples, ed.: Kansas Geological Survey, Bulletin 226, p. 67–80

Rutter, A. W., III, 1993, 3D seismic applications and implementation; *in,* Reservoir Description Workshop—Application of Underused Technologies, W. L. Watney and R. S. Sawin, comps.: University of Kansas, Technology Transfer Series 93–1, p. 353–360

Schlee, J. S., 1984, Interregional unconformities and hydrocarbon accumulation: American Association of Petroleum Geologists, Memoir 35, 184 p.

Steeples, D. W. (ed.), 1989, Geophysics in Kansas: Kansas Geological Survey, Bulletin 226, 312 p.

World Oil, 1994, U.S. oil and gas reserves hit 15-year lows: World Oil, v. 215, no. 2 (February), p. 84–85

Yarger, H. L., 1983, Regional interpretation of Kansas aeromagnetic data: Kansas Geological Survey, Geophysical Series 1, 35 p.

Yarger, H. L., 1989, Major magnetic features in Kansas and their possible geologic significance; *in*, Geophysics in Kansas, D. W. Steeples, ed.: Kansas Geological Survey, Bulletin 226, p. 197–213

Zeller, D. E., ed., 1968, The stratigraphic succession in Kansas: Kansas Geological Survey, Bulletin 189, 81 p.

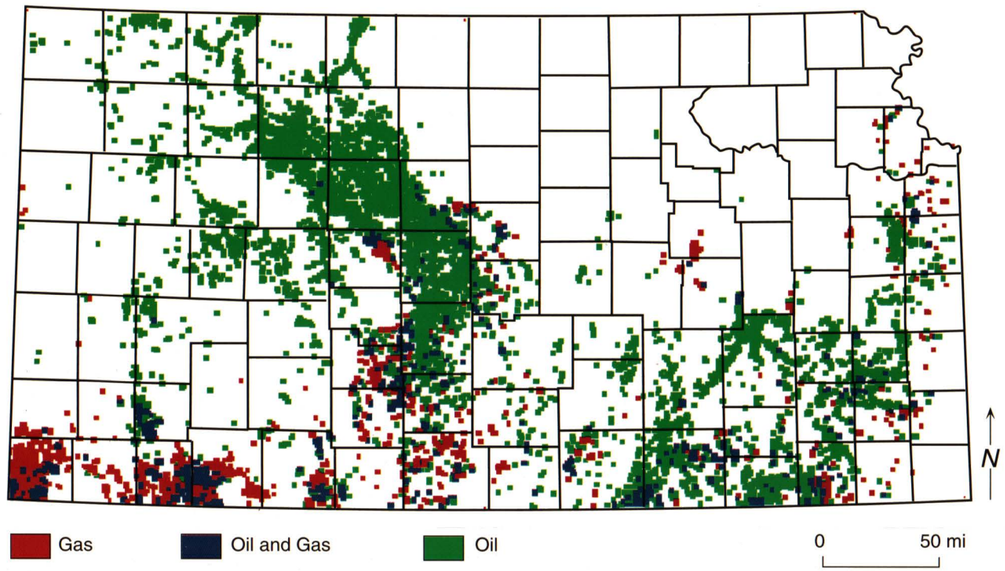

FIGURE 10—DISTRIBUTION OF PETROLEUM PRODUCTION FROM PENNSYLVANIAN ROCKS IN KANSAS (composited from data in Newell, Watney, Cheng, and Brownrigg, 1987).

Basement Tectonic Configuration in Kansas

D. L. Baars
Kansas Geological Survey, The University of Kansas, Lawrence, KS 66047

Abstract

The structure of the Precambrian basement of Kansas, midcontinent USA, is dominated by conjugate north-northeast- and northwest-trending wrench fault zones. North-northeast-trending faults of the Midcontinent Rift System (MRS) extend from Lake Superior across Kansas and into north-central Oklahoma. The fault zone widens from about 100 km (60 mi) in northeast Kansas to more than 160 km (96 mi) in south-central Kansas in a series of horsetail splays. North-northeast-trending structures of the MRS are displaced by about 80 km (48 mi) of dextral offset by the northwest-trending strike-slip fault zone.

Apparently penecontemporaneous northwest-trending wrench faults of the Bourbon Arch–Central Kansas uplift cross the state from southeast to northwest, offsetting MRS structures. The two conjugate wrench fault zones are complexly interrelated in central Kansas, where internal synthetic shears complicate axial horsts and grabens of the MRS. The Bourbon Arch is offset approximately 100 km (60 mi) by sinistral slip from the Central Kansas uplift along the MRS. The Humboldt fault zone at the eastern margin of the MRS was not offset significantly by northwest-trending faults, suggesting that the present-day expression of the southward-weakening fault zone was created during Pennsylvanian (Upper Carboniferous) rejuvenation of the basement fabric. Stratigraphic relationships record a history of repeated reactivation in Paleozoic time that strongly affected petroleum entrapment, with an especially strong pulse of uplift during Pennsylvanian time.

These rift zones are segments of continental-scale basement lineaments that are fundamental to the structural fabric of the North American basement. The Bourbon Arch–Central Kansas structural lane lies sub-parallel to the Olympic–Wichita lane that extends from southern Oklahoma to the northwest through the Paradox basin of eastern Utah, and the MRS lies sub-parallel to the Colorado Lineament which extends from the Grand Canyon in Arizona to the Lake Superior region. Thus, the basement of the western midcontinent and southern Rocky Mountains consists of large-scale fault zones that delineate suborthogonal basement blocks.

Introduction

The midcontinent and the state of Kansas, in particular, are generally believed to be geologically structureless like the scenery. Yet upon close examination of geophysical and subsurface data, the basement is found to be complexly faulted. In spite of earlier interpretations to the contrary, the basement of Kansas is here interpreted to be broken by wrench fault zones of regional proportions. These fault zones readily fit in a continental-scale structural fabric, which will be seen to delineate regional crustal blocks that together form the North American craton.

Basement Structure of Kansas

The Midcontinent Rift System (MRS) (sometimes referred to as the Central North American Rift System or Midcontinent Gravity High) has long been recognized from geophysical mapping to trend south-southwestward from Lake Superior into central Kansas in a snake-like curving pattern. Faults of this zone trend north-northeast–south-southwest across east-central Kansas, splaying outward toward the south (fig. 1). Lying parallel to the MRS immediately to the east is a complexly faulted positive feature known as the Nemaha uplift, bounded on the east by the Humboldt fault zone (Berendsen and Blair, 1986). In spite of its proximity and parallel trend, the Nemaha fault zone has generally been considered as a separate structure from the MRS, extending from southeastern Nebraska across eastern Kansas into north-central Oklahoma (Dolton and Finn, 1989).

Another prominent trend of basement faults crosses the MRS–Nemaha fault zone at near right angles. Numerous northwest-southeast-oriented faults extend from central Missouri into east-central Kansas, comprising what is often referred to as the Bourbon Arch complex (fig. 1). The Bourbon arch that affected lower to middle Paleozoic depositional patterns includes, and is bounded by, this zone of faults. The Bourbon arch complex appears to abut the Nemaha uplift. Another swarm of northwest-southeast faults in west-central Kansas marks a structurally high platform known as the Central Kansas uplift (CKU) (fig. 1). This faulted block appears to abut fault extensions of the MRS in central Kansas.

Subsurface mapping of lower Paleozoic rocks and the upper Precambrian surface reveals that the northwest-trending Bourbon arch fault zone complexly offsets faults of the Nemaha–MRS fault zone in east-central Kansas, breaking the basement into myriad suborthogonal fault blocks (fig. 1; Berendsen and Blair, 1986). Similarly, the southeastern extension of the Central Kansas uplift is complexly offset by faults that appear to be southerly extensions of the MRS (fig. 1). Geophysical maps, especially the second vertical derivative of gravity map (fig. 2), confirm these strongly intersecting relationships.

Berendsen and Blair (1986) interpreted the Nemaha–MRS fault system to exhibit sinistral strike-slip displacement along a regional wrench-fault zone, and this study confirms that interpretation. Many local offsetting relationships found on the Central Kansas uplift strongly suggest that dextral strike-slip movement has occurred along the northwest-trending fault zone as well.

In an effort to make order out of this chaos, the author has produced an interpretive sketch map (fig. 3) which demonstrates the present interpretation that the two fault trends intersect in central Kansas, each set displacing the other in their respective senses. The northwest-oriented Bourbon Arch-Central Kansas trend is offset sinistrally by Nemaha–MRS faults, and the Nemaha–MRS fault zone is offset in a dextral sense by the Bourbon Arch–Central Kansas faults. These zones of intersecting faults are further complicated by synthetic shears along the Nemaha uplift. That these faults displace one another suggests that movement of both sets was essentially penecontemporaneous. Thus, the intersection of the two major fault zones is interpreted as forming a conjugate set in central Kansas.

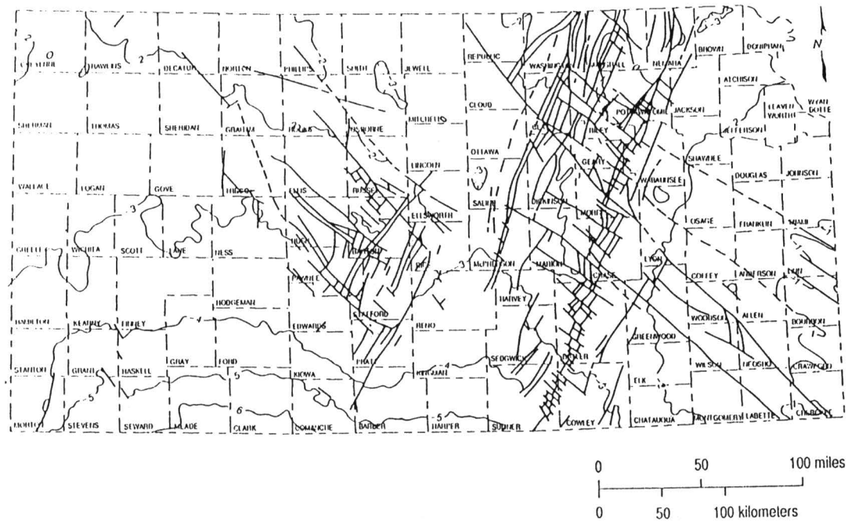

FIGURE 1—Map of the state of Kansas showing generalized fault patterns in the Precambrian basement as derived from subsurface studies. North-northeast–south-southwest faults are believed to be sinistral strike-slip faults and northwest-southeast structures are interpreted to be dextral strike-slip faults.

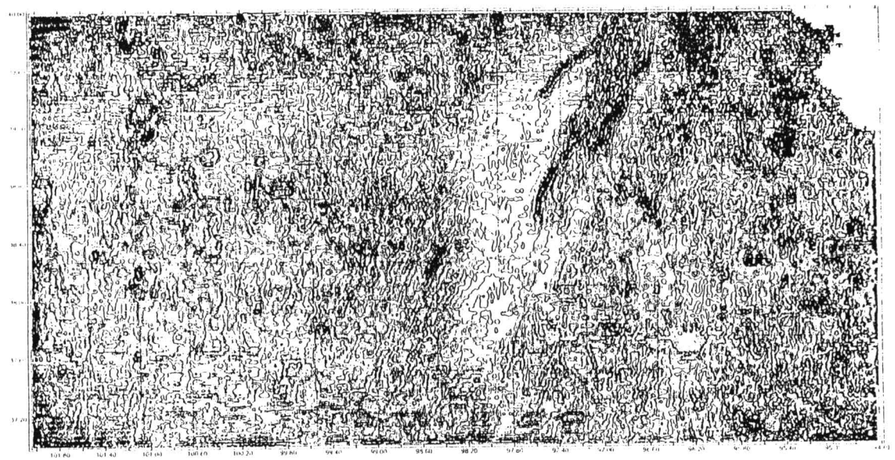

FIGURE 2—Second vertical derivative magnetic map of Kansas (reduced to the pole) compiled by the Kansas Geological Survey. The MRS is strongly apparent in the north-central part of the state, but other basement structures with north-northeast and northwest orientations are apparent. Compare with the basement structure map of fig. 1.

Regional Comparison

A similar intersection of northwest-southeast and northeast-southwest wrench fault zones was documented as occurring in the Paradox evaporite basin of southeastern Utah by Baars (1966) and Warner (1978). Warner cited evidence that the northeast-trending Colorado Lineament displays sinistral strike-slip offset, originating at about 1.7 Ga (middle Precambrian time). Baars and Ellingson (1984) further documented evidence that the northwest-trending Olympic–Wichita Lineament is a dextral wrench-fault zone of 1.6 to 1.7 Ga origin. As in Kansas, the intersecting wrench-fault zones appear to displace each other, forming a conjugate set. Stevenson and Baars (1986) interpreted the fault-bounded Paradox basin to be a large pull-apart basin of Pennsylvanian age, formed by reactivation along the northwesterly Olympic–Wichita Lineament, with extension facilitated by the northeasterly Colorado Lineament (fig. 4). The fault-bounded Uncompahgre uplift to the northeast supplied vast quantities of clastic sediments to the adjoining basin.

Although movement originated in middle Precambrian time, Baars (1966) documented strong evidence that movement along the Olympic–Wichita Lineament was rejuvenated in Late Cambrian, Late Devonian, Early Mississippian, and Middle Pennsylvanian time. Reactivation in Late Devonian time created shallow marine fault blocks upon which offshore sand bars formed and became petroleum reservoirs. Mississippian reactivation formed structurally controlled shoaling conditions that fostered development of Waulsortian banks, which upon dolomitization became excellent petroleum reservoirs (Baars, 1966). Further reactivation in Middle Pennsylvanian time again caused subtle shoals along the southern shelf of the Paradox basin that localized the development of algal bioherms that have produced prolific amounts of petroleum (Baars and Stevenson, 1982).

Regional Setting

The Olympic–Wichita Lineament, the key element in the origin of the Paradox basin, extends to the northwest at least across Utah, and has been interpreted (Baars, 1976) to be an extension of the Olympic–Wallowa Lineament of Wise (1963). It can be traced to the southeast into the fault complex of the southern Oklahoma aulacogen and beyond (Baars, 1976). The composite magnetic anomaly map of the United States (U.S. Geological Survey, 1982, *from* Hinze and Braile, 1988, plate 1B) clearly confirms these relationships. Thus, the Olympic–Wichita Lineament is a continental-scale structural feature interpreted to play a major role in the basement architecture of the North American craton (figs. 5 and 6).

The Pennsylvanian Paradox pull-apart basin lies along the Olympic–Wichita Lineament and is complimentary to a major fault-bounded uplift. In like fashion, the Pennsylvanian Anadarko and Arkoma basins of Oklahoma are intimately related to the same structural lineament, but lie in mirror-image to the Paradox basin. The uplifted sources of voluminous clastic sediments in southern Oklahoma occur to the south, and the deep structural basins are to the north of the fault zone (fig. 6). The deep basins of central Oklahoma are bounded generally to the north by a structurally controlled shallow shelf that lies along the Bourbon Arch–Central Kansas fault complex that in Kansas lies sub-parallel to the Olympic–Wichita Lineament (fig. 6). It is easy to interpret a close relationship between these Oklahoma basins and adjacent basement structures. (Perhaps these are also pull-apart basins?) As in the Paradox basin, Paleozoic rocks of the Kansas shelf of the Oklahoma basins show a long history of Paleozoic tectonic rejuvenations. Additionally, petroleum production from these strata is prolific.

Northern Midcontinent Basement Structure

Precambrian basement structures of the northern midcontinent are shown on fig. 5. To the north and east of Kansas, the structure has been generalized from Sims (1990). As previously discussed, the Midcontinent Rift System and the Central Plains Orogen are the principal structural features linking Kansas to the craton. It is noteworthy that the structural fabric of the northern midcontinent is, like the margins of the craton to the south and west, a network of northwest-southeast and northeast-southwest fault zones, many of which have been interpreted to be strike-slip structures (Sims, 1990). Thus, it appears that the basement structural fabric of the North American craton comprises several suborthogonal, fault-bounded blocks.

Figure 6 is a highly generalized map showing the relationships of Kansas basement structures to others of the midcontinent. Late Paleozoic fault-related basins are superimposed on the map to indicate their probable associations with basement structure. The interpretation shown on fig. 6 presents the MRS as a series of left-stepping en echelon fault zones as they appear to have occurred prior to extensional rifting. If this interpretation is correct, the MRS may consist of three originally distinctive compressional structures, later apparently joined by clockwise rotation of their associated crustal blocks, followed by late Precambrian relaxation of stress now exemplified by extension along the rift zone.

Such an interpretation of the MRS would explain the apparent age and structural discrepancies along the rift. Sims (1990, p. 5) depicts the northern rift as ". . . a medial horst of basalt-rhyolite flows and local overlying sedimentary basins that is flanked by red-beds, which compose clastic wedges along the margins of the rift." He (Sims, 1990) assigned an age of 1,000–1,200 Ma for basalts within the rift, or "about 1,100 Ma."

In contrast, the MRS in Kansas consists of numerous fault blocks (figs. 1 and 2), some of which contain predominantly basalts and others arkosic red beds; still others contain composite lithologies. Texaco recently drilled the Poersch #1 well within the MRS in southeastern Washington County, Kansas (SW SW sec. 31, T. 5 S., R. 5 E.), drilling and coring 8,454 ft (2,536 m) of Precambrian rocks. The upper 4,583 ft (1,3751 m) of Precambrian rock consisted of predominantly basalt and gabbro, with a few thin beds of arkose. The lower 3,871 ft (1,161 m) was predominently arkose with minor amounts of basalt and gabbro; the well bottomed in arkose (Berendsen et al., 1988). K-Ar dates by three different laboratories ranged from 587 to 800 Ma for a gabbro near the top of the Precambrian to 837–1,021 Ma for the deepest basalt encountered (Berendsen et al., 1988). Thus, rocks drilled in the deep test were considerably younger than the 1,100 Ma date for the northern MRS. Concern within the Kansas Geological Survey regarding the viability of these dates stems more from the younger age of the rocks in Kansas than of the quality of the dating process.

Discussion

A possible interpretation of the sequence of tectonic events that molded the basement of the midcontinent U.S.A. may be summarized as follows:

1) The crystalline basement was fractured to form orthogonal crustal blocks by northeast- and northwest-oriented faults in latest Archean or

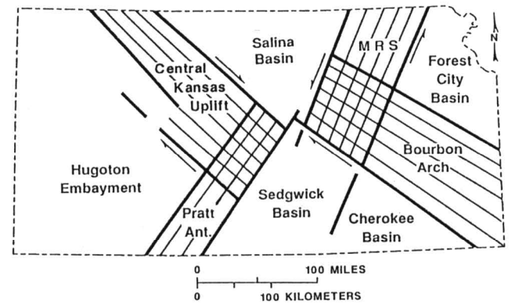

FIGURE 3—GROSSLY GENERALIZED DEPICTION SHOWING THE INTERPRETATION OF THE BASEMENT STRUCTURAL AND MAGNETIC MAPS OF FIGS. 1 AND 2. Structural fabrics are indicated by ruled patterns and interpreted sense of displacement shown with arrows. Where the structures cross in central Kansas, complex intersecting patterns result. The fault zones form basement uplifts that divide the region into five Paleozoic depositional basins.

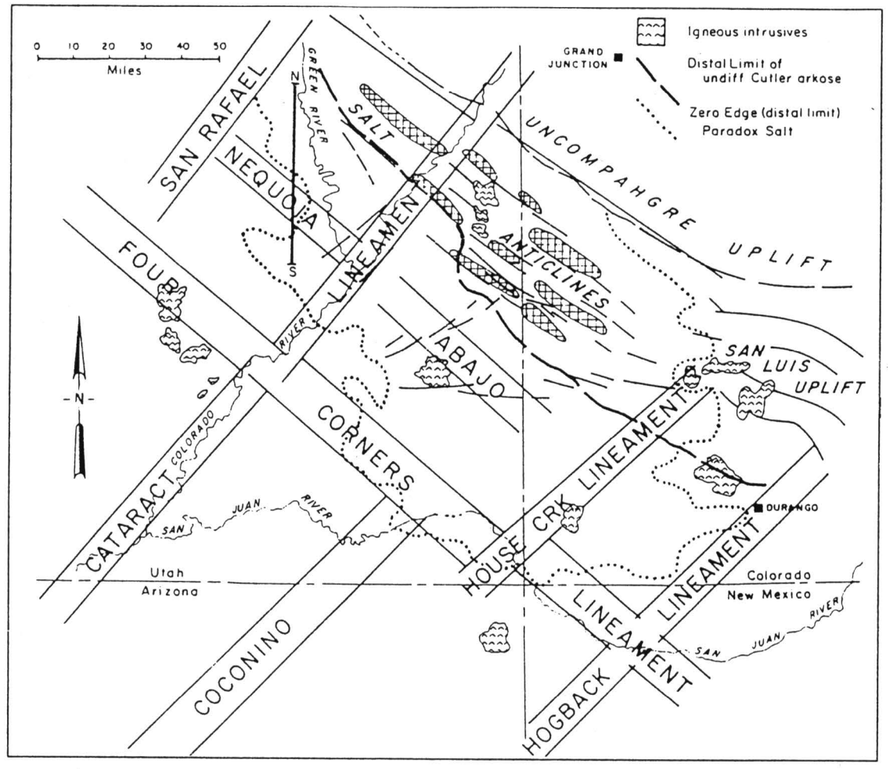

FIGURE 4—TECTONIC MAP OF THE PARADOX BASIN, SOUTHEASTERN UTAH AND SOUTHWESTERN COLORADO, FROM STEVENSON AND BAARS (1986). Northwesterly fault zones, indicated as basement "lineaments," are parts of the Olympic–Wichita Lineament, and northeasterly trends lie along the Colorado Lineament (see text). The Paradox evaporite basin of Pennsylvanian (Lower Carboniferous) age was interpreted to be a pull-apart basin. Compare this regmatic basement fabric with the regional structural pattern of fig. 6.

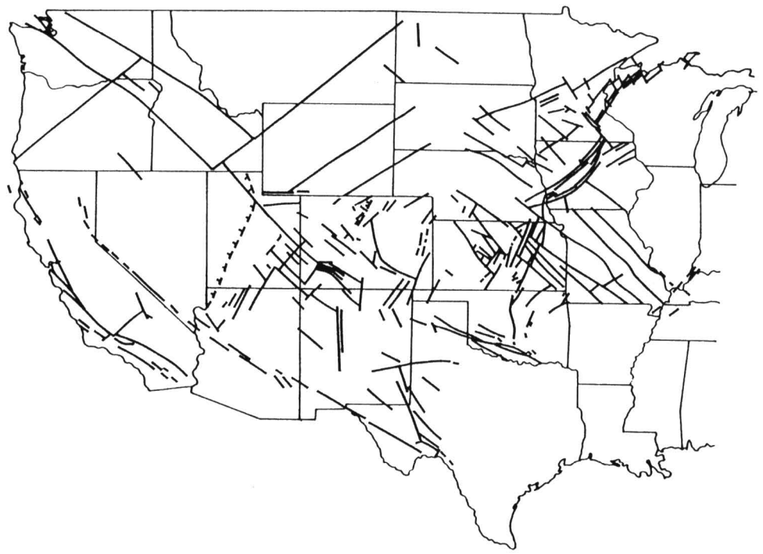

FIGURE 5—MAP OF THE WESTERN UNITED STATES SHOWING LOCATIONS OF SOME OF THE MOST SIGNIFICANT FAULT ZONES AND LINEAMENTS IN THE PRECAMBRIAN BASEMENT. Faults in the northern midcontinent, north of Kansas, are generalized from Sims (1990). Where sense of displacement has been determined, northwesterly structures are dextral and northeasterly structures are sinistral. In most cases, complex fault zones are shown as single lines.

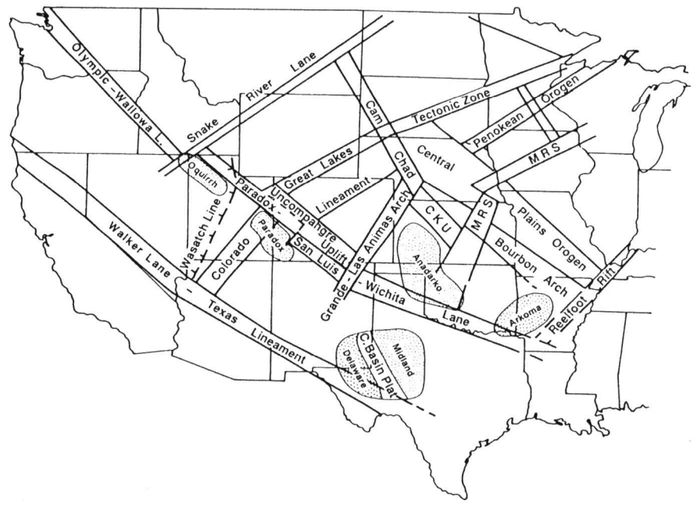

FIGURE 6—SUMMARY MAP SHOWING GENERALIZED BASEMENT STRUCTURAL ZONES OF FIG. 5, AND THE NAMES APPLIED TO THESE CONTINENTAL-SCALE TRENDS. Abreviations are: MRS = Midcontinent Rift System; CKU = Central Kansas uplift; Cam = Cambridge arch; Chad = Chadron arch. Note the obvious relationships of late Paleozoic depositional basins (Oquirrh, Paradox, Anadarko, and Arkoma) to the basement structural fabric. These are all fault-bounded basins of Pennsylvanian–Permian age formed by rejuvenation of basement structures during the Ancestral Rocky Mountains orogeny.

Early Proterozoic time (Sims, 1990) by north-south compressional strain.

2) Northeasterly strike-slip faults developed with sinistral sense of displacement; northwesterly faults were dextral. Master fault zones included the northeast-trending Colorado–Great Lakes tectonic zone, the Sierra Grande–Las Animas–Penokean trend, and the three left-stepping en echelon segments of the present-day MRS. Northwesterly master faults are the Texas–Walker Lane, the Olympic–Paradox–Wichita Lineament, and the Chadron–Cambridge–Bourbon arch trends.
3) Continued compression, or transpression, in the time frame 1,700–1,600 Ma started strike-slip dextral movement on the Olympic–Paradox–Wichita fault zone and consequent rotation of the large crustal blocks of the midcontinent. Thus, the apparent sinistral movement of faults that now offset the MRS in southern Minnesota and southeastern Nebraska respectively resulted from dextral rotation of crustal blocks.
4) By about 1,300 Ma, most of the transpressional stress was being released along the Texas Lineament–Walker Lane tectonic zone.
5) The compressional stress field began to relax by 1,100 Ma, and extension and volcanic activity along the MRS slowly worked southward from the Canadian Shield, ending in Kansas in latest Proterozoic time.
6) By Cambrian time, faults of the MRS apparently were locked and healed, perhaps because of the binding effects of basic igneous flows and intrusions. There is no evidence in Kansas to indicate that there was post-Proterozoic activity along the MRS except where faulting was not associated with late igneous activity, such as the Nemaha uplift–Humboldt fault zone and the southeastern Central Kansas uplift.
7) Minor intermittent activity along master faults continued throughout the lower Paleozoic, as indicated by subtle facies relationships in the sedimentary sequence.
8) By the beginning of Middle Pennsylvanian time, however, renewed intense tectonic activity, especially along the Olympic–Paradox–Wichita fault zone, created the major uplifts of the Ancestral Rocky Mountains and the complimentary deep Arkoma, Anadarko, Paradox, and Oquirrh basins. Faults of the Central Kansas–Bourbon Arch and Nemaha uplifts were reactivated, forming the northern shelves of the Oklahoma basins. Kluth and Coney (1981) blamed this tectonic convulsion on the collision of the South American–African plate with North America. However, it must be emphasized that this late Paleozoic event only reactivated existing basement structures.

Conclusions

The highly complex fault patterns of Kansas fit well with the continental-scale regmatic structure of the North American craton. When viewed at a continental scale, fault trends in Kansas are seen as segments of large-scale structural lanes that comprise the regional basement fabric. Although these structures originated in late Precambrian time, they were reactivated repeatedly throughout the Phanerozoic, affecting depositional and erosional patterns that localized petroleum reservoirs. Fault-controlled basement uplifts in Kansas comprise the complex northern shelves of the Oklahoma Pennsylvanian-age basins and are thus instrumental in controlling petroleum emplacement.

References

Baars, D. L., 1966, Pre-Pennsylvanian paleotectonics—Key to basin evolution and petroleum occurrences in Paradox basin, Utah and Colorado: American Association of Petroleum Geologists, Bulletin 50, p. 2,082–2,111

_____, 1976, The Colorado Plateau aulacogen, key to continental-scale basement rifting: 2nd International Conference on Basement Tectonics Proceedings, p. 157–164

Baars, D. L., and Ellingson, J. A., 1984, Geology of the western San Juan Mountains; *in*, Field Trip Guidebook, D. C. Brew, ed.: 37th Annual Meeting, Rocky Mountain Section, Geological Society of America, p. 1–45

Baars, D. L., and Stevenson, G. M., 1982, Subtle stratigraphic traps in Paleozoic rocks of Paradox basin; *in*, Deliberate Search for the Subtle Trap, M. T. Halbouty: American Association of Petroleum Geologists, Memoir 32, p. 131–158

Berendsen, P., and Blair, K. P., 1986, Subsurface structural maps over the Central North American Rift System (CNARS), central Kansas, with discussion: Kansas Geological Survey, Subsurface Geology Series 8, 16 p., 7 maps

Berendsen, P., Borcherding, R. M., Doveton, J., Gerhard, L., Newell, K. D., Steeples, D., and Watney, W. L., 1988, Texaco Poersch #1, Washington County, Kansas—Preliminary geologic report of the pre-Phanerozoic rocks: Kansas Geological Survey, Open-file Report 88–22, 116 p.

Dolton, G. L., and Finn, T. M., 1989, Petroleum geology of the Nemaha uplift, central midcontinent: U.S. Geological Survey, Open-file Report 88–450D, 39 p.

Kluth, C. G., and Coney, P. J., 1981, Plate tectonics of the Rocky Mountains: Geology, v. 9, p. 10–15

Hinze, W. J., and Braile, L. W., 1988, Geophysical aspects of the craton, U.S; *in*, Sedimentary Cover—North American Craton, U.S., L. L. Sloss, ed.: Boulder, Colorado, Geological Society of America, The Geology of North America, v. D–2, p. 5–24, plates

Sims, P. K., 1990, Precambrian basement map of the northern midcontinent, U.S.A.: U.S. Geological Survey, Map I–1853–A

Stevenson, G. M., and Baars, D. L., 1986, The Paradox—A pull-apart basin of Pennsylvanian age; *in*, Paleotectonics and Sedimentation in the Rocky Mountain Region, United States, J. A. Peterson, ed.: American Association of Petroleum Geologists, Memoir 41, p. 513–539

Warner, L. A., 1978, The Colorado Lineament—A Middle Precambrian wrench fault system: Geological Society of America, Bulletin 89, p. 161–171

Wise, D. U., 1963, An outrageous hypothesis for the tectonic pattern of the North American Cordillera: Geological Society of America, Bulletin 74, p. 357–362

Basement Control of Selected Oil and Gas Fields in Kansas as Determined by Detailed Residual Aeromagnetic Data

S. Parker Gay, Jr.
Applied Geophysics, Inc., Salt Lake City, UT 84111

Abstract

Basement control of Kansas oil and gas fields is shown to be very real and probably quite common. However, it is not possible to prove basement control with subsurface mapping, as few wells penetrate basement, nor with seismic, as the basement reflector is not always mappable. Residual aeromagnetics is the principal technique used in mapping basement, and it generally is employed only to outline the "basement fault block pattern," that is, the boundaries of the basement fault blocks. Trapping and reservoir-forming mechanisms, such as the presence or absence of basement hills and the amount and direction of throw on basement faults, must be determined independently from subsurface mapping or seismic studies. Nevertheless, magnetic basement mapping is a valuable exploration tool because it provides continuous large block coverage at low cost over both producing and nonproducing areas and furnishes many valuable exploration leads. These can be augmented with seismic or subsurface techniques for locating wells.

Introduction

This contribution is not intended to illustrate the geophysical parameters of a single Kansas oil or gas pool; rather, it is a discussion of a different approach to geological and geophysical thinking—basement control. Basement control can explain the presence of numerous oil and gas pools in Kansas, which, in turn, should prompt the discovery of additional pools using basement concepts. The understanding of basement control of structure in the sedimentary section has a long and seminal history in Kansas. Nevertheless, this history has been largely forgotten and the early concepts have been so effectively superseded by strain theory that basement control concepts are not widely used.

I will here discuss briefly some of the early history. Taylor (1917), writing of oilfield structures along the Nemaha Ridge in eastern Kansas, noted that " . . . the granite so far encountered has been found invariably under surface folds." His observations were noted by Moore (1920), state geologist of Kansas, 1916–1954, who proposed, that

> *The structure of the sedimentary rocks, then, appears to be controlled almost wholly by the nature of the hard granite which underlies the surface, and instead of folding by lateral pressure, it appears that the structures are the result of vertical settling or condensation of the sediments from compression by weight of overlying rocks.*

Moore deserves credit, along with Mehl and Blackwelder, all in 1920, for the nearly simultaneous recognition of compaction over basement topography as a cause of structure in the overlying sedimentary section. Acceptance of compaction theory was mixed in the decades of the 1920's, 30's, and 40's, but in 1949, the textbook, *Principles of Petroleum Geology*, by Professor Cecil G. Lalicker of the University of Kansas, was published with a full 20 pages devoted to the compaction phenomenon as a cause of structure and its value for petroleum exploration. This remained the most authoritative and extensive discussion of compaction for 40 years until a paper in the AAPG Bulletin in 1989 documented 30 basement hill cross sections from well data and demonstrated that all 30 basement hills resulted in compaction structures ("graviclines") in the overlying sedimentary section (Gay, 1989). Nine of these hills are located in Kansas and had been documented earlier by Walters (1946, 1953).

In spite of the rather auspicious Kansas-related beginnings of compaction theory and its later verification and thorough documentation, many present-day Kansas explorationists do not use the concept effectively, undoubtedly for the same reason stated by Blackwelder over 70 years ago: Structures are explained by "lateral compression," i.e., strain theory, because ". . . it is a predisposition inherited from our college courses" (Blackwelder, 1920).

If we do wish to use basement concepts, where do we go for advice? The above references, especially Lalicker, will suffice for a start, and I will here attempt to outline in a brief form the principal concepts.

Concepts of Basement Control

The 100% correlation of 30 basement hills with overlying compaction structures in the midcontinent (Gay, 1989) verified the concepts of the noted geologists of the 1920's, i.e., that compaction of the relatively soft sedimentary section over an irregular topography carved on the surface of the uncompactible crystalline basement results in a mimicking of the basement surface by the overlying sedimentary rocks. Structural highs appear over basement highs and structural lows over basement lows, although the amount of closure is much diminished, and structural development may cease at a prominent unconformity surface such as that developed at the top of the Mississippian section. Thus, it is not just isolated basement hills, or monadnocks, that affect the structure of the sedimentary section, it is the *entire paleotopography* of the basement.

Figure 1 is a map of structural high and low axes taken from a subsurface map with good well control in Pratt and Barber counties, Kansas (Williams, 1968). Figure 2 shows the axes of residual aeromagnetic highs and lows of the same area. These magnetic highs and lows reflect the *lithology* of the basement rocks because of differences in the magnetite content of the igneous and metamorphic rocks comprising the basement. These rock type changes and the generally sheared boundaries between them control the basement topography. Note the great similarity of the patterns in the two figures. Quantitative analysis resulted in a 74% correlation factor between the structural and basement alignments on the two maps. This demonstrates the pervasive basement topographic control of the structural axes, both highs and lows, in the lower parts of the sedimentary section in Kansas (and certainly elsewhere, as well).

The above concept opens up the exploration possibilities considerably. Now we must not only think of *structural closure* appearing over basement *highs*, we must also consider the possibility of fluvial deposits (Morrow channels, for example) occurring in structural-topographic *lows* on top of the Mississippian unconformity, or other unconformity surfaces in Kansas.

The second type of basement control, in addition to basement topographic control, is structural control, that is, faulting in the sedimentary section following old, reactivated basement faults. This is an old concept and adheres to the adage that "once a fault, always a fault." However, faults in the basement are not the type of sharp breaks we see in the sedimentary section. They are generally broad *shear zones* having widths of a half mile to a mile or more. These are the block boundaries of the "basement fault block pattern." Distances between basement shear zones vary considerably but are generally bracketed in the 2–5 mi (3–8 km) range. They occur in *sets* of parallel to sub-parallel fractures having different strike directions. They are of distinct ages and hence there are frequent terminations and truncations, and they are mappable with detailed residual aeromagnetics because of the rock type changes and magnetic susceptibility changes across them. These shear zones also generally erode low because they are intensely fractured, and this causes them to be visible on Landsat images of exposed basement, such as the Canadian Shield or other shield areas of the world. For emphasis, I summarize the above concepts in table 1.

Accepting these concepts of basement control, we can now proceed to the next step—the actual use of the concepts in exploration for oil and gas. First of all, in what ways does basement control affect hydrocarbon trapping and reservoir development?

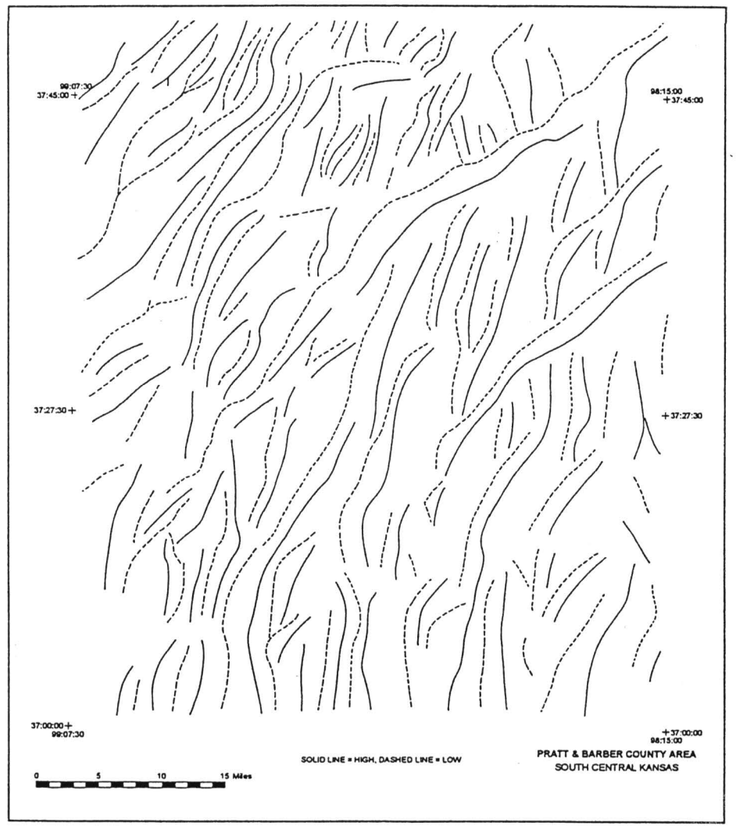

FIGURE 1—Axes of Simpson structural highs and lows, taken from Williams (1968).

An initial attempt at tabulating some of the ways this can occur is given in tables 2 and 3. Nineteen different geological mechanisms are shown. However, this must be considered an abbreviated list. Familiarity with hundreds, or thousands, of oil fields would be necessary for constructing a complete list, if such is possible. For example, in preparation for this paper a new type of reservoir not previously considered was found: oolite shoal development on a sea floor high over a reactivated basement fault (Collier Flats field, Comanche County, as described by Slamal, 1985; see fig. 13).

TABLE 1—TWO BASIC TYPES OF BASEMENT CONTROL ON THE OVERLYING SEDIMENTARY SECTION.

1. **Basement Topographic Control.** Structure is created in the overlying sedimentary section because of gravitational compaction of the sediments over the irregular basement topography. This results in many stratigraphic phenomena as well. (See, for example, Gay, 1989).

2. **Reactivated Basement Faults or Shear Zones.** Regional stresses reactivate some of the basement weakness zones, thus localizing structure, as well as causing stratigraphic effects in the overlying sedimentary section.

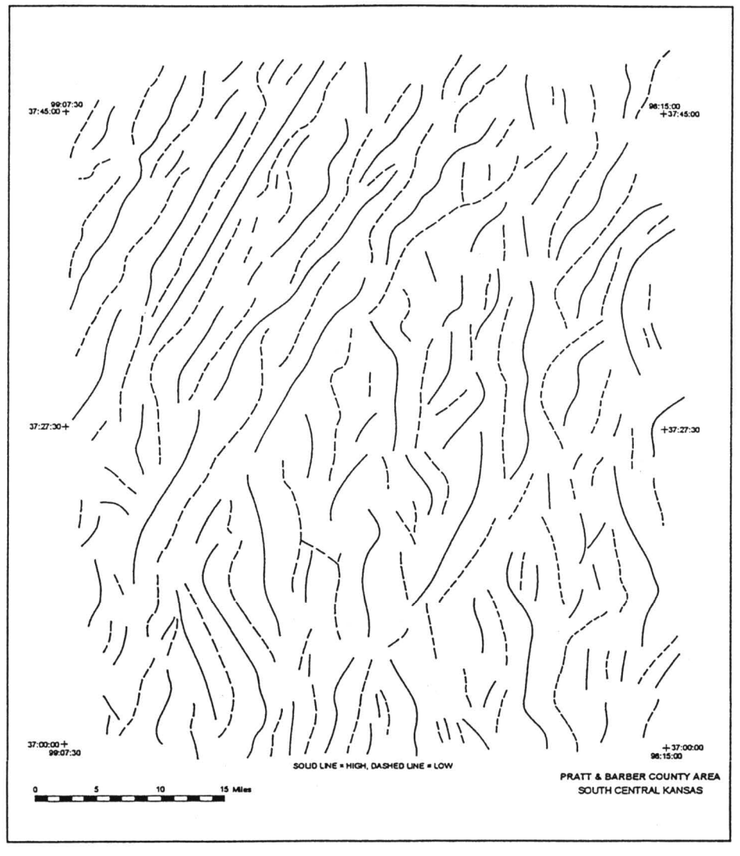

FIGURE 2—AXES OF RESIDUAL MAGNETIC HIGHS AND LOWS OF AREA OF FIG. 1, taken from proprietary aeromagnetic basement mapping by Applied Geophysics, Inc., 1982–83.

Concepts of Basement Geology

In order to utilize the above-described concepts of basement control on the structure and stratigraphy of the sedimentary section, it is helpful to understand a certain amount of basement, or Precambrian, geology. As a start, one could examine Landsat or SLAR images of outcropping basement areas worldwide ("shields") to get a feel for what the basement shear zones might look like underneath Kansas. However, it is not necessary to understand the details of Precambrian metamorphic and igneous petrology to grasp and apply basement concepts to exploration. Table 4 is a summary of sufficient information on basement geology to guide an exploration program.

The great complexity of basement structure results from active tectonism over the very long time span of the Precambrian Era, 4 billion years. This is approximately seven times longer than the time from the beginning of the Cambrian to the present. Not only this, but tectonism seems to increase as one goes back in earth time, i.e., plate tectonics is apparently slowing down, in spite of the fact that we are awed by the assemblage and breakup of Gondwana and Laurentia in the last 500 million years. A preliminary analysis of magnetic basement mapping in north-central Oklahoma–south-central Kansas revealed approximately eight major tectonic events that affected the Precambrian crust of the region (Gay, 1986). The great majority of these events, six and perhaps more, took place *prior to 1.4 billion years* ago. An emerging concept among students of Precambrian geology is that all the continents contain pieces of all the other continents due to the hectic pace of plate tectonics in the early stages of earth's history.

Some probable early Precambrian plate boundaries are visible in the residual magnetic data of the midcontinent region. Figure 3A is a banded contour version of residual magnetic data in south-central Kansas, covering approximately 3° of longitude and 1° of latitude. This figure is a regional map of the same magnetic data that are shown in the individual oil-field examples, figs. 4 through 13. It is made up of alternating bands of black, gray, and white between magnetic contour lines, rather than using the contour lines themselves. This type of presentation could also be called "variable density magnetics" and is extremely useful for seeing regional trends, or "sutures," in magnetic data.

Tectonic boundary A–A´ in fig. 3a, herein named the Argonia Suture, separates all northeast-trending basement blocks on the east from all north-trending basement blocks on the west. The area of northeast-trending blocks has previously been named the Sumner Terrane and the area of north-trending blocks the Sedgwick Terrane (fig. 3B) for the counties that fall within them (Gay, 1986). Sixty miles (100 km) to the west lies tectonic boundary B–B´, the Pratt Suture, which separates all northwest-trending

TABLE 2—TYPES OF TRAPS AND RESERVOIRS RESULTING FROM BASEMENT TOPOGRAPHIC CONTROL.

Direct
1. Positive structural closure over basement hills
2. Fluvial systems in low topography over basement lows
3. "Reverse dip" due to basement lows
4. Fracturing on flanks of basement hills
5. Pinchouts on flanks of basement hills

Indirect
6. Reefs and algal mounds on crests of graviclines
7. Clean sands, oolites, and carbonate grainstones on crests of graviclines
8. Pinchouts on flanks of graviclines

TABLE 3—TYPES OF TRAPS AND RESERVOIRS RESULTING FROM BASEMENT FAULT CONTROL.

Direct
1. Fault traps
2. Fractured reservoirs
3. Fractured and dolomitized limestones

Indirect
4. Folds over basement faults
5. Reefs and algal mounds along basement faults
6. Sand bars, oolite shoals, and carbonate grainstone development along basement faults
7. Fluvial systems located over basement faults (Low topography due to jointing)
8. Fluvial systems following fault scarps
9. Fluvial systems over down-dropped basement faults
10. Pinchouts over raised basement blocks
11. Reverse dip over basement faults

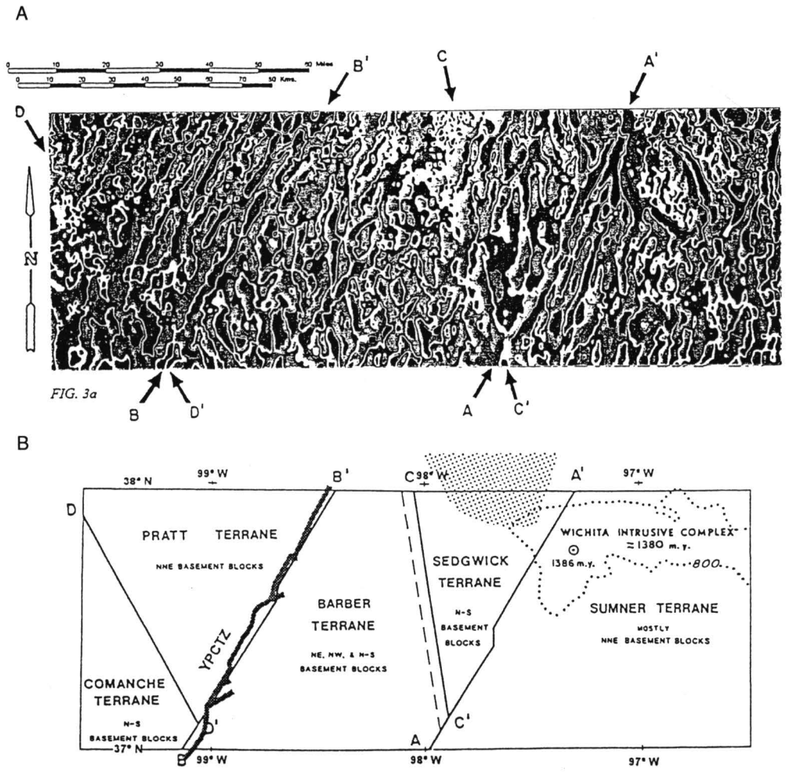

FIGURE 3A (top)—BANDED CONTOURS OF RESIDUAL MAGNETIC MAP OF PART OF SOUTH-CENTRAL KANSAS. Note the four obvious basement sutures (tectonic boundaries), as indicated by the arrows. 3B (bottom)—NAMES ARE GIVEN FOR THE VARIOUS PRECAMBRIAN TERRANES THAT ARE SEPARATED BY THE INDICATED SUTURES (from Gay, 1986, reproduced by permission of the Basement Tectonics Association). In the present paper, the sutures themselves are given names—A–A´, Argonia Suture; B–B´, Pratt Suture; C–C´, Pretty Prairie Suture; and D–D´, Joy Suture. Note the close correlation of the "Yellowstone–Peace Creek Tectonic Zone" (YPCTZ) with the Pratt Suture. It would be surprising if the Argonia Suture has not been similarly reactivated.

TABLE 4—BASEMENT FAULT BLOCK PATTERN—BASIC CONCEPTS.

1. Blocks of complexly faulted and folded metamorphic and igneous rocks are bounded by wide linear shear zones of crushed and broken mylonitized rock.
2. Individual blocks are composed of different rock types, or rocks of different metamorphic grade, and hence of different magnetic susceptibility. This makes it possible to map the block boundaries with residual high-resolution aeromagnetics.
3. Block boundaries generally fall into parallel sets, and several overlapping sets may exist in an area, resulting in a polygonal pattern for the individual blocks (H. Cloos, 1948).
4. Distances between parallel block boundaries generally vary between 3 and 8 km (2 mi and 5 mi) in all areas studied to date.
5. Later tectonic events reactivate the various fracture sets preferentially, according to their strike directions. Those most suited to relieving the imposed stress are the ones reactivated ("The New Basement Tectonics" -1972).
6. Erosion of the Precambrian surface generally results in topographic highs within the blocks and topographic lows following the block boundaries.

basement blocks of the Pratt Terrane on the west from the northeast, northwest, and north-south trends of the Barber Terrane on the east. The parallelism of A–A´ and B–B´ suggest a related origin, and one is reminded of the accreted terranes still active along the west coast of North America from California through Alaska. The ages of the Precambrian tectonic boundaries in fig. 3 must be considerably in excess of an age date of 1,386 Ma obtained within the Wichita intrusive complex shown on the east side of fig. 3, as the intrusive complex seems to be younger than A–A´. Even older are tectonic boundaries, C–C´ (Pretty Prairie Suture) and D–D´ (Joy Suture) which are truncated by A–A´ and B–B´ respectively. Certainly all the basement terranes, tectonic boundaries, and individual block boundaries were in place by Cambrian time and would have appeared much as they appear today in fig. 3.

The long strike length and great amount of inferred displacement of the tectonic boundaries in fig. 3 indicate that they are zones of greater than average weakness and as such, should be easily reactivated by later stress systems. This appears to be the case for the Pratt Suture, which is almost exactly coincident with the Pratt anticline or "Yellowstone–Peace Creek Tectonic Zone" (Berendsen and Blair, 1986; Slamal, personal communication, 1992). This is one of many zones in Kansas that are parallel to the Nemaha Ridge and are of latest Mississippian–early Pennsylvanian age. Perhaps such Mississippian–Pennsylvanian disruption also exists along the Argonia Suture (A–A´), but we have not examined subsurface data to investigate that possibility.

Mapping Basement Geology with Aeromagnetics

As outlined in table 4, basement tectonism juxtaposed rocks of differing magnetic susceptibilities across shear zones long before Cambrian time. It is this fact which allows us to map the shear zones with residual aeromagnetics. The shear zones thus fall on the magnetic gradients between the residual magnetic highs and lows. They are the principal zones of weakness in the basement that were reactivated by later (Paleozoic) tectonic events. Extensive comparison of reliable subsurface and seismic maps over large areas of the midcontinent and the Rocky Mountains at Applied Geophysics, Inc., have shown that fully 65–70% of the faults cutting the sedimentary section in these areas lie on magnetically mapped basement shear zones. Possibly the percentage of correlation would be higher if the mapped fault traces were more exact, but there are also cases where reliably defined faults cut through the interiors of basement blocks rather than following block boundaries. There are few absolutes in geology, but certainly a map of the basement fault block pattern is a good starting point for understanding the structure of an area.

Likewise, a map of the basement fault block pattern is an aid in locating basement topographic features. Basement shear zones (i.e., the edges of basement blocks) generally erode topographically low. That is why they are so evident on Landsat images of outcropping basement. This means that basement topographic highs generally fall within the block interiors, but where? Is the whole basement block a topographic high, is one edge higher, or are there several topographic highs within a single block? It is generally not possible to answer these questions with magnetics. In fact, some basement hills correspond to magnetic lows (see fig. 5). This would be the case where a basement hill is carved on a block that is less magnetic than surrounding blocks. Quartzite is one rock type that falls in the weakly magnetic category, and basement hills of quartzite are not uncommon in Kansas (Walters, 1953; J. Brewer, personal communication, 1983).

This brings up the problem of the ambiguity of magnetic data for mapping the vertical dimension; for example, attempting to determine whether a basement block is high or low or has a hill on it, or which side of a basement fault is up or down. Since the magnetic pattern is caused by the *lithology* of the basement rocks, neither of these problems is generally solvable with magnetics, especially in areas of low basement relief and limited fault throw, as in Kansas. In the highly regarded GSA Memoir 47, the first book ever written on aeromagnetic interpretation, it is stated: "Most magnetic anomalies arise from the lithology and not from the topography of the basement rock" (Vacquier et al., 1951, p. 8). In the third edition of *Introduction to Geophysical Prospecting,* a similar statement is made: "The magnetic relief observed over sedimentary basin areas is almost always controlled by the lithology of the basement rather than by its topography" (Dobrin, 1976, p. 534). On the other hand, the determination of the *edges* of magnetic anomalies (i.e., the boundaries of the basement blocks) or the horizontal dimensions, x and y, is *not* ambiguous.

It is recommended that the vertical dimension (z) be determined from subsurface or seismic data, which is precisely what these techniques measure. Thus, to obtain the best geologic picture of an area in all three dimensions (x, y, and z), one should integrate magnetic basement mapping with seismic and subsurface data. In reality, magnetics, like subsurface studies, must come before seismic, in order to determine the location of the most economic acquisition of seismic data as well as the necessary amount of data to obtain.

How does gravity surveying fit into this picture and when should it be employed? The author feels that in most cases gravity should be used like seismic as a follow-up tool run at a tight station-spacing of 200–500 ft (60–150 m) along specific profile lines, each a few miles long. In many cases, this could indicate whether a basement hill is present or which side of a fault is up. However, gravity is almost never used in this fashion. It is generally run on grids of 1 mi (1.6 km) spacing (sometimes with tighter spacing along roads) to give a regional picture. Here, it competes with aeromagnetics, which does a better and more detailed job of mapping the basement fault pattern. Aeromagnetic readings are spaced from tens of feet apart up to a maximum of 200 ft (60 m) along line, and this high density of data essentially defines the magnetic profile completely. The profile lines can be flown at any line spacing desired but are generally flown at a separation equal to one third to one half the depth to basement.

Many, or most, basement block boundaries are not readily defined by gravity as there is little contrast in the densities of the juxtaposed blocks. Overall, densities of basement rocks vary from about only 2.5 gms/cc to a high of 3.2 gms/cc (in rare cases)—a 28% change. However, magnetic susceptibilities of basement rocks routinely vary from 50 microcgs to about 5,000 microcgs. This is a 100 times change or 10,000%.

Selected Examples of Basement Control on Oil and Gas Fields in Kansas

The following pages show selected examples of known oil and gas fields in Kansas controlled, or apparently controlled, by basement features. All these examples are relatively clear-cut and straightforward. That is, the magnetic pattern conforms closely to an oil or gas field or some basement structure which apparently controls the subsurface structure or stratigraphy of the field. One could argue that the veracity of the presented cases is not proven and that the correlations may be fortuitous. On the other hand, one could never prove basement control anywhere at any time unless there were many wells to basement on a given trap or structure. Such a situation is unachievable in actual practice due to the limited number of wells to basement, and we must work with available data and the known principles of geology and geophysics to arrive at answers that satisfy the data in a logical manner. For the topographic aspects, it is important to remember scattered cases throughout the Midwest where there *were* sufficient wells to basement to define individual basement hills and to realize that compaction anticlines ("graviclines") were present in 30 out of 30 cases (Gay, 1989). For the structural aspects, we must keep in mind that about 65% of the well-documented faults in the sedimentary section that occur within the boundaries of aeromagnetic surveys coincide with residual magnetic gradients, that is, on magnetically mapped basement shear zones.

Moore SW Field, Pratt County, fig. 4

This example shows a structural high that coincides with a residual aeromagnetic high. For this reason it is considered a probable compaction structure ("gravicline") over a basement hill. Similar examples could be presented for Newbury field in Wabaunsee County, Coleman and Lake Creek fields in Montgomery County, Wellington field in Sumner County, and a number of others. Many additional fields correlate with residual aeromagnetic highs, but there is no published information indicating that they are structural fields.

Willowdale Field, Kingman County, fig. 5

This example shows a structural high that coincides with a residual aeromagnetic low. Note the near-straight line gradients on west, south, and east on both sets of

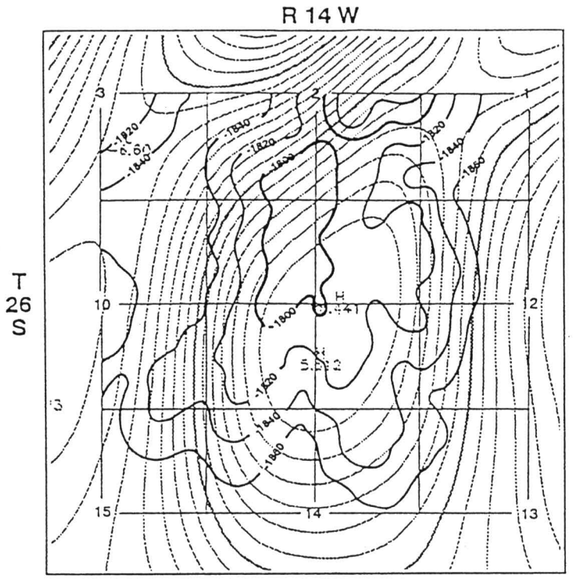

FIGURE 4—MOORE SW FIELD, PRATT COUNTY, A PROBABLE GRAVICLINE, as evidenced by the close correspondence of the Lansing structure contours (black) with the residual aeromagnetic high (gray). Structure is from Hellman (1985).

contours, indicating the existence of a probable underlying basement hill carved in a weakly magnetic basement rock, such as quartzite. Subsequent conversations in Wichita revealed that some exploration groups had previously noted the same phenomenon and used this concept as an exploration tool in Kansas (J. Brewer, personal conversation, 1983). Other similar correlations of structural highs with residual aeromagnetic lows have been noted for Bloom field in Barber County, Rosedale field in Kingman County, and Wiltex field in Harper County.

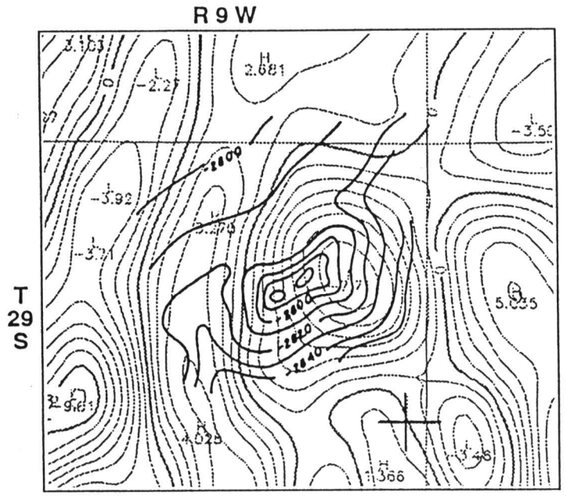

FIGURE 5—WILLOWDALE FIELD, KINGMAN COUNTY, A PROBABLE GRAVICLINE, as evidenced by the close correspondence of the Viola structure contours (black) with the residual aeromagnetic low (gray). Structure is from Cruce (1956).

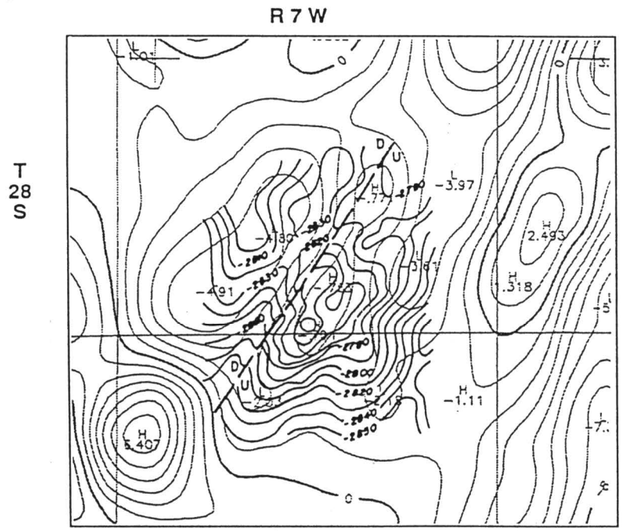

FIGURE 6—ALAMEDA FIELD, KINGMAN COUNTY, A PROBABLE GRAVICLINE, as evidenced by the close correspondence of the Viola structure contours (black) with the residual aeromagnetic high (gray). Structure is from King (1965).

Alameda Field, Kingman County, fig. 6

This is an interesting structure and could have been included with those in the first example (fig. 4) because it falls on a localized magnetic high. However, it is possible to interpret more of the basement geology here since the field falls precisely within a circular area of lower magnetic susceptibility than the area surrounding it. This is especially evident on the 3D stereo pair of the magnetic map. It is thus proposed that the area is underlain by a Precambrian igneous intrusion [4–5 mi (6.4–8 m) in diameter] onto which a basement hill was eroded. A down-to-the-northwest fault cuts all formations older than Pennsylvanian and coincides precisely with a 3- to 5-gamma residual magnetic gradient. This is typical of the fault correlations obtained with basement mapping where reliable geological data exists.

Coats Field, Pratt County, fig. 7

This example is included to illustrate a remarkable fault correlation, but there is reason to suspect that Coats field is a compaction structure over a basement hill. What else would cause a structure in south-central Kansas less than 1 mi (1.6 km) wide to have over 450 ft (135 m) of total vertical displacement on the Arbuckle? (Localized

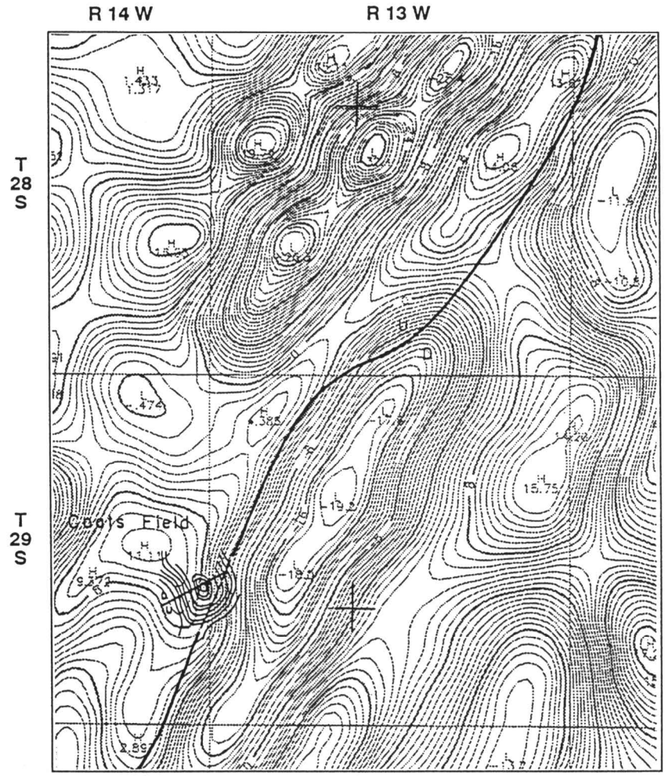

FIGURE 7—COATS FIELD, PRATT COUNTY, A POSSIBLE GRAVICLINE. Other possible graviclines would be the "corners" (noses) of the same magnetic high where Coats field is located. Structure (black) is on top of Arbuckle at a 50-ft (15-m) contour interval and is from Curtis (1956). Note the correlation of the long northeast fault, the deep manifestation of the shallow Pratt anticline, along the "Yellowstone–Peace Creek Tectonic Zone" with the residual magnetic gradients (gray).

basement "uplift," piston fashion, is not a viable tectonic mechanism.) Realizing that such a basement topographic high probably does exist on the edge of a 3 × 3 mi (4.8 × 4.8 km) wide basement block as mapped by the magnetic high (fig. 7), one might speculate that there is a basement rock type here which erodes to a "knobby" terrain (granite, perhaps?). The four "corners" of this block–NW, NE, SE, and SW–corresponding to the magnetic high thus become interesting places to use subsurface or seismic data to look for other structural highs. What is remarkable in fig. 7 is that the short NNE-trending fault within Coats field and the long seismically mapped fault underlying the Pratt anticline correlate precisely with residual magnetic gradients (i.e., the locations where one draws basement shear zones).

Stateline Trend, Wallace and Greeley Counties, Kansas, and Cheyenne and Kiowa Counties, Colorado, fig. 8

If high basement topography causes structural highs in the overlying sedimentary section, then low basement topography must result in overlying structural lows. It is

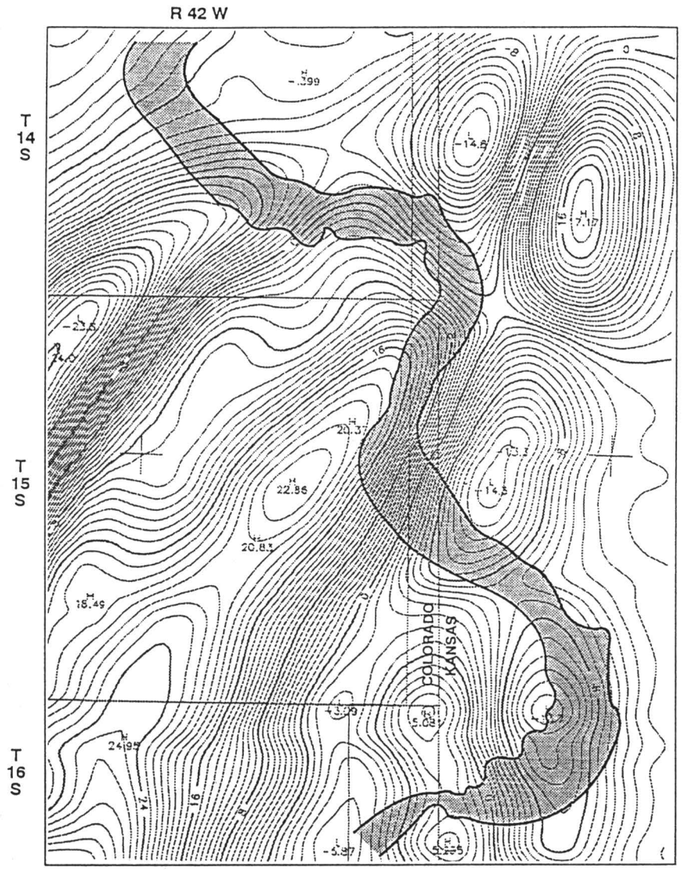

FIGURE 8—STATELINE TREND, WALLACE AND GREELEY COUNTIES, KANSAS, AND CHEYENNE AND KIOWA COUNTIES, COLORADO, superimposed on residual magnetic contours (gray). This prolific Pennsylvanian Morrow channel avoids residual magnetic highs and follows the magnetic lows and gradient areas, as do many similar channels in southeast Colorado.

possible then, through the process of erosion, that Mississippian structural lows in western Kansas–eastern Colorado became Pennsylvanian topographic lows. They would thus be favorable sites for the deposition of Morrow channel sands.

In 1985, one user of residual aeromagnetic data in southeast Colorado found an 85% correlation of Morrow channels with residual aeromagnetic lows. This suggests that there is a rock type in the basement of southeast Colorado that is magnetically weak and erodes topographically low. The Morrow channels there seem to follow magnetic lows and avoid magnetic highs. The subsequently discovered additions of Mt. Pearl and Siaana fields to the Sorrento Trend in Colorado, and the later discovery of the Stateline Trend along the Kansas–Colorado line, substantiated this observation. In fig. 8, the Stateline Trend is seen to bend sharply around a strong northeast-striking residual magnetic high and generally follows the magnetic gradients (i.e., the shear zones, which we expect to erode low) or the magnetic lows themselves. Thus, residual magnetics may be of some value in the search for new channels in the Morrow play, but again, only if integrated or followed up with other geological and geophysical information.

Gillian and O.S.A. Fields, Sedgwick County, fig. 9

Gillian field has been described as a fault trap on a structurally high horst block (Shawver, 1965a). O.S.A. field is an updip pinchout of the uppermost Simpson sandstone on this same block (Shawver, 1965b). A 1983 interpretation of a residual aeromagnetic survey covering this area precisely defined the west-bounding fault. A series of similar parallel faults, two of which are shown in fig. 9, have been equally well defined by the aeromagnetic data and present additional exploration opportunities. The logical follow-up would be detailed subsurface studies followed by seismic profiling over selected "look-alikes."

Ponca City Field, Kay County, Oklahoma, fig. 10

Many truly prolific oil fields have been found along the Nemaha structural system in eastern Kansas and north-central Oklahoma. The Ponca City field in Oklahoma [only 20 mi (32 km) south of the Kansas line] is included in this paper as a remarkable example of such a field. Figure 10 shows the location of the field relative to a strong residual magnetic gradient corresponding to a basement shear zone. Eastward-directed reverse fault movement of the shear zone (as shown in the sketch at the bottom) would explain the asymmetry of the fold. Such fields are common along the Nemaha Ridge, the Beaumont anticline, and other parallel trends in both Kansas and Oklahoma.

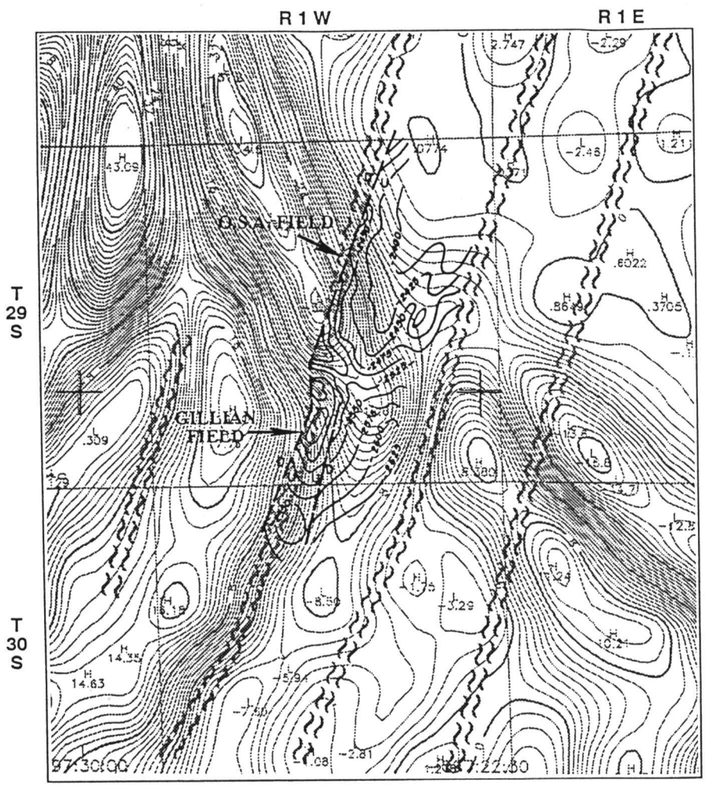

FIGURE 9—Gillian and O.S.A. fields, Sedgwick County. The west fault of Gillian field, which forms the trap, was exactly defined by a 1983 interpretation of the residual aeromagnetic map (gray contours). Structure contours (black) are on top of the Simpson Group, the producing horizon, and are from Sawver (1965a, b).

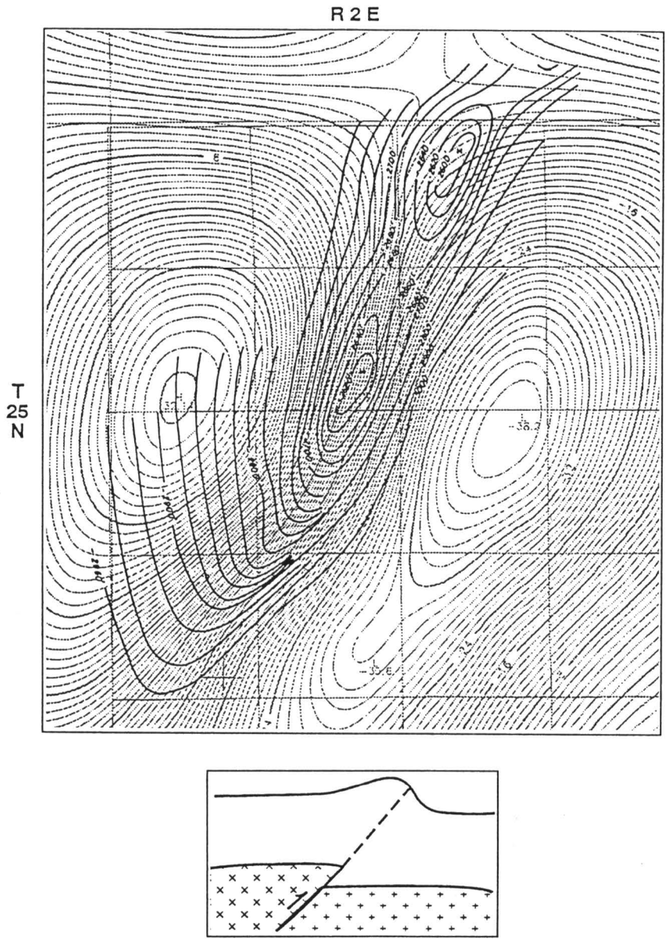

FIGURE 10—Ponca City field, Kay County, Oklahoma. Classic example of an asymmetric fold (black contours) over a basement shear zone defined by the steep gradient in the residual magnetic contours (gray). Reactivation of the shear zone by west-dipping reverse fault movement as in the sketch, is the probable cause of this structure. Mississippi lime structure contours are from Clark and Daniels (1929).

Davis Ranch Field, Wabaunsee County, fig. 11

This field [160 mi (256 km) northeast of the Ponca City, Oklahoma, field] is located on the "Alma Trend," which lies 10 mi (16 km) east of, and parallel to, the Nemaha Ridge. Davis Ranch field is a structural look-alike to the Ponca City field and is likewise a large producer falling along a magnetically mapped basement shear zone, although not precisely on it to the south. Auburn and John Creek to the south and Mill Creek to the north are similar fields located over basement faults.

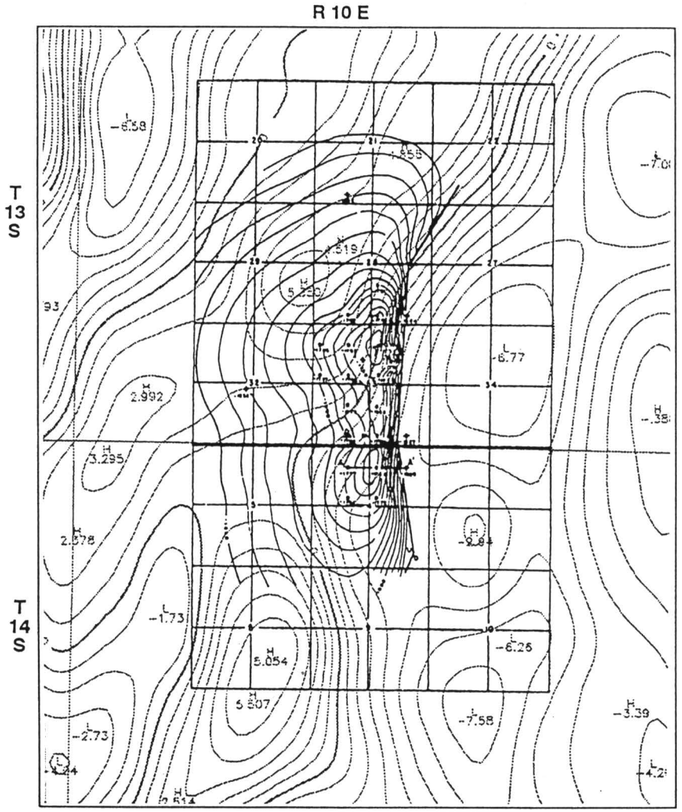

FIGURE 11—Davis Ranch field, Wabaunsee County. A Kansas analog to Ponca City field (fig. 10), 160 mi (256 km) north of Ponca City in the Alma Trend along the same Nemaha-related fault system. Black contours are top of Viola formation; gray contours are residual magnetics. Structure is from *Kansas Oil and Gas Fields*, vol. 3, 1960, p. 53.

Cunningham Field, Pratt and Kingman Counties, fig. 12

This structural field is similar to the Ponca City field and those of the Alma Trend just mentioned; however, it lies some 75 mi (120 km) west of the Nemaha Ridge along an apparent splay of the Yellowstone–Peace Creek Tectonic Zone. This zone is parallel to the Nemaha Ridge and apparently resulted from the same late-Mississippian compression as the Ponca City and Alma Trend fields. Note the excellent correlation of Cunningham field with the underlying magnetically mapped basement shear zone. Other Kansas fields that seem to fall in the same category are Weathered in Cowley County, North Yellowstone in Comanche County, and Bartholomew in Sedgwick County.

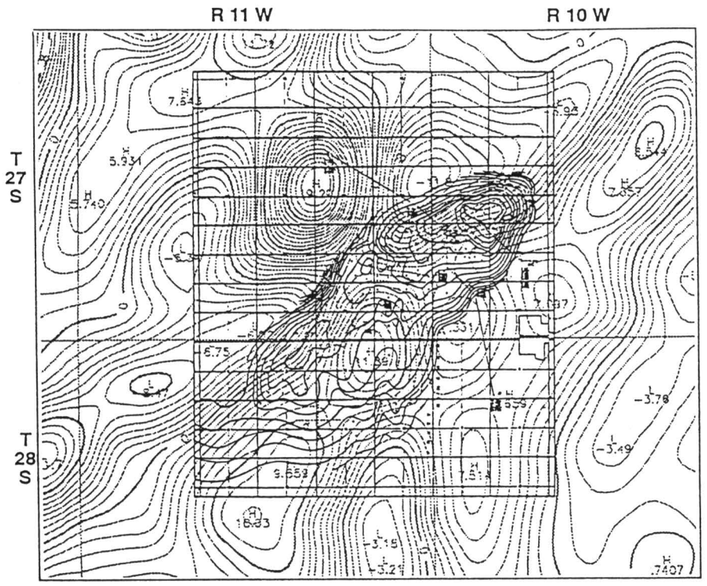

FIGURE 12—Cunningham field, Pratt and Kingman counties. Close correlation of the underlying basement shear zone with the asymmetric anticline indicates a probable reverse fault here, as in other similar fields in Kansas and Oklahoma. Black contours are on top of the Lansing formation; gray contours are residual magnetics. Structure is from Skelly Oil Company Geology Department, 1956.

Collier Flats Field, Comanche County, fig. 13

It is fitting to end this suite of field correlations with a stratigraphic example because many times it is stated that structure mapping of the basement is not relevant to certain exploration plays as they are "purely stratigraphic." Some examples of such stratigraphic plays lying along basement faults are the Shannon–Sussex–Ferguson offshore sandbars in the Powder River basin in Wyoming, the Muddy fluvial system of the Powder River basin, and the Desert Creek algal mounds of the Paradox basin in Colorado. Slamal (1985) described the Collier Flats field in Comanche County, Kansas, as an oolite shoal that developed on a "structurally high element." The field coincides almost precisely with a magnetically mapped basement shear zone, and Slamal states that this could have been vertically reactivated to produce a sea-floor high that localized the oolite development of Missourian age in the Swope Limestone of the Kansas City Group (Slamal, personal communication, 1992).

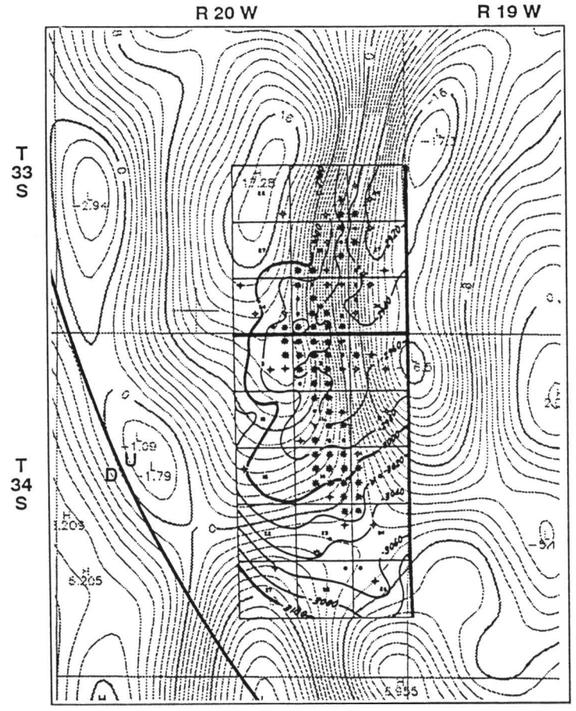

FIGURE 13—Collier Flats field, Comanche County. Production in this field is from an oolite shoal that evidently developed on a fault scarp over an underlying basement fault defined by the gradient in the residual magnetic contours (gray). Structure contours (black) are on top of Pennsylvanian Swope limestone. Structure and wells are from Slamal (1985).

Conclusions

This paper demonstrates two main points:

1) Basement control of oil and gas field traps and structures is highly prevalent, if not pervasive, in Kansas, and
2) Residual magnetic maps provide leads for exploration for these basement-controlled traps and structures.

The first point, that basement control exists, is academic if we cannot map the basement in order to take advantage of basement control. This factor illustrates why point number two is important. There is a means of mapping the basement to some degree, even if that means, residual aeromagnetics, is imperfect. Magnetics cannot locate basement hills with certainty, nor can it be determined which basement shear zones mapped have been offset by faulting and in what direction. Nevertheless, residual aeromagnetics can be used as a starting point, followed in favorable areas with other exploration tools.

In the writer's opinion, the quickest and surest way to use the concept of basement control as an exploration technique is to search for nearby analogs ("look-alikes") to known basement controlled fields. If Collier Flats field, for example, resulted from Pennsylvanian oolite deposition on a fault scarp over a basement fault, is it possible that similar features exist either along strike or on adjacent basement faults? Basement tectonic concepts indicate probable parallel faults two or three miles away on either side, and within this short distance the sedimentary processes may not have changed significantly. If Willowdale field is a gravicline over a basement hill carved in a quartzite block characterized by a residual magnetic low, are there other similar magnetic lows nearby? If Davis Ranch field is an asymmetrical fold over a reverse fault in the basement, surely the stresses caused other such structures along strike (or possibly parallel to it a few miles away).

When Applied Geophysics, Inc., first came to Wichita a decade ago to promote basement mapping with aeromagnetics, several prominent geologists told us: "We're beyond that stage in Kansas." Actually, the reverse appears be true. Many geologists in Kansas and in other parts of the United States have not yet reached "that stage," that is, the stage of understanding that extensive basement control is present in the sedimentary section and that there are ways and means of taking advantage of it. Those geologists who do will certainly discover additional important oil and gas reserves.

ACKNOWLEDGMENTS—The author wishes to acknowledge the continuing encouragement of William A. Miller in the preparation of this paper; the helpful discussions over the years with many Kansas geoscientists, especially R. Walters, A. James, T. Ray, and D. McGuire; and the valuable review and discussions by R. Slamal and D. Baars. The author also is greatly indebted to the staff at Applied Geophysics, Inc. (B. Opfermann, B. Hawley, P. Haslam, R. Andrus, B. Wallin, D. Pap, and F. Benjamin) for their useful assistance and innovative ideas in preparation of this paper.

References

Berendsen, P., and K. Blair, 1986, Subsurface structural maps over the CNARS with discussion: Kansas Geological Survey, Subsurface Geology Series 8, 20 p., 7 maps

Blackwelder, E., 1920, The origin of the central Kansas oil domes: American Association of Petroleum Geologists, Bulletin, v. 4, p. 89–94

Clark, S. K., and Daniels, J. I., 1929, Relation between structure and production in the Mervine, Ponca, Blackwell, and south Blackwell oil fields, Kay County, Oklahoma: American Association of Petroleum Geologists, Structure of Typical American Oil Fields, v.1, p. 158–175

Cloos, H., 1948, The ancient European basement blocks—preliminary note: American Geophysical Union, Transactions, v. 29, no. 1, p. 99–103

Cruce, J. D., 1956, Willowdale Pool: Kansas Geological Society, Kansas Oil and Gas Pools, v. 1, p. 95–97

Curtis, G. R., 1956, Coats field: Kansas Geological Society, Kansas Oil and Gas Pools, v. 1, p. 19–24

Dobrin, M. B., 1976, Introduction to geophysical prospecting, third ed.: McGraw–Hill, 630 p.

Gay, S. P., 1985, Gravitational compaction, a neglected mechanism in structural and stratigraphic studies: new evidence from midcontinent, U.S.A.: Applied Geophysics, Inc., Salt Lake City, 109 p.

_____, 1986, Relative timing of tectonic events in newly recognized Precambrian terranes in south-central Kansas, U.S.A., as determined by residual aeromagnetic data: Basement Tectonics Proceedings, v. 6, p. 153–167

_____, 1989, Gravitational compaction, a neglected mechanism in structural and stratigraphic studies: new evidence from midcontinent, U.S.A.: American Association of Petroleum Geologists, Bulletin, v. 73, p. 641–657

Hellman, T. D., 1985, Moore SW field: Kansas Geological Society, Kansas Oil and Gas Fields, v. 5, p. 175–181

King, C. R., 1965, Alameda field: Kansas Geological Society, Kansas Oil and Gas Fields, v. 4, p. 1–17

Lalicker, C. G., 1949, Principles of petroleum geology: New York, Appleton–Century–Crofts, 377 p.

Mehl, M. G., 1920, The influence of the differential compression of sediments on the attitude of bedded rocks (abs.): Science, New Series, v. 51, p. 520

Moore, R. C., 1920, The relation of the buried granite in Kansas to oil production: American Association of Petroleum Geologists, Bulletin, v. 4, p. 255–261

Shawver, D. D., 1965a, Gillian field: Kansas Geological Society, Kansas Oil and Gas Fields, v. 4, p. 78–87

_____, 1965b, O.S.A. field: Kansas Geological Society, Kansas Oil and Gas Fields, v. 4, p. 175–184

Skelly Oil Co., Geology Department, 1956, Cunningham field: Kansas Geological Society, Kansas Oil and Gas Fields, v. 1, p. 25–28

Slamal, R., 1985, Collier Flats field: Kansas Geological Society, Kansas Oil and Gas Fields, v. 5, p. 43–52

Taylor, C. H., 1917, The granites of Kansas: Bulletin of the Southwestern Association of Petroleum Geologists, v. 1, p. 111–126

Vacquier, V., Steenland, N. C., Henderson, R. G., and Zietz, I., 1951, Interpretation of aeromagnetic maps: Geological Society of America, Memoir 47, 151 p.

Walters, R. F., 1946, Buried Precambrian hills in northeastern Barton county, central Kansas: American Association of Petroleum Geologists, Bulletin, v. 30, p. 660–710

_____, 1953, Oil production from fractured Precambrian basement rocks in central Kansas: American Association of Petroleum Geologists, Bulletin, v. 37, p. 300–313

Williams, C. D., 1968, Pre-Permian geology of the Pratt anticline area in south-central Kansas: M.S. thesis, Wichita State University, 116 p.

Geophysical Model from Potential-field Data in Montgomery County, Kansas

Jianghai Xia
Kansas Geological Survey, The University of Kansas, Lawrence, KS 66047

Abstract

Potential-field data (gravity and aeromagnetic data with precision of 0.1 mGal and 3 nT, respectively) are inverted into density/magnetization distribution in the Precambrian basement of Montgomery County, Kansas, by a method of the iterative forward modeling of Xia and Sprowl (1992). The depth to the top of the Precambrian layer is determined by well data. The thickness of the layer is determined by trial-and-error such that the calculated density/magnetization models show reasonable correspondence with known geology. The inverted models agree with observed data to the root-mean-square error and the maximum deviation of 0.16 mGal and 1.4 mGal, respectively for gravity data, and of 5.3 nT and 18.8 nT, respectively, for magnetic data. The observed anomalies have been topographically corrected (for gravity data) and separated from the original anomaly (for gravity and magnetic data). The anomalies used for the inversion are obtained after subtracting the original anomaly's contribution by the subsurface terrane, which is modeled by well data. The inverted results show distribution of higher-than-average density/magnetization in the southwestern basement rock of the county, possibly due to an intrusion of granodiorite containing more than 3% of magnetite.

Introduction

Density and magnetization are physical properties that can change significantly from one rock type to another. Knowledge of the distribution of these properties within the ground can convey information about subsurface geology. Because each of these two properties is a source of potential-field anomalies, measuring potential fields at the surface makes it possible to infer the subsurface geology through an appropriate

The inversion of potential-field data does not have a unique solution because any observed potential-field data can be produced by an infinite number of possible sources (Dobrin and Savit, 1988). Therefore, the inversion consists essentially in finding a source in which certain parameter(s) may be adjusted to fit the observations. One technique for inversion of potential-field data is "inversion by iterative forward modeling." This technique repeats a sequence of direct calculation of the potential-field anomaly from a given model, comparison of the calculated and observed values, and modification of the model until a satisfactory agreement is reached between observed and calculated values (Dobrin and Savit, 1988). A number of methods have been developed for the forward calculation of potential fields from a model in two and three dimensions. Talwani et al. (1959) provides an efficient means of calculation for a two-dimensional model. Cady (1980) provides the modified Talwani method for so-called two-and-one-half-dimensional models, and Plouff (1976) described the method for three-dimensional models. Parker (1973) described a fast algorithm employing the Fourier-transform technique which can handle laterally varying density/magnetization distribution in a fixed layer. Because of the fast speed of the algorithm, this method is efficient to invert large data sets. Furthermore, Xia and Sprowl (1992) presented an approach for the iterative inversion which converges fast and stably and produces reliable solutions in most cases. They used Parker's formula for calculation of modeled anomaly, and Bouguer-slab and two-dimensional vertical dike formulas for modification of gravity and magnetic models, respectively. This project uses their method to invert the gravity and aeromagnetic data in Montgomery County, Kansas, into density/magnetization distribution of the Precambrian basement rock whose top and bottom surfaces, respectively, are defined by well data and known geology.

Potential-field data should be properly processed before any quantitative interpretation is attempted. One of the purposes of processing is to remove from the data all of the extraneous disturbances irrelevant to geological interpretations; such disturbances are due to changes in both elevation and latitude of stations, to meter drift, and to various other causes. Another purpose of processing is to isolate the (residual) anomaly from the target source of primary importance. This process is called regional-residual separation.

The gravity data that have been corrected for the effects from changes in elevation and latitude are usually called the Bouguer anomaly and often are used for geologic interpretations. However, this anomaly still contains extraneous disturbances due to topographic relief at the surface of measurement. Correction for these extraneous disturbances involves a vertical continuation of the data onto a common horizontal plane and is called topographic correction (Xia and Sprowl, 1991). A number of methods have been developed by several authors. Dampney (1969) described how to derive from the Bouguer anomaly an equivalent source of point masses on a horizontal plane (one point mass beneath each surface station) to reduce the data to that plane. However, he found that the error involved in this method is a function of depth of the equivalent source. Recently, Xia and Sprowl (1991) pointed out that the optimum depth of the equivalent source is that which maximizes the smoothness of the calculated anomaly between the data points. In addition, Xia et al. (1991) presented a fast and accurate technique using the fast Fourier transform to determine the equivalent source for a large data set. The gravity data used for this project are topographically corrected using Xia et al.'s technique (1991).

Extraction of the residual from the regional is done both with graphical and computational methods. The graphical method has the merit of allowing the interpreter to incorporate into the process his personal sense of "rightness" about the forms of the regional-residual anomalies (Dobrin and Savit, 1988). However, this method works well only under some limited situations and most of the processing work must be done manually. On the other hand, computational methods are fast and accurate without such a great reliance upon the exercise of judgment during the process. The most straightforward and commonly used approach is the polynomial-fitting method, the most flexible of the computational techniques. Here the observed data are fitted, usually by least squares, to the mathematically describable surface (regional surface) that most closely fits the data within a specified degree of detail. A method to determine, among various possible ones, the optimum order of polynomial that fits the regional surface was discussed by Abdelrahman et al. (1985). This project uses their method to separate the regional anomaly from the Bouguer anomaly and aeromagnetic data.

Data Processing

Gravity data were collected on the topographic surface with a spacing of 1.6 × 1.6 km (1 × 1 mi) in most of eastern Kansas and 1.6 × 3.2 km (1 × 2 mi) in western Kansas. The data are available in the data base at Kansas Geological Survey (Lam and Yarger, 1989). The precision of the data is about 0.1 mGal. Figure 1A shows the Bouguer gravity map in Montgomery County. The first correction to the data is topographic (Xia and Sprowl, 1991) in order to reduce the data onto a horizontal plane. Figure 1B is a topographically corrected Bouguer anomaly map using a method discussed by Xia et al.

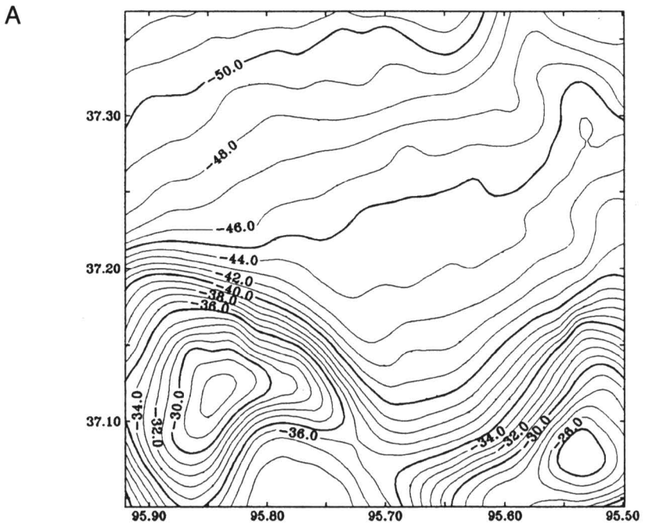

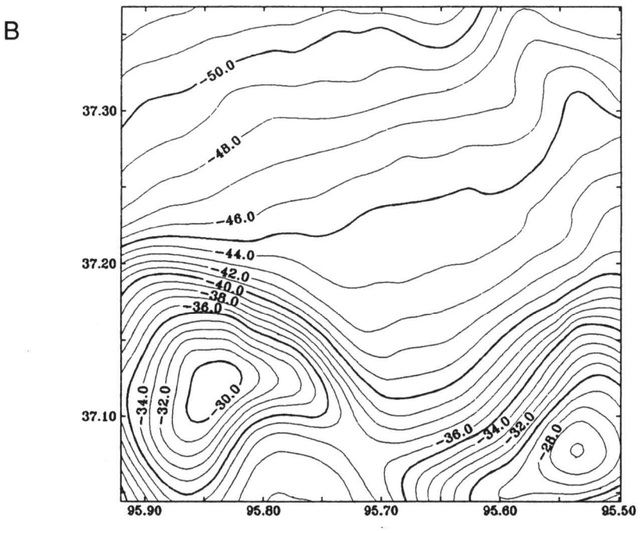

FIGURE 1—(A) Bouguer anomaly in Montgomery County, Kansas. Contour interval is 1 mGal. (B) Topographically corrected Bouguer anomaly on the level 700 m (2,297 ft) above sea level. Coordinates in figs. 1–15 are latitudes and longitudes.

(1991). After the correction, the data are on a horizontal plane of 700 m (2,297 ft) above sea level.

The second step of processing is to separate the anomaly. Abdelrahman et al.'s method (1985) is used to determine the optimum order of polynomial to separate the regional anomaly from the Bouguer anomaly. The overall similarity between each two successive residual maps was determined by calculating a correlation factor between the mapped variables. The correlation factors were computed using a formula given by Davis (1986, p. 40, Eq. 2.24, and p. 448). The lower order of two successive residual maps with the maximum value of the correlation factor was the optimum order of the polynomial to fit the regional surface. The correlation factor between the first-order and the second-order residuals is 0.9258, between the second-order and the third-order is 0.8102, and between the third-order and the fourth-order is 0.7468. Therefore, the optimum order of polynomial to fit the regional anomaly is 1. Figure 2 is the regional gravity map of the first-order polynomial trend, and fig. 3 is the residual Bouguer anomaly.

Aeromagnetic data were collected with a flight-line spacing of 3.2 km (2 mi) and a tie-line spacing of 32 km (20 mi). In eastern Kansas the airplane was flown at a fixed elevation 762 m (2,500 ft) above sea level. In western Kansas the flight elevation was 915 m (3,002 ft) above sea level in the eastern portion and 1,372 m (4,502 ft) above sea level in the westernmost quarter of the state. The precision of the data is about 3 nT. Details of the data were described by Yarger (1983, 1989). Figure 4 is the aeromagnetic map in Montgomery County. The datum in the county is 762 m (2,500 ft) above sea level. For the magnetic data, one step of processing is needed: anomaly separation. The correlation factor between the first-order and second-order residuals is 0.9027, between the second-order and third-order is 0.9605, and between the third-order and fourth-order is 0.8945. Therefore, the optimum order of polynomial to fit the regional anomaly is 2. Figure 5 is the regional magnetic map of the second-order polynomial trend, and fig. 6 is the residual magnetic anomaly.

In our study, all data are gridded into 24×23 matrix by SURFACE III (Sampson, 1988).

Anomalies Due to the Basement Terrane

Based on the well data (fig. 7B), we calculated potential-field anomalies caused by the modified Precambrian subsurface terrane shown in fig. 7A. Assuming that the rocks of the Precambrian basement are mostly granitic, the average density of the basement was chosen as 2.70 g/cm^3 (Garland, 1979). The rocks above the basement are shale, limestone, and sandstone, and the average density of these rocks is 2.43g/cm^3 (Garland, 1979) if the thickness of each is the same. Therefore, the density contrast of the interface would be 0.27g/cm^3 (= 2.70 – 2.43). We also assumed that the granitic rocks in the basement contained one percent of magnetite with the effective susceptibility K = 0.031 (SI units). Magnetization by the earth field of H = 40 A/m yields a magnetization of about 1.25 A/m (125 nT), which is an order-of-magnitude figure for polarization of

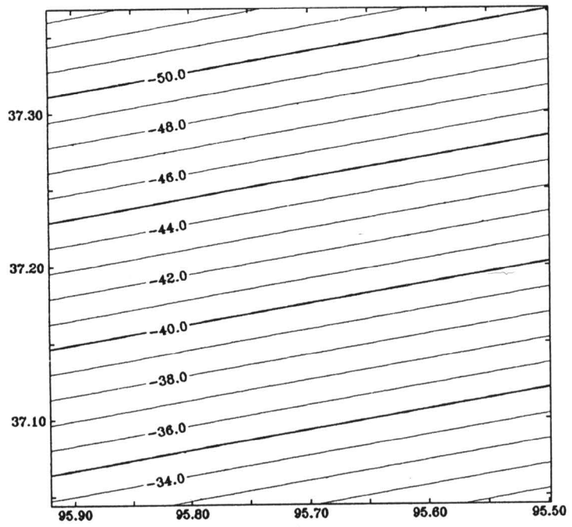

FIGUR E 2—FIRST-ORDER POLYNOMIAL REPRESENTS THE REGIONAL GRAVITY ANOMALY. Contour interval is 1 mGal.

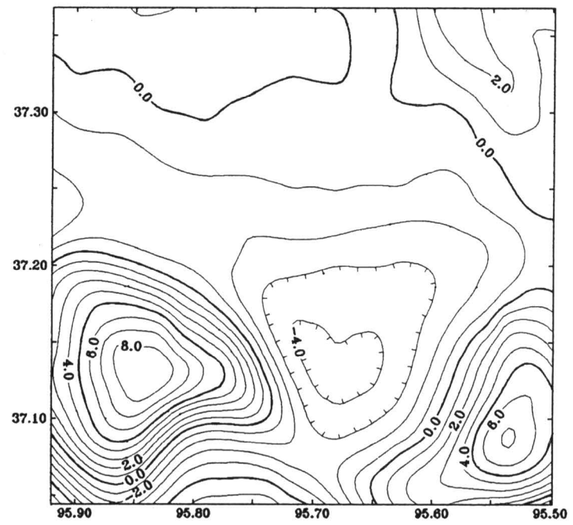

FIGURE 3—RESIDUAL GRAVITY ANOMALY. Contour interval is 1 mGal.

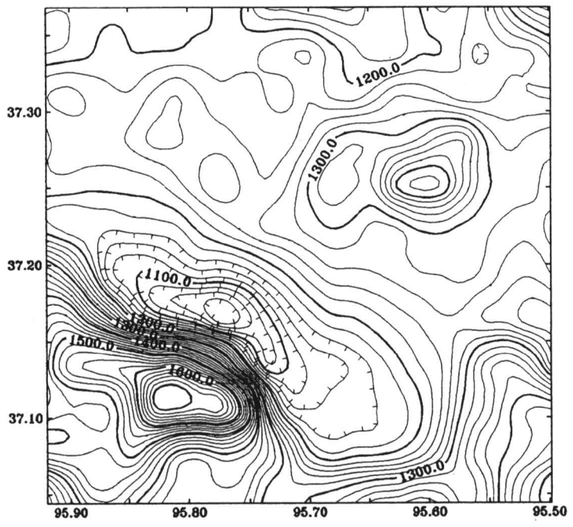

FIGUR E 4—AEROMAGNETIC ANOMALY IN MONTGOMERY COUNTY, KANSAS. Elevation of survey is 762 m (2,500 ft) above sea level; contour interval is 20 nT.

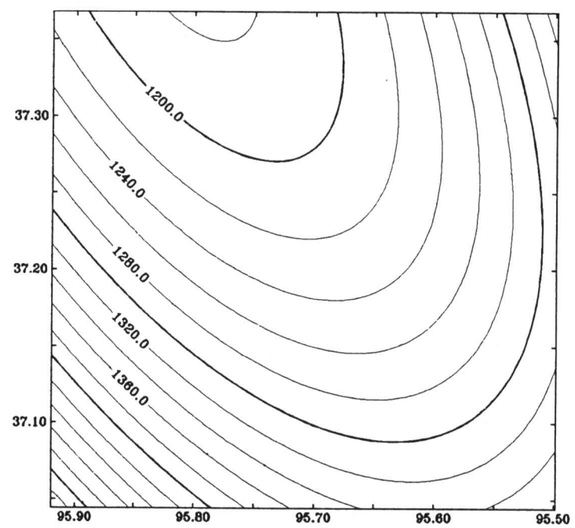

FiGURE 5—SECOND-ORDER POLYNOMIAL REPRESENTS THE REGIONAL MAGNETIC ANOMALY. Contour interval is 20 nT.

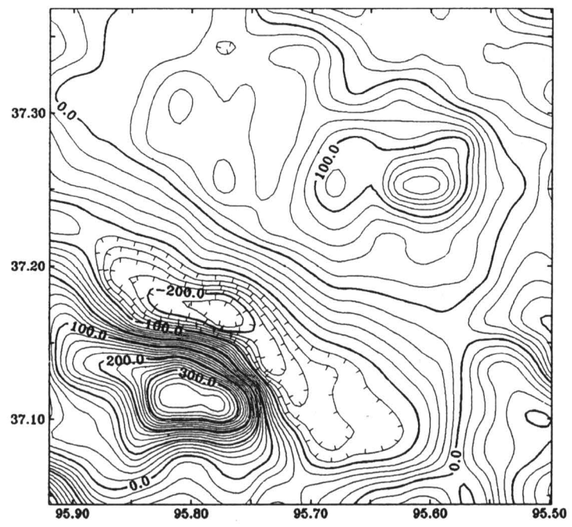

FIGURE 6—RESIDUAL MAGNETIC ANOMALY. Contour interval is 20 nT.

basement rocks commonly used in magnetic-model calculations (Nettleton, 1976). Because sedimentary rocks are usually nonmagnetic, we used 125 nT as the magnetization in modeling the magnetic interface.

Figure 8 is the modeled gravity anomaly based on the basement model (fig. 7) with the density contrast of 0.27g/cm^3. Figure 9 is the modeled magnetic anomaly of the basement structure (fig. 7) with the magnetization of 125 nT. Parker's (1973) formula (Eq. 1) was used to calculate the anomalies. The inclination and declination of magnetization of the modeled magnetic anomaly are 65° and 7°, respectively, which are the direction of the normal earth field in Kansas. These modeled anomalies show that the main anomalies in the county are not caused by the Precambrian basement structure. The modeled anomalies (figs. 8 and 9) are subtracted from the residual gravity anomaly (fig. 3) and residual magnetic anomaly (fig. 6). Then we obtain remaining anomalies shown in figs. 10 and 11, respectively, which are assumed to have been caused by lithological changes in the basement. We try to invert the anomalies into density/magnetization distribution in the basement.

A

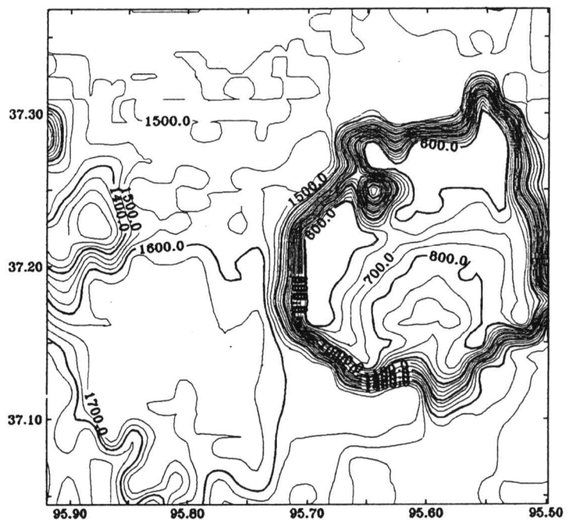

B

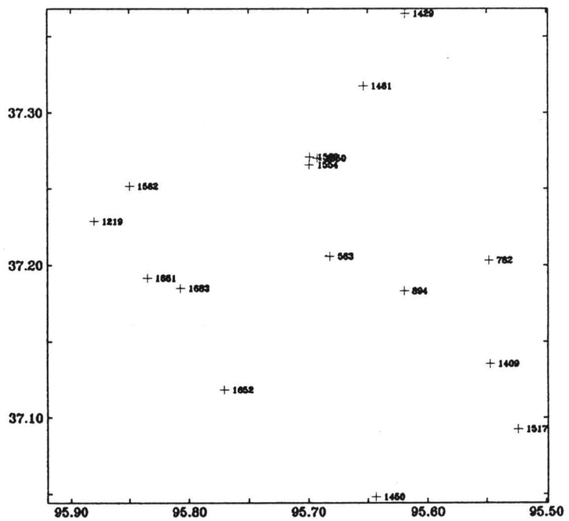

FIGURE 7— (A) MODEL OF DEPTH TO THE PRECAMBRIAN BASEMENT. Contour interval is 50 ft (15 km). (B) LOCATIONS OF THE WELL DATA; units are in feet.

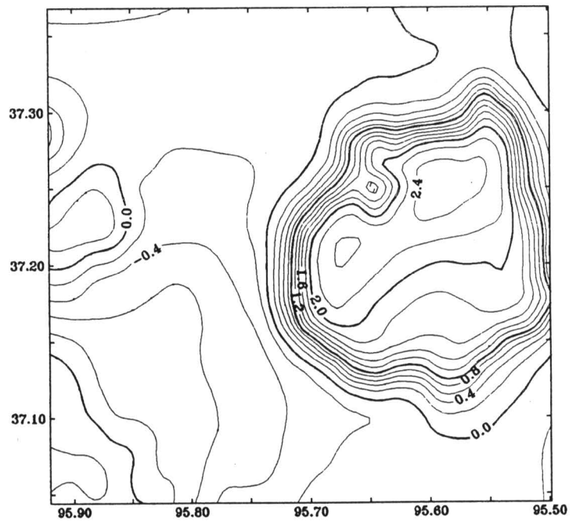

FIGURE 8—MODELED GRAVITY ANOMALY FROM THE BASEMENT MODEL (fig. 7A). Density contrast is 0.27 g/cm^3. Contour interval is 0.2 mGal.

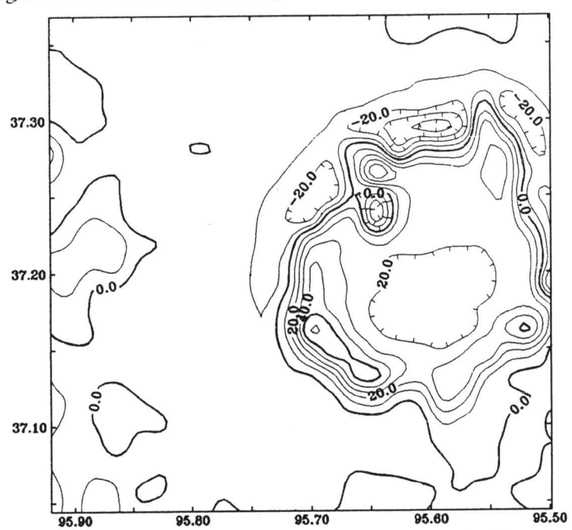

FIGURE 9—MODELED MAGNETIC ANOMALY FROM THE BASEMENT MODEL (fig. 7A). Magnetization is 125 nT, and inclination and declination of the magnetization are 65° and 7°, respectively. Contour interval is 10 nT.

Inversion of Potential-field Data

Xia and Sprowl's (1992) approach used in this study to invert the potential-field data is density/magnetization distribution within a layer. The computer program is described by Xia (1991). Calculation of a gravity anomaly field due to a material layer using Parker's formula (Eq. 1) requires three known functions: 1) the depth to the top of

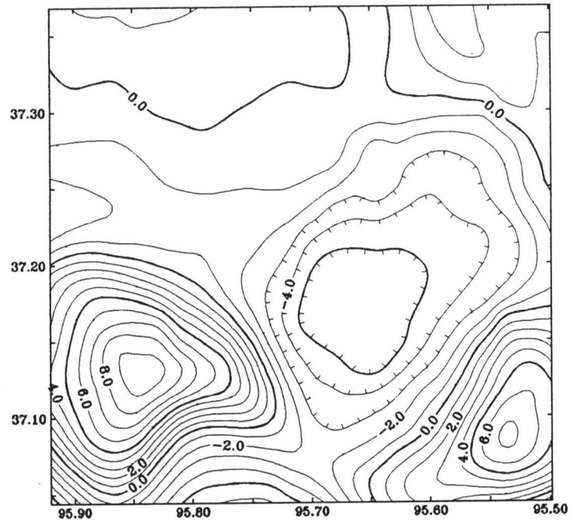

FIGURE 10—GRAVITY ANOMALY CAUSED BY LITHOLOGICAL CHANGE IN THE BASEMENT, which is equal to the residual gravity anomaly (fig. 3) subtracting the modeled anomaly from the basement structure (fig 8). Contour interval is 1.0 mGal.

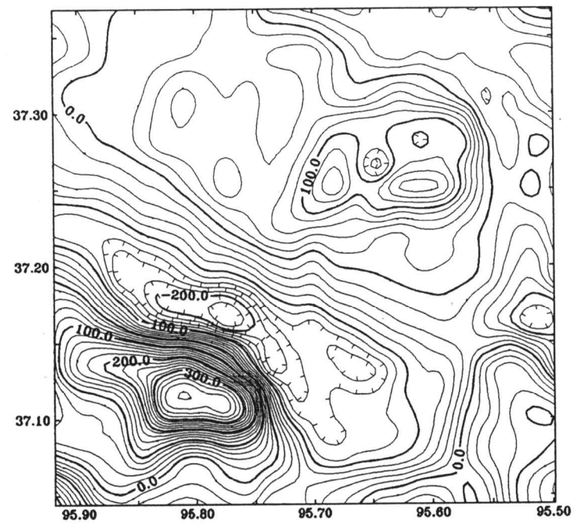

FIGURE 11—MAGNETIC ANOMALY CAUSED BY LITHOLOGICAL CHANGE IN THE BASEMENT, which is equal to the residual magnetic anomaly (fig. 6) subtracting the modeled anomaly from the basement structure (fig. 9). Contour interval is 20 nT.

the layer ($ZT = z_1$), 2) the depth to the bottom of the layer ($ZB = z_2$), and 3) the density distribution m:

$$F[h(x, y)] = 2\pi G \sum_{n=1}^{\infty} \frac{-|\vec{k}|^{n-1}}{n!} \times \tag{1}$$

$$\left\{ e^{-|\vec{k}|\delta_2} F[m(x, y)(z_2(x, y) - \delta_2)^n] - e^{-|\vec{k}|\delta_1} F[m(x, y)(z_1(x, y) - \delta_1)^n] \right\},$$

where G is the gravitational constant; $\vec{k}$ is a wave number vector; δ_1 and δ_2 are the average value of z_1 and z_2, respectively; and F is the Fourier transformation. For calculating magnetic anomalies, the formula is little different from Eq. 1 and m is magnetization distribution, the direction of which must be known. The forward series expansion of Parker's formula is uniformly convergent for any reasonable topographic relief functions, ZT and ZB (Parker, 1973).

Given ZT and ZB, the goal of inversion is to determine distribution function of density/magnetization m in the layer defined by ZT and ZB. The formulas that are used to modify the model after each iteration are listed below.

Case 1. Modifying the distribution of density in the layer:

$$\Delta\rho_i^k = (g_i - h_i^k) / 2\pi G(ZB_i - ZT_i), \tag{2}$$

where superscript k stands for the kth iteration and subscript i for the ith data point; g_i and h_i^k are the measured and calculated gravity anomalies, respectively; G is the gravitational constant; and $\Delta\rho$ is the density contrast.

Case 2. Modifying the distribution of magnetization in the layer:

$$\Delta J_i^k = (T_i - h_i^k) / 4\tan^{-1}(\Delta L / 2ZT_i^k), \tag{3}$$

where ZT_i^k, the depth of ZT below point i at the kth iteration; h_i^k and T_i are the calculated and measured total magnetic field anomalies, respectively; and ΔL is the average distance between data points, ΔJ_i^k is the modification to J_i^k, the magnetization below point i at the kth iteration.

Formula (2) is based on the Bouguer-slab formula. The formula (3) is simplified from the 2D vertical dike (Telford et al., 1982, p.166).

Two errors used to trace the iterative procedure are a root-mean-square error $RMS(k)$ at the kth iteration:

$$RMS(k) = \sqrt{\frac{1}{N}\sum_{i=1}^{N} (h_i^k - f_i)^2} \tag{4}$$

and the maximum deviation $MAXD(k)$ at the kth iteration

$$MAXD(k) = \max_{1 \le i \le N} |h_i^k - f_i| \tag{5}$$

where f_i is the measured anomaly at the ith point, and N is the total number of data points. These two errors can tell the differences between a modeled anomaly and a real anomaly. At least, one of them should be reduced after each iteration in order to obtain stable convergence of the inverse procedure.

The inversion approach consists of three steps:

1) Determine an initial model: initialize the model ρ (or J) to an average value and define ZT and ZB for the case 1 (or case 2), both of which are kept unchanged while solving for density (or magnetization) distribution;
2) Calculate the anomaly $h(x,y)$ by Parker's formula and estimate the RMS and $MAXD$ by Eqs. 4 and 5; if neither of these errors is reduced or the RMS reaches the accuracy threshold, the iterative procedure will be terminated, otherwise;
3) Modify the model by either Eq. 2 or Eq. 3, according to the type of anomaly, and then go to step 2.

Density/Magnetization Distribution in the Basement

The uniqueness of the inverse model of density/magnetization distribution is restricted by the uncertainty in the functions ZT and ZB. Obviously, the thinner the layer is, the larger the value of density/magnetization. In our study, depth to the bottom of layer ZB in the inverse procedure is flexible. This uncertainty is reduced by known rock types on several well stations. The inverse models should be consistent with these well data. Actually, we choose several different depths for each anomaly to find an acceptable model in geology because the inverse model should honor the rock types shown by the well data. We found that 2,500 m (8,202 ft) below sea level for gravity inversion and 1,200 m (3,937 ft) below sea level for magnetic inversion are reasonable choices of ZB.

Density distribution. We invert fig. 10 (gravity anomaly caused by lithological change) into density distribution within the basement. The upper surface of the layer ZT is the basement and the bottom surface ZB is chosen as 2,500 m (8,202 ft) below sea level. The two surfaces are kept unchanged while solving for density distribution. We initialize the density 2.67 g/cm^3, which is the average density of the continental crust. The initial RMS and $DMAX$ errors are 11.4 mGal and 28.5 mGal, respectively. After 20 iterations, the errors RMS is reduced to 0.16 mGal and $MAXD$ is reduced to 1.4 mGal. The final result, which represents the modified density distribution in the layer, is shown in fig. 12. The modeled gravity anomaly by lithological change is shown in fig. 13.

Magnetization distribution. We invert fig. 11 (magnetic anomaly caused by lithological change) into magnetization distribution. In this case, we define the upper surface of the layer ZT as the basement and the bottom ZB surface as 1,200 m (3,937 ft) below sea level. The two surfaces are kept unchanged while solving for magnetization distribution. The inclination and declination of the magnetization are 65° and 7°, respectively. We initialize magnetization 125 nT, which is the value of magnetization of the granitic rocks containing about 1% magnetite. RMS and $MAXD$ of the initial model are 97.2 nT and 393.3 nT, respectively. After 33 iterations, RMS is reduced to 5.3 nT and $MAXD$ is reduced to 18.8 nT. The final result, representing the modified magnetization distribution, is shown in fig. 14. The modeled magnetic anomaly by lithological change is shown in fig. 15.

Inverse procedure shows that two errors are reduced quickly and convergence of the iterations is stable. This shows that the formulas used to modify density/magnetization models work well.

Figures 12 and 14 show the inverse results. Density in most areas of fig. 12 is less than 2.80 g/cm^3, but in the southeastern part density is above 2.80 g/cm^3. According to Carmichael (1989, p. 163), densities greater than 2.80 g/cm^3 will separate basalt from granite. In the same area of fig. 14, the magnetization is above 400 nT, which is about three times the content of magnetite (3%) in the rocks in this area as in the normal granitic basement. According to Carmichael (1989) and Nettleton (1976), the fact of higher density and higher magnetization in the area could be caused by basaltic rocks. However, Steeples and Bickford (1981) pointed out that the Miami County core, which is granite, contains about 2% of magnetite by weight. The source rocks, therefore, that cause the potential-field anomaly in southwestern Montgomery County are probably an intrusion of granodiorite containing more than 3% of magnetite.

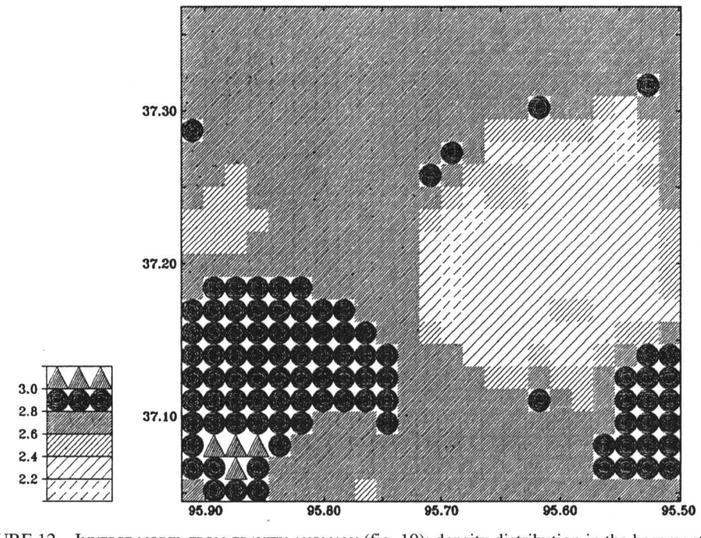

FIGURE 12—INVERSE MODEL FROM GRAVITY ANOMALY (fig. 10): density distribution in the basement rocks. Mapping interval is 0.2 g/cm^3.

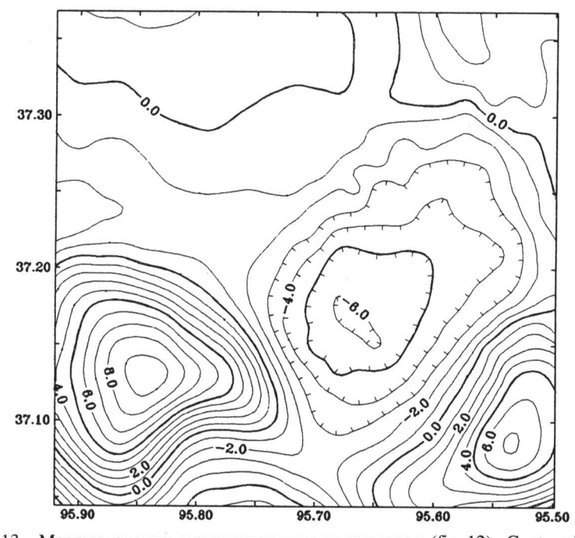

FIGURE 13—MODELED GRAVITY ANOMALY FROM THE INVERSE MODEL (fig. 12). Contour interval is 1.0 mGal. The RMS and $MAXD$ errors between figs. 10 and 13 are 0.16 mGal and 1.4 mGal, respectively.

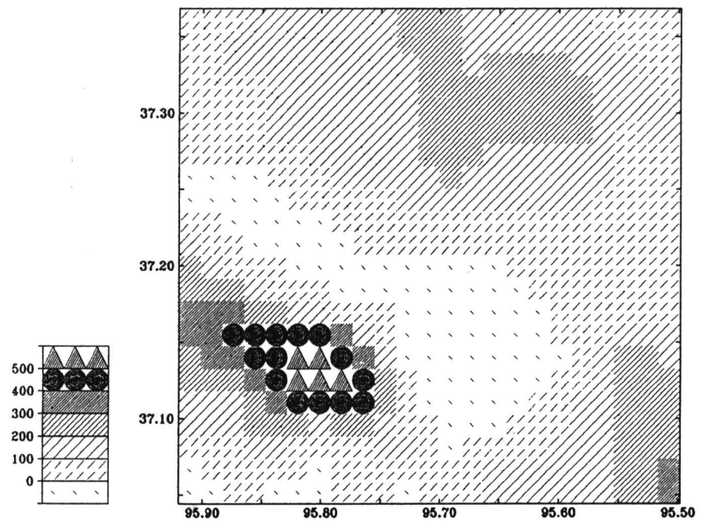

FIGURE 14—INVERSE MODEL FROM MAGNETIC ANOMALY (fig. 11); magnetization distribution in the basement rocks. Mapping interval is 100 nT.

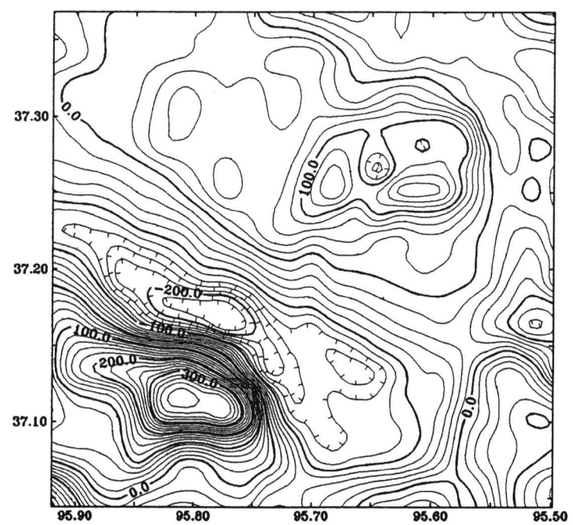

FIGURE 15—MODELED MAGNETIC ANOMALY FROM THE INVERSE MODEL (fig. 14). Contour interval is 20 nT. The *RMS* and *MAXD* errors between figs. 11 and 14 are 5.3 nT and 18.8 nT, respectively.

References

Abdelrahman, E. M., Riad, S., Refai, E., and Amin, Y., 1985, On the least-squares residual anomaly determination: Geophysics, v. 50, p. 473–480

Cady, J. W., 1980, Calculation of gravity and magnetic anomalies of finite-length right polygonal prisms: Geophysics, v. 45, p. 1,507–1,512

Carmichael, R. S. (ed.), 1989, Practical handbook of physical properties of rocks and minerals: CRC Press, Boca Raton, Florida, 741 p.

Davis, J. C., 1986, Statistics and data analysis in geology (2nd edition): New York, John Wiley & Sons, Inc., 646 p.

Dobrin, M. B., and Savit, C. H., 1988, Introduction to geophysical prospecting, 4th ed.: New York, McGraw-Hill, Inc., 867 p.

Garland, G. D., 1979, Introduction to geophysics—mantle, core, and crust: W. B. Saunders Company, 494 p.

Lam, C., and Yarger, H., 1989, State gravity map of Kansas: Kansas Geological Survey, Bulletin 226, p. 185–196

Nettleton, L. L., 1976, Gravity and magnetics in oil prospecting: New York, McGraw-Hill Book Company, 464 p.

Parker, R. L., 1973, The rapid calculation of potential anomalies: Geophysical Journal of the Royal Astronomical Society, v. 31, p. 447–455

Plouff, D., 1976, Gravity and magnetic fields of polygonal prisms and application to magnetic terrain corrections: Geophysics, v. 41, p. 727–741

Sampson, R., 1988, SURFACE III: Lawrence, Kansas, Interactive Concepts, Inc.

Steeples, D. W., and Bickford, M. E., 1981, Piggyback drilling in Kansas—an example for the Continental Scientific Drilling Program: Transactions of the American Geophysical Union, v. 62, p. 473–476

Talwani, M., Worzel, J. L., and Landisman, M., 1959, Rapid gravity computations for two-dimensional bodies with application to the Mendocino submarine fracture zone: Journal of Geophysical Research, v. 64, p. 49–59

Telford, W. M., Geldart, L. P., Sheriff, R. E., and Keys, D. A., 1976, Applied geophysics: Cambridge University Press, 859 p.

Xia. J., 1991, Computer program of inversion of potential-field data by iterative forward modeling: Kansas Geological Survey, Computer Program Series 91-2, 4 p., disk

Xia, J., and Sprowl, D. R., 1991, Correction of topographic distortions in gravity data: Geophysics, v. 56, p. 537–541

_____, 1992, Inversion of potential field data by iterative forward modeling in the wavenumber: Geophysics, v. 57, p. 126–130

Xia, J., Sprowl, D. R., and Adkins–Heljeson, D., 1991, A fast and accurate approach—correction of topographic distortions in potential-field data: Society of Exploration Geophysicists, 61st Annual Interntational Meeting, Expanded Abstracts, p. 626–629

Yarger, H. L., 1983, Regional interpretation of Kansas aeromagnetic data: Kansas Geological Survey, Geophysics Series 1, 35 p.

Yarger, H. L., 1989, Major magnetic features in Kansas and their possible geologic significance: Kansas Geological Survey, Bulletin 226, p. 197–207

Midcontinent Rift System in Northeastern Kansas

Timothy S. Woelk[1] and William J. Hinze[2]
[1]ARCO Oil & Gas Company, Houston, TX 77079, and [2]Department of Earth & Atmospheric Sciences, Purdue University, West Lafayette, IN 47907

Introduction

One of the major tectonic features of North America is the 1,100-Ma Midcontinent Rift System (MCR). This paleorift now lies largely buried under the thick Phanerozoic cover of the North American Craton; therefore, its trend, extent, and structural nature is detected only by geophysical means and the occasional deep drill hole. The rift was first reported in Kansas by Woollard (1943) as a result of his transcontinental gravity profile and was later to be known as the Midcontinent Gravity High. Subsequent aeromagnetic investigations showed a correlative magnetic anomaly and the feature was renamed the Midcontinent Geophysical Anomaly (MGA). The MGA is recognized as extending from Lake Superior to Kansas (Van Schmus and Hinze, 1985) and southerly into Oklahoma (Yarger, 1981). It is delineated by a positive central high and flanking minima on both gravity and magnetic maps. The rocks associated with the MGA crop out only in the Lake Superior Basin and comprise the classical association of bimodal volcanic, plutonic, and clastic sedimentary units of the "Keweenawan" suite (Morey and Green, 1982; Van Schmus and Hinze, 1985). It is primarily this association of a large volume of mafic and clastic rocks occurring along a long segmented belt which transects the regional pre-existing geologic pattern over most of its length that leads to the interpretation of the MGA and related segments as a rift (Hinze and Braile, 1988).

Growing interest in the Midcontinent Rift System over the past several years, fostered in part by the potential of this Keweenawan rift as a frontier hydrocarbon province, has led to an increased number of deeply penetrating seismic-reflection profiles over the structure. Two studies by the Consortium for Continental Reflection Profiling (COCORP) across the MCR in Kansas and Michigan (Brown et al., 1982; Brown et al., 1983; Serpa et al., 1984), and more recently, seismic lines acquired in Lake Superior as part of the Great Lakes International Multidisciplinary Program on Crustal Evolution (GLIMPCE) image a deep asymmetric central graben with prominent reflectors extending to depths of 30 km (18.6 mi) in places (Behrendt et al., 1988; Cannon et al., 1989). In addition, the seismic lines show that normal faulting played a prominent role in rift development before later compression changed them into high-angle reverse faults.

In 1984–85, Texaco, U.S.A. drilled a hole in northern Kansas (Berendsen et al., 1988) to test the petroleum potential of the clastic rock assemblage of the MCR. Texaco's interest was spurred in part by the results of the seismic-reflection investigation of the MCR conducted in northern Kansas by COCORP. These drill-hole data have added valuable constraints to understanding the structural style and tectonic evolution of the MCR in northeastern Kansas.

Potential-field Analysis

Study of the MCR in Kansas by direct observation is limited to a few scattered deep drill holes. Deep drill-hole data are useful in mapping basement lithology, but because holes rarely penetrate more than a few meters of basement they provide little structural information. Further complicating the matter, lithologies can be difficult to interpret due to the intensity of chemical weathering of the first few meters of the subcropping basement rocks (Lidiak and Hinze, 1988). To help overcome these difficulties, geophysical potential-field maps can be used to extrapolate basement lithology along gravity and magnetic trends from lithologies derived from basement holes. This information provides a useful regional context for localized investigations.

Gravity and magnetic studies played an important role in the early delineation of the MCR (Thiel, 1956; Lyons, 1959; Hinze, 1963; Hinze et al., 1973, 1982; King and Zietz, 1971; Oray et al., 1973) because these methods readily detect the large physical property contrasts associated with the Keweenawan rocks of the MCR (Klasner et al., 1979; Hinze et al., 1982; Hinze et al., 1992). The gravity and magnetic anomalies associated with the MCR are in general spatially correlative maxima and minima. Extrapolation of the Keweenawan rocks into the subsurface, in conjunction with seismic-reflection profiles, shows that the gravity and magnetic highs are derived from troughs filled with mafic volcanic and plutonic rocks as well as sedimentary rocks extending to depths greater than 15 km (9.3 mi) and up to 30 km (18.6 mi) in the Lake Superior basin (Hinze and Braile, 1988). The flanking minima are predominantly caused by clastic sedimentary rock basins. Recent investigations of the MCR have suggested that mafic intrusions permeating the crust below the rift contribute to the central maximum, and thickening of the crust contributes to the flanking minima.

The anomaly pattern of the MCR (fig. 1) is segmented, being disrupted at several locations. In southeastern Minnesota, the anomaly makes a sharp turn to the southeast extending to the Iowa border where it continues to the southwest. In southeastern Nebraska, the anomaly shifts abruptly to the east by about 60 km (37.3 mi), then continues into central Kansas. This en echelon pattern is defined in part by northwest-trending structural zones such as the Belle Plaine and associated faults in southeastern Minnesota (Chandler et al., 1989). In some rift models these faults are depicted as transform faults or accommodation zones separating rift segments (King and Zietz, 1971; Chase and Gilmer, 1973). However, they may simply be caused by pre-existing crustal faults which have disrupted the rift development.

The anomaly pattern broadens within the Lake Superior basin and the regional trend changes from NE-SW to NW-SE as it continues into Michigan. The MCR in southeastern Michigan intersects the Grenville Front Tectonic Zone (GFTZ)—a zone which separates high-grade metamorphic rocks of the Grenville Province from older adjacent provinces to the west—a result of the continent-continent collision of the 1.3–1.0 Ga Grenville Orogeny (Moore, 1986). The coincident age of the MCR and GFTZ coupled with the late-stage reverse movement of MCR faults has led to speculation that the rifting event terminated with the Grenville Orogeny.

On the Bouguer gravity map of the northeastern Kansas area (fig. 2), the most notable feature is the anomaly caused by the MCR. The feature extends from the northeast corner of the map (central Iowa) into southeastern Nebraska, where it is offset by about 60 km (37.3 mi), and then continues into Kansas. The basement surface lithology in the area between the rift segments in Nebraska and Kansas is predominantly a plutonic terrane of pre-Keweenawan granite gneiss and schist. The prominence of cataclastic rocks in southeastern Nebraska has led to the speculation of a crustal break in this area (Muehlberger et al., 1967), but because of the uncertain trend in the cataclasis, its association with the offset in the anomaly is conjectural (Lidiak, 1972).

The Iowa–Nebraska segment of the gravity anomaly is generally greater in magnitude and characterized by steeper gradients than those of the Kansas segment. In Kansas, the gravity gradient of the anomaly is steeper on the east side of the peak, and although its magnitude decreases to the southwest, the linear trend of the anomaly can be seen to extend into southern Kansas. In general, the gravity values to the east of the MCR in this area are lower than those to the west by about 10 mGal. This shift in the Bouguer gravity is observed as a broad positive gradient to the west in the high-cut (wavelengths greater than 8°) free-air gravity anomaly map of North America (von Frese et al., 1982) and other published anomaly maps (Simpson et al., 1986). Woelk (1989) accounts for the 10-mGal shift in modeling of the rift by a variation in the density of the upper crustal layer, whereas Lam (1986) indicates that the anomaly is related to crustal thickness variations and Simpson et al. (1986) suggest a possible correlation to a Precambrian suture along which the rift developed. However, mapping of the basement rocks by isotopic dating and lithology (Van Schmus et al., 1987) has failed to give evidence of a suture in the basement rocks predating the rifting event.

The magnetic anomaly map (fig. 3) is more complex than the gravity with many prominent anomalies. The MCR magnetic anomaly is not as smoothly varying as its gravity anomaly. In the Iowa–Nebraska segment, magnetic lows are present over the axis of the anomaly and the Kansas segment is of greater magnitude than that of the Iowa–Nebraska segment. The lows over the axial highs are probably caused by the

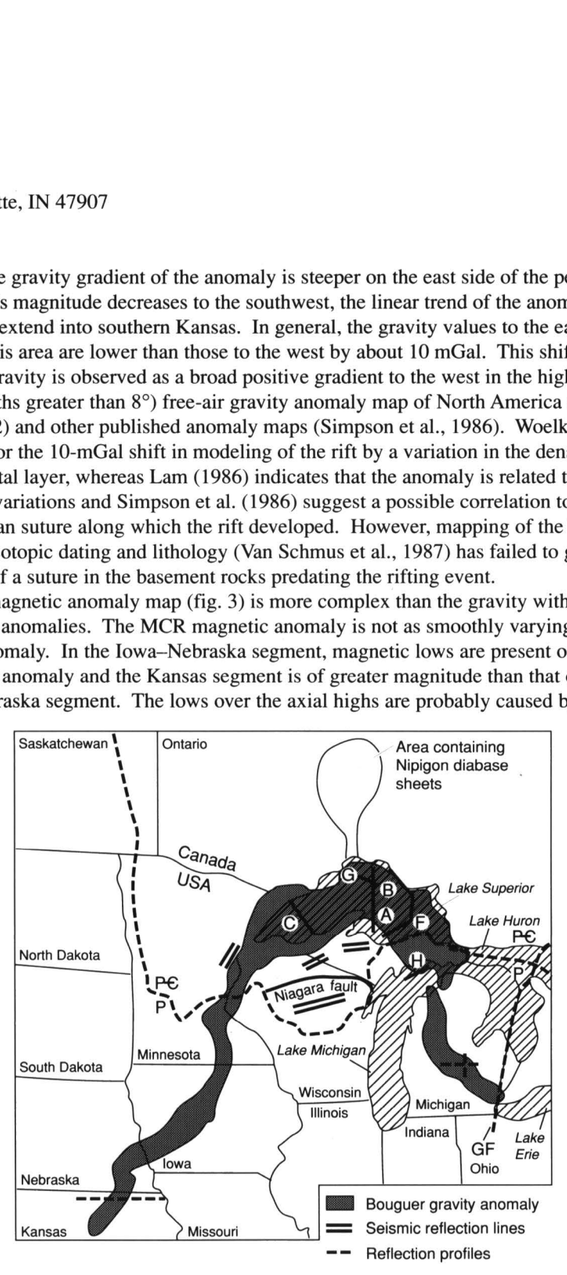

FIGURE 1—MAP SHOWING LOCATION OF THE POSITIVE BOUGUER GRAVITY ANOMALY (shaded) produced by rocks of the midcontinent rift and some major geologic features of the region. Heavy solid lines are seismic reflection profiles from the GLIMPCE program. Heavy dashed lines in Kansas and southern Michigan are locations of reflection profiles from COCORP. Short dashed line is contact of Phanerozoic (P) strata with Precambrian (Pε). Location and trend of Keweenawan diabase dike swarms shown schematically by heavy double lines. GF, Grenville Front (after Cannon et al., 1989).

remnants of the clastic-basin fill that originally blanketed the volcanic-filled troughs (King and Zietz, 1971).

The MCR magnetic anomaly terminates in central Kansas against a roughly linear trend of negative anomalies. The most prominent of these anomalies is the intense magnetic minimum in southern Kansas known as the Wichita Magnetic Low. Having no correlative gravity anomaly, this magnetic anomaly has been interpreted to occur along a east-west-trending Proterozoic suture zone (Yarger, 1981) with the Wichita Magnetic Low being a result of the contrast between two crustal blocks and large granitic plutons (Meyer, 1987). The series of roughly circular anomalies extending from northeastern Kansas into east-central Kansas are considered to be granitic plutons, possibly intruded along a zone of weakness that later influenced formation of the Forest City basin (Yarger, 1985).

Figure 4 is a second vertical derivative magnetic map of Kansas (after Yarger, 1985). The magnetic quiet zone that surrounds the magnetic high of the MCR corresponds to the proposed limit of a basin filled with Keweenawan clastic rocks (Yarger, 1985). Yarger (1985) has interpreted the lineations extending southwest from the quiet zone to correspond to block faulting and possibly to mafic dike intrusions that occurred during rifting. These lineations occur over an area of about 100 km (62 mi) in width, implying an extensive area of sub-rift crustal disturbance. This map also provides strong evidence for the continuation of the MCR south to at least the Kansas–Oklahoma border.

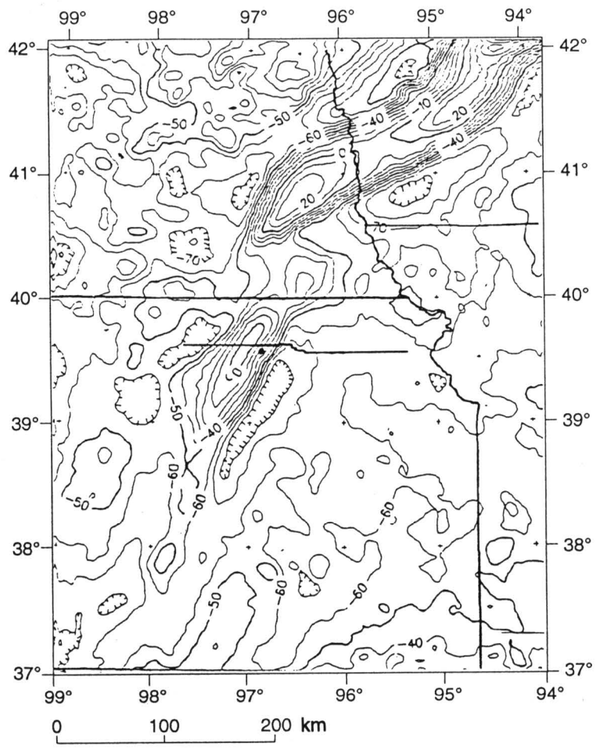

FIGURE 2—KANSAS LINE 1 AND TEXACO POERSCH #1 BOREHOLE (dot).

Geology

Keweenawan Stratigraphy

The igneous and clastic rocks associated with the MCR are exposed in the Lake Superior region and comprise the Keweenawan Supergroup. The Keweenawan Supergroup can be divided into two major suites: an igneous-sedimentary unit that occurs as primary basin fill, and a later sedimentary unit that occurs as late-stage fill of basins overlying the initial rock suite (Van Schmus and Hinze, 1985). Figure 5 shows the stratigraphic terminology and the time relationships along the MCR from Lake Superior to Kansas.

The Keweenawan volcanic rocks are composed of abundant olivine tholeiite, transitional basalts, basaltic andesites, rhyolites, and a few icelandites deposited into individual basins separated in space and perhaps time as the intensity and character of rifting fluctuated (Green, 1982). As a result of the time and space fluctuation of eruptions, individual flow units locally thicken and thin (Van Schmus and Hinze, 1985), but individual flow units have been traced over a distance of up to 90 km (56 mi) along strike. Thicknesses range from 1 m to 100 m (3.3 ft to 328 ft) with an average thickness of 10–30 m (33–98 ft) (Green, 1983).

The interflow sedimentary rocks make up approximately only 3% of the primary rift basin fill. They have been described as coarse, immature, polymictic, red-bed clastic

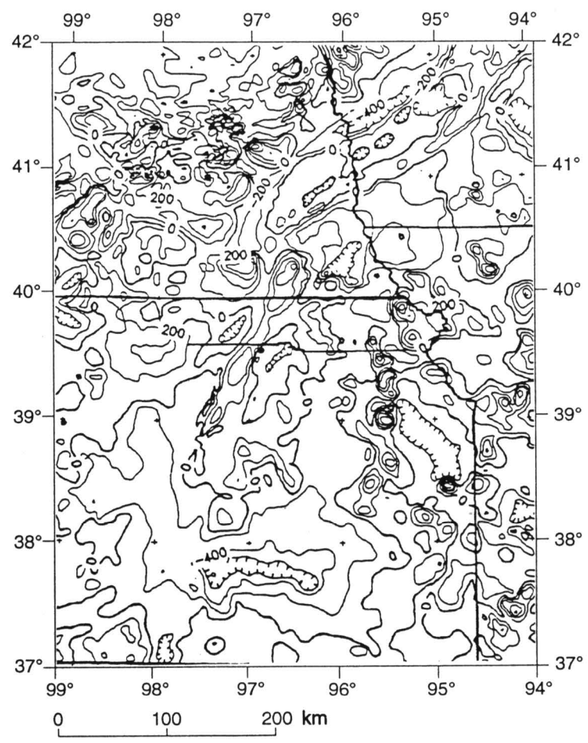

FIGURE 3—TOTAL INTENSITY MAGNETIC ANOMALY MAP OF STUDY AREA WITH LOCATION OF COCORP KANSAS LINE 1 AND TEXACO POERSCH #1 BOREHOLE (dot).

rocks interbedded within the Keweenawan lava pile (Merk and Jirsa, 1982). The interflow rocks were derived from three sources: subjacent lava flows; distant, uplifted Keweenawan volcanic and intrusive rocks; and pre-Keweenawan rocks adjoining the rift. Deposition was by streams flowing over the surfaces of the volcanic flows during short periods of volcanic quiescence (Van Schmus and Hinze, 1985).

The intrusive Keweenawan rocks of this unit are composed of dike swarms, diabase sills, small plutons, large cumulate bodies, and alkaline complexes. While the relationship of the alkaline complexes to the rift is not clear, the large gabbroic bodies and

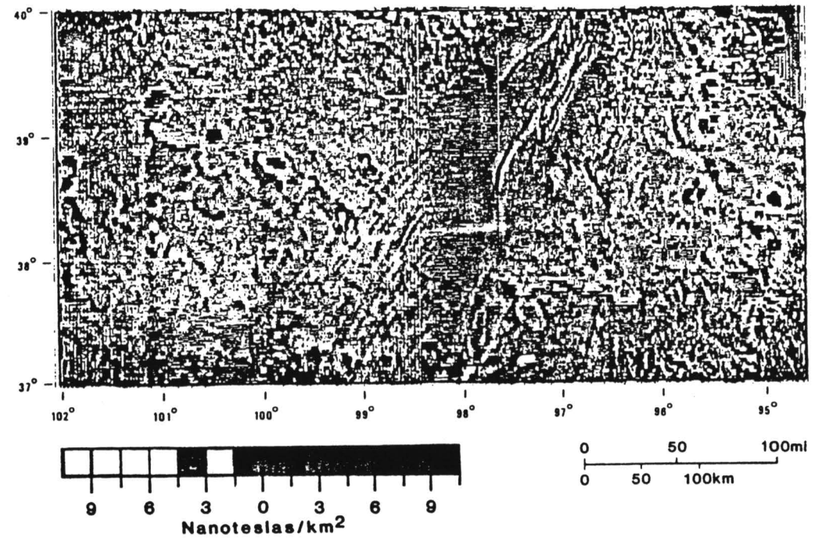

FIGURE 4—SECOND VERTICAL DERIVATIVE OF REDUCED-TO-THE-POLE TOTAL INTENSITY MAGNETIC ANOMALY MAP OF KANSAS (after Yarger, 1985).

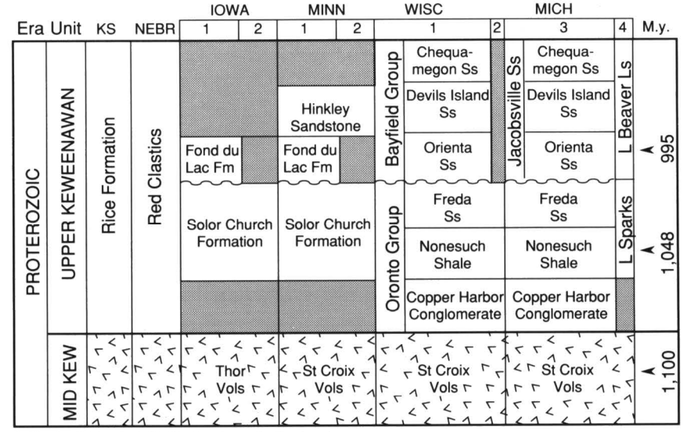

FIGURE 5—STRATIGRAPHIC TERMINOLOGY AND THE TIME RELATIONSHIPS ALONG MIDCONTINENT RIFT TREND (after Dickas, 1986).

basaltic sills and dikes are intimately associated with the Keweenawan volcanics (Van Schmus and Hinze, 1985).

The post-volcanic sedimentary rocks comprise the upper Keweenawan. They post-date active rifting, most likely being deposited in basins originating by vertical tectonic processes, such as broad crustal subsidence due to the excess mass of the volcanics (Van Schmus and Hinze, 1985) and thermal subsidence. In Kansas, these post-volcanic sedimentary rocks are called the "Rice Formation" (Scott, 1966 ; Berendsen et al., 1988).

Lithologically, the Rice Formation is predominantly an arkose or feldspathic sandstone with secondary amounts of micaceous and arenaceous green and red shale. Grains are rounded to subangular, frosted, and generally well sorted (Dickas, 1986 ; Berendsen et al., 1988). The Rice Formation contains limestone and dolomite interbedded with the sandstones and shales, suggesting marine or lacustrine influences (Scott, 1966; Berendsen et al., 1988).

Texaco Poersch #1 Borehole Lithology

The Texaco Poersch #1 borehole was drilled to a depth of 3,444 m (11,300 ft), making it the deepest borehole in Kansas and currently the second deepest penetration of the MCR after the Amoco 1 M. G. Eischeid borehole in Carroll County, Iowa (Berendsen et al., 1988; Anderson, 1990).

The Precambrian basement in the Poersch #1 borehole was encountered at 867 m (2,846 ft). The rocks from 867 m (2,845 ft) to total depth can be roughly divided into two distinct parts, or successions, of almost equal thickness (Berendsen et al., 1988) (fig. 6). The upper succession is dominated by mafic volcanic rocks and subordinate mafic and acidic intrusives, and the lower succession is dominated by arkose and subarkose with minor amounts of siltstone and shale (Berendsen et al., 1988).

The top of the upper, volcanic-dominated, succession is marked by a 88-m (288-ft)-thick gabbro unit that is in sharp contact with the overlying Phanerozoic rocks. Underlying the gabbro, the upper succession is composed of a 300-m (984-ft)-thick sequence of basalt flows, a 480-m (1,575-ft)-thick mixed volcanic-sedimentary sequence which is followed by a 400-m (1,312 ft)-thick sequence of basalt flows and another mixed package 120 m (394 ft) thick. Basalt flow tops were identifiable in all sequences from a reddish color of the rock which can be attributed to oxidation of the top of the flow (Berendsen et al., 1988). The sedimentary packages in the mixed sequences fine upward. Several pegmatites occur in this upper unit. They may all be related to the same intrusive event (Berendsen et al., 1988).

At a depth of 2,265 m (7,429 ft), the lower sedimentary-dominated succession was encountered. This unit can be divided into three sequences bounded by relatively thin mafic volcanic flows or intrusives (Berendsen et al., 1988). The upper sequence consists of about a dozen distinct sedimentary packages that can be characterized by fining upward (Berendsen et al., 1988). Sedimentary rocks in the middle sequence resemble the rocks of the upper sequence, but are consistently coarser grained (Berendsen et al., 1988). Grains of volcanic rock are more common in the lower sedimentary sequence and increase in abundance downward, possibly indicating the presence of flows slightly below the total depth of the hole (Berendsen et al, 1988).

The sedimentary and igneous rocks encountered in the Poersch borehole are decidedly synrift deposits (Berendsen et al., 1988). However, the order of their encounter in the borehole is opposite of what would be expected from the Lake Superior region stratigraphy. This suggests that the MCR in Kansas has been subject to the same late-stage reverse movement observed for northern segments of the rift.

Seismic Line Analysis

Between 1979 and 1981, COCORP recorded 317 km (197 mi) of deep seismic reflection profiles in northern Kansas. The principal purpose of this survey was to investigate the Midcontinent rift. The details of this 15-sec two-way travel time (TWT) reflection survey were provided by Brown et al. (1983) and Serpa et al. (1984).

Line 1 which images the MCR is shown in fig. 7. The upper 0.5 sec consist of relatively continuous and flat-lying reflectors that correspond to the Paleozoic section of the Forest City and Salina basins. These basins were part of the ancestral North Kansas basin and are now separated by the Nemaha Ridge (centered near vp (vibrating point) 1000). The Nemaha Ridge is bounded to the east by the Humboldt fault zone (near vp 900). By far the most prominent feature on the seismic profile is the MCR. Situated between vps 1400 and 2100, the MCR is characterized by high-amplitude reflections extending to about 4 sec which represent the Keweenawan synrift package. These reflections are believed to originate from seismic impedance contrasts between the volcanic and interflow sedimentary units or physical property contrasts within and between the volcanic flows. Above 5 sec relatively few reflections occur except for those from the MCR. This suggests that the upper crust in this area is primarily granitic terrane as supported by drill-hole data. Numerous strong, coherent reflections and diffractions occur below 5 sec. Brown et al. (1983) have suggested that these middle and lower crustal reflections are due to complex, three-dimensional fold and intrusion structures. These deep events are fewer in number and are less continuous under the main axial basin of the rift. This change in seismic character may be due to structural disturbance and igneous intrusion or it may be an artifact of reduced penetration through the axial basin. Moho reflections, expected at TWT of 11 to 13 sec are seemingly absent; however, the decrease in the number of reflections below 12 sec may represent a transition from crust to mantle. Although the Moho does not produce strong reflections, the reflections below 10 sec convey a sense of downwarp toward the center of the crust beneath the rift, suggesting thickening of the crust.

Interpretation of the upper rift structure was carried out using a reprocessed version of the upper 4 sec of line 1, used by Texaco, U.S.A. in their investigation of the rift (Berendsen et al., 1988; Woelk, 1989) In the reprocessed version, the reflectors from the axial basin are more coherent than in the original line, resulting in a more interpretable time section. Figure 8 shows the seismic interpretation superimposed on a line drawing of the reprocessed section; potential-field anomalies and lithologies from nearby basement drill hole are projected onto the section to provide additional control.

The western limit of the basalt basin is interpreted to be a reverse fault. This suggests that the dipping reflector package beneath vp 2000 images a ramp zone above a reverse fault. This arrangement is strikingly similar to what has been interpreted for seismic profiles across the MCR in Iowa, Wisconsin, and Minnesota (Chandler et al., 1989; Hinze et al., 1990). Thrusting of the basalt to its indicated position below the Phanerozoic cover is implied by both a magnetic high over vp 2000 and a correlative anomaly in the Bouguer gravity a short distance to the west. The offset between the gravity and magnetic highs may be attributed to the remanent magnetization of the basalts. Of the four boreholes that penetrated the basement along the trend of this ramp, three encountered mafic rocks while a fourth reported encountering granitic rock. The presence of granitic rock along this trend is problematic, but the predominance of mafic rocks along the trend, coupled with the potential-field anomalies, support the presented interpretation. The reflectors west of this fault are interpreted to be basalt. The depth extent of this unit is not clearly delineated; therefore, potential-field modeling was used to make this determination.

Moving easterly over the basin, a cross-cutting event can be seen between vps 1700 and 1750 at about 3 sec. Inspection of this event shows that reflectors on both sides of the event are clearly defined, and although the reflectors are clearly interrupted, they appear to correlate across the event without offset. This event is interpreted to be a result of seismic triplication (bow-tie) caused by basin geometry and not by geological structure. Serpa et al. (1984) noted that time migration did not resolve this cross-cutting relationship. However, this does not preclude the possibility of this event being a bowtie because time migration does not produce a true subsurface picture when the lateral velocity gradient is significant, as is the case with rifts. The resulting interpretation of the axial basin clearly resembles the structure and geometry that has been attributed to the MCR in previous investigations in Michigan (Brown et al., 1982; Fox, 1988), Lake Superior (Cannon et al., 1989), Iowa, Wisconsin, and Minnesota (Chandler et al., 1989). Individual volcanic units are traceable within the trough and appear to thicken toward

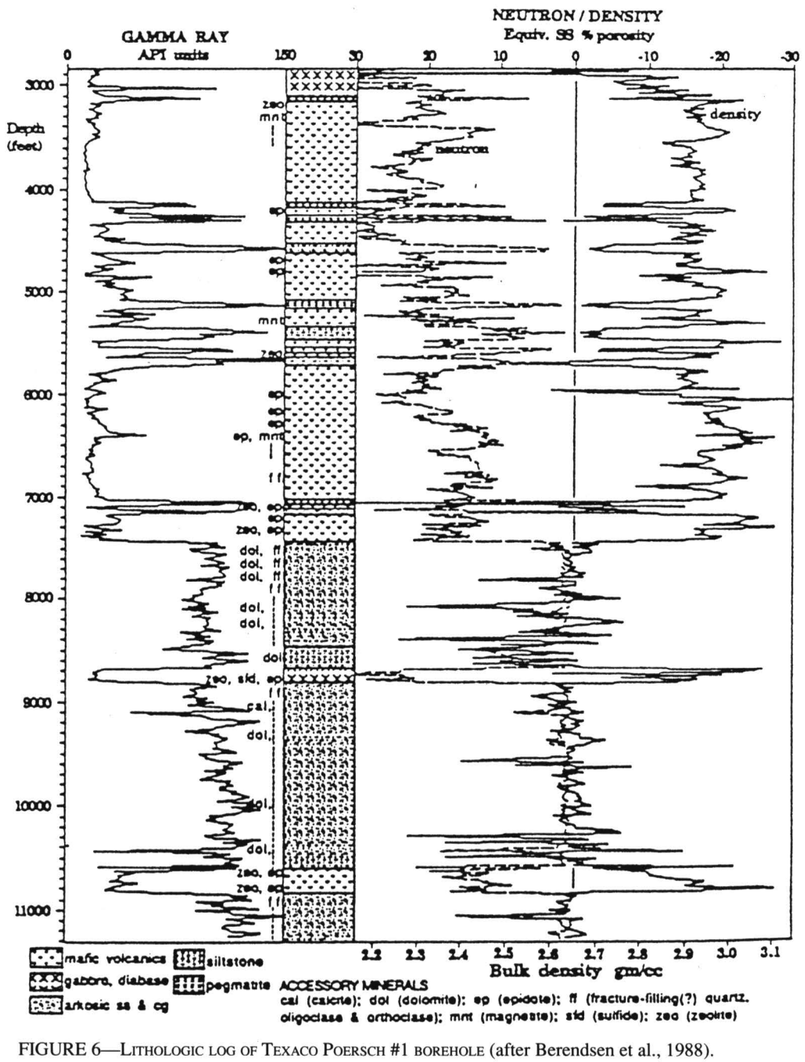

FIGURE 6—LITHOLOGIC LOG OF TEXACO POERSCH #1 BOREHOLE (after Berendsen et al., 1988).

the center of the basin, indicating that the rift basin was subsiding as it was being filled with synrift deposits. The bottom of the basin is difficult to determine in the seismic line. Further complicating the matter is the possibility that there is a lower unit of relatively homogeneous, less-reflective Keweenawan basalts, as observed elsewhere along the rift (Halls, 1978; Zhu and Brown, 1986; Chandler et al., 1989; Hinze et al., 1990).

One of the most interesting changes that is evident in the reprocessed line occurs east of vp 1650. The reflectors from the main basin are seen to be rising toward the structural high drilled by Texaco but are interrupted by a series of west-dipping reflectors at vp 1600. A change in the nature of the reflectors on either side of this west-dipping event also occurs; those to the east appear broken and disjointed in contrast to the continuity of the reflectors to the west. The series of west-dipping reflectors at vp 1600 are interpreted as a reverse fault. Projection of the Poersch borehole along strike suggests that the hole drilled through a reverse fault, thus providing an explanation for the transposed order of the dominant rock types from that observed elsewhere in the rift. The fault was not recognized in the log prepared from the drill-hole rock cuttings or in the wireline logs (Berendsen et al., 1988), but its presence is supported by a small magnetic high between vps 1550 and 1600 that has continuity along the strike of the rift. The offset between the magnetic high and the fault is probably due to the remanent magnetization of the basalt, but may also be influenced by the extent of the gabbroic intrusive that was encountered in the Poersch hole directly below the Phanerozoic rocks. This interpretation suggests that the curved reflections observed just below the fault plane are a result of impedance contrasts between the thin basalt flows and the large sedimentary packages encountered in the bottom half of the Poersch borehole.

Structural interpretation east of vp 1600 is difficult due to the lack of coherent reflectors. With the interpretation of a reverse fault beneath vp 1600, it is assumed that Keweenawan basalt is present at depth, below the synrift sedimentary rocks. This is supported by the increasing amount of volcanic rock grains noted at the bottom of the Poersch borehole. The magnitude and gradient of the gravity anomaly also suggest that high-density material is present below the bottom of the borehole and continuing east. Therefore, the top of a basalt body is interpreted to occur below the borehole and continuing east to the package of reflectors noted beneath vp 1500. The termination of the basalt body at this point is supported by the magnetic high between vps 1450 and 1500. Somanas and others (1989) proposed that this magnetic high was caused by an intrusive body apart from the rift rather than a thin edge. However, the corresponding gravity anomaly at this point reflects only a change in gradient rather than a high, suggesting that the basalt terminates at this point as previously modeled by Yarger (1980; *in* Hahn, 1980).

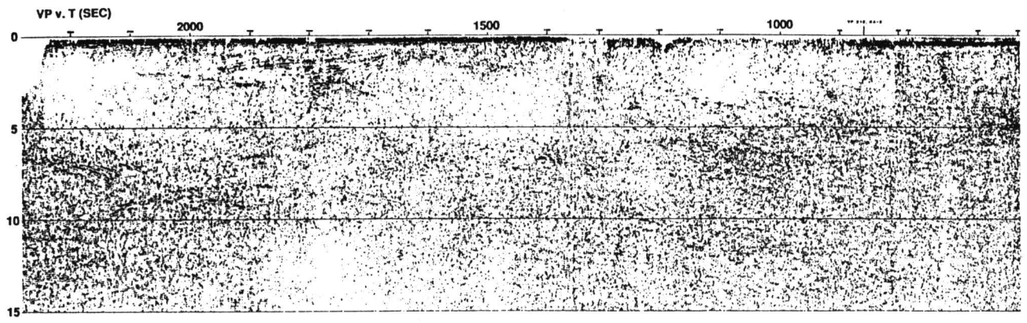

FIGURE 7—COCORP KANSAS SEISMIC REFLECTION LINE 1.

Profile Modeling

To further refine the interpretation initiated with the seismic-reflection profile, gravity and magnetic anomaly profiles were modeled along the COCORP line. It is possible to duplicate the observed gravity anomaly with bodies only in the upper 12 km of the crust using a geologic model similar to that shown in fig. 8. This model implies either that the outpouring of basalts occurred from a rather thin conduit leaving most of the crust undisturbed or that lower crustal intrusive bodies have negligible density contrast with the adjacent crust. However, a model incorporating the concept that the entire crust was disturbed by the rifting event also matches the observed anomaly as shown in fig. 9. Only the anomalous magnetic body at 6–7 sec was added to the gravity model to match the western margin of the magnetic profile. This model has the rift basin reaching a maximum depth of 9 km rather than 11.5 km where only the upper crust is involved. The throw on the reverse faults on either side of the rift basin is 3 km.

The model shown in fig. 9 is the preferred interpretation because it incorporates not only the gravity and magnetic modeling, but also the results of the seismic-reflection profiling and rock types encountered in the Poersch drill hole. Of special note is the regional thickening of the crust as suggested by the general downbowing of the deep seismic reflections. This model incorporates the concept that the entire crust is disturbed and intruded by dike swarms and igneous plutons, and although the crust is initially thinned, the crust is ultimately thickened by isostatic sinking. The magnetic modeling does not contribute to the lower crustal interpretation because most of the modeled magnetic anomaly is caused by bodies located within the upper 10 km of the crust. The crustal structure of this model is strikingly similar to the models proposed for the northern segments of the rift (e.g., Cannon et al., 1989; Hinze et al., 1992), arguing that there is homogeneity in structural style along the length of the rift. This conclusion is compatible with the recent U-Pb dating of the gabbro of the Texaco Poersch #1 hole (Van Schmus et al., 1990) that places the age of this intrusion (1,097.5 ± 3 Ma) in the middle of published U-Pb ages (1,086–1,108 Ma) for the Midcontinent rift igneous rocks in the Lake Superior region.

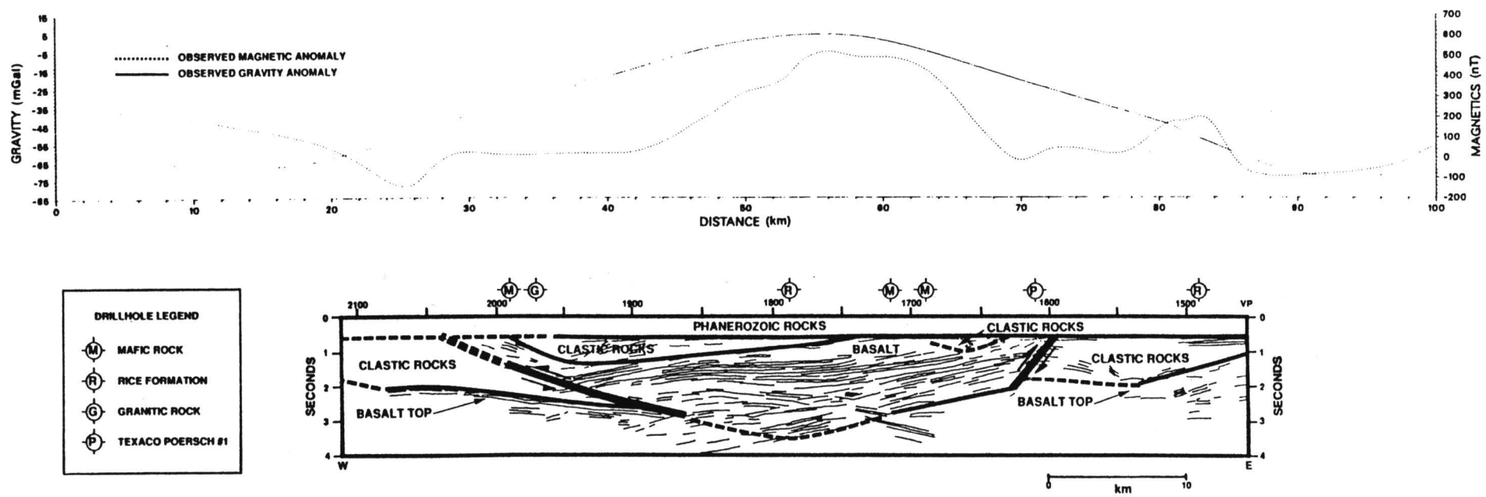

FIGURE 8—INTERPRETED STICK DIAGRAM OF REPROCESSED COCORP KANSAS LINE 1 WITH BOUGUER GRAVITY AND TOTAL INTENSITY MAGNETIC PROFILES PLOTTED. Location of nearby drill holes are projected along geologic strike.

Summary

The recently published data from Texaco, U.S.A.'s investigation of the MCR in northeastern Kansas have provided valuable information on the structural nature of the rift. Lithologic logs from the Texaco Poersch #1 borehole show that a transposed Keweenawan stratigraphy of gabbro and basalt overlying clastic rocks is present on the east side of the rift in Kansas in contrast to the rock sequence observed elsewhere in the MCR. This information, along with the density and velocity logs, provide constraints not available to previous interpretations of the seismic reflection and potential-field data. A reprocessed version of the upper 4 sec of COCORP seismic reflection Kansas Line 1 generated by Texaco, U.S.A. clearly images the axial trough of the MCR. This seismic line is interpreted to image the axial rift basin bounded by reverse faults. Projection of the Poersch #1 borehole along strike shows that Texaco, U.S.A. drilled through the eastern-bounding reverse fault accounting for the transposed order of lithology encountered in the borehole. Potential-field modeling supports the seismic interpretation of the rift structure. The resulting model of an axial rift basin bound by reverse faults is strikingly similar to interpretations proposed for northern segments of the rift, arguing that there is consistency in the structural style and tectonic evolution along the length of the rift system.

ACKNOWLEDGMENTS—Supported in part by National Science Foundation Grant EAR-8617315. We thank the Kansas Geological Survey (KGS) and Texaco USA for providing data used in this study. We also thank Don Steeples (The University of Kansas) and Pieter Berendsen (KGS) and Roger Borcherding (Texaco USA) for their assistance, and Lawrence W. Braile (Purdue University) for his advice on interpreting the seismic sections.

References

Anderson, R. R., 1990, Interpretations of geophysical data over the Midcontinent Rift System in the area of the M. G. Eischeid #1 petroleum test, Carroll County, Iowa; *in*, The Amoco M.G. Eischeid #1 deep petroleum test, Carroll County, Iowa, R. R. Anderson, ed.: Iowa Department of Natural Resources, Special Report Series, no.2, p. 27–38

Behrendt, J. C., Green, A. G., Cannon, W. F., Hutchinson, D. R., Lee, M., Milkereit, B., Agena, W. F., and Spencer, C., 1988, Crustal structure and deep rift basin of the Midcontinent Rift System—results from GLIMPCE deep seismic reflection profile: Geology, v. 16, p. 81–85

Berendsen, P., Borcherding, R. M., Doveton, J., Gerhard, L., Newell, K. D., Steeples, D., and Watney, W. L., 1988, Texaco Poersch #1; Washington County, Kansas—Preliminary geologic report of the pre-Phanerozoic rocks: Kansas Geological Survey, Open-file Report 88–22, 116 p.

Brown, L., Jenson, L., Oliver, J., Kaufman, S., and Steiner, D., 1982, Rift structure beneath the Michigan basin from COCORP profiling: Geology, v. 10, p. 645–649

Brown, L., Serpa, L., Setzer, T., Oliver, J., Kaufamn, S., Lillie, R., Steiner, D., and Steeples, D. W., 1983, Intracrustal complexity in the United States midcontinent—Preliminary results from COCORP surveys in northeastern Kansas: Geology, v. 11, p. 25–30

Cannon, W. F., Green, A. G., Hutchinson, D. R., Lee, M., Milkereit, B., Behrendt, J. C., Halls, H. C., Green, J. C., Dickas, A. B., Morey, G. B., Sutcliffe, R., and Spencer, C., 1989, The Midcontinent rift beneath Lake Superior from GLIMPCE seismic-reflection profiling: Tectonics, v. 8, p. 305–332

Chandler, V. W., McSwiggen, P. L., Morey, G. B., Hinze, W. J., and Anderson, R. R., 1989, Interpretation of seismic reflection, gravity, and magnetic data across the Middle Proterozoic Midcontinent rift system, northwestern Wisconsin, eastern Minnesota, and central Iowa: American Association of Petroleum Geologists, Bulletin, v. 73, p. 261–275

Chase, C. G., and Gilmer, T. H., 1973, Precambrian plate tectonics—the Midcontinent gravity high: Earth and Planetary Sciences, Letters, v. 21, p. 70–78

Dickas, A. B., 1986, Comparative Precambrian stratigraphy and structure along the Midcontinent rift: American Association of Petroleum Geologists, Bulletin, v. 70, p. 225–238

Fox, A. J., 1988, An integrated geophysical study of the southeastern extension of the Midcontinent rift system: M. S. thesis, Purdue University, 112 p.

Green, J. C., 1982, Geology of Keweenawan extrusive rocks; *in*, Geology and Tectonics of the Lake Superior Basin, R. J. Wold and W. J. Hinze, eds.: Geological Society of America, Memoir 156, p. 239–243

_____, 1983, Geologic and geochemical evidence for the nature and development of the Middle Proterozoic (Keweenawan) Midcontinent rift of North America; *in*, Processes of Continental Rifting, P. Morgan and B. H. Baker, eds.: Tectonophysics, v. 94, p. 413–437

Hahn, R. K., 1980, Upper mantle velocity structure in eastern Kansas from teleseismic p-wave residuals: M. S. thesis, University of Kansas, 84 p.; also available as Kansas Geological Survey, Open-file Report 80-14

Halls, H. C., 1978, The Late Precambrian central North American rift system—a survey of recent geological and geophysical investigations; *in*, Tectonics and Geophysics of Continental Rifts, I. B. Ramberg and E. R. Neumann, eds.: NATO Advanced Study Institute, v. 37, p. 111–123

Hinze, W. J., 1963, Regional gravity and magnetic anomaly maps of the Southern Peninsula of Michigan: Michigan Geological Survey, Report of Investigations, no. 1, 26 p.

Hinze, W. J., Kellogg, R. L., and O'Hara, N. W., 1975, Geophysical studies of basement geology of the Southern Peninsula of Michigan: American Association of Petroleum Geologists, Bulletin, v. 59, p. 1,562–1,584

Hinze, W. J., Wold, R. J., and O'Hara, N. W., 1982, Gravity and magnetic anomaly studies of Lake Superior; *in*, Geology and Tectonics of the Lake Superior Basin, R. J. Wold and W. J. Hinze, eds.: Geological Society of America, Memoir 156, p. 203–222

Hinze, W. J., and Braile, L. W., 1988, Geophysical aspects of the craton—U.S.; *in*, Sedimentary Cover—North American Craton, L. L. Sloss, ed.: Geological Society of America, The Geology of North America, D–2, p. 5–24

Hinze, W. J., Braile, L. W., and Chandler, V. W., 1990, A geophysical profile of the southern margin of the Midcontinent rift system in western Lake Superior: Tectonics, v. 9, p. 303–310

Hinze, W. J., Allen, D. J., Fox, A. J., Sunwood, D., Woelk, T. S., and Green, A. G., 1992, Geophysical investigations and crustal structures of the North American midcontinent rift system, Part C; *in*, Geodynamics of Rifting, P. Ziegler, ed.: Tectonophysics, v. 213, no. 1-2, p. 17-32

King, E. R., and Zietz, I., 1971, Aeromagnetic study of the Midcontinent gravity high of central United States: Geological Society of America, Bulletin, v. 82, p. 2,187–2,208

Klasner, J. S., Wold, R. J., Hinze, W. J., Bacon, L. O., O'Hara, N. W., and Berkson, J. M., 1979, Bouguer gravity anomaly map of the northern Michigan–Lake Superior region: U.S. Geological Survey, Geophysical Investigation Map GP–930, scale 1:1,000,000

Lam, C. K., 1986, Interpretation of statewide gravity survey of Kansas: Ph.D. thesis, University of Kansas, 213 p.

Lidiak, E. G., 1972, Precambrian rocks in the subsurface of Nebraska: Nebraska Geological Survey, Bulletin, no. 26, 41 p.

Lidiak, E. G., and Hinze, W. J., 1993, Grenville province in the subsurface of eastern United States; in, Precambrian—Conterminous U.S., ed, by J. C. Reed et al.: Geological Society of America, The Decade of North American Geology (DNAG), v. C–2, p. 353–365

Lyons, P. L., 1959, The Greenleaf anomaly, a significant gravity feature; *in*, Symposium of the Geophysics of Kansas, W. W. Hambleton, ed.: Kansas State Geological Survey, Bulletin 137, p. 105–120

Merk, G. P., and Jirsa, M. A., 1982, Provenance and tectonic significance of the Keweenawan interflow sedimentary rocks; *in*, Geology and Tectonics of the Lake Superior Basin, R. J. Wold and W. J. Hinze, eds: Geological Society of America, Memoir 156, p. 97–105

Meyer, W. V., 1987, The Wichita magnetic low, southeastern Kansas: M.S. thesis, Purdue University, 95 p.

Moore, J. M., 1986, Introduction—the "Greville Province" then and now; *in*, The Grenville Province, J. M. Moore, A. Davidson, and A. J. Baer, eds.: Geological Association of Canada, Special Paper 31, p. 1–11

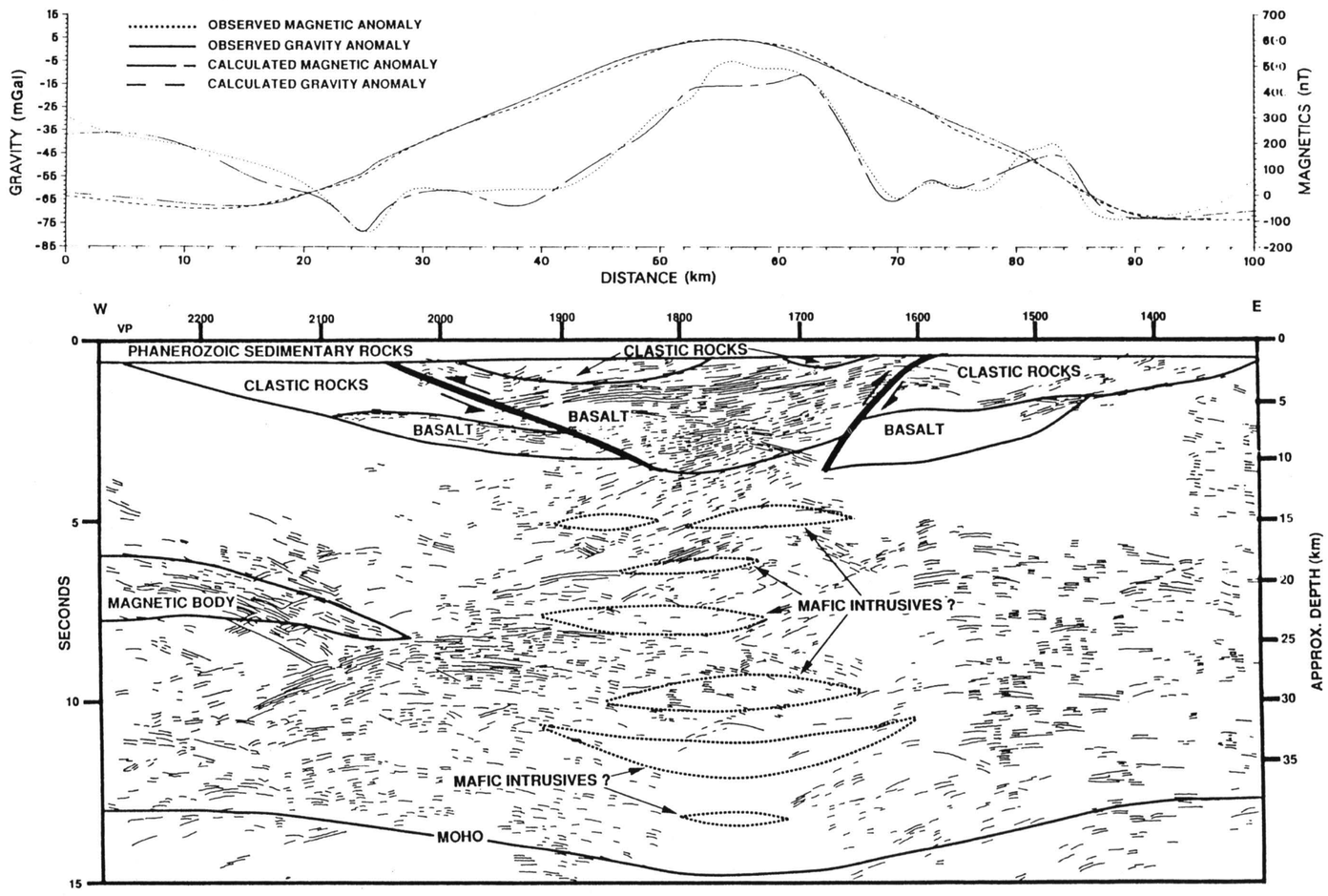

FIGURE 9—GEOLOGIC MODEL OF STICK DIAGRAM OF COCORP KANSAS LINE 1 WITH CALCULATED AND OBSERVED BOUGUER GRAVITY ANOMALY AND TOTAL INTENSITY MAGNETIC ANOMALY.

Morey, G. B., and Green, J. C., 1982, Status of the Keweenawan as a stratigraphic unit in the Lake Superior region; *in,* Geology and Tectonics of the Lake Superior Basin, R. J. Wold and W. J. Hinze, eds.: Geological Society of America, Memoir 156, p. 15–25

Muehlberger, W. R., Denison, R. E., and Lidiak, E. G., 1967, Basement rocks in continental interior of United States: American Association of Petroleum Geologists, Bulletin 51, p. 2,351–2,380

Oray, E., Hinze, W. J., and O'Hara, N. W., 1973, Gravity and magnetic evidence for the eastern termination of the Lake Superior syncline: Geological Society of America, Bulletin 84, p. 2,763–2,780

Scott, R. W., 1966, New Precambrian(?) formation in Kansas: American Association of Petroleum Geologists, Bulletin 50, p. 380–384

Serpa, L., Setzer, T., Farmer, H., Brown, L., Oliver, J., Kaufman, S., Sharp, J., and Steeples, D. W., 1984, Structure of the southern Keweenaw rift from COCORP surveys across the Midcontinent geophysical anomaly in northeastern Kansas: Tectonics, v. 3, p. 367–384

Simpson, R. W., Jachens, R. C., and Blakely, R. J., 1986, A new isostatic residual map of the conterminous United States with a discussion on the significance of isostatic residual anomalies: Journal of Geophysical Research, v. 91, p. 8,348–8,372

Somanas, C., Knapp, R. W., Yarger, H. L., and Steeples, D. W., 1989, Geophysical model of the midcontinent geophysical anomaly in northeastern Kansas; *in,* Geophysics in Kansas, D. W. Steeples, ed.: Kansas Geological Survey, Bulletin 226, p. 215–228

Thiel, E. C., 1956, Correlation of gravity anomalies with Keweenawan geology of Wisconsin and Minnesota: Geological Society of America, Bulletin 67, p. 1,079–1,100

Van Schmus, W. R., and Hinze, W. J., 1985, The Midcontinent Rift System: Annual Review of Earth and Planetary Sciences, v. 13, p. 345–383

Van Schmus, W. R., Bickford, M. E., and Zietz, I., 1987, Early and Middle Proterozoic provinces in the central United States; *in,* Proterozoic Lithospheric Evolution, A. Kroner, ed.: American Geophysical Union, Geodynamic Series, v. 17, p. 43–68

Van Schmus, W. R. , Martin, W. D., Sprowl, D. R., Geissman, J., and Berendsen, P., 1990, Age, Nd and Pb isotopic composition, and magnetic polarity for subsurface samples of the 1100 Ma Midcontinent rift: Geologic Society of America, Abstracts with Programs, v. 22, no. 7, p. A174

von Frese, R. R. B., Hinze, W. J., and Braile, L. W., 1982, Regional North American gravity and magnetic anomaly correlations: Geophysical Journal of Research, Astronomical Society,v. 69, p. 745–761

Woelk, T. S., 1989, An integrated geophysical study of the Midcontinent Rift System in northeastern Kansas: M.S. thesis, Purdue University, 74 p.

Woelk, T. S., and Hinze, W. J., 1991, Model of the Midcontinent Rift System in northeastern Kansas: Geology, v. 19, p. 277–280

Woollard, G. P., 1943, Transcontinental gravitational and magnetic profile of North America and its relation to geologic structure: Geological Society of America, Bulletin 54, p. 747–790

Yarger, H. L., 1981, Aeromagnetic survey of Kansas: EOS, American Geophysical Union, Transactions, v. 62, no. 17, p. 173–178

_____, 1985, Kansas basement study using spectrally filtered aeromagnetic data; *in,* The Utility of Regional Gravity and Magnetic Anomaly Maps, W. J. Hinze, ed.: Society of Exploration Geophysicists, p. 213–232

Zhu, T., and Brown, L. D., 1986, Consortium for Continental Reflection Profiling Michigan Survey—reprocessing and results: Journal of Geophysical Research, v. 91, p. 11,477–11,495

Forward Seismic Modeling—Applications and Utility

Neil L. Anderson,[1] Dennis E. Hedke,[2] and Ralph W. Knapp[1]
[1]Department of Geology and Geophysics, University of Missouri–Rolla, Rolla, MO 65401; [2]Consultant, Wichita, KS 67202; and
[3]formerly with Kansas Geological Survey, University of Kansas, Lawrence, KS 66047

Abstract

Geological bodies such as reefs, horst blocks, channel sandstones, faults, salt diapirs, deltaic complexes, etc., typically generate recognizable seismic signatures (or distinquishing seismo-geological features). The seismic signature of a geological body (a reef, for example) is composed of any and all features on the seismic data that can be confidently attributed to the presence of the reef.

Seismic signatures have two basic components: time-structure variations and character variations. The time-structure variation component is created by structural relief in the subsurface and velocity-generated, time-structural relief (pull-up/push-down effects). The character variation component consists of lateral changes in the amplitude and/or phase of specific events and lateral variations in the seismic image of specified units (typically corresponding to stratigraphic groups). The seismic image of a specified layer is the pattern of the sequence of events from the top to the base of that layer, inclusive.

Forward seismic modeling is the process through which a geologic section (subsurface depth/density/acoustic-velocity model) is transformed into a synthetic seismogram, thereby enabling the relationships between the subsurface and the corresponding synthetic seismogram to be deduced. Such modeling can elucidate the potential utility of the seismic technique prior to the acquisition of field seismic data and facilitate the interpretation of acquired data. Seismic modeling is typically done both before and after the acquisition of seismic field data. It aids the planning of an acquisition program and it is essential in interpretation, making correlation of the observed reflections with geologic interfaces possible, and verifying the seismic responses of deduced anomalies.

Introduction

Forward seismic modeling is the process through which a geologic section (subsurface model of one, two, or three dimensions) is transformed into a synthetic seismogram (synthetic seismic record). Depth and acoustic impedance (product of velocity and density) variations within the geologic section are converted to transit time and reflection amplitude, respectively (fig. 1). The relationship between the geologic section and the corresponding synthetic seismogram can then be deduced. Such modeling can elucidate the potential utility of the seismic technique prior to the acquisition of field seismic data and facilitate the interpretation of acquired data. Seismic modeling is typically done both before and after the acquisition of seismic field data. It aids the planning of an acquisition program, and it is essential in interpretation, making correlation of the observed reflections and geologic interfaces possible, and verifying the seismic responses of deduced anomalies.

Modeling Prior to the Acquisition of Seismic Data

Seismic surveys are usually designed with one or more geologic objectives in mind. Modeling is typically done prior to the acquisition of seismic data to ensure that the geologic objectives are potentially seismically visible and to ensure that appropriate field acquisition parameters are used.

Modeling prior to acquisition gives a good indication whether we will be able to resolve the geologic objective, assuming we manage to obtain good-quality field data. It can verify or refute whether geologic objectives can be seen within the limits of the field techniques that will be used. We will probably be able to identify our geologic objective on real seismic data if its seismic image can be resolved on synthetic seismograms.

Modeling after the Acquisition of Seismic Data

The seismic interpreter conceptually transforms seismic sections into geological sections. Reefs, horst blocks, channel sandstones, faults, salt diapirs, deltaic complexes, etc., are typical geologic targets, the seismic image of which the experienced explorer intuitively inverts (transforms seismic time sections into depth sections). The interpreted seismic data must result in geologic sections that are consistent with well log data and/or other geologic control.

Typically, synthetic seismic data are generated for all or part of a subsurface geologic section (as initially envisioned). The synthetic seismogram is compared to the real seismic data. When significant discrepancies are observed, the geologic section is modified (within the constraints imposed by other independent control) and a new synthetic seismogram is generated. This process is iteratively repeated, until the interpreter is satisfied with the correlation between the synthetic seismogram and the real seismic data, and is confident of the final interpretation.

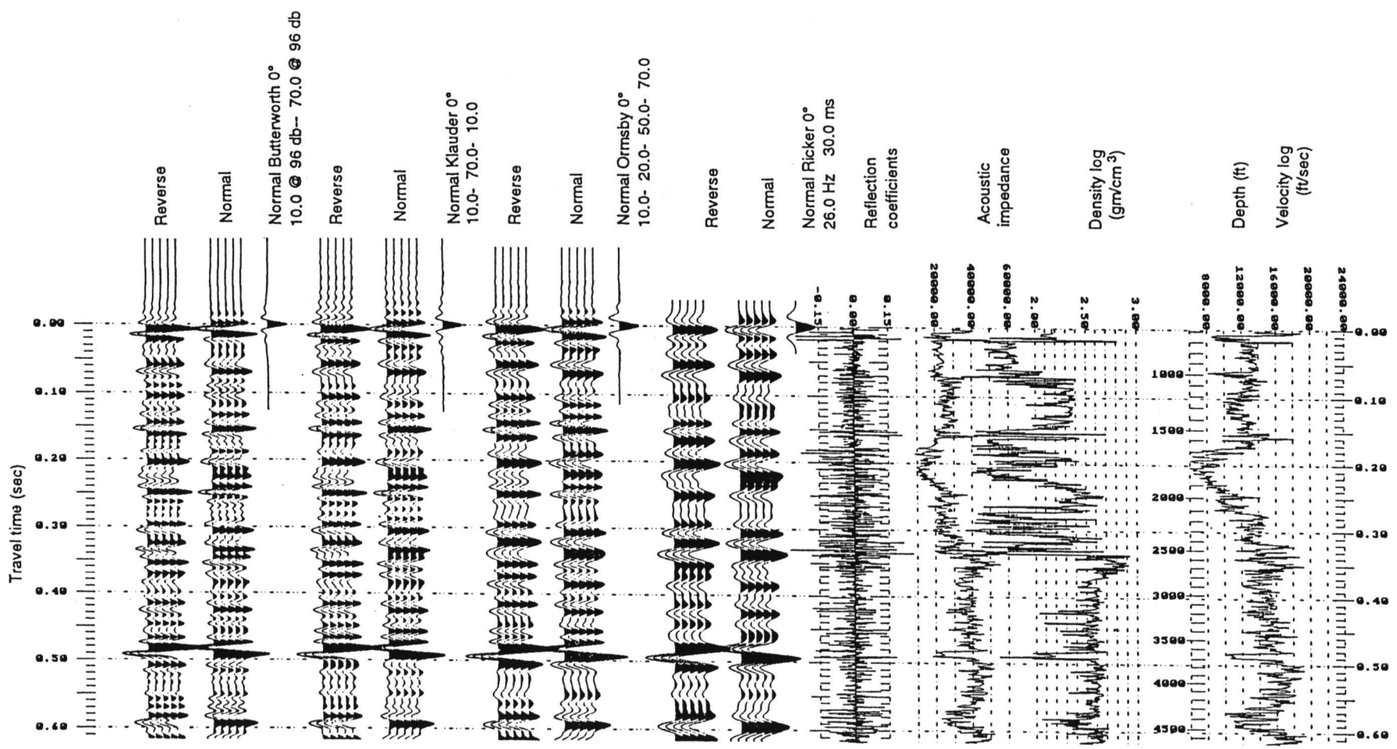

FIGURE 1—VELOCITY LOG, DENSITY LOG, ACOUSTIC IMPEDANCE CURVE (PRODUCT OF SEISMIC VELOCITY AND DENSITY), REFLECTION COEFFICIENT CURVE (ACOUSTIC IMPEDANCE CONTRAST) AND SUITE OF SYNTHETIC SEISMOGRAMS FOR THE SEC. 2, T. 30 S., R. 24 W. WELL. Each synthetic seismogram is generated by convolving the reflection coefficient curve with different type of zero-phase wavelet (ie. Ricker, Orsmby, Klauder, Butterworth). Such one-dimensional synthetic seismograms are generally used to correlate field seismic data to the subsurface geology. Note that in all of the figures, positive acoustic impedance contrasts (higher values with increasing depth) generate peaks (deflections to the right); the "arrival time"of a zero-phase wavelet is measured at the apex of the respective trough or peak. Transit time is two-way travel time.

Seismic Signature

Geological bodies or exploration targets such as reefs, horst blocks, channel sandstones, faults, salt diapirs, deltaic complexes, etc., typically generate recognizable seismic signatures (or distinquishing seismo-geological features). The seismic signature of a geological body, a reef, for example, is composed of any and all features on the seismic data which can be confidently attributed to the presence of the reef.

Seismic signatures have two basic components: time-structure variations and character variations (fig. 2).

1. The time-structure component is created by structural relief in the subsurface and velocity-generated, time-structural relief (pull-up/push-down effects).
2. The character variations component consists of lateral changes in the amplitude and/or phase of specific events, and lateral variations in the seismic image of specified units (typically corresponding to stratigraphic groups). The seismic image of a specified layer is the pattern of the sequence of events from the top to the base of that layer, inclusive.

Time-structural Component

The time-structural component of the seismic signature of a geological feature is due both to subsurface relief (fig. 3) and to velocity-generated, time-structural relief (figs. 4 and 5).

Subsurface relief may be the result of such features as primary depositional patterns, post-depositional deformation (faulting, folding, uplift, diapirism), erosion, salt dissolution, differential compaction, etc.

Velocity-generated, time-structural relief is primarily due to lateral facies variations and lateral variation in the thickness of a sediment of relatively uniform velocity. For example, the thickness of a channel sandstone can vary from 0 m to 30 m (0 ft to 100 ft) over a distance of less than a few hundred meters. Depending upon the velocity contrast between the channel sandstone and the encasing sediment, and associated structural relief, the pre-channel horizons may be "pulled-up" or "pushed down" beneath the channel facies.

When seismic modeling is done prior to data acquisition, the interpreter is attempting to determine whether the time-structural relief component of the seismic signature of the geological objective will be visible on field seismic data. When modeling is done after the acquisition of the data, the interpreter is trying to determine the nature of the geological feature that generated the observed pattern of time-structural relief.

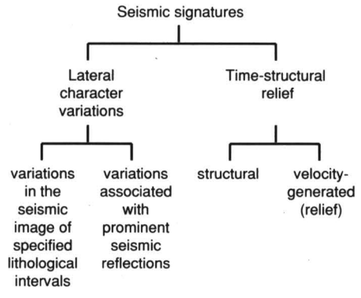

FIGURE 2—COMPONENTS OF THE SEISMIC SIGNATURE OF A GEOLOGICAL BODY CAN BE CATEGORIZED AS "LATERAL CHARACTER VARIATIONS" OR "TIME-STRUCTURAL RELIEF."

A word of caution: a component of time-structural relief on field seismic data can result from inappropriate statics corrections, too little care in processing, or over-zealous processing (figs. 6 and 7).

Character Variation Component

Character variations can be classified as lateral changes in amplitude and/or phase along a specific seismic event, or as lateral changes in the seismic image of a specified unit. Amplitude and/or phase variations typically occur as a result of constructive and destructive interference (figs. 8 and 9), lateral variation in acoustic impedance contrast (fig. 10), focusing and defocusing (fig. 11), diffractions (fig. 12) and differential attenuation. Lateral variations in the seismic image of a specified unit typically result from facies variation within that zone (e.g., reef to off-reef transition; fig. 12). Character variations that are independent of the body of interest are not considered to be components of the seismic signature of that body. These include interference from noise and some multiples (figs. 12 and 13).

When seismic modeling prior to data acquisition, the interpreter is attempting to determine whether the character variation component of the seismic signature of the geological objective will be seismically visible. When modeling after data acquisition, the interpreter is generally attempting to deduce the geological origin of an observed seismic anomaly.

Development of a Pre-acquisition Model

Seismic data are usually acquired to delineate a preconceived geological objective. Generally, the survey area has been selected on the basis of geological studies and is considered to be a favorable area with respect to the envisioned target. Pre-acquisition modeling consists of transforming the envisioned subsurface geologic section (subsurface model with units of depth, acoustic velocity, and density) into a synthetic seismic section (composed of space (0-, 1-, or 2-dimensions), time, and units of reflection amplitude). Typically, if the seismic signature of a geological target is not manifested on appropriately modeled synthetic seismograms, it will not be seen on field seismic data. Whether modeled features are interpretable on resultant seismic data depends largely upon the accuracy of the geologic section and the quality of the real seismic data (function of noise, multiple interference, acquisition parameters, quality of processing, etc.).

There are two types of pre-acquisition geologic sections—stratigraphic and structural. Both are designed on the basis of well control in the immediate vicinity of the study area, regional trends, the morphology, and acoustic impedance characteristics of features similar to the envisioned target. The stratigraphic and structural sections generally differ with respect to detail and ultimate purpose. Stratigraphic sections are designed to provide information with respect to the character variation component of the seismic signature of the envisioned anomaly. In contrast, structural sections are designed to illustrate the time-structural relief component. Typically, the stratigraphic section is restricted to that portion of the subsurface in the immediate vicinity of the envisioned geological anomaly, whereas the structural section usually extends from the surface to a depth below the features of interest.

Stratigraphic synthetic seismograms are generated in an effort to determine whether the character variation component of the seismic signature of the geological target will be seismically visible (figs. 1 and 13). Structural synthetic seismograms are usually generated in order to determine whether the time-structural component of the seismic signature of the geologic target will be visible (fig. 12).

In the case of the stratigraphic synthetic seismograms, modeled amplitude and phase variations along specific events and changes in the seismic image of layers are closely analyzed. In the case of the structural synthetic seismograms, the modeled seismic response to subsurface structure and velocity-generated time-structural relief are

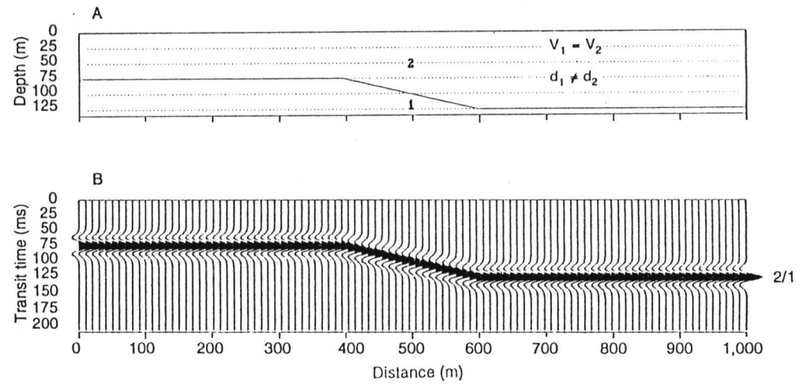

FIGURE 3—STRUCTURAL RELIEF IN THE SUBSURFACE IS MANIFESTED AS TIME-STRUCTURAL RELIEF ON SEISMIC DATA. In the upper illustration (geologic section), horizon 2/1 is displayed on a depth section; in the lower diagram (synthetic seismogram), horizon 2/1 is displayed on the corresponding time-section. The apex of the zero-phase Ricker wavelet peaks represents the arrival time of the event on the synthetic seismogram. The amplitude and polarity of the reflection is a function of the acoustic impedance contrast (product of velocity and density) between layers 2 and 1. In the process of "inversion," subsurface velocity functions and reflection amplitudes are used to convert seismic data into depth sections.

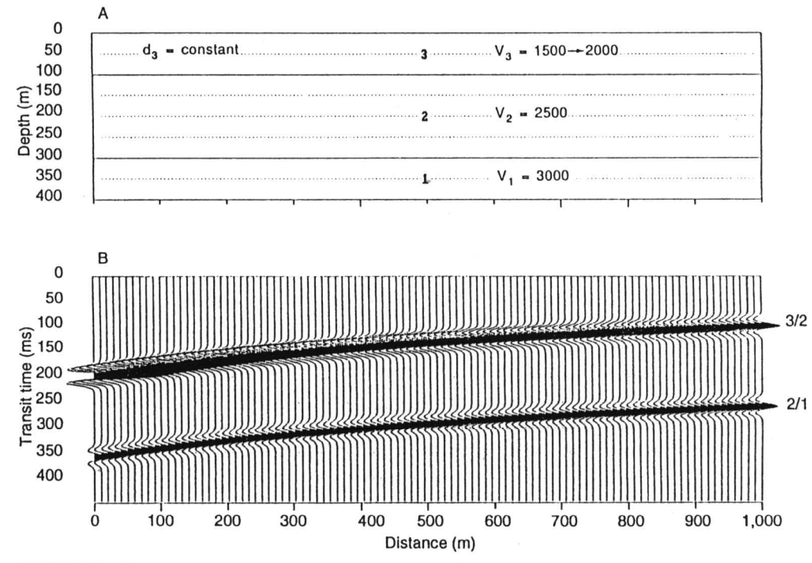

FIGURE 4—LATERAL VARIATIONS IN THE ACOUSTIC VELOCITY OF THE SUBSURFACE GENERATE TIME-STRUCTURAL RELIEF ON SEISMIC DATA. In the upper illustration (geologic section), horizons 2/1 and 3/2 are displayed on a depth section; in the lower diagram (synthetic seismogram), these horizons are displayed on the corresponding time-section. Note that the time-structural relief observed along the events (reflections) 3/2 and 2/1 are due to lateral velocity variations within layer 3.

analyzed. Based on these analyses, the interpreter decides whether the seismic signatures of the geological objective should be visible, assuming appropriate field acquisition parameters are employed, sufficiently good quality field data is obtained, and the data are properly processed.

Whether seismic signatures can be distinguished on the field data is a function of both the quality of the field data and signal/noise ratio of seismic data. Subtle or weak anomalies might only be seen on the final processed section. However, likely key marker horizons are noted on the synthetic seismograms and examined on common shot records (field seismograms) as a check of data quality.

Pre-acquisition modeling can be thought of as a precautionary measure—the seismic interpreter is attempting to safeguard against acquiring data in search of a target that is not likely to be visible on real seismic data and against using inappropriate field acquisition parameters.

Development of a Post-acquisition Model

Seismic data are usually acquired to delineate a preconceived geological objective. Generally, geologic sections (subsurface models) of such envisioned targets have been generated prior to data acquisition in order to ensure (within reason) that the seismic signature of the target will be visible on reasonable quality seismic data and as an aid to the design of field-acquisition parameters.

During post-acquisition modeling, the seismic interpreter, intuitively or otherwise, inverts the interpreted seismic data and develops a geological section using all available data as constraints. Such data would include acoustic and density log data, drilling and lithology data, stacking velocities, and check shot velocities. Experience and intuition will assist in refining modeled geologic sections.

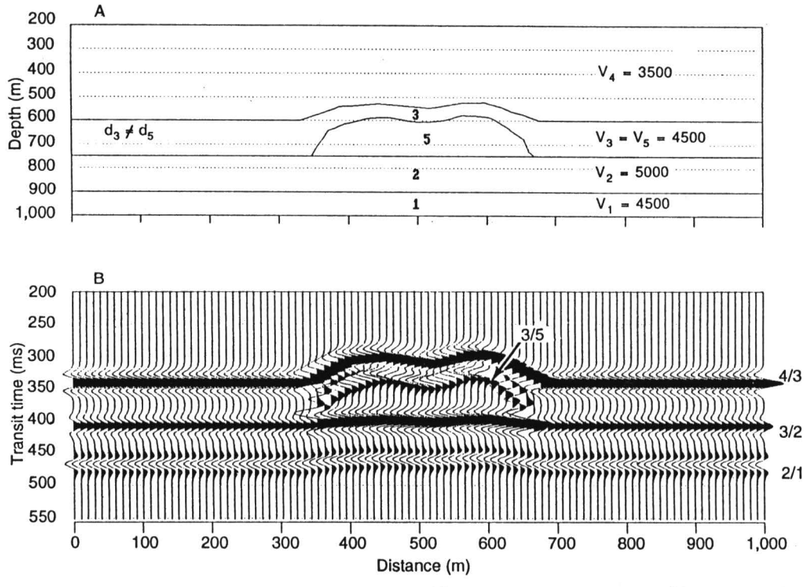

FIGURE 5—TIME-STRUCTURAL RELIEF ALONG EVENT 4/3 IS DUE TO STRUCTURAL RELIEF. Time-structural relief along event 2/1 is attributable to lateral variations in the thicknesses of the overlying layers.

A synthetic seismogram is generated by the interpreter for all or part of the geologic section and compared to the processed seismic data. When discrepancies are observed, the geologic section is modified and a new synthetic seismogram is generated. This process is iteratively repeated, until the interpreter is satisfied with the correlation between the synthetic seismogram and the real seismic data. Care must be taken to ensure that the final output is consistent with known geological constraints.

There are two complementary types of post-acquisition models—stratigraphic and structural. Both are designed on the basis of the inverted seismic data (intuitive or otherwise) and are constrained by available knowledge, including well log control, check shot velocities, regional trends and morphology, and acoustic impedance characteristics of related geological features. Stratigraphic models are generated to clarify the geological origin of the character variation component of an observed seismic anomaly. Structural models are generated to determine the origin of the time-structural component of an observed anomaly.

The stratigraphic synthetic seismogram enables amplitude and phase variation along specific events and variations in the seismic images of specific layers to be closely analyzed. Accuracy can depend on knowledge of the wavelet of the seismic energy pulse, that is, the response to a hypothetical isolated reflector. Using the structural

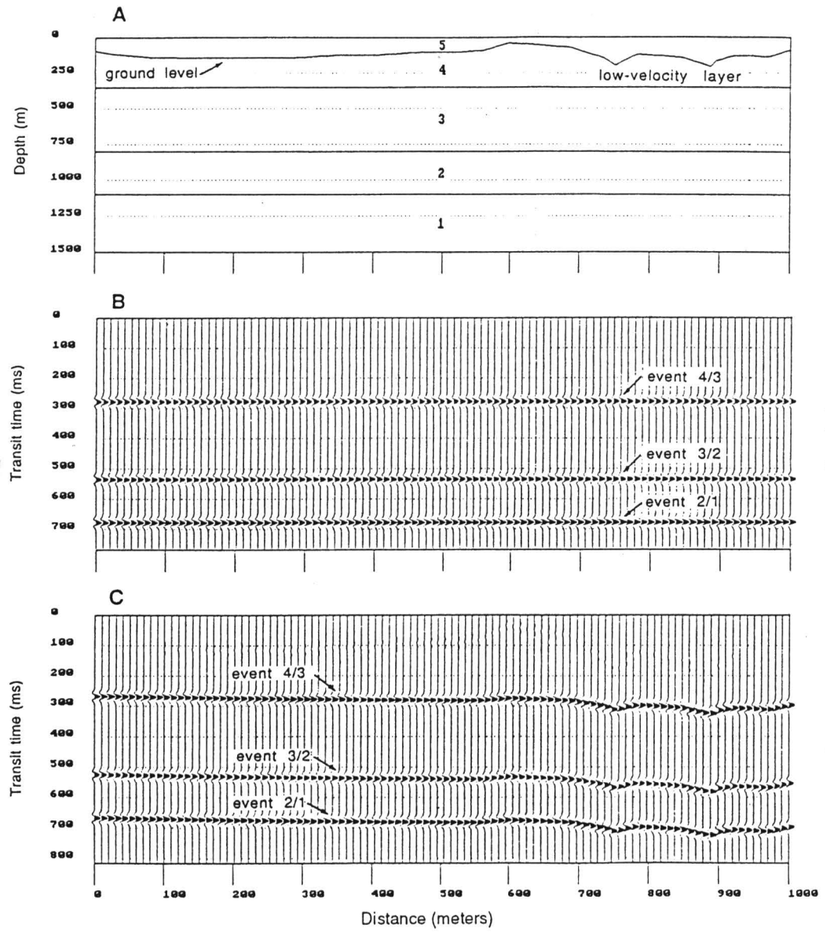

FIGURE 6—APPARENT TIME-STRUCTURAL RELIEF CAN BE CAUSED BY THE APPLICATION OF INACCURATE ELEVATION OR WEATHERING CORRECTIONS. Elevation corrections account for lateral changes in the surface elevation of shot and receiver locations; weathering corrections account for the lateral velocity variations which are characteristic of the shallow subsurface in many places.

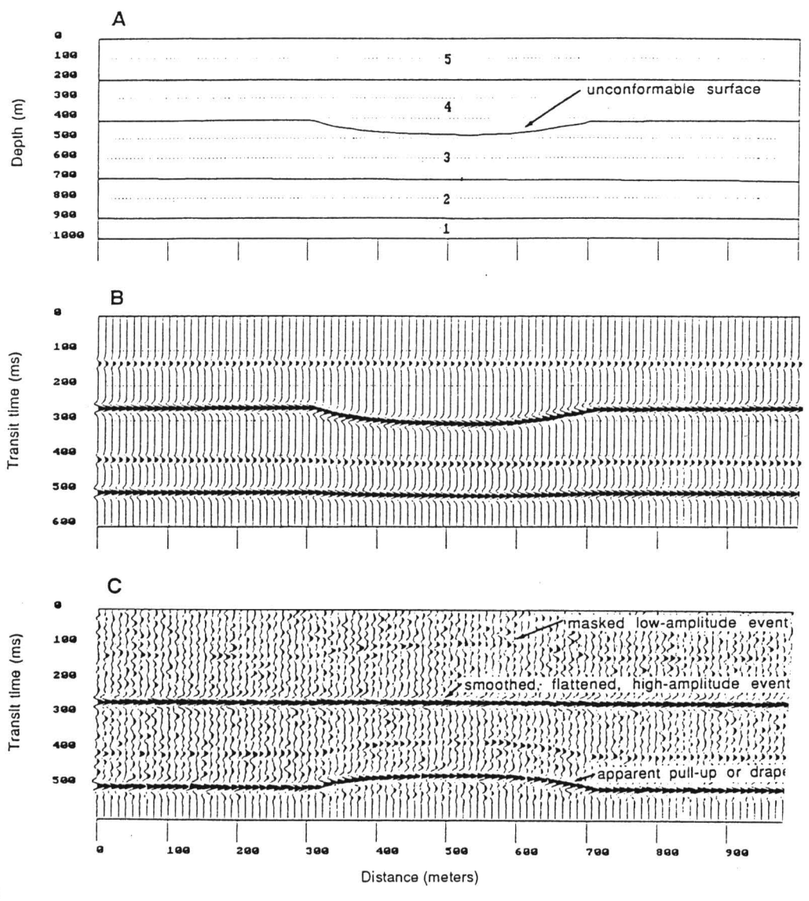

FIGURE 7—APPARENT TIME-STRUCTURAL RELIEF CAN BE AN ARTIFACT OF PROCESSING. In the middle diagram the geologic section has been properly transformed into a synthetic seismogram. The lower diagram is intended to illustrate the situation where a processor has used the high-amplitude reflection from the unconformable surface as a datum (20% noise has been superposed on the synthetic seismogram). As evidenced by the figures, such injudicious processing techniques can lead to erroneous interpretations.

synthetic seismograms, the interpreter attempts to deduce structural relief in the subsurface and to determine the velocity variations which produced the observed pattern of velocity-generated time-structural relief. This later seismogram depends on a stable wavelet on the real seismic data but is not dependent on identification of the wavelet form.

Post-acquisition modeling can similarly be thought of as a precautionary measure. The interpreter is attempting to ensure that anomalous features on the seismic data, in all probability, originate from geological features worthy of further evaluation (i.e., the acquisition of additional seismic control, drilling, etc.). The interpreter is attempting to avoid the gross error of an unrealistic interpretation.

Summary

Through forward seismic modeling, the interpreter can elucidate the potential utility of the seismic technique prior to the acquisition of field seismic data and thereafter facilitate the interpretation of acquired seismic data. Seismic modeling is typically done both before and after the acquisition of seismic field data. It aids the planning of an acquisition program, and it is essential in interpretation, making correlation of the observed reflections and geologic interfaces possible and verifying the seismic responses of deduced anomalies.

There are two basic types of forward models—stratigraphic and structural. Both are designed on the basis of well control in the immediate vicinity of the study area, regional trends, the morphology, and acoustic impedance characteristics of features similar to the envisioned target. The stratigraphic and structural synthetic seismograms generally differ with respect to detail and ultimate purpose. Stratigraphic synthetic seismograms are designed to provide information with respect to the character variation component of the seismic signature of the envisioned anomaly. In contrast, structural synthetic seismograms are designed to illustrate the time-structural relief component. Typically, the stratigraphic seismogram is restricted to that portion of the subsurface in the immediate vicinity of the envisioned geological anomaly, whereas the structural seismogram usually extends from the surface to a depth below the features of interest.

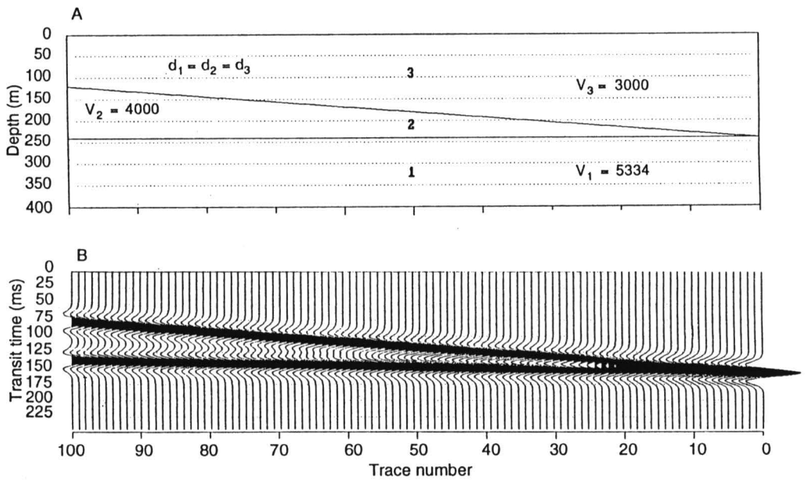

FIGURE 8—AMPLITUDE VARIATIONS CAN OCCUR AS A RESULT OF CONSTRUCTIVE INTERFERENCE OR "TUNING." On the synthetic seismogram, the reflections from horizons 3/2 and 2/1 are seen to visually merge as layer 2 pinches out from left to right. At trace 100 (one wavelength separation on geologic section), these events are distinct; from trace 99 to 50 (approximately one-half wavelength separation), the troughs which trail and precede the dominant peaks of the zero-phase Ricker wavelets increasingly constructively interfere. Thereafter, until the vicinity of trace 25, these same troughs destructively interfere with the dominant peaks to an increasing degree; the width of the wavelets appears to decrease and the apex of the upper and lower peaks (interpreted as the "arrival" time of the events) appears to be deflected upwards and downwards, respectively. Between traces 25 and 1, the dominant peaks begin to visually merge from a wide "doublet" into a single high-amplitude peak.

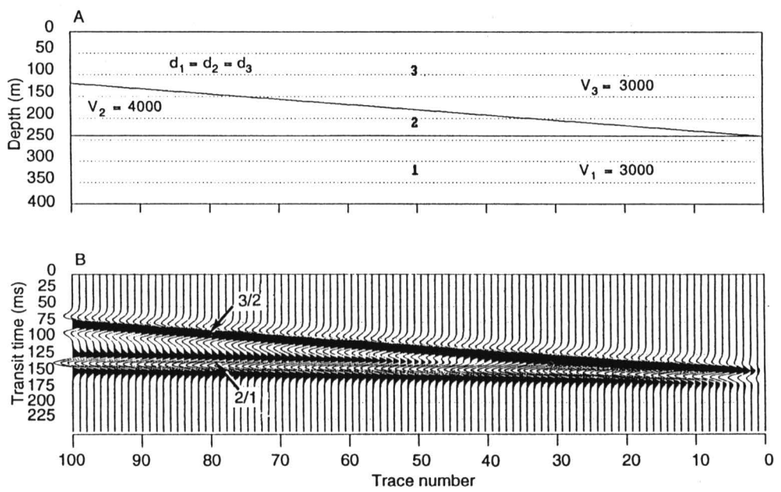

FIGURE 9—AMPLITUDE VARIATIONS CAN OCCUR AS A RESULT OF DESTRUCTIVE INTERFERENCE. On the synthetic seismogram, the equal amplitude and opposite polarity events 3/2 and 2/1 visually merge from left to right. At trace 1, these reflections superpose and cancel, yielding a null trace.

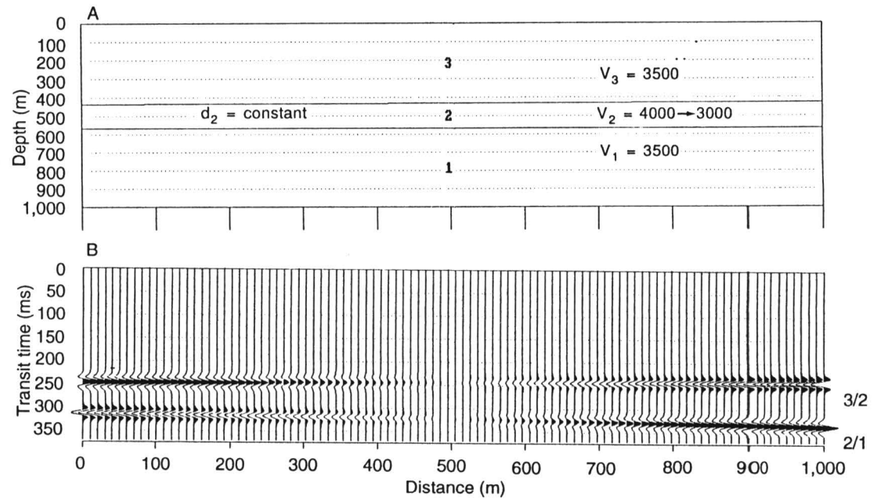

FIGURE 10—AMPLITUDE VARIATIONS ALONG A SPECIFIC REFLECTION CAN OCCUR AS A RESULT OF LATERAL CHANGES IN ACOUSTIC IMPEDANCE CONTRAST. In the model, the amplitudes and polarities of events 2/3 and 1/2 change from left to right as a result of a change in the seismic velocity of layer 2.

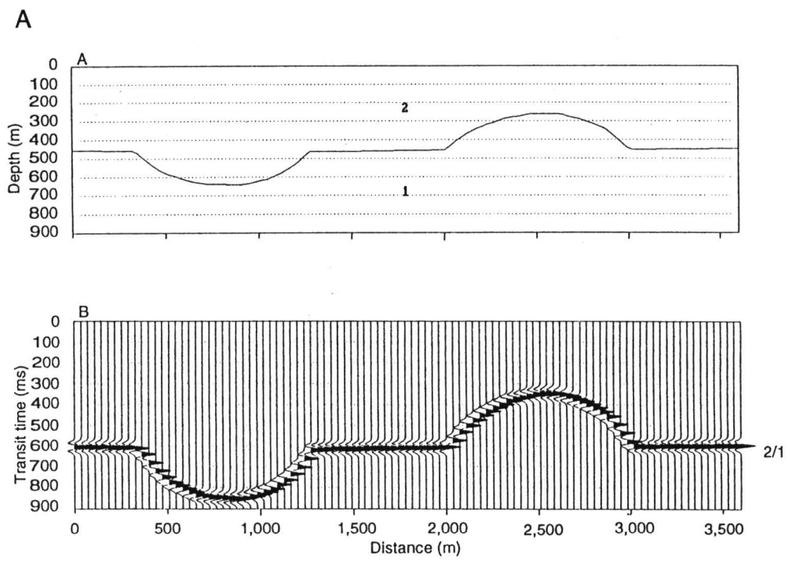

FIGURE 11A—GEOLOGIC SECTION AND CORRESPONDING VERTICAL INCIDENCE SYNTHETIC SEISMOGRAM (analogous to ideally migrated seismic data). Dipping surfaces are accurately located in time and space on this synthetic seismogram.

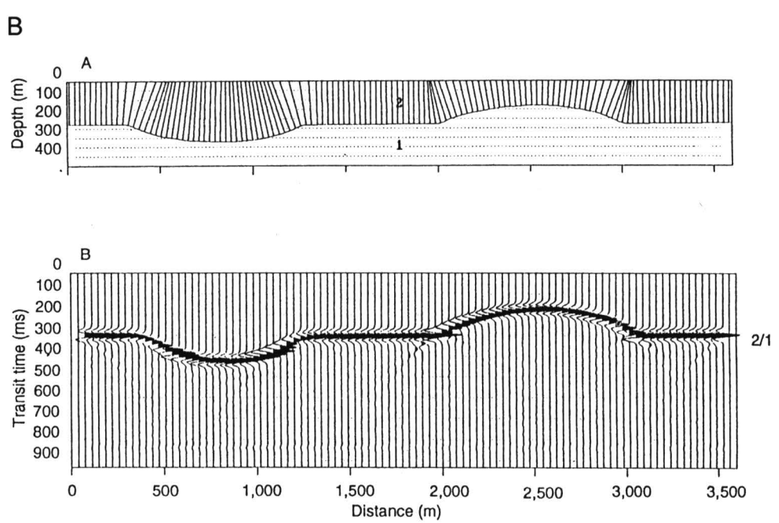

FIGURE 11B—GEOLOGIC SECTION AND CORRESPONDING DIFFRACTION SYNTHETIC SEISMOGRAM (analogous to non-migrated seismic data). Dipping surfaces are shifted in time and space; anticlinal structures are broadened and synclinal features are collapsed. Diffractions originating from discontinuities within the geologic section are superposed on the reflections. Note in this model the focal point of the syncline (as illustrated by the raypaths) is above ground level.

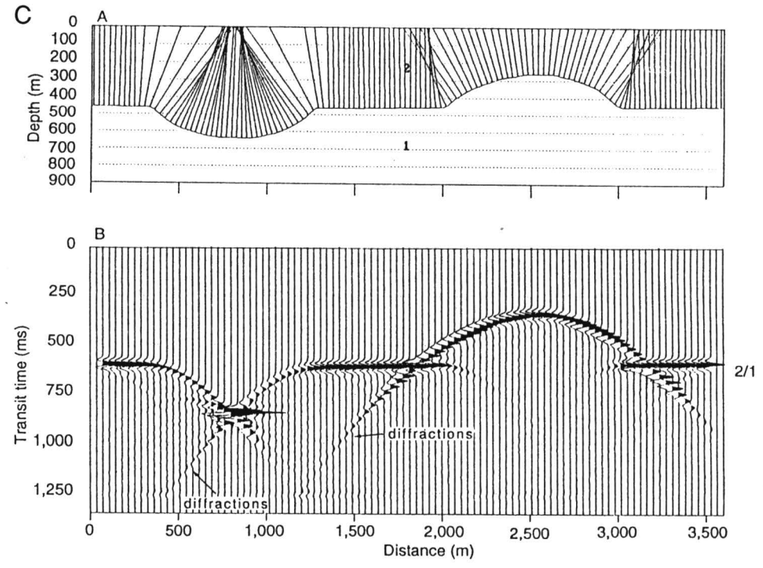

FIGURE 11C—IN THIS MODEL THE FOCAL POINT OF THE SYNCLINE IS NEAR GROUND LEVEL AT RECEIVER 75. As a result of focusing, the amplitude of the reflection on trace 75 is magnified. Diffractions originating from discontinuities within the geologic section are superposed on the reflections.

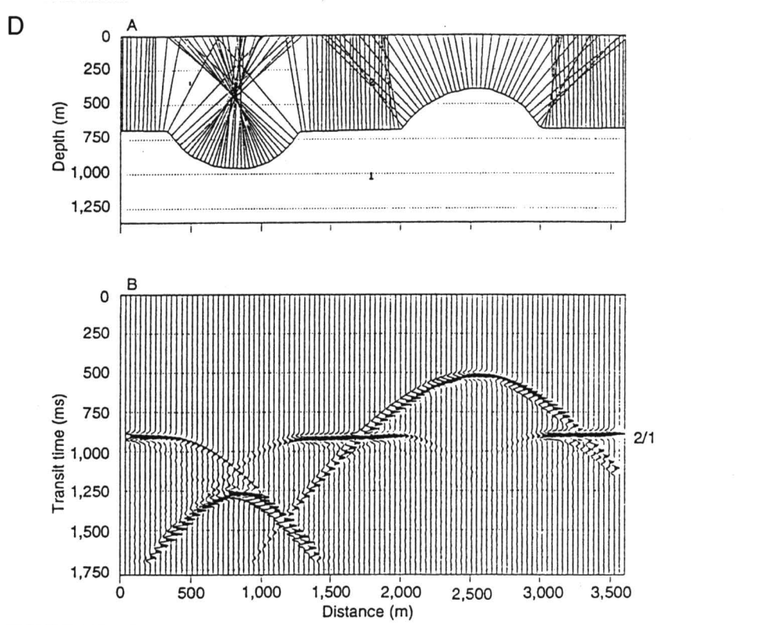

FIGURE 11D—IN THIS MODEL THE FOCAL POINT OF THE SYNCLINE IS SITUATED BELOW GROUND LEVEL. In this situation, the superposed reflections from the syncline and the diffractions emanating from the associated edge discontinuities are manifested as a classic "bow-tie."

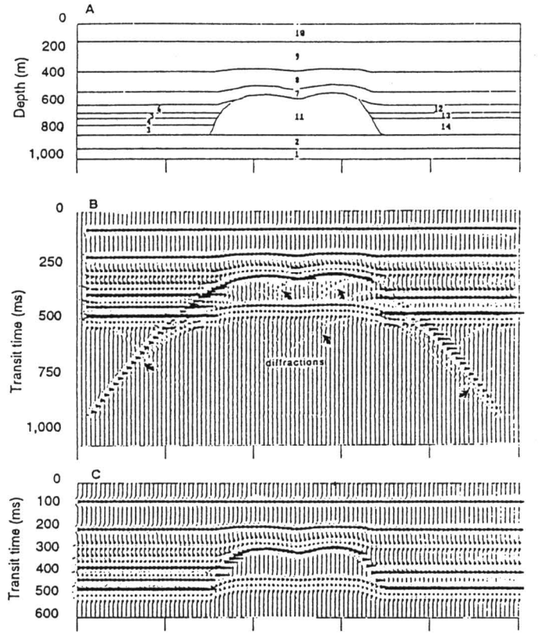

FIGURE 12A–E—GEOLOGIC MODEL AND CORRESPONDING SUITE OF SYNTHETIC SEISMOGRAMS. In **B**, a diffraction synthetic seismogram is shown. The diffractions originate from discontinuities associated with the surface of the reef and are considered to be part of the seismic image of the reef. In **C**, a vertical incidence synthetic seismogram is depicted. Note how definitively the seismic image of the reef can be differentiated from that of the laterally adjacent strata. In **D** and **E**, random noise has been superimposed on the vertical incidence synthetic seismogram. Noise (everything other than desired signal) is not considered to be part of the seismic signature. Frequency filtering, stacking, geophone arrays, and processing techniques are used to increase the signal-to-noise ratio. These two-dimensional synthetic seismograms are often generated in order to elucidate the utility of seismic technique with respect to exploration for an envisioned geologic target.

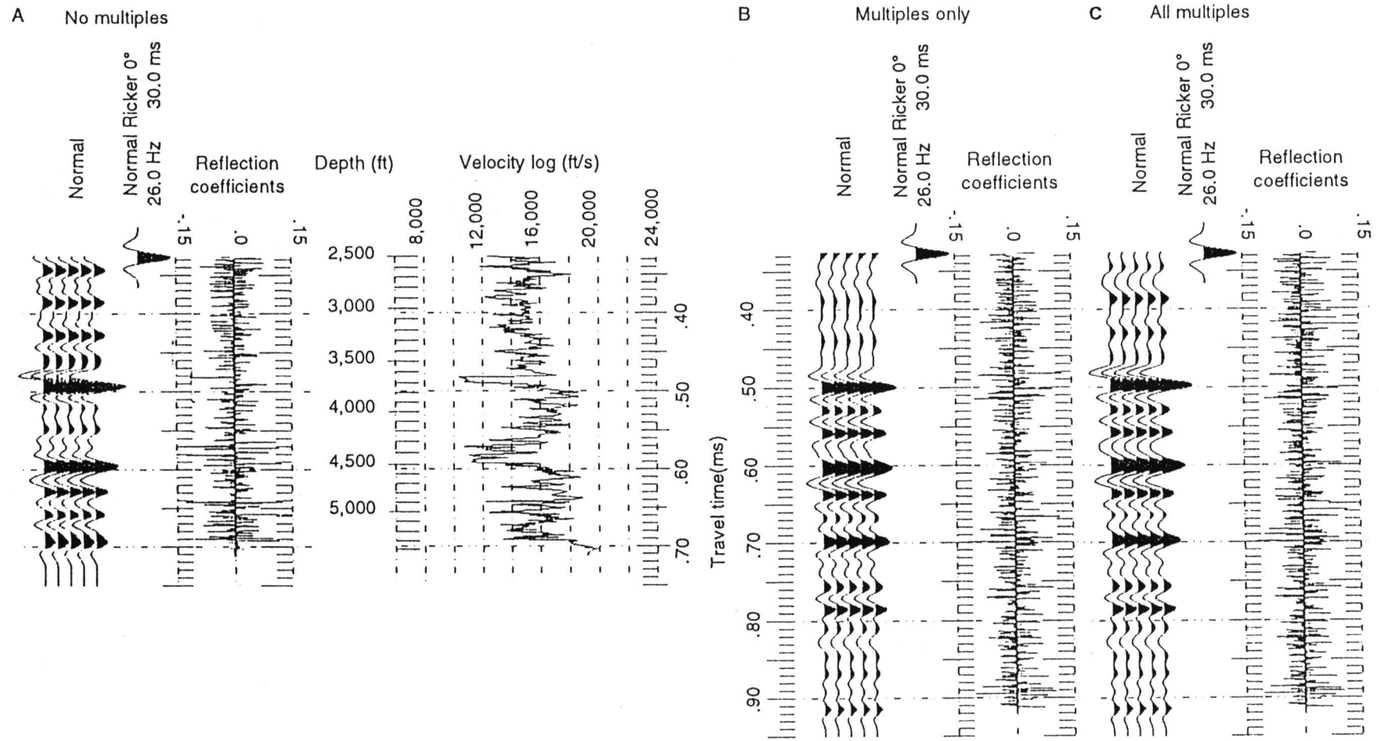

FIGURE 13A–C (right)—ONE DIMENSIONAL VELOCITY/DEPTH LOG (sec. 2, T. 30 S., R. 24 W. well) and corresponding suite of vertical incidence synthetic seismograms: **A**–primary reflections only, **B**–primary reflections and all multiples, and **C**–multiples only. Multiples can mask the seismic signature of a geologic target; they are generally considered to be noise. CDP stacking and processing techniques are used to reduce the relative amplitudes of multiple events.

Amplitude Variation with Offset

Ralph W. Knapp[1], Dennis E. Hedke[2], and Neil L. Anderson[3]
[1]formerly with Kansas Geological Survey, The University of Kansas, Lawrence, KS 66047; [2]Consultant, Wichita, KS 67202; and
[3]Department of Geology and Geophysics, University of Missouri–Rolla, Rolla, MO 65401

Abstract

Subsurface variation in the ratio compressional of *P*-wave velocity to shear (*S*-) wave velocity, V_p/V_s, yields an opportunity to observe amplitude variation with offset (AVO) effects. Ideally, such variations can be inverted to indicate lithology, porosity, constituent fluids, and/or presence of free gas. In practice, AVO techniques are somewhat limited by factors such as noisy data and actual subsurface materials.

One geological situation to which AVO techniques are ideally suited is the delineation of free gas-bearing sandstones. The dramatic decrease of V_p, relative to sandstone without gas, and the negligible change in V_s results in very large changes in V_p/V_s, i.e., Poisson's ratio. The AVO response is heavily dependent on that one parameter.

Data-quality control is critical with AVO measurements because many of the analyses are done with single trace common offset or CMP gathers, and measured amplitude response is very sensitive to noise. Data acquisition must include a large range of offsets, i.e., angles of incidence, ideally from 0 to 40°. A general rule of thumb is that far offsets need to be about 1.6 times the depth of the zone of interest. Recording of at least two components (vertical and radial) is desirable to rigorously derive true amplitude response of a *P*-wave reflection; however, the advantage of using a second component may not be truly cost-effective. Measured amplitude can be extremely accurate when corrected from offset information to an estimated true amplitude. Processing must maintain relative amplitude response of a reflection. This consideration affects and limits the use of AGC gain, deconvolution, and other space (trace) or time-adaptive processes. The display of AVO can be in the form of unstacked common offset gathers or CMP (CDP) gathers of instantaneous amplitude. Instantaneous amplitude compensates for phase-response differences on the peak amplitude of the reflection wavelet.

Introduction

Individual traces on conventional, common midpoint (CMP)-stacked (equivalently, common depth point (CDP)-stacked) seismic data are assumed to be representative of zero-offset (normal incidence) reflections. For deep targets (depth ≥ far offset), the assumption is fairly accurate. Consequently, common analysis is frequently based on normal-incidence modeling, which is relatively straight-forward because zero-offset rays do not have mode conversion. A vertically incident *P*-wave generates only a reflected *P*-wave and a transmitted *P*-wave. The amplitude of the reflected wave depends on the reflection coefficient, and the amplitude of the transmitted wave depends on the transmission coefficient. The signs of the coefficients indicate polarity of the resultant modes, relative to the incident wave:

$$\text{Reflection coefficient} = (Z_{i+1} - Z_i)/(Z_{i+1} + Z_i) = (1 - Z_i/Z_{i+1})/(1 + Z_i/Z_{i+1})$$

$$\text{Transmission coefficient} = 1 - R^2 = 4(Z_iZ_{i+1})/(Z_i + Z_{i+1})^2 = 4(Z_i/Z_{i+1})/(1 + Z_i/Z_{i+1})^2, \quad (1)$$

where subscripts indicate the layer number from the surface, Z is acoustic impedance, the product of rock density, ρ ,and rock velocity, V:

$$Z = \rho V. \quad (2)$$

AVO techniques exploit the fact that the seismic amplitude response of a reflection (energy) is a function of its angle of incidence. Non-zero offset rays have mode conversion which splits the incident energy; a *P*-wave incident on an interface generates the following:

- reflected *P*-wave
- reflected *S*-wave,
- transmitted *P*-wave
- transmitted *S*-wave (fig. 1).

Mode conversion is a fact of the physics of continuous media that require conservation of energy and momentum, i.e., continuity of stress and strain, or continuity of vertical and tangential displacement, across the interface. A *P*-wave that reaches the interface at a non-zero incident angle has components at right angles to the direction of hypothetical transmission and reflection *S*-waves that set up the generation of shear (*S*-) wave energy in these directions. It also has components parallel to hypothetical transmitted and reflected *P*-waves that set up the generation of compressional (*P*-) wave energy in these directions. Thus, with offset (incident angle), varying amounts of *P*-wave energy are lost to the generation of *S*-waves and the splitting of *P*-wave energy into reflected and transmitted components.

The amplitude of a reflected *P*-wave varies with offset according to the reflection coefficient, which is dependent on acoustic-impedance contrast (ratio of the products of velocity and density), and Snell's Law, which is dependent on velocity contrast (velocity ratio).

Velocity, Density, and Elastic Parameters of Rocks

In general, the product of velocity and density (acoustic impedance) is diagnostic of rock type; however, porosity complicates this value. One rock type at a particular porosity may have the same acoustic impedance as another rock type with different porosity.

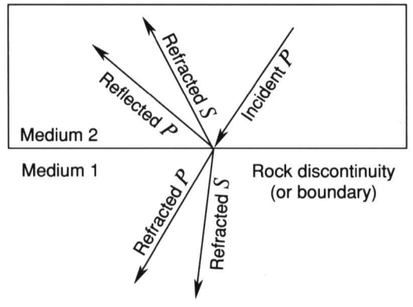

FIGURE 1—MODE CONVERSION BY INCIDENT *P*-WAVE.

Seismic velocities depend on the square root of a modulus divided by density:

P-wave velocity is related to the modulus of confined extension, *m*:

$$V_p = [m/\rho]^{1/2} \quad (3A)$$

S-wave velocity is related to only the shear modulus μ, and density ρ:

$$V_s = [\mu/\rho]^{1/2}. \quad (3B)$$

The modulus of confined extension, *m*, is similar in concept to Young's modulus *E*, the modulus of unconfined extension. Both describe extension of a body due to tensile strain. In an unconfined body, lateral constriction is permitted. In a confined body, it is not.

Confined extension is related to unconfined extension *E* by Poisson's ratio σ:

$$m = E\,(1 - \sigma)/[(1 - 2\sigma)(1 + \sigma)] \quad (4A)$$

$$= E\,(1.025 + 2\sigma 2) + 2\% \quad (4B)$$

Confined extension differs from unconfined extension by 10 to 40% (σ = 0.20–0.40, respectively). As materials get more rigid, relative to compressibility, i.e., lower values of σ, confined extension and unconfined extension become closer in value. (For σ = 0, the two are equal.)

One of the more common equations for *m* is:

$$m = k + 4/3m. \quad (5)$$

Thus,

$$V_p/V_s = [k/m + 4/3]^{1/2}. \quad (6)$$

where k is the bulk modulus.

Further, Poisson's ratio relates directly to V_p/V_s through the equation

$$\sigma = .5 - (V_s/V_p)^2/1 - (V_s/V_p)^2 \quad (7)$$

Poisson's ratio σ comes into play because it is dependent on the ratio V_p/V_s and, like density ρ, is relatively stable at depth under most circumstances. The two vary only slightly with rock type; in general, for sedimentary rocks, $0.3 < \sigma > 0.4$ ($\sigma \sim 0.35$) and $2.2 < \rho > 2.7$ ($\rho \sim 2.5$). Knowing or estimating constant values of σ and ρ, the first-order solution of the Zoeppritz (1919) equations is dependent only on the velocity ratio across the interface.

However, considering higher-order solutions of the Zoeppritz equations, AVO responses are theoretically sensitive to rock type. This is because the ratio of *P*-wave velocity to *S*-wave velocity, V_p/V_s, and σ are sensitive to lithology (fig. 2).

V_p/V_s measures the ratio of bulk modulus (incompressibility) to shear modulus. This can be a very subtle measurement and therefore difficult to derive by AVO methods. On the other hand, presence of gas in a reservoir causes a sufficiently dramatic contrast in the value of σ_i/σ_{i+1} that it may be practical to detect gas directly from AVO measurements. The presence of gas in a sandstone dramatically affects V_p but affects V_s only negligibly. Values of σ may change from between 0.3 and 0.4 in the overlying rock to about 0.1 in the gas sand. The ratio σ_1:σ_2 may be as great as 3:1 or 4:1. In general, in

the absence of gas, amplitude decreases very slightly with offset; however, in the presence of gas, the strong contrast in Poisson's ratio can cause amplitude to increase by more than 50% as angle of incidence increases from 0° to 30° or 40° (Ostrander, 1984). It is a radical change such as this that makes the use of AVO a viable diagnostic tool to determine the presence of gas. Figure 3 is a cross plot of V_p/V_s and ρ.

Knapp (1977) determined Poisson's ratio values of near **0.45** (V_p/V_s = 3.32, k/m = 10) for very shallow consolidated carbonates, about **0.4** (V_p/V_s = 2.5, k/m = 5) for the deeper portions of the shallow cyclothemic carbonate-shale section of southern Indiana, and **0.33** (V_p/V_s = 2.0, k/m = 2.67) for the Cambrian–Ordovician Simpson Sandstone. The values are consistent with the interval transit time ratio t_s/t_p seen on *P*-wave and *S*-wave reflection seismograms (Tatham, 1992).

King (1966), measuring sandstones at 5,000 psi pressure [equivalent to 3,000 m (9,999 ft) depth] and porosity varying from 19 to 25%, determined values of V_p/V_s [*s*] from 1.65 [**0.32**] to 1.77 [**0.36**] when filled with a salt solution (median value 1.71 [**0.35**]); 1.55 [**0.27**] to 1.69 [**0.34**] with kerosene in the pores (median value 1.6 [**0.30**], and bimodal values of 1.51 [**0.23**] and 1.58 [**0.29**] when dry (1.55 [**0.27**] average).

A

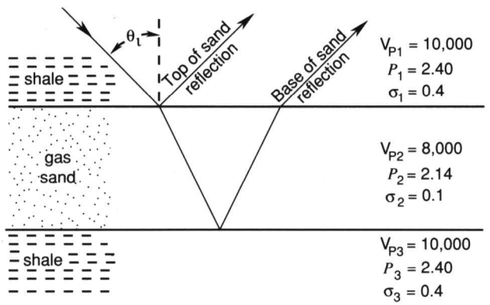

B

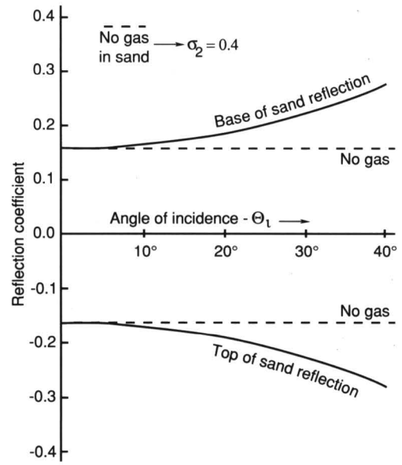

FIGURE 2—(A) SYNTHETIC GAS SAND MODEL. (B) COMPUTED APPARENT REFLECTION COEFFICIENT AS A FUNCTION OF OFFSET ANGLE (Ostrander, 1984).

Poisson's ratio values for the Green River Shale have been determined to vary between **0.22** and **0.30** (Podio et al., 1968). Hamilton (1976) measured Poisson's ratios of **0.45** to **0.50** for shallow marine sediments, with values decreasing with depth [600 m (2,000 ft) maximum depth]. For consolidated sediments, Gregory (1976) determined Poisson's ratio values of **0.20** to **0.30** when brine saturated and **0.20** to **0.14** when gas saturated. Domenico (1976 and 1977) determined values of about **0.40** for both unconsolidated sands and glass beads (38% porosity) when brine saturated and **0.10** when gas saturated.

Angle of Incidence

Angle of incidence q_i can be estimated from source-receiver offset X and reflector depth H using a simple straight ray-path assumption:

$$q_i = \tan^{-1}(X/2H). \tag{8}$$

This assumes that velocity does not substantially change with depth. Using Equation 5, the maximum angle of incidence is 26.6° when using the rule of thumb that maximum offset be equal to target depth. If velocity increases with depth, which generally is the case, angle of incidence will be under-estimated by source-receiver offset (Ostrander, 1984).

$V_p = (m/\rho)^{1/2}$ *P-wave*

$V_s = (\mu/\rho)^{1/2}$ *S-wave*

$$\sigma = .5 - (V_s/V_p)^2$$
$$1 - (V_s/V_p)^2$$

$$V_p/V_s = (1 - \sigma/0.5 - \sigma)^{1/2}$$

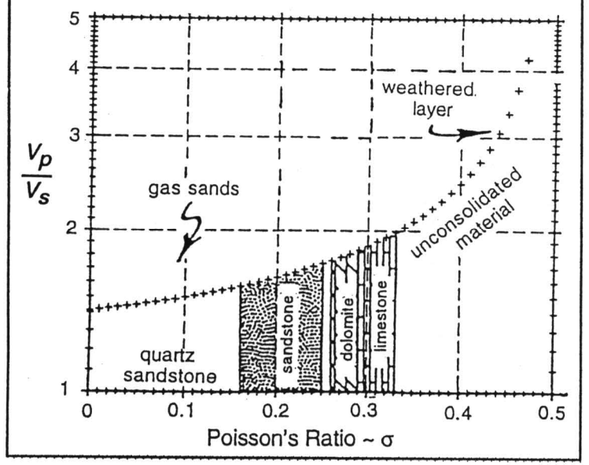

FIGURE 3—CROSS PLOT OF V_p/V_s AND ρ.

A better assumption is that velocity increases linearly with depth:

$$V_p = V_0 + \Delta V/\Delta H, \bullet H \tag{9}$$

where $\Delta V/\Delta H$, the rate of increase with depth, can be measured from sonic logs or estimated from stacking velocity. The equation for angle of incidence q_i versus offset X is:

$$q_i = \tan^{-1}\{(HX + V_0 X/k)/(H^2 + 2V_0 H/k - X^2/4)\}, \tag{10}$$
where $k = \Delta V/\Delta H$.

Using the example of Ostrander (1984), V_p = 1800 + 0.6 H m/sec, the angle of incidence is 34° when $H = X$ = 2,100 m (6,889 ft), Vp = 3,060m/sec at H = 2,100 m (6,889 ft).

The Range of AVO Effects in Gas Sands

Rutherford and Williams (1989) developed a useful working classification of gas sands which distinguishes on the basis of encasing materials and hence reflection coefficients which will be generated at various offsets (incident angle). Figure 4 summarizes sands as follows:

Class 1—High-impedance sands
Class 2—Nearly equivalent impedance sands
Class 3—Low-impedance sands

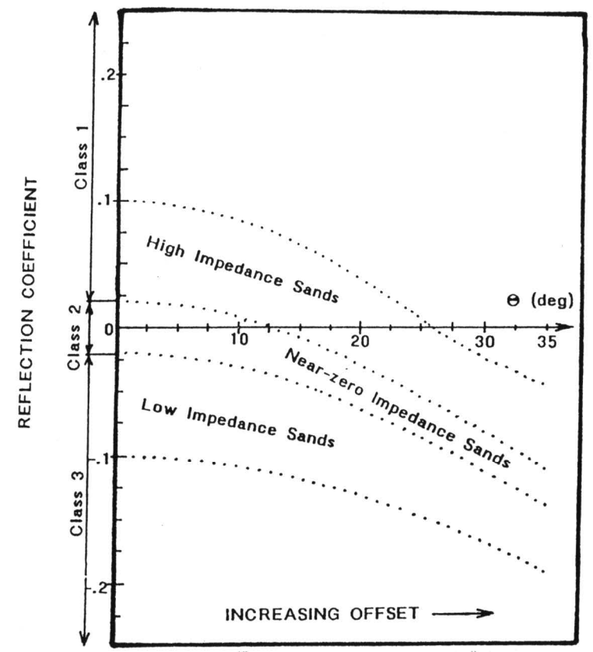

FIGURE 4—CLASSIFICATION OF GAS SANDS, BASED ON REFLECTION COEFFICIENT VARIATION WITH OFFSET (angle of incidence) as proposed by Rutherford and Williams, 1989. Midcontinent sands (Cherokee, Morrow) will tend to be Class 1, where phase reversal occurs at longer offsets.

In the example cited, Poisson's ratio and density for the gas sand were 0.15 and 2.0 g/cm^3, respectively; those for the shale were 0.38 and 2.4 g/cm^3. Note that in this case, Class 1 sands have a positive reflection coefficient (amplitude) until offset angle exceeds 25°. Class 2 sands can have positive amplitudes out to about 12°, but generally have negative coefficients; Class 3 sands have clearly negative amplitudes throughout.

Data Acquisition Considerations

Many acquisition-design considerations for AVO and conventional CMP reflection data are similar. One main difference is that AVO data are considered best when recorded by at least two components (vertical and radial), so that true amplitude of the reflection can be determined. However, true amplitude can be estimated from a single vertical component by using angle of incidence:

$$A_{est} = A_{meas}/\cos q_i. \qquad (11)$$

The accuracy of the estimate depends on the accuracy of q_i. The measurement of q_i is very insensitive to errors in the estimate of V_0 and fairly insensitive to errors in $\Delta V/\Delta H$. With 10% uncertainties in the estimates of V_0 and $\Delta V/\Delta H$, errors are generally within ±2%. With such low sensitivity, increased accuracy achieved by using a radial component, if indeed there is any increase, is probably not worth the increased cost of acquiring and processing a second component of data.

Another primary difference is that all possible care must be taken to minimize noise so that AVO analysis can be done with single, unstacked traces and a minimum of enhancement processing. It is also more important that maximum offset be large so that reflections with large angles of incidence are recorded. Minimum offset should be as small as possible, yet large enough to avoid adverse interference from the source. Surface sampling should always be designed such that equal sampling of both the surface and the subsurface is maintained by the geophones for all gathers of the data: common source (field recorder order), common receiver, common offset, and common midpoint (CMP).

The best configuration geometry is split-spread, half-integer offset (shooting between the gaps) (Knapp, 1985) with shots at every interval. Geophone and source arrays should be linear, equally weighted, and equal in length to the group interval. Alternatively, when using a point source, the receiver array can be linearly tapered and equal in length to twice the group interval (see Knapp, 1992). These configurations automatically satisfy sampling requirements. Other configurations, split-spread integer offset (shooting on gaps) and end-on, also require such array design; however, to have the subsurface evenly sampled in a CMP gather requires two-trace mixing of the data during processing (i.e., stack array processing, Morse and Hildebrandt, 1989).

Array length is designed to be as long as possible without adversely affecting high-frequency response at far offsets. This means that array length for a linear, equally weighted array should be less than V/f_{max}. Linearly tapered arrays are the auto-convolution of a linear, equally weighted array, the response when both source and geophones have the same linear array design. The length of a tapered array should be equal to two times that of the linear array. Array length is not deliberately designed to attenuate ground roll noise, although attenuation of high-frequency ground roll is a consequence of array application. Low-frequency ground roll noise is attenuated by use of low-cut frequency filtering. Group interval is designed to be equal to array length, or, if a sufficient number of channels is available, equal to $1/n\times$ the array length, where n is an integer.

Processing, Modeling, Display, and Analysis

Processing must be designed to maintain relative amplitude response laterally or, more exactly, down the normal moveout curves. Although this does not preclude the use of automatic gain control (AGC), the same function must be applied such that the gain applied to particular reflections is the same at all offsets. Use of deconvolution and other space or time adaptive processes have similar restrictions.

Data smoothing can help improve the accuracy of the measurement, but when overdone, it will change and smear the values. Such smoothing includes high-cut frequency filtering, trace-to-trace mixing of data in the CMP gather, record-to-record mixing of CMP gathers, and frequency-wave number filtering, a combination of all of the above. Judicious use of filtering may help reduce noise interference, but use of adaptive filters must maintain true relative amplitude response. Lateral mixing and wave number filtering of CMP records or common offset traces smear data spatially. This smearing must be very small with respect to lateral resolution. Lateral resolution can be estimated as the product of the vertical wavelet length in time and interval velocity of the target. Note that, contrary to common thought, lateral resolution is not related to Fresnel zone size (Knapp, 1991; Knapp, 1993). Mixing of CMP traces or common offset records smooths noise out of the measurement but must be small compared to the second derivative of AVO. Normal moveout correction is not done to avoid dispersion of the reflection by NMO stretch. Lateral alignment of a reflection is accomplished by a static shift.

An AVO display should be of instantaneous amplitude (square root of instantaneous energy) so that trace-to-trace phase differences within the wavelets does not influence measurement (Knapp, 1993). Polarity is determined from standard wiggle trace data, using CMP stacked data. Common offset (common incidence angle) displays are commonly most useful to make measurements. The alternative is to display unstacked CMP gathers.

Modeling and Data Example

Midcontinent Morrow Sandstones

While AVO responses can occur in a wide variety of rock types, current trends in application and research tend to be weighted toward sandstone reservoirs. This trend may evolve to include a greater emphasis on carbonate reservoirs, but the evidence presented here will be isolated to sandstones.

Figure 5, modified from Peddy et al. (1995), demonstrates how quick-look models can be generated to test anticipated AVO response from a Morrow sequence at a depth of about 8,300 ft. Utilizing sonic and density log control and applying an estimate for shear (S-) wave velocity, which then yields a Poisson ratio curve, synthetic offset

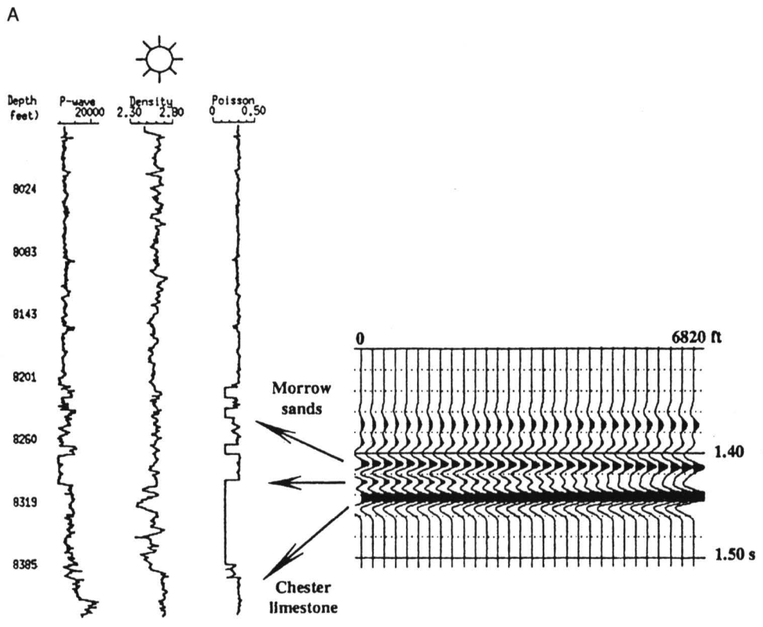

FIGURE 5A—Offset synthetic seismogram (CMP gather) demonstrating amplitude variation of gas sand at T = 1.430 sec. Note that P-wave velocity of Morrow sands is higher than overlying Morrow shale, while densities are nearly the same. Poisson's ratio of gas sand set at 0.15 for shale and Chester limestone ratio is set at about 0.35. Class 1 sand, based on Rutherford, 1989. Note offset range is 0–6,820 ft (2,046 m); sand depth is approximately 8,300 ft (2,490 m). Amplitude response of gas sand goes through complete phase reversal. (Modified from Peddy et al., 1995.)

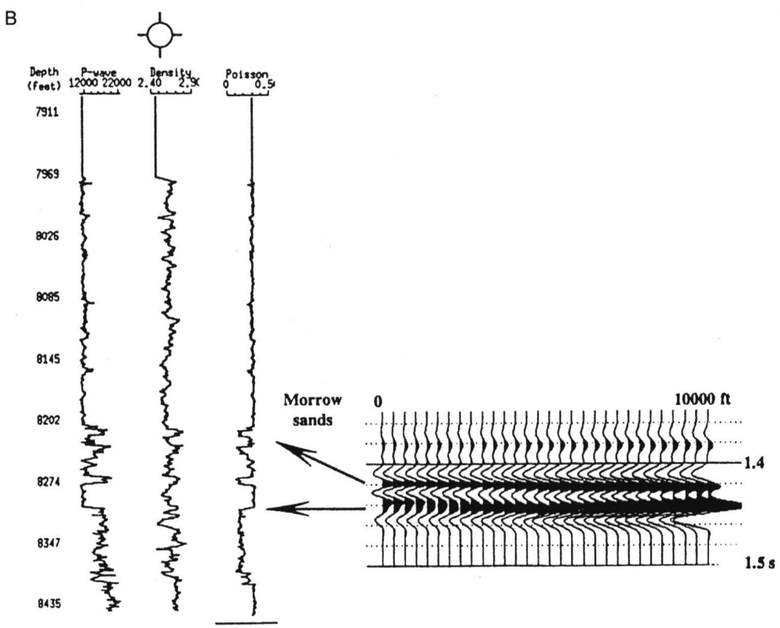

5B—Wet sand parameters substituted for gas sand in adjacent figure. Three thin sands interfere to produce a peak with an unchanging-to-slightly increasing AVO response at t = 1.430 sec. Chester limestone response is not included in this display. Note offset range is 0–10,000 ft (0-3,000 m). (Modified from Peddy et al., 1995.)

seismograms have been generated using a filter representative of their data. The two comparison models relate two changing phenomena. The offset seismogram on the left represents response from a gas sand, occurring at a time of 1.430 sec; the seismogram on the right represents a similar sequence, but with wet brine sand in place of gas sand. Note also that the wet sand model also reaches longer offsets, 10,000 ft as opposed to 6,820 ft for the gas sand.

The theoretical AVO response in the gas sand synthetic is evident as a peak amplitude event at 1.430 sec, which eventually diminishes and finally reverses polarity at an offset of about 5,000 ft. In contrast, the wet sand never generates a truly discernible event which would likely be AVO anomalous.

The real data example in fig. 6 demonstrates in significant detail that the theoretical response is well represented in the Morrow sand zone at about 1.430 sec. The panels shown here have been extracted from the processed data volume in a variety of offset ranges; each panel represents a set of trace gathers in close proximity to the known gas sand. This is a clear-cut case of a Class 1 sand.

Figure 7 demonstrates a very strong AVO response in a stacked section. In this case the gas sand has a much lower amplitude than the wet sand, a sample of Woodbine sand from east Texas. This is also a Class 1 sand, but note that the stacked response demonstrates amplitude dimming in the gas sand.

Recent research (Ross, 1995) now shows that Class 2 sands , i.e., sands with a 'nonbright-spot' or near-zero acoustic impedance can be further subdivided into those with phase reversals and those without. The reader is referred to this paper for an excellent discussion and case history with Gulf Coast examples.

Discussion and Summary

Consolidated sedimentary rocks generally vary in s from about 0.20 ($V_p/V_s = 1.66$, $k/m = 1.42$) to about 0.4 ($V_p/V_s = 2.5$). In general, Poisson's ratio, V_p/V_s and k/m decrease with depth, ostensibly because m increases faster than k with confining pressure. Carbonates have larger values of these parameters than shales, which have larger values than sandstones. Carbonates have the highest value of V_p and sandstones may have slightly greater values of V_p than shales, but are relatively close in value; the difference depends more on density differences than on bulk modulus differences. V_s is slightly larger for sandstone than carbonate; the difference is due more to density differences rather than to shear-strength differences. V_s is much smaller for shale, and differences are due to both shear-strength and density differences. Carbonates are relatively incompressible; shales are relatively compressible but also have relatively low shear strength; sandstones are relatively compressible but have shear strength similar to that of carbonates.

The determination of Poisson's ratio or V_p/V_s can be used to identify lithology, porosity, and/or presence of free gas.

The presence of free gas dramatically decreases V_p but affects V_s only negligibly, resulting in very small values of V_p/V_s and Poisson's ratio. It may decrease Poisson's ratio by a factor of 3 or 4 and V_p/V_s by a factor of 1.15 to 1.5. AVO increases as great as 50% from 0° to 40° of incidence angle are indicative of such large Poisson's ratio changes.

The ability to use AVO depends greatly on data quality, processing, processing integrity, and data display. All the steps must be designed to minimize noise and maintain the integrity of the AVO measurement.

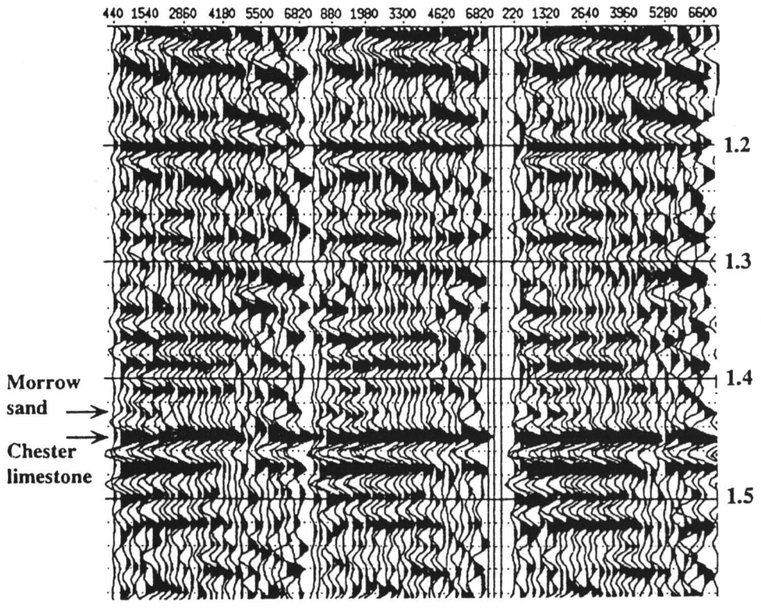

FIGURE 6—ACTUAL DATA VERIFYING PREDICTED MODEL RESPONSE FOR GAS SAND AT 1.430 SEC. The reflection from the Morrow sand diminishes rapidly with increasing offset. Panels taken represent nearby CMP gathers. In each case, offset increases to the right. (Modified from Peddy et al., 1995.)

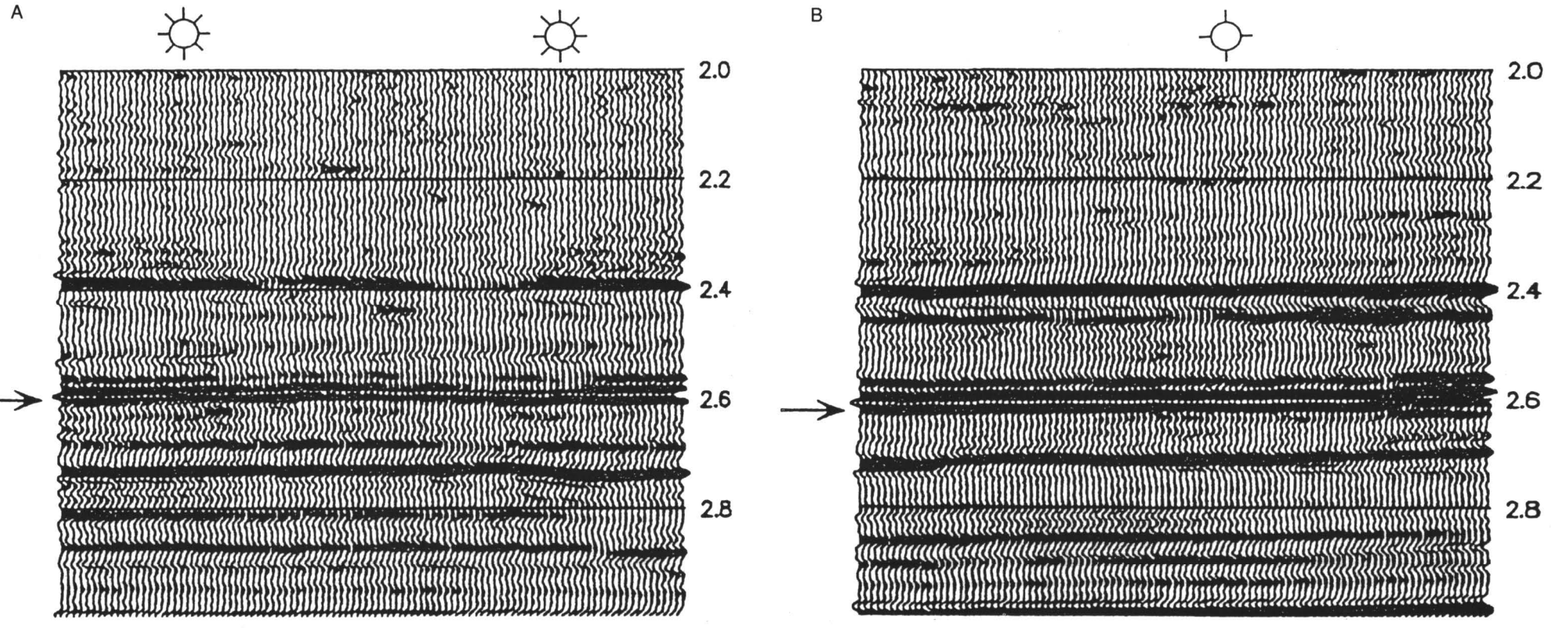

FIGURE 7—STACKED PROFILES DEMONSTRATING VARIATION IN AMPLITUDE RESPONSE BETWEEN THAT OBSERVED NEAR GAS WELLS AND THAT OF A DRY HOLE. (A) Stacked section containing gas wells; arrow indicates zone of interest, peak amplitude at 2.6 sec.

(B) Stacked section containing wet sand; amplitudes in the wet sand case are much higher than those for the gas sand. (Modified from Peddy et al., 1995.)

References

Domenico, S. N., 1976, Effect of brine-gas mixture on velocity in an unconsolidated sand: Geophysics, v. 41, no. 5, p. 882–894

_____, 1977, Elastic properties of unconsolidated sand: Geophysics, v. 42, no. 7, p. 1,339–1,368

Hermann, R. B., 1969, The structure of the Cincinnati arch as determined by short period Rayleigh waves: Bulletin of the Seismological Society of America, v. 59, p. 399–407

Knapp, R. W., 1977, Ellipticity of 0.4 to 2.4 Hertz Rayleigh waves with application to the study of near-surface structure: Ph.D. dissertation, Indiana University, 200 p.

_____, 1985, Use of half-integer offset with split-spread CDP seismic data: The Leading Edge, v. 5, no. 1, 13 p.

_____, 1991, Fresnel zone in the light of broad band data: Geophysics, v. 56, no. 3, p. 354–359

_____, 1992, The size of a reflection point: Canadian Society of Exploration Geophysicists, Calgary, May 5–8, p. 95

_____, 1993, Energy distribution in wavelets and implications on resolving power: Geophysics, v. 57, no. 1, p. 39–46

Koefoed, O., 1962, Reflection and transmission coefficients for plane waves: Geophysical Prospecting, v. 10, no. 3, p. 304–351

Morse, P. F., and Hildebrandt, G. F., 1989, Ground roll suppression by stack array: Geophysics, v. 54, no 3, p. 290

Muskat, M., and Meres, M. W., 1940, Reflection and transmission coefficients for plane waves in elastic media: Geophysics, v. 5, no. 2, p. 115–148

Ostrander, W. J., 1984, Plane wave reflection coefficients for gas sands: Geophysics, v. 49, no. 10, p. 1,637–1,641

Peddy, C. P., Sengupta, M. K., and Fashacht, T. L., 1995, AVO analysis in high-impedance sandstone reservoirs: The Leading Edge, v. 14, no. 8, p. 871–877

Podio, A. L., Gregory, A. R., and Gray, K. E., 1968, Dynamic properties of dry and water-saturated Green River Shale under stress: Society of Petroleum Engineers Journal, v. 8, no. 4, p. 389–404

Ross, C. P., and Kinman, D. L.,1995, Nonbright-spot AVO—two examples: Geophysics, v. 60, no. 5, p. 1,398–1,408

Rutherford, S. R., and Williams, R. H., 1989, Amplitude-versus-offset variations in gas sands: Geophysics, v. 54, no. 6, p. 680–688

Sheriff, R. E., 1991, Encyclopedic dictionary of exploration geophysics: Society of Exploration Geophysicists, Tulsa, 376 p.

Tatham, R. E., 1975, Surface wave dispersion applied to the detection of sedimentary basins: Geophysics, v. 40, no. 1, p. 40–55

_____, 1992, Current status of multicomponent seismic methods: Canadian Society of Exploration Geophysicists, Calgary, May 5–8, p. 54

Zoeppritz, K., 1919, Uber reflexion und durchgang seismischer wellen durch Unstetigkerlsflaschen: Berlin, Uber Erdbebenwellen VII B, Nachrichten der Konglichen Gesellschaft der Wissenschaften zu Gottingen, math–phys. K1, p. 57–84

Comparison of High-resolution and Conventional-resolution Seismic Data—Application to Cyclothems

Ralph W. Knapp[1] and Neil L. Anderson[2]
[1]formerly with Kansas Geological Survey, The University of Kansas, Lawrence, KS 66047; and
[2]Department of Geology and Geophysics, University of Missouri–Rolla, Rolla, MO 65401

Abstract

The interpreter who is used to conventional-resolution seismic data may be perplexed when confronted with high-resolution seismic data because conventional- and high-resolution data respond differently to the acoustic properties of the earth. For example, a high-amplitude, tuned, thin-bed reflection on a conventional seismic section may correspond to a low-amplitude, thick-bed event on a high-resolution section. Conversely, beds too thin to be effectively imaged by conventional data may be represented as high-amplitude, tuned reflections on high-resolution data. This may result in misidentification if the interpreter bases his stratigraphic correlations on amplitude response. Amplitude contrasts may also result from acoustic impedance gradients which generate high-amplitude reflections on conventional data but correspond to severely dimmed events on a high-resolution section. Lateral rugosity of the reflector surface and interference from adjacent thin layers can have a similar effect. As evidenced by models and seismic data incorporated into this paper, these factors result from the fact that conventional-resolution data and high-resolution data image different properties of the geologic strata.

Use of minimum-phase wavelets will cause time-correlation differences when data of different frequency content are compared and peaks or troughs rather than true wavelet onsets are picked. For this reason it is very important to ensure that data are processed to have zero-phase wavelets. Zero-phase wavelets also have the greatest resolving power; this is particularly important on high-resolution data. Because data of different frequency bands show different features of the earth, it may be advantageous in some situations to display each broad-band high-resolution section at a few different pass bands. Thus, features best imaged by conventional resolution are displayed and features best imaged by higher resolution are displayed.

Comparison of high-resolution data with conventional-resolution data and synthetic seismograms leads to inferences of vertical acoustic-impedance gradient and lateral surface rugosity. Vertical gradients on limestone surfaces, for example, may be related to porosity, and thus, recognition of their seismic signature may be an important interpretation tool.

Introduction

High-resolution seismic data contain higher frequencies than conventional seismic section data but are not necessarily broader in terms of octaves of frequency bandwidth. Typically, seismic data contain two or three octaves of data. As Knapp (1990) points out, resolution of seismic data that contain at least a couple of octaves of frequency bandwidth is dependent on the values of the highest frequencies of the data. The limiting of octave bandwidth is a function of the logistics of seismic-data acquisition, attenuation by the earth, and instrument dynamic range. When recording high-resolution data, it is difficult to record low frequencies, or it is generally not done. Because the size of arrays is limited, low-frequency noise such as ground roll is often attenuated using frequency filters. Low-cut filtering and gain amplification are jointly applied to bring high frequencies within the dynamic range of the recording instruments. If low frequencies saturate the instruments, high frequencies can not be recorded (Knapp and Steeples, 1986). Conventional seismic data use long arrays to remove ground roll but are unable to record high frequencies because long arrays attenuate high frequencies. Also, high-power sources used in conventional data recording characteristically generate relatively longer wavelength (i.e., lower frequency) data. Because attenuation reduces the amplitude of the high-frequency data relative to the low-frequency data such that it is below the dynamic range of the instruments, it is important that the amplitude of high frequencies be maximized relative to that of the low frequencies. Conventional seismic data are generally looking deeper into the earth so that attenuation of high frequencies is more severe.

Significant differences are noticed between high-resolution sections and conventional sections recorded over identical geologic strata. Distinctive reflections on a high-resolution section may be unnoticed on the low-resolution data because the beds are too thin for detection. This point is obvious because the objective of high-resolution is to image thin beds. Interestingly, however, prominent reflections on a conventional section may be severely muted on high-resolution data to the point where they may not be clearly identifiable. For instance, two limestones on a high-resolution section may have distinct reflection character differences, the thicker limestone being the one that is not well-imaged. There are several possible reasons for the differences. Most obvious is that on a seismic section, beds that correspond to tuning thickness will have the larger amplitude (Widess, 1973; Knapp, 1990). Tuning occurs when the thickness of the bed is approximately equal to one-fourth the apparent wavelength of the signal wavelet. Wavelength is equal to the interval velocity divided by the apparent frequency. Apparent frequency is the inverse of the time interval of one cycle (apparent period) of the wavelet. Tuning is constructive interference of the reflection from the base of a bed with the reflection from its top. Tuned thin beds on conventional data will be thick beds on high-frequency data. This will make a difference of perhaps a factor of two on the relative amplitude responses. But this factor does not account for all that is observed; there are two other possibilities.

High-resolution data, because they contain shorter wavelengths than conventional-resolution data, are more sensitive to vertical acoustic-impedance gradient and diffusive lateral rugosity of the reflection surface. Both of these factors cause a reduction of reflection amplitude. An acoustic-impedance gradient integrates the wavelet, causing a dispersion of the wavelet, lower frequency response, and lower amplitude response. It is possible that a reflector that has a strong response at low frequencies will be transparent to very high frequencies. Lateral rugosity causes a reduction in amplitude and/or dispersion of the wavelet, depending on mechanism of the rugosity. In fact, the response due to lateral rugosity can be identical to the response due to a vertical acoustic-impedance gradient. Without further information the two may be indistinguishable (Knapp, 1991). To distinguish the two, more geologic information is required; for instance, well logs will either confirm the gradient or not. If they do not, the inference is that the effect is due to lateral rugosity. Direct geological observation from outcrop or roadcut can also result in implications about reflection response. The misfortune is that frequently the two effects occur conjunctively. Unconformity surfaces are generally high-amplitude reflectors on conventional seismic data. Yet, by their nature, they generally have a weathered surface and are characterized by a velocity gradient. Generally, topographic highs exhibit more weathering. On the other hand lows may be infilled by detrital material. Thus, an unconformity may have both lateral rugosity and have a vertical gradient. This results in an even greater degree of amplitude reduction. Interference from adjacent interfering thin beds with lateral variation may also result in reduction of amplitude response. Vertical gradient may be related to porosity within carbonates. As such, recognition of the gradient may be useful as an exploration tool. A comparison of high-resolution data with conventional data or synthetic seismograms could help indicate the presence of a vertical velocity gradient.

Models

Thin Beds

Figure 1 shows the model response of a thin bed at different frequencies. At low frequencies (i.e., 25 Hz), the bed response is weak due to the destructive interference of the wavelet between the upper and the lower surfaces. For wavelets with long wavelengths, the positive reflection of the upper surface is partially masked by the negative reflection of the lower surface. At tuning (152 Hz), maximum amplitude response is seen. The trough from the upper positive reflection constructively interferes with the trough of the lower negative reflection. At high frequencies the response is that of a thick bed; the upper reflection and the lower reflection are separated by sufficient distance that the two reflections are effectively independent. The amplitude response of a thin bed can be nearly twice that of the response of a thick bed at high frequencies (i.e., 625 Hz) (Widess, 1973; Knapp, 1990).

The implication from the thin-bed model is that peak amplitude response will occur when design of the frequency response of the seismogram corresponds to tuning of the bed. Thicker beds will be better resolved with low-frequency, conventional sections. Thinner beds will be better resolved with high-frequency, high-resolution sections. The stronger reflections seen on the conventional seismogram will appear as weaker reflectors on the high-resolution section. One who is used to conventional seismic sections and the characteristic amplitude of particular horizons may misidentify a thin-bed horizon on a high-resolution section because it appears to have an anomalous reflection response.

Acoustic-impedance Gradient

Figure 2 is the model response of a uniform acoustic-impedance gradient as a function of frequency. Low frequencies (i.e., 20 Hz) with wavelengths longer than the zone of the velocity gradient are not affected by the velocity gradient. Reflection response dims as a function of frequency (i.e., above about 100 Hz) as the wavelet is integrated. The wavelet is broadened and appears as a lower frequency event. Amplitude response is reduced. At high frequencies (i.e., above 160 Hz), the reflections within the zone cancel and only the edge residuals are seen, showing top and bottom of the zone as weak reflectors. Even these reflections dim with frequency. At very high frequencies (i.e., 625 Hz), the horizon is effectively transparent.

A reflector with a graduated top may be a strong reflector on a conventional section and a weak reflector on a high-resolution section because of the acoustic-impedance gradient. Again, the interpreter used to conventional sections may misidentify horizons or think that data quality is poor because a reflection known to be prominent on conven-

tional data is weak or not detectable on the high-resolution section. This is a somewhat interesting paradox. The general intent of using a high-resolution survey is to image thinner and narrower targets. Yet the relative amplitude of the reflection of the target may be diminished by the nature of the target itself.

Lateral Rugosity

The effect of lateral rugosity depends on lateral resolution. Lateral resolution is dependent on a lateral wavelet (Berkhout, 1984; Claerbout, 1985). In addition to being sensitive to array size and the acoustic-impedance gradient of the earth, the lateral wavelet is dependent on frequency (Knapp, 1992). Thus, the higher frequencies (shorter wavelengths) of a high-resolution section are going to be more sensitive to lateral influences. A surface with short-wavelength, low-amplitude rugosity that may appear as a strong reflector on a conventional section may appear as a weak reflector on a high-resolution section. Interestingly, the synthetic seismogram that is constructed from a well log will also show a high-amplitude event because it is one-dimensional and is not affected by lateral influences. This effect alone provides evidence of lateral rugosity. Because lateral wavelets are very broad, migration will not influence the resolution of short-wavelength rugosity.

Figure 3 shows the influence of lateral rugosity. By misfortune, the effect is nearly identical to that of an acoustic-impedance gradient when the rugosity is smoothed by the lateral wavelet (Knapp, 1991). Although use of arrays will aggravate the problem, they are not the sole source of the broad lateral wavelet, so use of single geophones is not the answer to the problem (see Data Examples).

Interference of Adjacent Thin Layers

Interference from closely adjacent reflectors, such as sandstone channels, will also dim a reflection response because of interference. Although this effect exists on conventional seismic section, it will be aggravated on high-resolution section. The results are not necessarily dissimilar to the effects of lateral rugosity of the reflector surface except that channels may be large enough to be resolved and enhanced by migration. Figure 4 shows a section of a reflection response at different frequencies with channels present. The channel is modeled as an adjacent thin-bed reflector of reduced reflection coefficient. The effects of interference become more apparent as

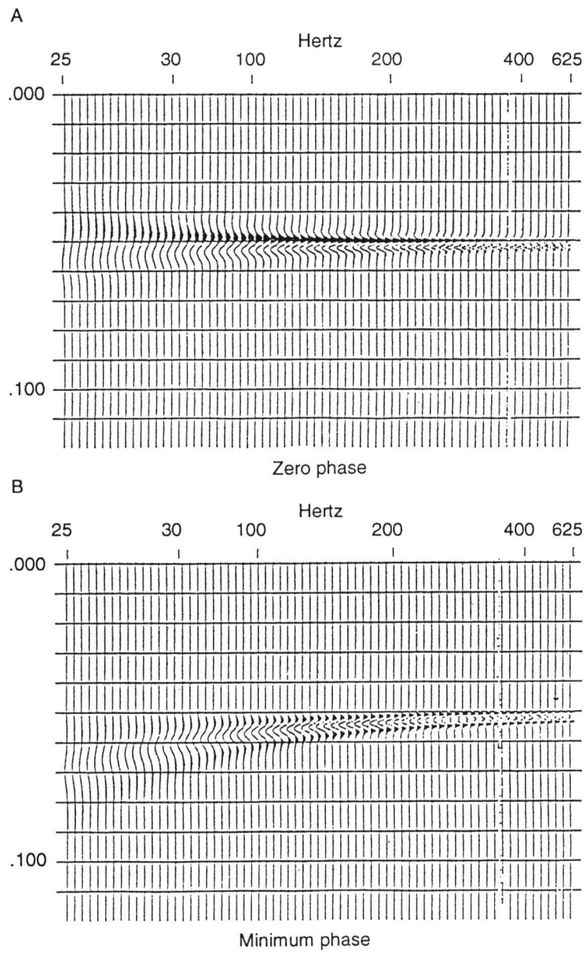

FIGURE 1—Response of a bed of constant thickness at different frequencies. Layer thickness is 2.5 msec, corresponding to 5 m at 4,000 m/sec: (A) zero-phase wavelet, (B) minimum-phase wavelet.

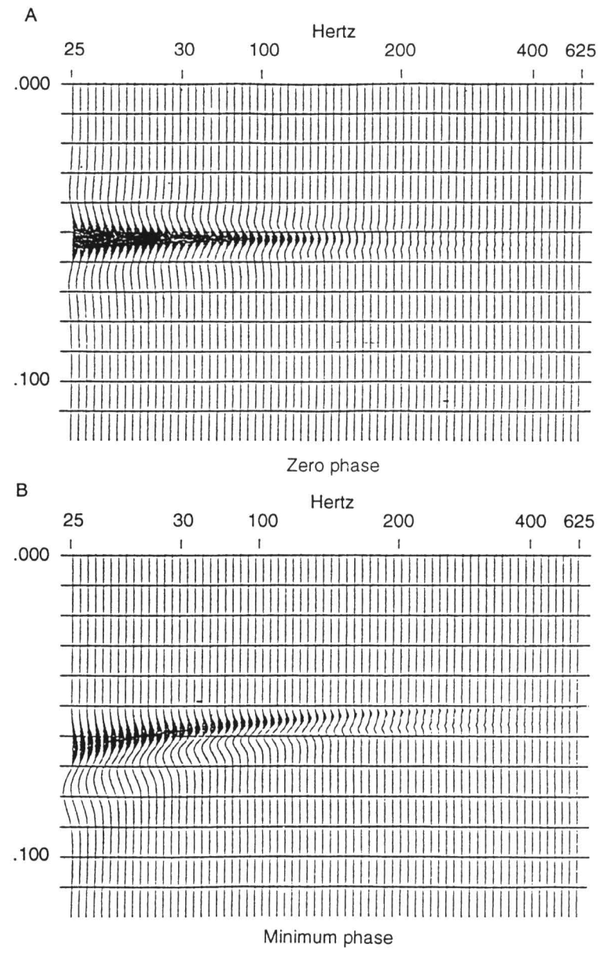

FIGURE 2—Response of a uniform acoustic-impedance gradient as a function of frequency. The zone is 5 msec thick, corresponding to 10 m at 4,000 m/sec: (A) zero-phase wavelet, (B) minimum-phase wavelet.

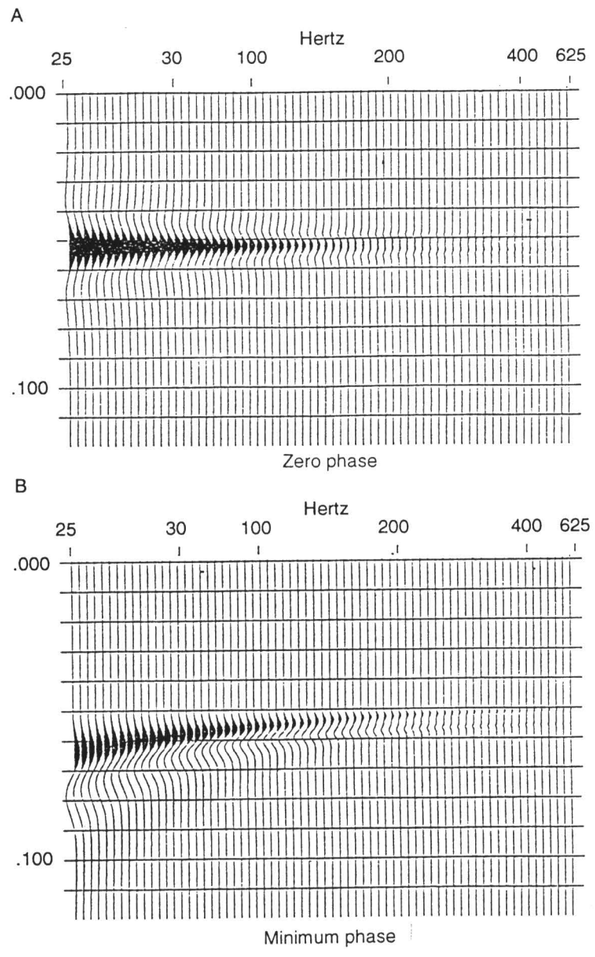

FIGURE 3—Models of lateral rugosity as functions of frequency: (A) zero-phase wavelet, (B) minimum-phase wavelet.

frequency increases. Dimming to 67% of the amplitude value at 25 Hz occurs between 200 and 300 Hz. Above 300 Hz, the presence of the thin layer becomes apparent in the response, and it amplifies in reflection strength as tuning begins to occur. Tuning frequency for the layer modeled is 1,000 Hz.

Wavelet Phase

Because the interpreter tends to choose a peak or a trough as the arrival of the event, interpretational errors are possible (see fig. 1). Structure is apparent on both the zero-phase section and on the minimum-phase section, although the thin-bed reflector is flat. On zero-phase data, interference of a thin bed (at frequencies below the tuning frequency) pushes the dominant peak up at the top of the reflector, apparently creating a positive feature (see Knapp, 1990). The lower trough is forced downward. Apparent thickness is greater than the true thickness (Widess, 1973). Actual position of the reflector is in the middle of the response.

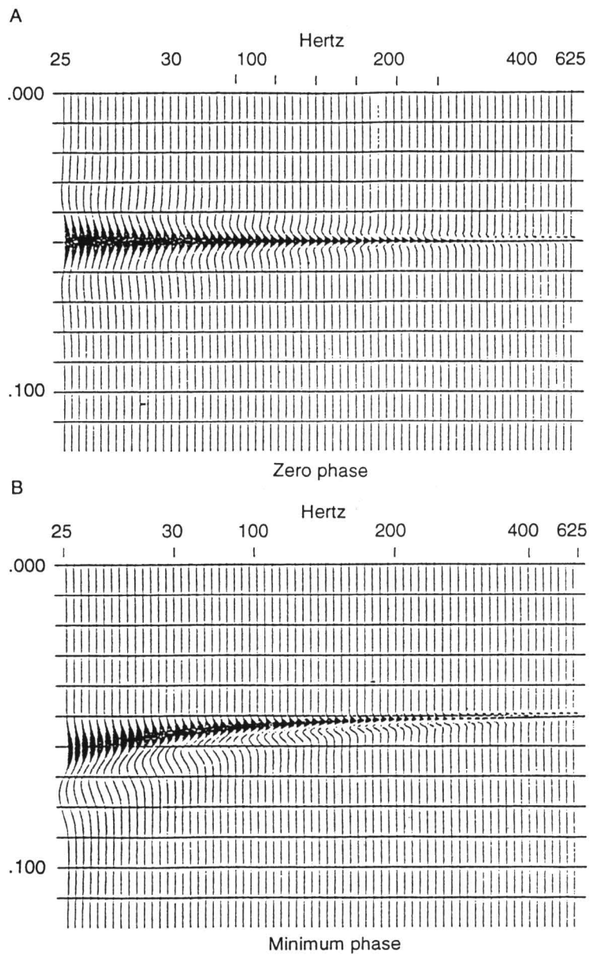

FIGURE 4—Model of interference from adjacent reflectors as a function of frequency: (A) zero-phase wavelet, (B) minimum-phase wavelet

The minimum-phase response has similar problems. Although the top of the bed can be identified from the onset of the wavelet, picking of the peak places the top below its true position. The error exists at all frequencies but is reduced at higher frequencies.

Figure 2 shows similar problems for the velocity gradient model. For the zero-phase wavelet, the peak is in the middle of the gradient interval for frequencies less than 200 Hz, and does not correspond to either the top of the main bed or the base of the underlying gradient. Timing errors will either be positive or negative depending on what the interpreter chooses the peak to represent. The time position of the reflector is too great if the top of the interval is identified and too small if the top of the layer is identified. At frequencies greater than 200 Hz, it is the zero-crossing that corresponds to the boundaries of the interval. Picking of either the peak or the trough results in small timing errors.

Problems are even greater for the minimum-phase model. Onset of the wavelet does not correspond to either the top of the interval or its bottom, although the approximation gets better at high frequencies. At high frequencies a peak approximately corresponds to the onset of the gradient and a trough to its termination, but again, timing is in error, except at the highest frequencies. Picks on the conventional section results in the time being too great. Picking a peak rather than onset greatly accentuates the timing error.

In comparing seismic sections with different frequency characteristics, mis-ties will occur, especially if the sections are minimum-phase. This is because the peaks and troughs of minimum-phase arrivals are deeper than true-time position of the reflector. Further, as the models demonstrate, thin bed and velocity gradient intervals disperse the arrival to deeper depth, an occurrence that is more severe with low frequencies than high frequencies. Except for the thin-bed response, reflections of zero-phase wavelets will generally arrive on time. Thin-bed interference, however, will pull up a zero-phase wavelet when bed thickness is less than the tuning thickness.

Attenuation: Frequency Decrease with Depth

In general, frequency response decreases with depth due to attenuation. This may result in mis-ties with a depth-to-time standard such as a velocity log. The problem is most severe in those cases where peaks or troughs are correlated on minimum-phase data. In this situation, the correlated deeper arrivals will be stretched in time, thus appearing to be too deep or leading to the conclusion that velocities are lower than true velocities. Thin beds and velocity gradients will also stretch the arrival downward. This effect will increase with decreasing frequency.

Zero-phase wavelets will result in correct timing regardless of frequency, except for the thin-bed situation where apparent pull-up will occur at frequencies less than tuning. The apparent pull-up will increase with decreasing frequency (fig. 1).

Data Examples

Upper Kansas City–Lansing Groups (Upper Pennsylvanian)

Figures 5 and 6 display a section of the upper Kansas City and Lansing Groups (Upper Pennsylvanian) with a velocity log from a nearby well and synthetic seismograms at several frequencies. The synthetic seismogram of fig. 5 with a 208-Hz Ricker wavelet suggests that the five limestones and four shales in the interval between South Bend and Farley limestones should be tuned, large-amplitude events on the high-resolution section. However, this does not fit the observation on the data. The Springhill and Farley limestones are relatively weak reflectors on the seismic section. From roadcut observations, the Springhill is known to have lateral surface roughness (Knapp, 1991; Knapp and French, 1991). This causes reduction of the amplitude response as discussed and illustrated in fig. 3. Sandstone layers in the overlying Bonner Springs Shale destructively interfere with the Farley event. This reduces both the amplitude of the peak corresponding to the Farley Limestone and the trough corresponding to the Bonner Springs Shale (see fig. 4).

The Argentine Limestone is dim on the seismic section (fig. 6) and shows lateral thickness variation and a reflector between the upper and lower units of the limestone bed. On the synthetic seismogram at high frequencies, it also appears to be a relatively low-amplitude event, because it is a thick bed and has split into two reflectors. At low frequencies it is a strong single reflector because its thickness tunes at between 50 and 90 Hz.

Conclusions

Models and real data show that there are geologic situations that may cause conceptual difficulties for an interpreter experienced only with conventional-resolution, low-frequency seismic sections when high-resolution, high-frequency seismic sections are encountered. The situations are thin beds, acoustic-impedance gradient, lateral rugosity, and interference from adjacent thin layers. It is a paradox that the value of high-resolution seismic data may be diminished in that high-amplitude, tuned reflections on a conventional seismic section will become low-amplitude, thick-bed reflections on a high-resolution section. In addition, acoustic-impedance gradients may dim an event which is manifested as a high-amplitude reflection on conventional data. Lateral rugosity and interference from adjacent layers can have a similar effect. Dimming can be so severe as to make the reflection transparent. In some cases all of these factors may be operating in conjunction; the fact is that high-resolution and conventional seismic data respond to different acoustic characteristics of the earth.

Thin-bed response can cause those horizons that generated strong, tuned reflections on conventional data to appear as relatively weak, thick-bed events on high-resolution data. This might cause the interpreter to misidentify a reflecting horizon. For example, a high-amplitude, thin-bed reflection on a conventional section could be miscorrelated with a high-amplitude, thin-bed reflection (of different origin) on high-resolution data. The Kansas City–Lansing example (figs. 5 and 6) illustrates such a case. The Wyandotte Limestone is a marker on the conventional section, and yet it is nearly transparent on the high-resolution data. However, other nearby reflectors, such as the contact between the Raytown Limestone and Liberty Memorial Shale, have a strong reflection response on the high-resolution section.

There are other situations which will cause amplitude dimming at higher frequencies. For example, an acoustic-impedance gradient may generate a high-amplitude reflection on a conventional section yet be transparent at high frequencies.

Lateral rugosity is sensitive to the frequency response of the data. At high frequencies, the dominant wavelength of the data approaches the dimensions of the rugosity and causes the reflection response to dim. The Springhill Limestone of the Lansing Group should be a medium-amplitude reflection according to the synthetic seismogram; however, as a result of surface roughness (diffusive rugosity), it is manifested as a weak event (figs. 5 and 6). The effects of rugosity can cause a response similar to that of a vertical acoustic-impedance gradient.

In the upper Kansas City Group, interference from thin sandstone layers in the Bonner Springs Shale causes dimming of the reflection response of the Farley Limestone (figs. 5 and 6). Without the sandstone layers, tuning would cause the Bonner Springs Shale and Farley Limestone to be a strong trough and peak combination. Instead, the trough has small reflectors representing the sandstone layers, reducing its amplitude, and the Farley Limestone is a relatively weak reflection.

Besides having lower resolution than zero-phase wavelets, minimum-phase wavelets cause frequency-dependent mis-ties of the data with depth in all the models shown. When that is coupled with the fact that frequency decreases with depth due to attenuation, this causes exaggeration of depth estimation, exaggeration of interval thickness, and underestimation of interval velocity.

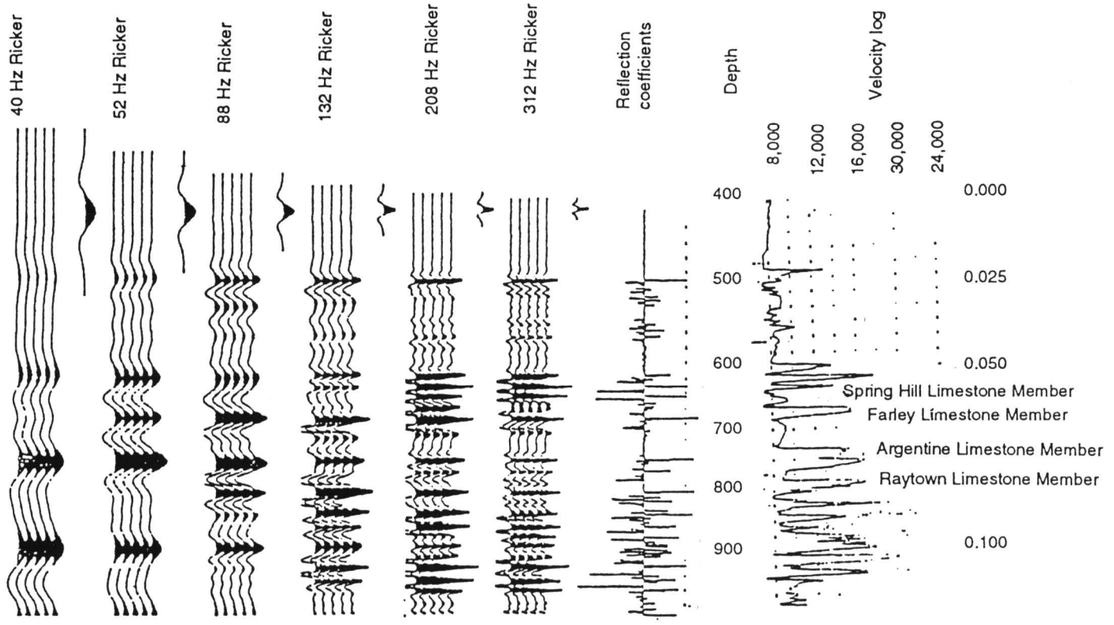

FIGURE 5—Upper Kansas City–Lansing, eastern Kansas, synthetic seismograms with different frequencies. The velocity log came from a well about 10 km from the seismic line (fig. 6).

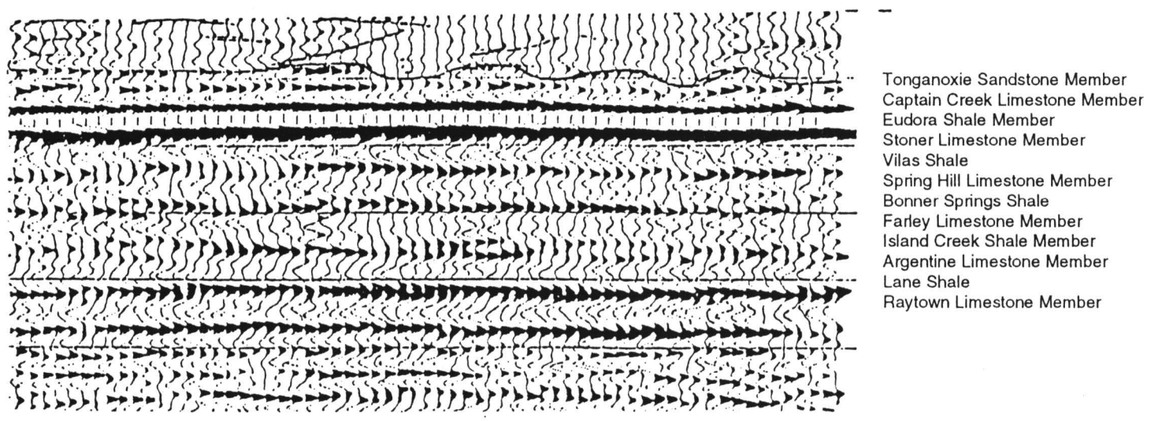

FIGURE 6—Seismic line highlighting Upper Kansas City–Lansing Groups. The Southbend Limestone (Upper Pennsylvanian, Lansing Group), which is on the well log, has been at least partially eroded and replaced by the overlying Tonganoxie, a local channel sandstone.

Seismic-data acquisition is carefully designed to use sources of minimum energy, minimum noise, and maximum frequency and bandwidth. Pre-emphasis filtering helps balance the data spectrum during acquisition. Use of multiple geophones increases sensitivity which allows smaller and higher frequency sources to be used, reduces random noise according to the square root of the number of geophones, and attenuates air-coupled wave noise by judicious spacing. Array size is designed to be the maximum possible without adversely affecting frequency response at long offsets. Group-to-group distance is set to be equal to array size, and arrays are linear to fit the stack-array concept of Morse and Hildebrandt (1989). The stack-array, the use of half-integer source offset (Knapp, 1985), and split spread geometry help reduce ground roll when data are stacked during processing. Source design also helps reduce ground roll. Data are gathered to the farthest offset possible that will avoid wide-angle reflections, and this is estimated to be about equal to the depth of the target reflector, but it is determined by field testing.

Wavelets are processed to be zero-phase or quadrature-phase because these phase designs have maximum resolving power and do not have the timing problems of other phase configurations (such as minimum-phase). Spectral whitening is used rather than deconvolution to balance the spectrum of the processed data because spiking deconvolution can adversely affect reflection character when the reflection coefficient series of the earth does not fit the presumption of randomness. Deconvolution, if used, is done judiciously and gently to remove specific problems such as multiples. Testing against synthetic seismograms can determine the degree of deconvolution that can be used without problems. Special care is taken in normal moveout, statics, residual normal moveout, residual statics, first arrival mutes, and mutes of normal moveout stretch to preserve the high-frequency quality of the field data and to show shallow reflections. For shallow data, moveout and stretch are particularly important because shallow data have more moveout than deeper data and the shallow section has a greater rate of change of velocity than the deeper part of the section.

Key reflectors can be shown at their greatest advantage by producing several sections with different pass bands. In this manner beds of different thicknesses can have a section with frequencies appropriate for tuning, creating maximum possible amplitude response and visibility, and characterizing bed thickness. Such sections would also indicate other features of the section such as acoustic-impedance gradients, lateral rugosity, and the presence adjacent of thin-bed interference.

References

Berkhout, A. J., 1974, Related properties of minimum-phase and zero-phase time functions: Geophysical Prospecting, v. 22, p. 683–709

_____, 1984, Seismic resolution—a quantitative analysis of resolving power of acoustical echo techniques: Geophysical Press, Amsterdam, 228 p.

Claerbout, J. F., 1985, Imaging the earth's interior: Oxford and Boston, Blackwell Scientific Publications, 398 p.

Hunter, J. A., Pullan, S. E., Burns, R. A., Gagne, R. M., and Good, R. L., 1984, Shallow seismic reflection mapping of the overburden-bedrock interface with the engineering seismograph—Some simple techniques: Geophysics, v. 49, p. 1,381–1,385

Knapp, R. W., 1985, Using half-integer source offset with split spread data: The Leading Edge, v. 5, no. 1, p. 66–69

_____, 1990, Vertical resolution of thick beds, thin beds, and thin-bed cyclothems: Geophysics, v. 55, p. 1,183–1,190

_____, 1991, Effects of surface roughness or diffusivity on migration, and lateral and vertical resolution (expanded abstract): Proceeding of the 2nd International Congress of the Brazilian Geophysical Society, p. 863–865

_____, 1992, The size of a reflection point: Proceedings of the Canadian Society of Exploration Geophysicists, p. 95

_____, 1993, Energy distribution in wavelets and implications on resolving power: Geophysics, v. 58, no. 1, p. 39–46

Knapp, R. W., and French, J. A., 1991, Features in Kansas cyclothems seen by high-resolution seismology; *in,* Sedimentary modeling—Computer simulation and methods for improved parameter definition, E. K. Franseen, W. L. Watney, C. G. St. C. Kendall, and W. C. Ross, eds.: Kansas Geological Survey, Bulletin 233, p. 111–121

Knapp, R. W., and Steeples, D. W., 1986, High-resolution common-depth-point reflection profiling—Field acquisition parameter design: Geophysics, v. 51, p. 283–294

Knapp, R. W., 1992, The size of a reflection point (abst.): Canadian Society of Exploration Geophysicists, Expanded Abstracts, p. 95

Morse, P. F., and Hildebrandt, G. F., 1989, Ground roll suppression by the stack-array: Geophysics, v. 54, p. 290–301

Widess, M. B., 1973, How thin is a thin bed?: Geophysics, v. 38, p. 1,176–1,180

Depositional and Stratigraphic Analysis of Kansas City Group Strata Utilizing High-resolution Seismic Imaging, Montgomery County, Kansas

Evan K. Franseen[1], Howard R. Feldman[2], Neil L. Anderson[3], and Richard D. Miller[1]
[1]Kansas Geological Survey, The University of Kansas, Lawrence, KS 66047; and
[3]Department of Geology and Geophysics, University of Missouri–Rolla, Rolla, MO 65401

Abstract

High-resolution seismic images were obtained of Missourian (Middle Pennsylvanian) strata in Montgomery County, Kansas. The interval imaged included the Mound Valley Limestone through Quivira Shale(?) (Kansas City Group). The length of the seismic line was approximately 400 m (0.25 mi). The 12-fold CDP production line was acquired using an end-on source/receiver geometry. Ground truth was determined using one core on the seismic line, several other cores taken near the line, and from nearby outcrops. A geologic model of the area and synthetic seismogram were used to confirm geologic interpretations. The seismic images revealed some known features, such as dramatic thinning of the Galesburg Shale, and some unknown features, such as channeling in what appears to be the upper part of the Nellie Bly Formation.

Introduction

The Kansas City Group (Upper Pennsylvanian, Missourian) in Montgomery County, Kansas (figs. 1 and 2) consists of alternating siliciclastic and carbonate rocks. The cyclic alternation of lithologies probably resulted largely from glacio-eustatic sea-level oscillations. The Drum Limestone of the Kansas City Group in Montgomery County has been the focus of ongoing studies because it contains an oolite body analogous to oolitic reservoirs in the Kansas City Group in central and western Kansas. The purpose of these studies has been to develop a detailed model of deposition and diagenesis of the Drum Limestone in order to better understand the origin of analogous petroleum reservoirs. To this end we have studied the Drum Limestone and associated units using data from outcrops, cores, geophysical well logs, and high-resolution seismic. In this report we present results from the first of three seismic lines shot along depositional dip in an area southwest of Independence, Kansas. The Drum Limestone is apparently absent in the area of this seismic line; however, the line does show details of pre- and post-Drum stratigraphy that influenced the ultimate development of reservoir-type facies.

FIGURE 1—Map of Kansas showing Montgomery County. In the study area, the Missourian succession represents the transition from a shelf to basinal environment. The succession thickens dramatically from north to south into the Arkoma basin. The transition from a shelf to basinal environment is characterized by the thickening of the siliciclastic sediment into the Arkoma basin. The limestone units, in contrast, generally thin from north to south in the basinal direction.

Geologic and Stratigraphic Setting

During deposition of the Kansas City Group, the area that is now Montgomery County was situated at a critical transition from a slowly subsiding shelf to the north, and a more rapidly subsiding basin to the south. North of Montgomery County, the Kansas City Group consists of continuous alternating carbonate and siliciclastic units. Many of the carbonate units contain localized thickenings due to oolitic buildups or phylloid algal reefs. South of the study area, the Kansas City Group thickens dramatically into the Arkoma basin. Limestones generally pinch out to the south as the siliciclastic units thicken.

The stratigraphic interval of interest in the study area extends from the Mound Valley Limestone to the Quivira Shale(?) (fig. 2). The Drum Limestone is generally under 5 m (16.5 ft) thick in the study area, but locally thickens to 20 m (66 ft) thick along a generally east-west trend (figs. 3 and 4). The thick zone of Drum Limestone is composed of porous oolite that is similar to petroleum reservoir facies. Thickness and facies changes in the Drum Limestone are interpreted to result from significant pre-Drum topography. Relief on the pre-Drum seafloor was apparently related to major thickness changes in the underlying sequence of rocks down to the Canville Limestone Member and possibly including the Galesburg Shale. The lowest unit that apparently influenced Drum deposition is the Galesburg Shale. In the area near the zone of thickened Drum, the Galesburg is thin (6.5 m; 21.5 ft) where the Drum is thickest, and thickens to a maximum of 19 m (63 ft) as the Drum thins to the north and south.

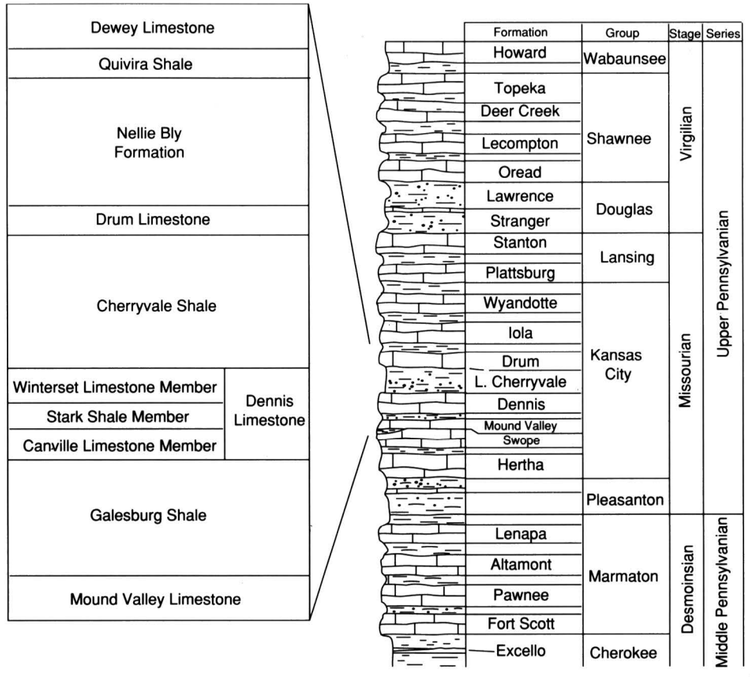

FIGURE 2—Generalized stratigraphy of the study interval.

Each of the next three significant units, the Winterset Limestone, Cherryvale Shale, and Drum Limestone, are thickest just basinward of the thickest underlying unit. During the deposition of each unit the depositional basin edge stepped basinward. For example, during Winterset deposition, the depositional shelf edge was in the area that is now southern Wilson County a few miles north of the Montgomery County border. The Winterset thins from nearly 30 m (99 ft) thick in central Wilson County to under 6 m (20 ft) thick in central Montgomery County (Watney et al., 1989). The Cherryvale Shale apparently filled in some of the low areas left from Winterset deposition and extended the depositional shelf edge to central Montgomery County. The Drum Limestone is thin, generally under 6 m (20 ft), where either the Cherryvale Shale or Winterset Limestone are thick, and increases in thickness up to 22.5 m (74 ft) as the Cherryvale Shale thins to the south where the Winterset Limestone is thin. Thus, deposition of the Drum Limestone extended the depositional shelf a few miles south of the Cherryvale Shale platform (fig. 3). However, this may not be true progradation, because sea-level fluctuations at this time resulted in a complex history of flooding and exposure of much of the study area (French et al., 1992; Watney et al., 1989).

The Nellie Bly(?) Formation overlies the Drum Limestone and consists of interbedded sandstone, siltstone, shale, and coal, and includes thin limestones in the upper portion. Ripple crossbedding, starved ripples, sediment loading, and soft-sediment deformation structures are all common features in these strata. There is a sharp, irregular erosional contact near the middle to base of the Nellie Bly(?) that can be traced throughout the study area on well logs and high-resolution seismic lines. This erosion surface is overlain by a fining-upward sequence of conglomerate, sandstone, and shale.

A black, platy shale (the Quivira Shale?), up to 3 m (10 ft) thick, lies directly above the Nellie Bly(?) Formation.

Inferred Depositional Environment

The Cherryvale Shale was part of a marine deltaic system that generally prograded to the south and southwest. The Cherryvale is distributed in one major lobe in the study area (fig. 3B). This lobe has a NE-SW axis, parallel to one direction of basement structures in the area, although this relationship remains enigmatic. The lobe of Cherryvale Shale thins abruptly to the south from 30 m (99 ft) to 6.5 m (21.5 ft) over a distance of about 1.6 km (1 mi) in the subsurface southwest of Independence. The southern and western edge of the Cherryvale lobe is interpreted as the depositional slope that was left after cessation of delta progradation, although some minor erosion occurred prior to, or

concomitant with, initial Drum deposition. Depositional environments of the Cherryvale are difficult to interpret because of the lack of sedimentary structures and the homogeneity of the shale. The relatively flat top of the Cherryvale lobe suggests that sediment accumulated up to local base level. It is likely that the sea was very shallow over the depositional shelf created by the Cherryvale delta.

The Drum Limestone marks the end of siliciclastic deposition and beginning of carbonate deposition in the study area. The lowest bed in the Drum Limestone is locally rich in fossils and shale clasts, and rests on an erosional surface on top of the Cherryvale Shale. This lowest limestone may represent deposition during a transgression and initial relative sea-level rise. Local scouring and/or channeling in lower Drum beds suggests relatively shallow-water conditions. Above the lowest limestone bed in the Drum are alternating shale and laminated carbonate mudstones. The paucity of bioturbation, fossils, and current structures all suggest a quiet, relatively deep-water environment of deposition. The alternating shale and laminated carbonate mudstone facies always occurs at the base of the Drum Limestone and gradually increases in thickness basinward. Above this facies is the main portion of the Drum Limestone, and it is this upper part that shows rapid facies and thickness changes in the study area.

Where the combined thickness of the Winterset Limestone (fig. 3A) and Cherryvale Shale (fig. 3B) are over 17 m (56 ft) thick, the Drum is a thin (generally under 3.5 m; 11.5 ft), tight (low porosity/permeability) limestone. Outcrops of the Drum in this area are composed of laminated carbonate mudstone, stromatolitic wackestone, and fossiliferous wackestone. Deposition in mostly normal marine water is evidenced by the abundant and diverse fauna in the wackestone and packstone.

Near the basinward edge of the Cherryvale Shale (where the Winterset Limestone is generally thin), the Drum increases in thickness and becomes more oolitic. Near the Cherryvale depositional shelf edge, the Drum typically consists of three units: a lower unit of alternating carbonate mudstone and shale, a middle unit composed of mudstone to fossiliferous wackestone, and an upper crossbedded oolitic unit. Evidence of erosion prior to oolite deposition is common, and a possible karst surface has been recognized indicating possible local subaerial exposure on top of the fossiliferous wackestone (Feldman and Franseen, 1991). Basinward of the break in slope of the Cherryvale, the Drum thickens abruptly to a maximum of 25 m (82.5 ft) in the subsurface. On outcrop and in cores, most of the Drum in this area is composed of crossbedded, fossiliferous, oolitic grainstone. Hamblin (1969) interpreted bimodal crossbed orientations in the Kansas City Group oolites to be the result of tidal currents. Crossbed orientations in the Drum oolite are also bimodal, but are dominated by southwest orientations, suggesting a setting dominated by ebb currents. Oolites were probably being generated in shallow water near the edge of the Cherryvale depositional shelf and transported basinward into lower-lying areas, possibly as a series of tidal deltas in some locations. The oolite is now preserved as several lobes extending basinward from the depositional shelf edge (compare figs. 3C and 4).

In basinward locations, south of the major oolitic accumulations, the exposed Drum is represented predominantly by unfossiliferous, laminated micrite and peloidal wackestone possibly reflecting a relatively deep, oxygen-starved environment. The Drum is locally absent in basinal areas in the subsurface. The distance of the transition from thin shelf limestone to thick oolite to thin basinal limestone is as little as 1 km (0.62 mi) in the subsurface. On outcrop this transition occurs over a distance of about 25–30 km (15–25 mi).

Apparently a minor flooding event followed Drum Limestone deposition, resulting in widespread deposition of the crossbedded sandstones and intervening shales of the Nellie Bly(?) Formation. However, a fall in relative sea level may be the cause of the laterally extensive erosion surfaces and channels that occur within the Nellie Bly(?), although no subaerial exposure features have been identified to date. Locally, the upper portion of the Drum Limestone appears to have been erosionally truncated. Current ripples, the lack of fossils, low-diversity trace fossil assemblages, and possible rhythmic tidal bedding suggest deposition in a shallow, estuarine environment for the Nellie Bly(?) Formation.

Deposition of the overlying black, platy shale (Quivira Shale?) likely represents the next major marine transgression.

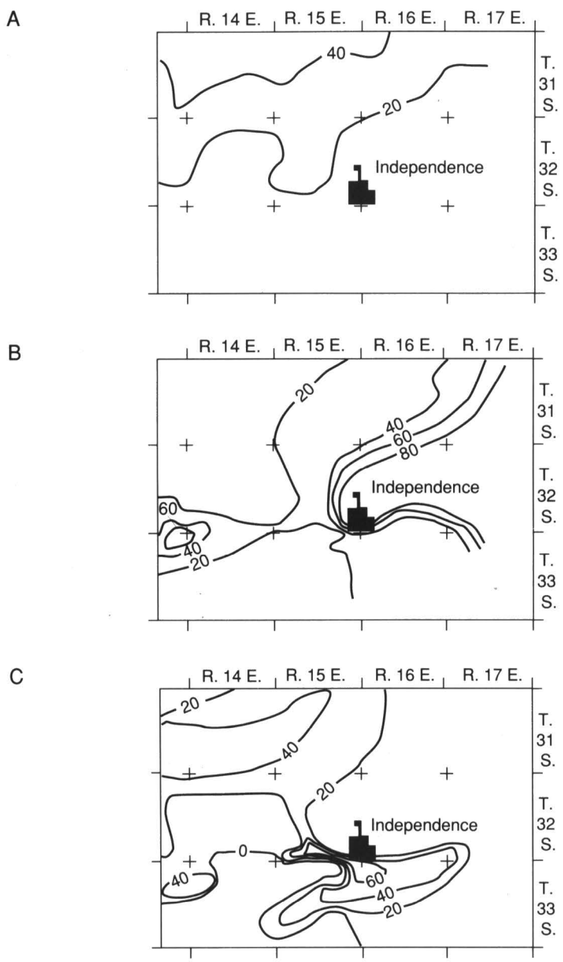

FIGURE 3—MAPS OF MONTGOMERY COUNTY SHOWING THICKNESS OF THE WINTERSET LIMESTONE (A), CHERRYVALE SHALE (B), AND DRUM LIMESTONE (C). Contour intervals are in feet.

Seismic Resolution

A high-resolution seismic-reflection study was conducted in the Drum Limestone study area in an effort to image geometric changes within Missourian stage strata at depths of up to 100 m (330 ft). These features are significant from both a geologic and geophysical perspective. Geologically, the nature of a truncation or pinch-out, either from erosion or a facies change, is important for determining the depositional history. Geophysically, a pinch-out or truncation represents an opportunity to quantify the practical thin-bed resolution of shallow high-resolution seismic reflection at this site.

This study highlights the geophysical aspects of quantifying practical thin-bed resolution. The data were acquired and processed to focus on a distinct shallow high-resolution seismic reflection at approximately 65 msec within the Galesburg Shale where the shale thins from 19 m (63 ft) to 7 m (23 ft).

The thin-bed resolving power of the CDP seismic-reflection technique is dependent upon the dominant frequency of the recorded reflection wavelet (Widess, 1973). Increasing the dominant frequency of recorded reflection signal involves: 1) generating a high-frequency source pulse, 2) sensing the signal with receivers with high voltage output, low noise, and a flat frequency response over the desired high frequencies, 3) recording the signal digitally on a seismograph with a large instantaneous dynamic range and electronically quiet analog filter and gain capabilities, and 4) optimizing the spread interval and receiver spacing for the target of interest (Knapp and Steeples, 1986). Criteria for resolving converging thin-bed sequences relies on observations of interference as evidenced by distortion of reflection waveforms (Ricker, 1953).

Practical resolution limits are dependent not only on recorded reflection frequencies but also on wavelet characteristics and noise. Zero-phase wavelets possess the highest resolving potential (Knapp, 1990). A known theoretical wavelet can be phase-filtered to zero phase. Successful application of deconvolution requires a statistically large number of unique reflection wavelets and data with a large signal-to-noise ratio (Yilmaz, 1987). Shallow high-resolution reflection data sets rarely have more than four to six reflections and are notoriously noisy (Steeples and Miller, 1990). Practical optimization of shallow high-resolution data sets by phase filtering to zero phase is generally not possible.

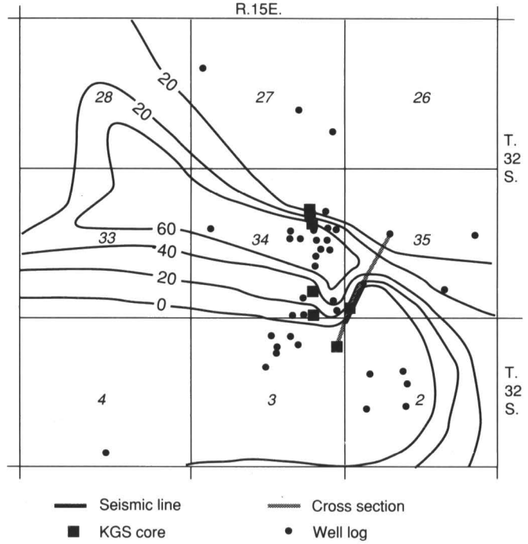

FIGURE 4—MAP OF STUDY AREA SHOWING THICKNESS OF DRUM LIMESTONE IN FEET AND LOCATION OF CROSS SECTION AND SEISMIC LINE. Our preferred interpretation, based on outcrop, seismic, and shallow well control is that the Drum Limestone was deposited as several(?) lobes elongated perpendicular to the edge of the Cherryvale delta. In our opinion, the example seismic line was shot between Drum Limestone lobes in an area of shale deposition only (fig. 5).

Field Procedures

Data for this study were acquired on an EG&G Geometrics 2401 seismograph. The seismograph amplifies, filters (analog), digitizes the analog signal into a 15-bit word, and stores the digital information on magnetic media. The selected low-cut filters have an 18-dB/octave rolloff from their indicated -3-dB point. Production lines were acquired with 100-Hz analog low-cut and 500-Hz analog high-cut filters. The 1,024 samples recorded per trace were at a 1/2-msec sampling interval. The dynamic range of the seismograph was more than adequate to record high-quality reflection information in the presence of source-generated and cultural noise at this site.

A series of walkaway-noise tests was conducted prior to acquisition of the production seismic lines. The spectral and total energy characteristics of the downhole .50-cal seismic source made it the source of choice at this site for this geologic target. The receiver array consisted of three 40-Hz geophones equally spaced over approximately 1 m (3.3 ft) and centered on each station. The receiver array was designed in an attempt to attenuate some of the source-generated noise (Steeples and Miller, 1990). Analysis of the noise tests allows acquisition parameters and equipment to be optimized for the site conditions.

The nominal 12-fold CDP production line was acquired using an end-on source/receiver geometry. Analysis of the walkaway data allowed determination of an optimum source-to-nearest-receiver offset of 17 m (56 ft) and source-to-farthest-receiver offset of 75 m (247.5 ft). A large component of direct and refracted wave energy inhibited closer source-to-receiver offsets. Near vertically incident recording minimizes normal move-out corrections and the associated stretch allowing a higher frequency, less distorted reflection wavelet to be recorded (Miller et al., 1990). The target reflector is approximately 75 m (247.5 ft) deep, which is within the optimum recording offset as evidenced by the walkaway-noise tests and general rules of thumb (Knapp and Steeples, 1986).

Data Processing

The CDP data were processed at the Kansas Geological Survey (KGS) using a proprietary set of algorithms developed by the KGS (Eavesdropper). Extreme care was used during the editing process to ensure removal of all non-seismic energy that could either be misinterpreted as reflections on stacked data or that hampered interpretations of real reflection events. Velocity analysis incorporated iterative constant-velocity stacking with detailed 1/5-wavelength surface-consistent statics to improve both accuracy of velocity corrections and time/depth conversion on interpreted cross sections. The main distinctions between the shallow high-resolution processing flow used on these data and most routine petroleum sequences relate to conservative use and application of correlation statics, precision required during velocity and spectral analysis, extra care during muting operations, and lack of deconvolution.

Modeling and Interpretation

As an aid to the interpretation of the seismic line (fig. 5), a geologic cross section (fig. 6), a corresponding two-dimensional geologic model (fig. 7), and a synthetic seismogram were generated (fig. 8). The geologic cross section is structurally consistent with well control (Clarkson #2 core; fig. 6) at trace 494 (fig. 5). The velocities and densities incorporated into the model (fig. 7) are consistent with the lithologies encountered in the Clarkson core, check shot survey data at the same well site, and stacking velocity control. The cross section in fig. 7 is presented as a reasonable representation of that portion of the subsurface imaged by the seismic control and illustrates some of the geometric details which characterize the Missourian stage strata in the study area.

The two-dimensional synthetic seismogram (fig. 8) was generated for the geologic model using Geophysical Micro-Computer Ltd. diffraction modeling software. A 5-msec, zero-phase, normal-polarity Ricker wavelet was used. The more prominent events on the synthetic seismogram have been labelled in order to facilitate comparisons between the geologic model, synthetic seismogram, and seismic line.

A comparison of the geologic model and the synthetic seismogram indicates that tops of the Mound Valley Limestone, Winterset Limestone, unnamed sandstone and a limestone in the upper Nellie Bly(?) Formation, and the base of the unnamed sandstone are manifested as relatively high-amplitude peaks on the synthetic seismogram (fig. 8). The base of the interpreted channel-fill, in contrast, is represented as a moderate-amplitude trough. Low-amplitude diffractions originate at the edges of these truncated horizons. The complexity of the central part of the synthetic seismogram is increased as a result of the non-vertical incident reflections from the base of the channel that collectively produce the observed classic "bow-tie" effect beneath the base of the channel.

The interpreted seismic line is presented as fig. 5. The labelled events were identified on the basis of the synthetic seismogram. The time-depths to the respective horizons are consistent with subsurface control at the Clarkson #2 well site, stacking velocities, and check shot survey control. The high degree of correlation between the geologic model, synthetic seismogram, and seismic line support the seismic interpretations presented.

As anticipated from the analysis of the synthetic seismogram, the tops of the Mound Valley Limestone, Winterset Limestone,

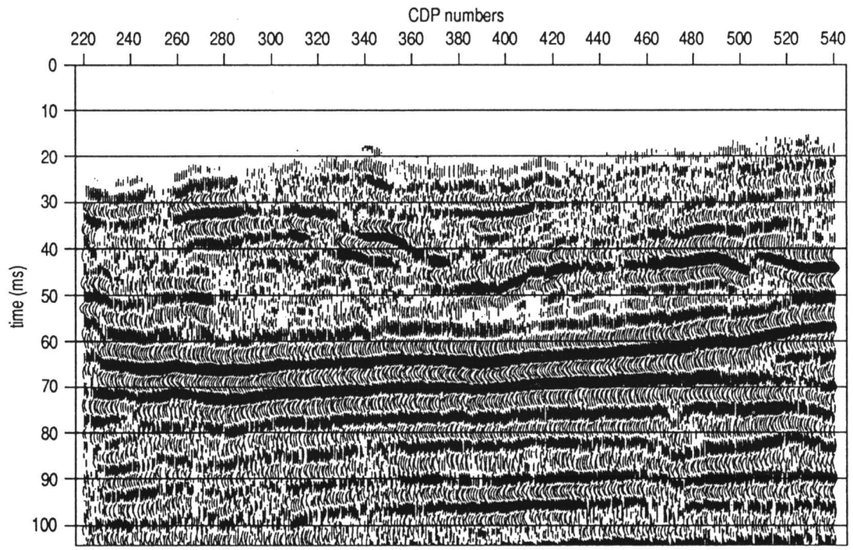

FIGURE 5—UNINTERPRETED AND INTERPRETED HIGH-RESOLUTION SEISMIC LINE. These data were acquired on an EG&G Geometrics 2401 seismograph using a downhole .50-cal seismic source and receiver arrays consisting of three 40-Hz geophones equally spaced over approximately 1 m and centered on each station. 1,024 samples recorded per trace were at a 1/2-msec sampling interval. Length of seismic line is about 0.4 km (0.25 mi).

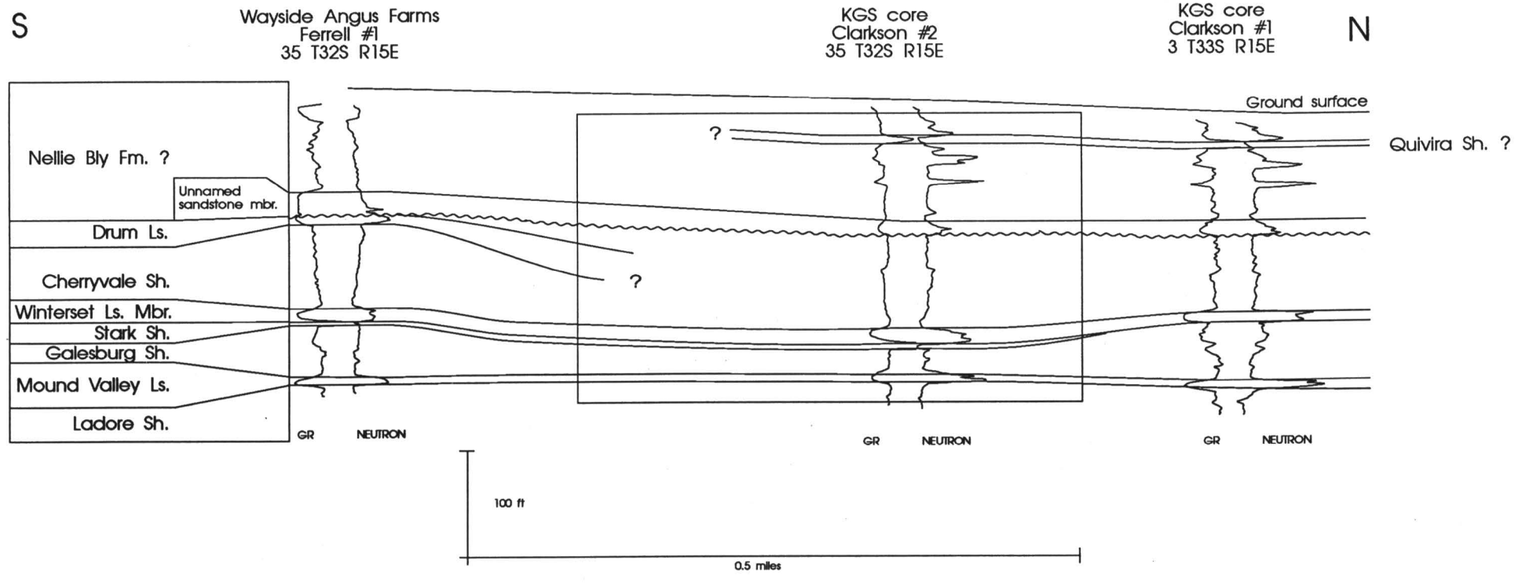

FIGURE 6—GEOLOGIC CROSS SECTION ALONG SEISMIC LINE BASED ON KGS CORES AND ONE OIL-WELL LOG. Box indicates approximate location and thickness of interval models for the synthetic seismic line.

unnamed sandstone and a limestone in the upper Nellie Bly(?) Formation, and the base of the unnamed sandstone correspond to relatively high-amplitude peaks on the seismic line. The Mound Valley Limestone, Winterset Limestone, unnamed sandstone, and Nellie Bly(?) Formation events appear to be correlatable across the seismic line. In contrast, the reflections from the top and base of the unnamed sandstone unit, as correlated, are truncated by an interpreted deeply incised and infilled channel. The base of the interpreted channel fill is correlated as a moderate-amplitude trough. The polarity of this event, and the subtle negative drape across the channel along the Nellie Bly(?) event, suggests that the channel fill is composed predominantly of compacted shales. This thesis has not been independently confirmed by drilling.

One striking feature on the example seismic line is the dramatic thinning of the Galesburg shale to the north (fig. 6; at about 65 msec, between the Winterset and Mound Valley Limestones). This is consistent with core and well-log data (fig. 6) and interpreted as confirmation of either the local depositional thinning or erosional thinning of the Galesburg Shale.

Also of significance is the apparent absence of the Drum Limestone along the entirety of the seismic line. (The absence of Drum Limestone at trace 494 has been confirmed by the Clarkson core.) Our preferred interpretation is that the Drum Limestone was not deposited in this part of the study area. Based on outcrop and shallow well control, we interpret the Drum Limestone to have been deposited as several(?) lobes elongated perpendicular to the edge of the Cherryvale delta. In our opinion, the example seismic line was shot between Drum Limestone lobes, in an area that received only shale deposition (fig. 4).

Analysis of cores and well logs in the study area suggests that the unnamed sandstone within the Nellie Bly(?) Formation rests unconformably on lower older units. The irregularity of this reflector on the seismic line and the interpreted channel are further evidence of the erosional nature of the lower contact and basal portion of the Nellie Bly(?) Formation.

The seismic line illustrates that stratigraphic complexity of the upper Nellie Bly(?) and overlying units indicated by lack of lateral continuity of events shallower than approximately 45 msec (fig. 5). This complexity is suggested in the geologic cross section by our inability to correlate the Quivira Shale(?) north of the Clarkson #2 core (fig. 6). A shale-filled channel is hypothesized as a partial explanation for the lack of continuity of shallow reflectors based on the similarity of the seismic line and synthetic model data (figs. 5, 7, and 8). Channeling in the Nellie Bly(?) Formation may explain the lateral discontinuity of thin limestone and sandstone beds shown on the well logs in fig. 6.

Summary and Conclusions

A 12-fold high-resolution seismic line was obtained along an 400-m-long (0.25-mi) line in central Montgomery County, Kansas. The interval from the Mound Valley Limestone to the Quivira Shale(?) was imaged. Ground truth was based on cores, well logs, and outcrops. These data in addition to interpretation of the seismic line were used to construct a simplified geologic model. The model was used to construct a synthetic seismic section. The synthetic section agrees well with the original seismic section. This technique revealed outcrop-scale features in the rocks, including one small channel in the Nellie Bly(?) Formation not previously suspected.

ACKNOWLEDGMENTS—This paper was prepared with the support of the U.S. Department of Energy (DOE Grant #DE–FG07–90BC14434). However, any opinions, findings, conclusions, or recommendations expressed herein are those of the authors and do not necessarily reflect the views of the DOE. We thank Jesse Clarkson and Warren Ferrell for allowing access to their land for the purposes of coring and seismic acquisition. We thank Dennis Hedke and Bill Miller for critical reviews and suggestions that improved the final manuscript.

References

Feldman, H. R., and Franseen, E. K., 1991, Stratigraphy and depositional history of the Drum Limestone and associated strata (Pennsylvanian) in the Independence, Kansas, area—A field trip guidebook and road log: Kansas Geological Survey, Open-file Report 91–45, 29 p.

French, J. A., Feldman, H. R., Watney, W. L., and Franseen, E. K., 1992, Stratigraphic architecture and facies distribution of upper Middle Carboniferous cyclic depositional sequences (cyclothems), southeastern Kansas, USA: Geological Society of America, Abstracts with Programs, v. 24, no. 4, p. 15

Hamblin, W.K., 1969, Marine paleocurrent directions in limestones of the Kansas City Group (Upper Pennsylvanian) in eastern Kansas: Kansas Geological Survey, Bulletin 194, pt. 2, 25 p.

Knapp, R. W., 1990, Vertical resolution of thick beds, thin beds, and thin-bed cyclothems: Geophysics, v. 55, p. 1,183–1,190

Knapp, R. W., and Steeples, D. W., 1986, High-resolution common depth point seismic-reflection profiling—field acquisition parameter design: Geophysics, v. 51, p. 283–294

Miller, R. D., Steeples, D. W., and Myers, P. B., 1990, Shallow seismic-reflection survey across the Meers fault, Oklahoma: Geological Society of America, Bulletin, v. 102, p. 18–25

Ricker, N.,1953, Wavelet contraction, wavelet expansion, and the control of seismic resolution: Geophysics, v. 18, p. 769–792

Steeples, D. W., and Miller, R. D., 1990, Seismic-reflection methods applied to engineering, environmental, and ground-water problems: Society of Exploration Geophysics, Volumes on Geotechnical and Environmental Geophysics, Stan Ward, ed., v. 1—Review and Tutorial, p. 1–30

Watney, W. L., French, J. A., and Franseen, E. K., eds., 1989, Sequence stratigraphic interpretations and modeling of cyclothems in the Upper Pennsylvanian (Missourian), Lansing and Kansas City Groups in eastern Kansas: Kansas Geological Society, Guidebook, 211 p.

Widess, M. B., 1973, How thin is a thin bed?: Geophysics, v. 38, p. 1,176–1,180

Yilmaz, O., 1987, Seismic data processing; S. M. Doherty, ed; *in*, Series—Investigations in Geophysics, no. 2, Edwin B. Neitzel, series ed.: Society of Exploration Geophysics, Tulsa, OK, 526 p.

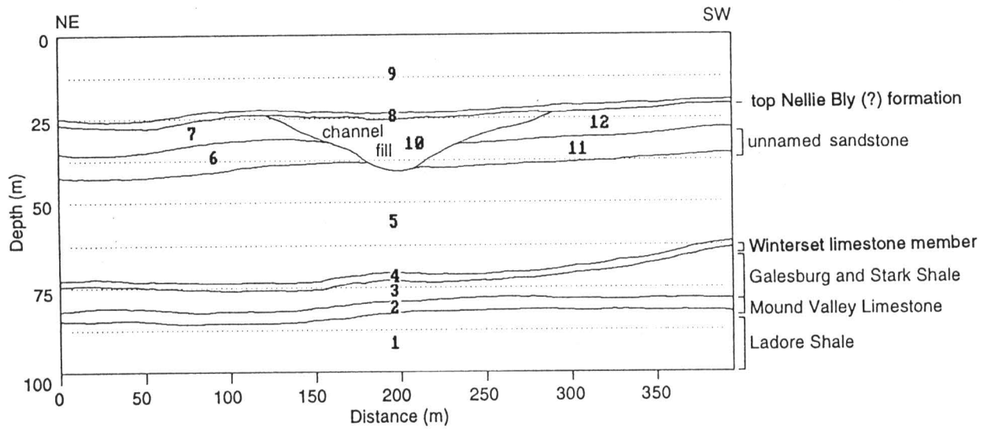

FIGURE 7—TWO-DIMENSIONAL GEOLOGIC CROSS SECTION. The geologic cross section is structurally consistent with well control (Clarkson #2 core) at trace 494 (fig 5). The velocities and densities incorporated into the model are consistent with the lithologies encountered in the Clarkson core, check shot survey data at the same well site, and stacking velocity control. This cross section is presented as a reasonable representation of that portion of the subsurface imaged by the seismic control and illustrates some of the geometric details which characterize the Missourian stage strata in the study area.

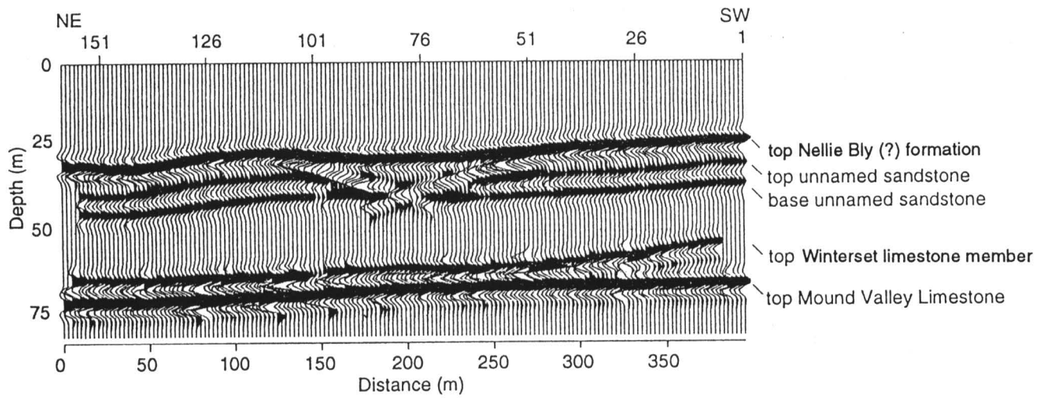

FIGURE 8—TWO-DIMENSIONAL SYNTHETIC SEISMOGRAM GENERATED FOR THE GEOLOGIC CROSS SECTION OF FIG. 6 USING GEOPHYSICAL MICRO-COMPUTER LTD. DIFFRACTION MODELING SOFTWARE. A 5-msec, zero-phase, normal-polarity Ricker wavelet was used. The more prominent events on the synthetic seismogram have been labelled in order to facilitate comparisons between the geologic model, synthetic seismogram, and seismic line.

Seismic Response of the East Flank of the Central Kansas Uplift, Rice County, Kansas

Nelda L. Haraldson[1], Ralph W. Knapp[2], and K. David Newell[3]
[1]Phillips Petroleum Resources, Ltd., Calgary, AB T2P 3N4;
[2]formerly with Kansas Geological Survey, The University of Kansas, Lawrence, KS 66047; and
[3] Kansas Geological Survey, The University of Kansas, Lawrence, KS 66047

Abstract

A 7-mi (11.2-km) seismic line across the Lyons anticline just south of Lyons, Rice County, Kansas, shows reflections to the depth of about 3,500 ft (1,070 m) corresponding to the Precambrian Rice Formation. The Lyons anticline is used as a gas storage facility.

Although data quality of reflections from the Precambrian is poor, the indication is that the Lyons anticline existed during the Late Proterozoic and that its initial uplift may be related to Keweenawan rifting. Cambrian–Ordovician Arbuckle Group reflections diverge away from the anticline, suggesting that deposition was contemporaneous with uplift. The Middle Ordovician Simpson Group and the Devonian–Mississippian Chattanooga Shale have distinctive reflection characters. Middle and Upper Ordovician Viola and Maquoketa Formations share a single response of a strong transitional, stretched, and positive-polarity peak.

Within the Chattanooga Shale is a thin limestone member which forms a distinct positive-polarity reflection. The limestone is seen to truncate over the crest of the Lyons anticline, and apparently thins eastward and is eventually replaced with siltstone.

In the Pennsylvanian, the Kansas City, Lansing, and Douglas Groups show a reflection aspect characteristic of a deposition system that is predominantly nonmarine clastic with an associated marginal-marine transport process. Reflections in the Shawnee Group have distinctive but modest amplitude and good continuity. Existence of a possible channel is apparent in the seismic response of the Kanwaka Shale. This feature would be rare to encounter and difficult to characterize if known only from drill data. In the Wabaunsee Group, the Howard Limestone forms a very prominent reflection.

The Lower Permian Admire, Council Grove, and Chase Groups have high-amplitude continuous reflections similar to the Wabaunsee, indicating lateral consistency across the section.

Introduction

Seven miles (11.2 km) of 12-fold MiniSOSIE (Barbier et al., 1976) seismic data were acquired during the summer of 1983 in Rice County, Kansas, along a line starting about 2 mi (3.2 km) south of the center of Lyons and proceeding eastward (fig. 1). Data-acquisition details are covered in table 1 and are discussed in Roehl et al. (1989). Reflections are detected to depths of approximately 3,500 ft (1,070 m) at times of 0.850 sec and correspond to Precambrian Rice Formation. Processing did not include migration.

Rice County is located on the western side of a broad structural saddle formed by the intersection of the Salina basin, the Central Kansas uplift, and the Sedgwick basin. Locally, geologic structures superimposed on the broad saddle generally strike north and north-northeast. The crest of the Central Kansas uplift is just west of the west edge of the seismic section. Deformation in the region began as early as Ordovician time and resulted in complex erosion, faulting, and folding, generally expressed as thickening and thinning and changing attitude of formations encountered in wells.

Uplift and erosion along the flanks of the ancestral Central Kansas uplift during Ordovician to Devonian time resulted in the removal of the Silurian–Devonian "Hunton" Group over much of Rice County and created a large valley named the McPherson Valley (Lee, 1956). Devonian–Mississippian Chattanooga Shale which fills the McPherson Valley reaches thicknesses in excess of 200 ft (61 m). Just west of the axis of the McPherson Valley is the Lyons anticline. This structure is one of a series of north-trending en echelon anticlines developed in western Rice County by accelerated deformation in Late Mississippian to Early Pennsylvanian time. Dip is variable on the east flank, but is, in general, about 2°. Reverse faulting on the west side of the anticline displaces lower Paleozoic strata in excess of 250 ft (75 m). This structure subcrops under the regional basal Pennsylvanian angular unconformity. Formerly a productive reservoir, the Lyons anticline is now used for storage of natural gas by Northern Natural Gas Co.

The original intent of the seismic line was to study the extent and character of a limestone bed within the Devonian–Mississippian Chattanooga Shale. Well log data indicate this limestone has a maximum thickness of about 70 ft (21 m) at the western edge of the section. It subcrops over the crest of the Lyons anticline and thins eastward from there. For further reference, fig. 2 shows the type log of Rice County.

Seismic Expression

General

The east-west seismic profile (fig. 3) runs roughly parallel to regional dip. Of particular interest in the area is the Lyons anticline centered at CMP 650, which is now used as a gas storage facility for Northern Natural Gas. Just east of the Lyons anticline is the McPherson Valley (Lee, 1956), beginning at CMP 680. These structures are particularly evident on fig. 4, a plot interpreted from well data with 5× vertical exaggeration. Several units, from the Cambrian–Ordovician Arbuckle Dolomite to Mississippian limestones, subcrop beneath a basal Pennsylvanian unconformity at about 0.600–0.630 sec (figs. 3b and 5). Likewise, there is a sub-Chattanooga unconformity where upper Ordovician Maquoketa Shale and middle Ordovician Viola Limestone subcrop (fig. 6).

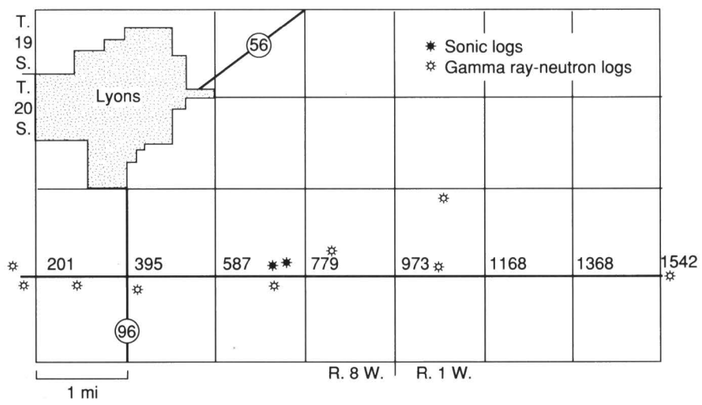

FIGURE 1—Location of Rice County seismic-reflection profile. CMP numbers are shown for each mile (section corner). CMP interval is nominally 27.5 ft (8.4 m).

Precambrian

The seismic response of the Precambrian section is poor, and reflections fade in and out with data quality (fig. 3A). The contact between Precambrian and Arbuckle dolomites is not seen on the section. Gravity and aeromagnetic information suggest that the top of the Precambrian in this area is Upper Keweenawan (Proterozoic) Rice Formation arkosic sandstones (Scott, 1966; Yarger, 1983; Yarger and Lam, 1982). According to COCORP results in northeastern Kansas (Brown et al., 1983; Serpa et al., 1984), this unit may contain few good reflectors. Thinning of a layer in the Rice Formation seen on the seismic section (fig. 7, CMP's 770–885, 0.800 to 0.840 sec) implies that the Lyons anticline existed during the Later Proterozoic with its initial uplift related to Keweenawan rifting.

Cambrian and Ordovician

The Cambrian–Ordovician Arbuckle Group is expressed seismically as a series of continuous, high-amplitude, parallel reflections (fig. 3, CMP's 185 to 290, 0.700 to ~0.800 sec and CMP's 730 to 780, 0.680 to ~0.800 sec). Divergence of the reflections away from the Lyons anticline suggests that deposition of the Arbuckle was contemporaneous with uplift of the anticline.

Above the Arbuckle, the seismic character of the Middle Ordovician Simpson Group is a trough of constant time thickness. It has a "noisy" character due to interbedding of shales, sandstones, and dolomites within the group. It is bracketed by strong positive-polarity peaks of the Middle Ordovician Viola above and Cambrian–Ordovician Arbuckle below. The Simpson Group response is distinguished from that of the lower part of the Devonian–Mississippian Chattanooga Shale because the seismic character of the Chattanooga Shale is a clean, relatively noise-free, trough event. The velocities of the Upper Ordovician Maquoketa are intermediate between the low-velocity Chattanooga above and the high-velocity Viola below. Consequently, the Maquoketa and Viola form a single response of a transitional, stretched (low apparent frequency) peak. This character is one of the strongest positive events on the section. The Maquoketa–Viola subcrops at the pre-Chattanooga unconformity at about CMP 690 (fig. 8). Figure 8 also illustrates the general seismic response of the Cambrian–Ordovician section.

Devonian and Mississippian

In this region, the Chattanooga Shale contains a thin limestone with a maximum thickness of about 70 ft (21 m) and thins eastward. Maximum thickness of the localized limestone within the Chattanooga (Lee, 1956) corresponds to the western edge of the seismic section. The limestone is missing under the eastern edge, being replaced by siltstones. The Chattanooga Shale is split into an upper and lower part by the limestone

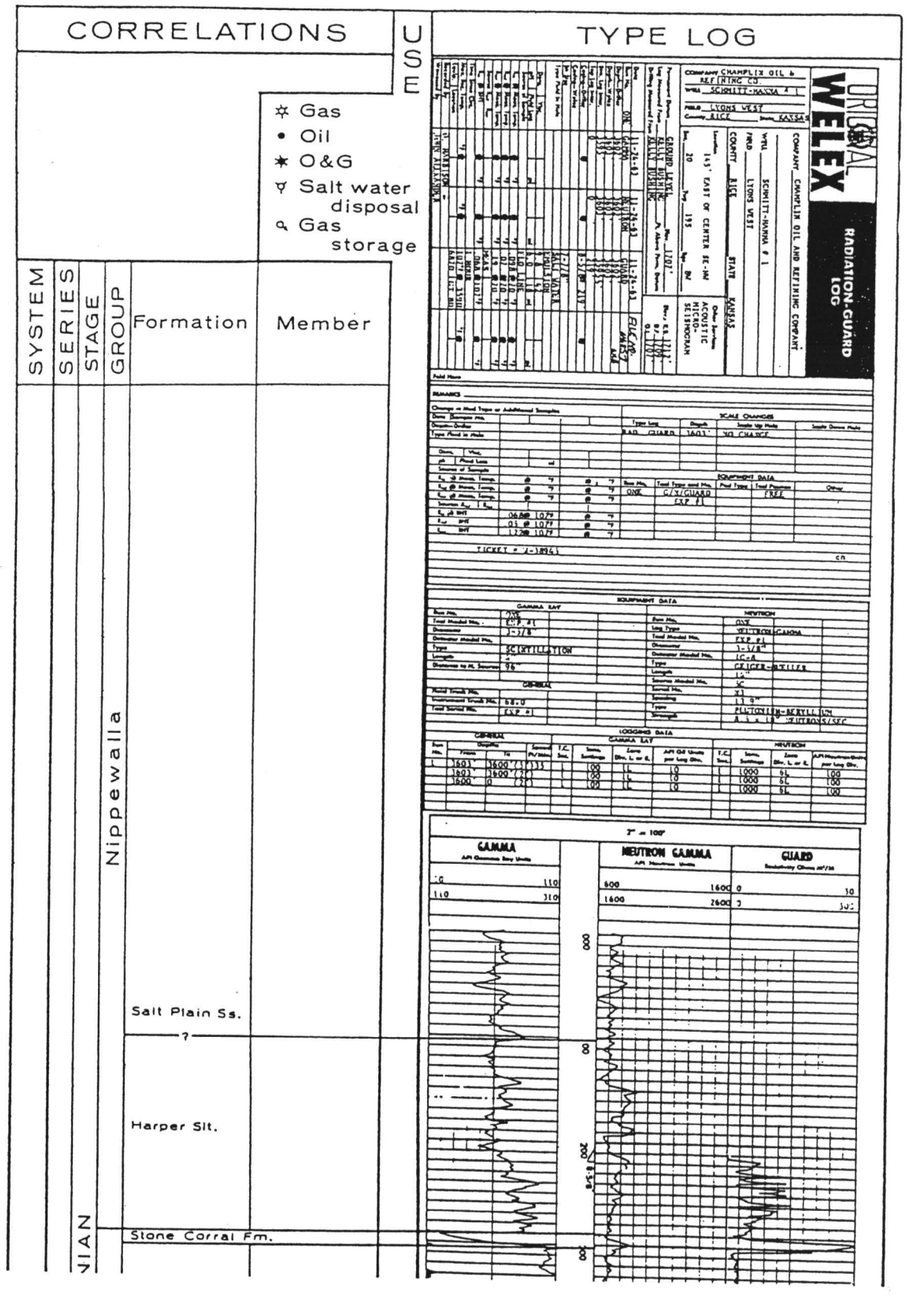

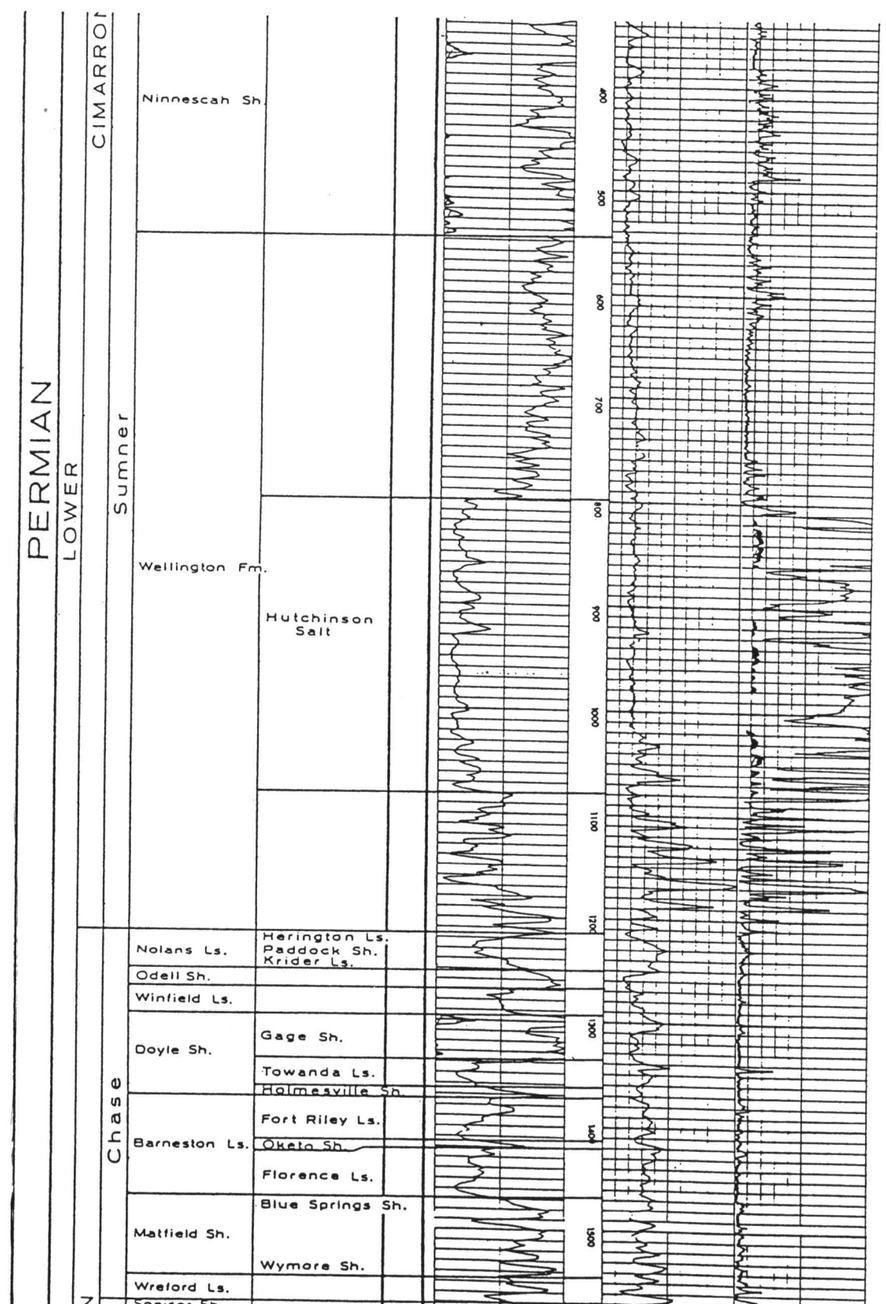

FIGURE 2—TYPE LOG OF RICE COUNTY, KANSAS (Harris et al., 1966).

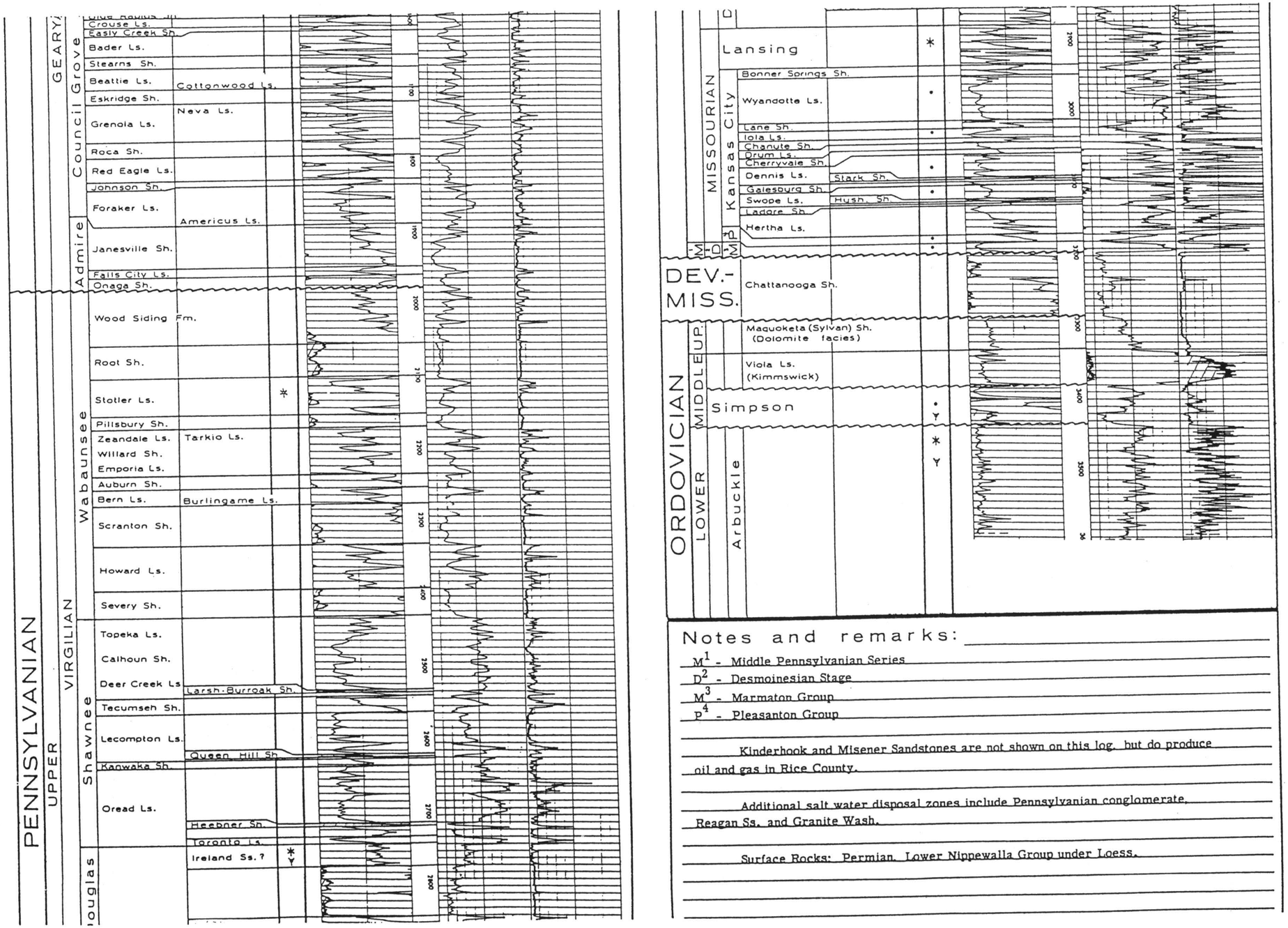

Notes and remarks:

M^1 - Middle Pennsylvanian Series
D^2 - Desmoinesian Stage
M^3 - Marmaton Group
P^4 - Pleasanton Group

Kinderhook and Misener Sandstones are not shown on this log, but do produce oil and gas in Rice County.

Additional salt water disposal zones include Pennsylvanian conglomerate, Reagan Ss. and Granite Wash.

Surface Rocks: Permian, Lower Nippewalla Group under Loess.

(Fig. 2 continued)

member. Throughout the section, the lower Chattanooga Shale maintains a constant time-thickness except where it is eroded over the Lyons anticline at the basal Pennsylvanian angular unconformity. The Misener Sandstone, the transgressive sandstone at the base of the Chattanooga Shale, is known from well control to be present in the vicinity of the Lyons anticline and westward from that point. Although it thins significantly eastward from the anticline, it is not seen in the seismic reflection character of the lower Chattanooga.

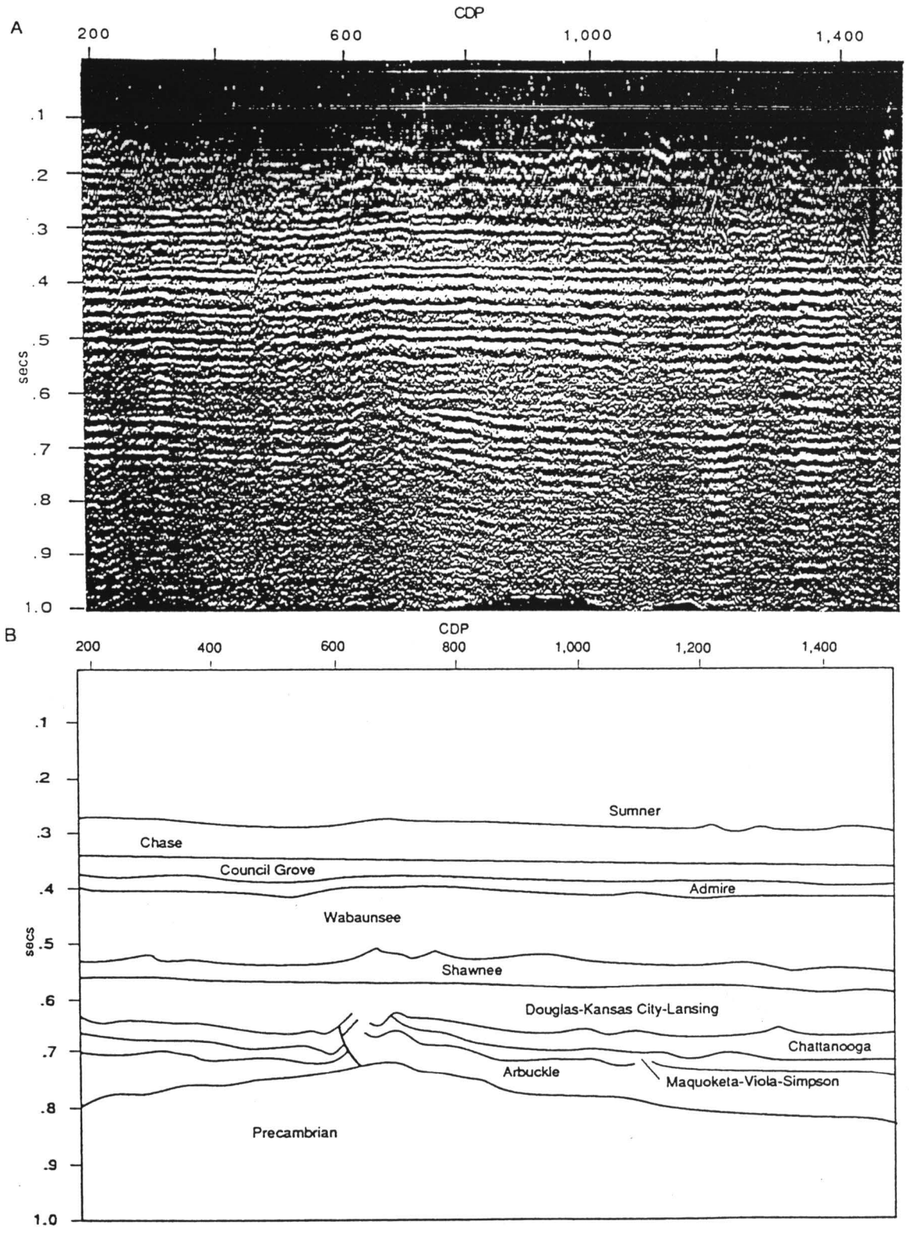

FIGURE 3—A) RICE COUNTY SEISMIC SECTION. B) GENERALIZED INTERPRETATION.

The Chattanooga limestone unit is one of the brightest positive-polarity reflections of the section where it is at its thickest, about 58 ft (18 m), at about CMP 800 (0.650 sec) (fig. 7). As the limestone thins eastward, the amplitude response dims. This is particularly apparent following the zones of excellent data quality (i.e., under CMP's 740–900, 1200–1240, and 1340–1420; figs. 8 and 9). Near CMP 1300 and eastward, the amplitude response of the Chattanooga limestone is very dim. It is either very thin or replaced with siltstone at this point. Westward of CMP 800 the Chattanooga limestone is locally truncated by erosion over the crest of the Lyons anticline. Westward from the Lyons anticline, the limestone member appears to thicken so as to be about the same thickness at CMP 300 as it is at CMP 800; i.e., it is about 58 ft (18 m), as estimated from amplitude response (fig. 3).

The upper Chattanooga Shale is expressed seismically as a broad pronounced trough. Eastward of CMP 1140, it begins to thicken dramatically. At CMP 1280 it bifurcates and a small intermediate peak (an artifact of the seismic wavelet) appears in its middle (fig. 9).

Pennsylvanian

The unconformity at the base of the Pennsylvanian is a low-amplitude event most easily identified by angular truncation of underlying strata. The Missourian-age Kansas City–Lansing and Virgilian-age Douglas Groups form a sequence of reflections having low amplitude and low continuity. This is probably indicative of parallel to slightly folded bedding that is characteristic of dominantly nonmarine clastic deposition by river currents and associated marginal-marine transport processes (Brown and Fisher, 1979). The interpretation is in general agreement with known stratigraphy of channel sandstones and shelf-margin limestone lenses and öolitic shoals that occur within these lower cyclothem units (Merriam, 1963). The Kansas City and Lansing Groups are composed primarily of limestone. Interbedded shales are too thin to be detected seismically. The Douglas Group is made up almost entirely of shales and channel sands. Similar to some of the interpretation given by Knapp and French (1991) and Knapp et al. (this volume, p. 53–56), marine limestone mounding, thin undetectable shales, and extensive erosional hiatuses combine to produce slightly chaotic, diffusive reflector characteristics for the given wavelength of the data, resulting in only nominal reflection amplitude for the three groups.

In the Shawnee Group (Virgilian), the Topeka and Lecompton limestones have modest-but-apparent seismic response. The intervening Calhoun Shale can be seen to vary across the section. Of particular interest in the Shawnee Group between CMP's 1330 and 1410 is a possible channel in the Kanwaka Shale (fig. 9). This anomaly helps illustrate the quality of the data.

In the Wabaunsee Group (Virgilian), the Howard Limestone forms one of the more prominent peaks on the section (fig. 9). Above the Scranton Limestone is the Stotler Limestone (fig. 10). Between these two limestones is a sequence of several discontinuous thin limestones and shales. In some cases interference of the reflections is constructive but in others it is destructive. The overall effect is a variable reflection character.

Permian

The Admire, Council Grove, and Chase Groups of the Lower Permian produce reflection configurations that are similar to the high-amplitude continuous reflections of

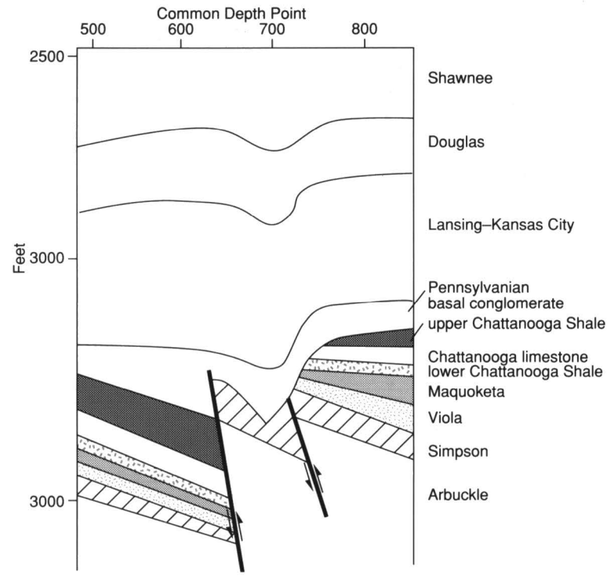

FIGURE 4—GEOLOGIC CROSS SECTION SHOWING PART OF LYONS ANTICLINE ALONG PART OF RICE COUNTY SEISMIC SECTION: 5× vertical exaggeration.

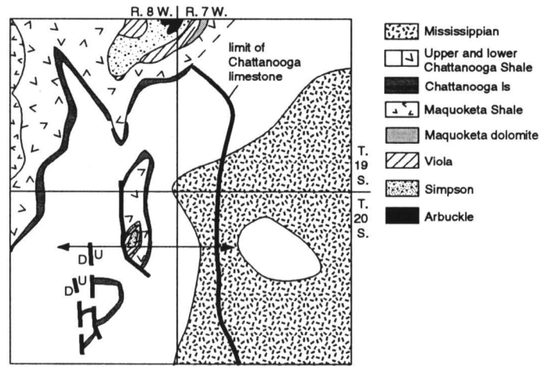

FIGURE 5—SUBCROP MAP AT THE BASAL PENNSYLVANIAN UNCONFORMITY. Heavy line indicates eastward extent of Chattanooga limestone unit within the Chattanooga Shale. Map is 12 × 12 mi (19.3 × 19.3 km). Location of the seismic line is marked by double-arrow line.

the Wabaunsee (fig. 10). Although individual thin beds may be unresolved, the high continuity of the reflections indicates lateral consistency of the reflectors across the section.

Summary and Conclusions

The seismic data basically confirm the interpretations derived from point-derived well geology. However, the continuity of the seismic line provides detailed resolution of the position and character of the stratigraphic and structural relationships. Reflectors of the Proterozoic Precambrian section are seen to have distinguishable characteristics that lend to the interpretation of structure and local stratigraphic continuity.

The growth history and geometry of the Lyons anticline is accurately expressed on the seismic section. The anticline was a large symmetric positive feature during Cambrian and Ordovician time and, perhaps, during late Precambrian. The crest was eroded prior to Simpson deposition, and growth was reactivated during Late Mississippian to Early Pennsylvanian as a smaller, asymmetrical, and highly folded and faulted positive feature. The basal Pennsylvanian angular unconformity truncates several lower Paleozoic units over the crest of the Lyons anticline.

The Chattanooga limestone is continuous across the section except where it subcrops at the Lyons anticline. It thins from west to east and is replaced in the vicinity of CMP's 1350 to 1360 by lithologies of lower seismic velocities (i.e., siltstones or shales).

Most resolvable Pennsylvanian and Permian cyclothems display consistent reflection character across the section, although bed thickness can be highly variable due to intercyclic erosion. In particular, the stratigraphic intervals between the Lecompton Limestone and the Calhoun Shale, and the Topeka Limestone and Severy Shale are very

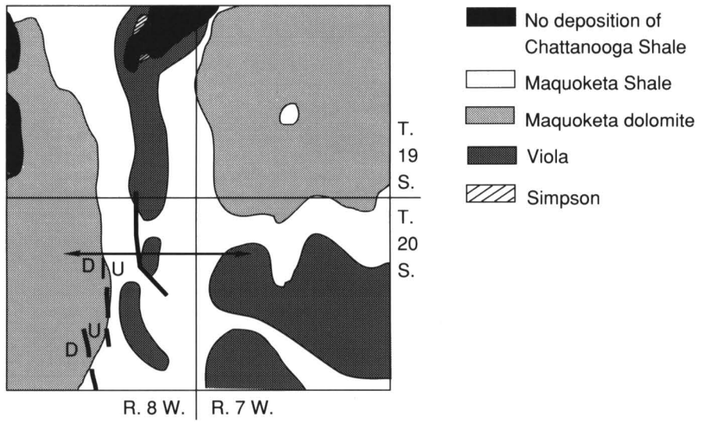

FIGURE 6—Subcrop map at the pre-Chattanooga unconformity. Dark areas indicate where Chattanooga Shale is absent due to later erosion at the basal Pennsylvanian unconformity. Subcropping Viola in the southeast quadrant of the map expresses the axis of the east-west-trending McPherson Valley. Map is 12 × 12 mi (19.3 × 19.3 km). Location of the seismic line is marked by the double-arrow line.

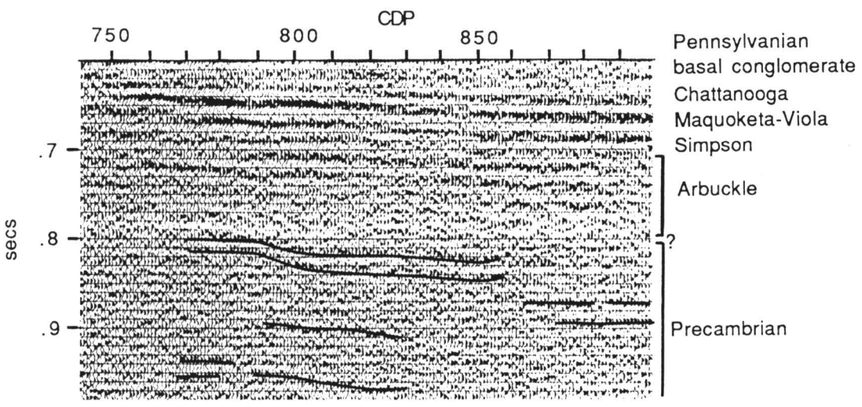

FIGURE 7—Detail of the Precambrian Rice Formation reflections between CMP's 740 and 900 (600–1,000 msec). Uplift of the anticline is indicated by dipping and thinning of the Rice Formation reflections.

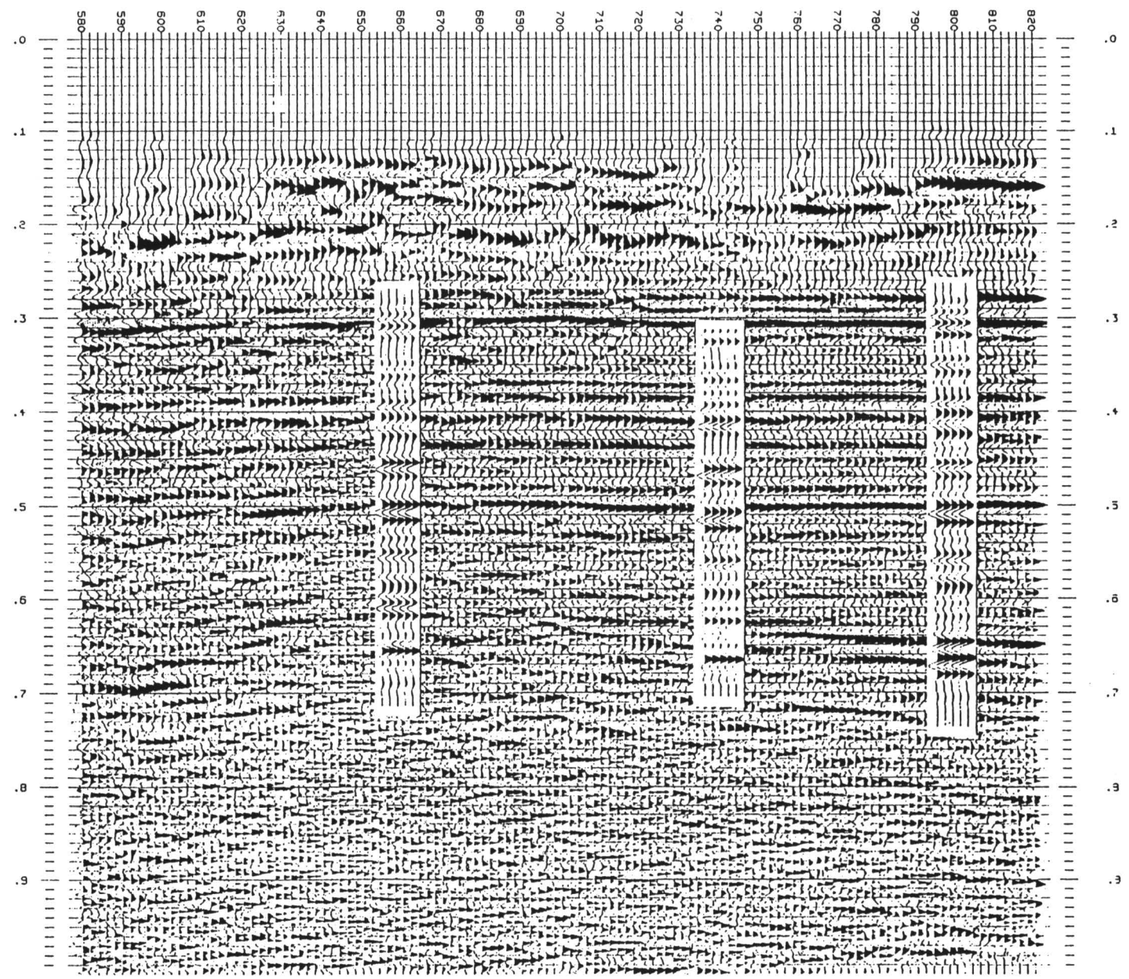

FIGURE 8—Detail in the vicinity of the Lyons anticline showing structures related to Late Mississippian–Early Pennsylvanian deformation. Correlation with three synthetic seismograms is shown.

TABLE 1—Seismic data-acquisition parameters.

Source type:	MiniSOSIE (Barbier et al., 1976) earth compactor
Vertical stack:	2,000 impulses/shotpoint
Record length:	1 second
Sample interval:	2 milliseconds
Source interval:	55 ft (17 m)
Source array:	55 ft (17 m) linear
Group interval:	55 ft (17 m)
Group array:	55 ft (17 m) linear
Recording geometry:	End-on, 24-channel, 12-fold CMP
CMP interval:	17.5 ft (8.4 m)
Near offset:	742.5 ft (226 m)
Far offset:	2,007.5 ft (612 m)
Filters:	low cut 55 Hz (24 dB/octave slope)
	high cut 125 Hz (24 dB/octave slope)
	notch 60 Hz (60 dB rejection)

variable. These thickness variations have short wavelengths and cannot be detected (or confirmed) by well control.

The advantage of the seismic detail is particularly illustrated by the display of the channel in the Kanwaka Shale. This channel is a potential producing reservoir, yet without the seismic line, detection by wells alone would have been solely by chance, and identification of its extent and character would have been impossible.

References

Barbier, M. G., Bondon, P., Mellinger, R., and Viallix, J. R., 1976, Mini-SOSIE for land seismology: Geophysical Prospecting, v. 24, p. 518–527

Brown, L., Serpa, L., Setzer, T., Oliver, J., Kaufman, S., Lillie, R., Steiner, D., and Steeples, D. W., 1983, Intracrustal complexity in the United States midcontinent—preliminary results from COCORP surveys in northeastern Kansas: Geology, v. 11., p. 25–30

Brown, L. F., and Fisher, W. L., 1979, Principles of seismic stratigraphic interpretation: American Association of Petroleum Geologists, table 5.2; *in,* Seismic Stratigraphy, R. E. Sheriff, ed. (1980): International Human Resource Development Corporation, Boston, p. 105–106

Harris, R. L., Stone, J. J., King, C. R., James, Alfred III, and Goebel, E. D., 1966, Type logs of Kansas, 1966, Rice County: Kansas Geological Survey

Knapp, R. W., and French, J., 1991, Features in Kansas cyclothems seen by high-resolution reflection seismology; *in,* Sedimentary Modeling—Computer Simulation and Methods for Improved Parameter Definition, E. K. Franseen, W. L. Watney, C. G. St.C. Kendall, and W. C. Ross, eds.: Kansas Geological Survey, Bulletin 233, p. 111–121

Lee, W., 1956, Stratigraphy and structural development of the Salina basin: Kansas Geological Survey, Bulletin 121, p. 1–151

Merriam, D. F., 1963, The geological history of Kansas: Kansas Geological Survey, Bulletin 162, 317 p.

Roehl, N. L., Knapp, R. W., and Newell, K. D., 1989, Seismic-reflection study in Rice County, Kansas; *in*, Geophysics in Kansas, D. W. Steeples, ed.: Kansas Geological Survey, Bulletin 226, p. 81–93

Scott, R. W., 1966, New Precambrian (?) formation in Kansas: American Association of Petroleum Geologists, Bulletin, v. 50, p. 380–384

Serpa, L., Setzer, T., Farmer, H., Brown, L., Oliver, J., Kaufman, S., Sharp, J., and Steeples, D. W., 1984, Structure of the southern Keweenawan rift from COCORP surveys across the Midcontinent Geophysical Anomaly in northeastern Kansas: Tectonics, v. 3, p. 367–384

Yarger, H. L., 1983, Regional interpretation of Kansas aeromagnetic data: Kansas Geological Survey, Geophysics Series 1, 35 p.

Yarger, H. L., and Lam, C., 1982, Gravity measurements in Kansas; *in*, Assessment of the Geothermal Resources of Kansas, D. W. Steeples and S. A. Stavnes, eds.: U.S. Department of Energy, Final report, Contract no. DE–AS07–79ET27204, p. 220–232

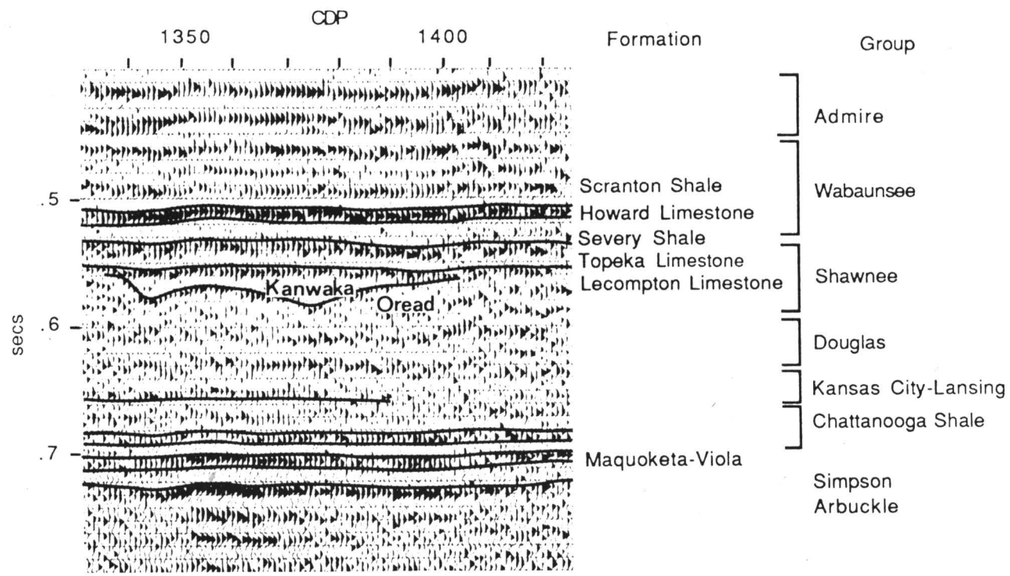

FIGURE 9—Detail of the eastern end of the seismic line showing stratigraphic relationships of Arbuckle through Wabaunsee Groups. Channel, presumably sand-filled, in the Kanwaka Shale shows erosion through several units to the Oread Limestone.

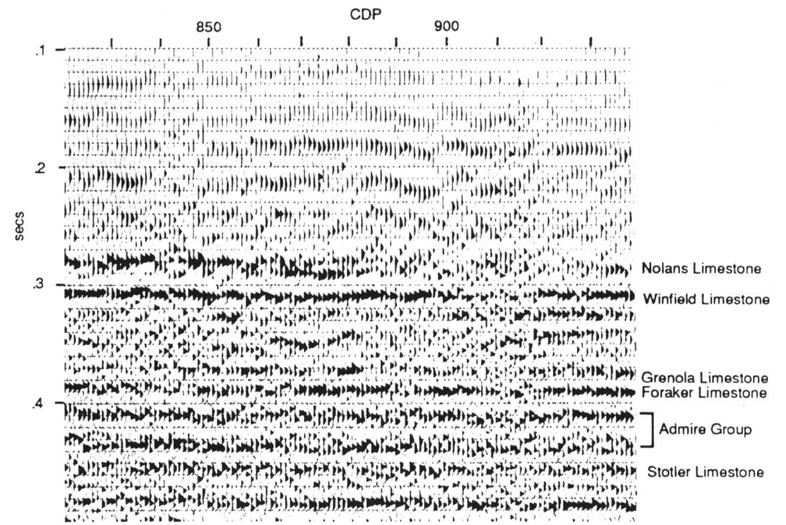

FIGURE 10—Detail showing stratigraphic relationships of Wabaunsee through Council Grove Groups. Interference patterns of thin shales and limestones create variable amplitude and character reflectors of the Admire Group and Foraker Limestone formation. The Nolan Limestone illustrates a stretched amplitude due to a transitional boundary.

Seismic Response of Pennsylvanian Cyclothems in Douglas County, Kansas

Ralph W. Knapp[1], W. Lynn Watney[2], and John A. French[1]
[1]formerly with the Kansas Geological Survey, The University of Kansas, Lawrence, KS 66047; and
[2]Kansas Geological Survey, The University of Kansas, Lawrence, KS 66047

Abstract

Middle and Upper Pennsylvanian cyclic sequences (cyclothems) in eastern Kansas are ineffectively imaged on standard petroleum-exploration reflection seismogram sections with frequency responses less than 80 Hz. The Kansas City and Lansing Groups, despite the number of interlayered high-contrast beds they contain, often cannot be distinguished and are grouped as a single characteristic response. However, the use of high-resolution reflection seismology, with dominant frequencies of 250–300 Hz and maximum frequencies to greater than 500 Hz, allows the detection of thin-bed units within the individual groups and formations to approximately 2-m thickness. Alternating thin limestones and shales that comprise cyclothems lead to resonance of the seismic wave. Geological cyclicity and reflection seismology harmonize, and carbonate units are recorded as peaks and siliciclastic units (mostly shales) are recorded as troughs. Further, seismic response is sensitive to such phenomena as the presence of intrabed sandstone lenses in shales and the surface roughness (diffusivity) of lithologic interfaces. The use of an instantaneous phase response display accentuates low-amplitude interbed features such as channels within sandstones and shales.

The ability of high-frequency seismic data to resolve features within the stratigraphically heterogeneous Pennsylvanian of eastern Kansas is demonstrated. To effectively image at the scale of variability of these strata (meters to tens of meters), resolution must be maximized and spurious noise minimized. Acquisition, processing, and display must all aim to this purpose. Small-scale features that are observed on a seismic section acquired across a geologically well-defined stratigraphic interval are documented, and observations of reflection character are correlated to observed geology.

Introduction

In 1986, a 70-m (230-ft)-long high-resolution seismic line was shot on the west campus of The University of Kansas (fig. 1). The data reveal a great deal about the seismic response of Kansas cyclothems. Details of the acquisition are published elsewhere (Knapp, 1988; Knapp and Müftüoglu, 1987; Knapp and Watney, 1987) and are summarized in table 1.

To detect thin beds requires short wavelengths (high frequencies). There is an inverse relationship between frequency content and thin-bed resolution (Knapp, 1990). The wavelength of frequencies in the wavelet must be within an order of magnitude of the thickness of a thin bed for detection to occur. Detection is maximized when bed thickness is one-fourth the wavelength of the dominant frequency. This is the tuning thickness (Widess, 1973). Dominant frequency is frequently about two-thirds of the maximum frequency contained in the wavelet-frequency bandwidth (Kallweit and Wood, 1982). Figure 2 shows that bed resolution improves dramatically with value of dominant frequency. In particular, with a dominant frequency of at least 200 Hz, detection of individual beds begins to occur. This is because tuning begins to occur at that point, at least for cyclic beds of the Upper Pennsylvanian in eastern Kansas. With frequencies of about 80 Hz or less ("typical" petroleum exploration data), reflection character associated with cyclothems has little to do with individual rock units. Rather, generalities are made about the groups, and, in particular, the Kansas City–Lansing Groups are typically paired as an event of some particular characteristic.

Seismic reflection is a differential process. That is, rather than being sensitive to lithologic processes, reflections are the consequence of changes (differences) in the acoustical impedance (product of density and velocity) of the rock. Because the seismic wavelet is band-limited, the reflection from an abrupt interface is smeared or spread in time. This dispersion is defined by vertical resolution (Knapp, 1990; Berkhout, 1984). Limitations in lateral resolution smear the horizontal character of the reflection response (Berkhout, 1984). Consequently, the vertical character of a reflection is modulated 1) according to the rate of lithologic change, i.e., vertical rate of change of the acoustic impedance and 2) according to the proximity of other reflecting surfaces that produce interfering reflections. Lateral changes in the reflector, such as reflection-surface roughness, likewise modulate the response at a reflection point; such effects are seen in these data. Migration, the correction of distortion due to reflector geometry, can correct for some of the problems of lateral interferences by removing the effects of diffractions and by moving reflectors to their correct position, but results are still strictly limited by lateral resolving power. Even migration reduces a point to what Claerbout (1985, p. 17) terms a "focus," i.e., a "point" with lateral and vertical dimension. For "layer cake" geology with smooth, thick-bed reflectors, the reflection character is regular and its amplitude and polarity represent the change in acoustic impedance. In this case, the results can be inverted to a geological interpretation with a maximum of ease, although calibration information is required. In general, however, reflection response is the complex interference of effects due to vertical and lateral geological changes. These effects limit interpretation capabilities.

Middle and Upper Pennsylvanian strata of eastern Kansas are characterized by cyclic lithologic sequences made up of alternating laterally persistent limestones, shales, and sandy shales. These cyclothems are typically 10–30 m (33–98 ft) thick, with individual members commonly less than a meter (3.3 ft) thick. Local development of sandstone channels and lenses, and coals is common in the thicker shales (Heckel, 1978; Heckel et al., 1979). Seismically, most beds appear as thin-bed responses (Knapp, 1990), corresponding to individual beds of limestone and shale. Consequently, the seismic section can be processed so that the shales appear as troughs and the limestones as peaks (fig. 3). Thickness cannot be directly measured but one can, in some cases, determine the thickness of a thin bed from its amplitude response (Widess, 1973) or its frequency (Knapp, 1990). The former method requires calibration by well log or other information and becomes unreliable when vertical or lateral changes of the reflector smear the response or when cyclothemic variation causes tuning of the reflector. The latter method depends on the cyclothemic tuning of the reflector and, depending on the degree of the tuning, may be very approximate. Both methods are employed to judge the thickness of a reflector bed.

Instantaneous phase emphasizes continuity of all reflectors, weak or strong. An important attribute of instantaneous phase is that amplitude is removed as a component, and reflectors, regardless of strength, have the same display weight. This is important in that a display of the recorded trace is scaled according to the amplitudes of the strongest reflections. CMP seismic data have a dynamic range of 40–60 dB (1:100 to 1:1000); a standard display has a dynamic range of about 20 dB (1:10). Accordingly, on a simple trace display, only the characteristics of the strongest reflections are obvious to the interpreter. This is important, of course, in terms of stratigraphic location and identification of marker horizons, but frequently it is the small subtle features and anomalies that are of true interest. The display of instantaneous phase enhances subtle features such as weak reflections and inflections on the stronger ones, and it is the most sophisticated of the devices one could employ to do so. Identification of relatively small-scale rock heterogeneity enhances the use of very high resolution seismic-reflection profiling for use in infracyclothemic seismic stratigraphic interpretation and use in near-surface reservoir analog investigations.

TABLE 1—Seismic-data acquisition parameters.

Source:	.50-caliber rifle fired into a auguered hole 30 in (76.2 cm) deep
Vertical stack:	1
Receivers:	Mark Products 40-D geophones, 100-Hz natural frequency, undamped
Arrays:	none, point source, and single geophone receivers.
Group interval:	2 m
Seismograph:	Input/Output DHR 2400, 24 channels
CMP stack fold:	12

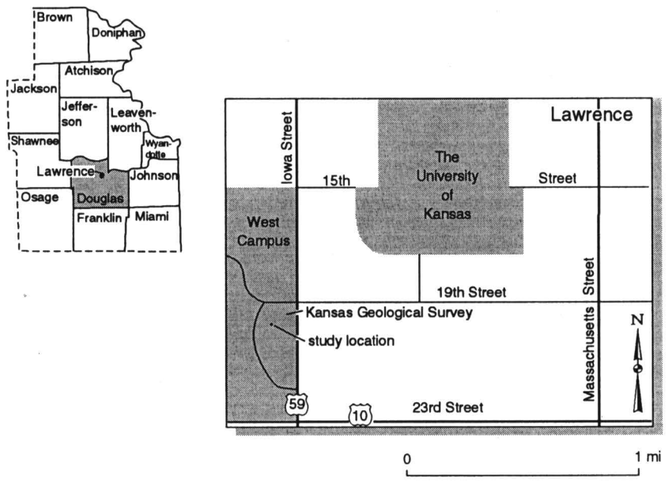

FIGURE 1—Location map of the seismic line. Total line length displayed in fig. 2 is 70 m (230 ft).

Instantaneous phase is determined from complex trace analysis (Taner et al., 1977). For smoothness, it is frequently the sine of the phase angle that is displayed. That is, values will vary from –1.00 (–90°, troughs) to +1.00 (+90°, peaks) with other angles cycling in-between.

Seismic Interpretation

The seismic section, correlated with a synthetic seismogram, and its general interpretation is shown on figs. 3 and 4. The synthetic seismogram is derived from a velocity log from a well about 10 km from the seismic line (DCL & FA #1, USGS–KGS, sec. 13, T. 12 S., R. 17 E., Douglas County). The fit is generally very good. Except for the lower Douglas Group, the response of the seismic section is one of thin beds where the troughs correspond to shales and the peaks to limestones. The general weakening of reflection strength with depth is due in part to distance from the surface and decreased signal-to-noise ratio, but also is due to a general decrease in reflection coefficient, i.e., changing geology from a carbonate rock-shale package in the Lansing, Kansas City, and Marmaton Groups above to a shaly sandstone-shale interval of the Cherokee Group below. Note the reduced contrast of the lithology below 150 msec, seen in the log of fig. 3. The reduction corresponds with the top of the Cherokee Group.

Stratigraphic nomenclature, which follows, is adapted from Watney et al. (1989).

Douglas Group (40 to 80 msec)

Only the lower half of the Douglas Group is recorded on the seismic section. The first strong reflector is the Haskell Limestone (47 msec), the basal member of the Lawrence Shale. The Haskell Limestone is 2 m (6.6 ft) thick and is displayed as a prominent peak. The remainder of the group is the Stranger Formation, the upper third of which contains very shaly sandstone and two thin coals. The two coals are the upper and lower Sibley coals. They are 0.3 m (1 ft) or less in thickness (Bowsher and Jewett, 1943), and they are resolved seismically as two distinctive troughs at 55 and 61 msec, respectively. It was demonstrated (Knapp and Müftüoglu, 1987) that despite the thinness of the coals, the acoustic-impedance contrast was great enough to cause a prominent reflection. They are easily detected. The lower two-thirds of the Stranger Formation is relatively clean Tonganoxie Sandstone.

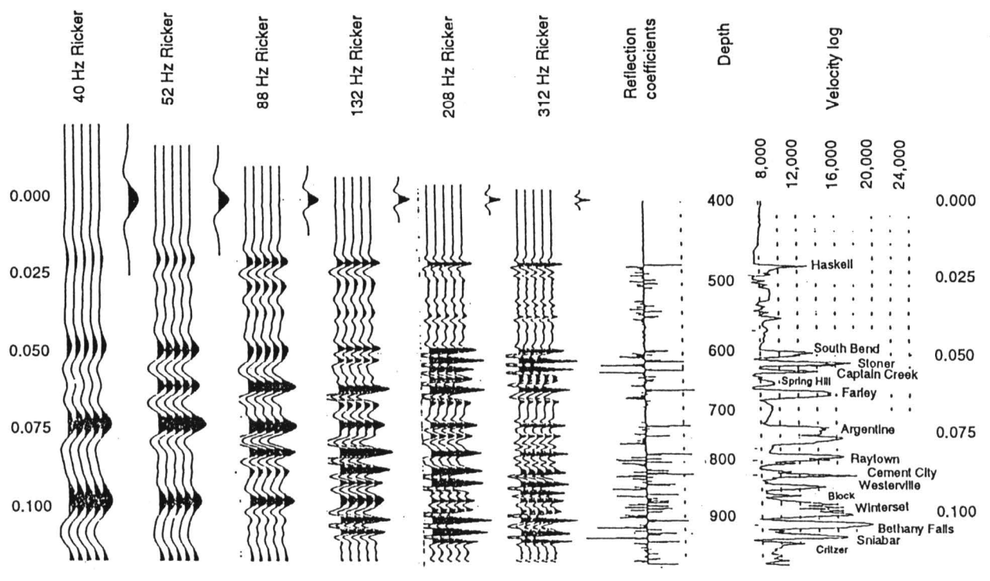

FIGURE 2—SYNTHETIC SEISMOGRAMS SHOWING THE RELATIONSHIP OF FREQUENCY AND BED DETECTION.

Sequence Stratigraphy of the Imaged Interval

The Tonganoxie Sandstone is a prominent fluvial to estuarine sandstone named after surface exposures near Tonganoxie, Kansas, in Leavenworth County (Moore et al., 1934), 20 km (12 mi) northeast of the seismic line. The sandstone from a core near the seismic line (KGS Fishpond #1) consists of 43 m (141 ft) of fine- to medium-grained crossbedded sandstone with rare thin shale and mudstone beds. This is the maximum known thickness of the sandstone. The city of Lawrence lies in a large buried valley in which the Tonganoxie Sandstone was deposited (Lins, 1950; Feldman et al., 1995). The valley cuts down from beneath the Haskell Limestone into the lower half of the Douglas Group and locally into the Stanton Limestone of the Lansing Group. The incised valley was mapped by Lins as 35 km (22 mi) wide near Lawrence along the outcrop belt and approximately 30 m (98 ft) deep.

The valley is generally filled to and beyond the valley walls with: 1) minor conglomerate at the base, 2) festooned cross stratified and massively bedded sandstone with abundant cut and fill structures, 3) thin-bedded argillaceous siltstone, sandstone, and silty shale, 4) silty shale and clay shale, and 5) coal (the upper Sibley coal which forms the uppermost bed of the Tonganoxie) (Lins, 1950). The coal can be correlated as essentially a continuous unit throughout the valley. Valley-fill strata beneath the coal range from amalgamated channel fills overlain by estuarine deposits while a marine limestone (Westphalia) overlies the coal (Lins, 1950; Feldman et al., 1995).

The Tonganoxie Valley trends northeast-southwest in the vicinity of Lawrence. A nearly continuous filled sandstone valley appears to have been mapped through the subsurface by Sanders (1959). The sandstone extends southward from Lawrence into southeastern Kansas until it crosses a carbonate shelf margin fringing the northern Arkoma basin. Several other elongate sandstone systems have been mapped by Sanders (1959) and Winchell (1957).

These sandstones apparently merge with the sheetlike Stalnaker sandstone in southern Kansas. The Stalnaker is located at a stratigraphic position equivalent to limestones in the Lansing Group (Winchell, 1957). The Stalnaker sandstone is interpreted as a lowstand deposit situated in the northern end of the Arkoma basin. Valley incision of the shelf to the north occurred during lowstand deposition. The Tonganoxie Valley in the Lawrence area, some 175 km (109 ft) from the shelf margin was progressively filled with sandstone, shale, coal, and eventually capped by marine limestone (Haskell Limestone) during a regional sea-level rise. The Haskell Limestone is a nearly continuous marker on both the shelf and basin in the northern midcontinent, reflecting regional base-level rise.

The underlying more regular carbonate-dominated cyclothems of the Lansing Group appear to have been deposited during a higher stand of sea level. Perhaps the siliciclastics of the Douglas Group, were better able to prograde out onto what was the carbonate platform when sea level was lower. In addition, lower stands of sea level probably encouraged valley incision such as the Tonganoxie Valley on the shelf (Watney et al., 1992). Uplift may have been responsible for both the fall in relative sea level and for introduction of the siliciclastics. However, cyclothems in the midcontinent can be correlated to equivalent cycles in western Kansas and on the Texas shelf (Boardman and Heckel, 1989; Watney et al., 1991) suggesting regional processes were important. Local expression of cyclicity may have been affected by local tectonism and sediment supply.

Instantaneous Phase

The instantaneous phase display (fig. 5) has removed the factor of amplitude (i.e., reflection strength) from the data; all reflections have the same display weight, regardless of strength. Figure 5 shows clearly the lateral continuity of the Haskell Limestone but, most importantly, shows internal channel structure within the Tonganoxie more clearly than the regular seismic trace section of fig. 3.

Lansing–Kansas City Groups (80–145 msec)

Particularly prominent in the Lansing–Kansas City Groups are the reflections of the Stanton Formation limestones (80–89 msec) and the Liberty Memorial Shale–Raytown Limestone combination (116 msec). Other prominent events include the Chanute Shale (120 msec) and the Bethany Falls Limestone–Hushpuckney Shale–Elm Branch Shale combination (135 msec).

In the Stanton Formation only the Stoner and Captain Creek Limestones are strongly detected (two peaks at 85 and 88 msec, respectively). The South Bend Limestone (81 msec) and the Rock Lake Shale have been cut by the Tonganoxie channel north of CMP 225, 253–260, and 275–280. The nature of the contact is prominently displayed on the instantaneous-phase section (fig. 5). The uniform, sandstone-free Eudora Shale (trough at 87 msec) contributes to the power of the reflector. Figure 5 shows the flatness of the reflecting surface at the top and bottom of the Stoner Limestone and the top of the Captain Creek. At almost 2-m (6.6-ft) thickness, the Eudora Shale can be considered to be a relatively thick bed because of its slow velocity. Because the limestones of the Stanton Formation are nearly twice as thick as the Eudora Shale and because their velocity is about twice as much, the wavelength thickness is equal for all three beds. This makes the situation for tuning nearly perfect; hence, the powerful, ringy result of about 300 Hz. This frequency response is exactly consistent with limestone thickness of 4 m (13 ft) and shale thickness of 2 m (6.6 ft). Tuning thickness (Widess, 1974) is one-fourth of the wavelength ($\lambda = V/f$). For the shale, .25 λ = 2 m = 2,400 m/sec/300 Hz; for the limestone, 0.25 λ = 4 m = 4,800 m/sec/300 Hz.

The sandstone- and siltstone-rich Vilas (95 msec) and Bonner Springs (102 msec) Shales are easily resolved on the amplitude and instantaneous phase sections (figs. 3 and 5). There is a strong lack of lateral continuity in the troughs of these reflectors. Both shales contain lenticular beds of siltstone and sandstone in nearby outcrops (Watney et al., 1989) Other than those two shales, the section is fairly laterally coherent to the Pleasanton Group beneath 140 msec.

The Cement City Limestone (118 msec), only 2 to 3 m (6.6–9.8 ft) thick, is a prominent reflector. Its frequency response (about 300 Hz) is consistent with its thickness. The Westerville Limestone (123 msec) is about 1 m (3.3 ft) thick, and waxes and wanes in strength across the section. (The unit is noted for local thickening up to 6 m (20 ft) due to grainstone buildups.] Its detection is marginal, and it represents the limit of detection for these data. The Westerville Limestone is a high-frequency event because it is so thin, and it is a low-amplitude event because it is thinner than the tuning thickness. Here, its apparent frequency is about 500 Hz. A limestone tuned to that frequency would have a thickness of about 2.4 m (7.9 ft). Amplitude response of the Westerville is about half the tuning amplitude; thus, its thickness is about half, i.e., 1.2 m (3.9 ft), or so. The Westerville interval displays good continuity in phase (fig. 5), despite its lateral variation in amplitude.

The reflections due to the Springhill (94 msec) and Argentine (106 msec) limestones are notably weaker on the seismic section than on the synthetic seismogram. The synthetic seismogram shows that according to vertical velocity contrast, these limestones should show strong positive reflectors. The seismic sections show very weak reflectors in their locations. The surfaces of these reflectors are known to have rough and diffusive surfaces in contrast to many of the other reflectors that are known to have flat, smooth surfaces (Knapp and French, 1991). The rugosity of the surfaces is due to subareal exposure, and the resulting roughness mutes reflection strength (Knapp, 1991). Diffusivity is a lateral effect, not a vertical effect, so it is not seen on the vertical sonic log. The anomalous response of the seismic section with respect to synthetic seismogram is diagnostic of lateral influence on the seismic data.

In all fairness, in this case, laterally variable sandstone content of the Vilas and Island Creek Shales is also a potential contributor to the observation. A lenticular crinoidal grainstone (sand-sized carbonate rock) ranging from 0 m to 1 m (0 ft–3.3 ft) in thickness is present at the base of the Island Creek Shale in nearby surface exposure (Watney et al., 1989). The grainstone rests on the Argentine or is separated from the Argentine Limestone by less than 0.5 m (1.6 ft) of shale. Similar lateral variations would variably attenuate the amplitude of the reflections along this surface.

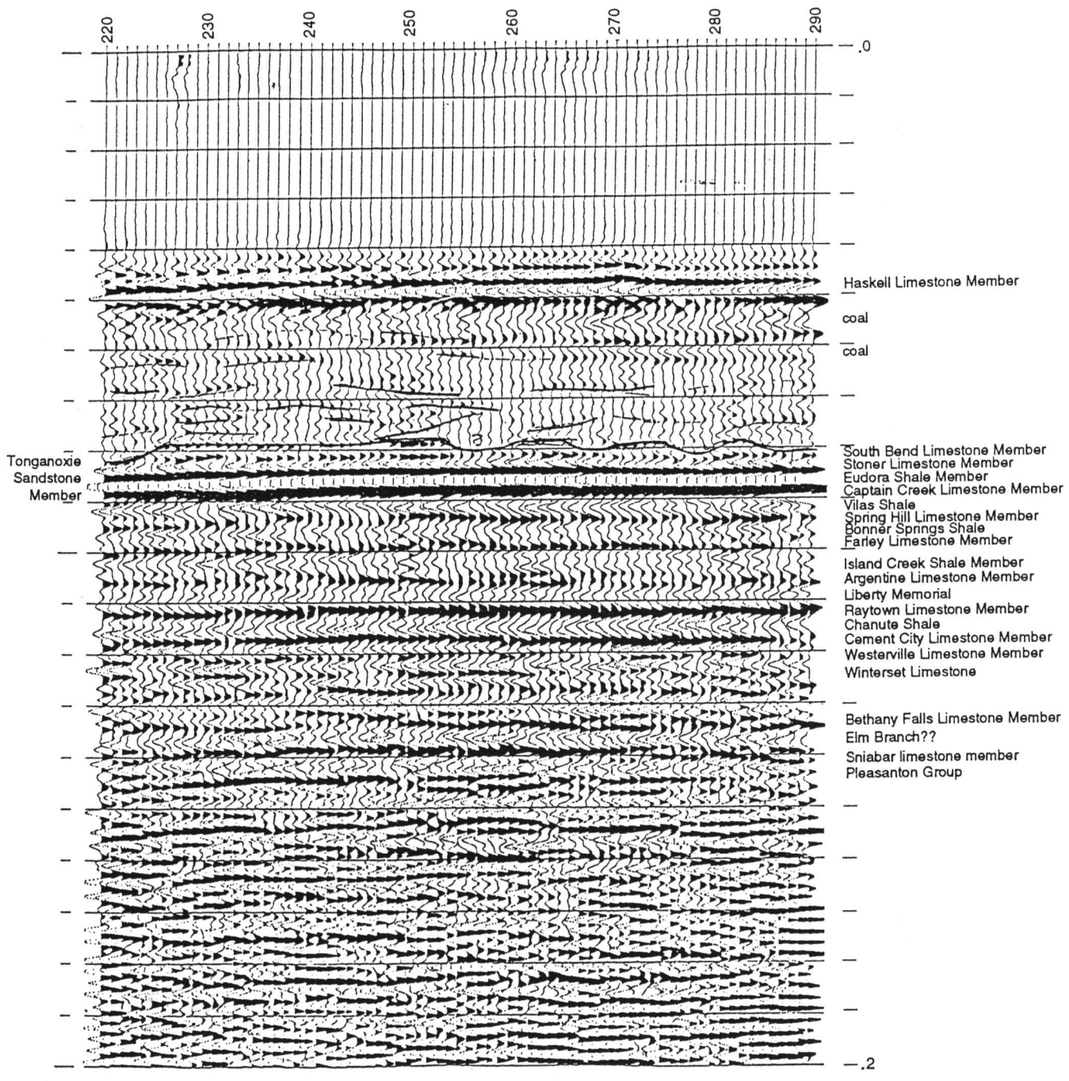

FIGURE 3—Seismic section acquired on west campus of The University of Kansas. Correlation with stratigraphic section from the area lines up peaks with limestones. Approximate depth in meters is given right of the section.

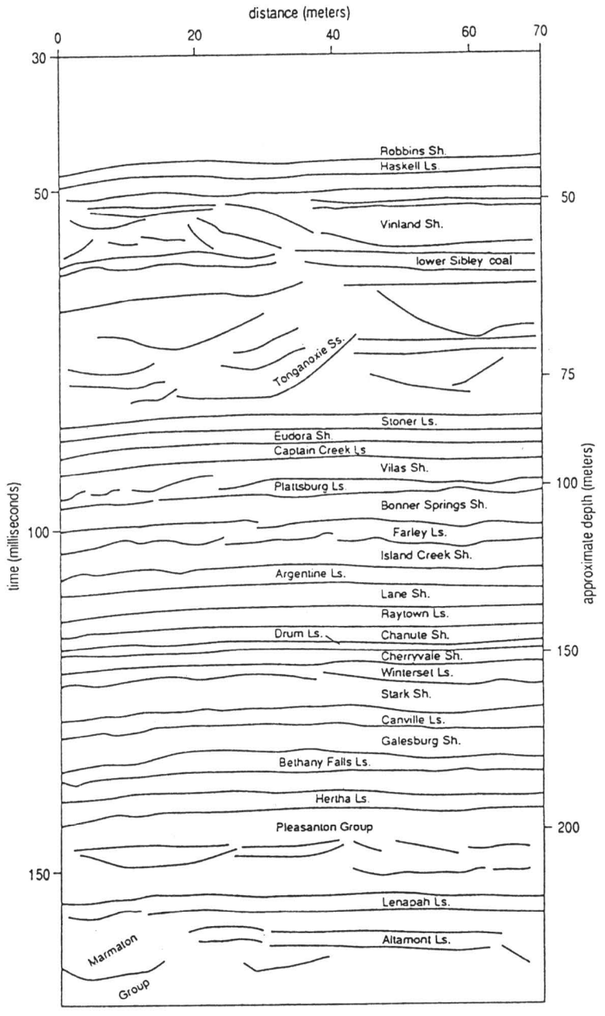

FIGURE 4—Interpretation of the seismic section of fig. 3.

Conclusions

The seismic-reflection response of the cyclothems of eastern Kansas to frequencies in the pass band of about 100 Hz to more than 500 Hz tends to tune to the thickness of the beds. Although Middle and Upper Pennsylvanian cyclothems of eastern Kansas are basically interbedded limestones and shales, and the seismic response is one of peak and trough for the cycle, the high-resolution seismic interpretation of their response is not quite that simple.

Reflection strength depends not only on rock contact type (i.e., shale-limestone and bed thickness), it depends also on the nature or diffusivity of the contact and/or on the presence of laterally irregular sandstone lenses and channels in the overlying shale. Clean shales and flat contacts result in strong reflectors. In this case, the actual strength and frequency response of the reflection depends on bed thickness. Rough contact surfaces and sandstone channels in the overlying shale can virtually obliterate a limestone reflector. In the cases seen with Bonner Springs and Vilas Shales, both conditions existed at the same time, so it is difficult to separate the effects.

Instantaneous phase specifically highlights the existence of lateral discontinuity. Emphasized in this process are coherent-but-curved "channel-looking" features and broken chaotic patterns suggesting lenticular or channel-form strata. In the display of instantaneous-phase, internal channel-form structures within the Tonganoxie Sandstone are more clearly seen, and the presence of sandstone lenses within the Vilas and Bonner Springs Shales is inferred as seen in nearby surface exposures of these strata. The high-resolution seismic section provides information about the sandstone content and uniformity of a shale. This determination is enhanced with instantaneous phase which is sensitive to low-amplitude reflections and lateral discontinuity. Instantaneous frequency demonstrates a realistic relationship between frequency value and thin-bed thickness when interval velocity is known. This property takes advantage of the tuning of the thin-bed cyclothems described by Knapp (1990).

The seismic section contains information about the lateral variability of the shale-limestone contact. From this, inferences can be made as to whether the bed surface was exposed to dissolution or erosion during subareal exposure or other processes that would have roughened the surface. The inhomogeneity of strata on top of a reflector surface such as sandstone in shale can also vary the seismic response by decreasing the sharpness of the reflection response. These observations show reasons why synthetic seismograms may fail to fit observed seismic data. Seismic reflections are affected by this lateral variability of the surface, whereas the synthetic seismogram is not. The effect of lateral discontinuity becomes more prominent at high frequencies (short wavelengths) because as wavelength approaches the dimensions of roughness, then diffusivity ceases to be negligible. Although lateral variation is observable on seismic data, as Knapp (1991) points out, it is difficult to characterize what is causing the observed result because of the smoothing or averaging effects of both the vertical and lateral wavelets.

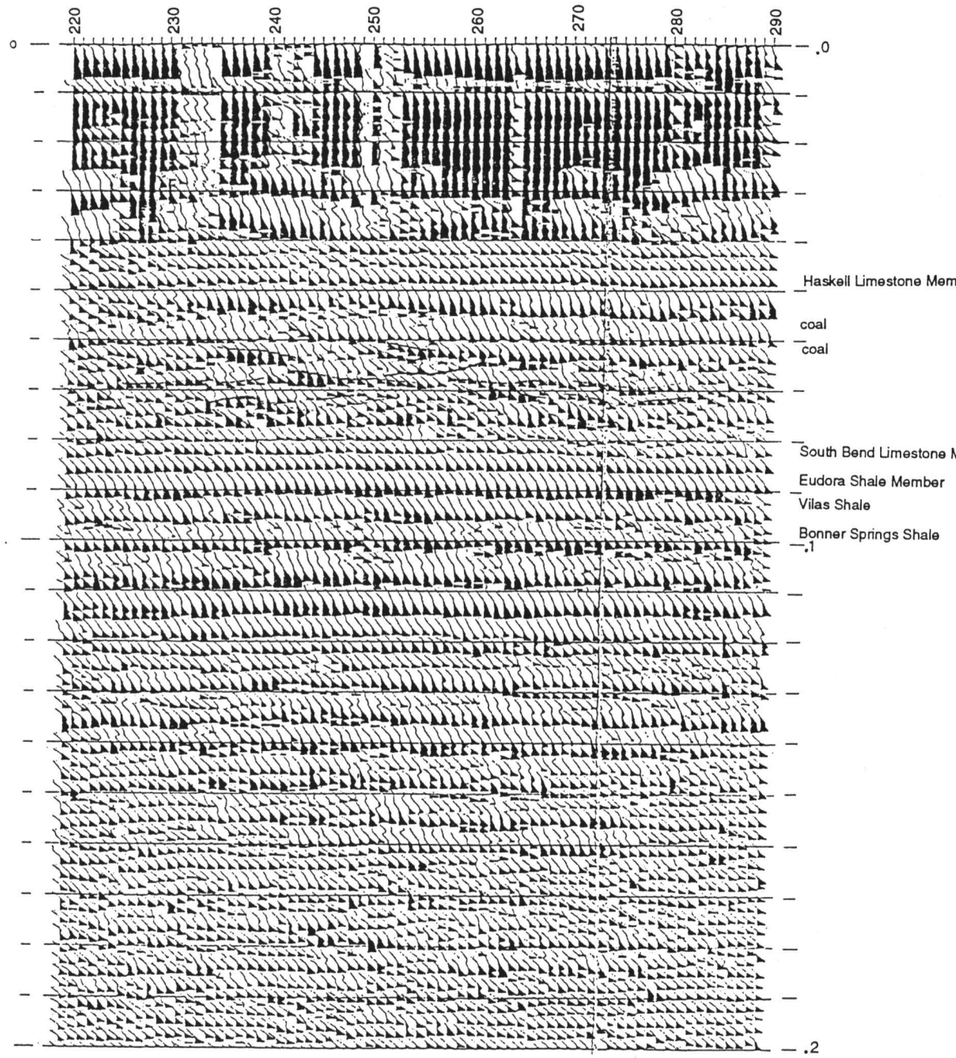

FIGURE 5—INSTANTANEOUS-PHASE DISPLAY.

Resolution power of the section is indicated by the clear resolution of the upper and lower Sibley coal, about 0.3 m (1 ft) thick each, at depths of about 50 m and 60 m (164 ft and 197 ft), respectively. Given the strength of the reflection from the 2-m (6.6-ft)-thick Haskell Limestone, it is evident that reflections from limestones thinner than 1 m (3.3 ft) are not difficult to detect in the shallow part of the section. In the deeper part of the section, the limits of detection are defined by the marginal detection of the Westerville Limestone, which is 1 m (3.3 ft) thick, at a depth of about 160 m (525 ft).

The seismic profile permits resolution of individual limestone and shale members of formations comprising the Lansing and Kansas City Groups. Thinner marine shales (condensed sections) such as the Hushpuckney and Stark shales are not seen except when the marine shale is thicker than 2 m (6.6 ft), e.g., Eudora Shale. Similarly, the transgressive limestones (flooding unit) are generally not resolved on the seismic profile due to thinness and proximity to the overlying highstand carbonate unit.

The Douglas Group presents a different type of geology with laterally discontinuous, lenticular and channel sandstones, thin limestones, and coal. The section imaged below the Haskell Limestone is situated in an incised valley filled primarily with Tonganoxie Sandstone overlain by a shale capped by the upper Sibley coal. Interval stratification probably representing some of the larger cut and fill structures in the Tonganoxie are clearly visible as well as the low-impedance coals.

Valley-fill sandstones of Morrow (Lower Pennsylvanian) age are important reservoirs in western Kansas. These results suggest that further studies of near-surface sites of these valley-filled sandstones may provide useful, cost-effective means of developing three-dimensional reservoir analogs.

ACKNOWLEDGMENTS—Ertan Müftüoglu aided in the acquisition of these data. He assisted on the crew while Jeff Treadway manned the seismograph. Ertan also did much of the work on whether or not we were detecting the Sibley coals. Brian Stephens aided in the initial interpretation of the data by helping with the correlation of the seismograms with well logs.

References

Berkhout, A. J., 1984, Seismic resolution: Geophysical Press, 228 p.

Boardman, D. R., II, and Heckel, P. H., 1989, Glacial-eustatic sea-level curve for early Late Pennsylvanian sequences in north-central Texas and biostratigraphic correlation with curve for midcontinent North America: Geology, v. 17, p. 802–805

Bowsher, A. L., and Jewett, J. M., 1943, Coal resources of the Douglas Group in east-central Kansas: Kansas Geological Survey, Bulletin 46, 94 p.

Claerbout, J. F., 1985, Imaging the earth's interior: Blackwell Scientific Publications, 398 p.

Feldman, H. R., Gibling, M. R., Archer, A. W., Wightman, W. G., and Lanier, W. P., 1995, Stratigraphic architecture of the Tonganoxie paleovalley fill (Lower Virgilian) in northeastern Kansas: American Association of Petroleum Geologists, Bulletin, v. 79, no., 7, p. 1,019–1,043

Heckel, P. H., 1978, Upper Pennsylvanian cyclothemic limestone facies in eastern Kansas: Kansas Geological Survey, Guidebook Series 2, 79 p.

Heckel, P. H., Brady, L. L., Ebanks, W. J., and Pabian, R. K., 1979, Pennsylvanian cyclic platform deposits of Kansas and Nebraska: Kansas Geological Survey, Guidebook Series 4, 79 p.

Knapp, R. W., 1988, High-resolution seismic data of Pennsylvanian cyclothems in Kansas: The Leading Edge, v. 7, no. 11, p. 24–27

_____, 1990, Vertical resolution of thick beds, thin beds, and thin-bed cyclothems: Geophysics, v. 55, no.9, p. 1,184–1,191

_____, 1991, Effects of surface roughness on migration—lateral and vertical resolution: 2nd Congress of the Brazilian Geophysical Society, Salvador, Bahia, Brazil

Knapp, R. W., and Müftüoglu, A. E., 1987, Detection of 30-cm-thick coals at depths of 50 and 60 meters by seismic reflection profiling: Society of Exploration Geophysicists, 57th Annual International Meeting and Exposition, Expanded Abstracts, p. 227–228

Knapp, R. W., and Watney, W. L., 1987, Seismic identification of Pennsylvanian cyclothems beneath Lawrence, Kansas: Society of Exploration Geophysicists, 57th Annual International Meeting and Exposition, Expanded Abstracts, p. 338–341

Knapp, R. W., and French, J., 1991, Features in Kansas cyclothems seen by high-resolution seismology; *in*, Sedimentary Modeling— Computer Simulation and Methods for Improved Parameter Definition, E. K. Franseen, W. L. Watney, C. G. St.C. Kendall, and W. C. Ross, eds.: Kansas Geological Survey, Bulletin 233, p. 111–121

Lins, T. W., 1950, Origin and environment of the Tonganoxie Sandstone in northeastern Kansas: Kansas Geological Survey, Bulletin 86, pt. 5

Moore, R. C., Elias, M. K., and Newell, N. D., 1934, Pennsylvanian and Permian rocks of Kansas: Kansas Geological Survey, Chart

Sanders, D. T., 1959, Sandstones of the Douglas and Pedee Groups in northeastern Kansas: Kansas Geological Survey, Bulletin 134, pt. 3, p. 125–159

Taner, M. T., Koelher, F., and Sheriff, R. E., 1979, Complex seismic trace analysis: Geophysics, v. 44, no. 6, p. 1,041–1,063

Watney, W. L., French, J. A., and Franseen, E. K., 1989, Sequence stratigraphic interpretations and modeling of cyclothems: Kansas Geological Society, Guidebook, 41st Annual Field Trip, 211 p.

Watney, W. L., Wong, J. C., and French, J. A., 1991, Computer simulation of Upper Pennsylvanian (Missourian) carbonate-dominated cycles in western Kansas; *in,* Sedimentary Modeling—Computer Simulations and Methods for Improved Parameter Definition, E. K. Franseen, W. L. Watney, C. G. St.C. Kendall, and W. C. Ross, eds.: Kansas Geological Survey, Bulletin 233, p. 415–430

Watney, W. L., French, J. A., Wong, J. C., Feldman, H. R., Franseen, E. K., and Guy, W. J., 1992, Sequence stratigraphy and stratigraphic modeling for improved understanding of midcontinent Paleozoic reservoirs (abs.): American Association of Petroleum Geologists, Bulletin, v. 76, no. 8, p. 1, 289

Widess, M. B., 1973, How thin is a thin bed?: Geophysics, v. 38, no. 6, p. 1,176–1,180

Winchell, R. L., 1957, Relationship of Lansing Group and the Tonganoxie ("Stalnaker") Sandstone in south-central Kansas: Kansas Geological Survey, Bulletin 127, pt. 4, p. 123–152

Seismic Signature of the Hutchinson Salt and Associated Dissolution Features

Neil L. Anderson[1], W. Lynn Watney[2], P. Allen Macfarlane[2], and Ralph W. Knapp[3]
[1]Department of Geology and Geophysics, University of Missouri–Rolla, Rolla, MO 65401; [2]Kansas Geological Survey, The University of Kansas, Lawrence, KS 66047; and
[3]formerly with Kansas Geological Survey, The University of Kansas, Lawrence, KS 66047

Abstract

The Hutchinson Salt Member of the Wellington Formation (Permian) is preserved throughout central and south-central Kansas as a more-or-less continuous body with net thicknesses of up to 560 ft (170 m). This salt has been extensively dissolved along its eastern margin due to contact with unconfined, undersaturated ground water during the Tertiary, Quaternary, and present. West of the main dissolutional edge, localized salt solution is occurring, probably associated with subsurface ground-water flow focused along structural conduits such as fractures and faults. Such solution has occurred in the past and in some areas is presently occurring.

In those areas where dissolution and associated deformation has not occurred, the Hutchinson Salt can generally be mapped on seismic data. Exceptions occur in those areas where the salt is too thin to be resolved given the effective bandwidth of the seismic data. Undeformed salt does not appreciably degrade the quality of seismic events of deeper origin.

In contrast, in those areas where significant leaching has occurred, the Hutchinson Salt can be difficult to map seismically. The reflection from the top of the remnant salt can be difficult to correlate as a result of excessive curvatures and surface irregularities, lateral variations in acoustic-impedance contrast, and superposed diffractions emanating from salt-related collapse features. The intra-salt and base salt events can be masked by diffractions as well as velocity-generated time-structural relief.

The recognition of velocity-generated time-structural relief along pre-salt events is particularly critical to the petroleum explorationist. It is imperative that the industry interpreter differentiate real structure from apparent structure on seismic data to preclude the possibility of drilling into non-existent structural closure along pre-salt horizons. The explorationist working in Kansas should be aware of the distribution of subsurface salts and the potential for leaching.

Introduction

The Hutchinson Salt Member (fig. 1) has been extensively dissolved along its eastern margin due to contact with unconfined, undersaturated ground water during the Tertary, Quaternary, and present. West of the main dissolutional edge, localized salt solution has occurred in the past and in some areas is presently occurring. Such sites are characterized by surface sinkholes and/or subsurface cavities. The more recent sinkholes (formed in the last last 100 years) are often associated with either salt mining or saltwater disposal and in some instances surface expressions developed in a matter of only hours or days (Walters, 1978). With respect to sinkholes of anthropogenic origin, it appears that the dissolution rate has been appreciably increased where boreholes penetrating the salt allow water to enter the salt beds, especially when surface meteoric water can pass through the salt into lower strata. Cavity formation may be substantial where the boreholes pass through or very near geologic structures that allow subsurface waters to naturally enter and dissolve the salt beds. The collapse of cavities as a result of salt dissolution in the subsurface has caused either gradual or catastrophic subsidence at ground level, and therefore has significant financial, environmental, and public safety implications.

Hutchinson Salt

The lower Leonardian Wellington Formation is the lowest unit of the Sumner Group, consisting of three members: a lower member of cyclic anhydrites and shale, the Hutchinson Salt, and an unnamed upper shale (Dellwig, 1963; Norton, 1939). The Wellington Formation is transitional between the cyclic marine limestone, dolomite, shale, and siltstone in the underlying Wolfcampian (Lower Permian) Chase Group and the overlying red-bed evaporites of the Ninnescah Shale and Stone Corral Formation. The overlying Ninnescah Shale is disconformable with the Wellington Formation in northern Kansas (Rascoe, 1968).

The Lower Leonardian-age Hutchinson Salt is a cyclic shelf deposit that accumulated on the northeastern extremity of an extensive evaporite facies tract, the southern edge of which is in West Texas (fig. 1). A belt of open and restricted shelf-margin and shelf carbonates of the Wichita Group lies south of the evaporite facies tract, rimming the northern edge of the Midland basin, then occupied by a deep Permian seaway (Watney, 1980; Watney et al., 1988).

The Hutchinson Salt consists of a stacked succession of many thin, but laterally extensive halite-dominated marine cycles (cyclic carbonate, sulfate, and halite). The halite-dominated cycles interfinger with and prograde over anhydrite beds southwestward towards the source of seawater (figs. 2 and 3). The cross sections of figs. 4 and 5 demonstrate this interstratification and correlation, while detailed core descriptions confirm the distinctive cyclicity of the evaporites. Watney (1980) and Watney et al. (1988) illustrate that the salt depocenter shifted southward progressively through time, as well as shrinking in areal distribution of the rock salt. Four bundles of multiple halite cycles are present and each younger set offlaps southward from the older set. Halite deposition covered a maximum of 37,000 mi² (96,000 km²). Total volume of this salt mass is estimated to be 1,100 mi³ (2,850 km³).

Although the net thickness of the rock salt (relatively pure halite) diminishes to the southwest, the total thickness of the salt-bearing interval increases uniformly toward the south-central map area (fig. 2). Thicknesses increase from less than 50 ft (17 m) on the north to over 550 ft (183 m) in the south, indicating maximum sediment accommodation space in the south due to greater subsidence. The subsidence area corresponds closely with the Anadarko basin and its shelf extensions, the Hugoton embayment and the Sedgwick basin. The overall salt basin covering two-thirds of Kansas, central Oklahoma, and part of the Texas Panhandle is oval shaped, bordered on the south by the Wichita uplift.

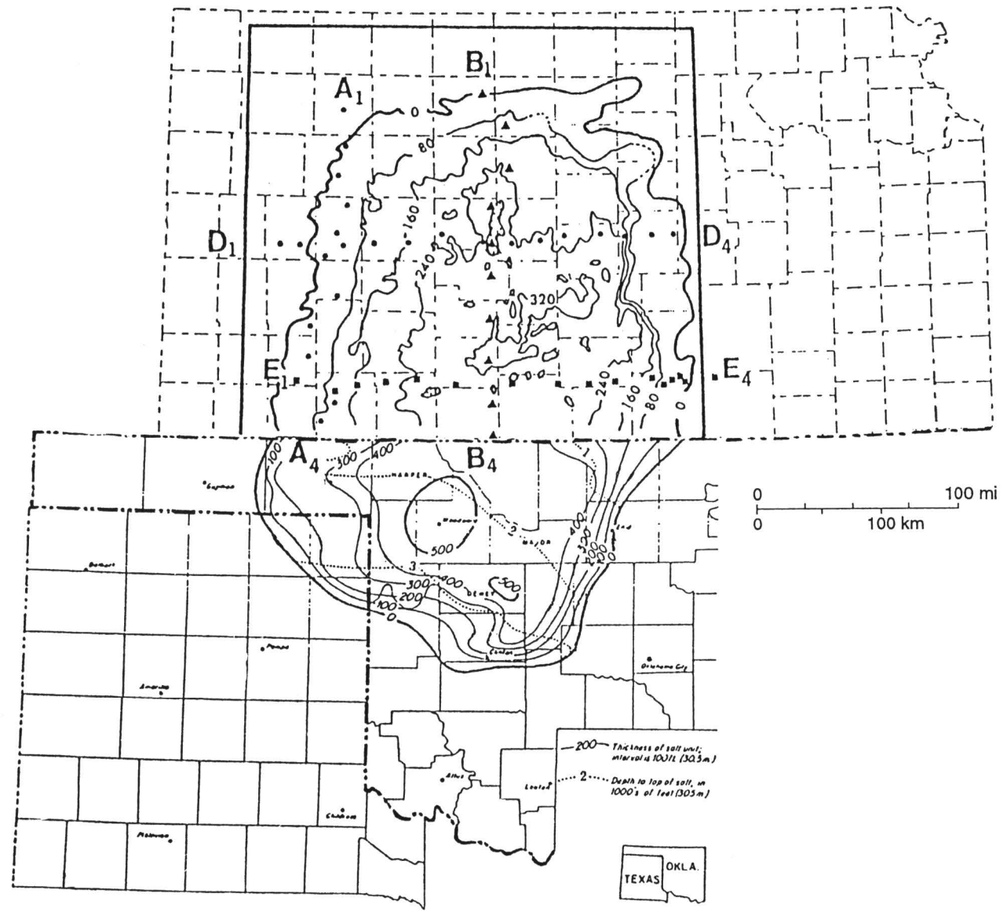

FIGURE 1—Distribution of Hutchinson Salt Member in Kansas, Oklahoma, and Texas. Kansas: net salt isopach with 80-ft (24-m) contour interval and outline of study area shown. Limit of Hutchinson Salt Member in Texas and Oklahoma from Johnson (1976).

Anhydrite beds increase in thickness and number southwestward across the map area at the expense of halite to the southern margin of the Anadarko basin in Oklahoma. Although thin magnesite beds are interstratified in the Hutchinson Salt, the carbonate facies tract does not become important except along the northern shelf of the Midland basin.

The net salt thickness of Hutchinson Salt conforms closely to the shape of the basin. However, younger layers, as previously mentioned, thicken and prograde basinward to the southwest, in part due to basin filling with shale to the north and east and an increasingly more proximal southerly restriction of the seaway (refer to cross sections). The location of the depocenter of the lower net salt unit in the extreme northeastern sector of the depression suggests that highest salinities were most distant from the source of seawater to the south. As the basin filled, the restriction of the basin increased and halite deposition migrated basinward.

The eastern edge of the Hutchinson Salt in central Kansas is a dissolution front occurring at shallow depths (<300 ft, 90 m). The front is expressed by a rapid decrease in thickness of salt from the top downwards (fig. 2). A lost circulation zone, numerous subsidence features, and brine seeps are associated with this solution edge as described by Walters (1978, 1980) and Gogel (1981).

The solution front extends from north to south for 90 mi (145 km) from near the city of Salina to just southwest of Wichita. South of this front the contours on the total net salt isopach map "open," and the structural contour map on top of the Hutchinson Salt again conforms to the adjacent mapped area (fig. 2).

The structural contour map on the top of the salt indicates a closed depression to the east of the solution front over the area in which the salt has been dissolved to only a small remnant layer at the base of the salt interval. As dissolution occurred, additional space was made available for new sediment. Thick Pliocene Equus beds and Recent Arkansas River sediment lie within this area where loss of sediment volume occurred by salt dissolution.

Although not identified by a zero contour, numerous areas between the zero salt line on the east and the solution front probably have zero salt in areas between control points. Furthermore, it is difficult to distinguish halite on petrophysical logs in this area because of the presence of gypsum and porous sandstones in the interval where halite may be present.

Salt distribution is decidedly very patchy in this area with further opportunity for minor solution and subsidence and contribution of dissolved ions to aquifer systems. The east-west cross sections D1–D4 and E1–E4 illustrate the solution front and the easterly depositional pinchout of salt into shale, respectively.

The contour lines of the total net salt isopach are rather irregular. What is mapped is a composite thickness of many individual layers of salt representing many cycles over a relatively large interval where shale and anhydrite layers interfinger with the salt and sometimes thicken quite dramatically at the expense of the salt. It was judged that the 40-ft contour interval is well within the precision of the log measurements used to obtain these data.

The contour map of the depth to the top of the Hutchinson Salt shows the measured depths taken from well logs. This map represents a combination of the earth's surface topography and the structural configuration of the upper surface of the salt interval. East-west trends of thinning represent major stream valleys at the earth's surface, such as the Saline and Smoky Hill rivers on the north end of the mapped area.

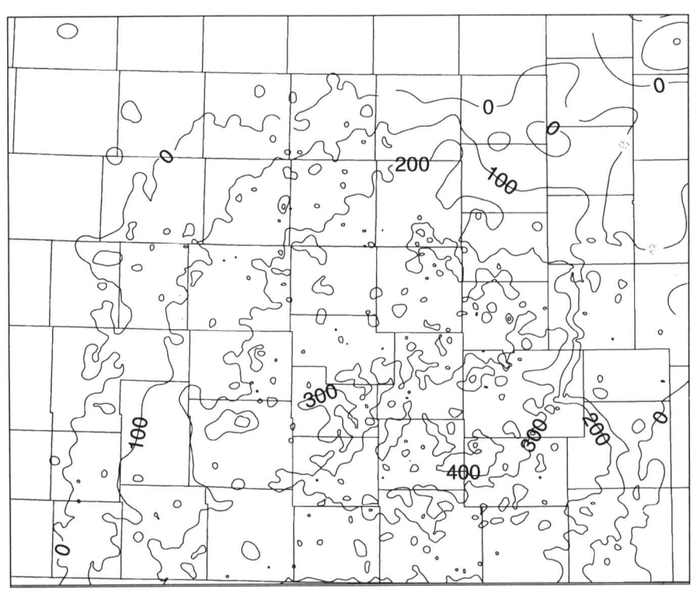

FIGURE 2—Total net salt isopach of the Hutchinson Salt Member of the Wellington Formation in Kansas. Contour interval is 40 ft (12 m); refer to fig. 1 for location.

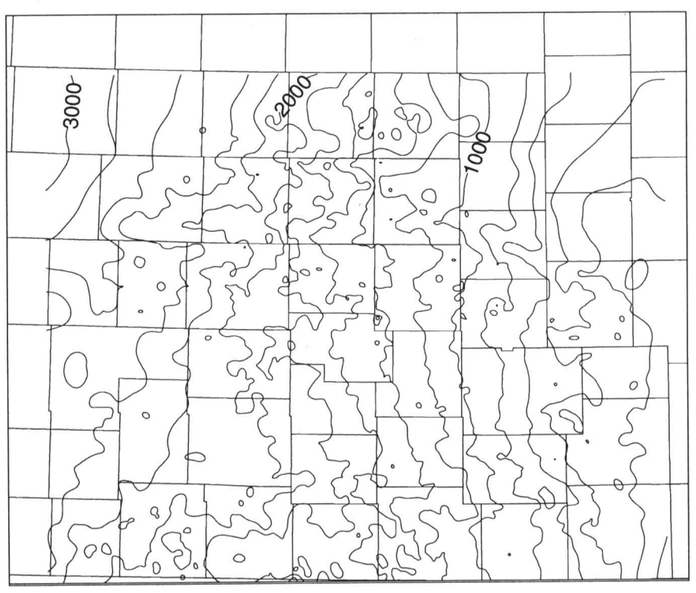

FIGURE 3—Depth to Hutchinson Salt Member of the Wellington Formation in Kansas. Contour interval is 50 ft (15 m); refer to fig. 1 for location.

Regional Hydrogeology and the Dissolution of the Hutchinson Salt

Examination of the salt-dissolution process in the context of the regional ground-water-flow system provides considerable insight into its natural and anthropogenically induced causes. Ground-water flow in the regional ground-water-flow system is northeastward from recharge areas in southwestern Kansas and southeastern Colorado to north-central Kansas (Macfarlane et al., 1992). Two primary flow paths that extend from the Sierra Grande uplift in southeastern Colorado into Kansas can be defined from the potentiometric surface map of the Dakota aquifer (fig. 6). One flow path parallels the outcrop and subcrop areas of the aquifer. The other flow path is northeastward through the confined portion of the Dakota aquifer and eastward into north-central Kansas. The regional flow system is recharged from precipitation moving downward to the water table. Most of the recharge to the regional flow system enters 1) in the upland areas of southeastern Colorado, through the upper Cretaceous aquitard; 2) in central Kansas, where it is thin and fractured; and 3) eastward of the Upper Cretaceous aquitard into unconfined aquifers. Elsewhere little recharge enters the system, especially where the Upper Cretaceous aquitard is thick (fig. 7). Belitz and Bredehoeft (1988) estimated that the Dakota aquifer receives 9.0 ft^3/sec through the Upper Cretaceous aquitard in the Denver basin in eastern Colorado and western and central Kansas, and 29.2 ft^3/sec in outcrop/subcrop areas in Kansas and southeastern Colorado. The principal discharge areas for the regional ground-water-flow system are in the Arkansas River valley in southeastern Colorado and extreme southwestern Kansas and many of the eastward-flowing river valleys in central Kansas. Belitz and Bredehoeft (1988) estimated the discharge from the Dakota aquifer to be 30.4 ft^3/sec.

Salt-affected reaches of streams, salt marshes, and springs in topographically lower areas, and wells flowing saltwater, are a common occurrence in central Kansas (Hay, 1890, 1891; Latta, 1949; Jordan et al., 1964; Hargadine et al., 1979; Gogel, 1981; Cobb, 1980; Gillespie and Hargadine, 1981; Sadeghipour et al., 1987; and Whittemore, 1984) (fig. 8). These occurrences of natural saltwater in shallow aquifers and surface waters and the geomorphic and structural effects are directly related to the movement of ground water in steady-state regional, intermediate, and local flow systems. Discharge areas of these systems are located primarily in stream valleys and are characterized by increases in hydraulic head and dissolved-solids concentration with depth below the water table. The increase of hydraulic head with depth causes cross-formational flows of more saline ground waters upward between aquifers. As a result, flowing wells that produce saltwater and other natural salt-related features are common (Toth, 1972, 1984; Kreitler et al., 1985). The occurrence of these hydrologic features suggest that: 1) central Kansas is included in the natural discharge area of the Permian aquifers that underlie much of western Kansas; 2) the Dakota aquifer is acting as a drain conducting saltwater from the Permian to the river valleys in parts of central Kansas; and 3) local flow systems conduct halite-solution brines from the Permian to overlying aquifers and surface waters. The local ground-water-flow systems are actively involved in the salt-dissolution process (Gogel, 1981; Johnson, 1976). Locally developed relief due to Cenozoic stream-valley erosion in these discharge areas creates local flow systems that help focus ground-water discharge into the valleys. Simultaneously freshwater recharge is added to the ground-water system, which is capable of dissolving bedded salts where present in the shallow subsurface.

There are two main types of salt-dissolution areas in Kansas: natural solution along the subcrop of salt beds, and new or aggravated solution caused by entrance of water

into salt beds via artificial penetrations. Natural solution occurs in a broad zone across the central part of the state and adversely affects ground- and surface-water quality as non-point source pollution as well as causing subsidence. Modern and ancient sinkhole development and faulting from natural causes in southwest and central parts of the state provide evidence that near-surface processes have been, and continue to be, active throughout the Cenozoic along the updip edge of the Hutchinson Salt and other evaporite-bearing strata (Frye, 1950). The front of the most active natural solution occurs along the subcrop of the Hutchinson Salt Member of the Permian Wellington Formation and extends from Dickinson County south to Sumner County. A second front exists in south-central Kansas along the edge of subcropping Ninnescah Shale. Saltwater contamination of ground and surface waters and generally slow subsidence development accompany the salt dissolution. The second type is more local and is associated with oil and gas boreholes or salt mining (Walters, 1978). Sinkhole formation resulting from a natural process of salt solution was first identified with the development of the Meade Sink, southwest Kansas, in 1879. Collapse due to solution resulting from anthropogenic activities was observed at Wichita in 1914 (Walters, 1978). The area of the greatest problems of salt dissolution related to anthropogenic activities occurs in a broad band west of the subcrop of the Wellington Formation from central to south-central Kansas. Subsidence over cavities formed in the salt are most rapid where a substantial thickness of unconsolidated surface deposits is present. Sink development associated with oil and gas activities has generally occurred where saltwater-disposal wells have allowed either disposed brine or aquifer water to flow across the salt section and produce a denser brine that flows to the disposal zone, usually the Arbuckle Group (Walters, 1978). In the last five decades, the Kansas Geological Survey has been involved in local investigations of sinkholes and other subsidence features from natural and anthropogenic causes in many parts of central Kansas. The local geology and site hydrology of many of these features are described in several Kansas Geological Survey publications, in particular Walters (1978). Most of the recent occurrences of subsidence and collapse have resulted from anthropogenic causes.

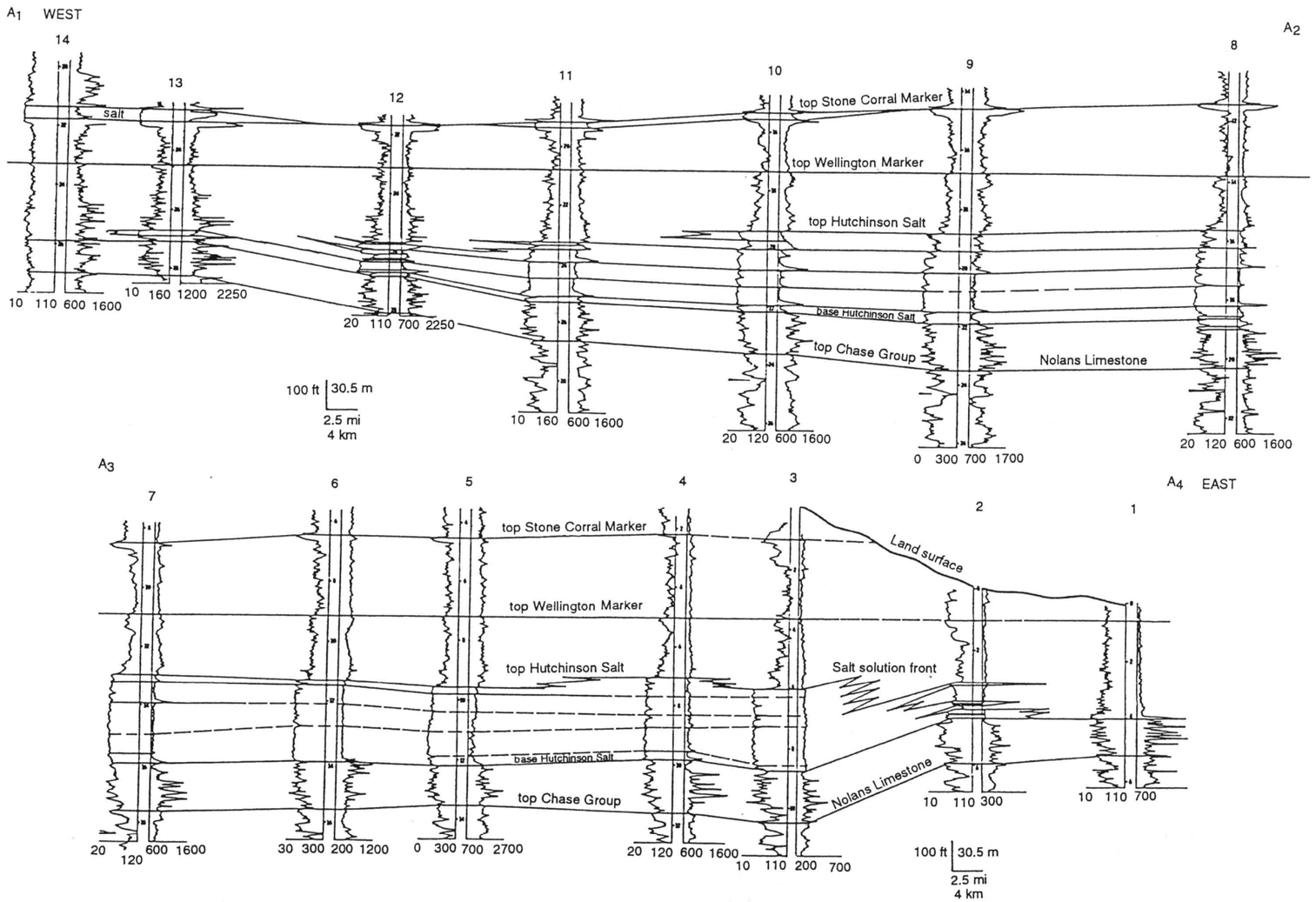

FIGURE 4—WEST-TO-EAST STRATIGRAPHIC CROSS SECTION A1–A4 OF HUTCHINSON SALT MEMBER OF WELLINGTON FORMATION COMPOSED OF GAMMA RAY/NEUTRON LOGS. Scale of logs are API units for gamma ray logs and counts per second and API units for neutron logs. Datum is on top of "Wellington Formation marker" above Hutchinson Salt. Stratigraphic markers include thin magnesite, anhydrite, and shale beds within Hutchinson Salt based on correlation of over 4,000 wells in central Kansas (Watney et al., 1988). The neutron in the boreholes encountered in the data base were usually washed out through the halite section. Consequently, the thicker drilling fluid section was recorded by the neutron log. As a result the anhydrite and carbonate in the interval usually were easily identified as beds with higher neutron count.

The eastern edge of the Hutchinson Salt in the vicinity of this cross section has undergone solution and is typified by an abrupt thinning of the halite into shale, "the lost circulation zone." The western margin of the section is situated along the basin margin of the salt and is typified by gradual thinning and eventually pinching out of the halite beds into shale. The upper halites pinchout farther into the basin than the underlying beds.

Seismic Signature of the Hutchinson Salt

In fig. 9, a suite of two one-dimensional synthetic seismograms for the sec. 2, T. 30 S., R. 25 W. well are presented. These seismograms were generated by convolving an edited version (the density log was clipped) of the reflection coefficient wavetrain (650–3,000-ft interval; 198.2–914.6-m interval) with the following zero-phase, Ricker wavelets of varying polarity and/or wavelength: 1) 30 msec, zero-phase, normal-polarity; 2) 30 msec, zero-phase, reverse-polarity; 3) 5 msec, zero-phase, normal-polarity; and 4) 5 msec, zero-phase, reverse-polarity. The 30-msec Ricker wavelet synthetic seismograms are presented as reasonable representations of conventional-resolution (26 Hz) CDP-stacked seismic data. The 5-msec Ricker wavelet synthetic seismograms, in contrast, are presented as reasonable representations of high-resolution (156 Hz) stacked (CDP) seismic data. As illustrated in fig. 9, the normal- and reverse-polarity displays are mirror images; troughs on the normal-polarity seismogram correlate to peaks on the reverse-polarity display. Definitions for these terms may be found in Anderson et al. (1993a,b) and Sheriff (1981).

The top and base of the Hutchinson Salt Member on the 30-msec wavelet, normal-polarity, synthetic seismograms (figs. 9 and 10) are represented (more-or-less) by moderate-amplitude peaks. As evidenced by these synthetic seismograms, from a reflection-seismic perspective, rock salt is enigmatic; although halite has a relatively high seismic velocity (4,200 m/sec), it has a low density (2,200 kg/m^3). (Typically, dense rocks have relatively high seismic velocities, and less dense rocks have lower seismic velocities.) The seismic image of the undeformed Hutchinson Salt can therefore be difficult to discriminate on conventional seismic data. The top of the rock salt, in particular, can be difficult to image; the Hutchinson Salt is overlain by denser shales of lower seismic velocity. Note that the synthetic seismic image of the Hutchinson Salt would be very different if only the velocity curve was used to calculate the reflection coefficient wavetrain.

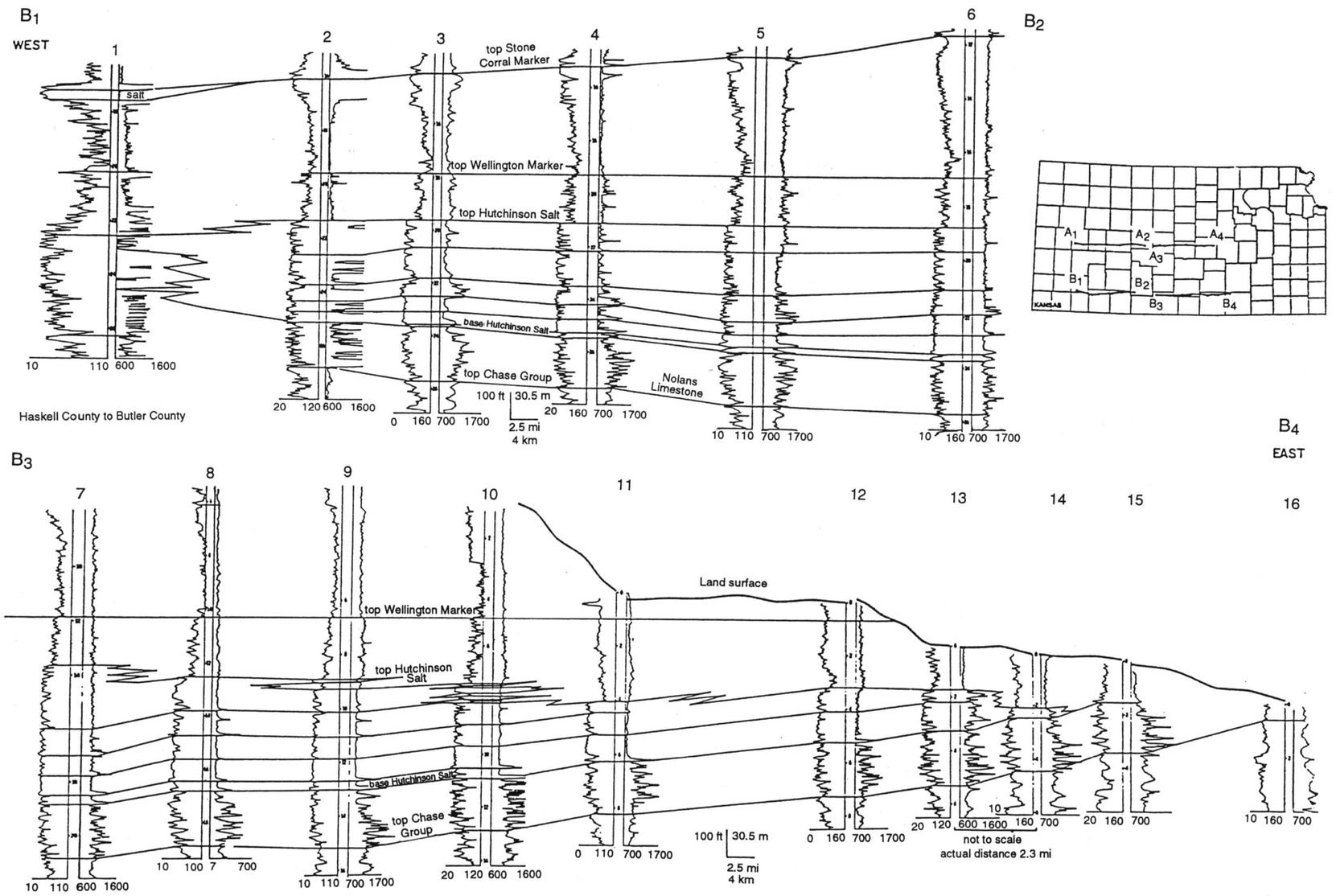

FIGURE 5—WEST-TO-EAST STRATIGRAPHIC CROSS SECTION B1–B4 OF HUTCHINSON SALT MEMBER OF WELLINGTON FORMATION. Datum is on top of "Wellington Formation marker" above Hutchinson Salt. Western reaches of salt basin along this line of section (in southwestern Kansas) are characterized by an abrupt transition from halite into a thick succession of anhydrite. In contrast, halite along the eastern margin of the line of section undergoes gradual thinning and pinchout into shale with the upper halites pinching out further into the basin.

The synthetic seismograms utilizing the 5-msec wavelet (fig. 10) were generated in order to model the seismic response of the Hutchinson Salt on high-resolution stacked (CDP) seismic data. Such data typically utilize frequencies on the order of 100–200 Hz. As illustrated by the synthetic seismogram (5-msec wavelet, normal-polarity), the top of the undeformed rock salt correlates to a low-amplitude peak; the base to a relatively high-amplitude peak. The Hutchinson Salt, between the top and base, is characterized by a series of relatively low-amplitude events, the product of interlayered halites, sulfates, and carbonates of variable acoustic impedance and thickness. Overall, the synthetic seismogram suggests that the seismic image of undeformed Hutchinson Salt can be readily discriminated on high-resolution seismic data. It should be noted that high-resolution sources have limited depth penetration, and that high-frequency input signal is rapidly attenuated with depth. As a result, the vertical resolution at depth (as suggested by the synthetic seismograms) might not be realized using current high-resolution seismic techniques.

In fig. 10, two one-dimensional synthetic seismograms for the sec. 2, T. 30 S., R. 25 W. well are presented. These seismograms were generated by convolving the unedited reflection coefficient wavetrain (650–5,400-ft interval; 198.2–1,646.3-m interval) with 30-msec, zero-phase Ricker wavelets of normal-and reverse-polarity, respectively. A comparison of figs. 9 and 10 shows the value of the judicious editing of sonic and density curves. The synthetic seismic images of the Hutchinson Salt on the edited and unedited seismograms are significantly different.

In fig. 11, a geologic cross section of a simplified salt-dissolution feature and corresponding two-dimensional, synthetic seismograms are presented. The seismograms were generated from the geologic cross section using 30-msec, zero-phase, normal-polarity Ricker wavelet, and vertical incidence and diffraction modeling techniques, respectively. The vertical incidence synthetic seismogram is somewhat analogous to ideally migrated stacked field seismic data; the diffraction synthetic seismogram, in contrast, is somewhat representative of non-migrated data. These synthetics illustrate several key components of the seismic signature of sinkholes.

As illustrated on the vertical incidence synthetic seismogram, each of the geologic horizons is represented by a reflection, the amplitude and phase of which is a function of the acoustic-impedance contrast across the respective horizon. Horizon 3/2 for example is manifested as a high-amplitude peak; the two-way travel time to the apex of the peak (at a specific trace) is equal to the depth to the horizon (at that trace location) divided by the average velocity to horizon 3/2 at that location.

As illustrated by the geologic cross section, the thicknesses of the post-salt layers vary in the vicinity of the sinkhole; as a result, the average seismic velocities to each of the horizons also vary. It is this lateral variation in average seismic velocity that creates the anomalous time-structural relief observed most readily on events 2/1, 3/2, and 4/3. These events are "pushed down" beneath the sinkhole, even though the corresponding horizons are seen to be more-or-less flat on the geologic cross section. (Note: if the average seismic velocity of the compensation sediment at the sinkhole site were higher than that of the dissolved rock salt, the underlying events would be "pulled up.")

Such velocity-generated, time-structural relief is typically associated with zones of salt dissolution. It is imperative that the interpreter differentiate velocity "pull-up" or "push-down" effects from those introduced by real subsurface structural relief. In the case of our model, it would be unfortunate if a well were drilled to the left of the time-structural anomaly along event 2/1, with the expectation of testing a closed structure along the corresponding horizon.

The diffraction synthetic seismogram in fig. 11 is analogous to non-migrated seismic data. These data differ from the vertical-incidence seismogram in that dipping surfaces are shifted in time and space; anticlinal structures are broadened and synclinal features are collapsed. In addition, diffractions originating from discontinuities within the geologic section are superposed on the primary events. Such diffractions can mask the seismic signature of pre-salt geologic targets. Fortunately, however, the masking effect of diffractions can be minimized by migration techniques; a process which (ideally) also shifts dipping events into their proper position in time and space. Ideally, migration would transform the diffraction seismogram into the vertical-incidence seismogram.

It should also be noted that the seismic image of the Hutchinson Salt is a function of both depth of burial and extent of deformation (dissolution). The interpreter must consider that the density and seismic velocity of subsurface rock salt is relatively constant, whereas the acoustic impedances of shales, clastics, and carbonates increase appreciably with depth of burial. As a result, the magnitudes of the reflections from the top and base of the Hutchinson Salt are depth dependent. In those areas where the Hutchinson Salt has been deformed, the character of the reflection can also vary significantly. For example, at one site the relative amplitude of the reflection from the top of the salt can be increased as a result of the fracturing of the overlying sediment. At another location, this reflection can be effectively masked by diffractions associated with dissoltion and subsidence.

Punkin Center Sink (Sec. 26, T. 23 S., R. 4 W.)

The county road east of Punkin Center in Reno County was closed due to a gradual yet persistent subsidence of an area of approximately 12 acres (5 hm^2). It is 5.6 km (3.5 mi) west of Burrton in the Burrton oil field. Since the original construction of the county road, approximately 3 m (10 ft) of vertical displacement has occurred (fig. 12). To ascertain the likely fate of the road, the Kansas Geological Survey was contracted by Reno County to do a seismic-reflection survey between August 8 and August 10, 1983 (Steeples et al., 1984). Two profiles were run intersecting at 90° on the western boundary of the surface depression (fig. 12). Profile 1 runs north-south and profile 2 runs east-west just south of the center of the sink. Over the sink, road-shoulder conditions were poor and geophone plants and source operations were hampered. This resulted in a reduction in the signal-to-noise ratio from CDP 845 to CDP 904 on line 2 (Steeples et al., 1984).

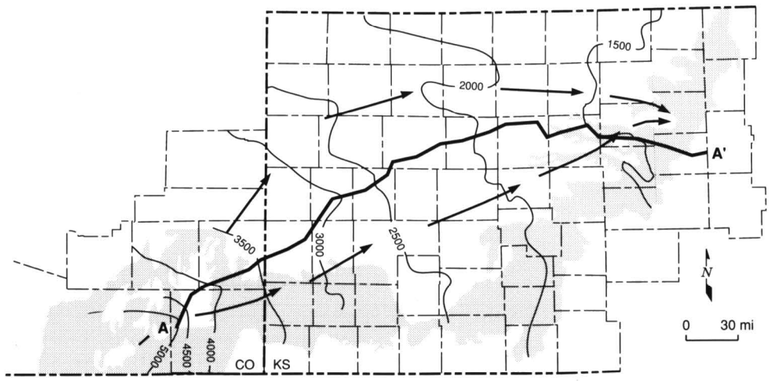

FIGURE 6—GROUND-WATER-FLOW DIRECTIONS IN THE INTERMEDIATE-SCALE SYSTEM IN SOUTHEASTERN COLORADO AND WESTERN KANSAS SUPERIMPOSED ON THE POTENTIOMETRIC SURFACE OF THE DAKOTA AQUIFER.

Regional geologic control indicates that in the vicinity of Punkin Center the shallow subsurface is composed of undifferentiated Pleistocene fluvial clastics (typical 40–60 m; 131–197 ft thick). The pre-Pleistocene subcrop is the Lower Permian-age Ninnescah Shale (Sumner Group), or in places of more extensive erosion, the underlying Wellington Formation. The Pleistocene strata are interpreted as fluvial in origin. They are reported to have been deposited within a north-south-trending valley carved by deeply incised river channels, the courses of which were at least locally controlled by the contemporaneous or earlier dissolution of the underlying Hutchinson Salt Member, Wellington Formation (Gogel, 1981).

Drillers logs from nearby wells indicate a high degree of variability in the thickness of the Hutchinson Salt at the Reno County site. This variability is not surprising since these salts have been totally leached at well sites just a few kilometers to the south and east. Indeed, the main salt-dissolution front (fig. 1) is generally mapped several kilometers to the east of the Punkin Center site (Gogel, 1981; Watney, 1980). The main dissolutional edge of the Hutchinson Salt in the vicinity of Punkin Center is more-or-less coincident with the southern extension of Voshell Ridge (Lam and Yarger, 1989).

A reverse-polarity display of seismic profile 1 is presented as fig. 13. (Increases in acoustic-impedance contrast are represented as troughs.) Several key seismic events have been correlated across these data. Unfortunately, since driller's logs in the area are old and not very reliable, and seismic velocity is not constrained by sonic logs or uphole tests, the seismic reflections cannot be directly correlated to specific geologic horizons. The correlations shown on the seismic section are therefore somewhat tentative. However, these interpretations are consistent with available geologic control and the accepted processes of salt dissolution. Layer C is interpreted to be the pre-Pleistocene subcrop; layers A and B, and D and E are thought to be seismically correlatable Permian and Pleistocene horizons, respectively.

Reflections thought to originate from the top (T) and base (B) of the Hutchinson Salt Member are labeled (fig. 13). This interpretation implies that the seismic line crosses two zones where the rock salts have been leached from the geologic record; elsewhere up to 40 m (20 msec) of rock salt are preserved. Note that the top of the Hutchinson Salt is manifested as a relatively high-amplitude event, probably as a result of the fracturing of the overlying strata.

The post-salt Permian events A and B effectively parallel the top salt event where present (and the base salt reflection elsewhere), supporting the thesis of post-depositional dissolution and implying that the leaching in the study area occurred after these strata had been deposited. Events C, D, and E in contrast are not time-structurally parallel to the top of the salt. The significance of this lack of parallelism can be demonstrated by an analysis of isochron values.

Consider first the isochron values A/C (two-way travel time between events A and C). (Recall that event C is interpreted to be the pre-Pleistocene Permian subcrop; event

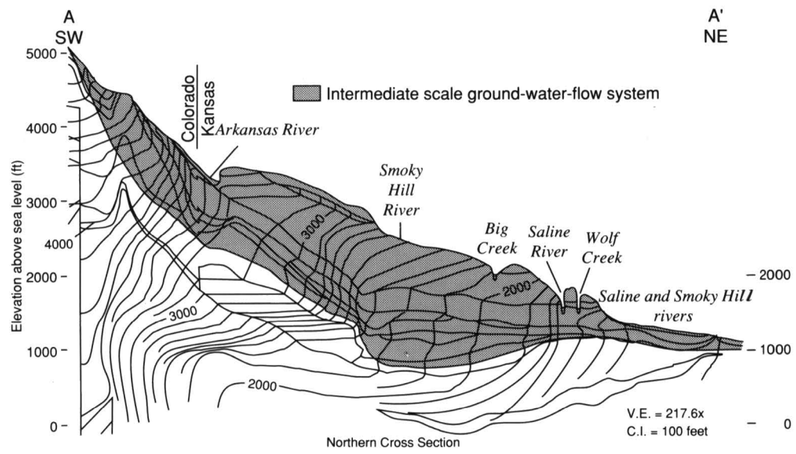

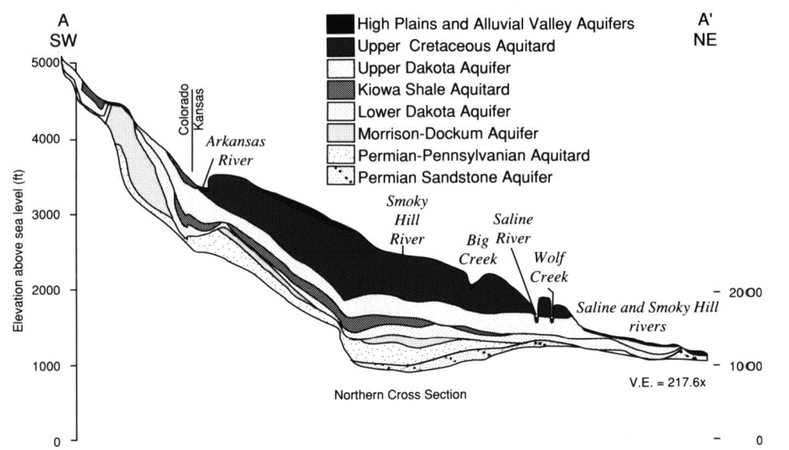

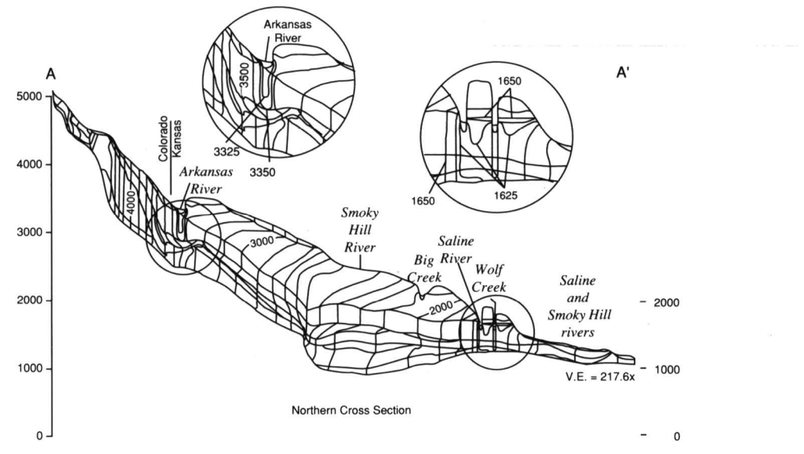

FIGURE 7—VERTICAL CROSS SECTION OF THE SHALLOW SUBSURFACE IN SOUTHEASTERN COLORADO AND WESTERN AND CENTRAL KANSAS SHOWING THE EQUIPOTENTIALS OF HYDRAULIC HEAD. Ground-water-flow direction is assumed to be from regions of higher to lower hydraulic head and normal to the orientation of the equipotentials. Vertical exaggeration—217.6×.

A is an underlying Permian horizon.) The A/C isochron values vary by up to 8 msec (12 m more-or-less) across the seismic section. The largest isochron values are observed within the distance interval 540–750 (where the rock salt is thin to absent) suggesting that a significant volume of the Hutchinson Salt was dissolved at this site prior to the onset of Pleistocene sedimentation. This interpretation is consistent with the thesis that the Pleistocene strata were deposited within deeply incised river channels, the courses of which were at least locally controlled by the contemporaneous or earlier dissolution of the underlying Hutchinson Salt. Alternatively, the observed variations in the A/C isochron values could be erosional in origin. The above-noted correlation between the A/C isochron values and the thickness of the remnant salt suggests that this alternative interpretation is less plausible.

The D/E isochron values also vary appreciably across the seismic line being about 30 msec greater within the distance interval 50–150 than across the thick remnant rock salt. This observation suggests that a significant volume of salt was dissolved within this distance after the deposition of horizon D and prior to the deposition of Unit E. Alternatively, Event D could represent the base of a deeply scoured channel.

These interpretations suggest that dissolution of the Hutchinson Salt occurred in the Punkin Center area during the Pleistocene and support the thesis that drainage patterns at that time were at least locally controlled by the contemporaneous leaching of the Permian salts. While surface observations and these seismic data indicate that the

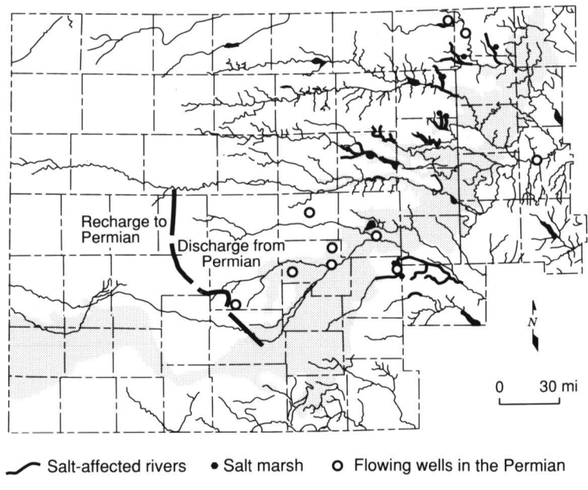

FIGURE 8—MAP SHOWING THE OCCURRENCE OF SALT MARSHES, FLOWING WELLS, AND AREAS OF SALTWATER INTRUSION INTO STREAMS ALL FROM NATURAL SOURCES IN CENTRAL KANSAS.

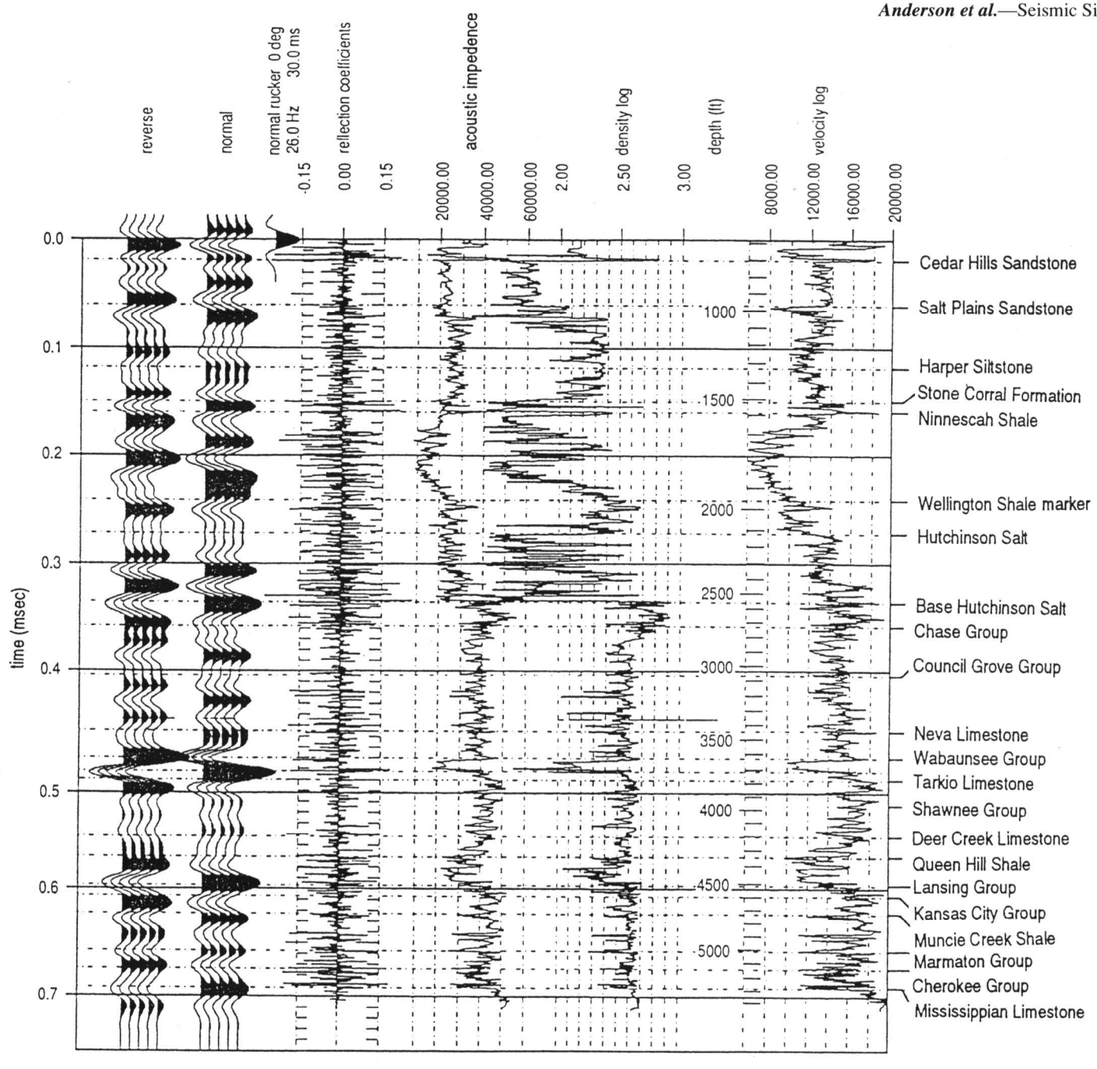

FIGURE 9—VELOCITY CURVE, EDITED DENSITY CURVE (minimum density of rock salt set at 2.2 g/cc), GAMMA RAY CURVE, ACOUSTIC-IMPEDANCE CURVE (product of seismic velocity and density), REFLECTION-COEFFICIENT CURVE (acoustic-impedance contrast) AND TWO SYNTHETIC SEISMOGRAMS FOR THE SEC. 2, T. 30 S., R. 25 W. WELL (Minneola field, Clark County). The synthetic seismograms were generated by convolving the reflection-coefficient curve with zero-phase 30-msec Ricker wavelets of normal- and reverse-polarity, respectively. By SEG convention, positive acoustic-impedance contrasts (higher values with increasing depth) generate peaks (deflections to the right); the "arrival time" of a zero-phase wavelet is measured at the apex of the respective trough or peak. Such one-dimensional synthetic seismograms are generally used to correlate field seismic data to the subsurface geology.

dissolution of the Hutchinson Salt is occurring and has occurred at various times in the geologic past, the lack of subsurface velocity control precludes the exact determination of the timing of the paleo-leaching. More specifically, without additional subsurface velocity control (e.g., sonic or check shot data), the interpreted ages of horizons A–E cannot be confirmed.

These seismic data not only provide information regarding the timing of the salt dissolution, they also give us insight into the process of leaching. Note for example, the interpreted curved displacement planes near the edges of the remnant rock salt. These fault planes suggest that leaching was initiated near the centers of the zones of the most extensive dissolution. (Very possibly, the earliest phases of dissolution were initiated along fractures associated with the ancestral Voshell Ridge.) In terms of particularly significant processes, the response of the adjacent sediment to the onset of dissolution appears to have been two-fold: 1) the remnant rock salt flowed (creep mechanisms) towards the zone of lower pressure, and 2) the overburden subsided into the developing voids and into those areas vacated by the creep of rock salt. The fracture planes which developed during the course of subsidence probably acted as conduits for inflowing freshwater and/or outflowing saline brines, and allowed for the gradual lateral migration of the salt-dissolution front. Note that the fault planes demarcate an upwards-expanding zone of measurable subsidence, a feature characteristic of gradual subsidence.

With respect to the hypothesis regarding the initiation of salt dissolution, it should be noted that there is no conclusive seismic evidence of vertical displacement along the pre-salt events. The time-structural relief present along these reflections is perhaps most readily attributed to velocity effects (due to the velocity contrast between the relatively high-velocity remnant rock salt and the lower-velocity compensation sediments). The noticeable loss in the coherency of the pre-salt events immediately beneath the central remnant rock salt is interpreted as a product of scattering and attenuation within a zone of current salt dissolution. (The surface is subsiding immediately to the east of this remnant body of rock salt; fig. 13.)

As evidenced by the seismic data, the top of the Hutchinson Salt and the post-salt (above approximately 200 msec) have been structurally deformed by the dissolution of the Hutchinson Salt and collapse of the overburden. Perhaps the most important observation that can be made from the analysis of the seismic data and surface observations is that at least three major episodes of sinkhole development have occurred. The most recent episode is still continuing. The earlier episodes, however, predate the

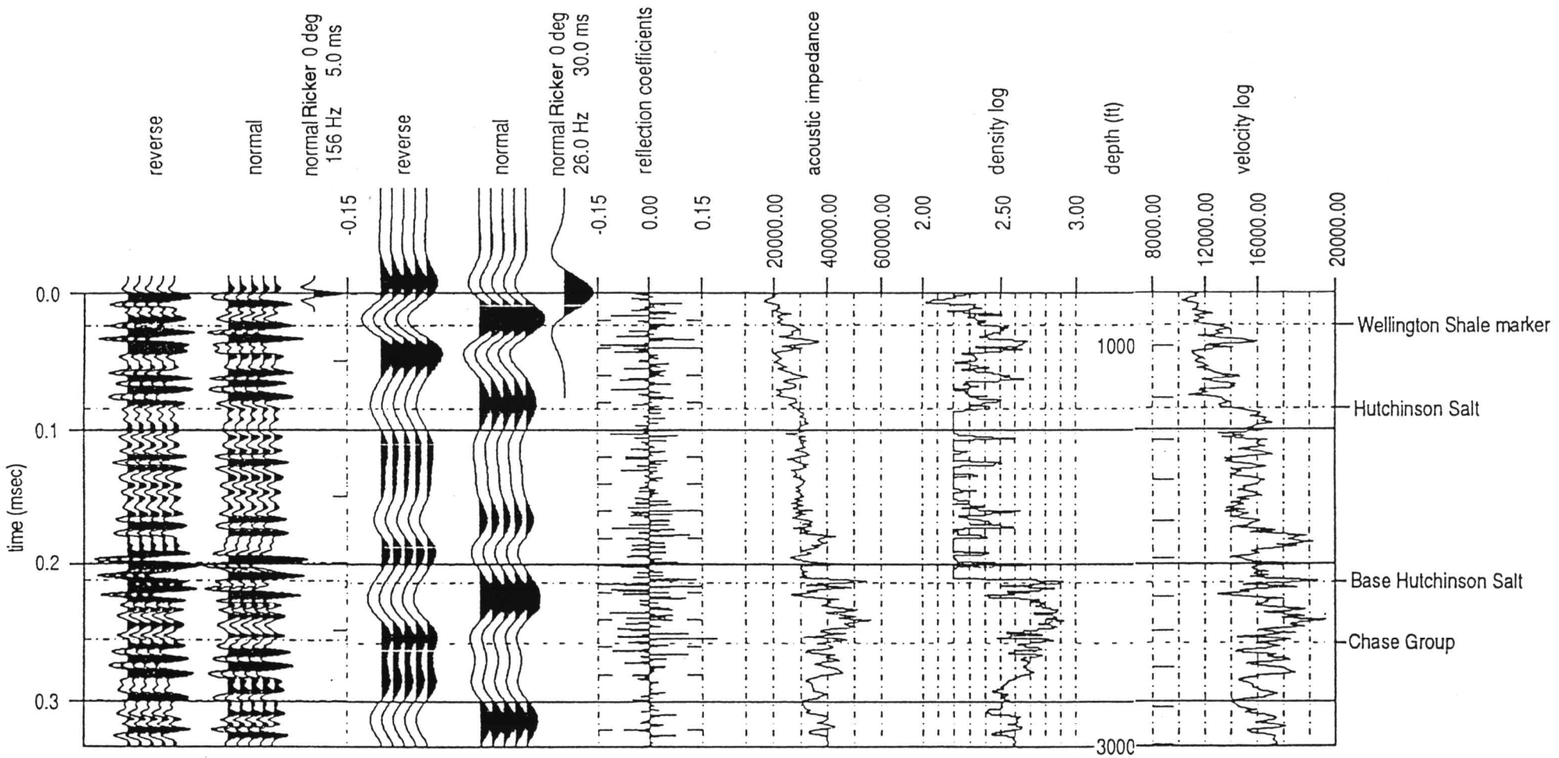

FIGURE 10—VELOCITY CURVE, UNEDITED DENSITY CURVE, GAMMA RAY CURVE, ACOUSTIC-IMPEDANCE CURVE, REFLECTION COEFFICIENT CURVE, AND TWO SYNTHETIC SEISMOGRAMS FOR THE SEC. 2, T. 30 S., R. 25 W. WELL (Minneola field, Clark County; 650–5,400-ft interval; 198.2–1,646.3-m interval). The synthetic seismograms were generated by convolving the reflection-coefficient curve with zero-phase, 5-msec Ricker wavelets of normal- and reverse-polarity respectively. As a result of caving and leaching, the densities of the rock salt and shallow shale intervals are anomalously low (less than 2.0 g/cc in places). A comparison of the synthetic seismograms of figs. 9 and 10 illustrates that such uncorrected and inaccurate readings significantly affect the synthetic seismic signature of the well-log suite. If the validity of the velocity-log readings have been similarly compromised, the unedited synthetic seismogram will not time-tie the processed seismic section.

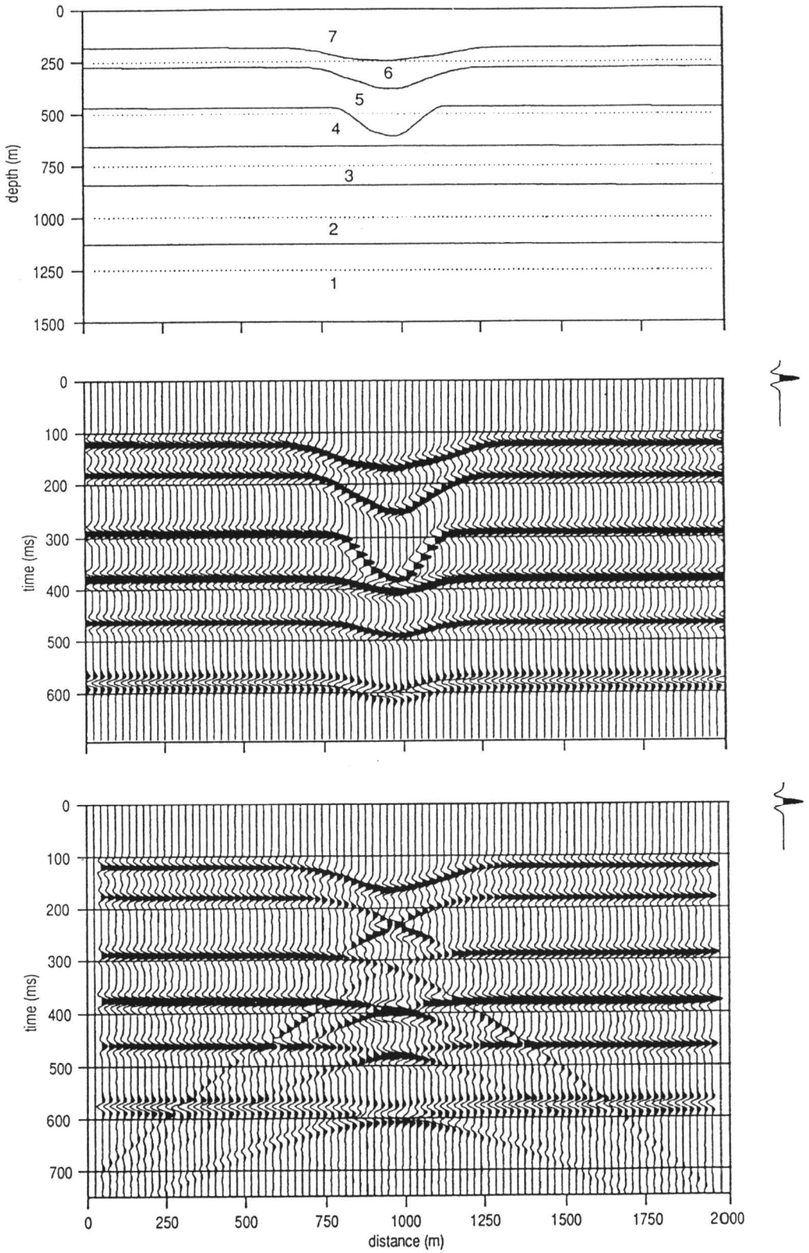

FIGURE 11—GEOLOGIC CROSS SECTION OF A SIMPLIFIED SALT-DISSOLUTION FEATURE AND CORRESPONDING TWO-DIMENSIONAL SYNTHETIC SEISMOGRAMS. The seismograms were generated from the geologic cross section, using 30-msec, zero-phase, normal-polarity Ricker wavelet, and vertical incidence and diffraction modeling techniques, respectively.

deposition of the base of the upper geologic layer (Pleistocene age Event E) correlated across the seismic section. This interpretation suggests that the hydraulic conditions necessary for dissolution of rock salt were present before any petroleum-exploration drilling occurred. The occurrence of paleo-sinkholes and a modern active adjacent sinkhole signifies that salt-dissolution sinkholes in Kansas can occur either naturally or as a result of inducement by drilling or mining.

Summary

Salt dissolution of both natural and anthropogenic origin has occurred and is still occurring in Kansas. Such leaching degrades the utility of the seismic technique and increases the potential for the misinterpretation of these geophysical data. As evidenced by the Punkin Sink seismic data, zones of extensive salt dissolution (including remnant salt and collapse structures) are characterized by diffractions and velocity-generated time-structural relief. The diffractions degrade the quality of the primary events; the apparent time-structural relief makes data processing more difficult and provides the opportunity for misinterpretations.

On a more positive note, the Punkin Sink data illustrate the utility of the seismic technique in terms of the elucidation of the processes and geological effects of leaching. The example data clearly demonstrate that dissolution of natural origin occurred in Kansas (at least during the Pleistocene). Surface observations indicate that subsidence (and presumably dissolution) is still occurring in the study area. These seismic data also suggest that the remnant rock salt creeps toward the zones of dissolution and that the zone of subsidence increases in areal extent at shallower depths.

References

Belitz, K., and Bredehoeft, J. D., 1988, Hydrodynamics of the Denver basin—explanation of subnormal fluid pressures: American Association of Petroleum Geologists, Bulletin, v. 72, p. 1,334–1,359

Cobb, P. M., 1980, The distribution and mechanisms of saltwater intrusion in the freshwater aquifer and in Rattlesnake Creek, Stafford County, Kansas: M.S. thesis, University of Kansas, Lawrence, 176 p.

Dellwig, L. F., 1963, Environment and mechanics of deposition of the Permian Hutchinson Salt Member of the Wellington Shale; *in,* Symposium on Salt: Northern Ohio Geological Society, Cleveland, p. 74–85

Frye, J. C., 1950, Origin of Kansas Great Plains depressions: Kansas Geological Survey, Bulletin 86, pt.1, p. 1–20

Gillespie, J. B., and Hargadine, G. D., 1981, Saline ground-water discharge to the Smoky Hill River between Salina and Abilene, central Kansas: U.S. Geological Survey, Water Resources Investigations 81–43, 72 p.

Gogel, T., 1981, Discharge of saltwater from Permian rocks to major stream-aquifer systems in central Kansas: Kansas Geological Survey, Chemical Quality Series 9, 60 p.

Hargadine, G. D., Balsters, R. G., and Luehiring, J., 1979, Mineral intrusion in Kansas surface waters—a technical report: Kansas Department of Health and Environment, Water Quality Management Section, 211 p.

Hay, R., 1890, Notes on some Kansas salt marshes: Transactions of the Twenty-second Meeting of the Kansas Academy of Science, 1889, p. 97–100

_____, 1891, Geology of Kansas salt: Seventh Biennial Report of the Kansas Board of Agriculture, p. 83–92

Johnson, K. S., 1976, Evaluation of Permian salt deposits in the Texas Panhandle and western Oklahoma for underground storage of radioactive wastes—Final report submitted to Union Carbide: Oak Ridge National Laboratories, 70 p.

Jordan, P. R., Jones, B. F., and Petri, L. R., 1964, Chemical quality of surface waters and sedimentation in the Saline River basin, Kansas: U.S. Geological Survey, Water-Supply Paper 1651, 90 p.

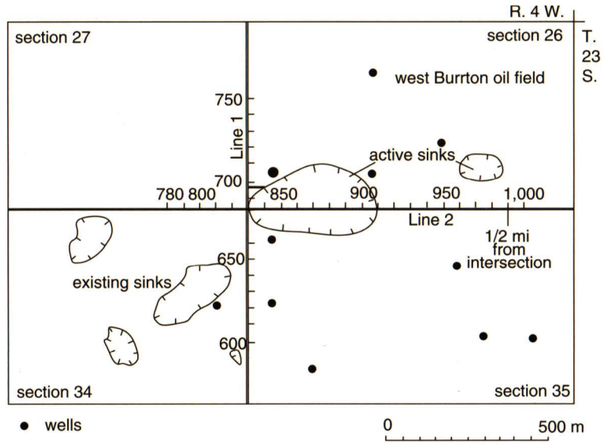

FIGURE 12—Location map for Punkin Center site, Reno County. Sinkhole sites and the locations of the seismic profiles are superposed.

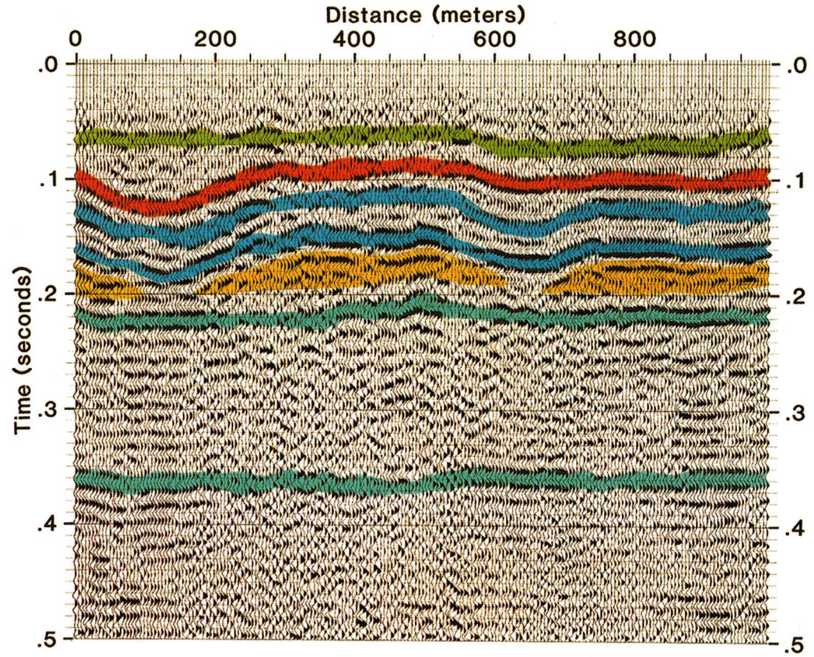

FIGURE 13—Interpreted reverse-polarity display of seismic profile 1.

Kreitler, C. W., Fisher, R. S., Senger, R. K., Hovorka, S. D., and Dutton, A. R., 1985, Hydrology of an evaporite aquitard: Proceedings of the 17th International Congress of International Association of Hydrogeologists on the Hydrogeology of Rocks of Low Permeability, Tucson, Arizona, v. 17, p. 150–168

Lam, C. K., and Yarger, H., 1989, State gravity map of Kansas; *in,* Geophysics in Kansas, D. W. Steeples, ed.: Kansas Geological Survey, Bulletin 226, p. 185–196

Latta, B. F., 1949, Ground-water conditions in the Smoky Hill valley in Saline, Dickinson, and Geary counties, Kansas: Kansas Geological Survey, Bulletin 84, 152 p.

Macfarlane, P. A., Whittemore, D. O., Chu, Tyan-Ming, Butler, J. J., Jr., Wade, A., Coleman, J., Doveton, J. H., Mitchell, J. E., and Kay, S., 1992, The Dakota Aquifer Program—annual report, FY91: Kansas Geological Survey, Open-file Report 92–1, 93 p.

Norton, G. H., 1939, Permian red beds of Kansas: American Association of Petroleum Geologists, Bulletin, v. 23, p. 1,751–1,859

Rascoe, B., Jr., 1968, Permian System of western midcontinent: The Mountain Geologist, v. 5, p. 127–138

Sadeghipour, J., Macfarlane, P. A., McElwee, C. D., and Kemblowski, M. W., 1987, Saltwater intrusion into alluvial aquifers—an evaluation of field methods and ground-water modeling techniques: Kansas Geological Survey, Open-file Report 87–6, 208 p.

Sheriff, R. E., 1981, Encyclopedic dictionary of exploration geophysics, 3rd ed.: Tulsa, Oklahoma, Society of Exploration Geophysicists, 376 p.

Steeples, D. W., Knapp, R. W., and Miller, R. D., 1984, Examination of sinkholes by reflection seismology; *in,* Sinkholes—Their Geology, Engineering and Environmental Impact, B. F. Beck, ed.: Proceedings of the First Multidisciplinary Conference on Sinkholes, Orlando, Florida, 15–17 October, p. 217–223

Toth, J., 1972, Properties and manifestations of regional ground-water movement: Proceedings of the 24th International Geological Congress, Montreal, Section 11, p. 153–163

_____, 1984, The role of regional gravity flow in the chemical and thermal evolution of ground water: Proceedings of the First Canadian/America Conference on Hydrogeology—Practical Applications of Ground Water Geochemistry, Banff, Alberta, Canada, National Water Well Association, Dublin, Ohio, p. 3–39

Walters, R. F., 1978, Land subsidence in central Kansas related to salt dissolution: Kansas Geological Survey, Bulletin 214, p. 1–32

_____, 1980, Solution and collapse features in the salt near Hutchinson, Kansas: South-central Section, Geological Society of America, Field Trip Notes, 10 p.

Watney, W. L., 1980, Maps and cross sections of the lower Permian Hutchinson Salt in Kansas: Kansas Geological Survey, Open-file Report 80–7, 10 p.

Watney, W. L., Berg, J. A., and Paul, S., 1988, Origin and distribution of the Hutchinson Salt (lower Leonardian) in Kansas; *in,* Permian Rocks of the Midcontinent, W. A. Morgan and J. A. Babcock, eds.: Midcontinent Society of Economic and Paleontologic Mineralogists, Special Publication No. 1, p. 113–135

Whittemore, D. O., 1984, Geochemical identification of salinity sources; *in,* Salinity in Watercourses and Reservoirs, R. H. French, ed.: Proceedings of the International Conference on State-of-the-Art Control of Salinity, Ann Arbor Science, Butterworth Publishers, Stoneham, MA, p. 505–514

Plastic Deformation and Dissolution of the Hutchinson Salt Member in Kansas

Neil L. Anderson[1], Ralph W. Knapp[2], Don W. Steeples[3], and Richard D. Miller[4]
[1]Department of Geology and Geophysics, University of Missouri–Rolla, Rolla, MO 65401; [2]formerly with the Kansas Geological Survey, The University of Kansas, Lawrence, KS 66047;
[3]Department of Geology, The University of Kansas, Lawrence, KS 66045; and [4]Kansas Geological Survey, The University of Kansas, Lawrence, KS 66047

Abstract

The Hutchinson Salt Member of the Permian Wellington Formation is preserved throughout south-central Kansas at subsurface depths of between 60 m and 760 m (197 ft and 2,494 ft), as a more-or-less contiguous body having maximum net thicknesses on the order of 170 m (558 ft). Within Kansas, the margins of the salt are depositional except for the updip eastern edge, which is dissolutional. Basinward of the present-day main eastern edge of the Hutchinson Salt, localized dissolution of both natural and anthropogenic origin has occurred. Such leaching has resulted in the formation of both surface sinkholes (e.g,. Janssen sink, Panning sink) and subsurface cavities (e.g., Knackstedt cavity).

Janssen sink is an example of slow and gradual surface subsidence, characterized by the predominantly ductile deformation of remnant salt. On seismic data, the feature is manifested as an upwards-expanding zone of measurable subsidence. Panning sink, in contrast, is an example of catastrophic surface subsidence. In cross section, the feature is presented as an inverted cone-shaped, vertically migrated collapse cavity (chimney).

The Knackstedt void is a bridged cavity, characterized by a vertically migrating collapse chimney, the roof of which is presently bridged above the original top of the salt. It is anticipated that this void will eventually close and that a surface sinkhole will develop on site. The nature of the sinkhole (i.e., gradual subsidence or catastrophic collapse) will be partially dependent upon: 1) the rate of continuing dissolution, 2) the rate of effective cavity closure due to creep and stoping, and 3) the shear strength of the post-salt strata.

Introduction

Rock salts exhibit unique physical properties and mechanical behavior. In situ, they are remarkably soluble, relatively impermeable and nonporous, almost incompressible, highly ductile, and rather easily deformed by creep (Baar, 1977).

In the presence of unsaturated waters, the dissolution of rock salt is essentially instantaneous, relative to the time-scale of the transport mechanisms (molecular diffusion, free convection, and forced convection). The plastic behavior of rock salt is demonstrated by salt glaciers and by flowage patterns observed in salt domes (Talbot and Jarvis, 1984; Richter-Bernburg, 1987).

Dissolution of rock salts in the subsurface can create pore space, differential stresses, creep and ultimately subsidence. There are two basic types (end members) of subsidence: 1) gradual subsidence characterized by relatively low rates of dissolution and the ductile deformation of remnant rock salt and 2) catastrophic subsidence characterized by relatively rapid rates of dissolution and brittle deformation of post-salt sediment (Ege, 1979; Rokar and Staudtmeister, 1985). Ductile deformation is typified by upward-expanding zones of subsidence. In contrast, brittle deformation is typified by a vertically propagating cavity or collapse chimney. Particularly in this later case, measurable surface subsidence may not occur; pending further dissolution, the cavity may be bridged effectively and/or infilled as a consequence of stoping.

Rock Salt Mechanics

Natural creep limits—limits of elastic behavior—of rock salts are extraordinarily small compared to most other rocks and are difficult to determine in the laboratory. Indeed, most researchers think that rock salt does not have a yield point; they conclude that over time, rock salt will eventually exhibit plastic deformation (i.e., creep). Total strain of rock salt is given by:

$$e = e_e + e_p + e_t + e_s + e_a$$

where e_e is elastic strain due to loading, e_p is plastic strain produced during loading, e_t is transient or primary creep strain, e_s is secondary or steady-state creep strain, and e_a is accelerating or tertiary creep strain. According to Carter and Hansen (1983), e_e and e_p are generally less than one percent (<1%) and are not particularly significant with respect to the long-term creep of rock salt. These authors also state that the accelerating creep strain e_a is generally observed at stresses above one-half of the short-term breaking strength in unconfined creep tests and in low-temperature, low-pressure triaxial creep tests. Under these conditions, microfracturing leads to macroscopic failure by faulting (glide mechanism).

Transient creep e_t (low-temperature creep mechanism, LT) is nonrecoverable and decelerating. This type of creep stems from constraints placed on dislocation glide at low temperatures, where diffusion rates are low and dislocations cannot surmount obstacles to glide and climb by cross slip. Each increment of strain makes further motion more difficult (strain hardening), thus creep rate decreases continuously with time.

According to Carter and Hansen (1983), steady-state creep e_s encompasses solution-precipitation creep, high-temperature (HT) creep, Cobble creep, and Nabarro–Herring (N–H) creep. HT creep can be thought of as nondecelerating LT creep. With respect to the HT mechanism, vacancy diffusion in the higher temperature regime is thought to allow for climb by dislocation intersection processes. In the same temperature regime, but at very low stresses, stress-induced bulk vacancy diffusion (Nabarro–Herring creep) or grain-boundary diffusion are thought to occur.

In the presence of water, solution-precipitation creep can occur within the low-temperature, low-pressure regime. This mechanism is described by Urai et al. (1986) as solution-transfer creep—a dynamic recrystallization process. Presence of even trace amounts of brine has a marked effect on the deformation of rock salt in laboratory tests. Tests on dry, dilated salt show more-or-less conventional dislocation creep behavior (glide). Brine-bearing samples, in contrast, show a marked weakening at low strain rates (low-differential stress). According to Urai et al. (1986), this is associated with dynamic recrystallization and a change of deformation mechanism to solution precipitation creep. These authors surmise that trace amounts of brine are present in rock salt in situ and that the presence of such fluid accounts for the observed discrepancy between typical laboratory and in situ observations. Rock salt under typical laboratory conditions (dry) deforms as an elasto-plastic; rock salt in situ deforms as a plastic. Indeed, the salt glaciers in Iran flow under gravitational stresses alone.

According to Jackson and Talbot (1986), strain rates for the in situ deformation of rock salt vary by over eight orders of magnitude from 10^{-8} sec^{-1} to 10^{-16} sec^{-1}. The most rapid rates are those of borehole closure during accelerating creep (10^{-8} sec^{-1}), mine closures and steady-state borehole closures (10^{-9} sec^{-1} to 10^{-11} sec^{-1}), and namakiers (salt glaciers; 10^{-8} sec^{-1} to 10^{-11} sec^{-1}). The rates of diapiric extrusion assisted by folding (10^{-13} sec^{-1}) and the rates for the most active phase of gravity-driven diapiric growth are significantly lower (10^{-8} sec^{-1} to 10^{-11} sec^{-1}). These rates are significantly lower than the strain rates at which laboratory specimens are typically tested (>10^{-7} sec^{-1}).

Dissolution and Mass Transport of Halite

Solubility of halite (359 g NaCl/1H_2O at 25°C) varies somewhat (depending upon temperature, pressure, and the concentrations of other solutes), but it is one to three orders of magnitude higher than the solubilities of anhydrite and limestone under normal ground-water conditions. Dissolution of rock salt is essentially instantaneous relative to the time scale of the transport process in the presence of unsaturated water. The rate of solid rock salt removal is therefore controlled by convective and/or diffusive flux of sodium and chloride ions away from a halite-bearing formation. Transport mechanisms include molecular diffusion, free convection, and forced convection.

Mass transport by diffusion is a very slow process. Davies (1989) cites the following example: in the situation where a halite unit is separated from an underlying freshwater aquifer by a 10-m (33-ft)-thick aquiclude having a *De* value of 10^{-11} m^2/sec, regional halite removal rate is on the order of 5 microns per year. In most natural situations, water in the aquifer has higher initial salinities, and *De* values of the aquiclude are a few orders of magnitude lower. Therefore, halite removal rates controlled by diffusion are typically much less than one micron per year.

According to Davies (1989), mass transport by free convection (driven by gravity acting on an inverted fluid density gradient) is much faster than transport by diffusion alone. Davies cites, as an example, a situation where a 1-m (3.3-ft)-wide fracture zone with a hydraulic conductivity of 10^{-4} cm/sec transects the aquiclude described in the previous paragraph. Localized halite-removal rate for this scenario is on the order of a few centimeters per year, which is orders of magnitude higher than the removal rate for diffusion alone.

Once salt-rich brine passes from a fracture zone into an underlying aquifer, the mode of mass transport is altered significantly. Forced convection through the aquifer, driven by a regional head gradient, becomes the primary transport mechanism. However, if the vertical component of the external head gradient is small, the vertical component of flow may still be primarily driven by buoyancy (Davies, 1989).

Brittle versus Ductile Subsidence

Salt is characterized by an ability to deform in either a ductile (plastic) or brittle manner, depending on temperature, stress state, and deformation rate. At temperatures expected for the salt dissolution-subsidence process, the primary ductile-deformation mechanisms for rock salt are dislocation glide (glide creep) at moderate differential stresses and moderate deformation rates, and solution-precipitation creep at low differential stresses and low deformation rates. If intercrystalline water penetrates the subsiding salt mass, deformation by intergranular liquid diffusion (solution-precipitation creep) is capable of producing strain rates that are orders of magnitude higher than are possible in relatively dry salt at the same stress states (Davies, 1989).

There are two basic types of subsidence in response to the dissolution of subsurface rock salt: 1) gradual subsidence characterized by relatively slow rates of dissolution and

ductile deformation of remnant rock salt, and 2) catastrophic subsidence characterized by relatively rapid rates of dissolution and brittle deformation of post-salt strata. These two types of subsidence represent the end members of a continuous range of subsidence processes. Ductile deformation typically generates an upward-expanding zone of subsidence; brittle deformation in contrast is characterized by an inverted, cone-shaped, vertically migrating collapse cavity (chimney). Whether measurable subsidence is expressed at the surface depends upon several factors including the timing of the dissolution, the areal extent and volume of the leached rock salt, the effect of stoping, the depth to the rock salt, and the response of the overburden. For example, measurable subsidence may not be exhibited by those sediments deposited after the latest phase of dissolution and associated collapse. In a second scenario, as a result of stoping, bridging, and rock-salt creep, the vertical migration of the collapse chimney could effectively cease, pending additional dissolution. Particularly in the former case, structural relief could be induced in the subsurface as a result of the compaction of the "compensation" sediments (Oliver and Cowper, 1983).

Example of Gradual Subsidence

Janssen sink is located in southern Ellsworth County about 13 mi (21 km) north of Lyons on K–14, about 3 mi (5 km) west of Geneseo (fig. 1). Gradual surface subsidence has been occurring about the Janssen "B" #6 well. Janssen "B" #6 was a production well in the Geneseo–Edwards oil field later converted to saltwater disposal. By 1988, about 3 m (10 ft) of subsidence had occurred; subsidence continues to occur at a rate on the order of 0.5 m/yr (Knapp et al., 1989)

In an effort to elucidate the subsurface morphology in the vicinity of the Janssen sink, two crossing seismic lines were acquired by the Kansas Geological Survey (figs. 1, 2, and 3). Good data quality of the two crossing seismic profiles allows a satisfactory interpretation of the present position of the Hutchinson Salt (Anderson et al., this volume, p. 57–65) and some overlying strata. Both sections show similar wavelet character of about 170 msec. Below 170 msec the data quality is poor with nothing more than subtle hints of primary reflectors continuous across the sections. As is illustrated on the seismic data, Janssen sink is characterized by an expanding zone of measurable subsidence.

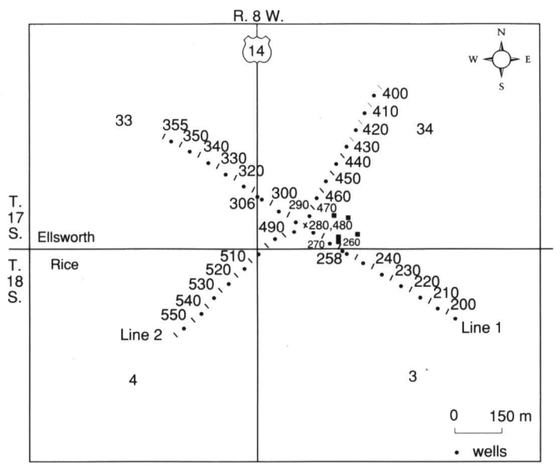

FIGURE 1—CDP-NUMBER LOCATION MAP OF JANSSEN SINK SEISMIC LINES IN ELLSWORTH COUNTY (Knapp et al., 1989). CDP interval is 5 m (16 ft).

Well logs from the area show the Stone Corral and the Hutchinson Salt at 120 m and 260 m (394 ft and 853 ft), respectively (Anderson et al., this volume, p. 57–65). There is about 45 m (148 ft) of relatively uniform salt underlying approximately 140 m (459 ft) of red-bed sequences of shale, limestone, sandstone, and anhydrite. Strong acoustic boundaries exist below 350 m (1,148 ft), but due to the lack of depth-penetration of seismic energy, identification and correlation of these events is tenuous at best.

Profile 1 traverses the sinkhole from southeast to northwest, intersecting the county road at CDP 258 and K–14 at CDP 306 (figs. 1 and 2). Surface expression of the sinkhole extends from CDP 270 to CDP 295 on profile 1. Modeling by Neely (1985) shows the Stone Corral to be the strongest reflector in the section (fig. 4). It is at about 140 msec at the flanks of the section. The top of the Hutchinson Salt is at about 220 msec and its bottom at about 240 msec.

Profile 2 (fig. 3) crosses the sink from northeast to southwest and crosses the county road and K–14 intersection from CDP's 504 to 508. As in profile 1, very strong reflectors can be identified above 140 msec (Stone Corral) with poor data quality below that two-way travel-time. The character of the energy present on the seismic section of profile 2 is easily matched with that on profile 1. CDP 480 on profile 2 and CDP 280 on profile 1 represent the same subsurface point. Displacement of the salt reflector between CDP 464 and 491 appears to be about 8 msec. This would imply between 8 m and 16 m of actual subsidence in the subsurface at the depth of the salt (using average seismic velocities for the post-salt strata of 2,000 m/sec and 4,000 m/sec, respectively).

Surface subsidence (on the order of 3 m; 10 ft) near the center of the sink is significantly less than the estimated relief near the top of the Hutchinson Salt (between 8 m and 16 m; 26 ft and 52 ft). There are several possible explanations: 1) As evidenced by the zone of subsidence, the areal extent of measurable subsidence increases at shallower depths; 2) Stoping of post-salt strata could have reduced the overall volume of subsidence at shallower depths; 3) The seismic estimates of subsurface structural relief near the center of the sinkhole could be high (seismic velocities could be lower than estimated due to subsidence-related fracturing).

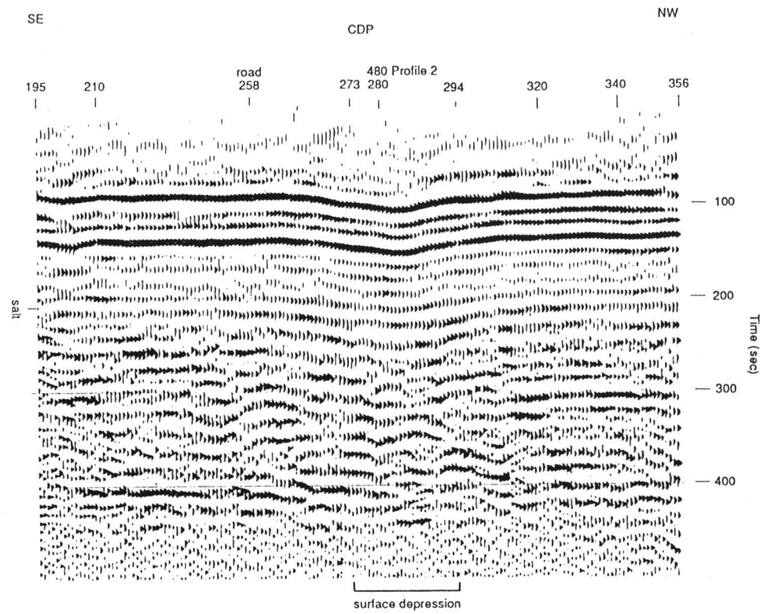

FIGURE 2—SEISMIC SECTION OF PROFILE 1 (after Knapp et al., 1989). The interpreted upwards-expanding zone of measurable subsidence is consistent with the gradual subsidence observed at the surface. Seismic control suggests that the zone of dissolution is more-or-less circular and symmetric, supporting the thesis that leaching was initiated by the inadvertent discharge of unsaturated (with respect to halite) oil-field brines through corroded pipe.

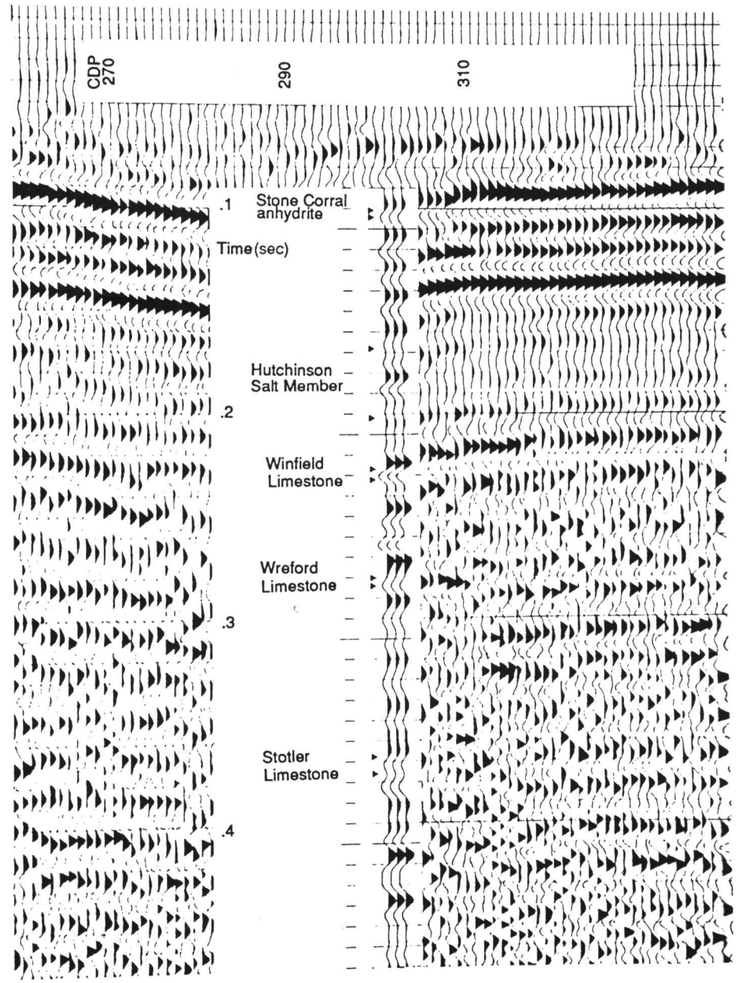

FIGURE 3—SEISMIC SECTION OF PROFILE 2 (after Knapp et al., 1989). The interpreted upwards-expanding zone of measurable subsidence is consistent with the gradual subsidence observed at the surface.

Example of Catastrophic Collapse (after Walters, 1978)

The top of the Hutchinson Salt Member in the Panning sink area (fig. 5) is at a depth of about 300 m (984 ft); it has a gross thickness (including shale and anhydrite interbeds) of about 100 m (328 ft). The rock salt is overlain by impermeable shales and, typically, by a shallow freshwater aquifer.

The principal reservoir facies in the Panning area, the Lower Ordovician Arbuckle dolomite at a depth of about 3,000 m (9,843 ft) is an enormously large aquifer with a strong water drive (fig. 6). Scores of wells in the Panning area produced 500 bbls or more of saltwater per day. Most of this salt is re-injected into the Arbuckle through high-volume, gravity-fed injection wells.

The disposed brine is unsaturated with respect to sodium chloride and corrosive to metals. Hence, within the disposal wells there is potential for appreciable salt dissolution, i.e., high energy input, large volumes of water unsaturated with respect to chlorides, and an enormous brine outlet in the Arbuckle dolomite.

The Panning sinkhole (figs. 5, 6, and 7) developed catastrophically around an abandoned oil well (Panning 11A) at that time in use as a saltwater-disposal well. The associated chimney can be described as an inverted, cone-shaped, vertically migrated collapse cavity. The following modified excerpt from Walters (1978) represents that author's reconstruction of the sequence of events that led to the formation of the Panning sinkhole.

September 1938 (fig. 6A): During the drilling of Panning 11A, freshwater-drilling fluid dissolved salt to a diameter of 1.37 m (4.49 ft). Note that the production casing did not reach this high up-hole.

1938–1943 (fig. 6B): No dissolution of salt took place while over 100,000 bbls of oil were being processed through tubing. Shale interbeds in the shale section collapsed and fell, accumulating in the void space from 367 m to 389 m (1,204 ft to 1,276 ft), just above the constriction in the hole size at the first anhydrite bed.

1943–1946 (fig. 6C): A cased-hole gamma-ray neutron log recorded in a nearby hole showed the static fluid level of the Arbuckle aquifer to be 278 m (912 ft) from the top of the hole. No salt dissolved in these years during which the well was temporarily abandoned as noncommercial after pumping 99% water due to the depletion of oil.

1946–1949 (fig. 6D): The well was converted for use as a saltwater disposal well by recementing the casing. Note the presence of cement opposite the lower salt section and the absence of cement opposite the upper salt section. No salt dissolved. Brine was disposed through tubing by gravity flow.

1949-1953 (fig. 7A): Tubing was removed from the well and brine was disposed directly down the casing. Corrosion resulted in casing leaks, permitting access for 72 gal/minute of brine, 14,000 ppm chlorides, to circulate across the salt face, then downward into the Arbuckle aquifer. A huge cavern, larger than 90 m (295 ft) in

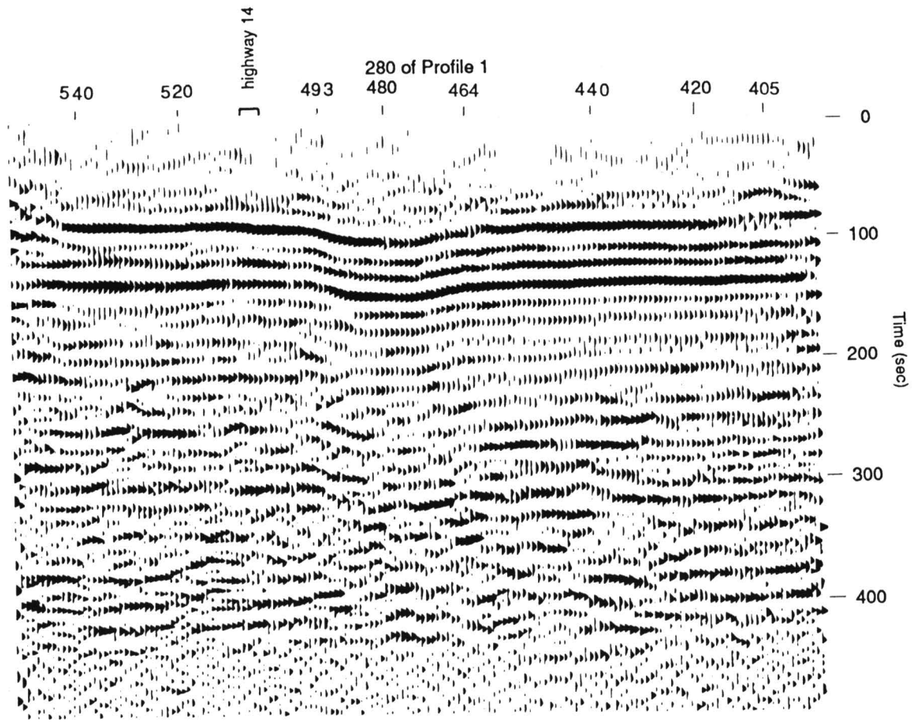

FIGURE 4—Comparison of processed field seismic and synthetic data for profile 1 (fig. 2; Neely, 1985).

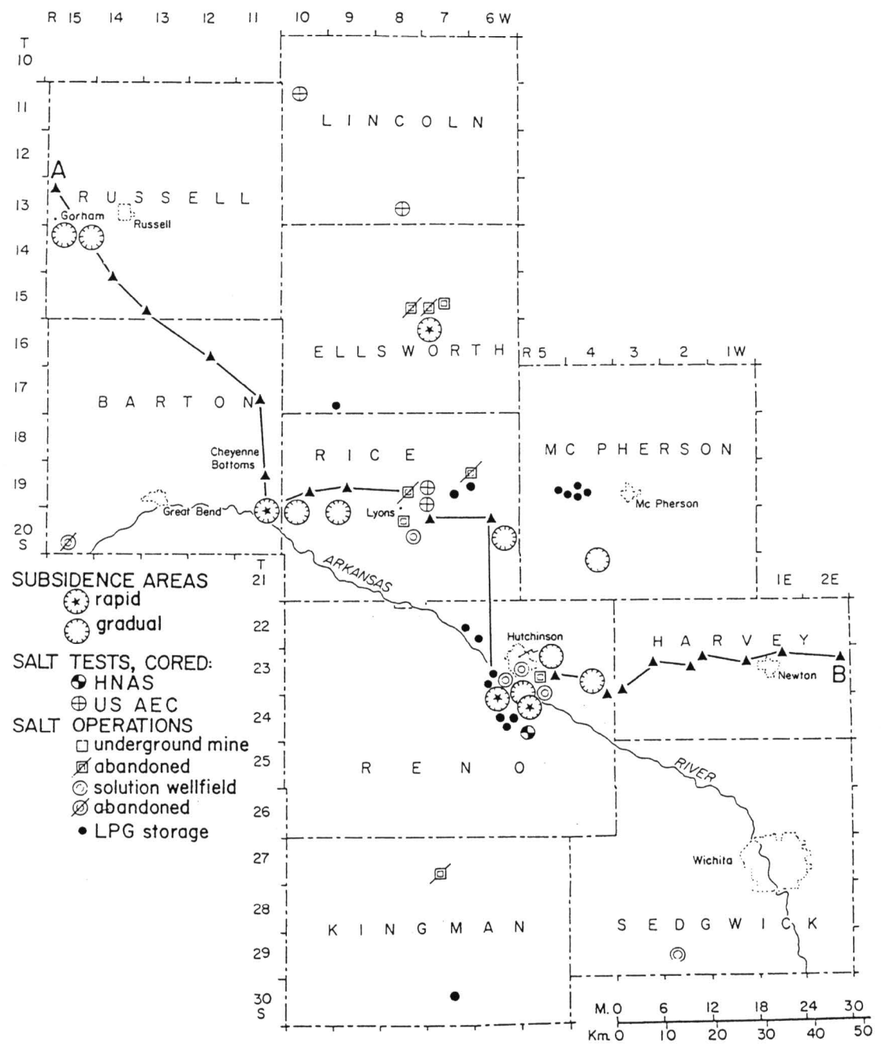

FIGURE 5—Index map showing the location of the Panning sink, Barton County (after Walters, 1978).

diameter, dissolved into the salt. Progressive falls of the shale interbeds and shale roof rocks partially filled the cavern. Successive roof falls caused the void space to gradually migrate upward to near the Stone Corral Anhydrite (depth 142 m; 466 ft), causing in turn, surface subsidence, ponding of water, and tilting of the derrick.

January 1959 (fig. 7B): The Panning 11A was abandoned but not plugged. The derrick was removed because surface subsidence caused it to tilt dangerously. With disposal-brine flow discontinued, salt dissolution ceased.

April 1959 (fig. 7C): The Panning 11A was plugged with 150 sacks of cement in the surface pipe to a depth of 58 m (190 ft), and the Arbuckle was bridged. There was no other plugging. The underground void space at shallow depth was now isolated from both the near surface and the Arbuckle aquifers. Brine in the void space drained downward gradually to reach equilibrium with the intermediate aquifers, leaving the near-surface void space unsupported by fluid and under vacuum.

April 24, 1959 (fig. 7D): When the uppermost keystone bedrock at a depth of 32 m (105 ft) fell into the newly drained shallow void space, the surface sinkhole formed rapidly in the three hours from 9:00 a.m. until noon, with lesser subsidence continuing to about 9:00 p.m. As the shallow void space filled with freshwater and air, falling material such as concrete derrick corner blocks fell into the narrow aperature and compressed, then ejected, the air. The casing collapsed and fell. At first, the loose sand and gravel moved downward in a freshwater slurry at a rate faster than the flow of the aquifer, forming a deep cone-shaped pit. As the void space filled, water accumulated in the surface sinkhole.

April 1959–1978 (fig. 7E): The circular sinkhole diameter near 100 m stabilized, forming a freshwater pond 20 m (66 ft) deep, volume near 57,000 m^3 (358,530 bbl). In the 17-year interval, the surrounding fence buckled downward and inward by only about 0.6 m (1.9 ft) on each side, indicating resumption of stable subsurface conditions. Transported sand and gravel filled the shallow space voided by roof falls. The former cavern in the salt is filled and plugged with fallen Permian shale and red beds; hence, it is thought that no further dissolution is occurring.

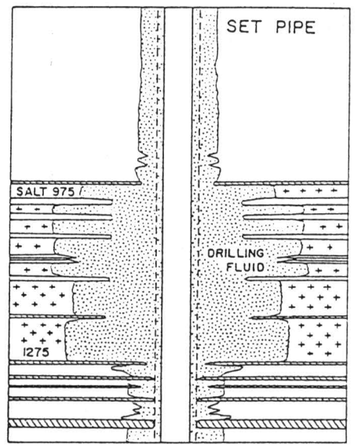

A-1938-SEPT.

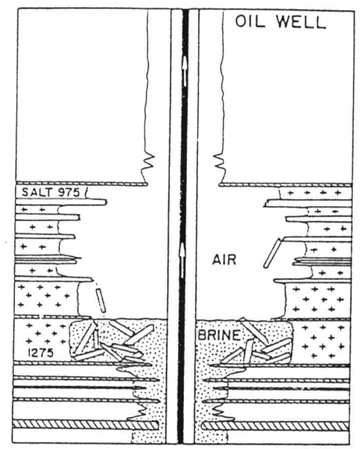

B-1938-1943

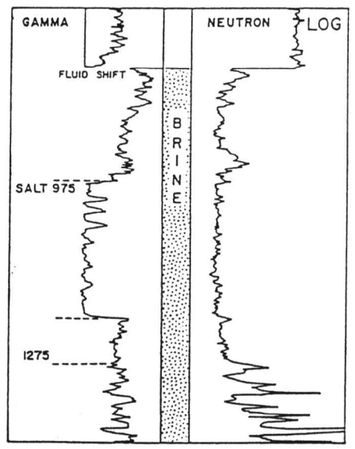

C-1943-1946

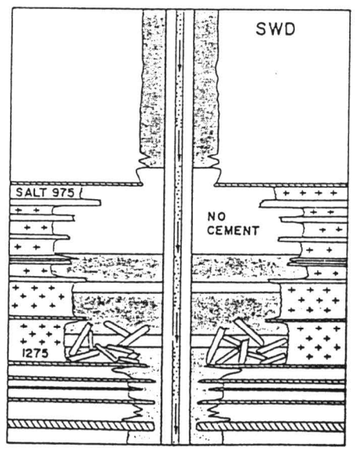

D-1946-1949

FIGURE 6—Diagram of salt section in Panning 11A (Walters, 1978).
A. After setting 6-inch (15.2-cm) oil-string casing.
B. Oil well. Oil is pumped up 2-inch tube.
C. Gamma-neutron log; tubing removed.
D. Saltwater-disposal well (SWD). Waste brine moving down 3-inch plastic-lined tube.

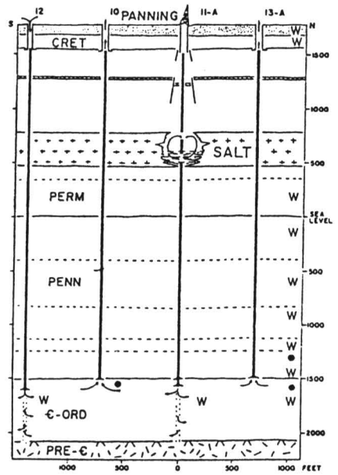

A-1949-1958

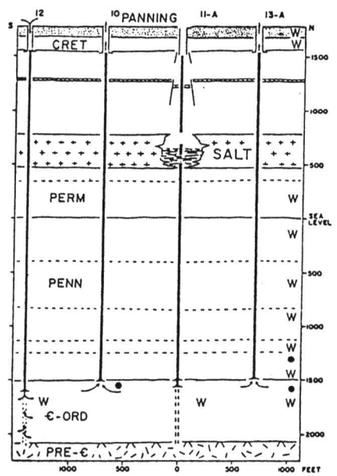

B-1959-JAN.

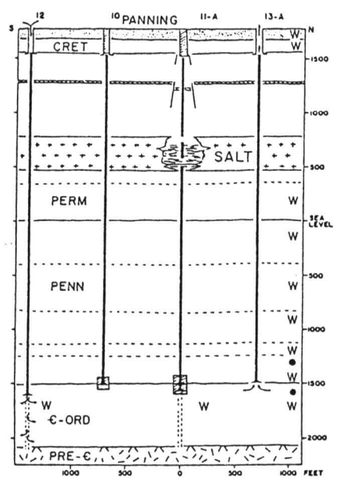

C-1959-APRIL 14

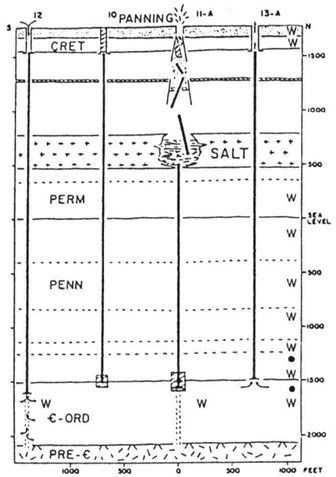

D-1959-APRIL 24

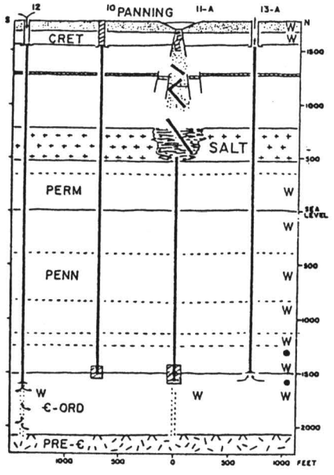

E-1959-PRESENT (1976)

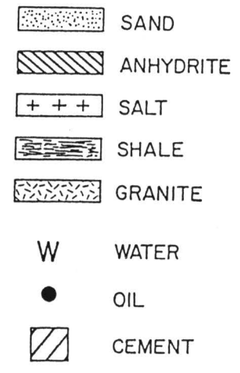

FIGURE 7—Cross section through the Panning 11A disposal well (Walters, 1978).
A. Waste brine moving down inside the 6-inch (15.2-cm) casing (plastic-lined tube removed) and circulating by Permian salt section through holes in casing.
B. Well abandoned; derrick removed.
C. Well plugged with cement in surface pipe, and "bridged" in Cambrian–Ordovician Arbuckle dolomite.
D. Sinkhole forming April 24, 1959.
E. 1959 to 1976, Legend for fig. 6.

Example of Bridging

The Hutchinson Salt in the Knackstedt area, McPherson County, Kansas (T. 20 S., R. 5 W.), extends from approximately 135 m to 210 m (443 ft to 689 ft) below the ground surface. At the Knackstedt saltwater-disposal well site, a bridged and air-filled, subsurface cavity was discovered when investigations into the loss of static water level resulted in a wireline video inspection of the well casing (fig. 8). The video discovered the absence of casing as well as any visible borehole walls between 97 m and 146 m (318 ft and 479 ft) in depth. The bottom of the borehole, which originally extended over 900 m (2,953 ft), was then plugged with neat cement. In an attempt to fill the void, 8400 m^3 (52,836 bbl) of gravel were poured into the well from the surface, raising the floor of the cavity to 135 m (443 ft), leaving approximately 38 m (125 ft) between the top of the gravel pile and the top of the air-filled void.

During the filling process, the hole was occasionally flushed with a saturated brine solution in an attempt to level the coning of the pile of material directly beneath the borehole opening in the ceiling of the void. No static fluid level was ever recorded after a brine-solution flush. Absence of a measurable water level in the hole at any time during the past several years, even though the alluvial sediments on the overlying shale roof contain a relatively shallow water table, suggests that the void is hydraulically connected to an aquifer with a hydrostatic head at least 160 m (525 ft) below the earth's surface. The aquifer could either be the intended oil-brine disposal horizon several hundred meters below the rock salt (the hole was filled with neat cement, rendering this unlikely) or a salt-solution zone extending laterally from the cavity location. The source of the waters causing most of the dissolution was probably unsaturated (with respect to halite) oil brine that escaped from the failed injection casing. Ground waters unsaturated with respect to halite could have been, and probably are, presently entering the large cavity. Therefore, this could be causing further dissolution expansion of its dimensions.

In an attempt to better define the morphology of the Knackstedt cavity, a preliminary seismic-reflection survey was conducted by the Kansas Geological Survey (fig. 9).

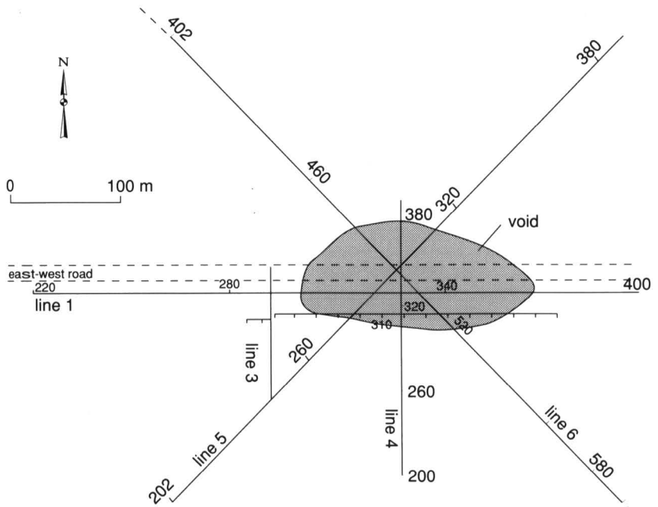

FIGURE 8—LOCATION MAP FOR THE KNACKSTEDT SITE (Miller et al., 1988). The saltwater-disposal well site, the seismic shotpoint lines, the map extent of the interpreted cavity, and other geographic information are superposed.

These data suggest that the cavity has a basal areal extent of about 20,000 m^2 (5 acres) (Miller et al., 1988).

Summary

Basinward of the present-day main eastern edge of the Hutchinson Salt, localized dissolution of both natural and anthropogenic origin has occurred. Such leaching has resulted in the formation of both surface sinkholes (e.g., Janssen sink, Panning sink) and subsurface cavities (e.g., Knackstedt cavity).

Janssen sink is an example of slow and gradual surface subsidence, characterized by the predominantly ductile deformation of the remnant salt. On seismic data, the feature is manifested as an upwards-expanding zone of measurable subsidence. Panning sink, in contrast, is an example of catastrophic surface subsidence. In cross section, the feature is presented as an inverted cone-shaped, vertically migrated collapse cavity (chimney).

The Knackstedt void is a bridged cavity, characterized by a vertically migrating collapse chimney, the roof of which is presently bridged above the original top of the salt. It is anticipated that this void will eventually close and that a surface sinkhole will develop on site. The nature of the sinkhole (i.e., gradual subsidence or catastrophic collapse) will be partially dependent upon: 1) the rate of continuing dissolution, 2) the rate of effective cavity closure due to creep and stoping, and 3) the shear strength of the post-salt strata.

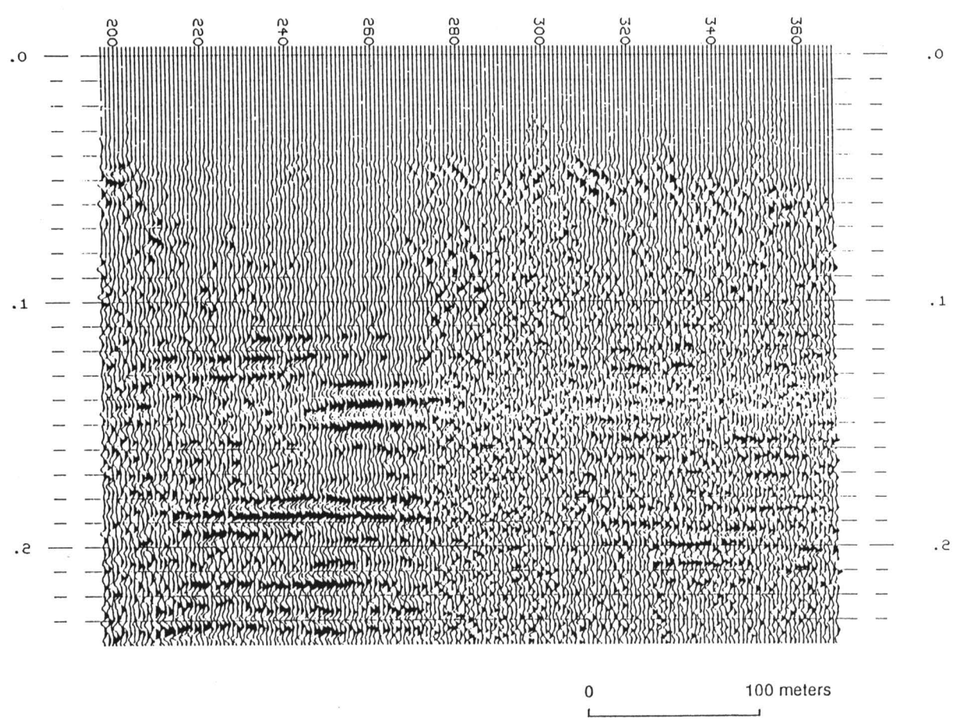

FIGURE 9—SEISMIC SECTION FOR LINE 6 (Miller et al., 1988). The interpreted cavity location is from trace 275 to 316.

References

Baar, C. A., 1977, Applied salt-rock mechanics 1: Elsevier Scientific Publishing Company, 294 p.

Carter, N. L., and Hansen, F. D., 1983, Creep of rock salt: Tectonophysics, v. 92, p. 275–333

Davies, P. B., 1989, Assessing deep-seated dissolution-subsidence hazards at radioactive-waste repository sites in bedded salt; *in,* Richard H. Jahns Memorial Volume, A. M. Burnham et al., eds.: Engineering Geology, v. 27, p. 467–487

Ege, J. R., 1979, Surface subsidence and collapse in relation to extraction of salt and other soluable evaporites: U.S. Geological Survey, Open-file Report 79-1666

Jackson, M. P. A., and Talbot, C. J., 1986, External shapes, strain rates, and dynamics of salt structures: Bulletin Geological Society of America, v. 97, p. 305–323

Knapp, R. W., Steeples, D. W., Miller, R. D., and McElwee, C. D., 1989, Seismic reflection at sinkholes; *in,* Geophysics in Kansas, D. W. Steeples, ed.: Kansas Geological Survey, Bulletin 226, p. 95–116

Miller, R. D., Steeples, D. W., Myers, P., and Somanas, D., 1988, Seismic reflection surveys at the Knackstedt saltwater disposal well: Kansas Geological Survey, Open-file Report 88-31, 24 p.

Neeley, G. W., 1985, Waters' method synthetic seismograms applied to seismic-reflection modeling: M. S. thesis, The University of Kansas; also available as Kansas Geological Survey, Open-file Report 85–25, 82 p.

Oliver, J. A., and Cowper, N. W., 1983, Wabamun salt removal and shale compaction effects, Rumsey area, Alberta: Bulletin of Canadian Society of Pétroleum Geology, v. 31, p. 161–168

Richter–Bernburg, G., 1987, Deformation within salt bodies: Dynamical Geology of Salt and Related Structures, p. 39–75

Rokar, R. B., and Staudtmeister, K., 1985, Creep rupture criteria for rock salt; *in,* Sixth International Symposium on Salt, B. C. Schreiber and H. L. Harner, eds.: Salt Institute Inc., Virginia, v. 1, p. 455–462

Talbot, C. J., and Jarvis, R. J., 1984, Age, budget, and dynamics of an active salt extrusion in Iran: Journal of Structural Geology, v. 6, p. 521–533

Urai, J. L., Spiers, C. J., Zwart, H. J., and Lister, G. S., 1986, Weakening of rock salt by water during long-term creep: Nature, v. 324, p. 554–557

Walters, R. F., 1978, Land subsidence in central Kansas related to salt dissolution: Kansas Geological Survey, Bulletin 214, 82 p.

Shallow Seismic-reflection Study of a Salt-dissolution Subsidence Feature in Stafford County, Kansas

Richard D. Miller[1], Don W. Steeples[2], and Thomas V. Weis[3]
[1]Kansas Geological Survey, The University of Kansas, Lawrence, KS 66047; [2]Department of Geology, The University of Kansas, Lawrence, KS 66045; and
[3]formerly with Kansas Geological Survey, now with Normandy Exploration Limited, Kent Town, South Australia

Abstract

Seismic-reflection surveying was successfully used to define subsidence of the Stone Corral anhydrite in Stafford County, Kansas, in response to dissolution of the 85-m (279-ft)-thick Permian-aged Hutchinson Salt at a depth of approximately 340 m (1,116 ft). Gradual formation of a surface depression around the Siefkes "A" No. 6 abandoned oil-field-brine disposal well in Stafford County, Kansas, led to a 12-fold CDP seismic survey to define the potential extent and amount of future surface subsidence. Several reflections interpreted on the CDP stacked sections possess dominant frequencies in excess of 100 Hz. Reflections can be interpreted on stacked sections at two-way times from 80 msec (approximate depth of 70 m; 230 ft) to 220 msec (approximate depth of 200 m; 656 ft). The Stone Corral anhydrite reflection is present between 200 and 220 msec on all three seismic lines and possesses a maximum of 20 msec (35 m assuming 1,770 m/sec seismic velocity) of relative subsidence. The March 1990 subsurface dissolution boundary, as defined by the Stone Corral anhydrite, suggested a potential four-fold increase in the surface area of the sinkhole encompassing part of both an east-west and a north-south county road.

Introduction

Subsurface dissolution of salt beds represents a hazard to surface and subsurface structures in many parts of the world. Natural or anthropogenic subsidence can occur either gradually or catastrophically (Walters, 1977). Determination of potential extent of future surface subsidence allows more accurate damage estimates and rehabilitation requirements.

Seismic-reflection techniques have successfully detected the presence and extent of subsurface dissolution prior to and during surface subsidence (Steeples et al., 1986, 1987; Miller et al., 1985; Knapp et al., 1989). The technique offers a powerful method of imaging portions of the subsurface in the vicinity of some subsidence features. The successful use of the technique depends on several key conditions. First and foremost is the existence of acoustic velocity and/or density contrasts between geologic units in the subsurface. The Stone Corral anhydrite fulfills this condition, having a large acoustic velocity and density contrast with surrounding siltstones, silty sandstones, and shales. The second condition relates to the ability of the near-surface to propagate a high-frequency seismic signal. Finally, the acquisition parameters and recording equipment must be compatible with the proposed target and required resolution of the survey.

Geologic Setting and Subsidence

Several major salt basins exist throughout North America (fig. 1) (Ege, 1984). The Hutchinson Salt Member of the Permian Wellington Formation underlies a significant portion of south-central Kansas (fig. 2) (Walters, 1977). The thickness of the salt increases from depositional edges on the west and north, an erosional edge on the east, and a facies change on the south to a maximum thickness of over 170 m (558 ft) in north-central Oklahoma. The increased thickness of the Hutchinson Salt is due to increased quantities of salt as well as more and thicker interbedded anhydrites. Thickness of the salt in the vicinity of the Siefkes subsidence is approximately 75–85 m (246–279 ft) (figs. 3 and 5) (Watney, 1980). Cross section A–A´ shows the distribution of salt along an east-west profile located 6 mi (9.6 km) north of the Siefkes subsidence feature (fig. 6) (Watney, 1980). The Siefkes subsidence is located approximately 120 km (72 mi) west of the Hutchinson Salt dissolution front (figs. 3 and 6) (Watney, 1980).

The stratigraphic section overlying the Hutchinson Salt Formation at the Siefkes well location is the target of this seismic-reflection survey (fig. 5). Overlying the salt are approximately 70 m (230 ft) of the upper Wellington Formation shales with minor carbonates, 80 m (262 ft) of the Ninnescah Shale with minor carbonates, and 6 m (20 ft) of Stone Corral anhydrite at a depth of 186 m (610 ft). The Stone Corral is a key seismic marker horizon in central Kansas. The depression of the Stone Corral, resulting from dissolution of the underlying Hutchinson Salt, is used to map the lateral extent of the Siefkes subsidence feature in the subsurface. Overlying the Stone Corral is approximately 70 m (230 ft) of Harper Sandstone, 80 m (262 ft) of Salt Plain Sandstone, and 41 m (135 ft) of Quaternary unconsolidated sediments.

Salt dissolution can result in various rates of surface subsidence. The dissolution process remains active as long as flowing unsaturated brine solution or freshwater is in contact with a salt bed. This results in the formation of a void, generally water filled, within the salt bed. Depending on the size of the void and the competency of the overlying sedimentary section, either a void or a closed collapse feature migrates upward at varying rates. The result is a catastrophic collapse or gradual subsidence when the effect of the dissolution feature reaches the surface.

Natural dissolution of the Hutchinson Salt is not uncommon in Kansas (Ege, 1984). Surface subsidence associated with natural salt dissolution occurred in Meade County, Kansas, in 1879. Faults extending through the Pleistocene sediments (sediments containing freshwater under hydrostatic pressure) are postulated as the conduits for flow instigating the salt dissolution that eventually resulted in the Meade County sinkhole (Frye and Schoff, 1942). Paleo-sinkholes resulting from dissolution of the Hutchinson Salt prior to Pleistocene deposition have been discovered with high-resolution seismic-reflection surveys (Steeples et al., 1984). Natural dissolution of the Hutchinson Salt may have been occurring to some degree in some localities since deposition.

FIGURE 1—Major salt basins of North America (Ege, 1984).

Land subsidence associated with salt mining and petroleum-related brine disposal has been documented in Kansas for at least the last 70 years (Walters, 1977). In cases related to solution salt mining, sinkholes generally have been the result of roof rock failure. Casing failure or faulty surface grouting have allowed petroleum by-product disposal wells to become conduits to the Hutchinson Salt (unsaturated brine solutions). Sinkholes related to brine-disposal wells result from roof failure similar to sinkholes associated with solution mining of salt.

Siefkes Subsidence Feature

The Siefkes subsidence feature is located in NE NE NE sec. 3, T. 22 S., R. 12 W. in Stafford County, Kansas (fig. 3). The gradually forming, anthropogenic subsidence feature is centered on the plugged Siefkes "A" No. 6 saltwater-disposal well (fig. 4). A rough visual estimate of surface subsidence as of 1990 indicated the feature had approximate dimensions of 75 m by 85 m (246 ft by 279 ft) laterally with about 0.5 m (1.6 ft) maximum vertical displacement (fig. 4). This is a minimum estimate since visually determining the outer edges of a shallow subsidence feature is difficult.

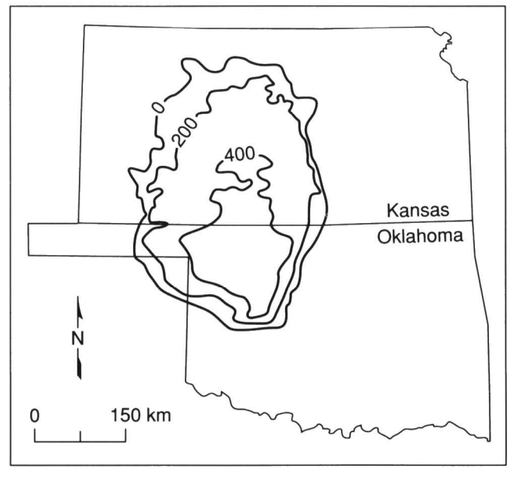

FIGURE 2—Areal extent and thickness of Hutchinson Salt Member (Walters, 1977).

The Siefkes "A" No. 6 drillhole was completed in November 1939. It penetrates the Hutchinson Salt Member of the Wellington Formation from 344 m to 416 m (1,129 ft to 1,365 ft) in depth. The drillhole has a total depth of 1,100 m (3,609 ft) and terminates in the Arbuckle Formation. The well was converted to a saltwater-disposal well in 1950 (Korphage, personal communication, 1992). Unsaturated fluids eventually reached the Hutchinson Salt either through corroded casing or along the outside of the casing. The well passed a mechanical integrity test as late as 1986, but due to evidence of surface subsidence, it was plugged in 1988 (Morris, personal communication, 1992). The onset of dissolution of the Hutchinson Salt and the time required for the subsidence to have developed a noticeable surface expression is unknown.

Field Parameters

Three CDP seismic-reflection lines were acquired with nominal 24-fold redundancy (fig. 4). The lines were roughly centered on and intersect at the Siefkes "A" No. 6 inactive brine-disposal well. Lines 1 and 2 were acquired during March 1989 with line 3 acquired in March 1990. The original two lines (1 and 2) were collected with extremely dry near-surface conditions and abnormally high winds. It was determined after digital processing of data from lines 1 and 2 that more subsurface information was needed east of the north-south county road. The third line was then acquired using the results of lines 1 and 2 to determine line length and location.

An extensive series of walkaway-noise tests was conducted prior to production acquisition (table 1). The compacted near-surface material made it impossible to use the downhole .50-cal seismic source (the source of choice at this site, for this geologic target) and forced the use of an above-ground silenced .50-cal gun. The .50-cal silencer reduces source-generated air-coupled waves and acts as a containment device for stray debris. The surface configuration of the .50 cal is less energetic and does not generate the high frequency and broad bandwidth signal possible with the .50 cal in the downhole mode (Steeples et al., 1987). The receiver array consisted of three 40-Hz geophones equally spaced over approximately 1 m (3.3 ft) and centered on each station. The receiver array was designed in an attempt to attenuate the source-generated noise. The acquisition parameters and equipment for lines 1 and 2 were optimized for the less-than-ideal site conditions.

Significant changes in the near-surface conditions during the March 1990 survey necessitated a new set of walkaway-noise tests for line 3 (table 1). Improved near-surface conditions allowed the use of the .50-cal downhole gun. In the downhole configuration of the .50 cal, the gun barrel is lowered down an augered hole approximately 6 cm (2.4 inches) in diameter and 0.6 m (2 ft) deep. The downhole placement of the barrel greatly reduces both the source-generated air-coupled waves and the thickness of low-velocity, highly attenuative near-surface material through which seismic energy must travel. Station spacing was identical to the 1989 survey as were the receiver arrays and source/receiver geometries. Consistent with the 1989 survey, the acquisition parameters and equipment were optimized to the site conditions and geologic target.

The source/receiver geometry on all three lines resulted in a nominal 24-fold data set. Most shot locations were occupied twice, once pushing the 24-channel spread from low-numbered stations to high-numbered stations and then reversed, pushing the same spread from high-numbered stations to low-numbered stations. This acquisition procedure results in a pseudo 48-channel symmetric (with respect to the source location) split-spread geometry with two consecutive groups of 24 channels separated by three stations.

The 24-channel data were analog-filtered, amplified, A/D-converted (11 bit plus sign), and recorded on an Input/Output DHR-2400 seismograph. Analog low-cut filters helped to enhance the data bandwidth by decreasing the amount of low-frequency noise, allowing increased gaining of incoming post-filtered high-frequency signal. The analog low-cut filters selected have a 24 dB/octave roll-off with a -3 dB point of 110 Hz for line 3 and 55 Hz for lines 1 and 2. The relatively severe analog low-cut filtering increased the dominant reflection frequencies and therefore improved the potential vertical- and horizontal-bed resolution.

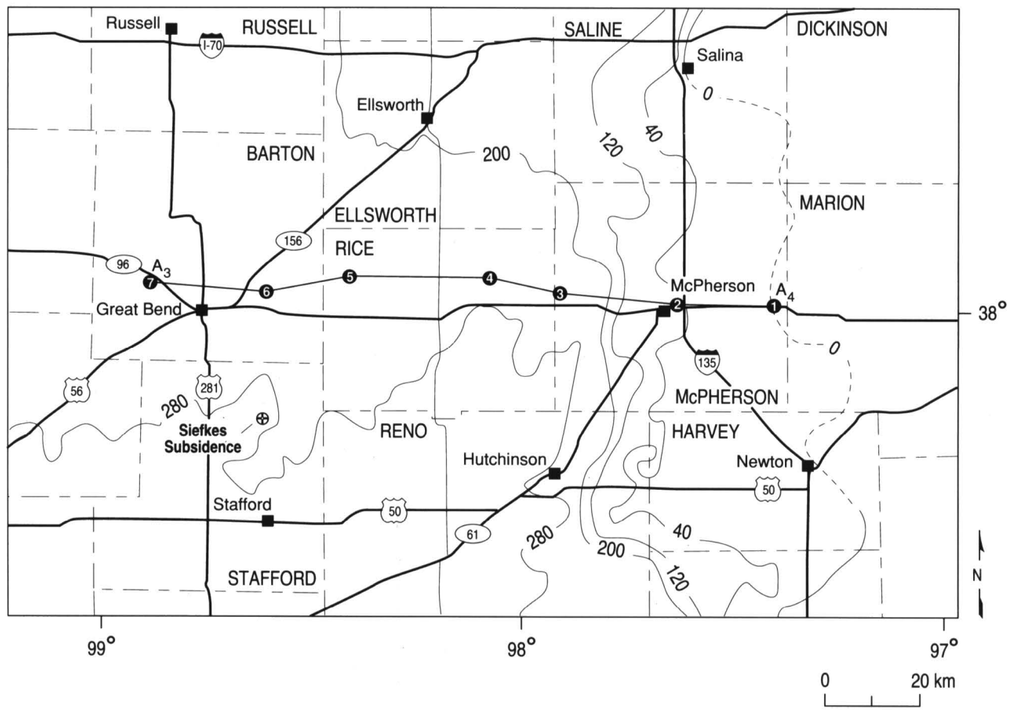

FIGURE 3—SIEFKES SUBSIDENCE LOCATION MAP, INCLUDING HUTCHINSON SALT THICKNESS CONTOURS and drillhole cross section location (Watney, 1980).

TABLE 1—CRITICAL ACQUISITION PARAMETERS.

	3/90	3/91
Station increment	5 m (16.5 ft)	same as 3/90
Receiver array length	1.5 m (4.9 ft)	same as 3/90
Split-spread intervals*	10 - 125 m (33–412.5 ft)	same as 3/90
Source	.50 cal surface	.50 cal downhole
Receivers	L28E Mark Prod.	same as 3/90

*Source-to-nearest-and-farthest-receiver distance

TABLE 2—CDP SEISMIC PROCESSING STEPS.

Format to SEG-Y
Dead and noisy trace edit
Trace balancing (AGC)
First-arrival muting
Surgical muting of coherent noise
CDP sort
Datum statics correction
NMO correction
Surface-consistent statics
Bandpass filtering
CDP stack

Data Processing

The CDP data were processed at the KGS using a proprietary set of algorithms developed by Sytech Co. The processing flow was very similar to routine petroleum sequences with the exception of the severity and accuracy of the muting processes and the emphasis placed on near-surface velocity analysis (table 2). Extreme care was used during the editing processes to ensure removal of all non-seismic energy that could either be misinterpreted as reflections on stacked data or that hampered interpretations of real reflection events. Velocity analysis incorporated iterative constant velocity stacking with detailed surface-consistent statics to improve both accuracy of velocity corrections and time/depth conversion on interpreted cross sections. The general processing flow resulted in a nominal 24-fold CDP stacked section for each of the three survey lines.

Results

Reflection energy can be identified on raw field data in a time window between about 80 msec and 400 msec (fig. 7). Differentiation of reflection energy from seismic noise on field files is essential for confident and consistent interpretation of stacked seismic sections. Refraction arrivals, present as the first breaks (first source-generated energy recorded) on seismograms, were removed with a severe first-arrival mute. Low-velocity linear arrivals that can be identified on the nearest-to-the-source trace at about 50 msec and on the farthest-from-the-source trace at about 400 msec are source-

generated air-coupled waves. Air-coupled waves were surgically removed from all shot gathers. Ground roll is the low-frequency energy clearly visible on inside traces between 10 m and 40 m (33 ft and 131 ft) source offset. The low-frequency characteristics of the ground roll make attenuation with a properly designed bandpass filter very effective. Dominant frequency of reflection energy is in excess of 100 Hz.

Reflections from the Stone Corral anhydrite can be clearly identified at about 210 msec on most field files (fig. 7). The apparent reverse moveout on the Stone Corral reflection on this field file is interpreted to be the result of roof failure of a previous salt-dissolution void. Stone Corral reflections on seismograms from areas with competent salt would appear hyperbolic with a very subtle downward curvature at increasing receiver-to-source offsets. The reflection energy interpretable on this seismogram clearly indicates subsurface collapse. A synthetic seismogram calculated from the nearby Sittner "A" No. 1 acoustic-velocity log supports the interpretation of the field file (fig. 8). The strongest reflector on the synthetic seismogram is the Stone Corral. The absolute two-way travel time of the Stone Corral reflector calculated from the synthetic seismogram is unknown because the acoustic log used to generate it was not recorded above a depth of 76 m (250 ft). However, the amplitude of the Stone Corral reflection is significantly larger than any other reflection occurring between 76 m (250 ft) and 457 m (1,500 ft) on the synthetic seismogram. This supports the interpretation that the large amplitude 210-msec reflections observed on lines 1, 2, and 3 (figs. 9, 10, and 11) are from the Stone Corral. By comparing the drill log (fig. 5) with the field file plot (fig. 7), a stacking velocity of 1,800 m/sec is calculated. This is consistent with the results of the velocity analysis carried out during processing.

The top of the Hutchinson Salt does not generate a large amplitude reflection on the synthetic seismogram (fig. 8). In fact, it is a weaker reflector than is indicated by the synthetic seismogram because the low density-high velocity combination of salt results in a small acoustic-impedance contrast with the surrounding low velocity-high density shales. No density log is available for the Sittner "A" No. 1 drillhole, so the large acoustic velocity of the salt is not modified by the salt's low density, and the synthetic seismogram overestimates the salt response. Figure 7 confirms that the top of the Hutchinson Salt is not a good reflector.

Seismic line 1 was acquired with a maximum record length of 250 msec (fig. 9). The target on line 1 was the top of the Stone Corral. Faulting and subsidence interpreted on the Stone Corral is assumed to be the result of dissolution of the salt. Normal faults forming horst and graben structures can be interpreted from the 12-msec depression of the Stone Corral reflection. Subtle coherent reflection events observed between CDPs 225 and 275 above the Stone Corral are most likely from within the Harper and Salt Plain Sandstones. The lack of coherent events between the Stone Corral and the surface from CDPs 275 to 325 is related to the poor near-surface and environmental conditions. Dissolution in the subsurface extends from approximately CDPs 220 to 320 on line 1.

Seismic line 2 was acquired with a maximum record length of 500 msec (fig. 10). Coherent reflection information is identifiable between approximately 70 and 320 msec. The overall data quality on line 2 is better than line 1 due to decreased wind noise. The near-surface conditions were consistent for both lines 1 and 2. The Stone Corral reflection can be identified across the entire line. A depression of up to 20 msec is observed on the Stone Corral reflector. Several reflection events between the Stone Corral and the surface are interpreted as coming from within the Harper and Salt Plain Sandstones and are across the entire expanse of line 2. The interpretative line drawing clearly shows the extent of faulting and the relatively uniform nature of the subsidence in the subsurface. The severity of reflector slump observed on line 2 appears to increase with depth. This apparent decrease in subsidence upward from the salt is probably related to differential expansion, although it could be related to velocity anomalies related to slumping into the cavity. The predominant structural features on line 2 are the series of normal fault blocks that bound the graben formed as a result of dissolution and subsidence.

Line 3 was acquired east-west and is the most conclusive of the three seismic lines (fig. 11). The dominant frequency of the Stone Corral reflection is clearly in excess of 100 Hz. Subsurface subsidence on line 3 extends from CDP 250 to 340. Normal faults offset the Stone Corral reflection across the entire subsidence area. The maximum depression of the Stone Corral reflection is 20 msec. Only the normal fault interpreted at approximately CDP 325 offsets the 80-msec reflecting event. The 80-msec reflection is the shallowest interpreted reflector at a depth of approximately 50 m (164 ft). Several high-frequency events are interpreted between the 80-msec reflection and the approximately 200-msec Stone Corral reflection. The relatively uniform, gradual slump of reflectors overlying the dissolved salt can be observed on all three lines.

The 20-msec depression of the Stone Corral reflector visible on lines 2 and 3 (figs. 10 and 11) represents the Siefkes subsidence feature in the subsurface. By using an 1,800-m/sec stacking velocity, calculation of a 35-m (115-ft) maximum vertical displacement of the Stone Corral is possible. If the stacking velocity within the zone of subsidence is reduced by the collapse and fracturing of the sediments overlying the salt, the resulting vertical displacement would be proportionately less than 35 m (115 ft).

The potential future surficial expression of dissolution voids in the Hutchinson Salt can be extrapolated from interpretations on the Stone Corral reflection (fig. 12). The dashed portions of the interpreted future sinkhole represent speculative interpolation between control points on the associated seismic lines. The apparent eastward elongation of the future sinkhole along line 3 indicates subsidence of the Stone Corral reflector was probably active along the eastern edge between March 1989 and March 1990. This ongoing subsidence of the Stone Corral may be indicative of active dissolution or delayed roof failure along the eastern portion of the salt void.

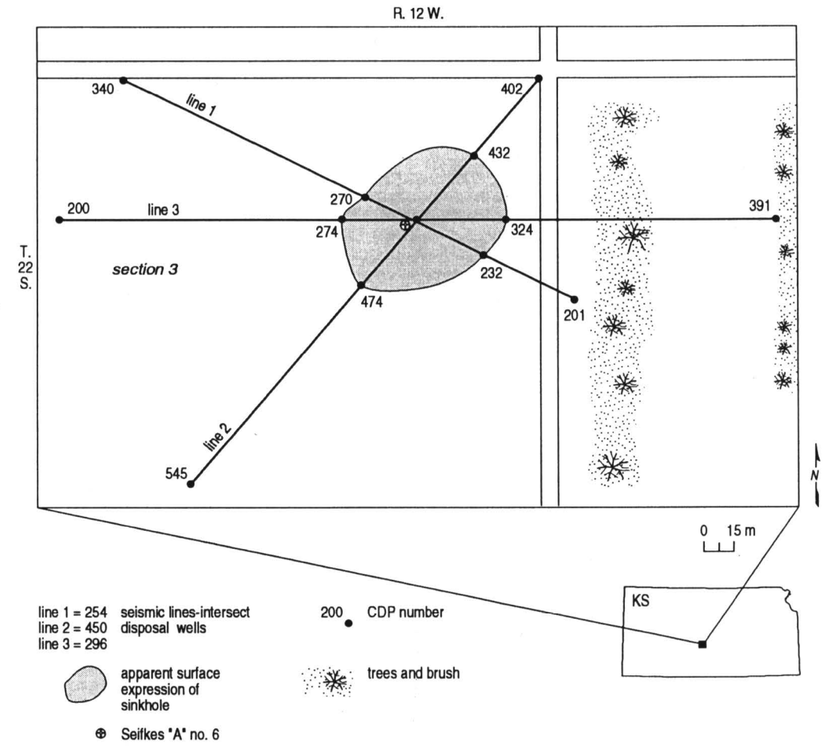

FIGURE 4—SITE MAP INDICATING LOCATION OF THREE SEISMIC LINES AND APPROXIMATE AREAL EXTENT OF THE SUBSIDENCE.

Conclusions

Optimum recording parameters for each line were selected after two separate extensive series of walkaway-noise tests, one for each survey (table 1) (Steeples and Miller, 1990). Adverse near-surface and environmental conditions, detrimentally affecting both geophone plants and propagation of high-frequency seismic-reflection information, strongly contributed to a low signal-to-noise ratio on the 1989 survey. Improved site conditions on the 1990 survey allowed use of the downhole .50-cal gun and 110-Hz low-cut filters, which (in comparison to the 1989 survey) resulted in reduced levels of recorded environmental, instrument, and non-seismic reflection noise.

The subsurface subsidence associated with this Siefkes subsidence feature (at least as indicated by the Stone Corral anhydrite) seems to have been active as of March 1990. Extrapolation of the present subsurface dissolution boundaries (as interpreted from the Stone Corral reflection) suggests a potential four-fold increase in the surface area of the present-day sinkhole. At some time in the future, this sinkhole could include part of the east-west and north-south county roads. Dissolution of the salt, as interpreted from seismic data, appears to be

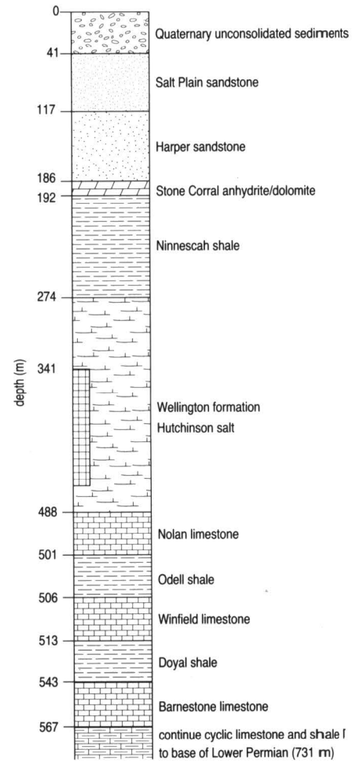

FIGURE 5—STRATIGRAPHIC SECTION FROM SIEFKES "A" NO. 6 GAMMA RAY/NEUTRON LOG.

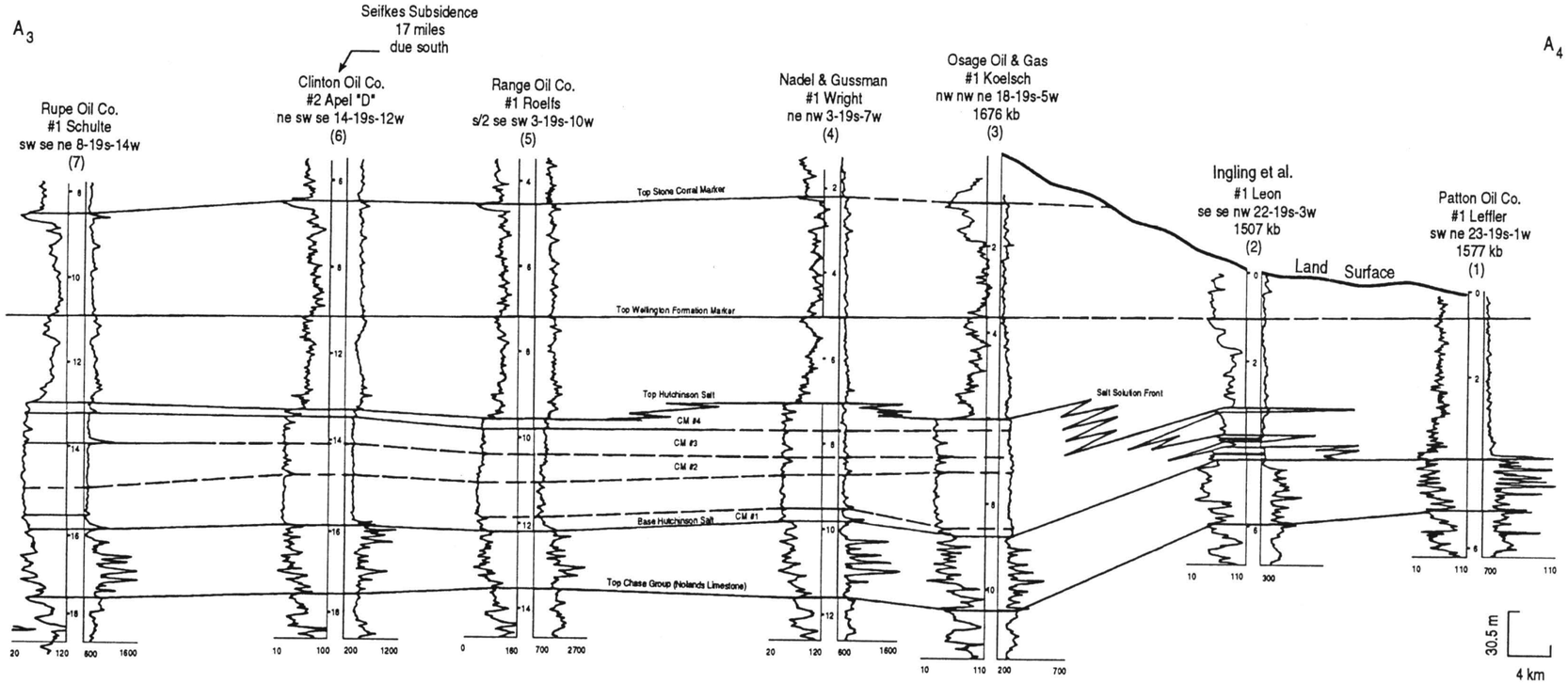

Open file August, 1980
W. L. Watney
Kansas Geological Survey

West to east stratigraphic cross section
Scott County to McPherson County, Kansas
Hutchinson Salt Member, Wellington Formation
Datum: Top Wellington formation marker
Logs: Gamma Ray-Neutron (API Units)

FIGURE 6—DRILLHOLE CROSS SECTION A3–A4 THROUGH BARTON, RICE, AND MCPHERSON COUNTIES, KANSAS (Watney, 1980).

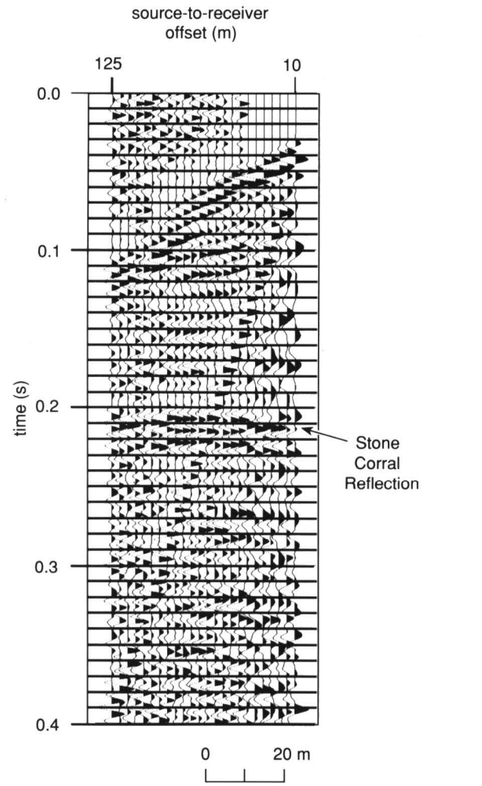

FIGURE 7—24-CHANNEL FIELD FILE WITH STONE CORRAL REFLECTION INDICATED.

slightly asymmetric to the west with respect to the surface location of the abandoned disposal well.

There is no reason to suspect the apparent eastward growth of the subsurface dissolution front has terminated. The actual subsurface dissolution front could be well east of the north-south county road that intersects line 1. It is also not unreasonable to suggest that the northeast boundary (as interpreted from line 2) may now be several tens-of-meters closer to the intersection of the two county roads. No seismic evidence exists (on the three seismic lines reported here) to suggest the surficial expression of the subsurface subsidence will reach the intersection of the north-south and east-west county roads. The north-south county road will eventually be affected by the salt dissolution which has already resulted in subsurface subsidence (as interpreted on the Stone Corral anhydrite) several tens-of-meters east of the road.

The interpreted subsurface subsidence on the western boundary appears to be consistent over the span of time between the two seismic surveys. Topographic evidence seems to suggest surface subsidence is presently active along the western boundary. There is no seismic evidence to suggest westward expansion of subsurface subsidence.

The apparent subsurface growth of the dissolution front to the east with no apparent associated surface subsidence suggests delay between roof failure of the salt unit and surficial expression. The apparent elongation of the surface expression of the sinkhole to the west between the two seismic surveys with no obvious associated subsurface growth is probably related as well to a delay. The delay between roof collapse and surface subsidence is probably not uniform for all parts of the sinkhole. Alternatively, the rate of dissolution may vary with azimuth from the center of the sinkhole, in which case the elongation noted above may not be indicative of active dissolution.

The results derived from interpretations of the three seismic lines suggest a continued gradual subsiding of the surface around the abandoned disposal well. Due to the apparent active nature of the subsurface subsidence, the maximum future surficial expression of the salt voids and associated roof collapse cannot be ascertained from the three seismic lines collected between March 1989 and March 1990. There appears to be either continued subsurface growth of salt voids to the east or delayed roof failure of previously existing voids in the salt. A return visit to this site in approximately two to three years with the intent of acquiring data along line 3 should yield far more insight into subsurface growth and rate of roof failure.

ACKNOWLEDGMENTS—We wish to thank Randie Grantham, George Coyle, and Mubarik Ali for their assistance with data acquisition. We would like to extend a special thanks to Dean A. Keiswetter for his assistance during acquisition. Also, the work of Esther Price and Mary Brohammer in manuscript preparation and Pat Acker's quality graphics are greatly appreciated. Funding was provided in part by a contract with Quinoco Petroleum.

References

Ege, J. R., 1984, Formation of solution-subsidence sinkholes above salt beds: U.S. Geological Survey, Circular 897, 11 p.

Frye, J. C., and Schoff, S. L., 1942, Deep-seated solution in the Meade basin and vicinity, Kansas and Oklahoma: American Geophysical Union, Transactions, v. 23, pt. 1, p. 35–39

Knapp, R. W., Steeples, D. W., Miller, R. D., and McElwee, C. D., 1989, Seismic reflection surveys at sinkholes in central Kansas; *in,* Geophysics in Kansas, D. W. Steeples, ed.: Kansas Geological Survey, Bulletin 226, p. 95–116

Miller, R. D., Steeples, D. W., and Treadway, J. A., 1985, Seismic-reflection survey of a sinkhole in Ellsworth County, Kansas: Society of Exploration Geophysicists, 55th annual meeting, Washington, D.C., Technical Program Abstracts and Biographies [Exp. Abs.], p. 154–156

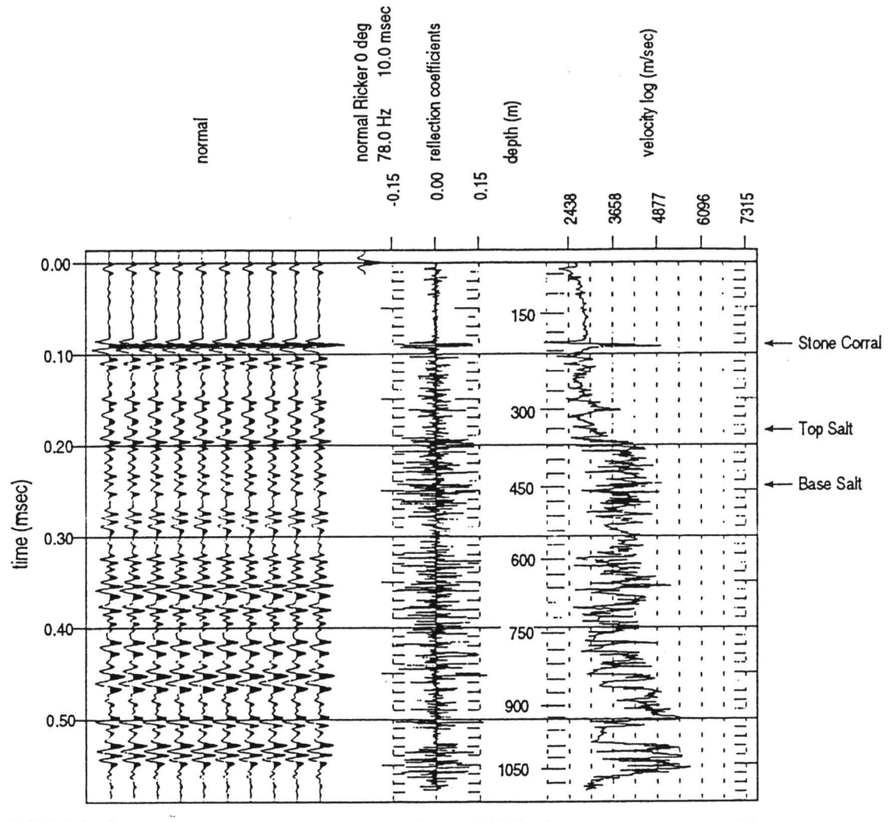

FIGURE 8—SYNTHETIC SEISMOGRAM CALCULATED FROM SITTNER "A" NO. 1 ACOUSTIC VELOCITY LOG. The Stone Corral reflection is indicated.

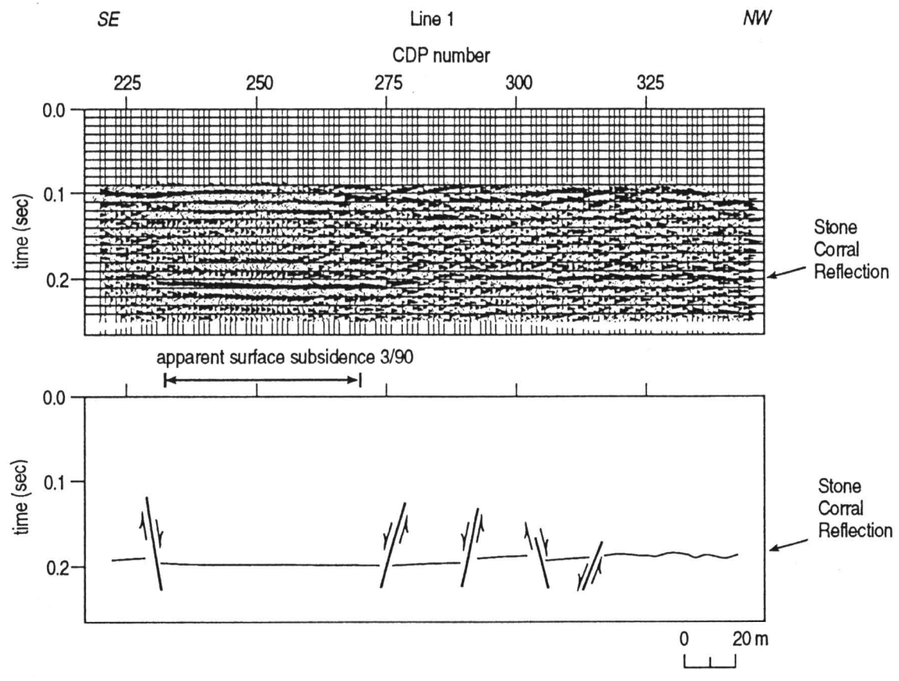

FIGURE 9—PSEUDO 24-FOLD STACK SEISMIC SECTION OF LINE 1 WITH ASSOCIATED INTERPRETIVE LINE DRAWING. The Stone Corral reflection is indicated.

Steeples, D. W., Knapp, R. W., and Miller, R. D., 1984, Examination of sinkholes by seismic reflection; *in,* Sinkholes—Their Geology, Engineering, and Environmental Impact, Barry Beck, ed.: A. A. Balkema, Boston, p. 217–224

Steeples, D. W., Knapp, R. W., and McElwee, C. D., 1986, Seismic reflection investigations of sinkholes beneath Interstate Highway 70 in Kansas: Geophysics, v. 51, p. 295–301

Steeples, D. W., Miller, R. D., and Knapp, R. W., 1987, Downhole .50-caliber rifle—an advance in high-resolution seismic sources [Exp. Abs.]; *in,* Technical Program Abstracts and Biographies: Society of Exploration Geophysicists, 57th Annual Meeting, p. 76–78

Steeples, D. W., and Miller, R. D., 1990, Seismic-reflection methods applied to engineering, environmental, and ground-water problems: Society of Exploration Geophysicists, volumes on Geotechnical and Environmental Geophysics, Stan Ward, ed., Vol. 1—Review and Tutorial, 1–30

Walters, R. F., 1977, Land subsidence in central Kansas related to salt dissolution: Kansas Geological Survey, Bulletin 214, 82 p.

Watney, L., 1980, Maps and cross sections of the Lower Permian Hutchinson Salt in Kansas: Kansas Geological Survey, Open-file Report 80–7

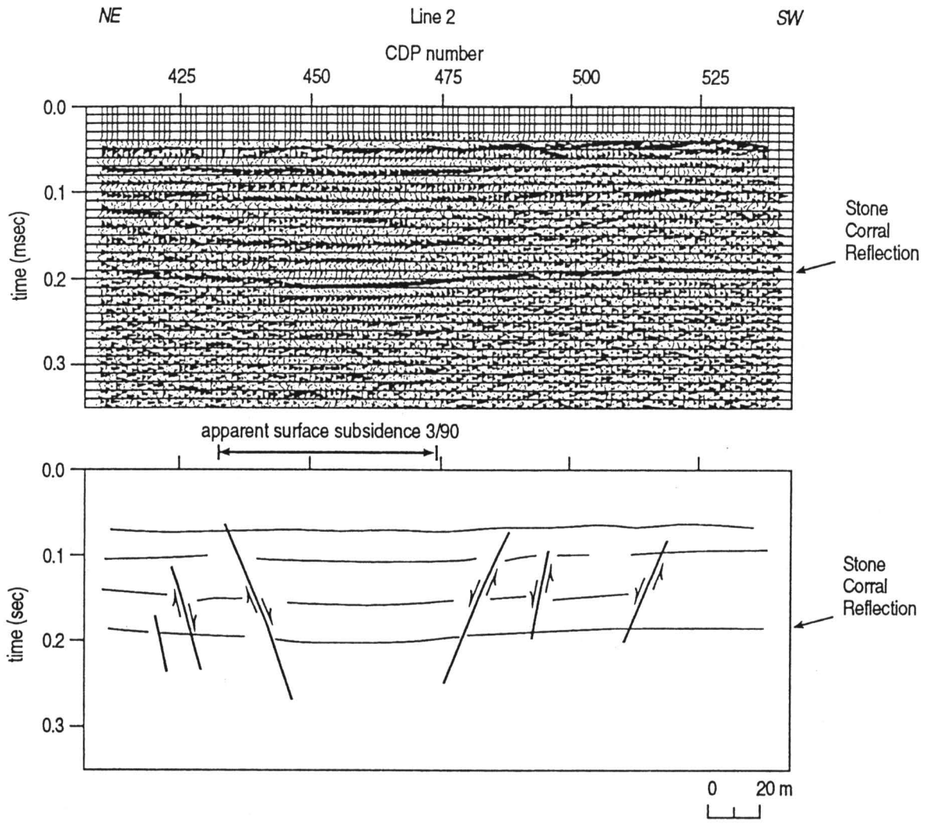

FIGURE 10—PSEUDO 24-FOLD STACK SEISMIC SECTION OF LINE 2 WITH ASSOCIATED INTERPRETIVE LINE DRAWING. The Stone Corral reflection is indicated.

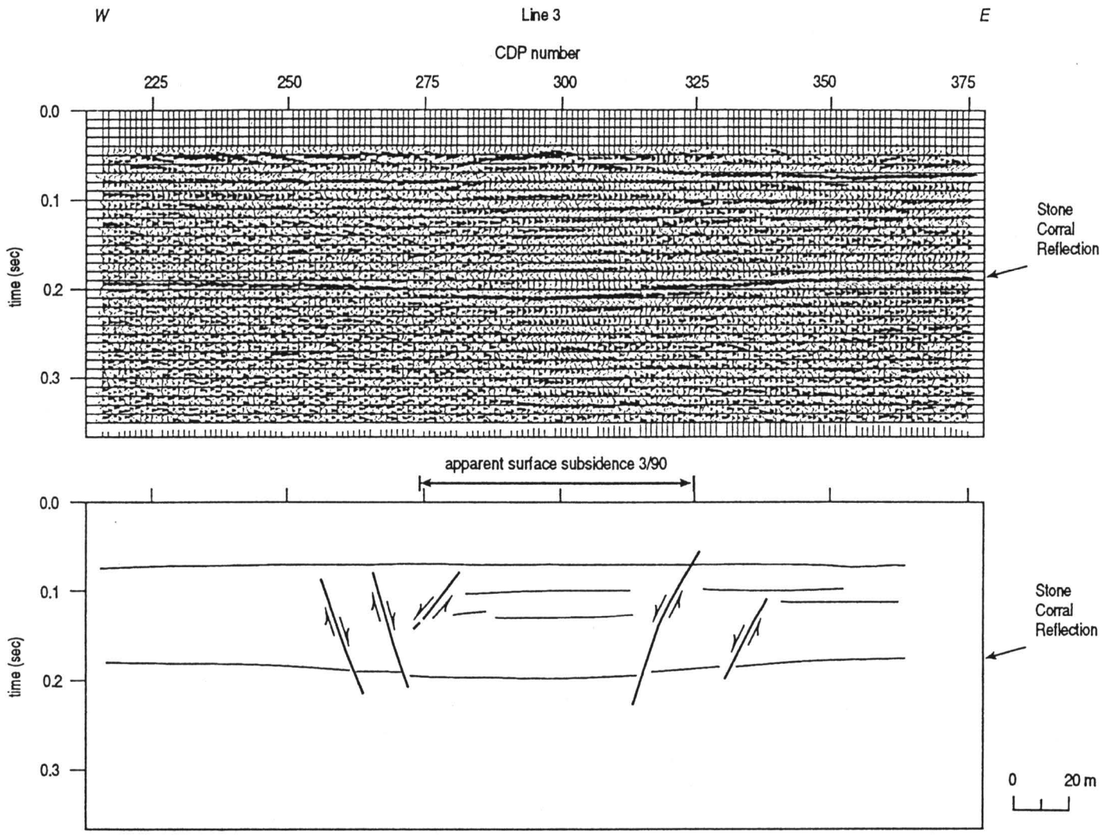

FIGURE 11—PSEUDO 24-FOLD STACK SEISMIC SECTION OF LINE 3 WITH ASSOCIATED INTERPRETIVE LINE DRAWING. The Stone Corral reflection is indicated.

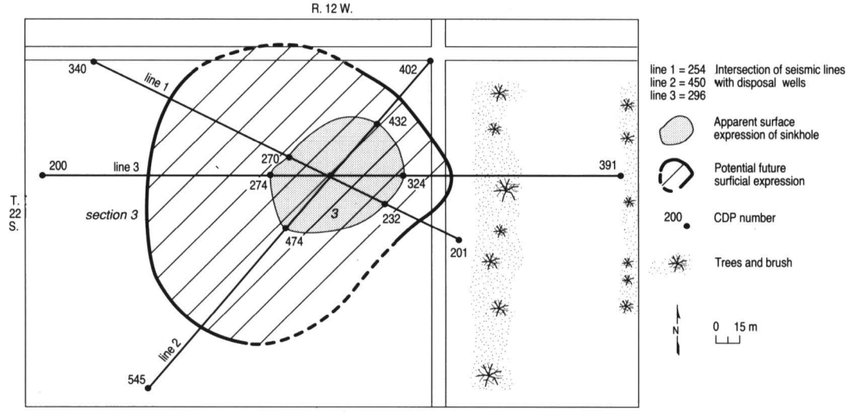

FIGURE 12—SITE MAP SHOWING PRESENT AND POTENTIAL SURFACE SUBSIDENCE AT SIEFKES.

Cheyenne Bottoms Basin—Geophysical Study of a Natural Land-sink Area in Central Kansas

Dean Keiswetter[1], Rob Sporry[2], Neil L. Anderson[3], Tom McClain[4], and Richard D. Miller[5]
[1]Geophex, Ltd., Raleigh, NC 27603; [2]International Institute for Aerospace Surveys and Earth Sciences, Delft, Netherlands; [3]Department of Geology and Geophysics, University of Missouri–Rolla, Rolla, MO 65401;
[4]formerly with Kansas Geological Survey, The University of Kansas, Lawrence, KS 66047; and [5]Kansas Geological Survey, The University of Kansas, Lawrence, KS 66047

Abstract

The Cheyenne Bottoms basin is an elliptical, natural land-sink feature totaling approximately 16,600 ha (41,000 acres). The basin is bounded on the north, south, and west by 35-m (115-ft)-high Cretaceous limestone and sandstone bluffs and on the east and southeast by Pleistocene sand dunes and alluvium. Cheyenne Bottoms is considered the most important ecosystem in Kansas and is one of the most important migration points for shorebirds in North America.

The origin of Cheyenne Bottoms is disputed. Understanding the subsurface structure and potential salt-related mechanisms responsible for the wetlands may help identify tectonic controls important for shallow oil/gas pools. A single, high-resolution CDP line was acquired at Cheyenne Bottoms to test the feasibility of using the seismic-reflection technique to resolve subsurface structures.

Seismic data and geologic well control suggest that the Cheyenne Bottoms area is a natural land-sink, the result of faulting, salt dissolution, and rock-salt creep. The authors' preferred interpretation is that regional faulting during the Pleistocene allowed for the vertical circulation of ground waters, thereby initiating the dissolution of the Hutchinson Salt Member. Salt dissolution, as envisioned, would have been most extensive in the immediate vicinity of the faults. In those areas peripheral to the sites of extensive leaching, rock-salt creep probably occurred. This process entails the creep of rock salt from zones of high pressure (no significant leaching) towards zones of lower pressure (sites of active dissolution or void space).

As a consequence of faulting, the pre-Hutchinson Salt horizons are structurally low in the Cheyenne Bottoms area. As a result of faulting, salt dissolution, and rock-salt creep, the top of the Hutchinson Salt Member and the post-Hutchinson Salt horizons (including the present surface) are also structurally low.

Introduction

Cheyenne Bottoms, located in east-central Barton County, Kansas, is an elliptical, natural land-sink feature (fig. 1) totaling approximately 16,600 ha (41,000 acres). The basin is bounded on the north, south, and west by 35-m (115-ft)-high Cretaceous limestone and sandstone bluffs and on the east and southeast by Pleistocene sand dunes and alluvium (fig. 1). Within this basin, a 7,690-ha (19,000-acre) wetlands lies along the southeastern edge of the sink. The Kansas Department of Wildlife and Parks has maintained the marsh region since 1950, when a system of canals was constructed to divert surface drainage into five pools. Due in part to the rapidly declining marsh regions in the United States, Cheyenne Bottoms is the most important ecosystem in Kansas and among the most important migration points for shorebirds in North America (Wentz, 1990). Water depth in the pools fluctuates with the seasons but seldom exceeds 0.6 m (2 ft).

The origin of the Cheyenne Bottoms basin has been attributed to structural movement (Bayne, 1977) and salt dissolution/subsidence (Johnson, 1901; Bass, 1926; Latta, 1950). The seismic data incorporated into this paper were collected in an effort to verify the presence (or absence) of faults and associated salt-dissolution features.

Geology

Unconsolidated Pleistocene and Holocene alluvial sediments are anomalously thick in the Cheyenne Bottoms basin. In the immediate vicinity of the seismic line, the thickness of these strata are on the order of 35 m (115 ft). The Pleistocene sediments were deposited within the paleo-Chase Channel system (Bayne and Fent, 1963); the Holocene strata are Blood Creek and Deception Creek sediment.

Although deposition of the Ogallala Formation occurred in the Cheyenne Bottoms area during the Tertiary, erosional processes dominated, and no remnant Tertiary rock is preserved. The erosional activities during the Tertiary and regional faulting and associated salt dissolution processes have largely shaped the current bedrock topography.

The Cretaceous Graneros Shale and Dakota Sandstone underlie Tertiary strata within Cheyenne Bottoms and crop out elsewhere, effectively rimming the basin (fig. 2).

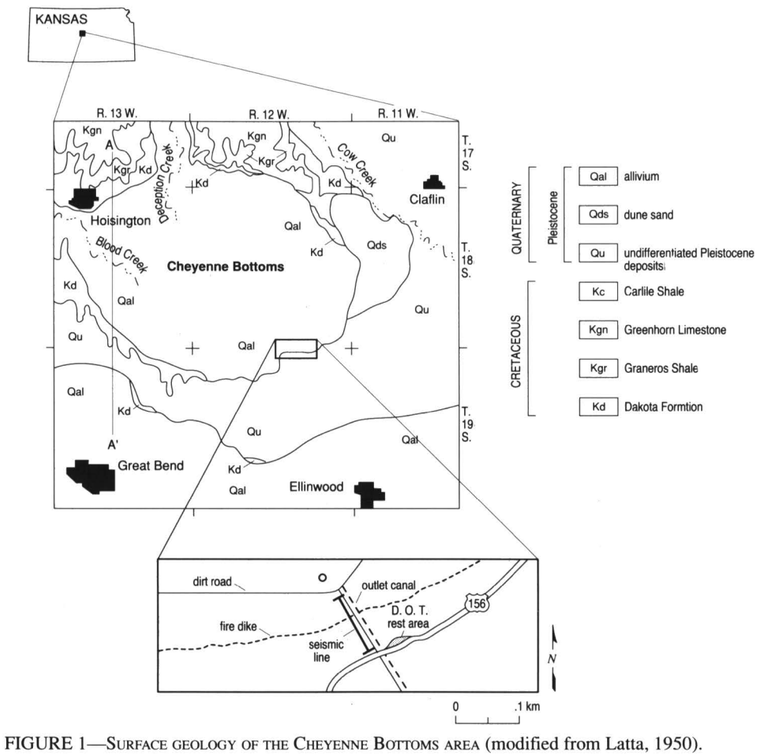

FIGURE 1—SURFACE GEOLOGY OF THE CHEYENNE BOTTOMS AREA (modified from Latta, 1950).

The contour map of the bedrock surface (fig. 3) shows a well-defined erosional channel, the course of which is thought to have been influenced by contemporaneous faulting and salt-related subsidence. The bedrock channel slopes to the southeast at about 1.2 m/km (2.4 ft/mi). Basin walls rise approximately 45 m (148 ft) to the south, west, and north.

Pre-Mesozoic units are represented in the Cheyenne Bottoms area by a sequence of alternating marine limestone, shale, and sandstone (Zeller, 1968; Bayne, 1977; Merriam, 1968). Key strata from a geophysical perspective are the Permian-age Stone Corral Formation of the Sumner Group and the Hutchinson Salt Member of the Wellington Formation. In the Cheyenne Bottoms area, the Stone Corral Formation is composed of dolomite and anhydrite. The Hutchinson Salt Member is composed principally of halite with minor interbeds of anhydrite, dolomite, and shale.

The Stone Corral Formation dips regionally towards the northwest. Within the study area, however, the top of this unit is anomalously (up to 6 m; 20 ft) structurally low relative to the regional trend and defines a basin, the areal extent of which is consistent with the surface area of the Cheyenne Bottoms basin (figs. 4 and 1). The structural low at the Stone Corral level rises abruptly to the northwest where a local anticlinal fold is present. A domelike high is located to the south of the basin in the northwest corner of T. 19 S., R. 12 W.

Similar structural features are observed at the top of the Hutchinson Salt Member (fig. 5). The top of this unit is as much as 9 m (30 ft) structurally low, relative to its regional trend, and is bound to the northwest by a localized high. The domelike high to the south of the basin is similarly distinct on the Hutchinson Salt structure map (fig. 5). Bayne (1977) noted that borehole information to the top of the Hutchinson Salt Member within the Cheyenne Bottoms area is sparse and that additional data could potentially change the extent and shape of the basin feature.

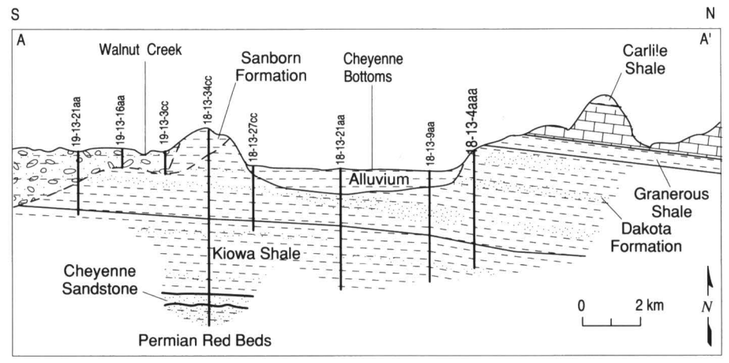

FIGURE 2—GEOLOGIC CROSS SECTION (Latta, 1950), location of cross section is indicated on fig. 1.

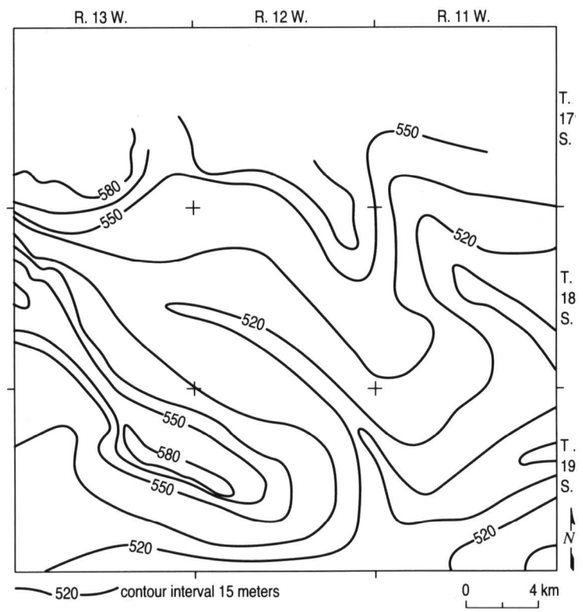

FIGURE 3—Contour map of the bedrock surface (data from Latta, 1950; contoured by Bayne, 1977).

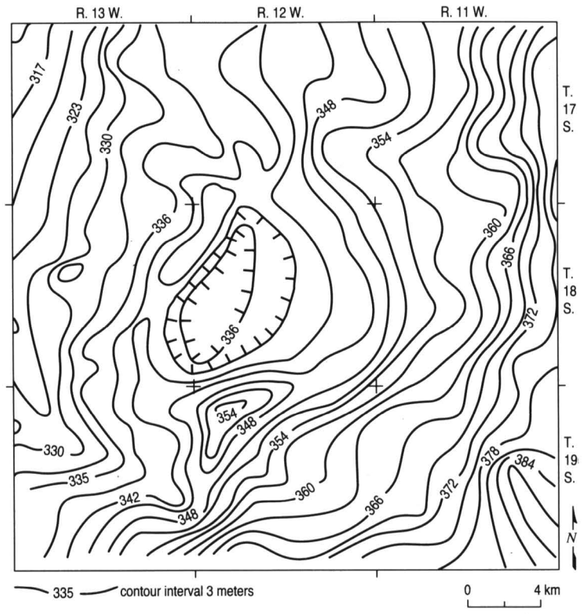

FIGURE 4—Contour map of the top of the Stone Corral Formation (Bayne, 1977).

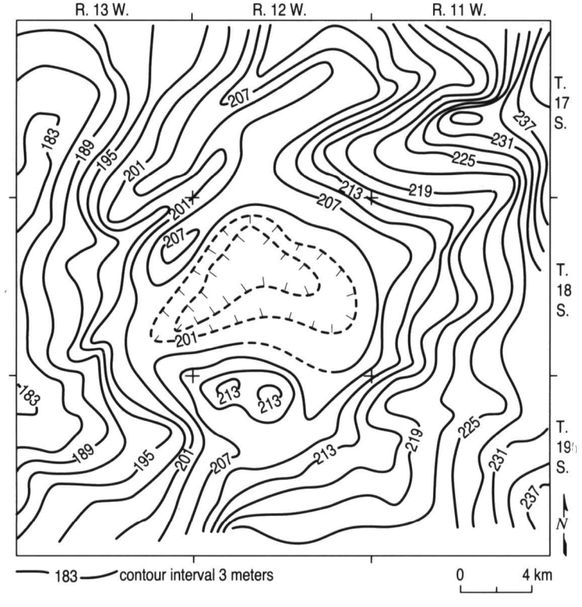

FIGURE 5—Contour map of the top of the Hutchinson Salt Member (Bayne, 1977).

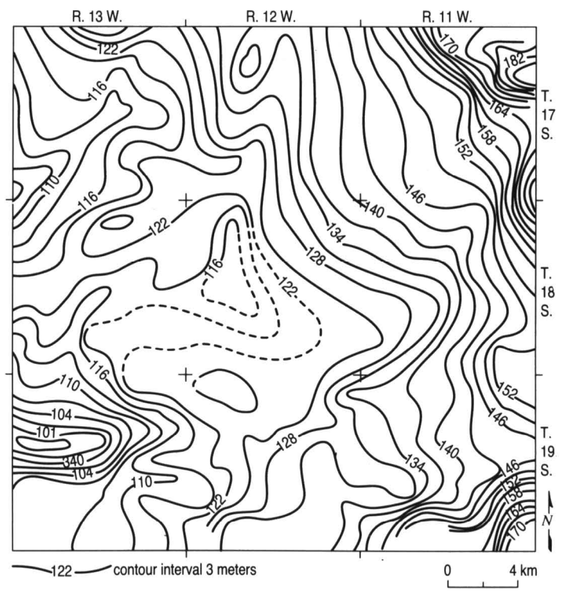

FIGURE 6—Contour map of the base of the Hutchinson Salt Member (Bayne, 1977).

Structure at the base of the Hutchinson Salt Member (fig. 6) is similar but of lesser magnitude than that at the tops of the Hutchinson Salt and Stone Corral. The domelike high to the south of the Cheyenne Bottoms basin is still present but reduced in relief. The bounding structure to the west of the basin is present but is larger and shifted to the west.

The patterns of structural relief observed at the top of the Stone Corral and at the top and base of the Hutchinson Member are consistent with the thesis that the Cheyenne Bottoms basin is partially the result of faulting and salt-related subsidence.

Data Acquisition

In an effort to elucidate the geologic origin of the Cheyenne Bottoms basin, seismic data were acquired adjacent to the edge of the marsh along an outlet canal (fig. 1; sec. 34, T. 18 S, R. 12 W.). The location of the CDP line was chosen based on proximity to well data (geologic control), accessibility to field vehicles, and quiet environmental conditions. The saturated, alluvial media provided excellent geophone–near surface coupling. Routine acquisition procedures such as consistent firing procedures; deeply rooted, vertical geophone plants; and manicuring the source and geophone locations to remove surface vegetation maximized recorded frequency response and helped attenuate unwanted source-generated noise.

An Input/Output 2400 DHR seismograph was used to analog filter, amplify, A/D convert (11 bits plus sign), and record the seismic data. These data were displayed on paper plots during acquisition and stored on magnetic media in a modified SEG-Y format. The selected sample interval was 0.5 msec and record length was 500 msec. Analog low-cut filters with a 24 dB/octave roll off and a –3 dB point of 220 Hz were used; the severe analog low-cut filters improved the resolution, decreased the effects of ground roll, and allowed the depth interval of interest to be imaged. The receiver array consisted of 3–40 Hz Mark Product L-28E geophones (with a damping factor of 0.7), wired in series, evenly spaced over 0.6 m (2 ft), and centered on 1.2 m (4 ft) stations. The geophone array was designed to enhance signal levels and attenuate source-generated noise. The fixed gain amplification, 72-dB instantaneous dynamic range, and 24-channel recording capabilities make the DHR 2400 competitive for target-oriented studies.

Walkaway-noise Tests

A series of walkaway-noise tests were conducted to optimize acquisition parameters (fig. 7A, B). Source to receiver offsets ranged from 2 m to 246 m (6.6 ft to 807 ft), with three-geophone arrays centered on 1.2-m (4-ft) group spacings. Placement of the source in a 1-m (3.3-ft) hole to avoid wave attenuation by the weathered layer was possible due to the water-saturated, alluvial, near-surface media. The broad band characteristics and high energy output of the downhole .50-caliber rifle (Steeples et al., 1987) made it the source of choice at this site.

Analog low-cut filters shape the recorded spectrum, resulting in data with a higher dominant frequency and broader bandwidth than data recorded with no low-cut filters (Steeples, 1990). Increasing the dominant frequency and broadening the frequency spectrum of reflection energy improves resolution (Widess, 1973). During testing procedures, open (no low-cut filter), 110-Hz (fig. 7A, C), 220-Hz (fig. 7B, C), and 340-Hz low-cut filters were tested. As the low-cut filter is increased, noticeable increases in dominant frequency are observed (figs. 7A–C) The 220-Hz low-cut filters were selected

for production acquisition based on an in-field analysis of shot records. Subsequent processing and display indicate that a low-cut filter with a lower corner frequency may allow the Paleozoic sequence to be better imaged.

The survey produced excellent data; on several of the noise spreads (figs. 7A, B), hyperbolic reflection events can be identified as early as 20 msec; others can be observed between 30 and 200 msec, with several less defined reflections, between 200 and 300 msec.

Data Processing

The Cheyenne Bottoms data were processed on an Intel 80386-based microcomputer using *Eavesdropper* (a seismic-data-processing package developed and marketed by the Kansas Geological Survey). The processing flow is displayed in table 1. Special care was taken during trace editing, surgical muting, and velocity analysis. Deconvolution and migration processes were not applied. No corrections for elevation were made due to the relatively flat topography along the seismic line. During the processing flow, each step was visually inspected in an effort to ensure that processing artifacts were not introduced.

Velocity analysis is critical during high-resolution seismic-data processing. Inaccurate stacking velocities will effectively lower the frequency content of the stacked section and result in unreliable time-to-depth conversions. Due to the highly variable weathered layer, stacking velocities varied considerably both laterally as well as vertically. After visual inspection of velocity panels, the velocity function shown in table 2 was selected.

Spectral analysis techniques were used to define appropriate digital filters. Digital frequency filters are often critical in verifying reflection events. These data are of sufficient quality that digital filtering simply enhanced shallow events while enabling deeper events to be resolved. After the spectral analysis, a band pass filter of 75 to 250 Hz was applied to the final stack (corner frequencies 35, 75, 250, 400 Hz). The ground-roll energy was sufficiently reduced during the digital filtering and stacking processes such that no other procedures (such as surgical muting) were required.

Borehole Data/Modeling

In fig. 8 a one-dimensional synthetic seismogram for a well near the Cheyenne Bottoms area (sec. 28, T. 19 S., R. 11 W.) is presented. This seismogram was generated by convolving an edited version (the pseudo-density log was modified as per figure caption) of the reflection coefficient wavetrain (250–1,570-ft interval; 76.2–479-m interval) with zero-phase, 5-msec wavelength Ricker wavelets of both normal and reverse polarity. The synthetic seismogram is presented as a reasonable representation

TABLE 1—GENERALIZED PROCESSING SEQUENCE used to generate the CDP stack.

Raw data
↓
Conversion to SEG-Y format
↓
Bad trace editing
↓
Surgical muting of first arrivals and air-wave energy
↓
Frequency filter
↓
CDP sorting
↓
Velocity analysis
↓
NMO correction
↓
Automatic static corrections to apply surface-consistent statics
↓
Residual static corrections
↓
CDP stack
↓
Trace balancing

A

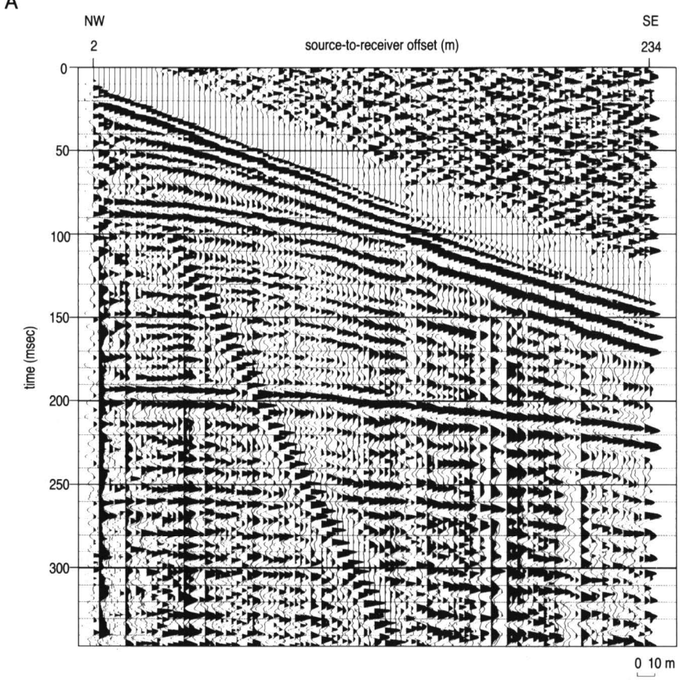

B

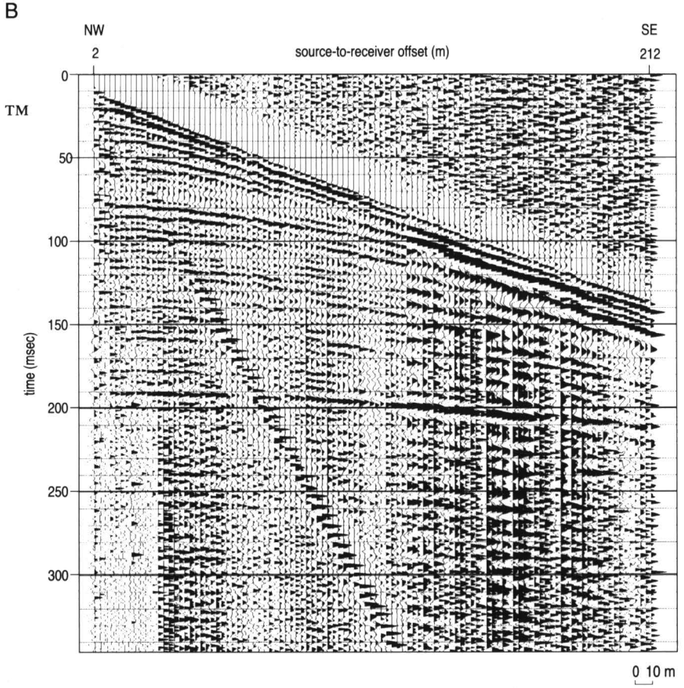

C

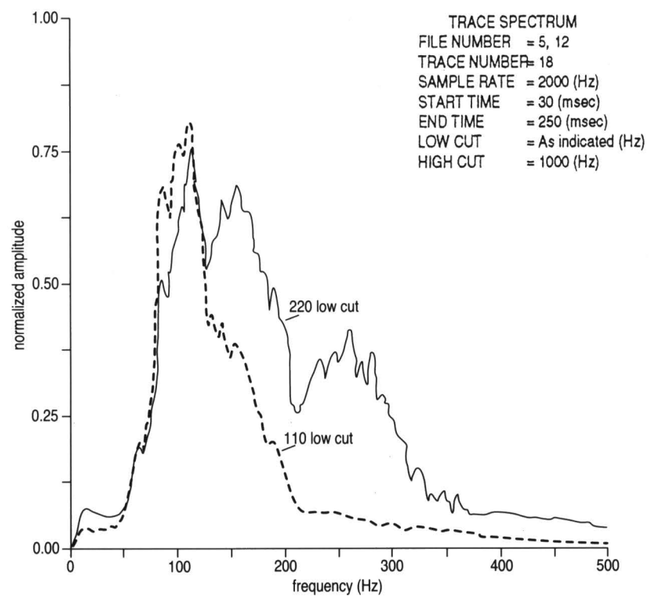

FIGURE 7—A) WALKAWAY-NOISE SPREAD ACQUIRED WITH THE 110-HZ LOW-CUT FILTERS.

B) WALKAWAY-NOISE SPREAD ACQUIRED WITH THE 220-HZ LOW-CUT FILTERS. Source-to-near offset is 2 m (6.6 ft) for both the walkaways; trace spacing is 2 m (6.6 ft).

C) COMPARISON OF FREQUENCY VS. AMPLITUDE SPECTRA for data acquired with different low-cut filters (110 vs. 220 Hz as shown).

TABLE 2—VELOCITY FUNCTIONS AS A FUNCTION OF LOCATION AND TIME. The velocity value is the average velocity from the surface to the specific time.

Station 210		Station 220		Station 235		Station 250	
Time (msec)	Velocity (m/sec)	Time (msec)	Velocity (m/sec)	Time (msec)	Velocity (m/sec)	Time (msec)	Velocity (m/sec)
30	1200	30	1200	30	1200	30	1200
40	1375	40	1350	40	1350	40	1300
55	1600	55	1475	55	1450	60	1400
80	1700	80	1700	85	1700	80	1600
130	1750	130	1700	100	1800	120	1700
150	1800	155	2100	130	1800	155	1700
190	2300	185	2500	155	1900	185	2000
300	3000	300	3000	185	2000	300	3000
				300	3000		

Station 265		Station 272		Station 280		Station 290	
Time (msec)	Velocity (m/sec)	Time (msec)	Velocity (m/sec)	Time (msec)	Velocity (m/sec)	Time (msec)	Velocity (m/sec)
30	1250	30	1250	30	1275	30	1200
40	1300	40	1350	40	1500	40	1350
55	1400	55	1500	50	1400	50	1450
80	1600	80	1700	75	1500	75	1600
120	1600	125	1700	110	1600	130	1600
155	1900	150	1900	120	1800	140	1800
185	2000	185	2100	150	2000	190	2300
300	3000	300	3000	185	2100	300	3000
				300	3000		

of high-resolution (156 Hz) CDP-stacked seismic data. As is illustrated in fig. 8, the normal- and reverse-polarity displays are mirror images; troughs on the normal-polarity seismogram correlate to peaks on the reverse-polarity display. Definitions for these terms may be found in Anderson et al. (1992a) and Sheriff (1991).

The top and base of the Hutchinson Salt Member on the normal-polarity synthetic seismogram (fig. 8) are represented by moderate-amplitude peaks. The Hutchinson Salt Member, between the top and base, is characterized by a series of relatively low- to moderate-amplitude events, the product of interlayered halites, sulfates, shales, and carbonates of variable acoustic impedance and thickness. Overall, the synthetic seismogram suggests that the seismic image of undeformed Hutchinson Salt Member can be readily discriminated on high-resolution seismic data. It should be noted that high-resolution sources have limited depth penetration and that high-frequency input signal is rapidly attenuated with depth. As a result, the vertical resolution at depth (as suggested by the synthetic seismogram) might not be realized using current high-resolution seismic techniques.

As evidenced by this synthetic seismogram, from a reflection-seismic perspective, rock salt is a bit of an enigma; although halite has a relatively high seismic velocity (4,200 m/sec), it has a low density (2,200 kg/m^3). (Typically, dense rocks have relatively high seismic velocities, and less dense rocks have lower seismic velocities.) The top of the rock salt in particular can be difficult to image; the Hutchinson Salt Member is overlain by denser shales of lower seismic velocity. Note that the synthetic seismic image of the Hutchinson Salt Member would be very different if only the velocity curve was used to calculate the reflection coefficient wavetrain.

As illustrated on the synthetic seismogram, the reflections from the top and base of the Stone Corral are manifested as a high-amplitude peak and high-amplitude trough, respectively. The seismic signature of the Blaine Formation (thin anhydrite, the top of which is not represented on the synthetic seismogram) is similarly characterized by a high-amplitude peak-trough combination.

Sonic log control was not acquired above the Blaine Formation. As a result the base Pleistocene and the base Cretaceous are not imaged on the synthetic seismogram. Our experience elsewhere in central Kansas and the geologic/lithologic control in the study area suggests that these interfaces will be manifested as moderate- to high-amplitude peaks on zero-phase, normal-polarity seismic data. As a result of erosion, these seismic events also can exhibit significant lateral time-structural relief relative to the adjacent conformably bedded strata.

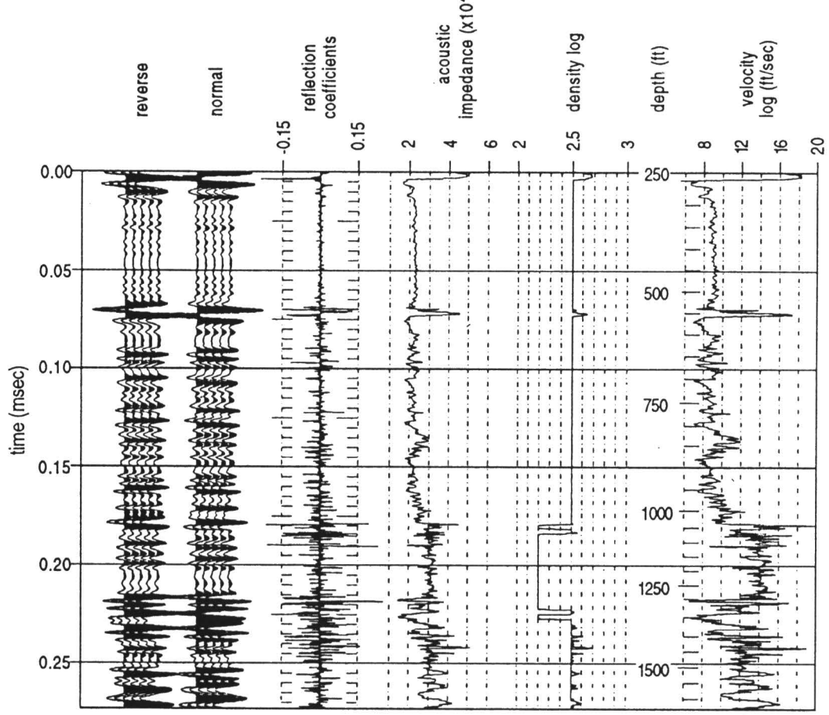

FIGURE 8—MODELING FROM BOREHOLE INFORMATION.

Seismic Data

Correlation of the synthetic seismic data with the normal-polarity CDP stacked seismic data is quite good (fig. 9). Well-log information, stacking velocity control, and the synthetic seismogram have enabled confident identifications of several key reflections.

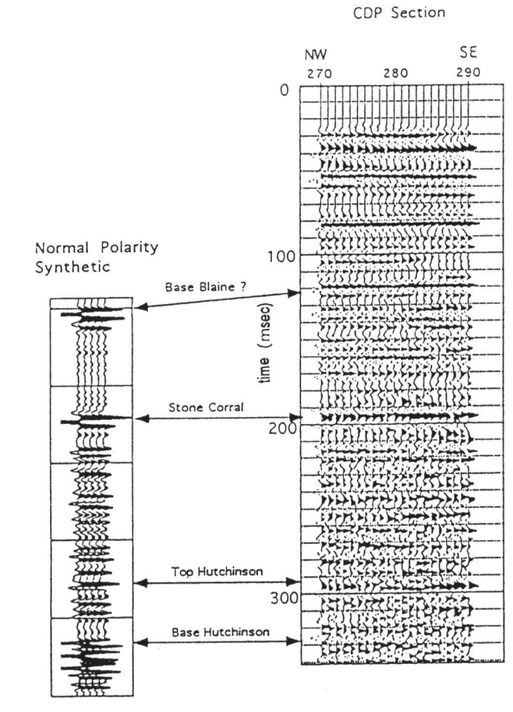

FIGURE 9—CORRELATION OF SYNTHETIC TRACE TO SEISMIC SECTION. Borehole data are from a well approximately 10 km (6.2 mi) southeast of Cheyenne Bottoms.

The shallowest labeled event is the pre-Pleistocene subcrop (fig. 10A, B). This undulating surface is erosional and represents the contact between the largely unconsolidated Pleistocene fluvial sediment and the underlying Cretaceous strata. This event conforms to driller logs for a well (sec. 29, T. 18 S., R. 12 W.) where the Dakota Formation is marked by the presence of gray shales and coal chips at a depth of around 35 m (115 ft). This event and the overlying inter-Pleistocene reflections are relatively time-structurally low to the north of CDP 250 (1–3 msec). This pattern of relief is consistent with erosion and the post-depositional compaction of the Pleistocene infill, supporting Haworth's (1897) thesis that Cheyenne Bottoms is a product of the Pleistocene sedimentary processes. Alternatively, the observed time-structural low could have been accentuated by either late-stage faulting, salt dissolution, and/or salt creep.

The base Cretaceous, base Blaine, top Stone Corral, and top Hutchinson Salt events are time-structurally low (1–2 msec) to the north of trace 250, supporting the thesis of late-stage faulting, dissolution, and/or creep. The base Hutchinson Salt event, in contrast, appears to be relatively flat (fig. 10C), suggesting that the time-structural relief observed along the shallower horizons is at least partially attributable to the recent thinning of the Hutchinson Salt.

On the basis of the seismic data, the preferred interpretation is that as a result of rock-salt creep, the Hutchinson Salt is several msec (5 m or so; 16 ft) thinner to the north of trace 250 than to the south. We submit that these salts are actually being leached to the north of the seismic line and that the observed thinning is the result of rock-salt creep towards the zone of active and/or recent dissolution.

From a regional perspective, we suggest that faulting during Pleistocene time initiated the dissolution of the Hutchinson Salt to the north of the seismic line. (As a consequence of this faulting, the pre-Hutchinson horizons are structurally low in the Cheyenne Bottoms area.) The leaching of Hutchinson Salt caused surface subsidence and influenced the regional drainage pattern to the extent that the Cheyenne Bottoms area was incised by deeply cutting stream channels. Erosional downcutting was accentuated by salt dissolution; hence, the base Pleistocene is anonymously low and the Pleistocene fill anonymously thick in the area. In those areas peripheral to the sites of extensive leaching, rock-salt creep occurred. This process, as envisioned by the authors, entails the creep of rock salt from zones of high pressure (no significant leaching) towards zones of lower pressure (sites of active dissolution or void space).

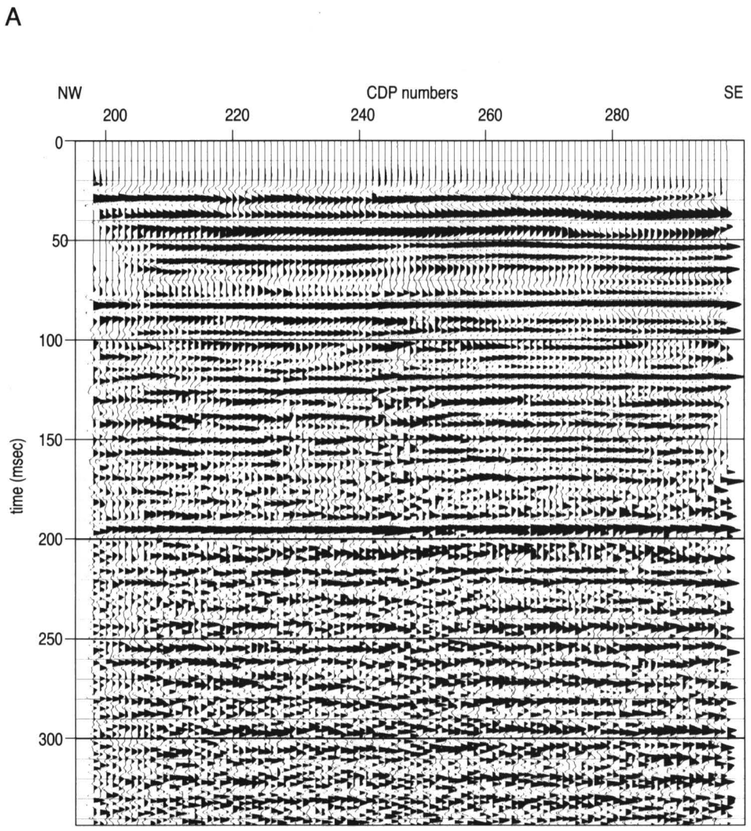

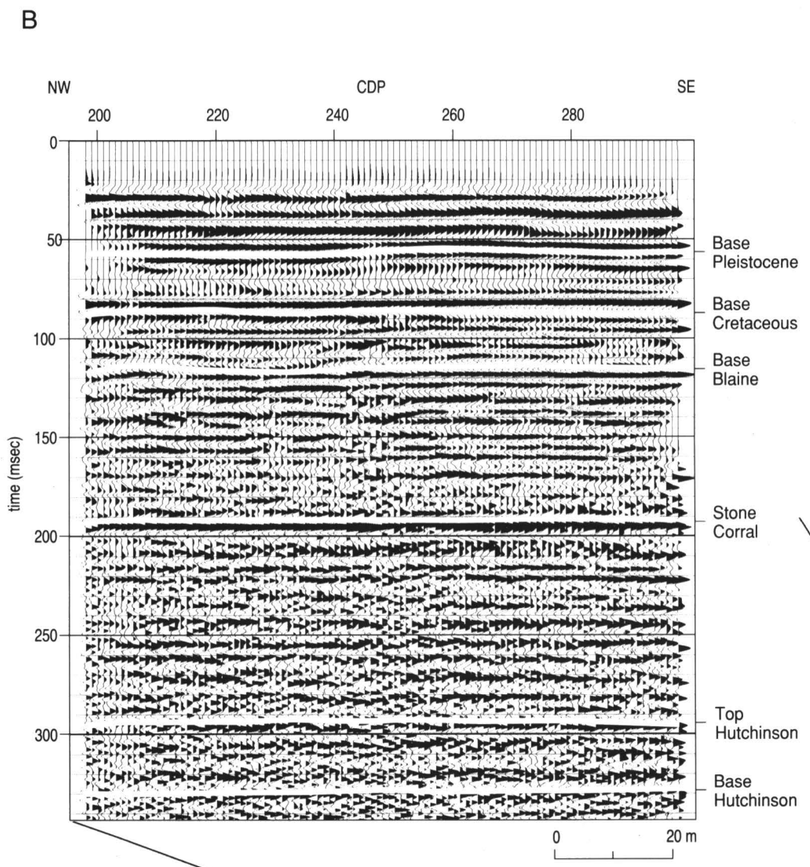

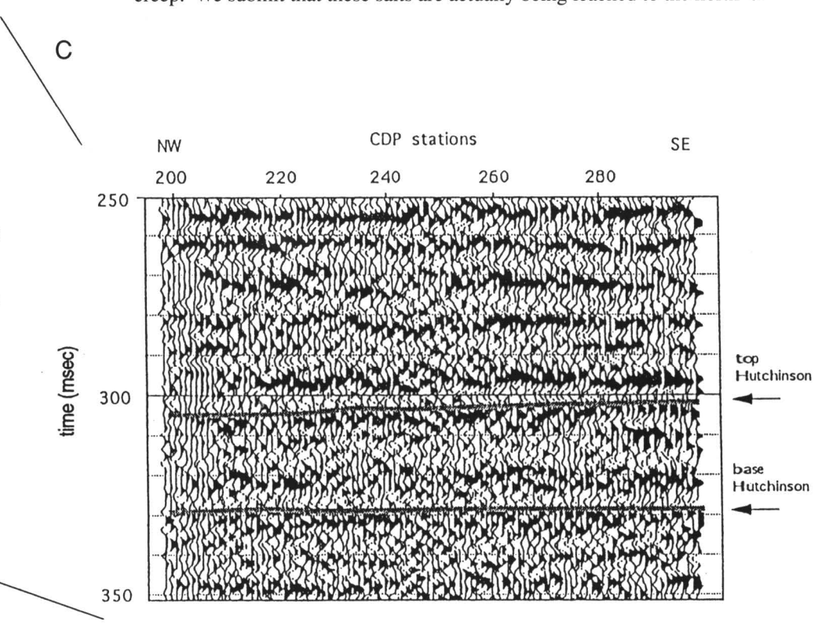

FIGURE 10—CDP STACKED SECTION OF THE SEISMIC DATA (A) AND INTERPRETATIONS (B) AND (C).

Summary

Seismic data (figs. 10A–C) were acquired near the southeastern periphery of the Cheyenne Bottoms area in an effort to elucidate the geologic origin of the basin. Our interpretation of these data suggests that the Hutchinson Salt Member thins along the length of the line (from southeast to northwest) by about 5 m (16 ft) as the result of rock-salt creep. We submit that these salts are actually being leached to the north of

the seismic line and that the observed thinning is the result of rock-salt creep towards the zone of active and/or recent dissolution.

This interpretation is consistent with the generally accepted thesis that Cheyenne Bottoms is a natural land-sink, caused by regional faulting and the associated dissolution of the Hutchinson Salt. Our interpretation differs from these previously published concepts in that we provide seismic evidence that (at least in places) the Hutchinson Salt thins about the periphery of the Cheyenne Bottoms area. This thinning is herein attributed to rock-salt creep.

These high-quality seismic data suggest that a regional high-resolution seismic study could successfully image the Hutchinson Salt Member within Cheyenne Bottoms and better our understanding of the timing of tectonic activity responsible for the fracturing patterns observed. A study of this nature could potentially provide key information regarding the origin of Cheyenne Bottoms, salt dissolution and associated subsidence could be verified, and fault/fracture zones could be located. We anticipate acquiring additional seismic data with modern technology and techniques which would provide equal if not better resolution with very little (if any) environmental impact on the ecosystem.

ACKNOWLEDGMENTS—The authors thank Karl Grover, Kansas Fish and Game Commission, for assistance during the planning stages, and Pat Acker for preparing the quality graphics.

References

Bass, N. W., 1926, Geological investigations in western Kansas: Kansas Geological Survey, Bulletin 11, 96 p.

Bayne, C. K., 1977, Geology and structure of Cheyenne Bottoms, Barton County, Kansas: Kansas Geological Survey, Bulletin 211, 12 p.

Bayne, C. K., and Fent, O. S., 1963, The drainage history of the upper Kansas River basin: Kansas Academy of Science, Transactions, v. 66, p. 363–377

Haworth, E., 1897, Physiography of western Kansas: Kansas University Geological Survey, v. 2, p. 11–49

Johnson, W. D., 1901, The high plains and their utilization: U.S. Geological Survey, 21st Annual Report, p. 601–741

Latta, B. F., 1950, Geology and ground-water resources of Barton County, Kansas: Kansas Geological Survey, Bulletin 88, 228 p.

Merriam, D. F., 1968, The geologic history of Kansas: Kansas Geological Survey, Bulletin 162, 317 p.

Sheriff, R. E., 1991, Encyclopedic dictionary of exploration geophysics: Society of Exploration Geophysists, 376 p.

Steeples, D. W., Miller, R. D., and Knapp, R. W., 1987, Downhole .50-caliber rifle—an advance in high-resolution seismic sources (exp. abs.); *in,* Technical Program Abstracts and Biographies: Society of Exploration Geophysicists, 57th Annual Meeting, p. 76–78

Steeples, D. W., 1990, Early spectral shaping boosts data quality: Oil and Gas Journal Special, p. 49–55

Wentz, A. W., 1990, An introduction to Cheyenne Bottoms; *in,* Cheyenne Bottoms—Jewel of the Prairie: Kansas Department of Wildlife and Parks

Widess, M. B., 1973, How thin is a thin bed?: Geophysics, v. 38, p. 176–1,180

Zeller, D. E., 1968, The stratigraphic succession in Kansas: Kansas Geological Survey, Bulletin 189, 81 p.

Feasibility and Resolution of Shallow Seismic-reflection Techniques in Northwestern Franklin, Southeastern Douglas, and Osage Counties in Kansas

Richard D. Miller[1] and Thomas V. Weis[2]
[1]Kansas Geological Survey, The University of Kansas, Lawrence, KS 66047; and
[2]formerly with Kansas Geological Survey, now with Normandy Exploration Limited, Kent Town, South Australia

Abstract

Seismic reflection can be effectively used in east-central Kansas to delineate subsurface features significant to hydrologists, petroleum geologists, and petroleum engineers. Eight high-resolution seismic lines were acquired within a three-county area in east-central Kansas. Dominant frequencies of reflections from this area ranged from 140 to 350 Hz, yielding vertical resolution limits between 1 m and 3 m (3.3 ft to 10 ft) to depths in excess of 200 m (656 ft). Synthetic seismic traces and well geology were incorporated into interpretations of reflection events. Seismic data from the east, north, and west portions of the study area are of excellent quality and can be correlated with the synthetic seismograms and from line to line based on wavelet character and reflection-time intervals.

Introduction

Seismic reflection surveys have been successfully used to delineate subsurface features relevant to petroleum exploration for nearly 70 years. The effective use of the technique for shallow applications depends on several key conditions. The most critical is the existence of acoustic velocity and/or density contrasts in the subsurface. The second relates to the ability of the near-surface to propagate high-frequency seismic signals. Finally, the acquisition parameters and recording equipment must be compatible with the proposed target, resolution requirements, and environmental constraints of the survey. Recent developments associated with the use of the technique to evaluate environmental sites have enhanced the potential of the technique for cost-effective application throughout Kansas (Steeples and Miller, 1990).

Shallow, high-resolution seismic-reflection profiles can be useful both in characterizing shallow structures or anomalies and extending features identifiable in outcrop and surface excavation into the upper several hundred meters of the subsurface. The high-resolution seismic-reflection method has only recently developed into a practical and effective tool for identifying shallow (<100 m; 328 ft) structures (Hunter et al., 1984; Jongerius and Helbig, 1988; Treadway et al., 1988; Miller et al., 1989, 1990; Gochioco and Cotten, 1989; Miller and Steeples, 1991; Goforth and Hayward, 1992). The shallow seismic-reflection technique is inexpensive (compared to drilling) and can increase the horizontal resolution and often decrease the number of drillholes by an order of magnitude. Seismic reflection is an extremely effective technique for detecting faults and interpreting stratigraphic relationships; depth can only be estimated and lithologies only inferred without confirmation drilling, however.

High-resolution CDP seismic-reflection data were collected at eight different sites in east-central Kansas to determine stratigraphic consistency and appraise resolution potential of the technique (fig. 1). The seismic lines possessed data with varying signal-to-noise ratios as well as dominant-frequency content. Correlation and analysis of the interpreted reflecting events from line to line was similar to single-point seismic techniques (McGuire and Miller, 1989). The lines were all CDP-processed in a consistent fashion to enhance any wavelet characteristics unique to particular geologic interfaces. The consistent character and frequency of the seismic energy recorded in this area and the synthetic seismogram allowed extensive stratigraphic interpretations and confident correlation between the various seismic lines.

Geologic Setting

Cyclic Upper and Middle Pennsylvanian limestone and shale sequences with minor sandstone units dominate the study area (fig. 2). These units are characteristic of the transgressive-regressive "Kansas" cyclothems that resulted from the rise and fall of sea level over the northern midcontinent shelf during Early to Middle Pennsylvanian time (Heckel, 1988).

The uppermost stratigraphic unit identified as a seismic reflector in this study is the Deer Creek Limestone. It occurs near the middle of the Upper Pennsylvanian Shawnee Group, and is primarily limestone, but consists of a series of alternating limestones and shales. Moving stratigraphically downward in the Shawnee Group, the Tecumseh Shale, the Lecompton Limestone, the Kanwaka Shale, and the Oread Limestone continue this cyclic limestone-shale-limestone pattern (O'Conner, 1955; Ball et al., 1963; Zeller, 1968). The Lecompton and Oread Limestone formations provide good seismic reflectors in this study area (fig. 3).

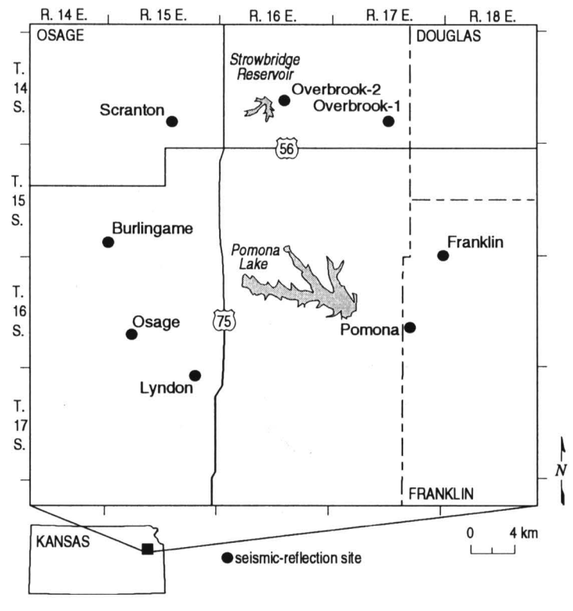

FIGURE 1—SITE MAP OF STUDY AREA WITH THE EIGHT SEISMIC-PROFILE LOCATIONS INDICATED.

The Douglas Group, consisting of the upper Lawrence Formation and the lower Stranger Formation, is stratigraphically below the Shawnee Group. It does not have the internal cyclic character of the overlying Shawnee Group described above. It is primarily shale and channel sandstones with minor limestone and coal beds (O'Connor, 1955; Ball et al., 1963; Zeller, 1968). The Amazonia Limestone, the Ireland Sandstone, and the Haskell Limestone members provide identifiable seismic reflectors within the Lawrence Formation (fig. 4). No reflectors were identified within the Stranger Formation.

The next lower group in the stratigraphic column is the Lansing Group. It is primarily limestone but has the internal cyclic limestone-shale character similar to the Shawnee Group described above. It consists of, from top to bottom, the Stanton Limestone, the Vilas Shale, and the Plattsburg Limestone (O'Connor, 1955; Ball et al., 1963; Zeller, 1968). The Lansing Group results in an identifiable group of seismic reflections in this study area (fig. 3).

As we move down the stratigraphic column, the Kansas City Group is a cyclic package of limestones, shales, and sandstones. From top to bottom it

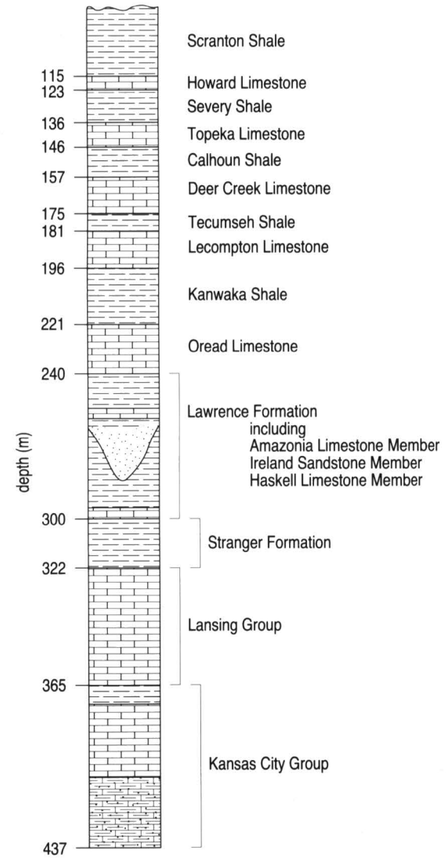

FIGURE 2—LITHOLOGIC SECTION, DEPTHS ARE FROM OSAGE CITY #4 DRILL HOLE.

consists of the Bonner Springs Shale, the thick Wyandotte Limestone, the Lane Shale, the Iola Limestone, the Chanute Shale, the Drum Limestone, the Cherryvale Shale, the Dennis Limestone, the Galesburg Shale, the Swope Limestone, the Ladore Shale, and the Hertha Limestone (O'Connor, 1955; Ball et al., 1963; Zeller, 1968). The alternating limestones and shales result in an identifiable group of reflectors shown in fig. 3.

Below the Kansas City Group, at the base of the Upper Pennsylvanian Series is the Pleasanton Group, which is primarily shales and sands (O'Connor, 1955; Ball et al., 1963; Zeller, 1968). No reflectors have been identified from within the Pleasanton Group.

Below the Pleasanton is the Marmaton Group, which occurs at the top of the Middle Pennsylvanian Series. The Marmaton Group consists of alternating limestones, shales, and sandstones (O'Connor, 1955; Ball et al., 1963; Zeller, 1968). Seismic reflectors interpreted to be from within the Marmaton occur at the east end of the study area.

The sedimentary section described above has a gentle 1° dip to the west-northwest. This results in the observation of stratigraphically higher reflectors to the west and lower to the east. Superimposed on this gentle westward dip is the topographic relief of the study area. A maximum 300 ft (91 m) of relief from ridge tops to valley floors occurs in the area (Wilson et al., 1986). The observed seismic sections are a function of the east-west position within the study area and the local elevation of the survey line.

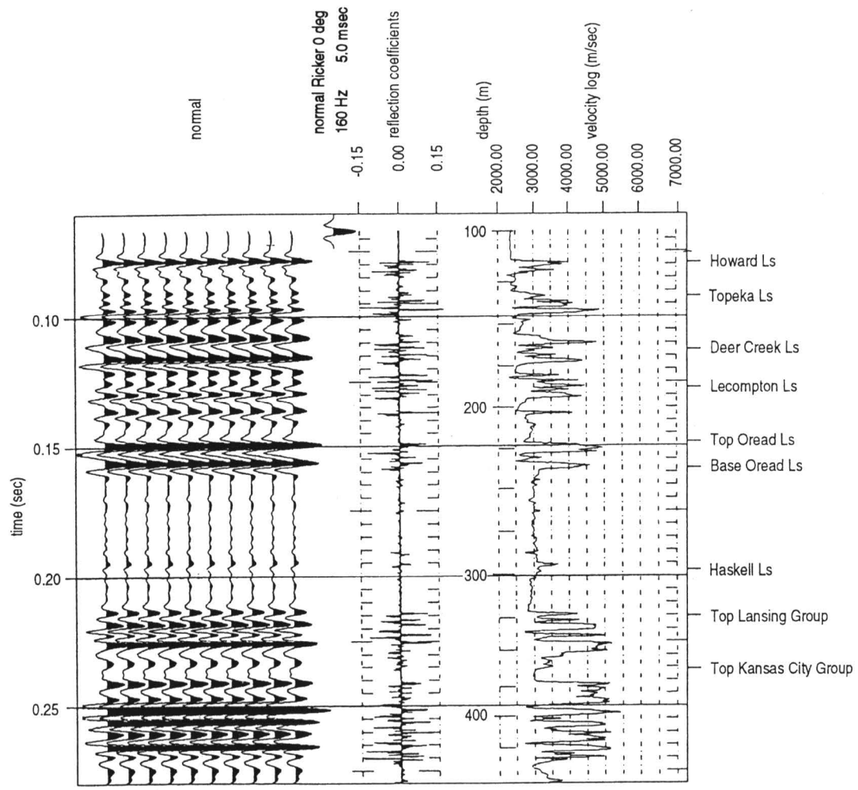

FIGURE 3—SYNTHETIC SEISMOGRAM FROM OSAGE CITY #4 ACOUSTIC-VELOCITY LOG.

Data Acquisition

All data were acquired with an I/O DHR-2400 seismograph. The 24-channel data were analog filtered, amplified, A/D converted (11 bits plus sign), and recorded on 9-track magnetic tape in a demultiplexed format. Generally, two shots were recorded at 1/4-msec sampling interval (2,000-Hz alias frequency) with a total listening time of 250 msec at each shot location. The 36 dB/octave roll-off analog low-cut filters selected during acquisition have at the –3 dB point a dominant frequency from 220 to 340 Hz depending on the specific site characteristics and depth of interest. The selection of the analog low-cut filters was based on dominant and maximum reflection frequencies recorded during walkaway-noise testing.

Selection of the type, number, orientation, and spacing of sources and receivers for each line was intended to maximize recorded data and its resolution potential while maintaining as much consistency as possible in wavelet characteristics. Data for this study were recorded with two single Mark Products L-40A 100-Hz geophones wired in series and planted in a small (<1-m; 3.3-ft) inline array. Modified .30-06 and .50-caliber hunting rifles were used as projectile energy sources. Subterrain detonation of these rifles increased ground coupling and reduced air-coupled waves. Determination of the appropriate energy source was based on target depth and surface conditions (i.e., attenuation). The source and receiver station spacing was optimized according to each site's target-depth range and near-surface velocity. All the seismic data presented here were collected over a two-week period.

Data Processing

The 24-channel seismic-reflection data were processed into 12-fold CDP stacked sections using algorithms and a processing flow designed to enhance the high-frequency portion of the seismic traces. The critical steps in the processing flow include first-arrival muting, air-blast muting, bad-trace editing, common-depth-point (CDP) sorting, bandpass filtering, automatic surface-consistent statics, normal moveout velocity correction, Automatic Grain Control (AGC) trace scaling, and CDP stacking. Each seismic line was processed individually with the order and parameters selected for each of the previous steps optimized for each line.

Unique data characteristics, related to near-surface conditions on certain lines, required specific processing techniques to enhance reflections and improve line-to-line correlations. Some of the line-specific techniques used included trace mixing (whole CDPs), auto-shaping deconvolution, auto-predictive deconvolution, time-varying filtering, and predictive deconvolution. These techniques were used conservatively to retain as much consistency between lines as possible.

Interpreted Seismic Data

The final stacked sections used for interpreting the subsurface geology have signal-to-noise ratios that allow confident and consistent correlation of reflections from section to section and from actual traces to synthetic traces (derived from geophysical well logs). The dominant frequency of the unprocessed field data varies from 140 to 350 Hz, depending on site characteristics and recording parameters. Reflections are interpreted on the seismic sections and correlated to either group, formation, or member based on signal-to-noise ratios and resolution. Reflections or apparent reflections not correlated to particular geologic interfaces do not have high confidence matches with the synthetic seismic traces and/or the stratigraphic column from this area. Reflections interpreted on stacked seismic sections equate to geologic interfaces that range from the base of the Deer Creek Limestone (Shawnee Group) to below the base of the Kansas City Group, possibly within the Marmaton Group (fig. 2).

Seismic-reflection events interpreted to represent significant geologic features are enhanced on the seismic sections (figs. 4–10). Specific groups, formations, or members were correlated to reflection arrivals based on time/depth, wavelet characteristics,

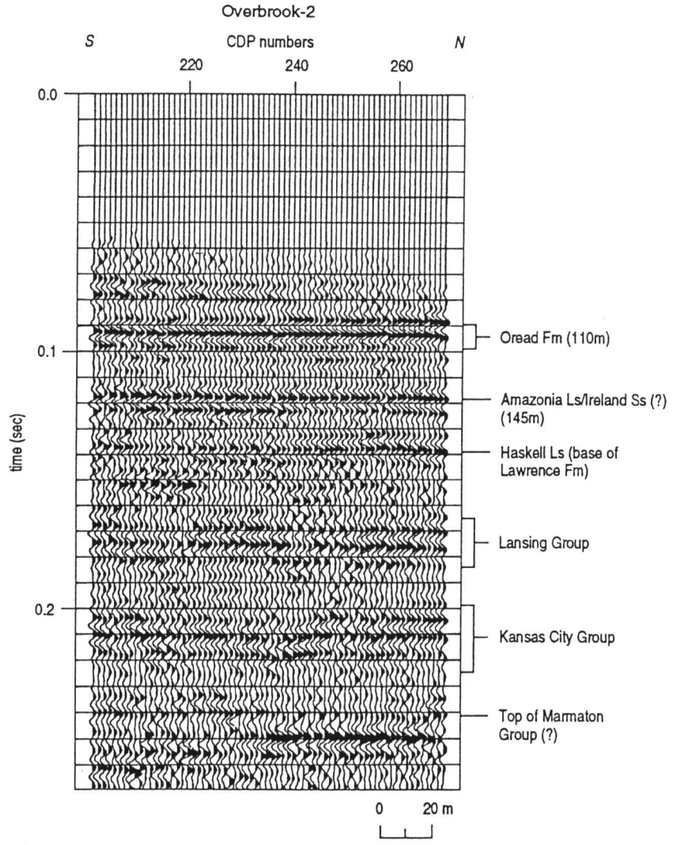

FIGURE 4—INTERPRETED 12-FOLD SEISMIC-REFLECTION PROFILE FROM NEAR SCRANTON, KANSAS. The reflection from the Oread is at approximately 92 msec (110 m) and the reflection from the base of the Lawrence is at approximately 140 msec (168 m).

surrounding reflection events, and drill/log data. A synthetic seismogram was generated using the acoustic-velocity log from the Osage City #4 drillhole located to the west and downdip of the survey area (sec. 4, T. 15 S., R. 13 W.; fig. 3). Interpretations are intended to highlight orientation and stratigraphic features of reflectors within the upper 350 m in this area. Correlating seismic data with minimal well control, significant distance between lines, and no acoustical marker horizons forced strong dependence on matching of acoustic properties.

The Overbrook-2 seismic line possesses several localized geologic features (fig. 4). Several strong reflecting events are present between 80 and 250 msec. An unidentified reflection at about 80 msec dips about 5° to the north relative to the flat-lying Oread Formation at about 90 msec. Two subtle erosional/depositional features can be interpreted in reflections between 130 and 220 msec. A 2-msec high in the Haskell Limestone at about CDP 260 represents about a 2–2.5-m (6.6–8.2-ft)-change in elevation over a distance of slightly more than 25 m (82 ft). A 1-msec channel in the top of the Kansas City Group is present at CDP 235 and equates to a cut about 1.5 m (5 ft) deep and 35 m (115 ft) across. Dominant frequency of data on this line is approximately 175 to 200 Hz, which suggests vertical resolution of about 1.5 m to 2 m (5 ft to 6.6 ft). The cyclic nature of the reflecting events is very consistent with the regional geology as determined by drilling and outcrop studies (Heckel et al., 1979).

The Overbrook-1 seismic line has a slightly lower dominant frequency than Overbrook-2 but contains a potential erosional/depositional feature at the contact between the Lansing and Kansas City Groups. Gentle undulations in the Amazonia Limestone (75 m; 246 ft) and the Haskell Limestone (105 m; 345 ft) are evident above the top of the Lansing Group. Erosional features at the base of the Ireland Sandstone on the south end of the line can be inferred at approximately 85 msec. An apparent lens or pinch-out between units within the Lansing Group and the top of the Kansas City Group can be interpreted between CDP 200 and 240 at a depth of about 150 msec. The feature appears to be the result of erosion of the top of the Kansas City and subsequent deposition and eventual channel filling. The feature has expression at the basal contact of the Lansing Group and is thickest (~15 m; 49 ft) at the southernmost end of the line. The minimum vertical resolution potential of this data set is about 2.5–3 m (8–10 ft).

The Franklin seismic line is stratigraphically lower in the section and possesses the greatest resolution potential of all the lines acquired (fig. 6). Reflections across the entire section are relatively flat with little indication of either structural or stratigraphic change or anomalies. The shallowest reflection is probably from the Haskell Limestone (25 m; 82 ft). A thick section of Tonganoxie Sandstone (within the Stranger Formation) present on this line just beneath the Haskell Limestone is not evident in this quantity on any of the other seven lines. This could be a large channel feature. Between the top of the Marmaton Group and the basal contact of the Kansas City Group, a pinch-out can be interpreted. This line possesses resolution potential of less than 1 m in certain parts of the section.

The Pomona section lacks the high signal-to-noise ratio in the upper 100 msec of the record present on other data from this study (fig. 7). The top of the Kansas City Group is the first quality reflection interpretable on the seismic section. The shallower reflections (top of the Lansing Group and the Haskell Limestone) did not stack in as a direct result of a limestone layer very close to the ground surface that adversely affected the seismic energy. As with the Franklin section, little variation can be observed across the section. The maximum potential resolution within the Kansas City Group on this section is about 2 m (6.6 ft).

Stratigraphic changes can be observed within several units on the Lyndon seismic section (fig. 8). Thinning can be interpreted at the top of the Oread Formation (65

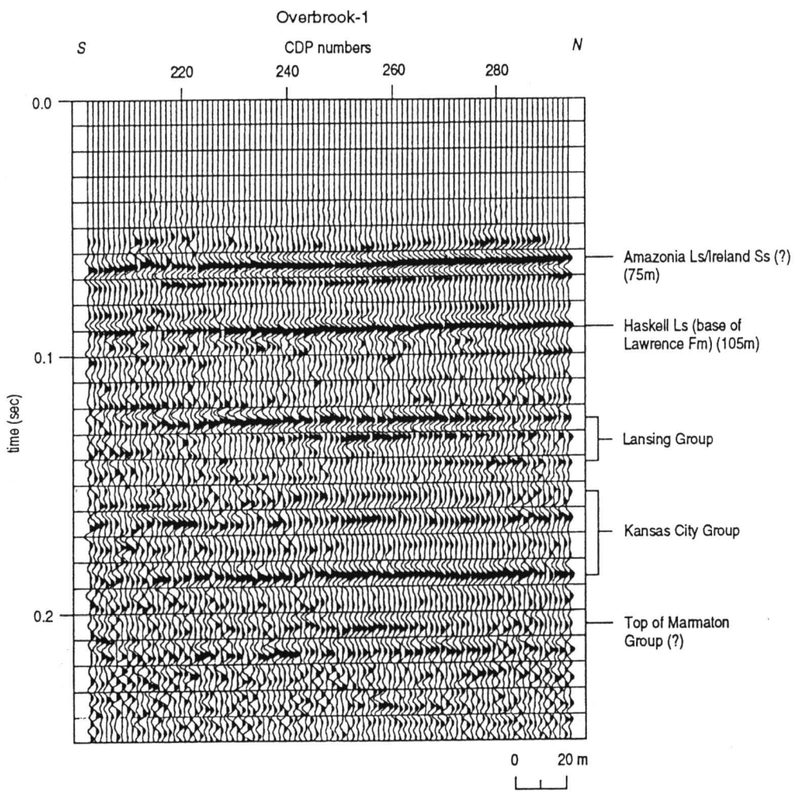

FIGURE 5—Interpreted 12-fold seismic-reflection profile from near Burlingame, Kansas. The reflection from the base of the Lawrence is at approximately 89 msec (105 m) and the reflection from the top of the Lansing Group is at approximately 125 msec (150 m).

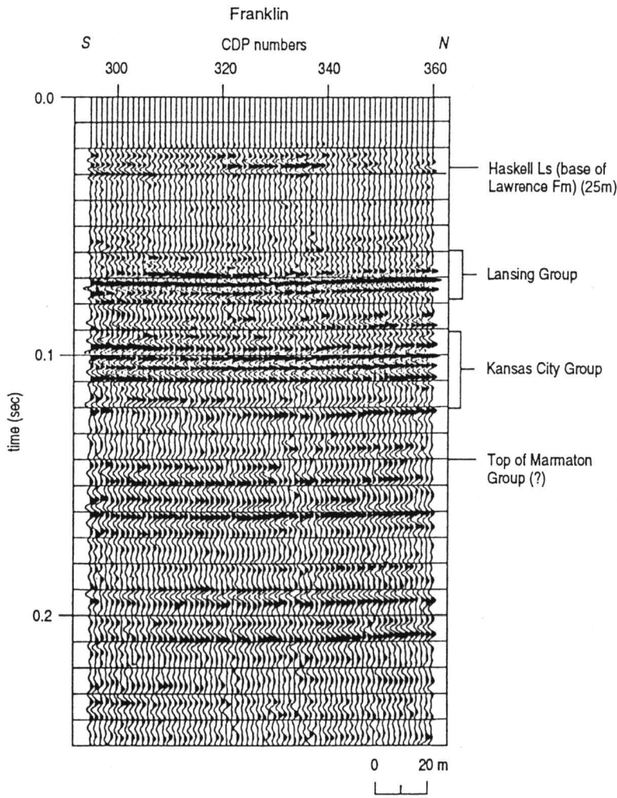

FIGURE 6—Interpreted 12-fold seismic-reflection profile from near Lyndon, Kansas. The reflections at approximately 70 msec (80 m) are interpreted to be from the Lansing Group and the reflections at approximately 100 msec (120 m) are interpreted to be from the Kansas City Group.

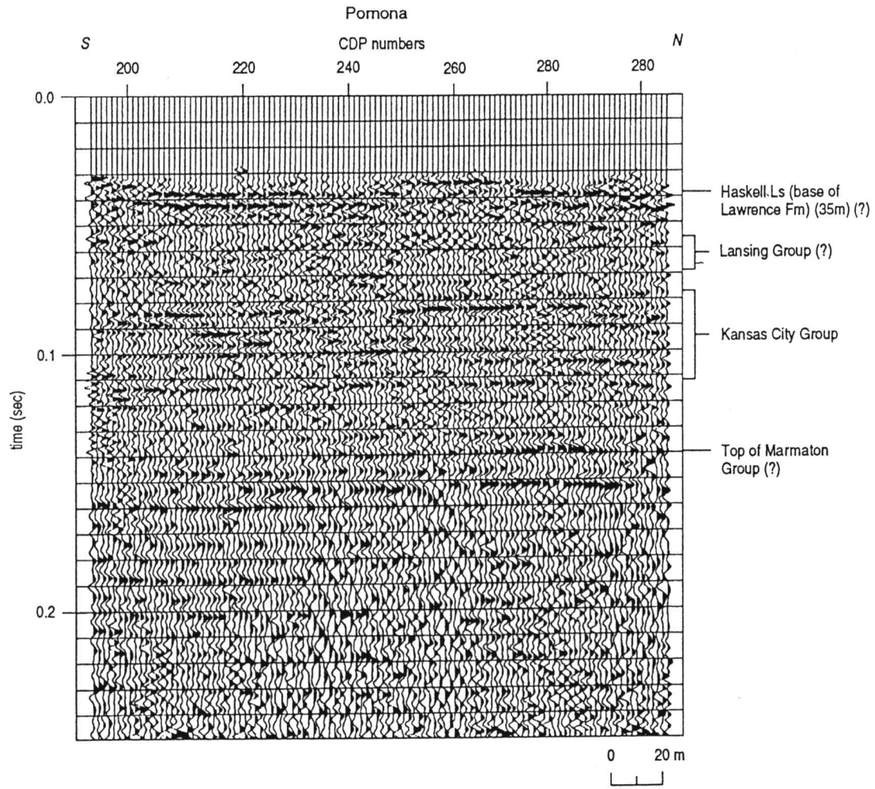

FIGURE 7—Interpreted 12-fold seismic-reflection profile from near Overbrook, Kansas. The reflection from the base of the Lawrence is at approximately 40 msec (45 ft) and the reflection from the top of the Kansas City Group is at approximately 80 msec (100 ft).

msec), top of the Lansing to base of the Haskell (130 msec), base of the Lansing to top of the Kansas City (165 msec), and within the Kansas City Group (200 msec). There appears to be a regional 1° dip in reflecting events on this line. The minimum vertical resolution on this line is about 1–1.5 m (3.3–5 ft).

The Osage City seismic line is structurally/stratigraphically the most variable (fig. 9). A very well defined lens/pinch-out/channel can be interpreted at the base of the Oread Formation within what is identified as the Amazonia Limestone or Ireland Sandstone. The channel within the Amazonia Limestone/Ireland Sandstone is the most significant feature of its type delineated during this study. The channel appears to be 150–200 m (492–656 ft) across with a maximum depth of 5–7 m (16–23 ft). Several stratigraphic anomalies are present within the Lansing Group. Subtle undulating beds are evident within the Kansas City Group between CDP 225 and 250 at a depth of 210 msec. The apparent dip or pull-up on the north end of the line is probably related to low fold and uncompensated near-surface static. The maximum vertical resolution on this line is 1–1.5 m (3.3–5 ft).

The Burlingame seismic line possesses the lowest dominant reflection frequencies and therefore the lowest resolution potential of the eight lines (fig. 10). Two stratigraphic features of potential interest can be interpreted on the section at 90 msec and 180 msec. These features both seem to be mounds probably associated with depositional anomalies. These highs are both about 2–3 m (6.6–10 ft) vertical and 20–25 m (66–82 ft) horizontal. The shallower high (90 msec) may be the edge of a pinch-out or lens extending beyond the end of the survey line to the north. Within the Kansas City Group, significant changes in reflection wavelet characteristics seem to occur, possibly indicative of thickness changes in bedding within that horizon. The vertical resolution potential of this data set is around 3 m (9.8 ft).

The Scranton seismic data is stratigraphically higher in the section and, therefore, has the potential to image all the major geologic interfaces observed on the previous seven lines (fig. 11). Very few unique or anomalous features can be interpreted on this section. This section displays the cyclic layer-cake stratigraphy that is regionally consistent in most of eastern Kansas. Across the section as a whole, very subtle deviations from horizontal bedding can be observed as in previous sections. The Lansing Group is relatively distinct, but reflections from within the Lawrence Group (beneath the Oread Formation) do not possess the necessary spectral properties to resolve layering as clearly as other seismic sections in this study. The Kansas City Group is sufficiently deep that the signal-to-noise ratio does not permit much in the way of stratigraphic interpretations. The vertical resolution potential of this data set ranges from 1.5 to 2.5 m (5-8 ft).

Conclusions

The seismic data collected from this area are on the average very high quality with thin-bed resolution ranging from 1 to 4 m. Seismic data from the east, north, and west portions of the study area are of excellent quality and can be correlated with the synthetic seismograms and from line to line based on wavelet character and reflection-time intervals. The seismic data from the southwest part of the area have slightly different signal characteristics in comparison to the other data sets. However, reflection-time intervals, stacking velocities, and the synthetic seismogram reflections can be identified and correlated from well data. Seismic data from the southeast portion of the study area do not possess the very high signal-to-noise ratio of lines from other parts of the study area. This is most likely due to the near-surface repetitive limestone sequences seen in outcrop all over the southern portion of the study area. Confidence in interpreting many of the apparent subtle stratigraphic and/or structural features on these seismic data as real (and not static or uncompensated velocity) comes from qualitative comparisons of the interpreted feature reflections above and below.

Seismic reflection can be cost-effective in delineating subsurface features significant to hydrologists, petroleum geologists, and petroleum engineers in this area. Petro-

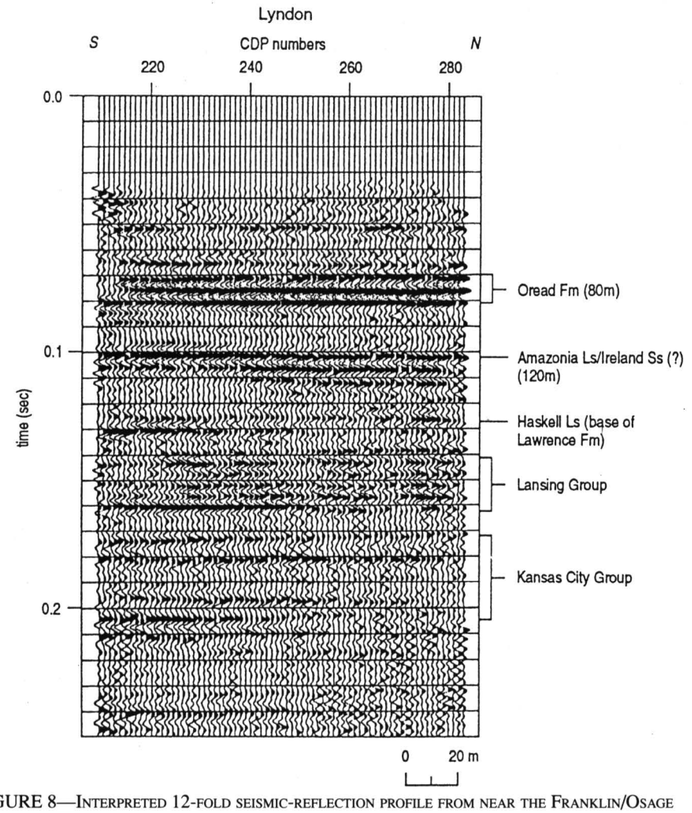

FIGURE 8—Interpreted 12-fold seismic-reflection profile from near the Franklin/Osage County, Kansas, boundary. The reflection from the base of the Oread is at approximately 80 msec (100 m) and the reflection from the base of the Lawrence is at approximately 127 msec (150 m).

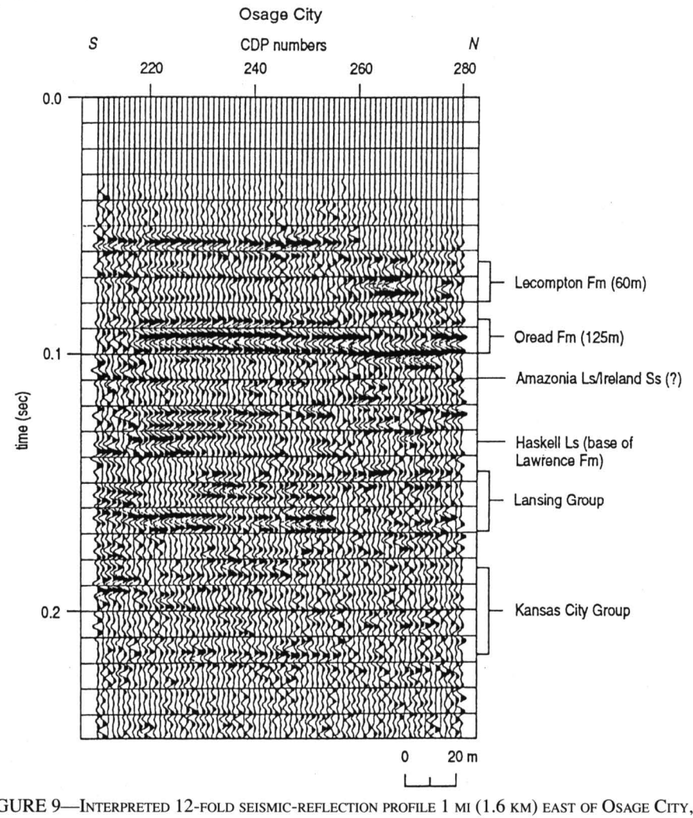

FIGURE 9—Interpreted 12-fold seismic-reflection profile 1 mi (1.6 km) east of Osage City, Kansas. The reflection from the base of the Oread is at approximately 100 msec (120 m) and the reflection from the base of the Lawrence is at approximately 134 msec (160 m).

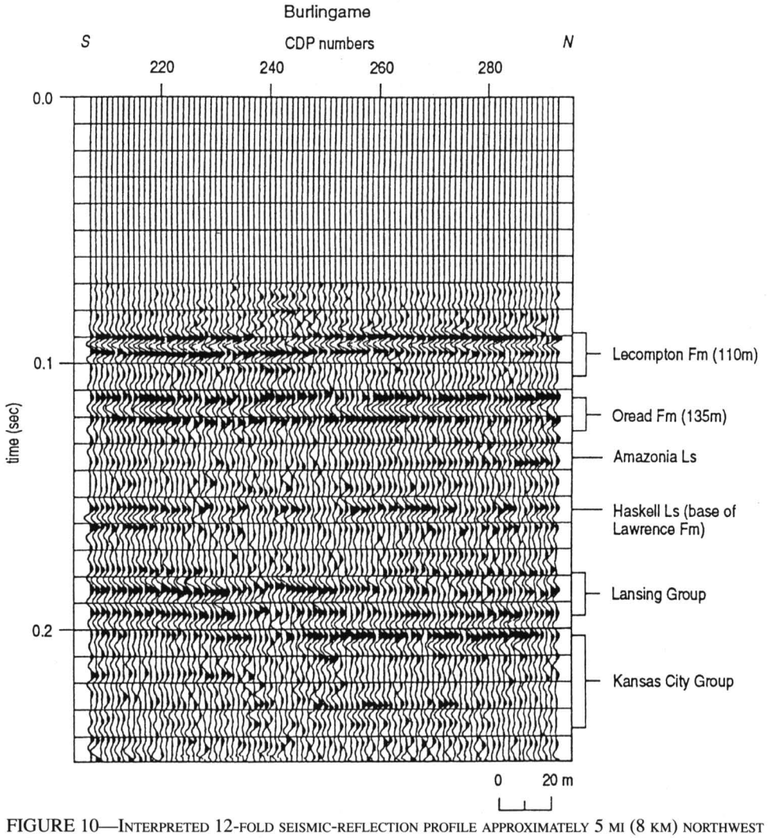

FIGURE 10—Interpreted 12-fold seismic-reflection profile approximately 5 mi (8 km) northwest of Overbrook, Kansas. The reflection from the base of the Oread is at approximately 122 msec (145 m) and the reflection from the base of the Lawrence is at approximately 154 msec (185 m).

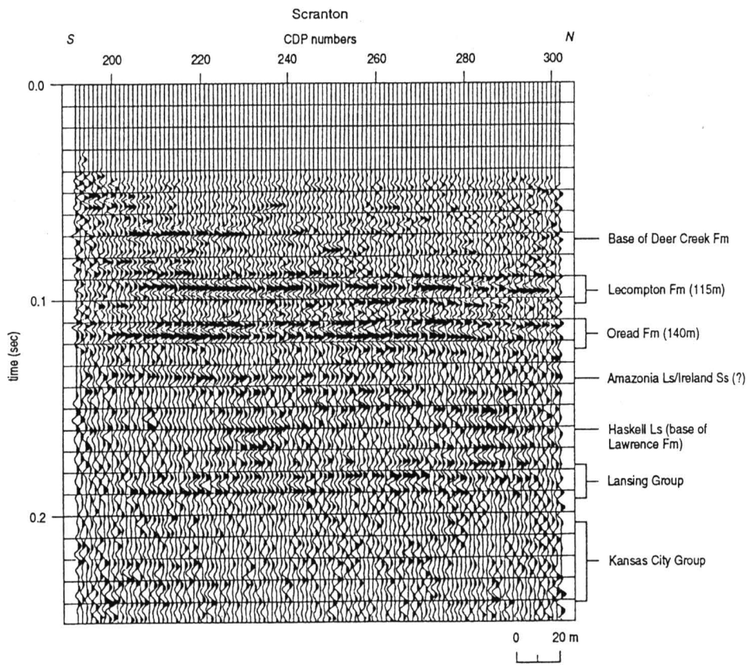

FIGURE 11—Interpreted 12-fold seismic-reflection profile near Pomona, Kansas. The reflection from the Oread is at 120 msec (145 m). The base of the Lawrence is interpreted to be at approximately 160 msec (190 m).

leum exploration targets in eastern Kansas with horizontal extent less than 20 m (66 ft) and vertical expression less than 3 m (10 ft) at depths of 100–350 m (330-1,155 ft) could be routinely delineated using this method. Detection and mapping of channel systems with seismic reflection could greatly enhance identification of ground-water availability and production in east-central Kansas. Model parameters necessary for enhanced recovery systems could be improved if zone geometries could be resolved within 2 m (6.6 ft) vertically and 10 m (33 ft) horizontally. This data set suggests that seismic reflection could greatly benefit most subsurface exploration and/or exploitation in east-central Kansas.

Acknowledgments—We wish to thank Don Steeples, Jeff Treadway, Bradley Birkelo, Paul Myers, and Andrew Kalik for their work on this project. Thanks also go to Mary Brohammer for her manuscript preparation, Pat Acker for her graphic design, and the anonymous reviewers who contributed to the quality of this finished article.

References

Ball, S. M., Ball, M. M., and Laughlin, D. J., 1963, Geology of Franklin County, Kansas: Kansas Geological Survey, Bulletin 163, 57 p.

Gochioco, L. M., and Cotten, S. A., 1989, Locating faults in underground coal mines using high-resolution seismic-reflection techniques: Geophysics, v. 54, p. 1,521–1,527

Goforth, T., and Hayward, C., 1992, Seismic reflection investigations of a bedrock surface buried under alluvium: Geophysics, v. 57, p. 1,217–1,227

Heckel, P. H., 1988, Classic "Kansas" cyclothems: Geological Society of America, Centennial Field Guide–South-central Section, p. 43–56

Hunter, J. A., Pullan, S. E., Burns, R. A., Gagne, R. M., and Good, R. S., 1984, Shallow seismic-reflection mapping of the overburden-bedrock interface with the engineering seismograph—some simple techniques: Geophysics, v. 49, p. 1,381–1,385

Jongerius, P., and Helbig, K., 1988, Onshore high-resolution seismic profiling applied to sedimentology: Geophysics, v. 53, p. 1,276–1,283

McGuire, D., and Miller, B., 1989, The utility of single-point seismic data; *in*, Symposium on Geophysics in Kansas, D.W. Steeples, ed.: Kansas Geological Survey, Bulletin 226, p. 1–8

Miller, R. D., Steeples, D. W., and Brannan, M., 1989, Mapping a bedrock surface under dry alluvium with shallow seismic reflections: Geophysics, v. 54, p. 1,528–1,534

Miller, R. D., Steeples, D. W., and Myers, P. B., 1990, Shallow seismic-reflection survey across the Meers fault, Oklahoma: Geological Society of America, Bulletin 102, p. 18–25

Miller, R. D., and Steeples, D. W., 1991, Detecting voids in a 0.6-m coal seam, 7 m deep, using seismic reflection: Geoexploration, Elsevier Science Publishers B.V., Amsterdam, The Netherlands, v. 28, p. 109–119

O'Connor, H. G., 1955, Geology, mineral resources, and ground-water resources of Osage County, Kansas: Kansas Geological Survey, Vol. 13, part 1, 50 p.

Steeples, D. W., and Miller, R. D., 1990, Seismic-reflection methods applied to engineering, environmental, and ground-water problems; *in*, Vol. 1: Review and Tutorial, Stan Ward, ed.: Society of Exploration Geophysicists, Investigations in Geophysics No. 5, p. 1–30

Treadway, J. A., Steeples, D. W., and Miller, R. D., 1988, Shallow seismic study of a fault scarp near Borah Peak, Idaho: Journal of Geophysical Research, v. 93, no. B6, p. 6,325–6,337

Wilson, F. W., O'Connor, H. G., Paul, S., and Chaffee, P. K., 1986, A feasibility study of sites for the proposed superconducting super collider in Kansas, preliminary geographical, geological, and geotechnical assessments: Kansas Geological Survey, Open-file Report 87–16, 18 p.

Zeller, D. E. (ed.), 1968, The stratigraphic succession in Kansas: Kansas Geological Survey, Bulletin 189, 81 p.

Garfield Prospect, Lippelmann Field, Decatur County, Kansas

Michael L. Crouch
Murfin Drilling Co.,Wichita, KS 67202

Introduction

The Lippelmann field is located in the east-central portion of Decatur County, Kansas. The initial test, the Murfin Drilling Company #1-16 Lippelmann, was drilled in August 1982. Development drilling began immediately after the discovery well, and the field was developed by September 1984. A total of five successful oil wells have been drilled in the Lippelmann field with production coming from the Pennsylvanian Oread, Lansing, and Pawnee–Cherokee formations. Production has been approximately 356,166 BO as of June 1992, with the ultimate recovery projected at 554,732 BO.

Regional Geology

In Decatur County, Pennsylvanian oil is trapped in structures along the southern extension of the Cambridge arch (fig. 1). The Cambridge Arch is located in Norton and Decatur counties and covers only about 1,000 mi² (2,589 km²) in western Kansas. It is a large, northwest-trending anticlinal feature that extends northward into Nebraska and is separated by a structural saddle from the Central Kansas uplift to the southeast. Structural movement occurred along the Cambridge Arch in pre-Mississippian, pre-Desmoinesian post-Mississippian, and Mesozoic time.

Prospect Geology

The Garfield prospect was originated in a general geological evaluation of R. 26 W. from T. 2 S. to T. 5 S. done in August 1980 (fig. 2). The original evaluations were done by mapping the Lansing structure and the Anyhdrite to Lansing isopach. Several areas of interest were identified due to holes with shows of hydrocarbon and structural and isopach mapping which indicated a test could be drilled in a more favorable position with the aid of seismic information.

Several prospects in T. 3 S. were of the quality to have acreage checks performed. The first was located around secs. 5 and 6 due to a possible structural anomaly set up by holes in sec. 32, sec. 5, sec. 6, sec. 12, and sec. 7. Another was located in secs. 3, 4, 9, and 10 generated by a well in sec. 9 with a slight show in the Lansing–Kansas City.

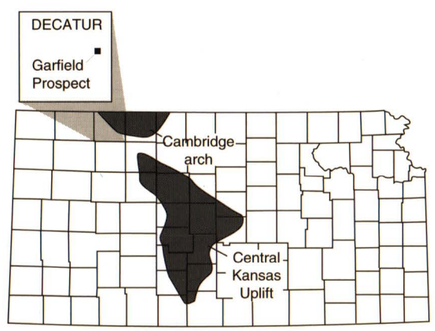

FIGURE 1—Location of Garfield prospect, Lippelman field, Decatur County, Kansas.

The third prospect, the Garfield prospect, was built on a test that recovered free oil from the Lansing in sec. 19 and an anomalously high hole in sec.17, resulting in a prospect in secs. 17, 18, 19, and 20.

On the Garfield prospect, Murfin Drilling Company obtained acreage in secs. 19, 20, and 29, and we also obtained all of sec. 16, which was not part of the original geological ideal. The dry hole in the NE NE NE sec. 17 was the only control point for our lead and had only show of gas in the upper Lansing. The hole was drilled by Consolidated Oil and Gas and John O. Farmer in 1970, with three DST's. The DST in the upper Lansing had 480 ft (146 m) of gas in the pipe with mud and water and good reservoir pressures. The Lansing was at -949 ft (-289 m) and the Anydrite to Lansing interval was 1,401 ft (427 m).

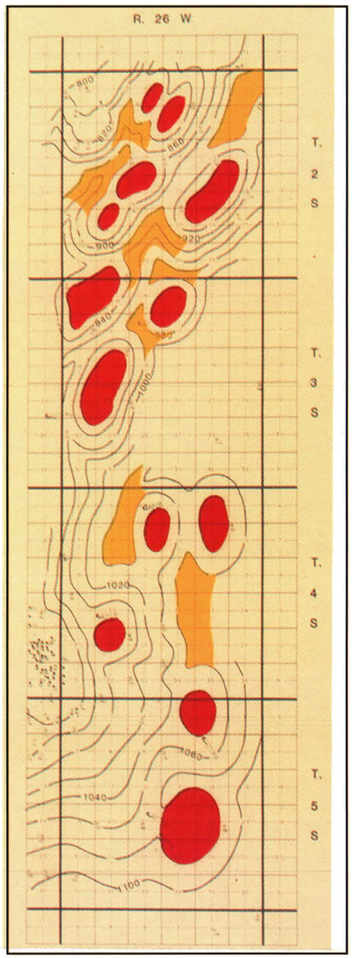

FIGURE 2A—Lansing structure.

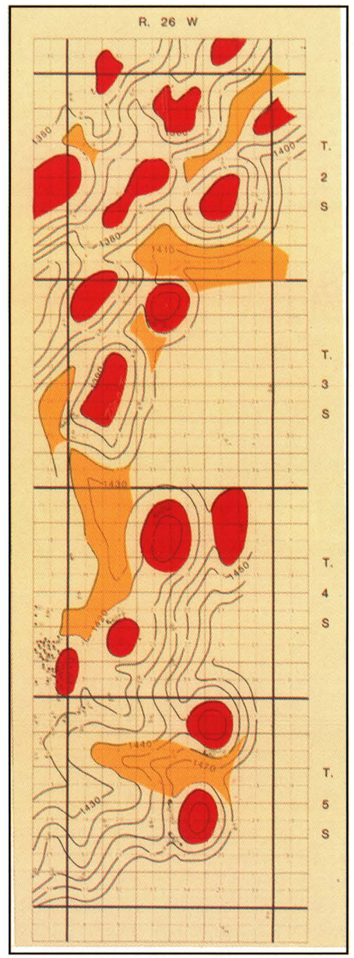

FIGURE 2B—Anhydrite to Lansing isopach, 7/24/80.

Prospect Geophysics

The geophysical method used to investigate the prospect was correlation point seismic information. The seismic records were evaluated with an Anhydrite Time Structure map used in conjunction with isochron maps to various reflectors below the anydrite.

Seismic program was assigned to evaluated sec. 16. This prospect was termed the Garfield prospect, and the acreage to the southwest termed the Tacha prospect. The following discussion will be limited to sec. 16 and the resulting development around the Garfield prospect. Shot points were assigned on a diagonal 20-acre (8-hm²) pattern on sec. 16 and also a shot point on the Consolidated Oil & Gas and J. O. Farmer hole in the NE NE NE sec. 17. The original program on the Garfield prospect consisted of 33 points. The seismic program was shot by Reliance Exploration of Wichita, Kansas, using 180-ft (55-m) shot holes loaded with 5–10 lbs of charge for the "A" shot. A second shot for each hole was recorded at approximately 60 ft (18 m) with 2 1/2 lbs of charge. The records were 12 traces, split-spread recorded with a 50_2–130 filter and computed to a 2,500-ft (762-m) above-sea-level datum. The records were displayed on photographic paper, and no tape records were recorded. The identification of the various horizons was accomplished by using regional velocities since no synthetic seismogram was available in the area. The resulting interpretation is presented in the next four figures. The graphic display of these maps, and all following sets of maps, is a 3D view of sec. 16 as seen from above and from the northwest with the Consolidated Farmer well shown as a bore hole with a synthetic seismogram displayed beside the hole. The synthetic seismogram was generated from the Murfin #1-16 Lippelmann, which was drilled after the original interpretation was completed. Figure 3 shows the shot points as

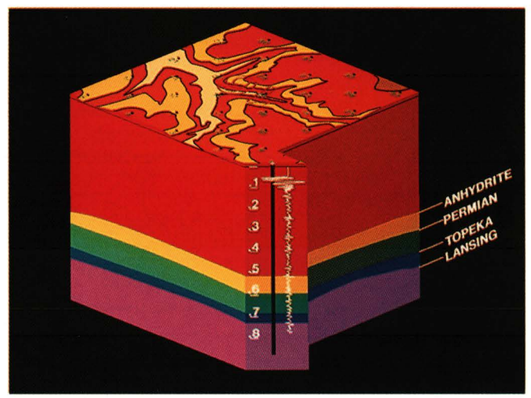

FIGURE 3—Murfin Drilling Co., Garfield Prospect, Decatur County, T. 3 S., R. 36 W.

spotted on the surface elevation. The layers indicate the various horizons picked on the correlation points, which include the Topeka and Lansing formations. Figure 4 represents a surface of the anydrite below a datum of 2,500 ft (762 m) with a 0.005-sec contour interval. A positive feature can be seen on the Anhydrite Time Structure in the northwest portion of sec. 16 around shot points 2, 3, 4, 7, 8, and 11. Figure 5 represents the Topeka surface below the flattened Anhydrite Time Structure. The contour interval is 0.002 sec. As presented in the figure, a thin is seen to include shot points 1, 6, and 8. Figure 6 represents the surface of the Lansing below the flattened anhydrite. The thin in sec. 16, offsetting the well in 17 is somewhat larger. The general trend is a thin running northwest to southeast.

A location was selected at the SE NW NW sec. 16 and the Murfin Drilling Company #1-16 Lippelmann was spudded 8–28–82 and completed as an oil well. The first DST in the Oread recovered 30 ft (9 m) of clean gassy oil, 120 ft (37 m) of mud-cut oil, 400 ft (122 m) of highly oil-cut mud, and 360 ft (110 m) of muddy water (fig. 7).

The second DST (3,506–3,550 ft, 1,069–1,082 m; Lansing C, D, and E) recovered 1,100 ft (335 m) of gas in pipe, 630 ft (192 m) of clean gassy oil, and 780 ft (238 m) of frothy oil with good pressures.

The third DST in the Cherokee (3,823–3,850 ft; 1,165–1,173 m) recovered 20 ft (6 m) of heavy oil-cut mud and 1,310 ft (400 m) of slightly oil-cut saltwater.

The Lansing formation was penetrated as a subsea datum of -923 ft (-281 m) and the Anhydrite to Lansing interval at 1,390 ft (424 m), which represents 11 ft (3.4 m) of thinning to the well in sec. 17.

Figure 7 also presents a sample record correlated to a synthetic seismogram generated from the Murfin #1-16 Lippelmann along with the logs from the test and the DST results.

Since the N/2 and the S/2 of sec. 16 were separate leases, it was decided by Murfin Drilling Company to drill the Murfin "B" #1-16 in the south half, located in NE NW

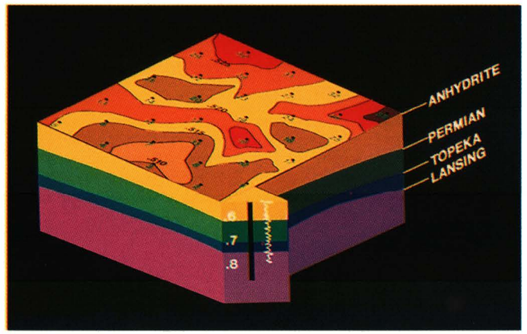

FIGURE 4—Anhydrite time surface.

FIGURE 5—Anhydrite to Topeka time surface.

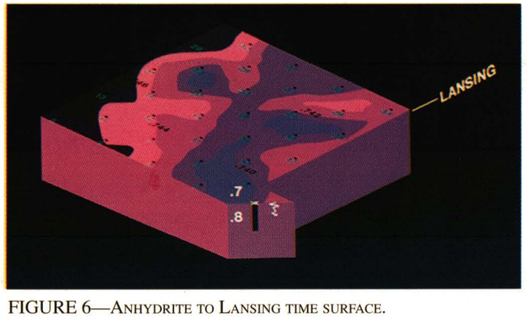

FIGURE 6—Anhydrite to Lansing time surface.

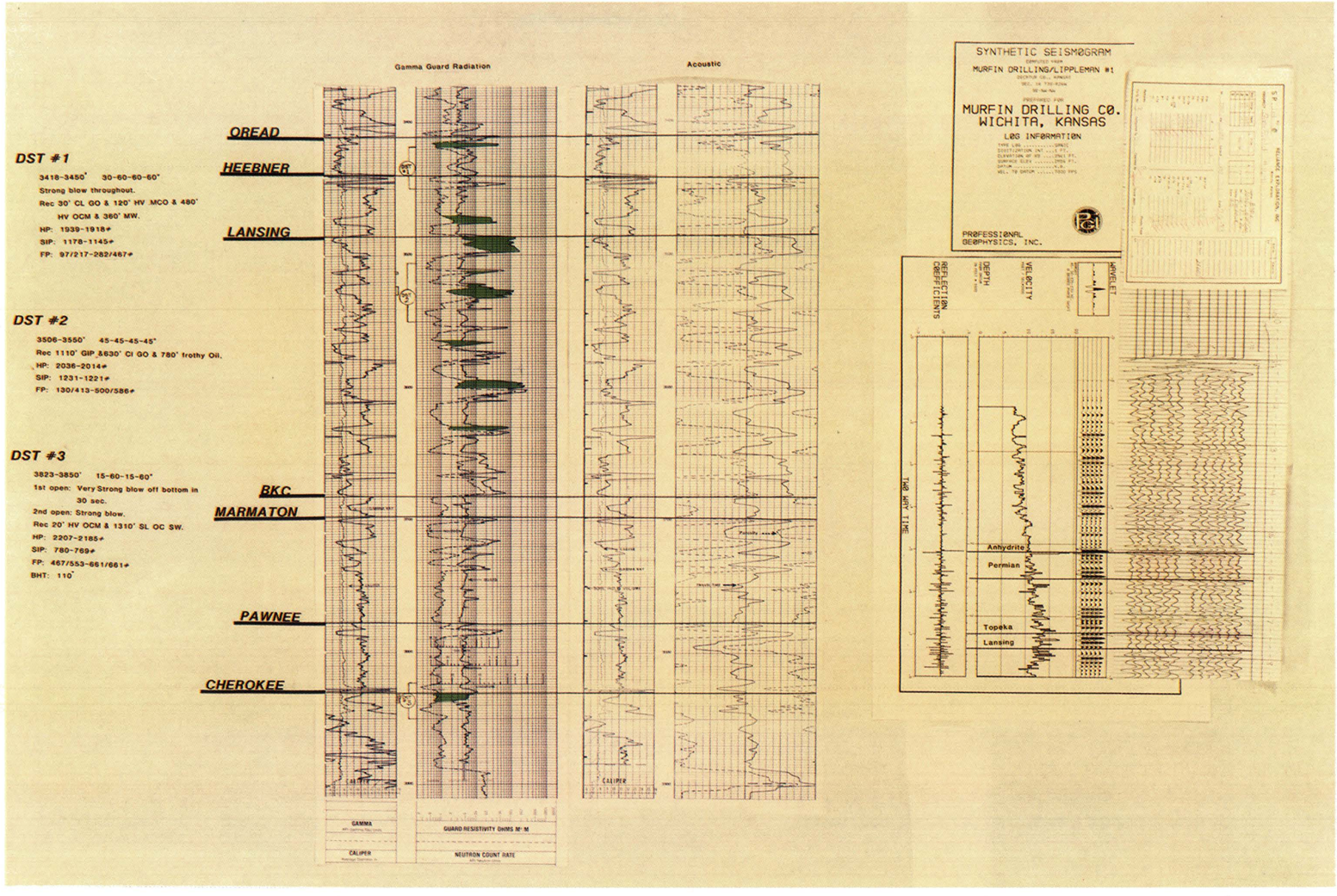

FIGURE 7—Synthetic seismogram of Lippelmann #1.

SW, just north of shot point #18. The well was spudded on August 28, 1982, and ran low all the way down to total depth (TD). The hole had a Lansing datum of -947 ft (-289 m) and an Anhydrite to Lansing datum interval of 1,397 ft (426 m) (fig. 8).

Three tests were run during the drilling, but no shows of oil or gas were recovered except for some very slightly oil-cut mud out of the Oread.

With our initial success, we felt that the features in the NW sec. 16 needed to be refined with shot points on 10-acre (4-hm^2) locations. The new program resulted in 25 more shot points. The second round of shooting put the charge for the "A" shot at

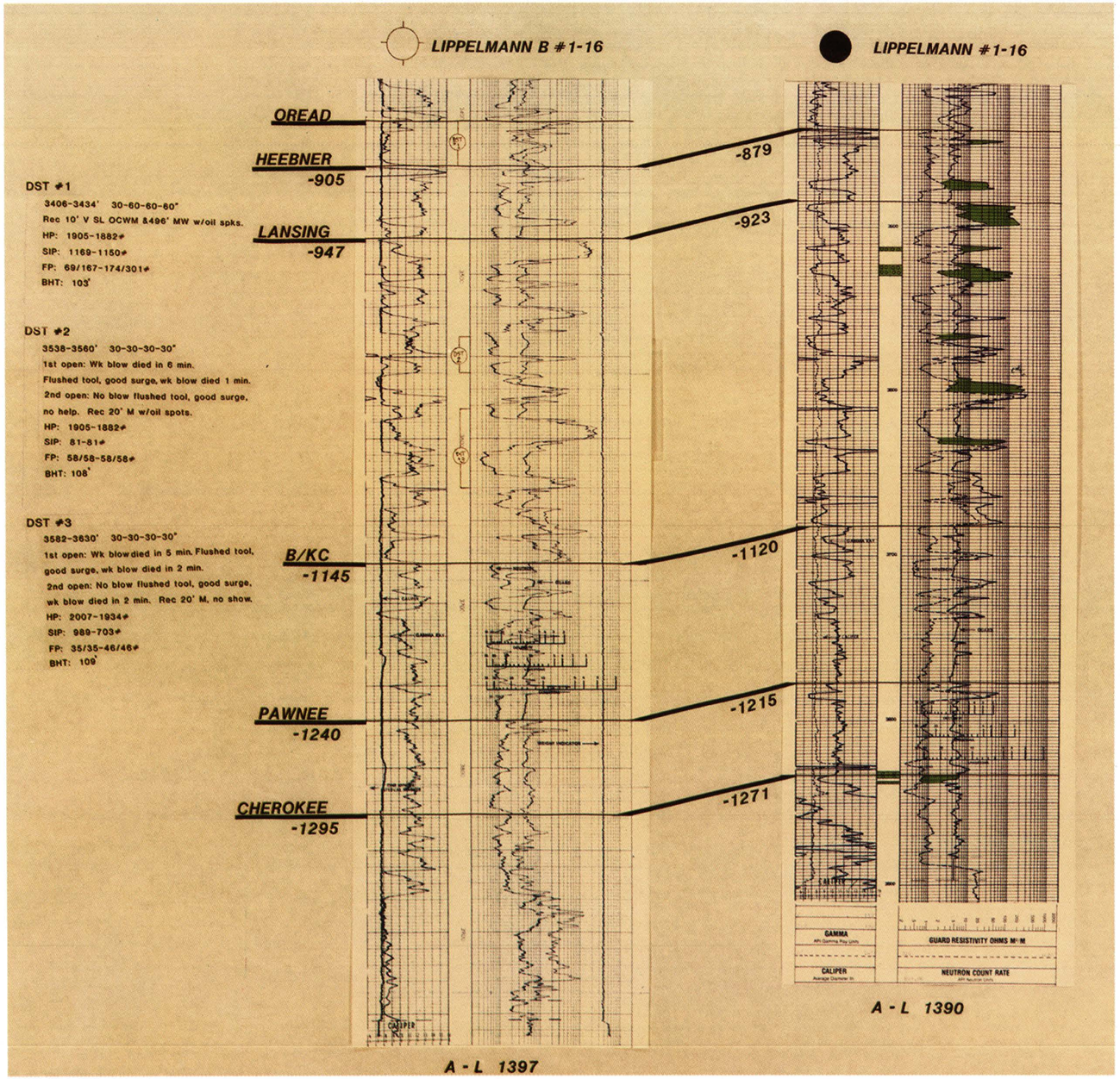

FIGURE 8—Synthetic seismogram of Lippelmann B #1–16 and Lippelmann #1–16.

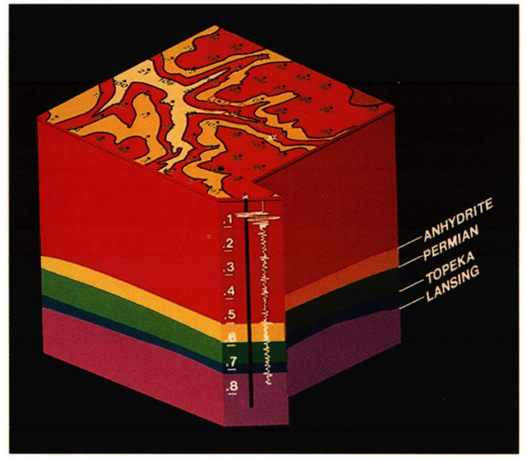

FIGURE 9—Garfield Prospect.

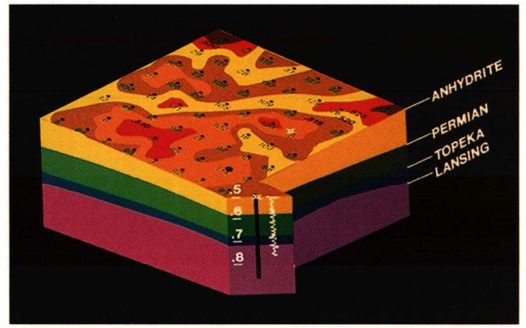

FIGURE 10—Anhydrite time surface.

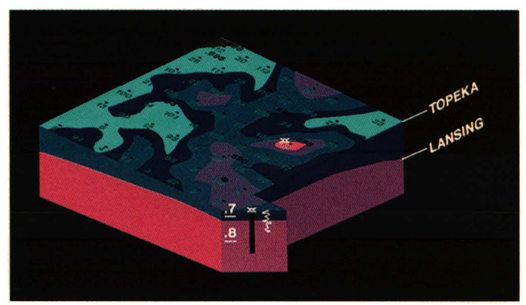

FIGURE 11—Anhydrite to Topeka time surface.

approximately 250 ft (76 m) and the "B" shot was detonated at approximately 100 ft (30 m). Charge sizes increased to 15 lbs on the "A" shot and 10 lbs on the "B" shot. The filter setting and geophone layout were consistent with the first round of shooting. The same graphical display as above is presented with the new shot points filled in on 10-acre (4-hm^2) spots.

Figure 9 indicates the location of the infill points along with the initial two tests drilled by Murfin Drilling Company. The #1-16 Lippelmann is displayed at shot point 114 and the Murfin "B" 1-16 is displayed between shot points 18 and 103. Figure 10 is a display of the Anhydrite Time Structure indicating a large positive area in the N/2 sec. 16. Figure 11 displays the Topeka structure below a flattened Anhydrite and again shows a positive feature running northwest-southeast across the section. Figure 12 indicates the same structural configuration on top of the Lansing.

Shot points in the NW sec. 16 (114, 92, 95, and 97) appeared to be high and thin on all maps. The Murfin Drilling Company #2-16 Lippelmann (shot point #92 NW NE NW) and the #3-16 Lippelmann (shot point #97 NW SE NW) were staked on those shot points.

The #2 Lippelmann was spudded on July 28, 1983, and drilled to total depth with seven DST's being performed. Figure 13 shows the resulting log, in cross section form, from the Lippelmann #2-16 and the DST's. The Lansing was penetrated at -933 ft (-284 m) and the Anhydrite to Lansing interval was 1,396 ft (426 m). Pipe was set.

The #3 Lippelmann was spudded on August 7, 1983, and drilled to total depth with one DST (fig. 14). The Lansing was penetrated at -936 ft (-285 m) with an interval of 1,397 ft (426 m).

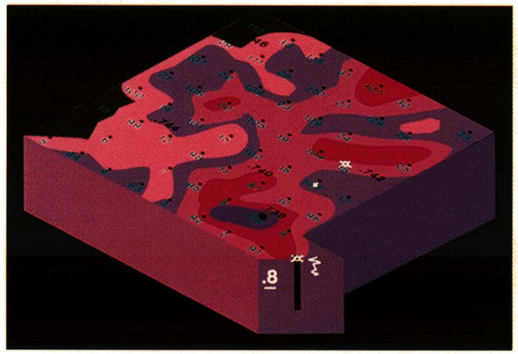

FIGURE 12—Anhydrite to Lansing time surface.

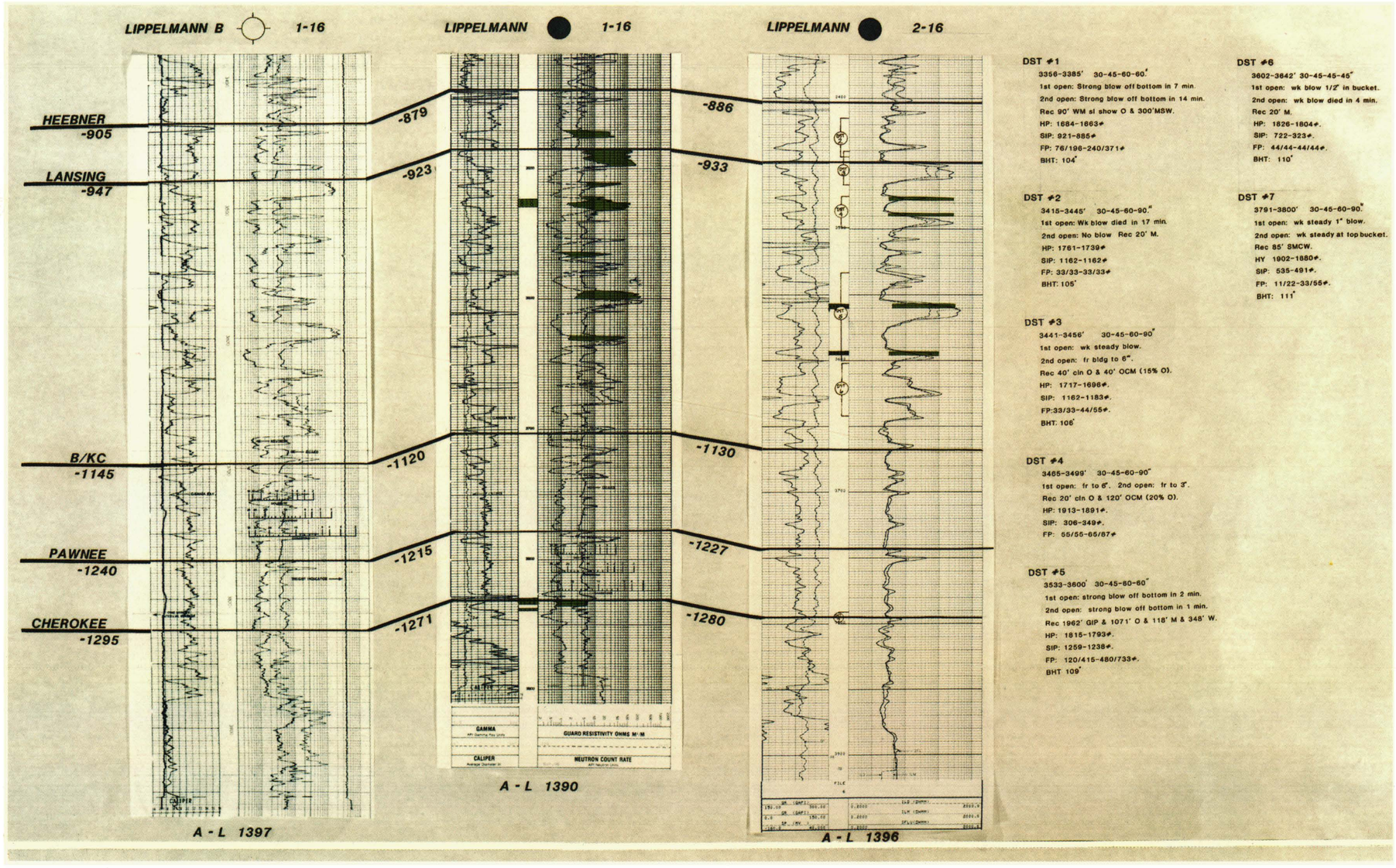

FIGURE 13—Synthetic seismogram of Lippelmann B #1–16, Lippelmann #1–16, and Lippelmann #2–16.

Murfin Drilling obtained a farm-out from Diamond Shamrock in the S/2 sec. 9 and decided to shoot a diagonal 20-pattern (nine more points) there (figs. 15–18 are a result of that interpretation). The wells which had been drilled previous to the additional shooting are displayed on the maps in figs. 15–18. Murfin Drilling Company had also renewed the lease on the S/2 sec. 16 from Mr. Lippelmann on a six-month term.

Because of the resulting interpretation, it was decided to offset to the original three wells somewhere in the SW sec. 9 and also at a possible location on a high thin spot in the S/2 sec. 16. After an evaluation of the interpretation, Murfin Drilling Company decided to drill near the SE SE SW sec. 16 between shot points 27 and 127. This seemed to be on the feature running northwest/southeast and also on a somewhat positive Anhydrite.

The Murfin "B" #2-16 was spudded on November 14, 1983, and drilled to depth with no tests or shows and TD in the Lansing without reaching the base of the Kansas City. The Lansing was at -967 ft (-295 m) and the Anhydrite to Lansing interval was 1,400 ft (427 m). Figure 19 indicates the relationship of the Murfin "B" #2-16 to the wells drilled earlier on the prospect.

Several more shot points (5) were now programmed in the S/2 sec. 9 to obtain 10-acre coverage over the area on the proposed 1-9 Shirley. The resulting interpretation as shown in figs. 20–23 located the Murfin #1-9 Shirley on the same diagonal 20 pattern (SE SW SW) north of the #1-16 Lippelmann (at shot point #141). The Murfin #1-9 Shirley was spudded on November 20, 1983. The Lansing was cut at -927 ft (-278 m) and the interval was 1,393 ft (425 m). Pipe was set (fig. 20).

Production from the Lippelmann field through June 1992 has been 249,333 BO from the Lippelmann lease and 106,833 BO from the Shirley lease with the ultimate recovery projected at 429, 873 BO from the Lippelmann lease and 124,859 BO from the Shirley lease.

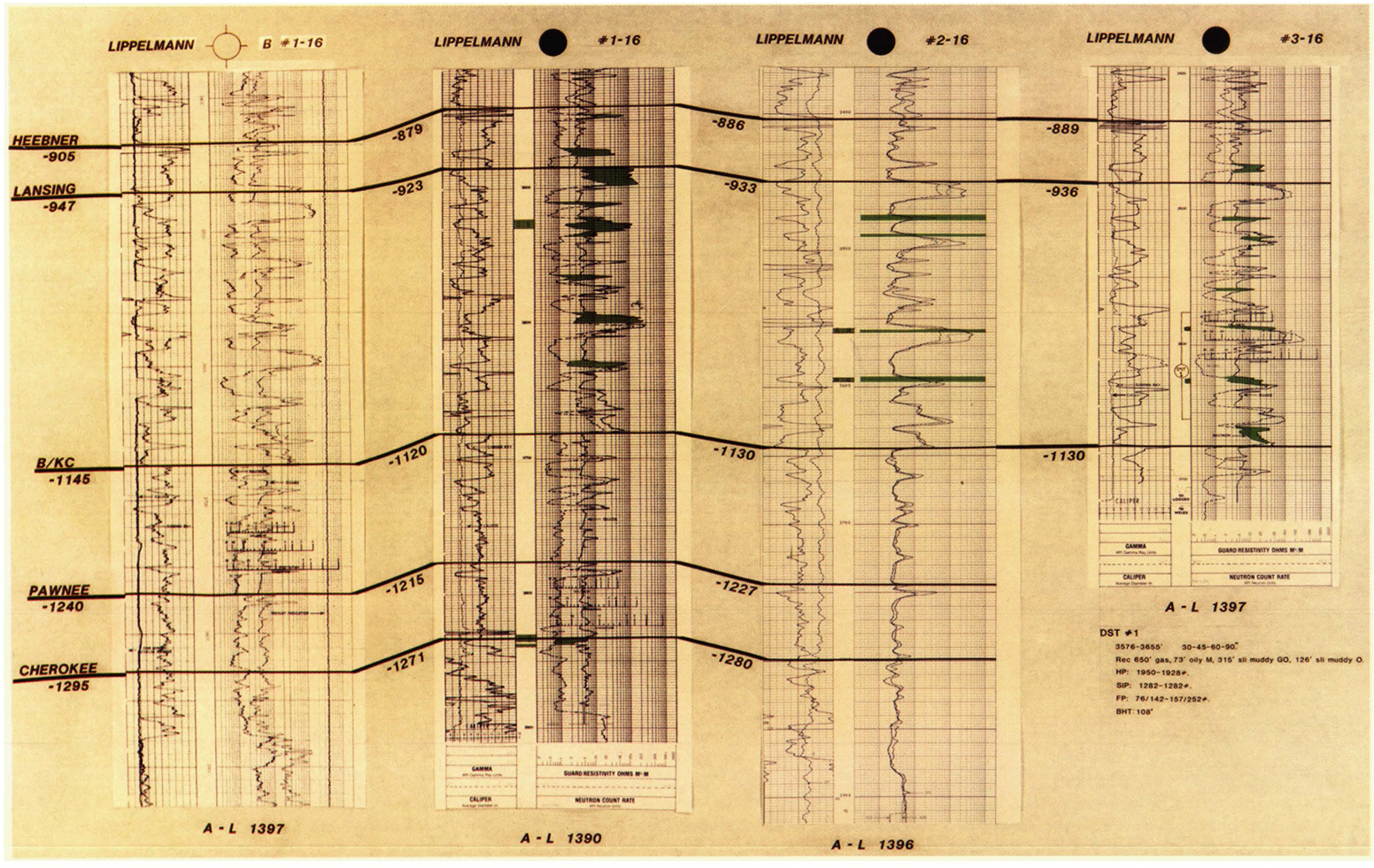

FIGURE 14—Synthetic seismogram of Lippelmann B #1–16, Lippelmann #1–16, Lippelmann #2–16, and Lippelmann #3–16.

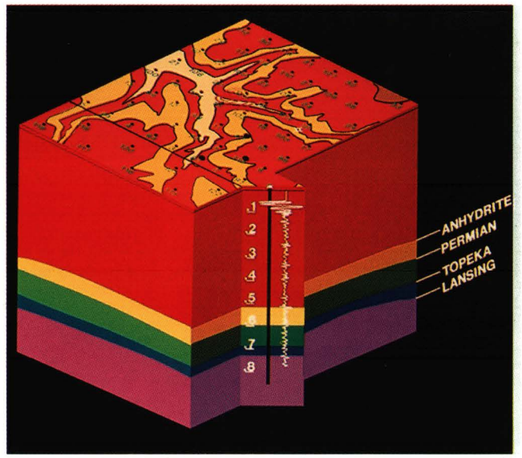

FIGURE 15—Garfield Prospect, Decatur County.

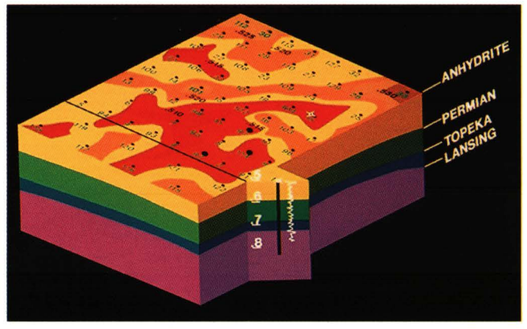

FIGURE 16—Anhydrite time surface.

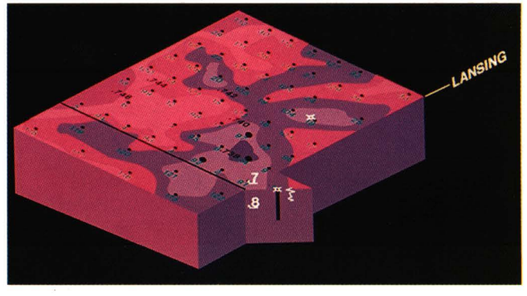

FIGURE 17—Anhydrite to Lansing time surface.

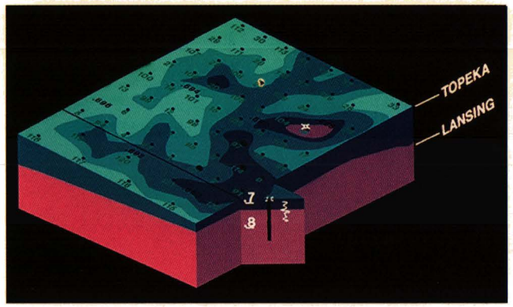

FIGURE 18—Anhydrite to Topeka time surface.

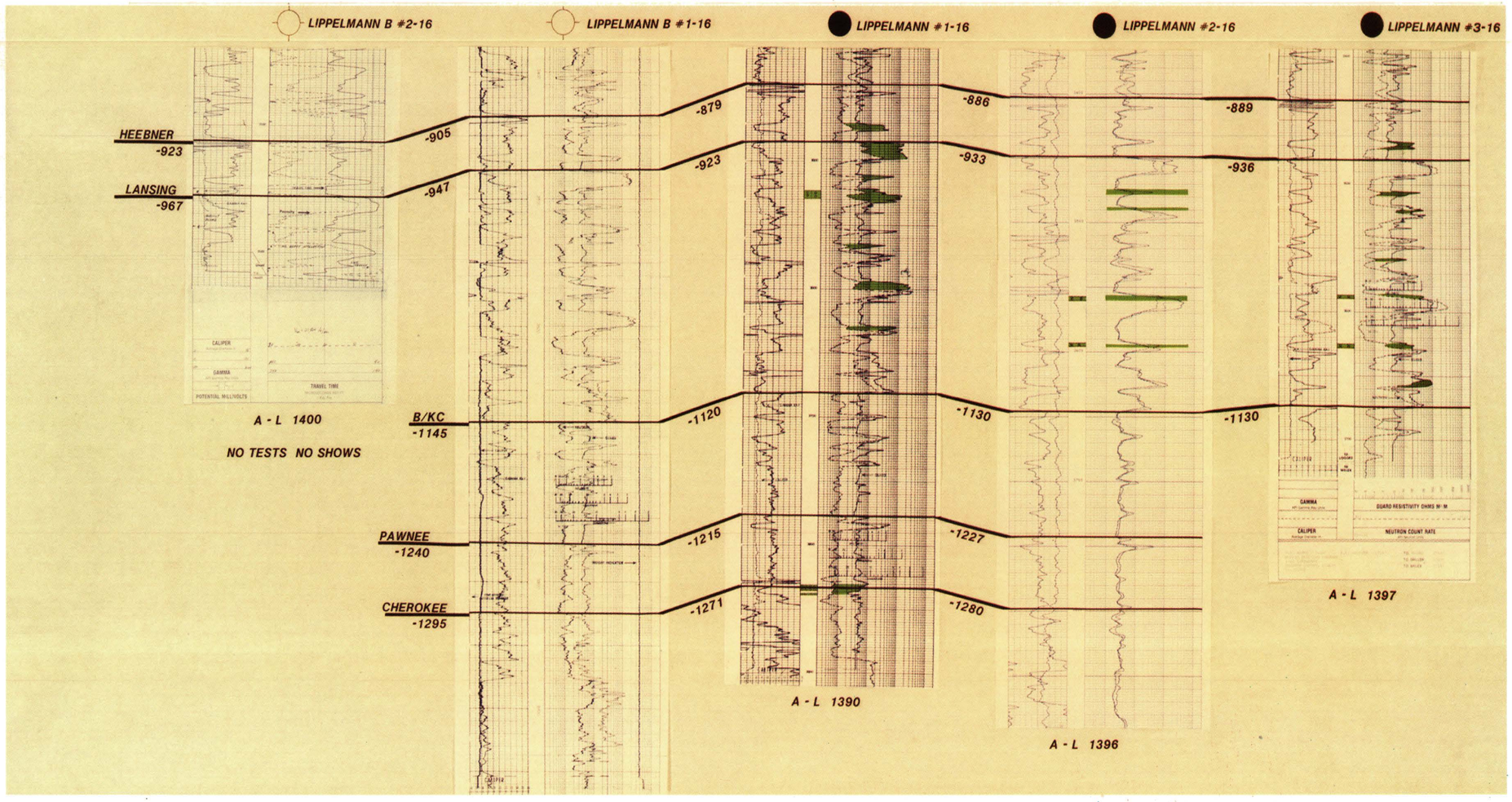

FIGURE 19—Garfield Prospect, Decatur County.

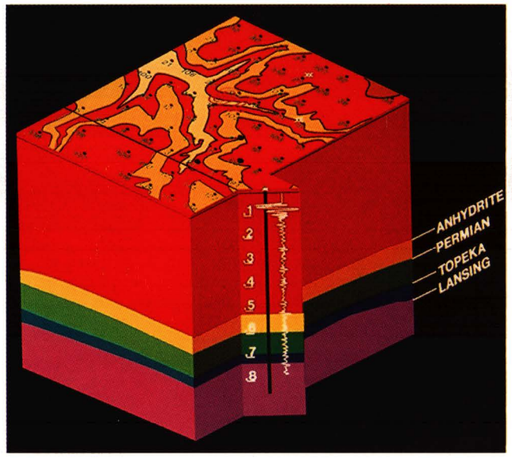

FIGURE 20 (LEFT)—SYNTHETIC SEISMOGRAM OF LIPPELMANN B #2–16, LIPPELMANN B #116, LIPPELMANN #1–16, LIPPELMANN #2–16, AND LIPPELMANN #3–16.

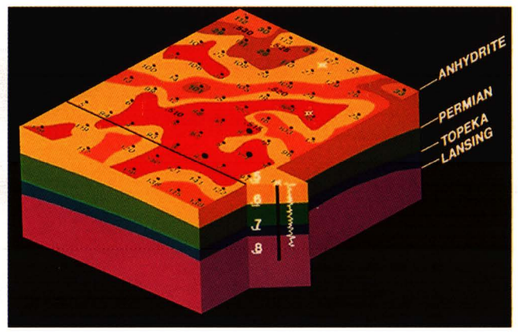

FIGURE 21—ANHYDRITE TIME SURFACE.

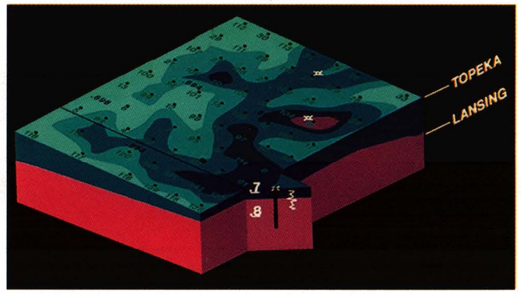

FIGURE 22—ANHYDRITE TO TOPEKA TIME SURFACE.

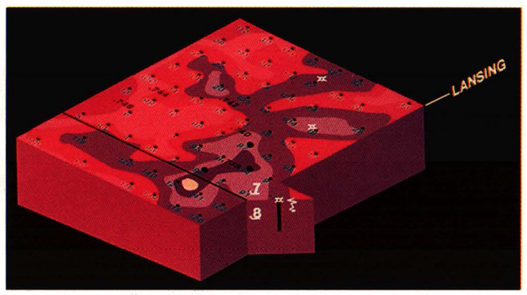

FIGURE 23—ANHYDRITE TO LANSING TIME SURFACE.

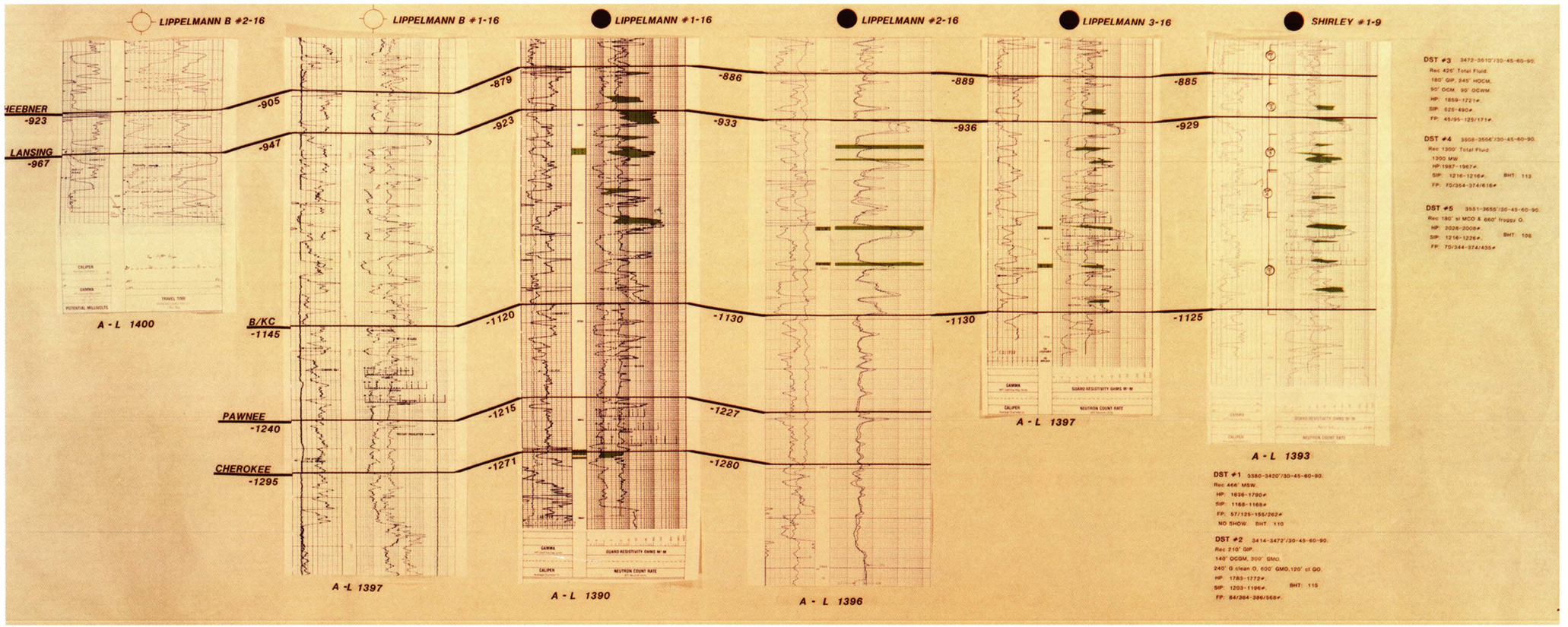

FIGURE 24—SYNTHETIC SEISMOGRAM OF LIPPELMANN B #2–16, LIPPELMANN B #1–16, LIPPELMANN #1–16, LIPPELMANN #2–16, LIPPELMANN #3–16, AND SHIRLEY #1–9.

Minneola Complex, Ford and Clark Counties, Kansas

Stacy L. Clark
Double Eagle Enterprises, Tulsa, OK 74103

Introduction

The stratigraphy of the Morrow Series in southwest Kansas consists of sandstones and shales, with the shales acting as source and seal and the sandstones forming the reservoir facies. Within the Minneola complex, the upper limit of the Morrowan is defined by the base of the "Thirteen Finger limestone" (where present) or the base of the Inola limestone. The base of the Morrowan is the Mississippian–Pennsylvanian unconformity (fig. 1). The Morrowan interval ranges from 5 to 120 ft (2 to 37 m) in thickness in the Minneola complex (fig. 2) and thickens south-southwest toward the Anadarko basin.

The Morrowan sandstones and siltstones are lenticular and range in thickness up to 15 ft (5 m). The sandstones are very fine grained, clean, subrounded to rounded, cemented by calcite, and commonly glauconitic (Robinson, 1983). Quartz averages over 90% of the framework minerals, chert averages 3%, and glauconite, feldspar, and sedimentary rock fragments account for 1% or less of the total volume. The framework minerals are cemented by ankerite, calcite, quartz, clay minerals, and pyrite, of which carbonate minerals and quartz are the most common. Associated interbedded shales and siltstones are dark gray to black, ranging from 20 to 50 ft (6 to 15 m) in thickness. Occasionally, at the base of the Morrowan, a conglomeratic sandstone up to 20 ft (6 m) thick is present. Porosities range normally 1–4% in the unproductive tight sands and 12–18% in the productive sands.

At the close of Mississippian–Chesteran time, the sea regressed and the northern shelf of the Anadarko basin was subaerially exposed. Fluvial drainage systems developed in the Early Pennsylvanian around the flanks of the Hugoton embayment and on the northern shelf of the Anadarko basin; sediment was eroded from the Central Kansas uplift and transported into the area. Marine transgression into the area during Morrowan time resulted in the deposition of conglomeratic basal sandstones and marine shales. Following several transgressive-regressive cycles and the deposition of sporadically distributed lower and middle nonproductive Morrowan sandstones, the uppermost and major productive Morrowan sandstone was deposited during the final transgressive phase. Figure 3 illustrates the thickness and distribution of the productive sandstones in the study area.

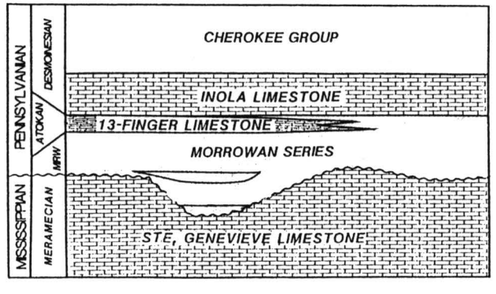

FIGURE 1—IDEALIZED STRATIGRAPHIC SECTION FOR MINNEOLA IN NORTHERN CLARK AND SOUTHERN FORD COUNTIES, KANSAS.

These uppermost productive Morrowan sandstones have been interpreted by Doyel (1985) to be strike-valley sandstones, reworked and redeposited in a marginal marine environment during the transgression of Early Pennsylvanian seas. Busch (1974) described the geometry of strike-valley sandstones as 1) being controlled by predepositional topography of tilted alternating resistant and nonresistant strata, 2) lengths up to "many" (Busch, 1974) miles for individual sand bodies, 3) very asymmetric in cross sections having a teardrop profile, and 4) having widths ranging from 0.5 to 1 mi (0.8 to 1.6 km). Morrowan sandstone geometry in the Minneola complex fails to satisfy three of four of Busch's (1974) geometric criteria for strike-valley sandstones.

Within the study area, the Morrowan sandstones and shales lie unconformably on the lithologically uniform, resistant Ste. Genevieve Limestone. Subsurface mapping indicates that the predepositional topography of the Mississippian surface locally was eroded not into escarpments or cuestas that parallel strike, but into a gently sloping surface cut by Early Pennsylvanian drainage channels, which roughly parallel present-day regional dip to the south-southwest. Regionally, the geologically ideal location for the deposition of strike-valley sandstones would be on the alternating resistant-nonresistant strata of the Mississippian Chester formation, which subcrops approximately 6 mi (10 km) south of the study area. In contrast to strike-valley sandstones, the Morrowan sandstones in the study area are rarely laterally continuous along strike for more than 1–1.5 mi (1.6–2.4 km). In addition, the sandstones are symmetric and lenticular or pod-like rather than asymmetric and teardrop in configuration (fig. 3). The sandstones maintain widths ranging from 0.5 to 1 mi (0.8–1.6 km). Although the stratigraphy is consistent with marginal marine deposition, the geometric inconsistencies open the possibility for other depositional model alternatives.

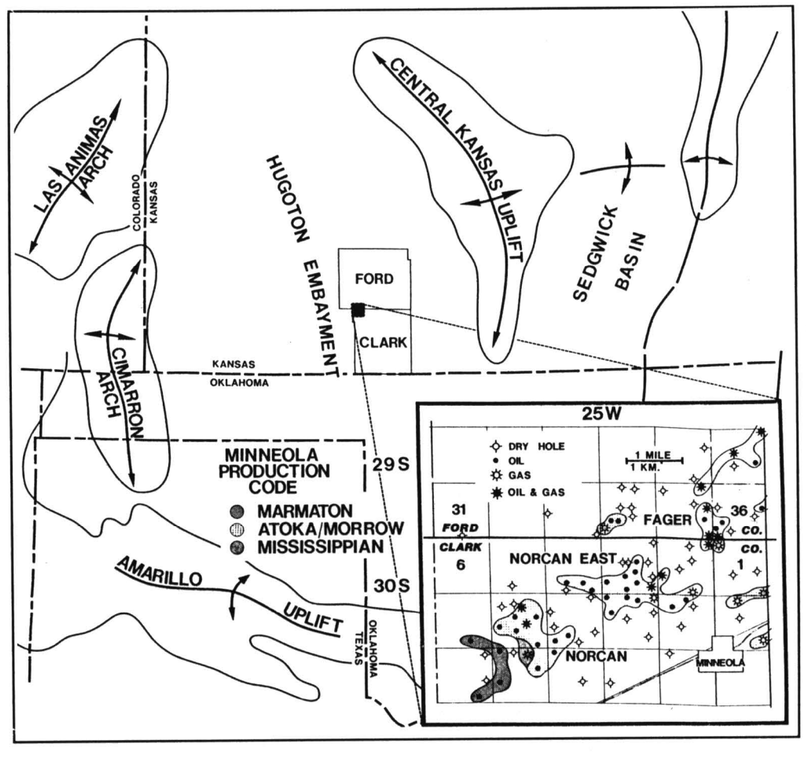

FIGURE 2—INDEX MAP OF STUDY AREA SHOWING MAJOR TECTONIC FEATURES. Individual fields and associated production of Minneola complex are shown in insert.

The uppermost productive Morrowan sandstones in the study area are interpreted to be barrier bars or shelf sandstones (Tillman et al., 1985) deposited during stillstands of a transgressive sea. The barrier bar sandstones deposited during stillstand "2" of fig. 3 are represented in the stratigraphic cross section of fig. 4. These sandstones are 5–15 ft (2–5 m) thick and are best preserved within the former fluvial channels due to differential compaction during deposition. Deposition of the sandstones on Mississippian highs outside the channels resulted in very thin (less than 5 ft or 2 m), tight sandstone. The barrier bar sandstones were covered by marine shales and marine shelf carbonates of the Cherokee Group as transgression continued.

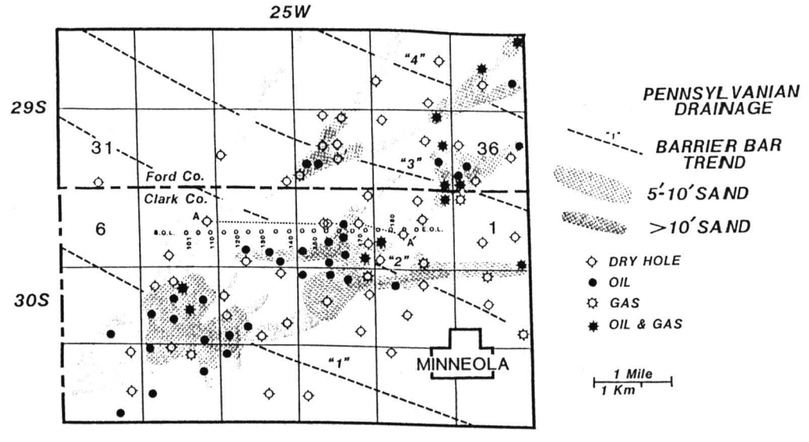

FIGURE 3—MAJOR LOWER PENNSYLVANIAN DRAINAGES AS INTERPRETED FROM SEISMIC. Barrier-bar sand accumulations and trends marked "1," "2," "3," and "4" are mapped from well control in Clark and Ford counties, Kansas.

Minneola Complex

Introduction

The Minneola complex, located in northwestern Clark and southwestern Ford counties, Kansas, consists of northeast-southwest-trending oil fields that produce almost entirely from sandstones of Morrowan age: Norcan, Norcan East, and Fager fields. The complex currently consists of 54 producing oil and gas wells, of which 50 wells produce from Morrowan sandstones at depths of 5,100–5,300 ft (1,554–1,615 m). Here, the sandstones range in thickness from 3 to 16 ft (1–5 m). Two Morrowan wells have some minor commingled gas production from the Mississippian. The remaining four wells produce oil from limestones in the Marmaton Group. Closure is present on these limestones as a result of draping over Mississippian erosional remnants. Total recoverable reserves for the Minneola complex are estimated to be 2.5 million bbl of oil and 6 billion ft^3 of gas. Morrowan sandstone production was first established in southeast Clark County, Kansas, with the discovery of the Harper Ranch field in 1953. Discovery of the Lexington field in east-central Clark County by Mesa Petroleum in 1977 extended Morrow production approximately 20 mi (32 km) north. The discovery by Ladd in 1980 of the Minneola complex extended known Morrowan sandstone production 25 mi (40 km) west.

The Morrowan sandstones at Lexington field and the Minneola complex accumulated under similar conditions. The thickest Morrowan sandstones were deposited in narrow channel cuts on the weathered, eroded Mississippian surface, a situation which created excellent stratigraphic traps for petroleum accumulations. Early exploration drilling by Mesa at Lexington for these traps was primarily guided by limited subsurface control. However, seismic data became increasingly important as development drilling proceeded at the Lexington field after Morrowan production was found to be associated with seismic anomalies. The discovery well in the Minneola complex, Ladd 1-8 Norton, sec. 8, T. 30 S., R. 25 W., was drilled on an anomaly (recognized on 12-fold Vibroseis seismic) similar to those drilled at Lexington field. Subsequent development drilling in the Minneola complex relied on the integration of seismic data with subsurface geologic analysis.

Geologic Cross Section

The locations of the five wells incorporated into the geologic cross section (fig. 4) and the example seismic section (see fig. 8) are superimposed in fig. 3. All five wells are within 330 ft (100 m) of the seismic line and penetrate the Mississippian limestone. The cross section illustrates the relationship between productive/potentially productive 50–100 ft (15–30 m) channel cuts and the nonproductive regionally thin, less than 20-ft (6-m) Morrow shale-filled section.

The westernmost well, Banks Oil #1-5 Belden, cuts approximately 50 ft (15 m) of Morrow channel fill and encountered 6 ft (2 m) of middle Morrowan nonproductive wet sandstone. Nearly 8,000 ft (2,460 m) to the east, the Santa Fe #1-3 Boucher is stratigraphically high on the Mississippian and encountered no Morrowan sandstone. The central well 990 ft to the east, Ladd #2-3 Fager, encountered approximately 10 ft (3 m) of Morrowan sandstone, which was deposited in a 40-ft (12-m) channel and initially produced 246 BOPD. The Murfin #1-3 Fager, 990 ft (305 m) east, is stratigraphically high and again encountered no productive Morrowan sand. The easternmost well, the Murfin #2-2 Hall, cuts 56 ft (17 m) of Morrow channel fill but encountered no productive Morrowan sandstone.

Based on the depositional model, drilling in Early Pennsylvanian channels is no guarantee that upper sandstones will be encountered. Between still-stands, marine shales and fine siltstone were deposited. These depositional relationships are illustrated in fig. 4 by the poorly developed upper sandstone in the Banks Oil #1-5 Belden and the Murfin #2-2 Hall, both of which were drilled on either side of a productive upper Morrowan sandstone. The nonproductive fine siltstones and sandstones found in these wells are tight (5% porosity) since they were not reworked during deposition.

Seismic Section

Determining the position of the Mississippian–Pennsylvanian unconformity on the regional seismic data is critical. To perform this task, synthetic seismograms were generated from available sonic logs and tied to the seismic line. Once the position of the Mississippian–Pennsylvanian unconformity on the seismic data is established, anomalous changes in wavelet character (amplitude, frequency, and polarity) along this interface can be identified and mapped. Changes in lithology and thickness in the Morrowan section are associated with seismic anomalies in the Minneola complex.

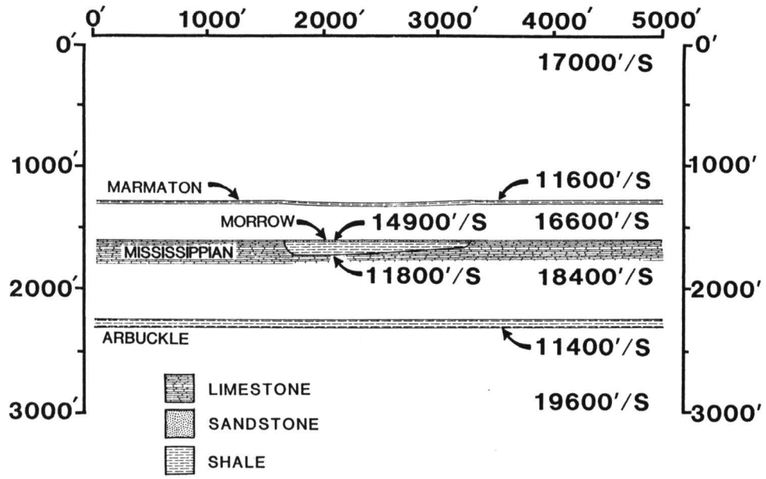

FIGURE 5—IDEALIZED GEOLOGIC AND VELOCITY MODEL OF EARLY PENNSYLVANIAN CHANNEL FOUND IN MINNEOLA COMPLEX FILLED BY MORROWAN SANDSTONES AND SHALES.

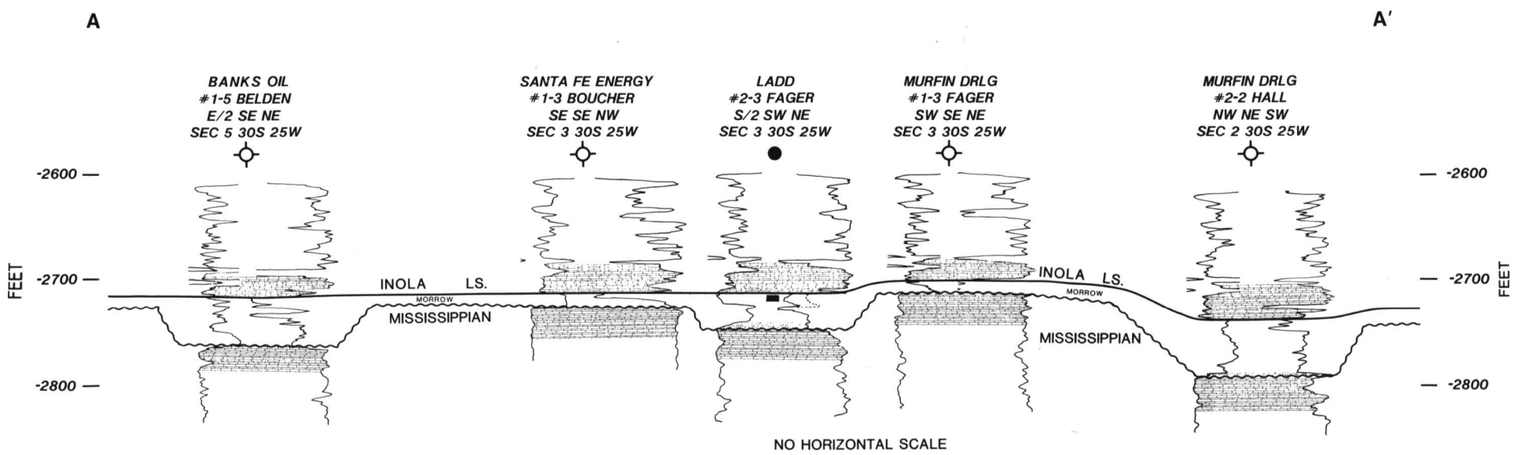

FIGURE 4—STRUCTURAL CROSS SECTION SHOWING THE STRATIGRAPHIC/DEPOSITIONAL RELATIONSHIPS OF INDIVIDUAL MORROWAN SANDSTONES. Section datum is -2700 ft (-823 m). Location of cross section shown in fig. 3.

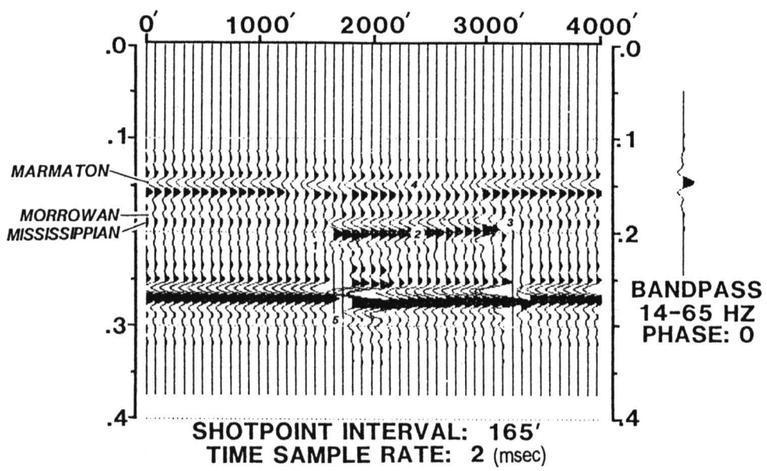

FIGURE 6—SEISMIC RESPONSE OF GEOLOGIC-VELOCITY MODEL OF FIG. 5, ILLUSTRATING ANOMALIES ASSOCIATED WITH MINNEOLA COMPLEX.

Exploration and development success was contingent upon recognizing several seismic anomalies associated directly with the Lower Pennsylvanian drainage and the stratigraphy of the Morrowan section. These anomalies, listed in order of relative importance, are 1) diffractions, 2) amplitude anomalies, 3) polarity reversals, 4) sagging of the Marmaton reflector due to differential compaction, and 5) breakup or faulting of underlying Viola–Arbuckle reflectors. Note that the appearance of these anomalies is highly influenced by the angle at which the seismic data was shot in relation to the channel cut, the thickness and type of sediment (percentage of shale vs. percentage of limestone), and the morphology of the Lower Pennsylvanian channels, that is, those with steep sides vs. those with gentle slopes.

Figures 5, 6, and 7 represent the geologic input, seismic responses, and vertical incident ray tracing from an underlying reflector, respectively, of an idealized geologic model of an asymmetrical channel filled with Morrowan clastics. The channel depicted in fig. 5 is 60 ft (18 m) deep on the left, thinning to 20 ft (6 m) on the right. The channel is filled with shale and 10 ft (3 m) of sandstone overlying the shale. The model was run on an IBM-PC compatible Mira System using Mira software. After reflection coefficients were generated, they were convolved with zero-phase 14–65 Hz bandpass wavelet and plotted at normal polarity to match processing parameters of proprietary seismic data.

The first anomaly, diffractions (marked #1 on fig. 6) caused by the sharp channel edges that act as a point source (Trorey, 1961), is the most noticeable feature on the seismic line. Unfortunately, the Mira ray-trace modeling program currently does not have the capabilities for generating diffractors. However, Neidell and Poggiagliolmi (1977) discussed the wave-theory model response for sandstone bodies of varying lateral extent and their relationship to Fresnel zone size. This work is directly related to the generation of diffractions caused by channel edges currently observed on seismic data. (A field example will be reviewed in detail.)

The second anomaly (marked #2 on fig. 6), a high-amplitude bright spot, is present between 1,670 and 3,000 ft (509 m and 914 m) at 200 msec on fig. 6. This anomaly is caused by increased acoustic impedance due to additional slower velocity sands and shales filling the channel and overlying faster Mississippian limestones. Normally, the interface between the Cherokee and Morrowan shales (10 ft or 3 m or less) and the Mississippian is a very weak seismic event. The addition of low-velocity sands and shales in the Early Pennsylvanian channels causes a strong acoustic interface with the Mississippian limestones, resulting in localized amplitude anomalies. Note that as channel depth decreases and the clastic fill thins, the bright spots decrease in amplitude.

In conjunction with amplitude anomalies, apparent polarity reversals (marked #3 on fig. 6) are observed at the channel edges at the top of Mississippian reflectors (fig. 6). The Cherokee–Morrowan–Mississippian reflector, which is normally a very weak peak, becomes a strong trough over the Early Pennsylvanian channels at 190 msec. This change is due again to the additional 60–100 ft (18–30 m) of clastic section in the channel and results in an 8–12-msec time shift or polarity reversal. Diffractions, strong amplitudes, and polarity reversals are the most frequently observed anomalies associated with pre-Pennsylvanian channels.

The other two anomalies are less commonly observed. The first is the sagging and loss of amplitude in the overlying Marmaton reflector (marked #4 on fig. 6). This sagging (at 155 msec on fig. 6) is in response to differential compaction of sediments deposited over more compactible shales and sands deposited within the channel. The second of these less commonly observed seismic anomalies is the breakup and/or faulting of the Viola–Arbuckle reflectors at 260 msec (marked #5 on fig. 6). These reflectors are generally a continuous, strong peak-trough-peak sequence located approximately 103 msec below the top of the Mississippian event. The cause for the breakup of these seismic events is not clear. Faulting or fracturing in the pre-Pennsylvanian section possibly controlled development of the Early Pennsylvanian drainage patterns. Fault systems interpreted on Ladd proprietary seismic data several miles southwest of the Minneola complex appear to be associated with the Early Pennsylvanian drainage patterns. A second explanation for the apparent "faulting" below channels is seismic ray-path geometry. Seismic ray-trace modeling indicates imaging problems occur as wave fronts (returning from underlying reflectors) encounter the edges of deep, steep-sided channels (fig. 7). This encounter causes "breaks" in the underlying Viola–Arbuckle reflectors which, although they appear to be faults in fig. 6 at 270 msec, are in fact the product of ray-path geometry.

Although many examples of the previously described anomalies have been identified on the available seismic data base, the following example was chosen based on its proximity to well control. The seismic line is 12-fold, consisting of a 20–100 Hz upsweep and three inline vibrators. The array was 48 channel, with 165-ft (50-m) group and 330-ft (100-m) shotpoint intervals. The location of the line (fig. 3) cuts nearly perpendicularly to several Early Pennsylvanian channels and passes 330 ft (101 m) south of four key wells and 330 ft (101 m) north of the other.

Figure 8 is the unmigrated final stack (migrated data were not available). The interval of interest is located between 950 and 1,000 msec, with the top of the Mississippian at approximately 970 msec. Accurately identifying the top of the Mississippian is important to avoid misinterpretation of Early Pennsylvanian channeling anomalies. This section has several key anomalies associated with Early Pennsylvanian drainage. The first example is the amplitude anomalies located at both the eastern and western ends of the line, SP 103–110 and SP 178–188 at 980 msec, which correspond to Early Pennsylvanian channel cuts identified on the geologic cross section. The amplitude anomalies (indicated by #1 on fig. 8) associated with the Banks #1-5 Belden and Murfin #2-2 Hall wells indicate that additional clastic section was deposited locally in a channel cut. Modeling indicates amplitude anomalies associated with Early Pennsylvanian channeling events are dependent upon several of the following variables: 1) depth of channel cut, 2) types of lithologies filling the channel, and 3) the types and variability of overlying and underlying lithologies. Diffractions (indicated by #2 on fig. 8) appear to be associated with the Banks #1-5 Belden well, which suggests a sharp channel cut. Both anomalies located on either side of the seismic line have polarity reversals (indicated by #3 on fig. 8) present at the channel edges at the top of the Mississippian reflector. The second example is located between SP 155 and SP 170 at 980 msec. The convex shape of the reflector suggests diffractions off the channel edges. Proper migration of these

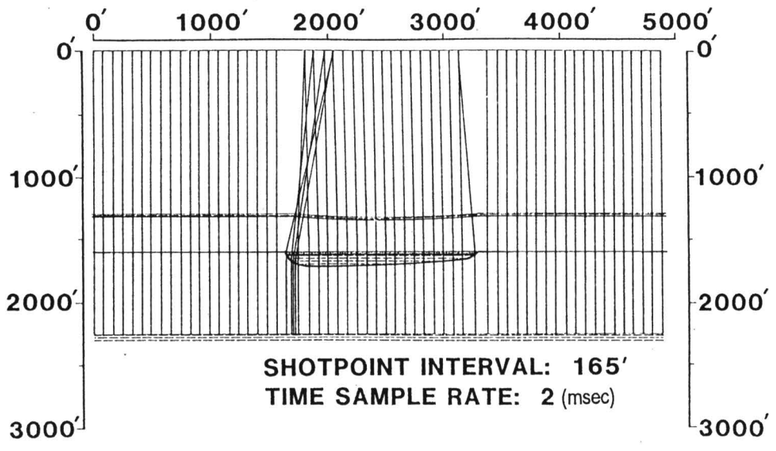

FIGURE 7—NORMAL-INCIDENT RAY TRACING FROM VIOLA–ARBUCKLE REFLECTORS ILLUSTRATING CONVERGENT RAY PATHS CAUSED BY EDGES OF STEEP-SIDED CHANNELS.

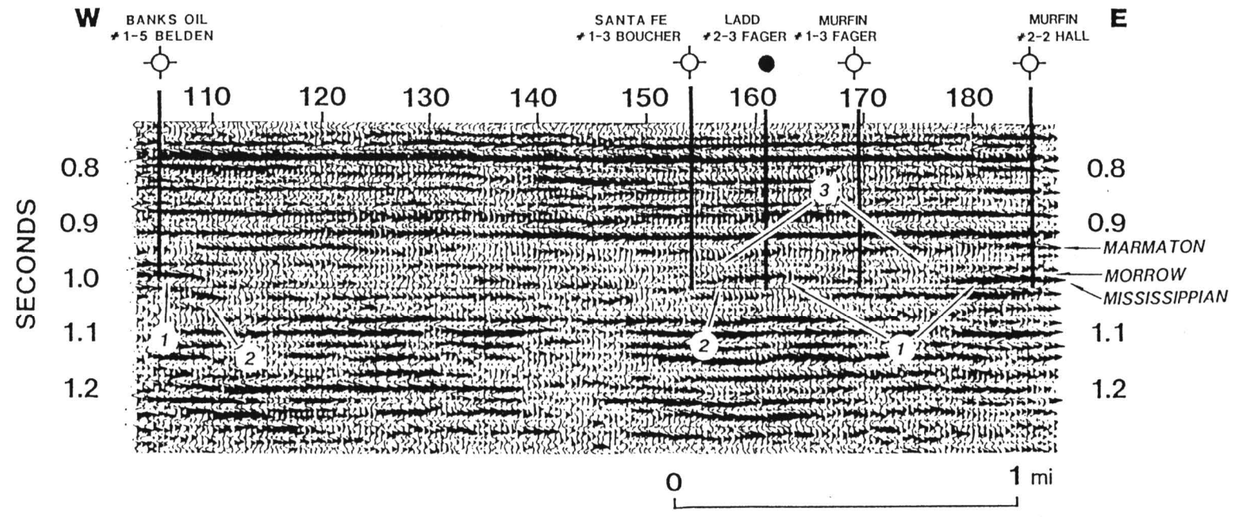

FIGURE 8—EAST-WEST SEISMIC LINE ILLUSTRATING EXAMPLES OF DIFFRACTIONS, AMPLITUDE ANOMALIES, AND POLARITY REVERSALS ASSOCIATED WITH LOWER PENNSYLVANIAN CHANNELING. Stippled pattern marks Mississippian/Pennsylvanian unconformity.

data will collapse those diffractions into their correct orientation and reduce the risk of missing the channel by drilling diffraction events on nonmigrated data.

The amplitude of this event would be further enhanced by migration, which would move additional energy into its proper location. The weakness of amplitude in this case is due to the fact that only 20 ft (6 m) of additional Morrow section was deposited in this shallow cut and higher velocity sandstone replaces lower velocity shale, reducing the reflection coefficient of the event. Modeling indicates strong amplitude events do not occur until more than 50 ft (15 m) of additional clastic section is deposited. This is the case at the Banks and Murfin wells located at the far ends of the cross section.

The abrupt break in the weak peak that marks the top of the Mississippian contrasts sharply with the strong trough over the channel event (fig. 8). This apparent polarity reversal is attributed to the increased thickness of sandstones and shales found in the Morrowan channel as opposed to adjacent faster velocity Mississippian limestones. This particular seismic line does not illustrate either sagging of the overlying Marmaton events or the breakup and/or faulting of the underlying Viola–Arbuckle reflectors.

Conclusions

Oil and gas production in the fields of the Minneola complex are controlled by the development of reservoir-quality Morrowan sandstones. Sandstone development was controlled by the interaction of two geological events. First, during regression of the Mississippian Chesterian sea, fluvial drainage channels were incised into the Mississippian limestone surface; later, cyclic Early Pennsylvanian marine transgressions caused the deposition of marine sandstones, the greatest thicknesses of which were concentrated in lows in the earlier developed drainage patterns. The paleodrainage systems are manifested on CDP seismic data as a variety of anomalies: 1) diffractions, 2) amplitude anomalies, 3) apparent polarity reversals, 4) sagging of overlying reflectors, and 5) apparent "faulting" in the pre-Mississippian section.

References

Busch, D. A., 1974, Stratigraphic traps in sandstones—exploration techniques: American Association of Petroleum Geologists, Memoir 21, p. 67–71

Doyel, D. R., 1985, Norcan field study; *in*, Kansas Oil and Gas Fields, v. 5: Kansas Geological Society, p. 215–222

Neidell, N. S., and Poggiagliolmi, E., 1977, Stratigraphic modeling and interpretation—geophysical principles and techniques; *in*, Seismic Stratigraphy—Applications to Hydrocarbon Exploration, C. E. Payton, ed.: American Association of Petroleum Geologists, Memoir 26, p. 389–416

Robinson, R. J., 1983, Geochemical investigation of diagenetic history of Pennsylvanian Morrowan sandstone, Lexington field, Clark County, Kansas; M. S. thesis, Kansas State University, Manhattan, 66 p.

Tillman, R. W., Swift, D. J. P., and Walker, R. G., 1985, Shelf sands and sandstone reservoirs: Society of Economic Paleontologists and Mineralogists, Short Course Notes 13, 708 p.

Trorey, A. W., 1961, A simple theory for seismic diffractions: Geophysics, v. 35, p. 762–784

Roland SE Field, Rush County, Kansas

David W. Ballard and Kevin K. Reinschmidt
Balcron Oil, Billings, MT 59104

Introduction

Roland SE field is located in the northwest portion of Rush County, Kansas (fig. 1). Although the field was discovered in 1968, it was not effectively developed until 1988. At the present time, there are 10 producing wells at Roland SE. Production is from the Cambrian–Ordovician Arbuckle Group with the exception of one well, Baldwin #1–36, which produces from the Pennsylvanian Lansing Group (fig. 2). Ultimate recovery at Roland SE is projected to be 444,000 BO, with the average well producing 44,000 BO.

The Arbuckle dolomite is an excellent reservoir at Roland SE field, as illustrated by 6 ft of Arbuckle core from the House #3–36. Measured porosities average 23.7% while the average permeability is 1,540.7 millidarcies.

Regional Geology

In Rush County, oil is trapped within closed structures along the irregular Arbuckle subcrop, a major angular unconformity (fig. 3). Rush County is located on the western flank of the Central Kansas uplift. The uplift comprises several anticlines or horsts that were created by uplift of Precambrian basement granites and quartzites during late Mississippian time.

Rush Rib is the local northwest-southeast-trending structure that sets up the Arbuckle play in Rush County. Arbuckle beds are truncated and overlain by Pennsylvanian rocks along each flank. Arbuckle rocks are absent on the crest of the rib, where Precambrian basement rocks are in direct contact with Pennsylvanian strata (fig. 3).

During pre-Pennsylvanian time the uplifted rib was subject to extensive karstification. The karst topography resulted in a series of paleotopographic closed structures that are the main target for oil exploration.

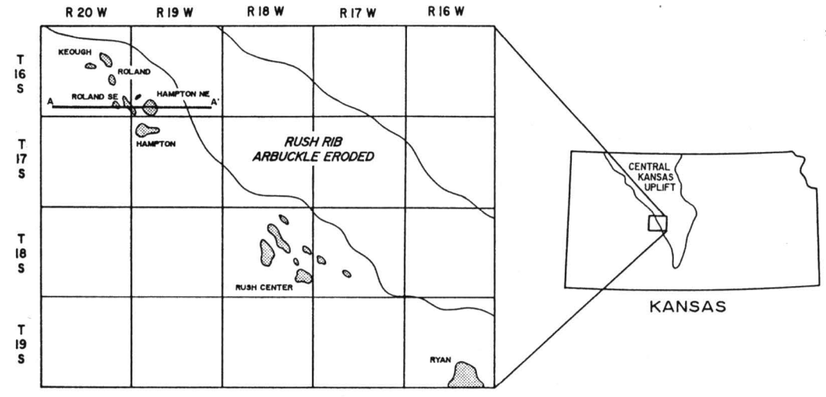

FIGURE 1—RUSH COUNTY ARBUCKLE PRODUCTION.

These ancient hills are pitted with various sized sinkholes and bisected by larger sink valleys. Deposition of the overlying Pennsylvanian Cherokee Group followed. The Cherokee is a conglomerate of varicolored shales and chert that filled in the sink features and provide the impermeable cap rock for the Arbuckle reservoirs.

Due to differential compaction, Pennsylvanian and Permian beds are structurally closed across paleotopographic Arbuckle highs (fig. 3). Most of this compaction-related structure occurs within the Marmaton and Cherokee intervals. However, sizable Arbuckle hills affect strata as high as the Permian Stone Corral anhydrite. Many Pennsylvanian Lansing–Kansas City reservoirs owe their structure to this compaction process. Larger Arbuckle structures are identifiable as thins with isopach mapping of the Stone Corral anhydrite to the Marmaton interval (fig. 3).

Prospect Geology

Production at Roland SE was initiated upon the completion of the Rock Island Oil and Refining Company #5 Littler well (SE SW NW sec. 31, T. 16 S., R. 19 W.). Subsequent unsuccessful tests to the north and west seemed to indicate that the well was associated with production at Hampton NE field. An Arbuckle structure was inferred just west of the Littler #5 well (fig. 4). The prospect was supported by the presence of two nearby show wells, the Littler #7 (NW SW NW sec. 31, T. 16 S., R. 19 W.) and the #1 Littler "B" (NE NE SE sec. 36, T. 16 S., R. 20 W.), both of which recovered free oil from drill-stem tests within the Arbuckle (fig. 2).

In March of 1988, Balcron Oil drilled the #1–36 Baldwin (NW SE NE sec. 36, T. 16 S., R. 20 W.). Although the Arbuckle was structurally low and nonproductive, pay was established within the Lansing. No shows were encountered in the Arbuckle, but a nearby structure seemed likely based on presence of closure at the Lansing horizon.

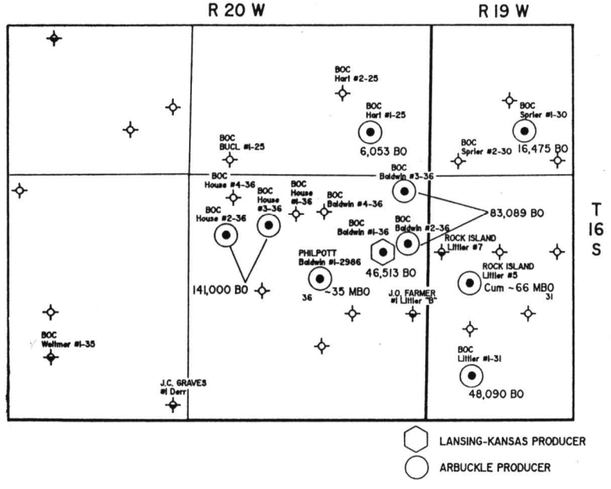

FIGURE 2—PRODUCTION MAP, ESTIMATED ULTIMATE RECOVERIES.

Subsequent drilling of the #2–36 Baldwin, just east of the #1-36 Baldwin, resulted in the discovery of additional Arbuckle production at Roland SE.

Figure 5 represents the updated version of the Arbuckle structure. Roland SE, as interpreted, comprises three separate structural reservoirs created by the very irregular Arbuckle paleotopography. Although the three distinct pools are structurally separated, they share a common oil-water contact at -1,774 ft.

The isopach map of the Stone Corral anhydrite–Marmaton interval (fig. 6) illustrates a general thin, due to compaction, across the Roland SE feature. The isopach thin corroborates with the deeper Arbuckle structure, but fails to identify the dissected Arbuckle horizon. In retrospect, the anhydrite–Marmaton isopach appears to be a very useful tool for exploration, both geologically and seismically, but has limited use when determining development locations.

Cross section B–B′ (fig. 7) shows the off-structure thickening in the Cherokee conglomerate that has filled in the Arbuckle low. An inverse relationship is seen

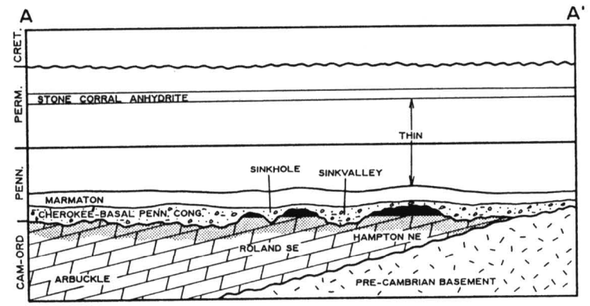

FIGURE 3—CROSS SECTION A–A'; NOT TO SCALE.

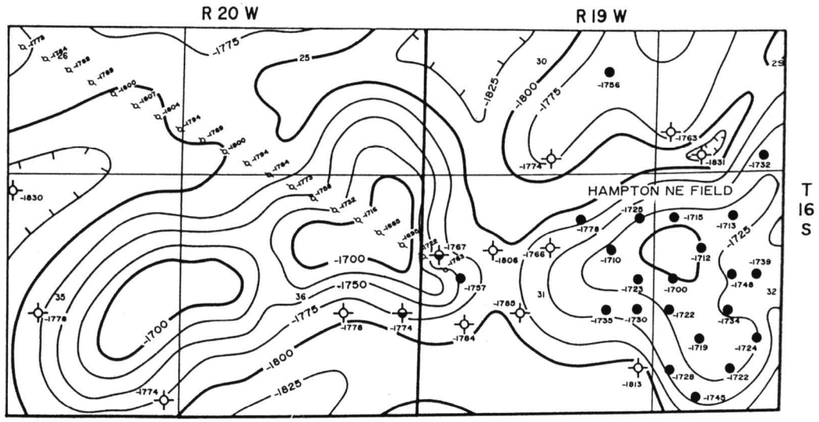

FIGURE 4—PRE-DISCOVERY ARBUCKLE STRUCTURE, MAY 1988; contour interval = 25 ft (7.6 m).

between the Cherokee thickness and the anhydrite–Marmaton isopach values of the two Baldwin wells. This is attributed to the amount of chert in the conglomerate. The author's experience has been that, in many cases, Arbuckle sinkholes are filled with chert-rich conglomerates that are less susceptible to compaction. In this manner, local Arbuckle lows can be masked within a relatively larger Arbuckle structure.

Geophysical Overview

After the Baldwin #1–36 wildcat was drilled, the decision was made to use more detailed CDP seismic control to position wells. Seismic data were acquired in three phases and resulted in an irregular seismic grid that covered nearly every selected drill site. All data are 15-fold and were acquired using a Vibroseis source and 60-channel recording equipment. Vibrator source points were spaced at 165 ft (50 m) with geophone groups at 82.5 ft (25 m). Data were shot using a symmetrical split spread with a maximum spread length of 2,640 ft (805 m). Vibrator sweeps ranged from 14 to 96 Hz over 12 secs.

Seismic-record quality is generally excellent in the area. Several strong seismic horizons exist, allowing the seismic data to be confidently tied to sonic log synthetic seismograms. Figure 8 shows Line HW–1 correlated to the synthetic seismogram from the Baldwin #1-36 well. The strong reflectors are the Stone Corral Anhydrite, Topeka Limestone, base Kansas City, and Marmaton. The Lansing and Arbuckle horizons are generally seismically mappable but are manifested as much weaker reflections.

Resolution of the Arbuckle reflection is dependent on the Cherokee being sufficiently thick to allow visual separation from the higher amplitude Marmaton reflector. Figure 9 illustrates the effect of Cherokee thickness on Arbuckle resolution and the amplitude of the Cherokee "peak" (on reverse polarity data). Intervals thicker than 45 ft (13 m) show complete resolution with no interference between the Marmaton and the Arbuckle. Partial resolution occurs between 45 ft and 10 ft (13 m and 3 m) where the Arbuckle trough does not track the horizon top exactly but the Cherokee peak shows diminishing amplitude.

An additional limitation to the resolution of Arbuckle and Cherokee horizons occurs at those sites where the sinkhole width is narrow. The Fresnel zone, which contributes to a reflection, calculates to approximately 700 ft (213 m) for depths at Roland SE. For sinkholes less than 700 ft (213 m) wide, interference from the adjacent terrain prevents the observed seismic character from matching the character modeled from sonic logs.

Mapping Methods

Primary mapping methods include isochron maps for the anhydrite to Marmaton and the anhydrite to Arbuckle intervals, and seismic-character analysis for the Cherokee "peak." Isochron maps are preferred rather than time-structure maps in order to avoid artificial highs created from near-surface velocity changes. Exaggerated seismic profiles of interpreted horizons are used to provide a convenient display of subtle isochron thinning.

The Stone Corral anhydrite–Arbuckle isochron map (fig. 10) is believed to be the most reasonable proxy for Arbuckle structure, though it is limited in areas where the Cherokee is thin. The map identifies three closed thin trends which correspond to the producing structures. Each is approximately 0.005 secs thinner than the closest dry hole and 0.010 secs thinner than adjacent lows.

Since the Arbuckle reflection is not entirely reliable in resolving Arbuckle structure where the Cherokee is thin, the Stone Corral anhydrite–Marmaton isochron map (fig. 11) is created as a check on the Arbuckle interpretation. Though this interval in fig. 11 shows considerably less thinning than the anhydrite–Arbuckle map (fig. 10), the reflection strength of the Marmaton allows for more confidence in the data. The closed thins bounded by the 0.385 contour generally coincide with the producing area, but do not define the flanks of the structures as clearly. Relief measures 0.003 secs or less above edge wells, and 0.005 secs above adjacent lows.

Development History

Because the Baldwin #1–36 appeared to be a near miss in the Arbuckle reservoir, Line HW-1 was acquired to look for a nearby location that would be structurally higher at the Arbuckle. After correlating the seismic data to the well log synthetic, it was apparent that a better location was present only 600 ft (183 m) to the east where the Arbuckle event gained 6 msecs of time-structure relief. Additional positive indicators included 2 msecs of thinning in the anhydrite–Marmaton interval and a slight decrease in amplitude of the Cherokee peak. The ensuing Baldwin #2-36 was the Arbuckle discovery well, 30 ft (9.1 m) higher at the Arbuckle level and 39 ft (11.9 m) thinner in the Cherokee relative to #1–36.

After the Baldwin #2–36 success, the seismic criteria for selecting drill sites were established and an additional grid of seismic data was acquired. Line HW–4 best characterizes the field because seven wells were drilled on or close to the line. Figure 11

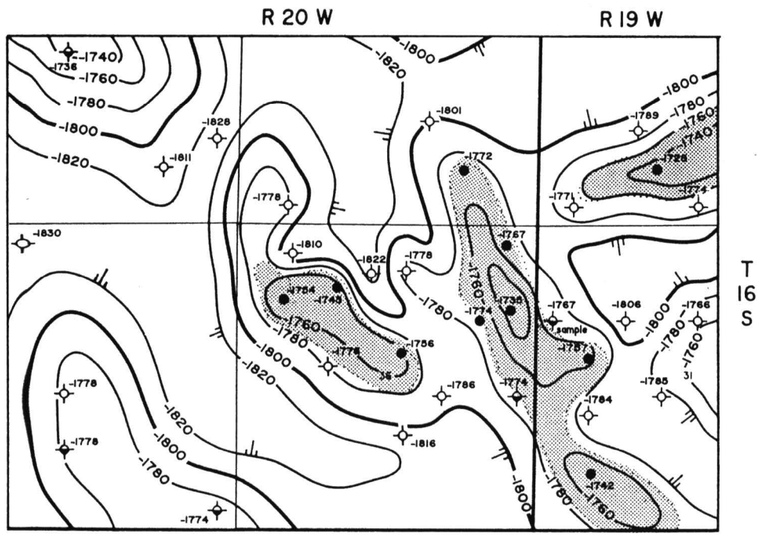

FIGURE 5—ARBUCKLE STRUCTURE; contour interval = 20 ft.

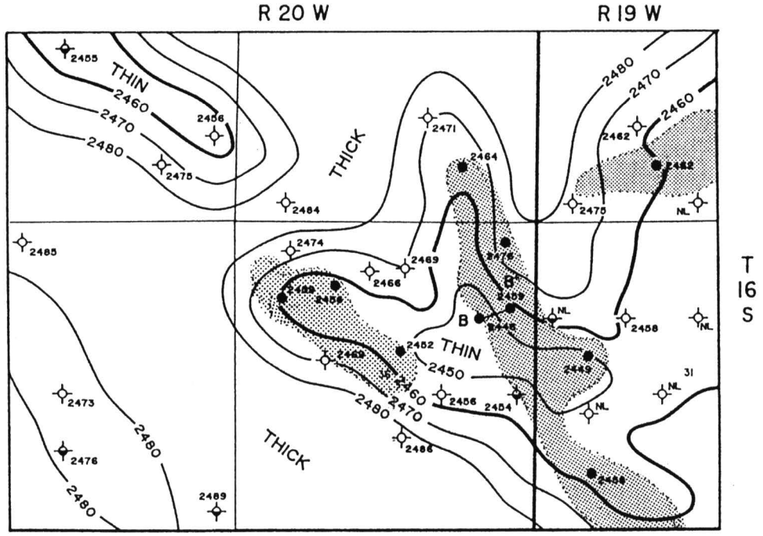

FIGURE 6—ISOPACH MAP, STONE CORRAL–MARMATON; contour interval = 10 ft.

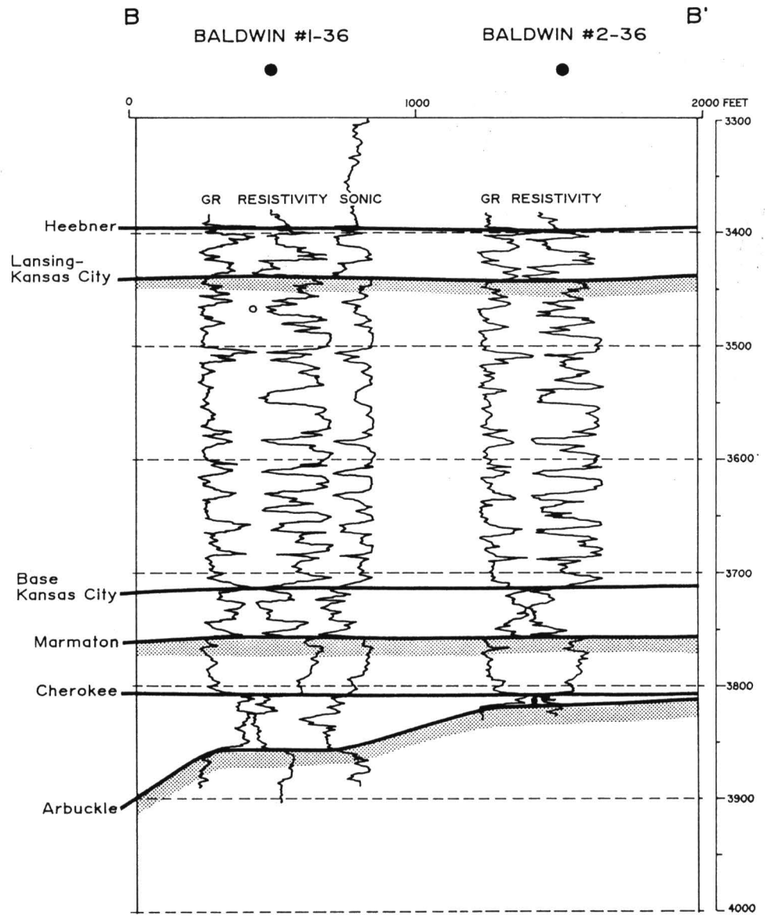

FIGURE 7—TYPE LOG CROSS SECTION.

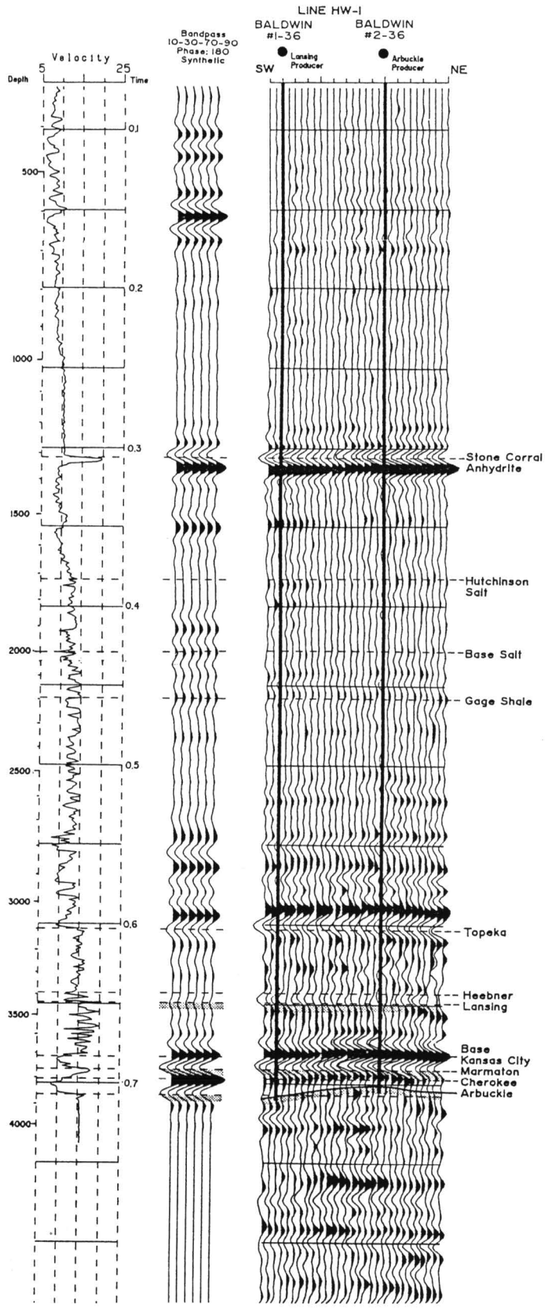

FIGURE 8—LINE HW-I CORRELATED TO THE BALDWIN #1–36 SYNTHETIC SEISMOGRAM (REVERSE POLARITY).

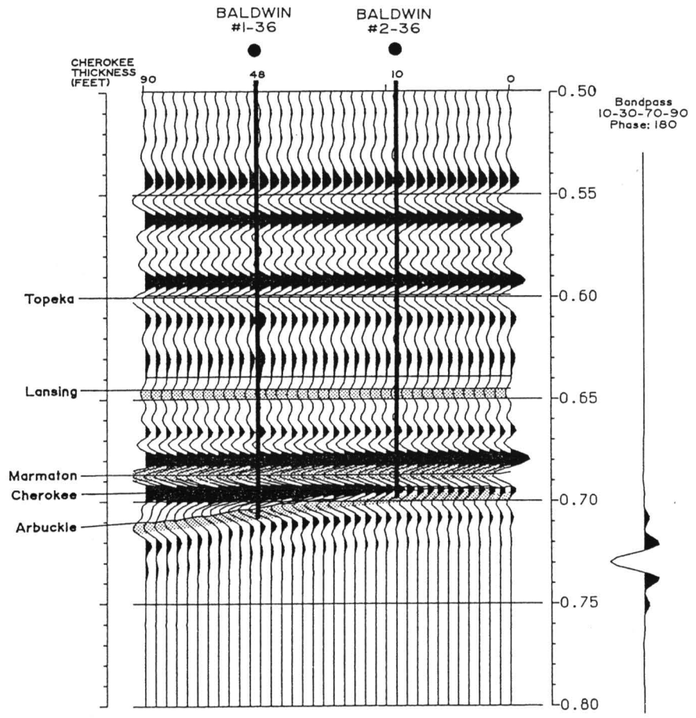

FIGURE 9—SEISMIC MODEL WITH VARYING CHEROKEE THICKNESS.

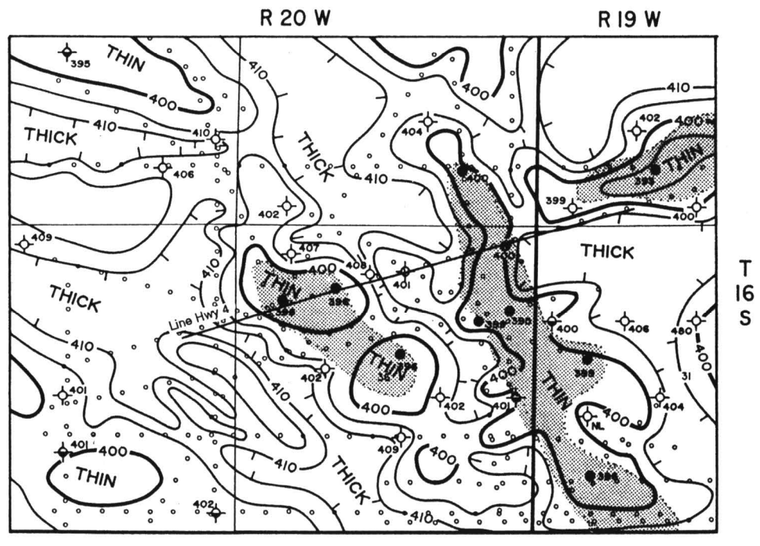

FIGURE 10—ISOCHRON MAP, STONE CORRAL ANHYDRITE–ARBUCKLE; contour interval = 5 msec, interval velocity = 6.35 ft/msec.

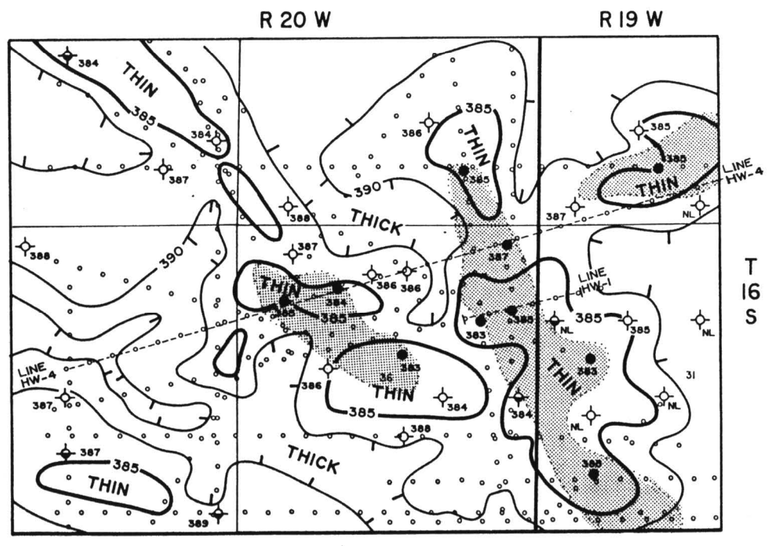

FIGURE 11–ISOCHRON MAP, STONE CORRAL ANHYDRITE–MARMATON; contour interval = 5 msec, interval velocity = 6.4 ft/msec.

shows this line and a vertically exaggerated display of the interpretation to illustrate interval thinning across the line. The western half of Line HW–4 clearly exhibits all of the seismic characteristics established by the Baldwin case history and seismic modeling. The interpreted time section shows that the producing House #2–36 and #3–36 are located on Marmaton and Arbuckle thins. Additionally, the Cherokee peak is significantly lower amplitude at the House wells than the area to the southwest.

The first development location drilled was the House #1–36, chosen because the Cherokee peak dims to near zero amplitude and the anhydrite–Arbuckle interval mapped as the thinnest location in the field. Although this location looked extremely safe based on seismic character, the well ran extremely low in the Arbuckle and encountered 80 ft of the Cherokee. The predominance of chert in the Cherokee indicated that a sinkhole was encountered rather than a regional Arbuckle low. A re-evaluation of the seismic line determined that the sinkhole was approximately 400 ft (122 m) wide and that good locations existed to the west. The apparent seismic character for the sinkhole is only a few traces wide and is substantially different from the character over the rest of the structure.

The House #2–36 was the second development well drilled, and 18 ft (5.5 m) of Cherokee was encountered over a productive Arbuckle structure. Similarity of the seismic character and interval thinning prompted drilling of the House #3-36 producer. This well was drilled only 580 ft (177 m) from the House #1-36 and ran 77 ft (23.5 m) higher on the Arbuckle structure. The area east of the sinkhole was tested by the Baldwin #4-36. The Baldwin #4-36 ran 44 ft (13.4 m) high relative to the House #1-36, but was not high enough to produce.

Regional thinning of the Cherokee to the east of the Baldwin #4-36 results in poor resolution of the Arbuckle reflection at the Spreier locations in sec. 30. The #2-30 has only 8 ft (2.4 m) of Cherokee, yet is too low to produce in the Arbuckle. Since the Arbuckle reflection is unresolvable in sec. 30, the anhydrite–Marmaton isochron is the only useful seismic map in this area.

The development experience at Roland SE showed that seismic imaging of the dissected Arbuckle structure was reasonably successful. Limitations include the

sinkholes which are narrower than a Fresnel zone and mapping edge locations where the relief is only 1–3 msecs over nearby dry holes. Although Balcron Oil's development success rate was only 50% using the seismic method, none of the seven Arbuckle wells would likely have been drilled without acquiring the CDP seismic grid. The seismic dollars spent on the project total $120,000 for 30.4 mi (48.9 km) of data. This represents $0.41/bbl for the 294,000 bbls of estimated Arbuckle reserves. The total drilling and seismic cost per barrel is $3.74.

Conclusions

Roland SE field is a cluster of three structurally trapped Arbuckle reservoirs. The structural configuration is largely formed by remnant paleotopographic features on a karsted erosional surface including narrow sinkholes, wider erosional valleys, and intervening highs with relatively flat tops and sharp, irregular edges. The remnant topography was filled with the deposition of the Cherokee red shales and chert conglomerates, which provided a seal for the underlying porous carbonates. Differential compaction of the shales with burial resulted in isopach thins overlying Arbuckle highs. The seismic expression of the Arbuckle highs are a lower amplitude Cherokee reflection and isochron thins in the Stone Corral anhydrite–Marmaton and Stone Corral anhydrite–Arbuckle intervals. Since the structures are narrow and highly irregular, a detailed seismic grid was cost effective in minimizing dryholes and recognizing drill sites. After drilling an unsuccessful Arbuckle wildcat, the CDP seismic method allowed Balcron Oil to find seven Arbuckle wells not likely to have been discovered otherwise.

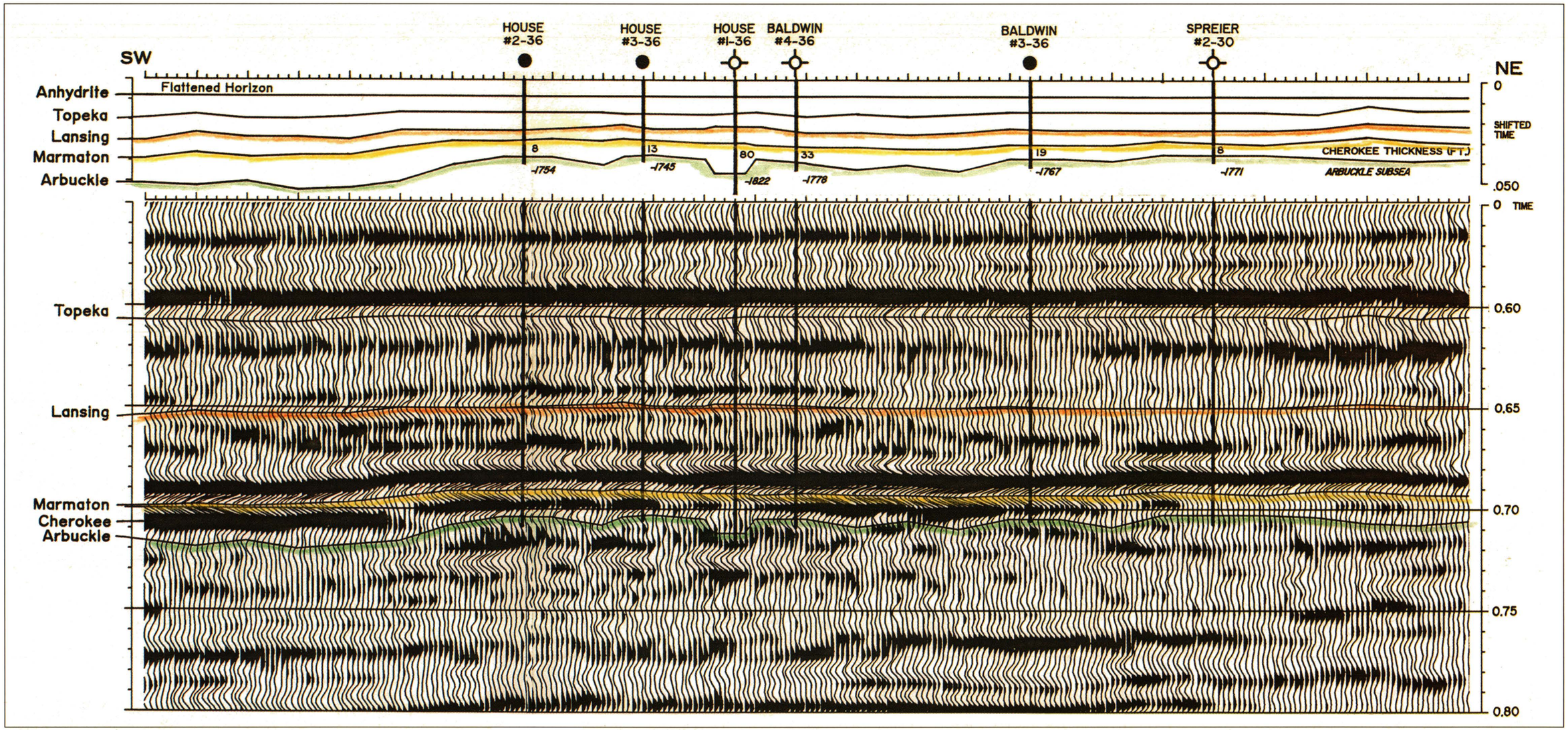

FIGURE 12—LINE HW–4 AND INTERPRETED TIME SECTION (flattened on anhydrite).

Seismic Expression of a Subtle Stratigraphic Trap, Lexington Field, Clark County, Kansas

Larry J. Richardson[1] and Dennis E. Hedke[2]
[1]Pickrell Drilling Co., Inc., Wichita, KS 67202; and
[2]Consultant, Wichita, KS 67202

Abstract

Lexington field is located in northeastern Clark County, Kansas, principally in secs. 19 and 20, T. 31 S., R. 21 W. Geologically, the field is situated on the northeastern shelf of the Hugoton embayment of the Anadarko basin, near the eastern limit of Morrowan Stage deposition. The field has yielded over 4 million bbls of oil and about 4 BCF gas from combined Morrow and Mississippian reservoirs. Fluvial sandstones within the Morrow section are responsible for over 96% of the oil and about 75% of the gas produced from the field.

Productive Morrow sandstones within the field were deposited in a deeply incised fluvial channel. The Morrow trap is stratigraphic with reservoir sandstones being effectively encased in impermeable shales. Mississippian production, in contrast, is primarily related to the development of highly fossiliferous zones which have reservoir-quality porosity over a limited area. This anomalous porosity is erosionally absent in the productive Morrow channel region. Productive Mississippian wells are situated on both sides of the channel.

The discovery well in the field was drilled on a structural high with the Mississippian and Ordovician as potential reservoir targets. Morrow reserves were fortuitously encountered during field development.

The seismic expression of the channel environment is somewhat subtle. After-the-fact modeling is of assistance in characterizing the Morrow–Mississippian interface. Conventional data evaluation, coupled with trace-attribute analysis, has resulted in a fairly comprehensive understanding of this complex subsurface system.

Introduction

The Lexington field discovery by Mesa Petroleum in 1977 (discovery well: Mesa 1–19 Seacat, SW SE sec. 19, T. 31 S., R. 21 W.) did not receive excessive industry attention (figs. 1 and 2). The initial Mississippian production of 94 BOPD and 603 MCFGPD were good numbers for probable commercial production, but not overly so. However, the December 1978 Morrowan "re-discovery" with flowing potential of 984 BOPD and 374 MCFGPD rekindled a heated exploration play which had already resulted in significant Morrow production at Harper Ranch and other proximal fields. Final field extents and a production index map are provided in fig. 3.

An excellent paper by Emery and Sutterlin (1986) provides insight regarding depositional environments in the Morrowan section. Included in that paper are numerous subsurface maps and discussion related to the structural and depositional history of the Lexington area. Additional reservoir insights and production data are given by Wilkins (1985). Related research pertaining to regional Morrowan deposition is given by Swanson (1979).

The major focus in this paper is the reexamination of the subsurface work in light of all released well data and available seismic control. Our efforts are concentrated on Morrowan stratigraphy and seismic expression. The seismic profile incorporated in this paper crosses a "typical" estuarine channel sandstone reservoir. The exact location of the seismic profile made available for the study is not shown in order to preserve the proprietary integrity to the current data owners (Samson Resources, Tulsa, Oklahoma).

Geological Maps/Cross Section

The estuarine channel into which the Morrow reservoir sandstones at Lexington field were deposited is the product of regional uplift which either precipitated or substantially enhanced the erosional intensity at the Mississippian unconformity. Relief on the unconformable surface has been defined by drilling to be as much as 150 ft (45 m) over a distance of 1/4 mi (1/2 km) (fig. 4), indicating a dip rate of about 600 ft/mi (114 m/km), or about a 6.5° incline from channel "bluff" to channel "bottom." Long, narrow channel segments and abrupt local offsets in the Mississippian incisement reasonably suggest fault control.

A variety of sediments have filled in the postulated estuarine environment. According to Emery and Sutterlin (1986), four subfacies of the productive Morrow sandstone are recognized:

1) supratidal
2) intertidal
3) channel bank
4) tidal channel.

The gross stratigraphic interval attributable to the Morrow section (base Inola-top Mississippian) ranges from a minimum of about 6 ft (1.8 m) on unscoured Mississippian ridges to a maximum of about 117 ft (35 m) near the depocenter of the channel. The map configuration of the Morrow interval is an inverse image of the Mississippian surface (fig. 5).

Encased within this interval, sandstones of variable lateral extent and thickness occur. The maximum sandstone thickness attained is about 40 ft (12 m) (fig. 6).

At the base Inola (top Morrow shale) marker, structure is greatly subdued owing to the relatively level channel infilling (fig. 7). Some evidence of differential compaction of shale and sandstone material is suggested within the channel. At Lansing time (map not shown), little more than a nominal re-entrant of contours gives a hint of the structural sag over the channel.

Structural log profile A–A´ shows the morphology and infilling of the channel (fig. 8). The productive channel well in this cross section is the original Morrow "rediscovery." Note that at the west end of the cross section, the well with the highest Mississippian datum is not productive in any zone. Apparently, porosity/permeability are the predominant controls for Mississippian production.

Synthetic Modeling

After the fact modeling was accomplished by digitizing sonic log data from a well which is representative of conditions in the vicinity of the seismic profile. A full-length synthetic seismogram for this well is given with horizon picks on fig. 9. This seismogram was generated using parameters designed to match the data as originally acquired: sample rate of 4 msec, frequency bandwidth 17–56 Hz.

An additional seismogram segment highlighting particularly the section from Cherokee through Mississippian was generated with sonic and density data, with identical filter and parameters as the full-length seismogram and is used as a basis for the simplified 44-trace model (fig. 10). The model illustrates in graphic detail the synthetic seismic response predicted when the scoured Mississippian surface has been filled with a maximum of 106 ft (32 m) of Morrow sediments. Model traces on the extreme left and right represent the reflection sequence predicted when only a thin veneer (8 ft, 2.4 m) of

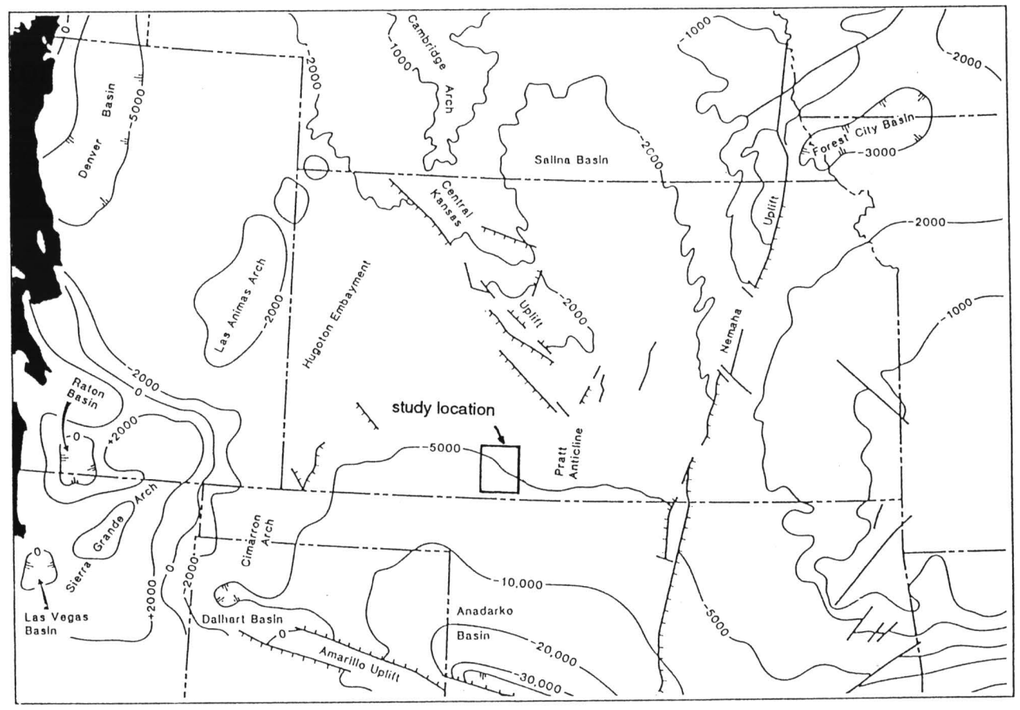

FIGURE 1—Regional location map showing project proximity to geologic provinces.

Morrow rests on the Mississippian. Upon comparing the model to actual processed results, one can see encouraging agreement and some moderate departures from actual data. One possible explanation for some of these deviations may be related to amplitude variation with offset (AVO) effects. The synthetic model was developed on the basis of "zero offset" conditions. The maximum offset utilized in processing this dataset was 5,720 ft (1,716 m).

Whatever the case for relative deviations from theoretical models, this simplified model demonstrates our improving ability to extract challenging anomalies from such a dataset. Bear in mind also that modern data acquisition has a minimum 2-msec base sample rate as compared to the 4-msec rate of these data.

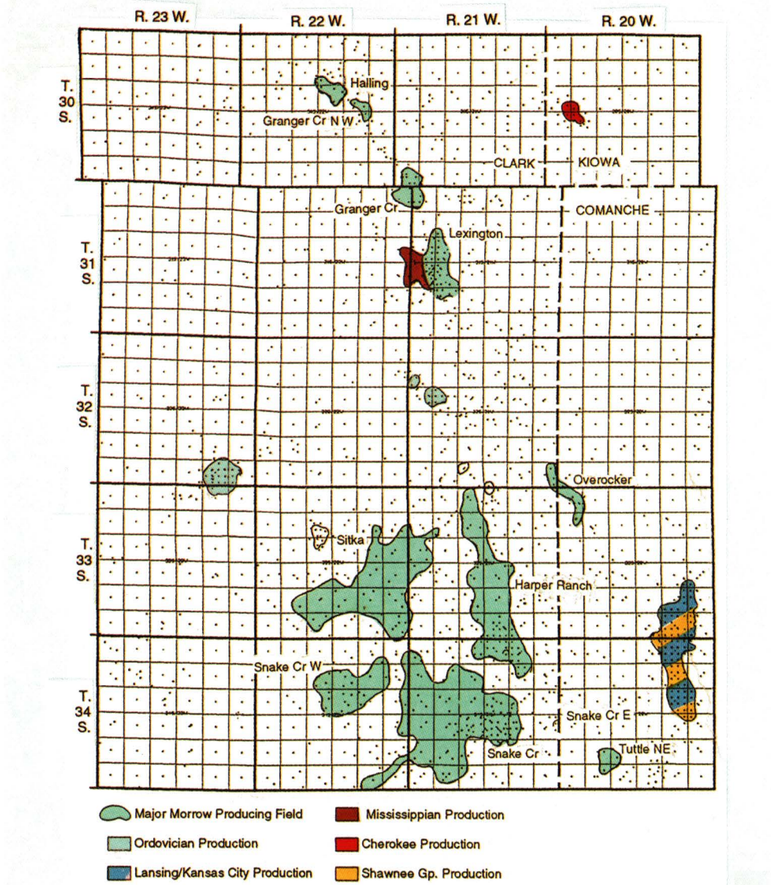

FIGURE 2—PRODUCTION INDEX MAP, HIGHLIGHTING MORROW PRODUCTION.

Seismic Profiles

Representative uninterpreted and interpreted stacked seismic sections presented in figs. 11 and 12, respectively, illustrate the seismic signature of the Morrow channel sandstones at Lexington field. As mentioned previously, proprietary constraints prevent revealing the exact line location. The west end of the profile is left. Polarity of the data is normal. Several select wells have been judiciously tied to the seismic profile.

By today's standard, the data were acquired using a relatively low-frequency input pilot of 17–56 Hz. In spite of this limitation, the seismic stratigraphic signature of the channel anomaly, while subtle at first look, becomes more discernible with successive passes of data analysis. Evidence corroborating the anomaly occurs as follows:

A) Over the range of shotpoints 142–115, a higher amplitude peak develops at the base of Morrow/top of Mississippian interface. This effect is noticeable on conventional profiles at about 1,025 msec. Notice that the Morrow/Mississippian interface is seismically very dim outside the channel zone.

B) Instantaneous frequency content of the dataset (fig. 13) demonstrates significant contrast in the channel zone. Lower frequency sediments occur as green and yellow immediately below the Morrow shale event. Notice that the theoretical response of the top Morrow in the channel suggests a moderate amplitude event should appear immediately above the Morrow shale. Real data show this condition to be only weakly and intermittently developed. The high

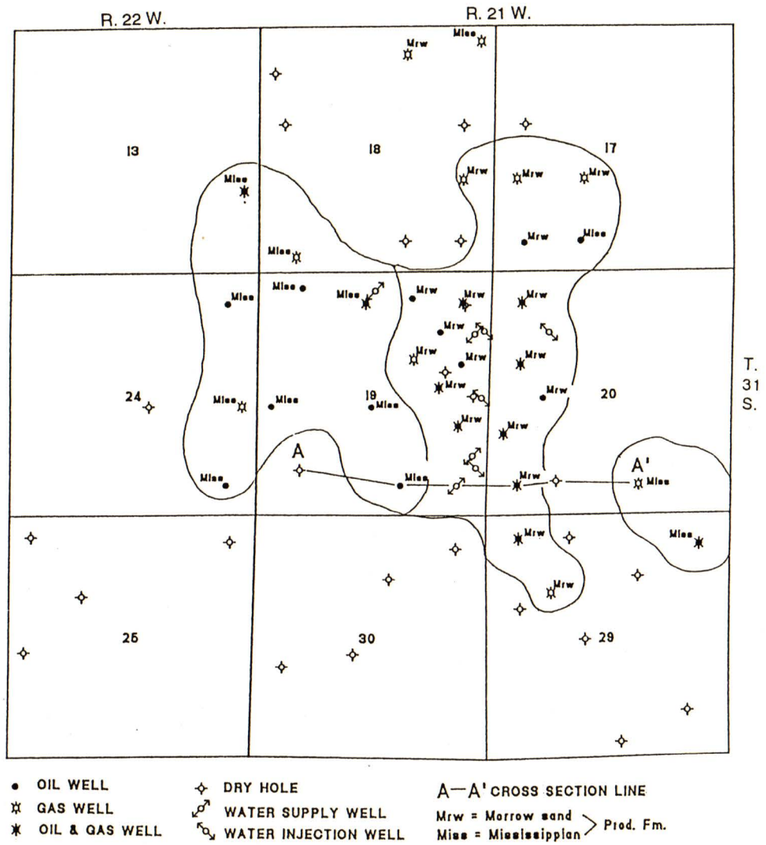

FIGURE 3—LEXINGTON FIELD EXTENTS AND LOCAL PRODUCTION INDEX, contour interval = 20 ft (6 m).

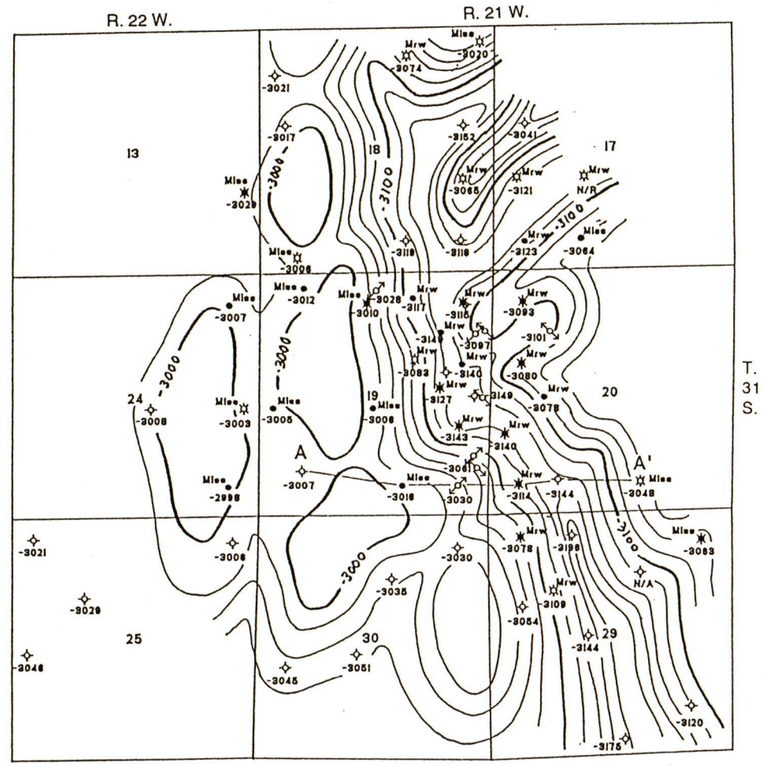

FIGURE 4—GEOLOGIC STRUCTURE, TOP MISSISSIPPIAN, contour interval = 20 ft (6 m).

amplitude zone occurring at the top of the model is equivalent to the event just below the Stark shale on the actual data.

C) The attribute of instantaneous phase is shown in fig. 14. Notice that Morrow channel sediments occur predominantly as blue and green colored, in contrast to the largely yellow-green materials outside the channel environment.

As a final note concerning overall seismic response, note that the Viola event, occurring at about 1,130 msec, largely parallels the Mississippian surface, whereas Morrow and younger sediments show some sense of draping over channel infilling.

Summary/Discussion

Data provided for review and examination in this study are valuable for several reasons: 1) the structural content of the reprocessed data holds a high level of integrity against actual well ties; 2) the stratigraphic content, while lacking modern resolution, is still of considerable value in relating to actual geology; and 3) calculation of instanta-

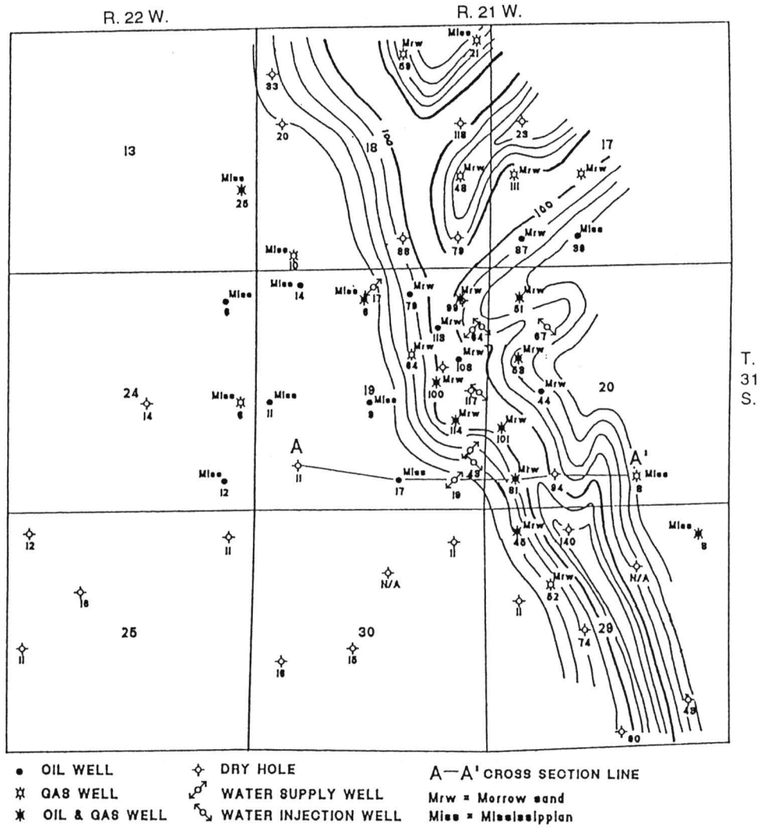

FIGURE 5—ISOPACH MAP, BASE INOLA TO TOP MISSISSIPPIAN, contour interval = 20 ft (6 m).

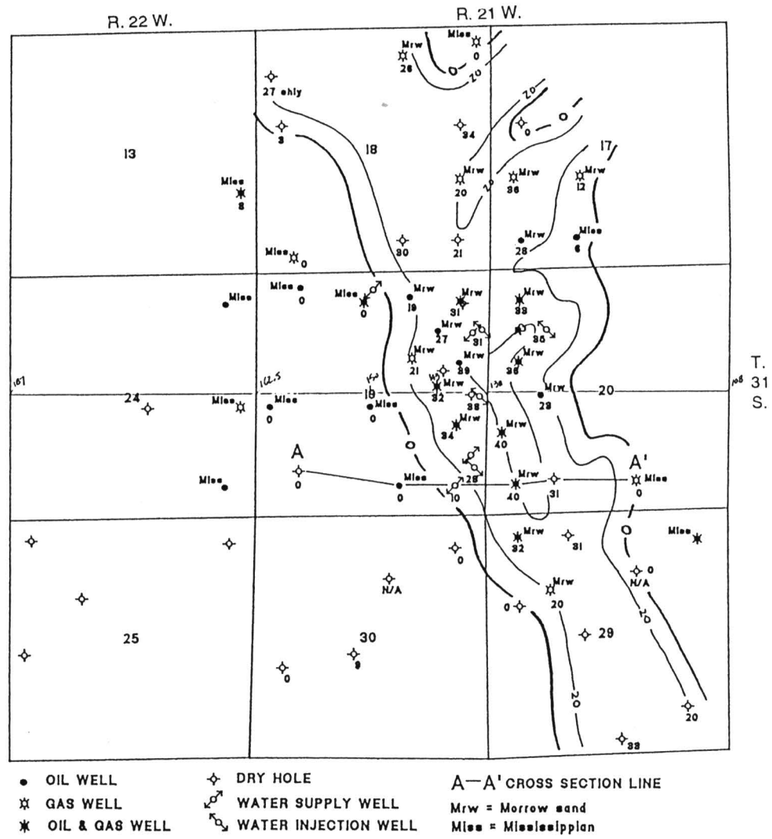

FIGURE 6—ISOPACH MAP, MORROW SAND, contour interval = 20 ft (6 m).

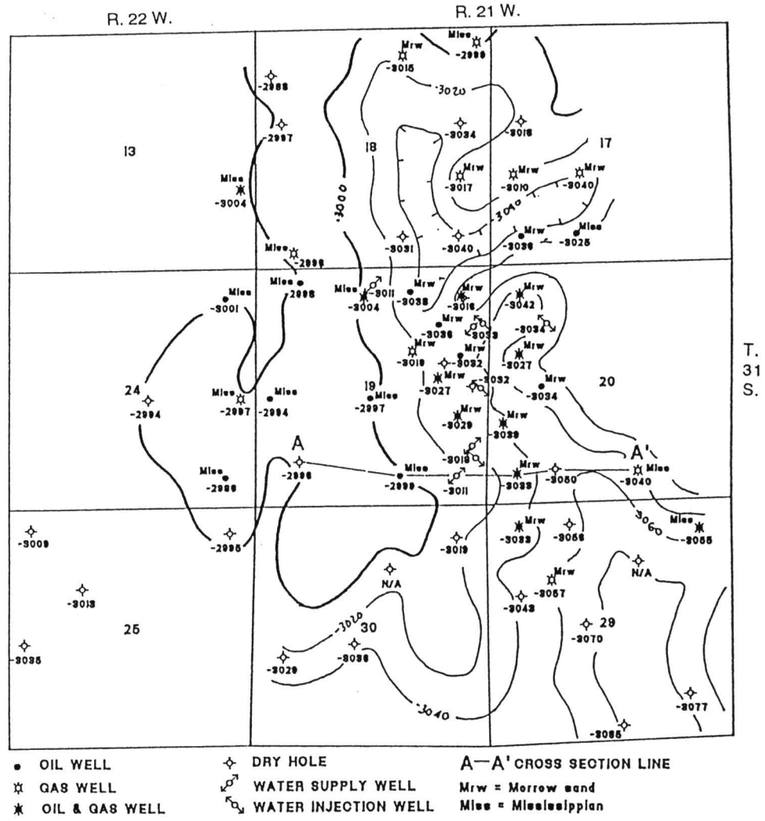

FIGURE 7—GEOLOGIC STRUCTURE, BASE INOLA (TOP MORROW), contour interval = 20 ft (6 m).

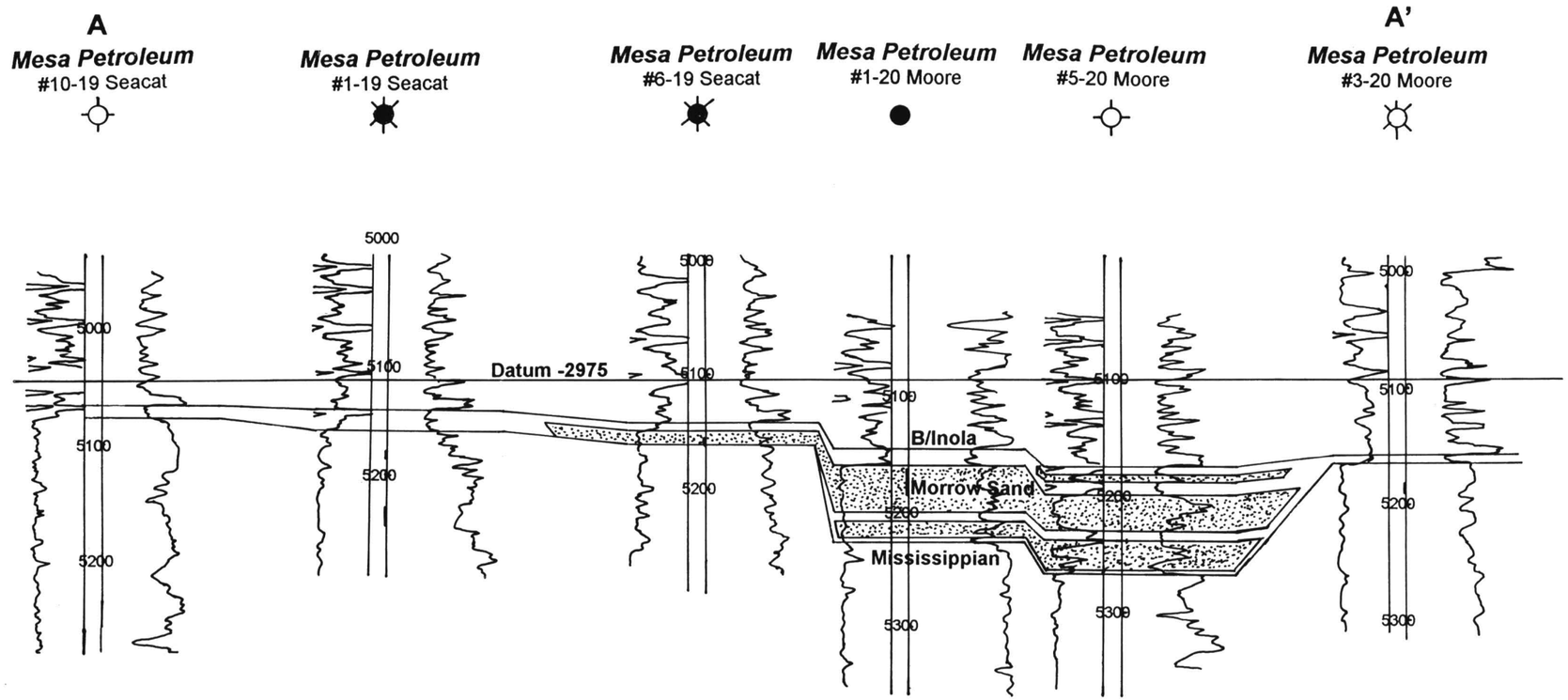

FIGURE 8—Structural log cross section A-A′.

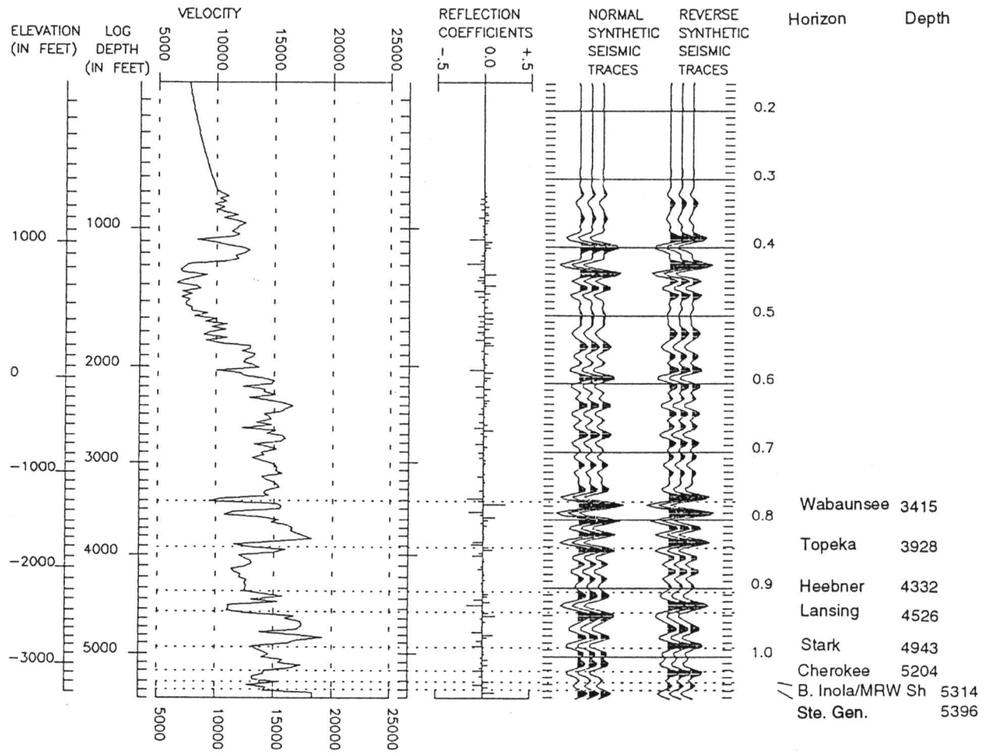

FIGURE 9—SYNTHETIC SEISMOGRAM, Mesa Petroleum Moore 1–20, SW SW sec. 20, T. 31 S., R. 21 W. Filtered at 14–17/50–56 Hz.

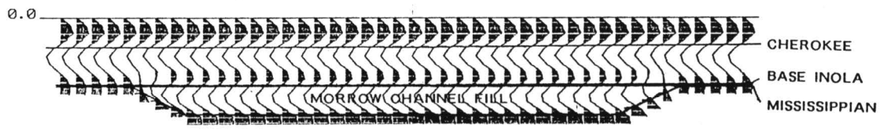

FIGURE 10—TWO-DIMENSIONAL MODEL DERIVED FROM SONIC AND DENSITY LOGS, Mesa Petroleum Seacat 7–19, 1,900 ft (570 m) FSL and 510 ft (153 m) FEL, sec. 19, T. 31 S., R. 21 W. Maximum channel thickness = 106 ft (31 m); Morrow thickness outside channel = 8 ft (2.4 m).

neous attributes also yields encouraging agreement to known anomalies.

ACKNOWLEDGMENTS—The writers greatly appreciate the initial contribution and approval for data release by Mesa Petroleum, Amarillo, Texas. Later contribution of actual field tapes for reprocessing and workstation evaluation was approved by current data owners, Samson Resources, Tulsa, Oklahoma. Reprocessing was provided by Production Geophysical Services (PGS), Englewood, Colorado.

References

Emery, M., and Sutterlin, P. G., 1986, Characterization of a Morrowan sandstone reservoir, Lexington field, Clark County, Kansas: Shale Shaker, Oklahoma City Geological Society, v. 37, no. 2, p. 18–33 (also appears in the American Association of Petroleum Geologists, Treatise of Petroleum Geology, Atlas of Oil and Gas Fields, Stratigraphic Traps II)

Swanson, D. C., 1979, Deltaic deposits in the Pennsylvanian upper Morrow formation of the Anadarko basin; *in*, Pennsylvanian Sandstones of the Midcontinent, N. J. Hyne, ed.: Tulsa Geological Society, Special Publication No. 1, p. 115–168

Wilkins, G. C., 1985, Lexington field; *in*, Kansas Oil and Gas Fields, P. G. Gerlach and T. Hansen, eds.: Kansas Geological Society, v. V, p. 159–166

Appendix

Acquisition and Processing Parameters

Acquisition (Western Geophysical, June 1977)

Source:	Vibroseis, four vibrators times 16 sweeps
Pilot:	17–56 Hz, 7 sec
Sample rate:	4 msec
VP interval:	220 ft (66 m)
Group interval:	220 ft (66 m)
Seismometers/group:	36
Spread:	Split
Near offset:	660 ft (198 m)
Maximum offset:	5,720 ft (1,716 m)
Filters:	out/out
Instruments:	DFS–3
No. channels:	48
Nominal fold:	24

Processing (Production Geophysical Services, January 1992)

- Trace edit
- Spherical divergence correction using area velocity function
- Refraction statics using Green Mountain method
- Surface consistent deconvolution: shot/receiver/offset 160 msec operator length
- Zero phase whitening 17–60 Hz
- Geometry statics update: refraction + datum statics
- Velocity analysis: three passes every 50 CDPs
- Surface consistent statics: window 250–1,050 msec
- Inverse spherical divergence using area velocity function
- Model-based spherical divergence using final velocities
- CDP consistent statics: window 450–1,400 msec, 7-sec maximum
- Stack: root N compensation
- Zero-phase whitening 17–60 Hz
- Post-stack filter 18/72–55/120 Hz/dB
- Scale: Gain -3 dB

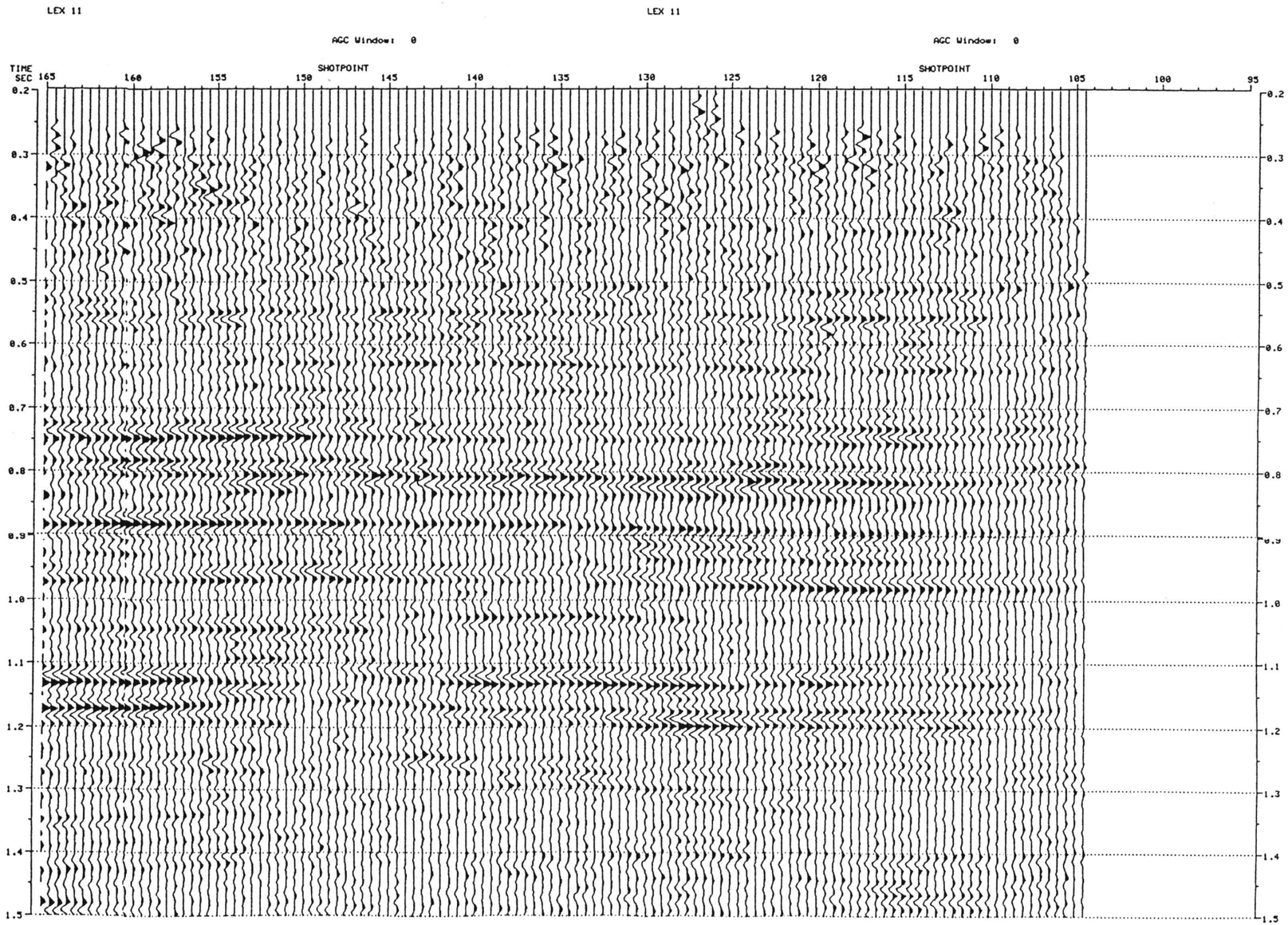

FIGURE 11—Representative seismic profile from study area. Group interval = shot interval = 220 ft (66 m). Nominal 24 fold. Datum = 2,900; velocity = 10,000 ft/sec.

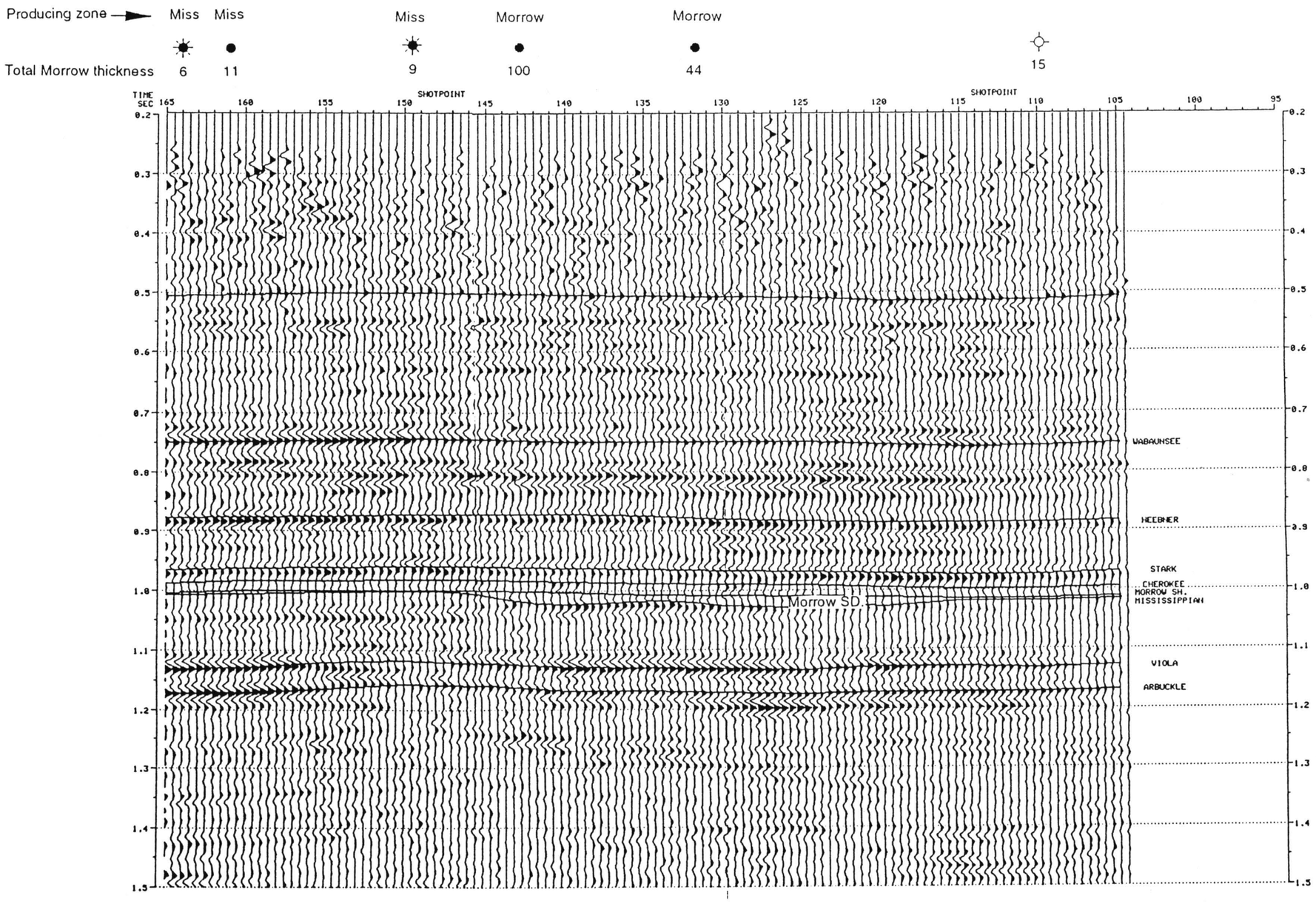

FIGURE 12—ANNOTATED CONVENTIONAL STACKED PROFILE. Note amplitude buildup at approximately 1,025 msec, between stations 145–115.

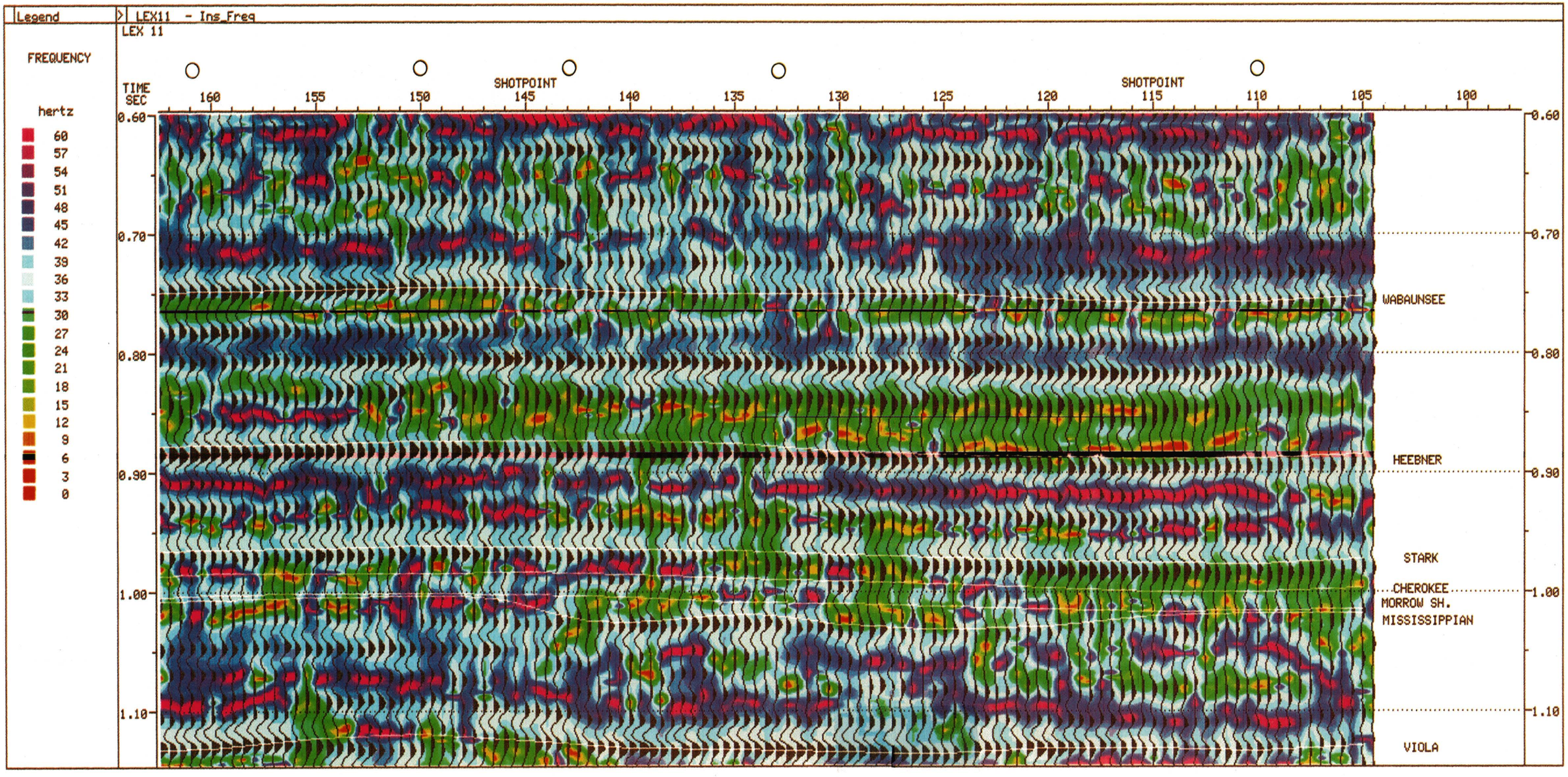

FIGURE 13—Instantaneous frequency display of previous conventional stacked data; note frequency anomalies especially between stations 142–135 and 130–124.

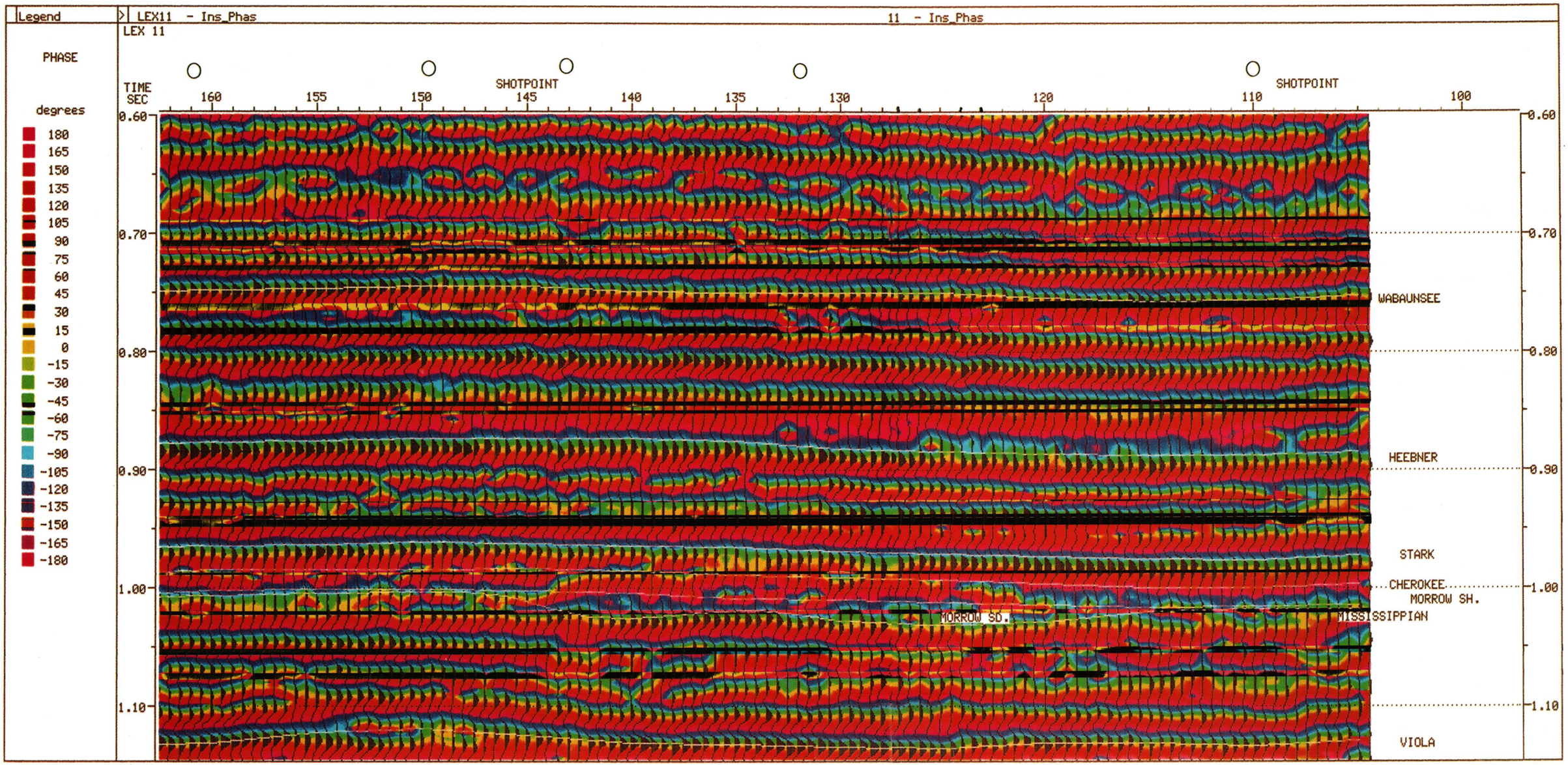

FIGURE 14—Instantaneous phase display; note anomalous character between stations 142–120.

Seismic Expression of the Damme Field, Finney County, Kansas

William A. Miller[1], Mark G. Lehrer[2], and Carmen J. Porter[2]
[1]Canyon Energy, Inc., Denver, CO 80202; and
[2]Texaco USA, Denver, CO 80237

Abstract

Damme field, located in Finney County, Kansas, produces oil from Mississippian and Pennsylvanian carbonates and sandstones. Trapping is due to both structure and stratigraphy. First discovered in 1951, this field has produced 15 million barrels of oil and is still producing today.

The structural nature of Damme field is readily observed on CDP-seismic data acquired over the field. The erosional topography on the Mississippian (pre-Pennsylvanian) unconformity reveals a fault-bounded structure, and thick Morrow deposits fill in the surrounding paleotopographic lows. The influence of basement block faulting is suggested by the seismic data as well as by aeromagnetic data in the area. The structural relief is rapidly attentuated in the overlying Pennsylvanian section, and the buried paleotopography is described very well by mapping of the Permian to Mississippian interval.

This paper describes the seismic expression of Damme field with modern CDP seismic, and contrasts this expression with the predicted model response generated from well-log information in the field. The basement influence is also examined as described by published aeromagnetics and Precambrian structure maps.

Introduction

The causal relationship between Mississippian and Morrowan paleotopography and sedimentology, basement structure, and their corresponding seismic expression has long been of critical importance in the successful exploration beneath the Hugoton embayment of southwest Kansas. Unfortunately, because of rapid lithology changes in the Permian and Pennsylvanian sections and the frequent occurrence of near-surface velocity anomalies, the direct interpretation of these relationships from seismic data has often proved difficult. This paper will examine seismic data over a producing field in the area, Damme field, and demonstrate how interval-mapping and forward-modeling techniques can aid in the seismic interpretation. Regional aeromagnetic data are also considered in the interpretation.

Damme field is located in T. 21 and 22 S., R. 33 W., Finney County, Kansas. It is one of a series of northwest-southeast-trending fields in the northeastern portion of the Hugoton embayment (fig. 1), which produce primarily from Mississippian St. Louis oolitic shoals associated with present-day Mississippian structures. Other fields in the area include Pleasant Prairie (Finney and Haskell counties), Ingalls (Gray County), Nunn (Finney County), Lakin (Kearny County), and Shallow Water (Scott County).

Damme field has produced over 15 million bbls of oil from 148 wells since its discovery in 1951. Producing zones include the Pennsylvanian Ft. Scott, Marmaton, and Morrow formations, in addition to the Mississippian St. Louis formation. The trapping mechanism has been described as combination structural and stratigraphic (Schmidlapp, 1959).

Discovery

The Damme field discovery well, the #1 Damme, was drilled by W. L. Hartman and was based on regional subsurface geology (Schmidlapp, 1959). The #1 Damme (SE SE NW sec. 21, T. 22 S., R. 33 W.) was completed in April 1951, for an initial reported production potential of 1795 BOPD out of the Mississippian St. Louis. The Finnup field was discovered 2 mi (3.2 km), southeast of this well with the drilling of the W. L. Hartman–Finnup #1 (NE NE NW sec. 34, T. 22 S., R. 33 W.) in August 1953. The Finnup #1 had a reported initial production potential of 434 BOPD out of the St. Louis.

Development of this area revealed that the original Damme and Finnup fields were part of the same anticline that makes up the Damme field as seen today. Subsequent drilling established production in the Morrow sandstones, and in the Marmaton and Ft. Scott carbonates.

Structural Setting

The Damme field area was part of a relatively stable platform throughout much of the Paleozoic. The region was part of the Southwest Kansas basin during late Devonian–early Mississippian time, with the structurally positive ancestral Central Kansas uplift removed far to the northeast (Merriam, 1963). This area developed into the Hugoton embayment of the Anadarko basin in later Mississippian time. This embayment, bounded to the west and north by the Las Animas Arch–Sierra Grande uplift, and to the east by the Central Kansas uplift, opens southward from the Damme field area into a slightly deeper, more open-marine platform or shelf as evidenced by thickening of the strata into the deep Hugoton area (Handford, 1988).

The Central Kansas uplift continued to be a positive feature while the Hugoton subsided during a major change in structural development near the end of Mississippian time (Merriam, 1963). A pre-Pennsylvanian unconformity developed as the seas regressed, creating an erosional surface with sufficient paleotopography to control much of the oil and gas production across Kansas. This unconformity has been a primary mapping objective for most seismic work in Kansas. In the Damme field area, the top of the Mississippian is the pre-Pennsylvanian unconformity, and throughout this discussion the two will be used synonymously. This is not the case over the Central Kansas uplift, however, where the Mississippian is completely eroded away placing Ordovician rocks at the unconformity.

The present day Mississippian structure of Damme field is a northwest-southeast-trending, southward-plunging anticline (fig. 2). This long, narrow feature is faulted on the east and is similar to other southward-plunging anticlines around the embayment on which Mississippian production is found, such as Pleasant Prairie and Nunn fields (Merriam, 1963). There is over 100 ft (30 m) of relief across the anticline in the east-west direction and up to 75 ft (23 m) of closure formed in the northwest-southeast direction down the axis of the anticline.

The paleotopographic nature of the Damme field structure is revealed by mapping the thickness of the Lower Pennsylvanian Morrow formation (fig. 3), as well as the interval from the Permian Stone Corral (also referred to as the Cimarron) anhydrite to the Mississippian (fig. 4). The Morrow formation consists of sandstones and shales deposited on the unconformity and filling in the topography. This was ultimately transgressed by Pennsylvanian seas, which deposited shelf carbonates over a long period of relative tectonic inactivity. The Morrow deposits thicken by over 50 ft (15 m) to the west of the anticline and by over 200 ft (61 m) on the faulted east side (fig. 5), revealing the magnitude of the paleotopography. The Morrow channels run in several different directions around the paleotopographic high. The Stone Corral to Mississippian interval likewise shows 50 ft (15 m) of relief over the anticline, generally mirroring the buried topography.

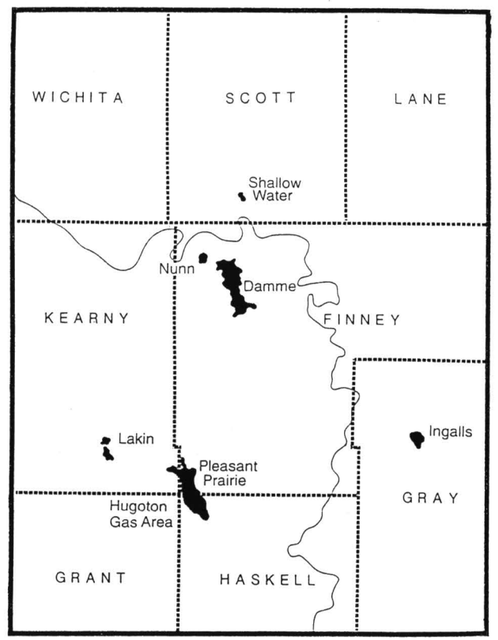

FIGURE 1—Regional index map showing the location of Damme field and other key Mississippian fields in the area.

Stratigraphic Setting

Much of North America during Mississippian time was covered by epeiric seas which deposited widespread shallow-marine limestones (Handford, 1988). Oolitic shoals accumulated on the ramps, shelves, and rimmed edges of these carbonate platforms. The St. Louis oolitic grainstones at Damme field, as well as those of other major St. Louis producing fields in the Hugoton embayment, trend northwest-southeast in a direction which most probably parallels depositional strike. They are interpreted to have been deposited on a shallow-marine shelf. The St. Louis reservoirs at Damme field represent a grainstone-shoal environment which built up over a muddy open-marine sea floor (Handford, 1988).

The Morrowan sandstone reservoirs at Damme field developed as a result of the fluvial and estuarine processes which occurred in response to the regression of the Mississippian sea from the area. These sandstone reservoirs tend to occur on the flanks of the Mississippian paleotopographic highs and probably represent deposition consistent with a valley-fill model.

The Pennsylvanian Marmaton and Ft. Scott reservoirs developed as the Pennsylvanian seas transgressed the buried topography. These carbonates typically represent algal mound/oolitic shoal build-ups in a restricted shelf environment and their porosity development seems to correlate directly to the structure at Damme field.

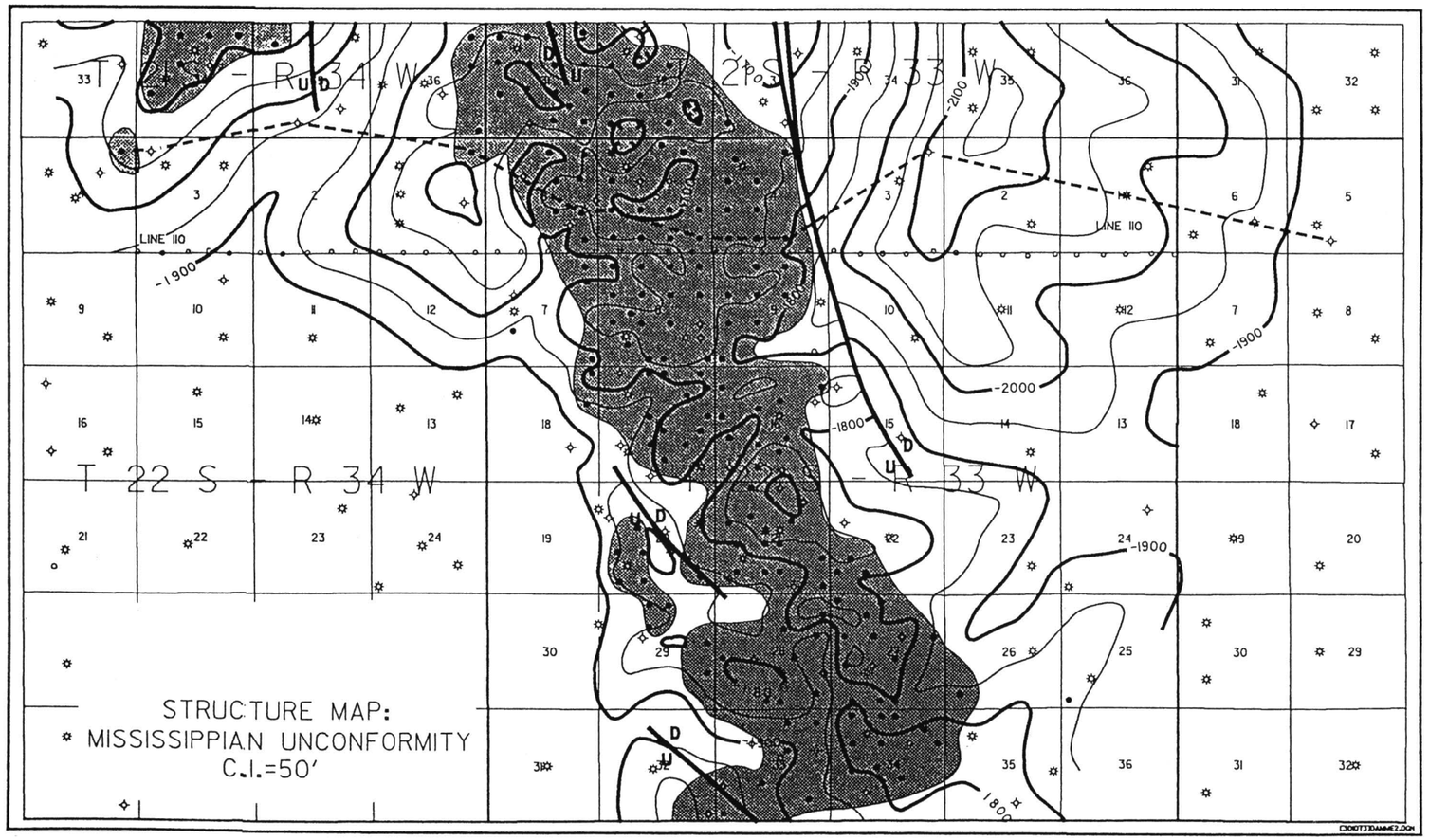

FIGURE 2—Structure on the Mississippian (pre-Pennsylvanian) unconformity at Damme field. Green shading indicates the productive area of the field.

Seismic Response

A number of geologic formations in the Damme field area are good seismic reflecting events and are regionally mappable with seismic data (fig. 6). These include the Permian Stone Corral (Cimarron), the Pennsylvanian Wabaunsee (Stotler limestone), Lansing, Ft. Scott, and Morrow, and of particular importance the top of the Mississsippian unconformity.

Cyclic carbonate deposition continued into the Permian until the area became increasingly more restricted, leading to the widespread deposition of the Cimarron (Stone Corral) anhydrite. The net effect of this depositional history was to infill and attenuate, if not completely mask, the buried structures on the pre-Pennsylvanian unconformity. A comparison of regional maps constructed on top of the Mississippian rocks with maps on the Pennsylvanian Lansing and Permian Stone Corral formations illustrates this dramatically in the Damme field area (Merriam, 1963). As a consequence, a common exploration approach to using seismic data in Kansas is to construct interval, or isochron, maps from the Stone Corral to Mississippian, or an upper Pennsylvanian formation to the Mississippian to identify the buried erosional topography. The identification of paleostructures as well as paleodrainage patterns on this surface is important in the exploration of western Kansas.

From a seismic perspective, interval mapping is not only a logical mapping approach but a necessary alternative to time structure mapping in Kansas. While the direct mapping of the pre-Pennsylvanian unconformity using time structure would be desirable, the amount of structural time relief is on the same order as uncertainties in the travel times due to varying near-surface velocities. Interval velocities at depth, such as from the Stone Corral to the Mississippian, tend to be more stable and do not display the significant lateral variations typical of the near-surface velocities. Consequently, interval time maps from the Stone Corral or upper Pennsylvanian to the Mississippian tend to be more reliable and are consistent with the geologic model of buried pre-Pennsylvanian structures.

Seismic Model

The nature of the buried paleotopography and the thickening of the Morrow section is readily apparent off the crest of the paleostructure (fig. 5), especially in the drainage to the east. The rapid attenuation of structure in the overlying section is illustrated as the Marmaton section shows only slight thickening off the crest.

Seismic modeling was accomplished by first creating an interpolated log cross section using sonic logs across the field (fig. 7). Unfortunately, this section does not exactly parallel the geologic cross section (fig. 5), but was constructed to illustrate the same type of observed paleotopography. The input section was flattened on the upper Pennsylvanian Wabaunsee (Stotler limestone), and only the lower portion is shown in order to focus on the Mississippian. The modeled seismic response (fig. 8) was generated using a zero-phase bandpass-filtered wavelet of 10–20–50–70 Hz. This section is also flattened on the Wabaunsee to illustrate the nature of the paleotopography. The Mississippian surface shows the most dramatic relief. The thickness of the overlying Morrow reflects the paleotopography, thinning to less than 50 ft (15 m) over the crest of the paleostructure and thickening off on the flank. The seismic model shows an ampli-

tude loss of the Morrow event as it thins over the crest of the anticline. The marked north-south drainage observed east of the field (figs. 2 and 3), where the Morrow thickens to over 250 ft (76 m), is the most striking feature on the model. The paleostructural time relief (two-way) from the Wabaunsee to Mississippian is approximately 15 msec from the crest to the west flank, or about 112 ft (34 m) at an interval velocity of 15,000 ft/sec (4,545 m/sec) suggested from sonic log velocities. The relief into the deep east-bounding drainage is over 30 msec.

Most of the compensation of the paleotopography on the Mississippian is taken up in the Morrow section, though some relief is still apparent at the base of the Kansas City (BKC). Any indication of structural relief is very subtle at the Lansing event.

Seismic Data

A 24-fold CDP seismic line, line 110 (figs. 2–4), oriented east-west across Damme field, was utilized in examining the seismic response of the field. These data were acquired in 1980 using a vibroseis source, 48-channel recording, and a group and shotpoint interval of 110 ft (33 m).

The data were reprocessed in 1991 in an attempt to extract the maximum amount of stratigraphic information, especially with respect to Mississippian St. Louis zones. While the reprocessing improved the data resolution markedly from original versions, the data ultimately were only suitable for interval mapping to reconstruct the Mississippian paleotopography. Changes in the Morrow section thickness were also apparent.

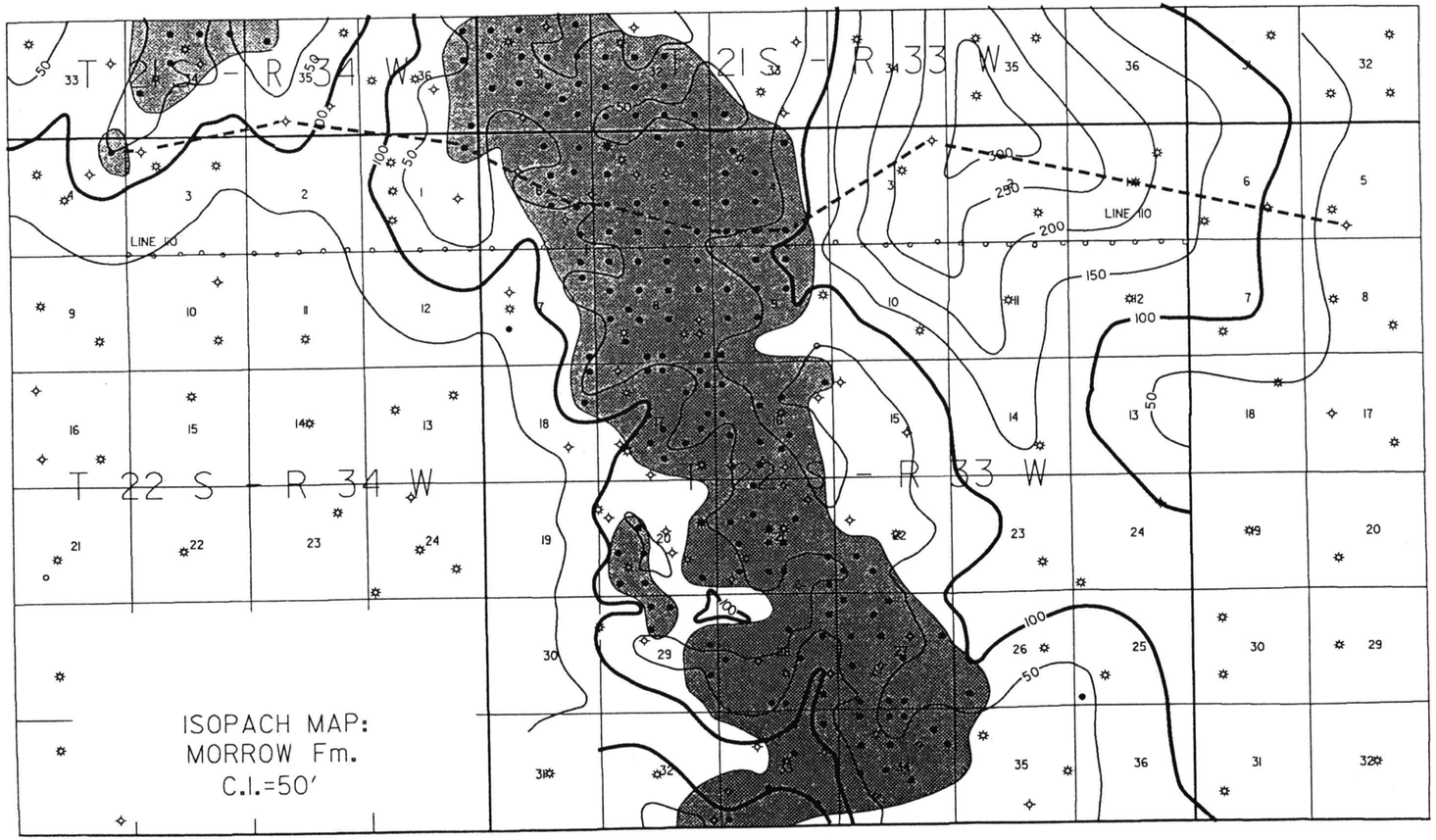

FIGURE 3—Isopach of the Pennsylvanian Morrow formation at Damme field.

In order to facilitate an examination of the buried Mississippian paleotopography, Line 110 was flattened on the Cimarron (Stone Corral) anyhydrite (fig. 9). The Cimarron anhydrite, Wabaunsee, Lansing, Morrow, and Mississippian horizons are indicated on the section. The Morrow section has been highlighted to accentuate the topography on the Mississippian.

As predicted by the model study, the most striking feature on the section is the relief on the Mississippian and the corresponding thickness changes in the Morrow. From the crest of the structure to the west there is approximately 10–12 msec of time relief on the Mississippian. To the east, the deep drainage is observed where the Morrow thickens dramatically to over 250 ft (76 m).

The expression of the Mississippian paleostructure is attenuated in the overlying geologic section. Subtle relief on the Wabaunsee is observed on Line 110 across the top of Damme field, and relief is still subtle at the Lansing horizon. The Lansing to Morrow interval, inclusive of the Marmaton, is observed to thicken off the crest of the Mississippian paleostructure.

A detailed display was extracted from the full section of Line 110 and plotted to approximately the same scale as the seismic model (fig. 10). This portion of Line 110 was similarly flattened on the Wabaunsee. Only every other trace was plotted to make the horizontal scaling and resolution comparable to the model traces for the purposes of analysis. The time relief on the Mississippian from the crest of the paleostructure to the west flank is about 10 msec. The amplitude loss of the Morrow event observed on the model as it thins across the paleostructure is not as dramatic on the seismic data of Line 110. One potential difference is due to the fact that the seismic model is not constructed from exactly the same portion of the field crossed by Line 110.

The thick Morrow drainage to the east of Damme field is observed on the detailed section (fig. 10), though the authors will readily admit that without the available well control the correlation to the lower leg of the anomaly may not have been obvious from the data. Part of this interpretation problem is due to a lack of good edge definition of the anomaly. Loss of good edge definition of the west side of the anomaly is primarily due to its juxtapostion with the fault bounding the east side of Damme field. The east side of the deep drainage anomaly is not so readily explained. One possibility is that this east edge of the anomaly is much sharper than we have represented, and the edge was not properly imaged seismically even though the data were migrated. This is, in part, a shortcoming of the acquisition parameters of the data. Regardless, the Mississippian paleostructure is still obvious on the data section, and the utility of the seismic data for exploring for this type of feature should be readily apparent.

More locally, a thickening of the Morrow is observed west of the crest of the paleostructure on the detailed seismic section (fig. 10), and it rapidly thins again to the west. This corresponds to the Morrow thick identified from well control and trending south to north into secs. 6 and 7, T. 22 S., R. 33 W. (fig. 3). As observed on the seismic data, the Morrow thins into secs. 1 and 12, T. 22 S., R. 34 W. Ironically, the subtle drainage patterns as identified by Morrow thickening are more obvious on these data than the dramatic thickening to the east.

Interpretation of Deep Structural Elements

Handford (1988) pointed out in his article on the Mississippian ooid grainstone reservoirs of Damme field that the lack of well penetrations below the St. Louis precluded an interpretation on the deeper stratigraphic units at Damme field. To this end, seismic data can provide some insight into the tectonic controls on the field. Many models for grainstone shoal deposition have an underlying structural mechanism which influenced water depth and sea-floor topography. There is an obvious correlation between St. Louis "B" zone oolitic development with the Mississippian structure and, perhaps more importantly, with the Mississippian paleotopography inferred from the Morrow isopach. It is not unreasonable to postulate that this paleotopography is an expression of an older structure which likely had an influence on the "B" zone shoaling. Additionally, an underlying structural framework often controls subsequent erosional frameworks, such as in the Morrow.

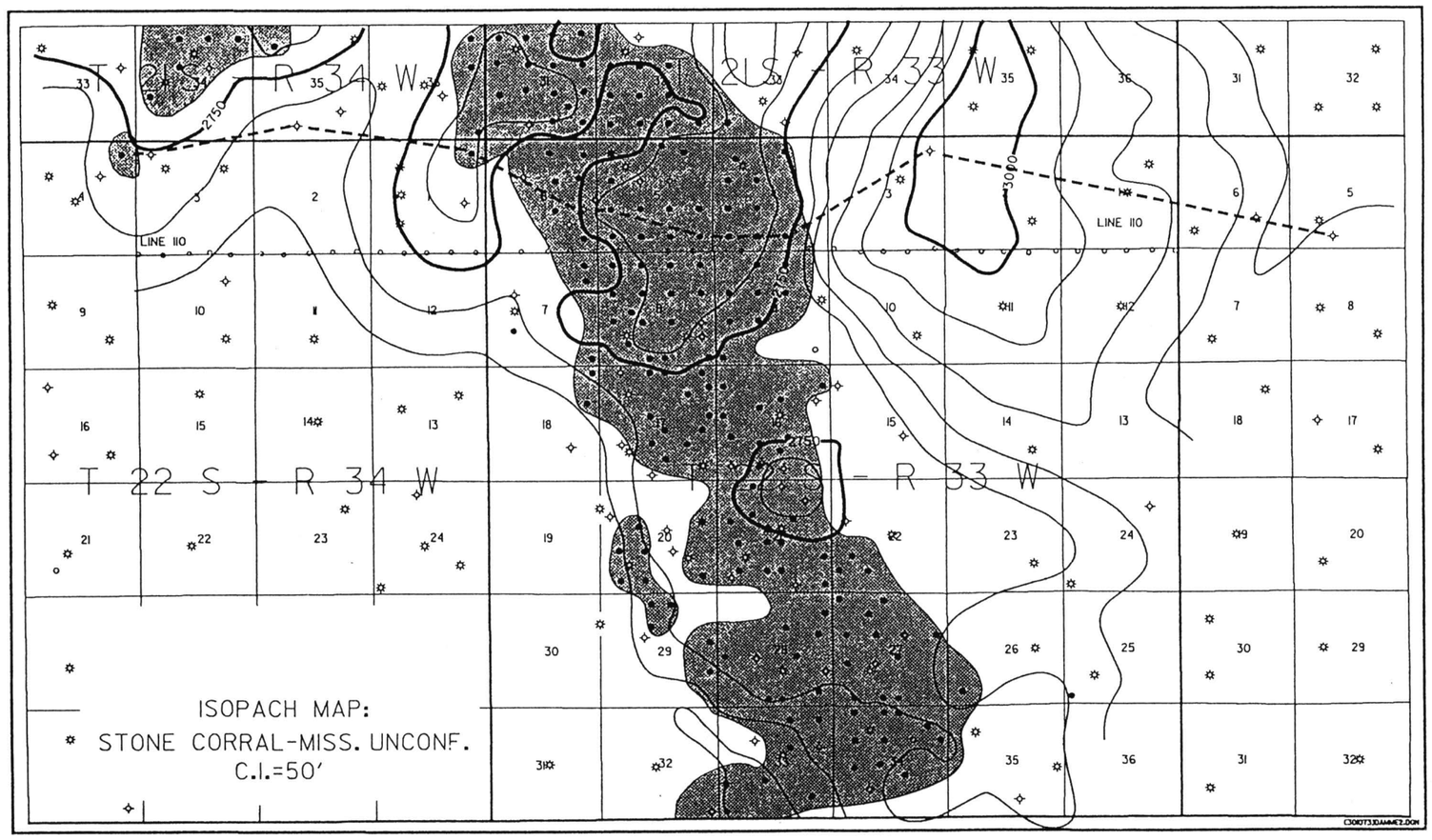

FIGURE 4—Isopach from the Permian Stone Corral (Cimarron) Anhydrite to the Mississippian unconformity.

Figure 11 shows one possible interpretation of the pre-Mississippian deep section of Line 110. The Precambrian surface was projected into the data on the basis of the estimated Precambrian structure in the area as constructed by Cole (1976) and published by Bickford et al. (1979). The Ordovician surface is estimated from regional well penetrations. As previously noted, there are no deep well penetrations in the immediate Damme field area to conclusively establish these correlations.

The pre-Mississippian section is interpreted to be influenced by basement-seated block faulting. There are varying degrees of throw on individual faults, with the most dramatic vertical change on the fault bounding the east side of Damme field. There is a strong coincidence of the deep north-south Morrow thick on the east side of the field with a downthrown basement block. The highest basement blocks correspond to the main part of Damme field. The local thickening of the Morrow previously described on the west side of Damme field in secs. 6 and 7, T. 22 S., R. 33 W., is coincident with interpreted block-fault edges.

The thickness of the St. Louis "B" zone mapped from well control (fig. 12) shows some interesting correlations with the interpreted fault blocks. The limits of the St. Louis "B" zone as defined by isopach mapping are superimposed across the top of the Line 110 seismic section (fig. 11). The Precambrian surface shows a general west-to-east ramping up into the field and terminating against the east fault. The Ordovician surface mirrors the Precambrian, for the most part, but appears to reach its highest point (relative to the Stone Corral datum this section is flattened on) just to the west of the field axis, from where it rolls off slightly to the east. The highest point of the Ordovician is coincident with a small upthrown block interpreted on the data, and the thickest "B" zone development occurs on the west side of this block.

Since the block faulting is interpreted as basement related, it seemed logical to examine any available aeromagnetic data to support this idea. Figure 13 is a portion of the Kansas aeromagnetic map (Yarger et al., 1981) superimposed on the index map (fig. 1). Of immediate interest is the pronounced northwest-southeast-trending aeromagnetic feature that aligns with the east edge of Damme field. Yarger (1983) has pointed out the persistence of this northwest-southeast lineament trend across western Kansas. It would be logical to conclude that this lineament defines a basement boundary which correlates to the basement block faulting interpreted on the seismic data. The observation that the throw interpreted from the seismic data on the basement block faulting is opposite to the

sense of the magnetic intensity across the lineament suggests that the aeromagnetic feature is related to a compositional boundary in the basement. Such a boundary would be a likely zone of weakness across which fault displacement could occur. Certainly a more thorough analysis and modeling of the magnetic data profiles and available gravity data would be necessary in order to support such a conclusion.

The potential basement influence on Damme field was suggested by Cole (1976) and Bickford et al. (1979) in the construction of the topography on the basement surface for Kansas (fig. 14). Damme field can be seen to lie along an interpreted southeast-plunging basement anticline. Other Mississippian fields in the area such as Lakin (Kearny County) and Pleasant Prairie (Finney and Haskell counties) correlate to similar interpreted basement features.

Summary

The seismic data examined over Damme field clearly demonstrate how mapping of the paleotopography on the pre-Pennsylvanian unconformity can be accomplished using CDP seismic data. This buried topography can be identified from an analysis of interval times between key horizons such as the Permian Stone Corral (Cimarron) anhydrite and

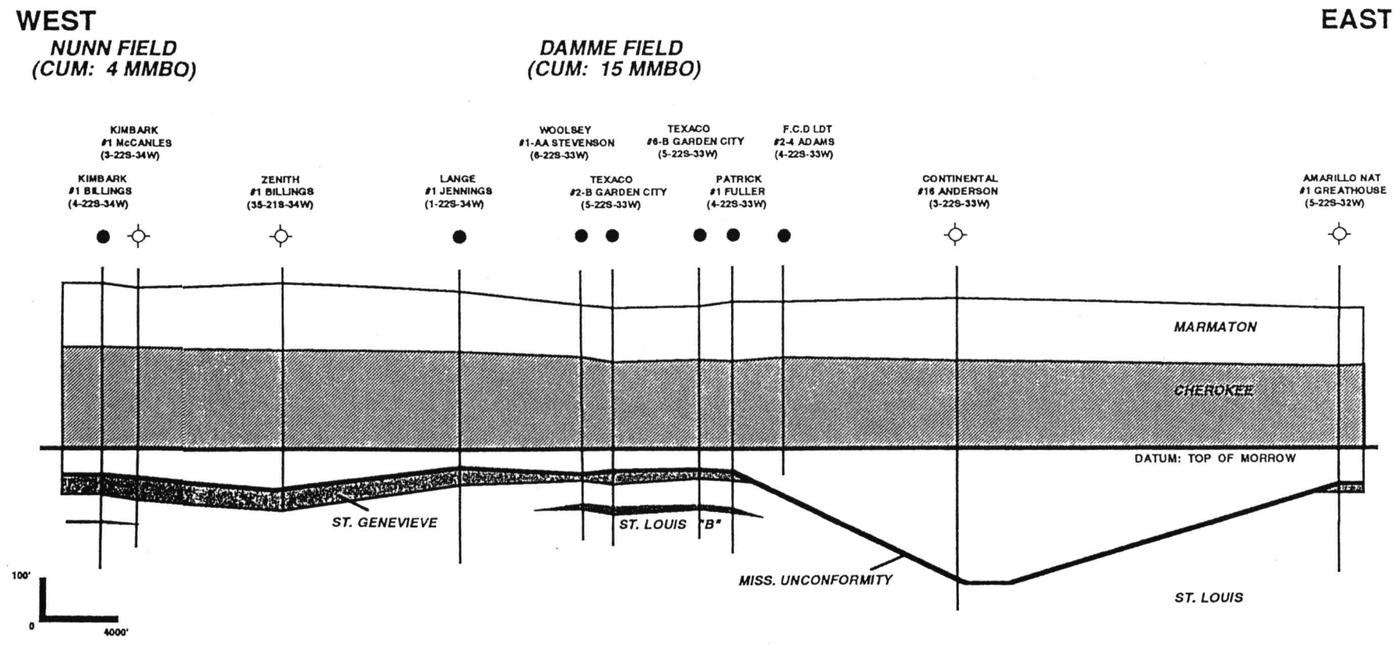

FIGURE 5—EAST-WEST STRATIGRAPHIC CROSS SECTION ACROSS DAMME FIELD. (Location shown as blue dashed line on figs. 2, 3, 4, and 12.)

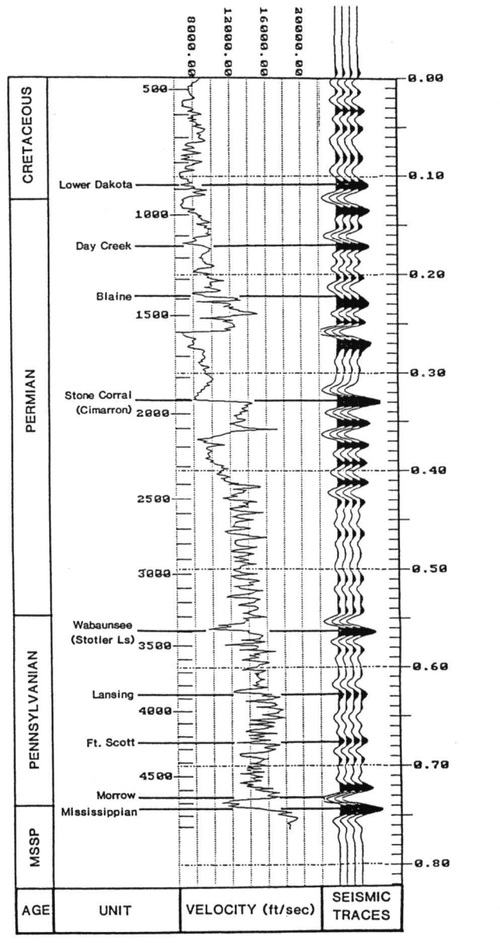

FIGURE 6—TYPICAL SEISMIC RESPONSE OF THE GEOLOGIC SECTION IN THE DAMME FIELD AREA. Synthetic traces generated with a 10–20–50–70 Hz zero-phase wavelet.

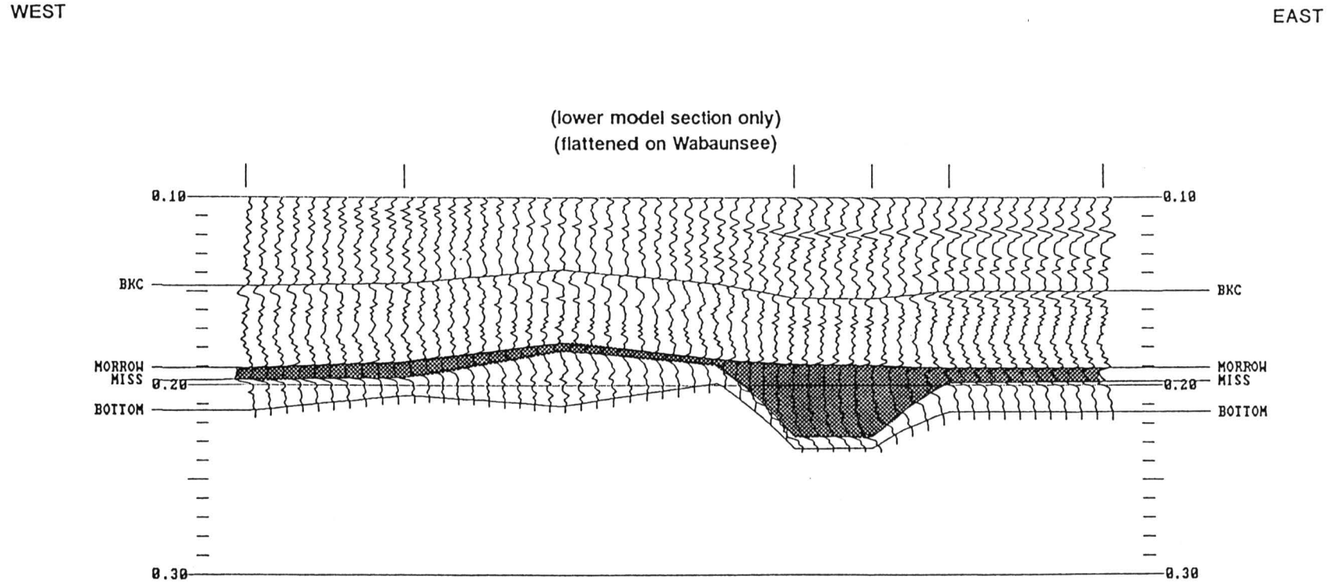

FIGURE 7—EAST-WEST STRATIGRAPHIC CROSS SECTION OF INTERPOLATED SONIC LOG TRACES CONSTRUCTED ACROSS DAMME FIELD. Used as input for seismic model of fig. 8. (Only lower portion of section is shown to focus on Mississippian.)

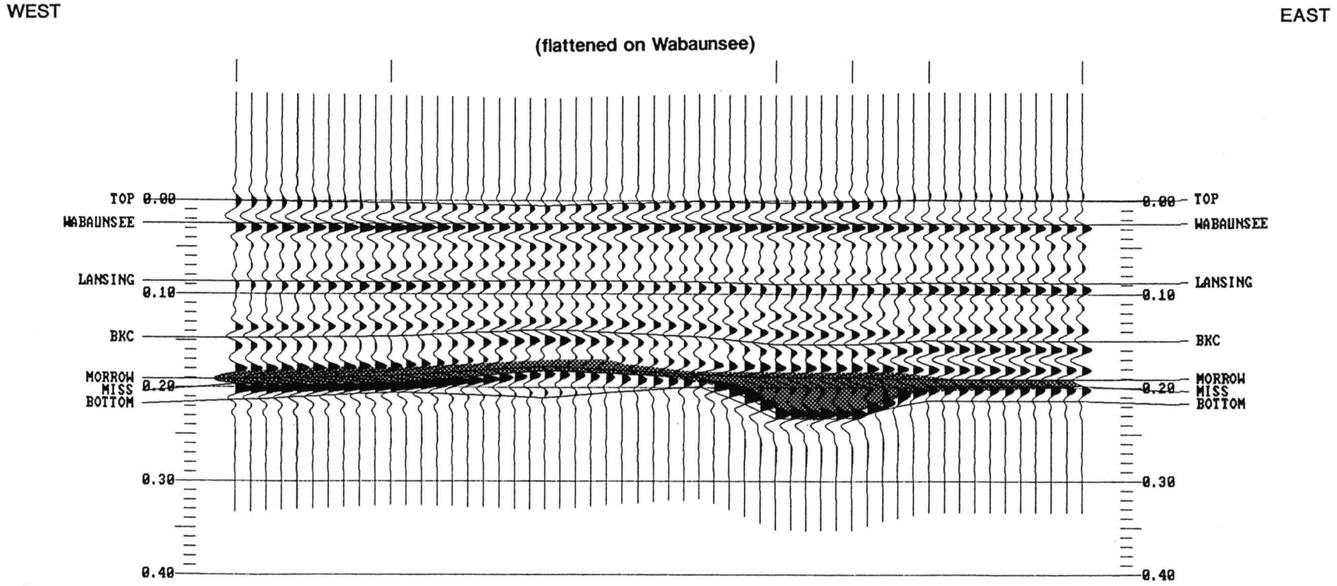

FIGURE 8—SEISMIC MODEL OF DAMME FIELD GENERATED FROM INPUT LOG SECTION OF FIG. 7 BY CONVOLVING WITH A 10–20–50–70 HZ ZERO-PHASE WAVELET.

the Mississippian unconformity. Flattening seismic sections on the Stone Corral facilitates the identification and presentation of these features.

The Morrow section overlying the Mississippian thickens and thins in relation to the paleotopography on the Mississippian at Damme field. This could be directly observed on the seismic data, making it possible to map the erosional framework of the Morrow over and around the Mississippian paleotopographic highs. The Morrow sandstones tend to produce in areas flanking the paleotopographic highs. Since the highs influence Mississippian, Ft. Scott, and Marmaton production, an accurate reconstruction of the paleotopography by seismic methods can help make both the exploration for these targets as well as their development more successful.

Seismic data offer some insights into the influence of deeper structure and tectonics on the development of key stratigraphic facies at Damme field. There was a noticeable coincidence between the distribution of St. Louis "B" zone shoaling and deeper basement fault blocks. A similar coincidence could be observed between Morrowan drainage patterns and the basement faulting. The block faulting might be related to a northwest-southeast lineament trend observed on aeromagnetic data, a trend also suggested by previous work on mapping the topography on the basement surface.

We caution that we offer these comments purely as observations of coincidence between different data sets. A more rigorous study integrating gravity and magnetic modeling and analysis, geologic field studies over similar producing structures, and regional seismic data is necessary before firmly concluding that causal relationships exist. Certainly the observations made are both encouraging and intriguing.

ACKNOWLEDGMENTS—The authors would like to express their appreciation to Texaco USA for permitting the publication of this paper, for providing invaluable data, and for assisting with preparation of figures. Robert A. Peterson of Texaco provided invaluable computer drafting assistance. Particular thanks go to Terry Elzi of Echo Geophysical, Denver, Colorado, for providing the reprocessing of the seismic data, and to John Beury III, of Paragon Geophysical, Wichita, Kansas, for helping introduce all the individuals who would contribute to this paper. A final thanks is due the Kansas Geological Survey for their patience during the lengthy preparation of this paper, a time made all the longer by these trying times in our industry.

References

Bickford, M. E., Harrower, K. L., Nusbaum, R. L., Thomas, J. J., and Nelson, G. E., 1979, Preliminary geologic map of the Precambrian basement rocks of Kansas: Kansas Geologic Survey, Map M–9, scale 1:500,000

Cole, V. B., 1976, Configuration of the top of Precambrian rocks in Kansas: Kansas Geological Survey, Map M–7, scale 1:500,000

Handford, C. R., 1988, Review of carbonate sand-belt deposition of ooid grainstones and application to Mississippian reservoir, Damme field, southwestern Kansas: American Association of Petroleum Geologists, Bulletin, v. 72, no. 10, p. 1,184–1,199

Merriam, D. F., 1963, The geologic history of Kansas: Kansas Geological Survey, Bulletin 162, 317 p.

Schmidlapp, R. L., 1959, Damme and Finnup fields: Kansas Geological Society, Kansas Oil and Gas Fields, Western Kansas, v. 2, p. 8–12

Yarger, H. L., 1983, Regional interpretation of Kansas aeromagnetic data: Kansas Geological Survey, Geophysics Series 1, p. 1–35

Yarger, H. L., Robertson, R. R., Martin, J. A., Ng, K., Sooby, R. L., and Wentland, R. L., 1981, Aeromagnetic map of Kansas: Kansas Geological Survey, Map M–16, scale 1:500,000

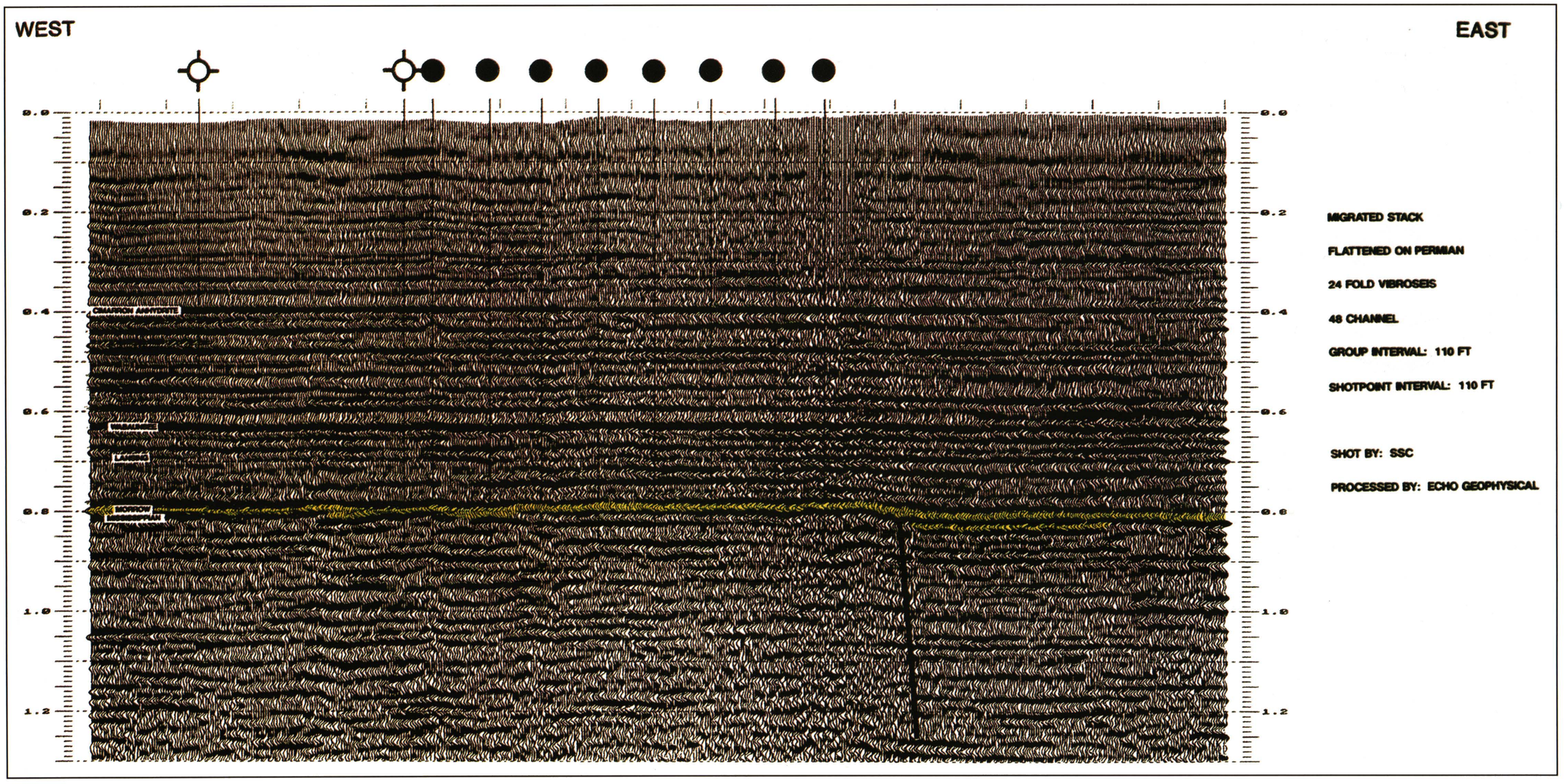

FIGURE 9—East-west seismic line 110 across Damme field, flattened on the Permian Cimarron (Stone Corral) Anhydrite. Morrow formation is highlighted to accentuate the Mississippian unconformity.

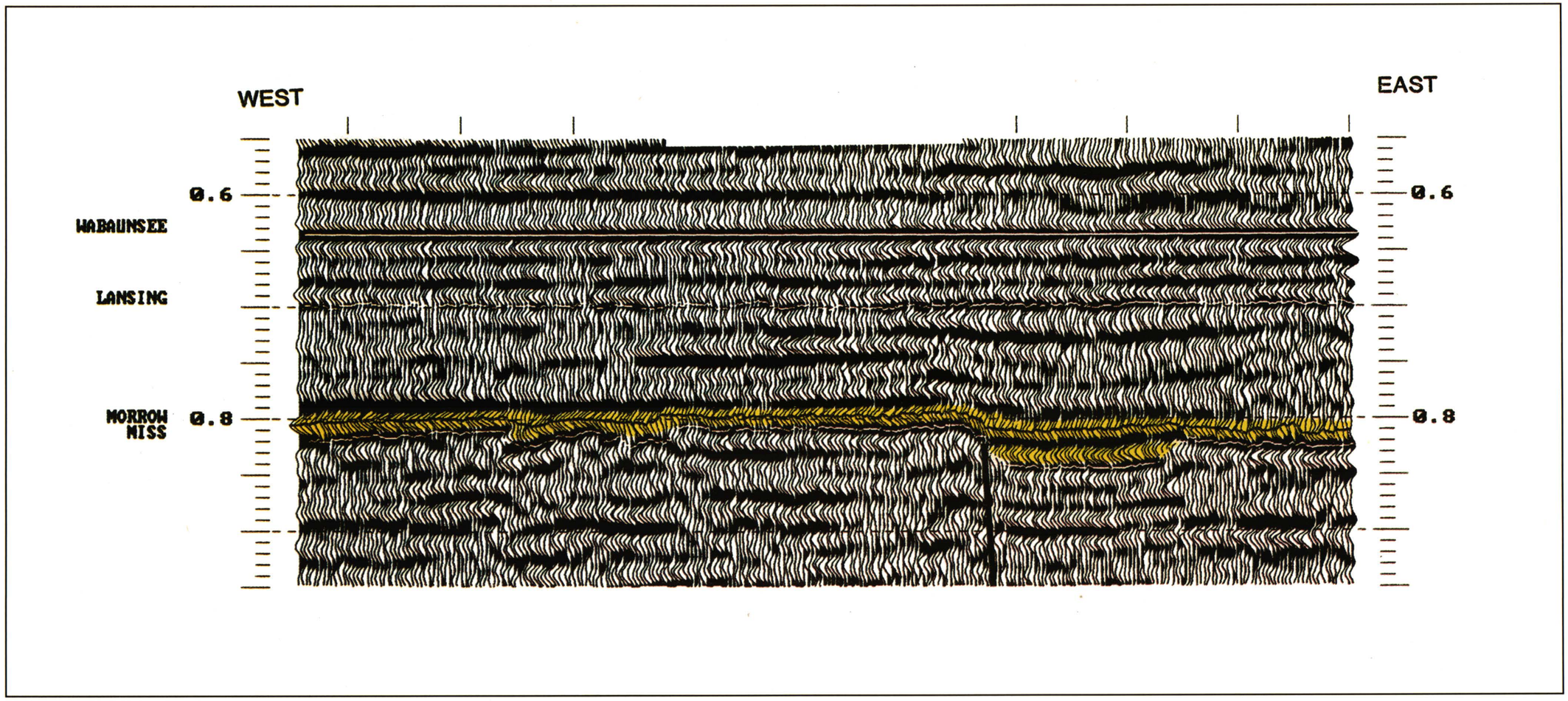

FIGURE 10—Portion of Seismic line 110 replotted and flattened on the Pennsylvanian Wabaunsee (Stotler limestone) for comparison with seismic model of fig. 8.

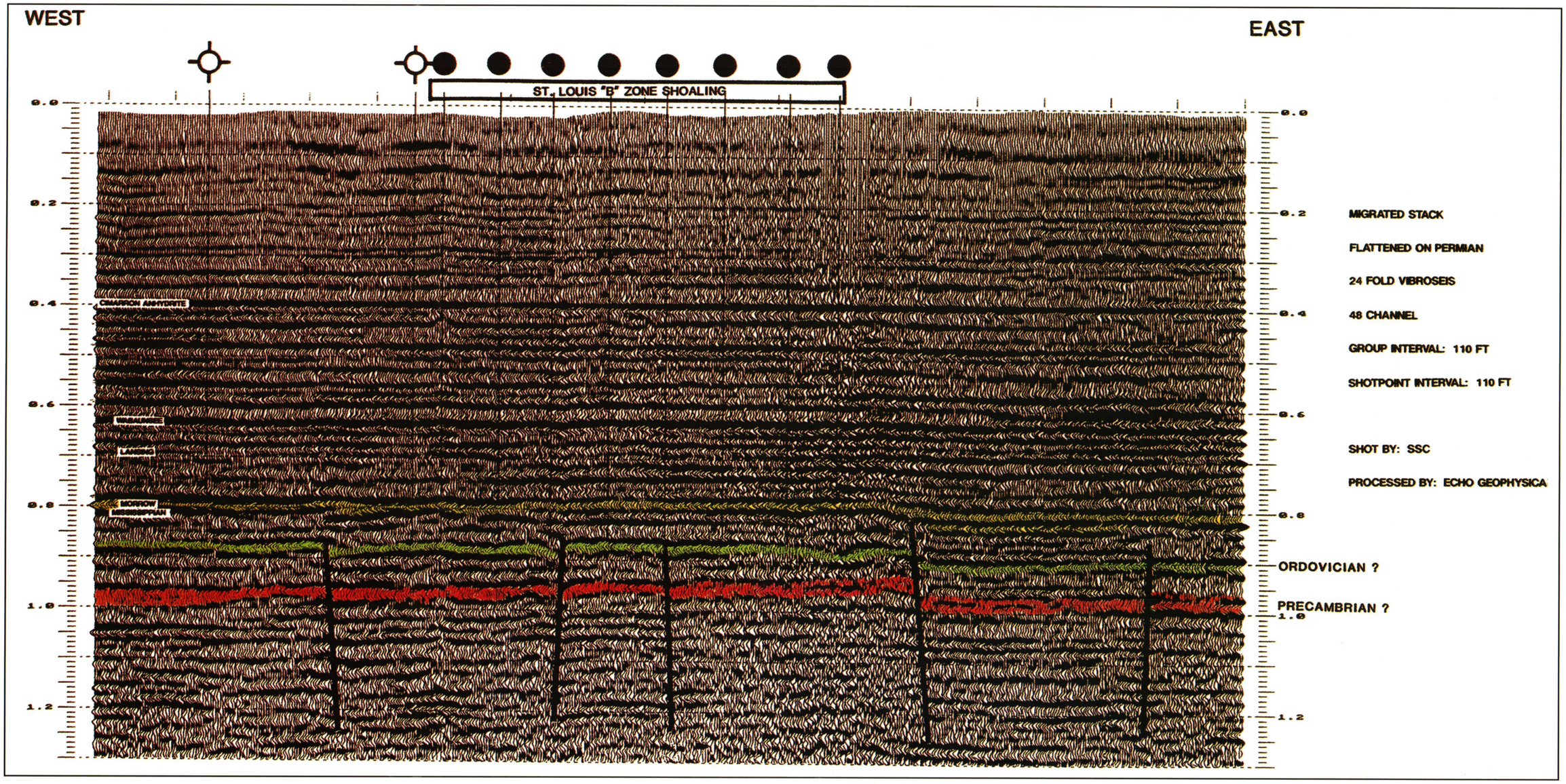

FIGURE 11—Seismic line 110 shown with a basement interpretation. The limit of the St. Louis "B" zone is shown across the top of the section.

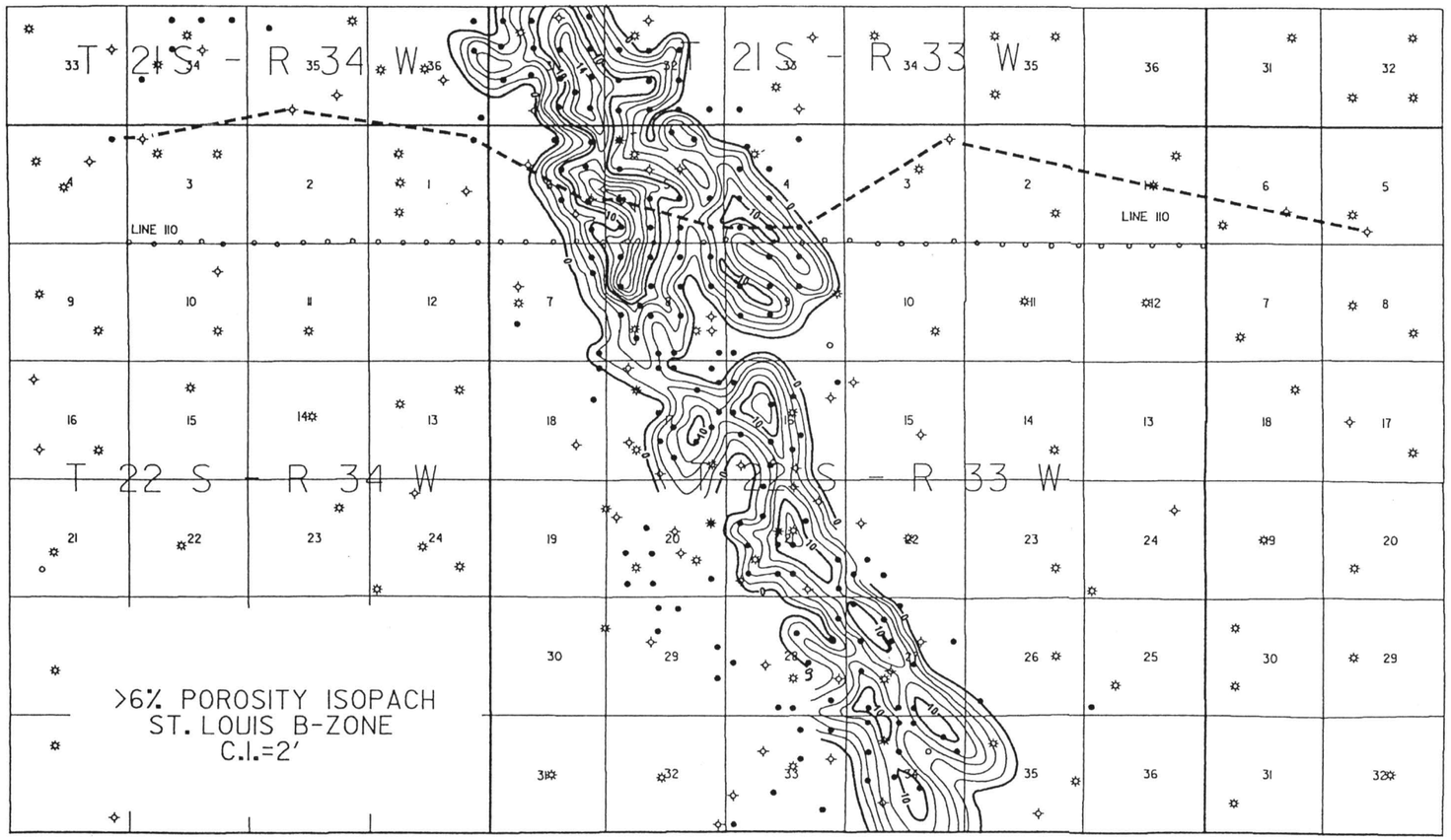

FIGURE 12—Porosity isopach of the St. Louis "B" zone at Damme field.

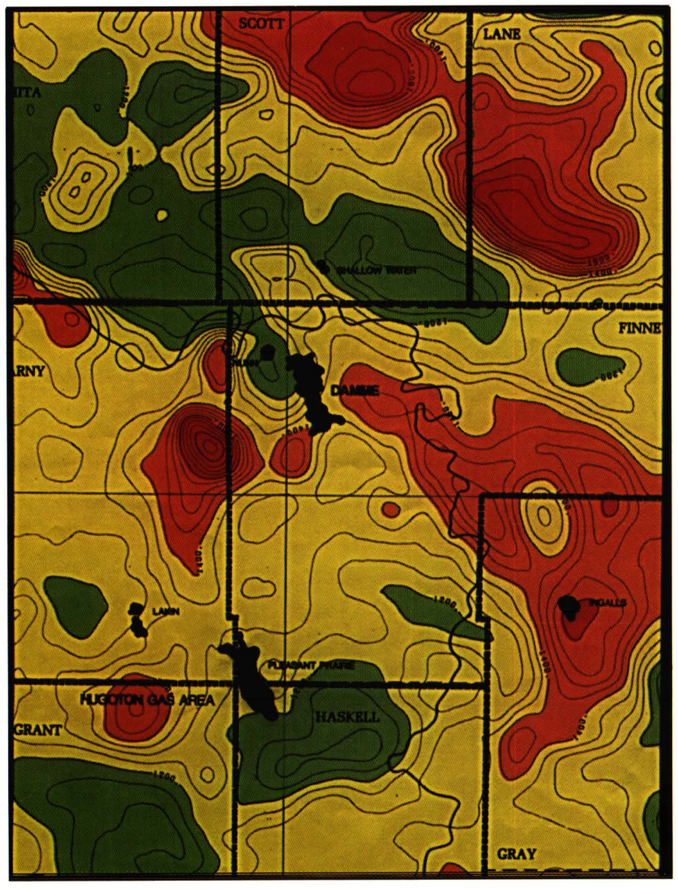

FIGURE 13—Portion of the Kansas aeromagnetic map with Damme field and other key Mississippian fields indicated (after Yarger et al., 1981).

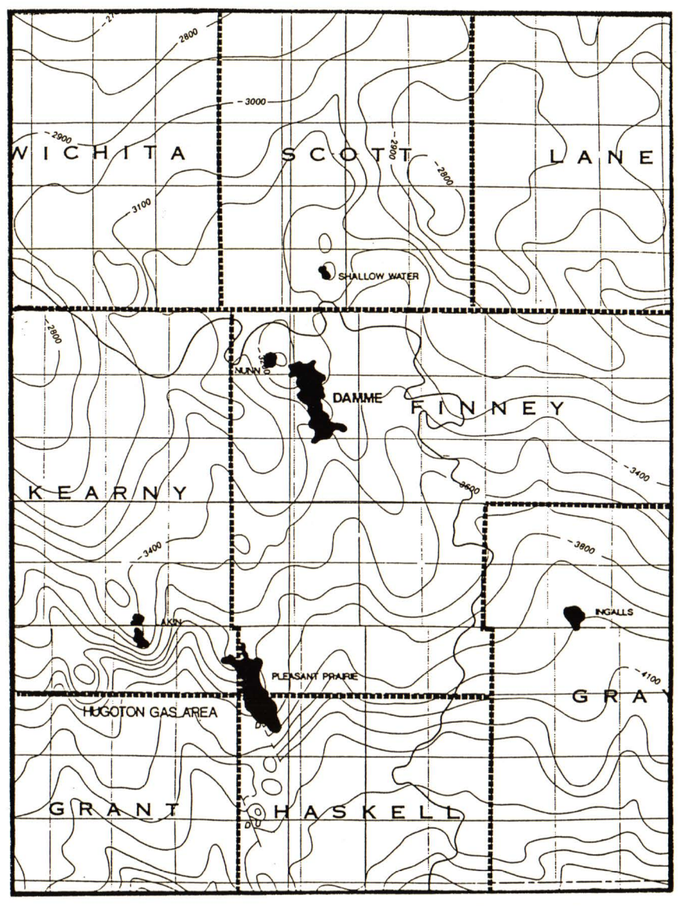

FIGURE 14—Portion of the Precambrian basement map of Kansas with Damme field and other key Mississippian fields indicated (after Bickford et al., 1979).

Stockholm SW Field, Greeley/Wallace Counties, Kansas

William A. Miller[1], Emily M. Hundley–Goff[2], and Lawrence G. Brown[3]
[1]Canyon Energy, Inc., Denver, CO 80202; [2]Geographix, Denver, CO 80202; and
[3]Consulting Geologist, Parker, CO 80134

Abstract

Stockholm SW field was the first Morrow oil field discovered in what is referred to as the Stateline trend. This 30-mi (48-km) trend is located along the border between Kansas and Colorado and includes western Wallace and Greeley counties, Kansas, and eastern Cheyenne and Kiowa counties, Colorado. Oil is produced out of Lower Pennsylvanian Morrow valley-fill sandstones from more than 250 producing wells comprising 10 fields.

While not utilized in the original discovery of Stockholm SW field, geophysics has played a significant role in the exploration for and development of all subsequent fields in the trend. The incisement of valleys into the underlying carbonates has created a thick Morrow sequence directly mappable with modern seismic techniques. Hundreds of miles of seismic data have been acquired along the Stateline trend in the exploration for Morrow reservoirs, and 3D seismic has proved valuable in field development. Aeromagnetic data provide clues as to the basement influence on Morrow drainage patterns. The use of these data and the key geologic elements of the play are the focus of this paper.

Introduction

Stockholm Southwest (SW) field is located in T. 15 and 16 S., R. 42 and 43 W. of Greeley and Wallace counties, Kansas, and in T. 16 S., R. 41 W. of Cheyenne County, Colorado. The field is part of a major oil-producing trend which lies on a regionally stable Paleozoic platform which developed in the northern reaches of the Hugoton embayment of the evolving Anadarko basin (fig. 1). This trend lies east of the prominent Las Animas Arch and extends for 30 mi (48.3 km) north and south of Stockholm SW field, straddling the Colorado/Kansas border. It has been informally named the Stateline trend and consists of 10 oil fields, all of which produce from a sequence of Lower Pennsylvanian Morrow fluvial valley-fill sandstones. Stockholm SW was the first oil field discovered in this trend. Other fields in the Stateline trend include Harper Ranch, North Arapahoe, Arapahoe, Arapahoekan, Frontera, Second Wind, Jace, Moore–Johnson, and Sidney.

The primary pay at Stockholm SW field is the Stockholm sandstone, which is stratigraphically the lowest sandstone in the upper Morrow Series at Stockholm SW. The Johannes sandstone, found stratigraphically immediately above the Stockholm sandstone, is a secondary pay at Stockholm SW.

Discovery

Prior to the 1970's, all of the Morrow production in southeast Colorado, excluding southeast Baca County, was gas with associated condensate. In 1971, Koch Exploration Company completed the first Morrow oil well in the area at Smoky Hill field in Kit Carson County, Colorado. The well proved to be noncommercial and did not attract much industry attention. In the middle to late 1970's, Texas Oil and Gas Production Corp. (TXO) began a detailed examination of petrophysical well logs in southeast Colorado and western Kansas, looking for possible by-passed productive zones. As part of this exploration effort, TXO drilled the Evans No. 1 "E" in December 1978, a twin to the R.G. Smith–Evans No. 1, a dry hole located in the NE NE SE sec. 11, T. 16 S., R. 43 W., of Greeley County, Kansas. The original Evans No. 1 was drilled and abandoned in 1969, and no cores or drill-stem tests were taken. This well penetrated 27 ft (8.2 m) of Stockholm sandstone with no shows of oil reported in the samples. In the twin to the dry hole, the TXO wellsite geologist logged oil shows in the Stockholm sandstone, which was drill-stem tested and recovered 550 ft (167.8 m) of oil and gas, 1,000 ft (305 m) of mud-cut oil, 500 ft (152.5 m) of oil and mud, and 100 ft (30.5 m) of oil and water. In March 1979, the well was completed in the Stockholm sandstone for an IPP of 82 BOPD and 528 MCFGPD.

The TXO–Evans No. 1 "E" became the first commercial Morrow oil well in the entire southeast Colorado and immediate stateline area north of T. 24 S. Previously, Morrow sandstones in the area had only produced low-BTU gas. Soon after the discovery of the Stockholm SW field, oil production was established in the Sorrento field 50 mi (80 km) to the west of Stockholm SW field (fig. 1).

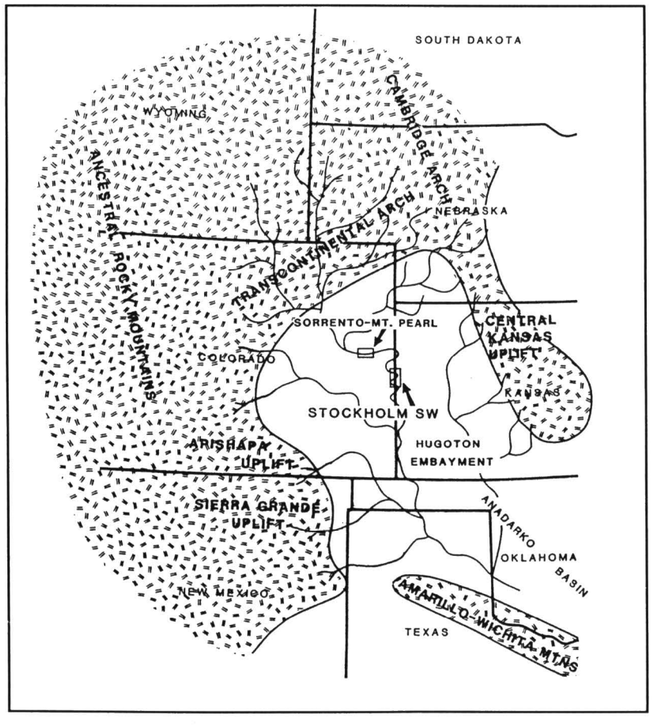

FIGURE 1—MORROW PALEOGEOGRAPHY MAP. This figure shows areas of crystalline basement uplift, hypothetical Morrow drainage systems, the Hugoton embayment, and the Anadarko basin as they are postulated to have appeared during Morrow time. It also serves as a regional index map for this paper (modified after Swanson, 1979).

The initial development of the Stockholm SW field proceeded in an east-west direction from the discovery well. The pace of development slowed as dry holes were encountered at the eastern and western margins of the field, which suggested a lack of further sandstone deposition. In July 1985, TXO drilled the Bergquist No. 1 in the SW SW NE sec 6, T. 16 S., R. 42 W., of Greeley County, Kansas, a northeast stepout to Stockholm SW of over 1/2 mi (0.8 km). This well initially flowed 800 BOPD and was significant in that it showed a dramatic northward turn of the Stockholm sandstone trend and suggested that Stockholm SW drained a much larger area than originally thought. The pace of development proceeded quickly after the successful completion of the Bergquist No. 1. The TXO–Wallace No. 1 "R," drilled in March 1987 in the C W/2 sec. 29, T. 15 S., R. 42 W., of Wallace County, Kansas, was another stepout to the north and was significant in that it was drilled solely on the basis of seismic information. Seismic data would prove instrumental in the subsequent development and exploration in the trend.

Three significant wildcats drilled in 1987 would cause activity in the trend to expand dramatically to the north of the Stockholm SW field. The Medallion–Arapahoe No. 27–1 was drilled in the SE NW sec. 27, T. 15 S., R. 42 W., of Cheyenne County, Colorado, and completed as a Stockholm sandstone oil well. It rejuvenated the Arapahoe field originally discovered by TXO in April 1978, a field that was producing low-BTU gas and oil from the Johannes sandstone. The Frontera field was discovered with the drilling of the Mull–Stateline Ranch No. 1 in the NW NW sec. 18, T. 15 S., R. 41 W., of Cheyenne County, Colorado. A short time later, TXO drilled the discovery well of the Arapahoekan field, the Hibbert No. 1 "A" in the NE NW NW sec. 1, T. 15 S., R. 43 W., of Wallace County, Kansas.

Production to the south of the Stockholm SW field was first initiated with the discovery of the Second Wind field in July 1988. The discovery well, the TXO–Kriss No. 1 "A," was drilled in the NE NW sec. 18, T. 16 S., R. 41 W., of Cheyenne County, Colorado, and completed as a Stockholm sandstone oil well. The Stateline trend currently comprises 10 fields over an area extending from T. 12 S., R. 43 W., of Cheyenne County, Colorado, to T. 18 S., R. 43 W., of Greeley County, Kansas.

Structural Setting

The sandstones of the Stockholm SW field were deposited during a time of relatively minor structural activity in the immediate area. Major paleogeographic features during Morrowan time were the Transcontinental Arch to the north, the Central Kansas uplift to the east, the Ancestral Rocky Mountains to the west, and the still developing Anadarko basin to the extreme south. This structural setting created the regional northwest to southeast drainage into the Anadarko observed during Morrowan time (fig. 1).

Geophysical data indicate a high degree of faulting and fracturing in the underlying Mississippian carbonates which appear to be basement seated. The pre-Morrowan structural activity developed a conjugate framework of fault and fracture trends oriented northeast and northwest across the Stateline trend. These northeast and northwest trends are evident throughout the Rocky Mountain region and are believed to be related to regional wrench-fault tectonics (Stone, 1968). Although significant structural activity

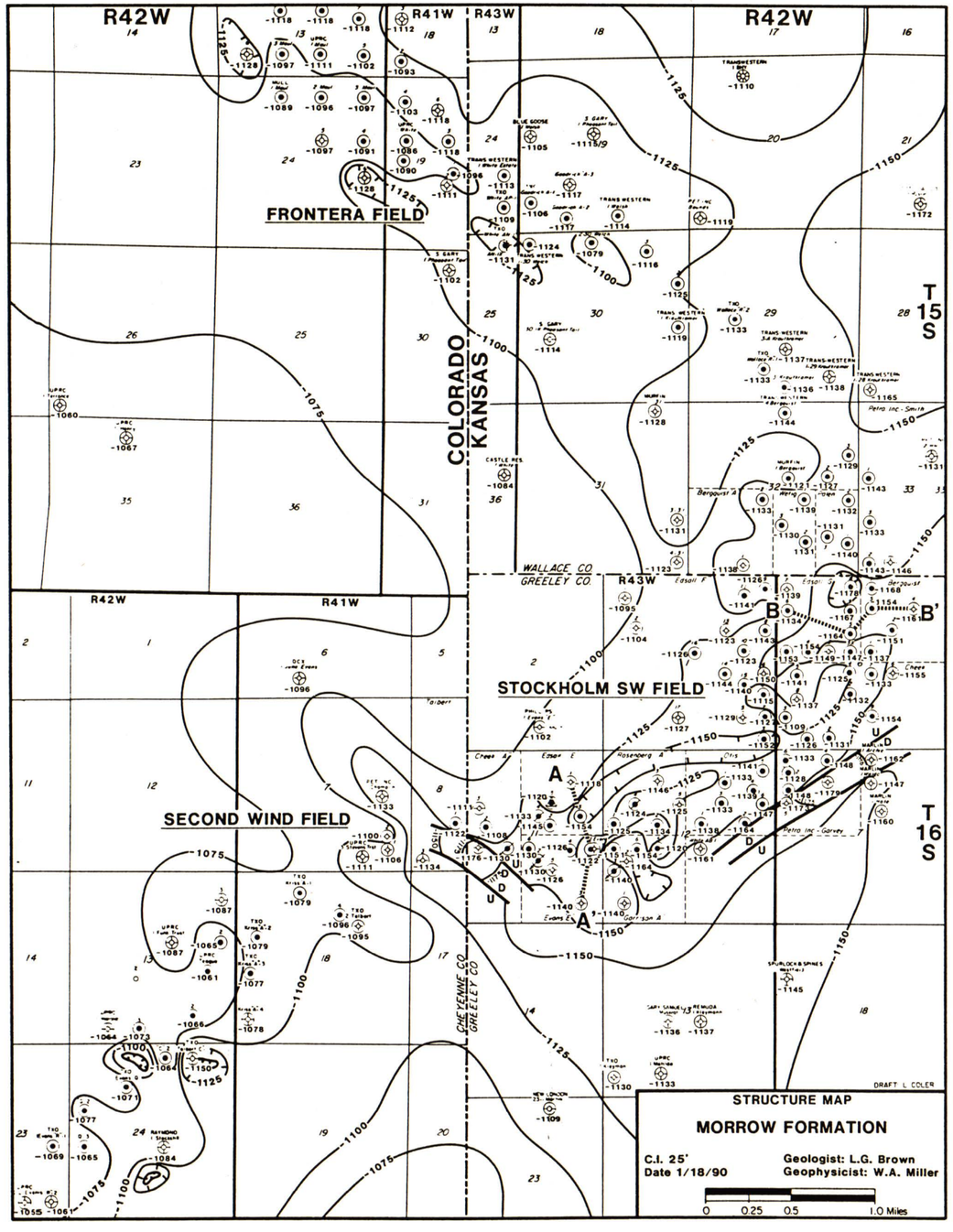

FIGURE 2—Structure map, top Morrow Formation.

along these trends appears to have ceased during Morrowan time, subtle expressions of these trends seem to have influenced the direction of Morrow drainage in local areas. Specifically, the pronounced westward bend of the Stockholm SW field into T. 16 S., R. 43 W., is postulated to have been the result of the Morrow channel system encountering a low-relief escarpment feature (fig. 2).

Post-Morrowan structural activity appears to have reactivated some of the pre-existing fault trends. The most significant reactivation appears to have occurred during the Laramide Orogeny. The south side of the Stockholm SW field is bounded by post-Morrowan faults which are parallel to, but not coincident with, the thick Morrow section and suggest rejuvenation of a fault framework that had previously influenced drainage during Morrowan time (fig. 2). The sense of the movement, however, appears to have reversed from pre-Morrowan to post-Morrowan time, perhaps due to a subsequent change in the orientation of the regional stress field. A lack of consistent deep log data has made an accurate reconstruction of this timing difficult. Regional aeromagnetic data indicate that the Stockholm SW field is positioned near a dramatic intrabasement compositional contact, a probable zone of weakness during tectonic activity (fig. 3).

Stockholm SW field is located on a regionally west-to-east tilted surface which developed as a result of movement during the Laramide Orogeny. The regional Stockholm sandstone trend is parallel to structural strike as defined by mapping the structure on the top of the Morrow Formation. A significant aspect of structure in the Stockholm SW field and along the Stateline trend is the occurrence of local structural depressions which often contain wet, nonproductive sandstone. Seismic data have shown these to be fault related. Development 3D seismic to the southwest of Stockholm SW field in the Second Wind field suggests that, in some instances, these faults led to the creation of collapse features in the Mississippian as small as 20 acres (8.1 ha) in areal extent (fig. 2). These features, which are post-Morrowan in occurrence, can display as much as 100 ft (30.5 m) of relief. Recognition and avoidance of these structural features is important in field development.

Stratigraphic Setting

The Morrow Formation in the Stockholm SW field is subdivided into the sandstone, siltstone, and shale of the upper Morrow and the carbonate and shale of the lower Morrow. All of the oil and gas production in the Stockholm SW field is from upper Morrow sandstones. The primary hydrocarbon reservoir is the Stockholm sandstone, with additional hydrocarbon reservoirs occurring in the Johannes and other overlying sandstones (fig. 4). The Morrow is underlain by Mississippian carbonates and overlain by carbonates and shales of the Pennsylvanian Atoka formation.

Regionally, the Stockholm SW field is situated on a stable Paleozoic platform which extended north from the Anadarko basin. The older Mississippian formations sequentially subcrop to the north with increasing distance from the Anadarko basin. In the Stockholm SW area, the Ste. Genevieve limestone is the youngest Mississippian formation present. It is a slightly arenaceous, cream to tan, micro-oolitic wackestone. The Ste. Genevieve is very thin at Stockholm SW and near its subcrop limit. Consequently, the St. Louis limestone is more often the Mississippian formation penetrated. The St. Louis is a massive, very dense, tight, dark-gray crinoidal wackestone. The lower Morrow limestone rests unconformably on top of the Mississippian at Stockholm SW field and is deposited on the topography developed on this unconformity. The lower Morrow limestone is a very tight, argillaceous, glauconitic, crinoidal wackestone which is typically interbedded with thin marine shales. Regionally, the lower Morrow section

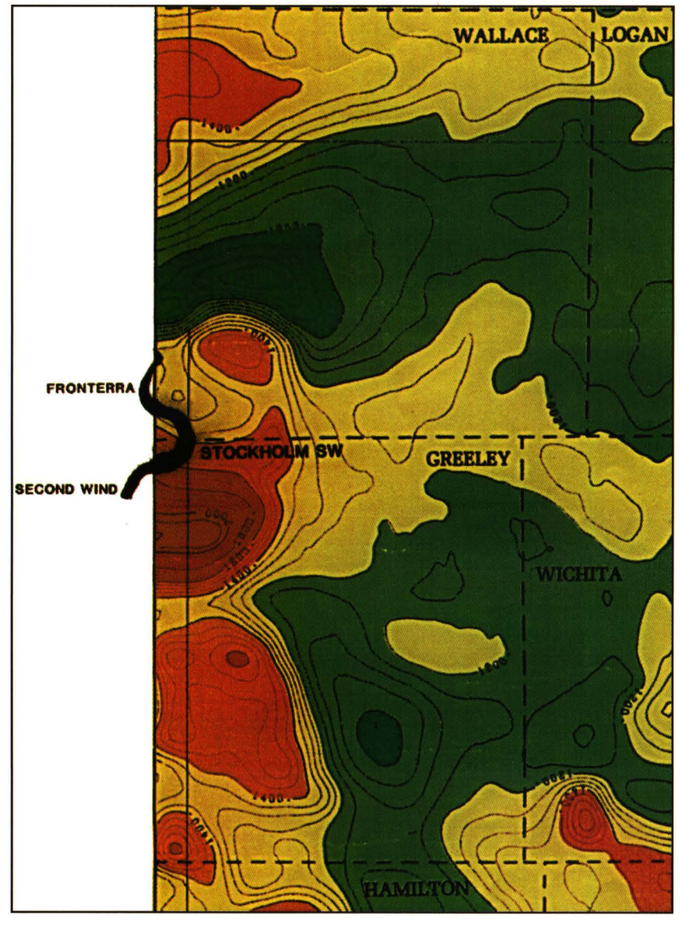

FIGURE 3—Portion of the Kansas aeromagnetic map in the Stockholm SW field area (after Yarger et al., 1981).

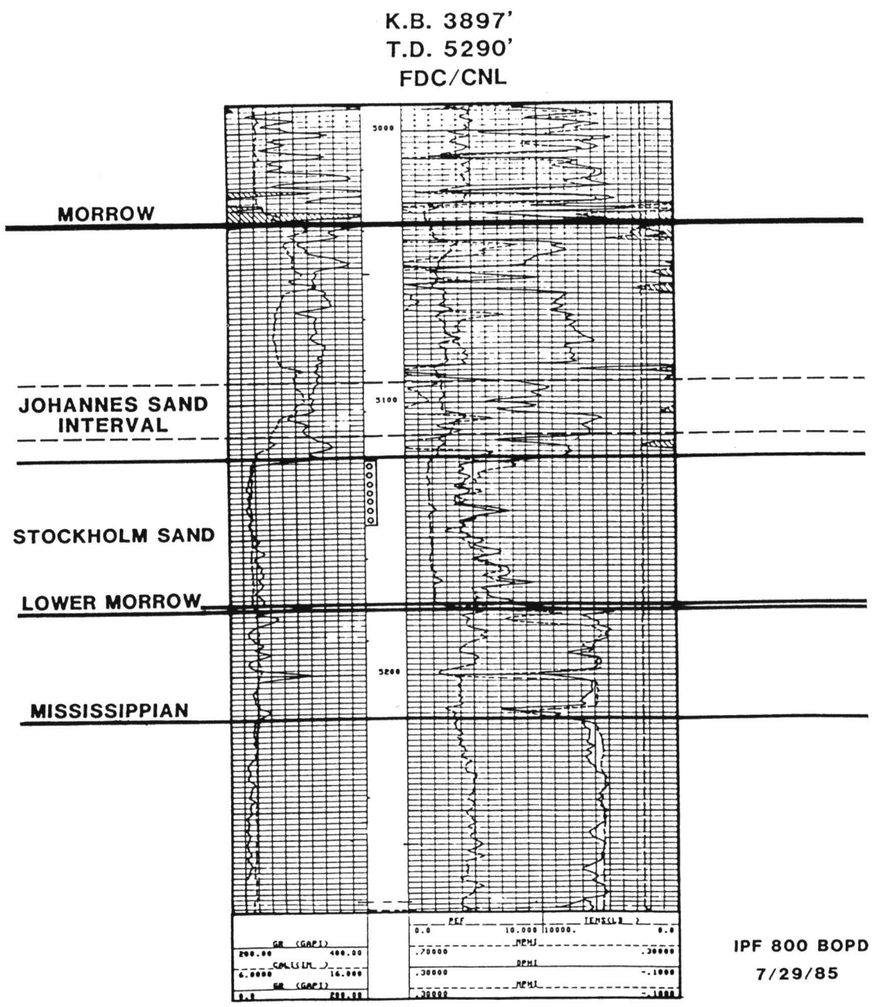

FIGURE 4—Type log, TXO–Bergquist No. 1, SW SW NE sec. 6, T. 16 S., R. 42 W., Greeley County, Kansas.

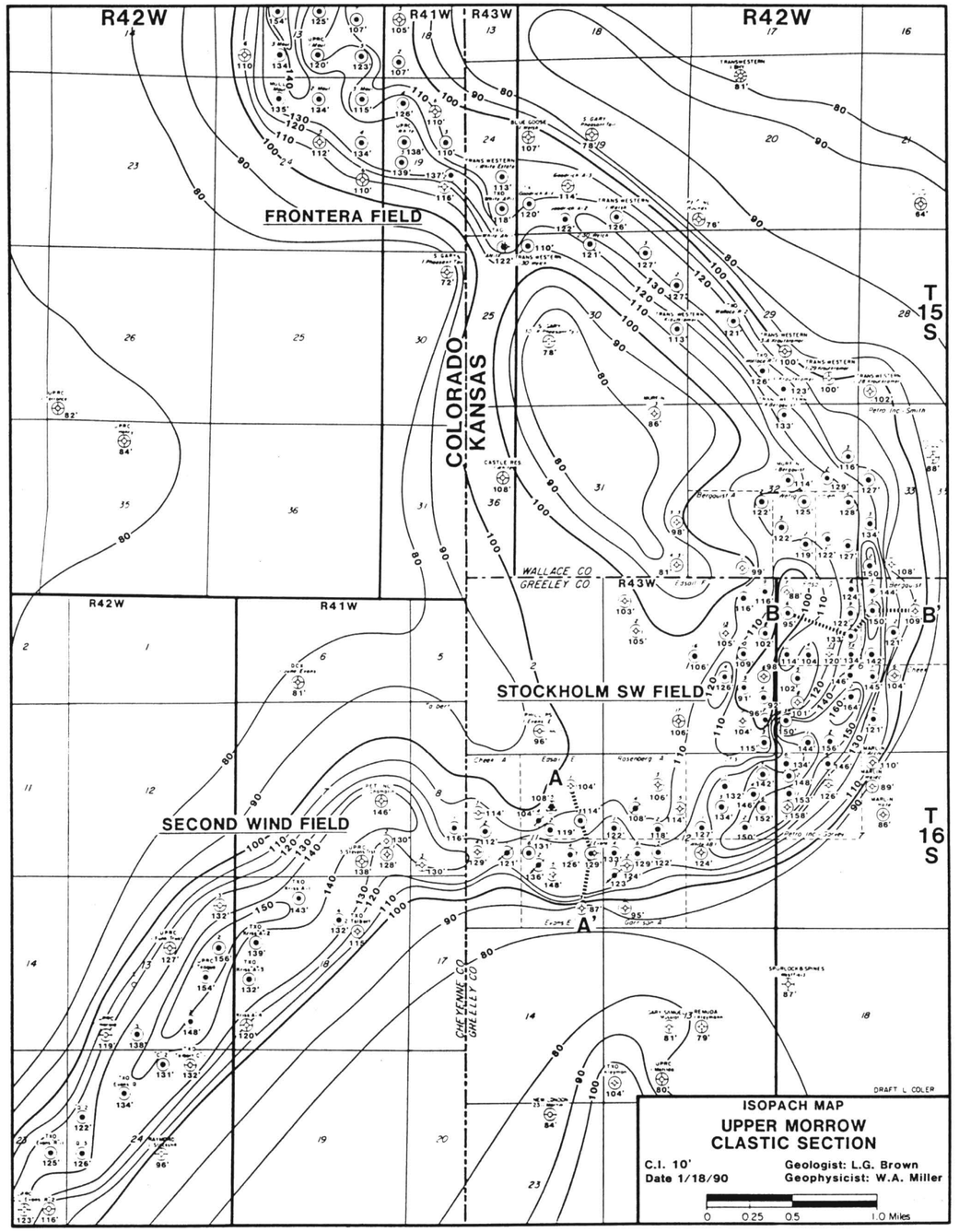

FIGURE 5—Isopach map, upper Morrow section.

thickens dramatically to the south into southwest Kansas and the Anadarko basin (Swanson, 1979). The top of the lower Morrow is overlain unconformably by the upper Morrow, and this erosional surface can create deep channel incisements into the lower Morrow. At Stockholm SW, the lower Morrow thickness ranges from 0 to 70 ft (0–21.4 m) and varies as a function of both unconformities.

The upper Morrow section in the vicinity of the Stockholm SW field consists predominantly of marine and nonmarine clastic rocks with an occasionally isolated thin, lenticular limestone bed. Average thickness of the upper Morrow is approximately 85 ft (25.9 m) in this area. Paleontological data from the upper Morrow indicate a depositional environment which ranged from shallow, open and restricted marine shelf to estuarine. The late Morrowan Anadarko sea experienced numerous episodic fluctuations in sea level which were related to global glacial events documented in the Pennsylvanian (Vail, 1977). When the Anadarko sea withdrew during a regressive phase, the Morrowan shelf sediments were subaerially exposed. Upper Morrowan fluvial systems subsequently flowed out across these exposed mud flats enroute to the Anadarko basin.

The Stockholm fluvial system created a deep incisement, or valley, into the lower Morrow limestone. In portions of the field, the lower Morrow limestone has been completely eroded and the Stockholm sandstone lies unconformably on the Mississippian. The Stockholm SW valley was subsequently back-filled with fluvial and estuarine sediments during a transgression of the Anadarko sea. The upper Morrow is up to 150 ft (45.8 m) thick in the areas of the erosional valleys (fig. 5). The Stockholm SW valley-fill system is approximately 0.5 mi (0.8 km) in width, gently meandering and non-avulving, and it experienced virtually continuous sand sedimentation along its thalweg.

The primary producing sandstone at Stockholm SW occurs at the base of the upper Morrow clastic section approximately 100 ft (30.5 m) below the top of the Morrow and is locally referred to as the Stockholm sandstone (figs. 6 and 7). The Stockholm sandstone is a fine- to coarse-grained quartz arenite and, in part, a gravel-sized conglomerate. It consists of multiple fining-upward sequences but tends to be coarsest at the base. The Stockholm sandstone reservoir consists of stacked sequences of fluvial point-bars and massive sandstones up to 61 ft (18.6 m) thick, which accumulated under estuarine conditions during marine transgressive periods.

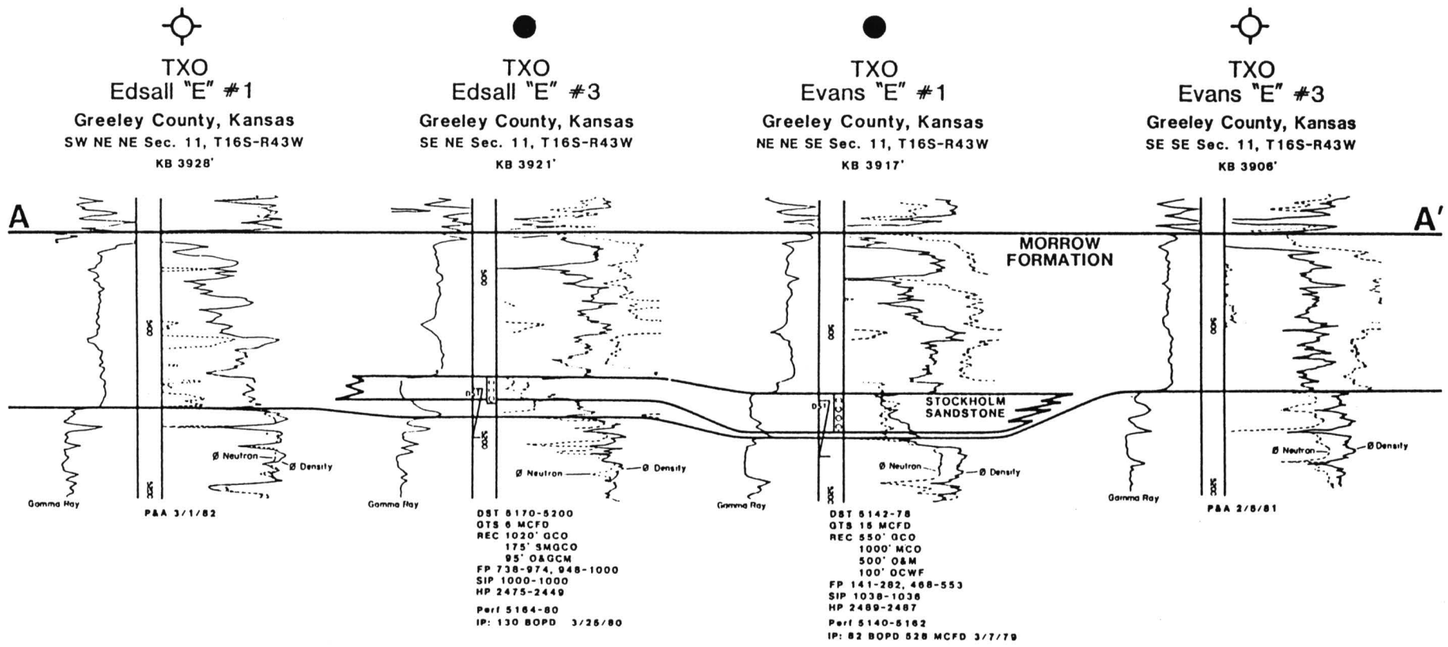

FIGURE 6—STRATIGRAPHIC CROSS SECTION A–A′. Datum is the top of the Morrow Formation. Note channel incisement into underlying lower Morrow carbonates.

Younger fluvial systems, active during post-Stockholm regressive pulses, tend to sub-parallel the pre-established Stockholm valley-fill system. These younger systems deposited the Johannes sandstone and other upper Morrow sandstones. The top of the Johannes sandstone is typically separated from the Stockholm sandstone by approximately 35 ft (10.8 m; fig. 4); however, in some areas of the field the Johannes sandstone lies in contact with the Stockholm sandstone. The Johannes consists predominantly of a series of discrete overlapping point-bars.

Exploration and Development Concepts

The Stockholm SW reservoir was initially interpreted as a marine-bar sandstone. The ubiquitous glauconite present coupled with coarsening-upwards log profiles was misleading to early geologic modeling and exploration. The key to exploration for the Stockholm sandstone was the recognition that it was related to a deeply incised valley-fill system. Various sandstone units in the upper Morrow section must therefore be correlated down from the top of the upper Morrow shale, or any other consistent regional marker in the upper Morrow section, rather than up from the top of the lower Morrow limestone (fig. 6). Employment of this model has greatly enhanced the ability of the explorationist to accurately explore for and develop this trend. After lying virtually dormant for approximately eight years, exploration and development along the Stateline trend greatly accelerated as a depositional model of the Stockholm sandstone integrated with the use of seismic data began to be understood and used effectively. Wildcat drilling extended the trend approximately 30 mi (48.3 km) with the discovery of several major fields both to the north and to the south.

A key element in the exploration for, and the development of, Stockholm sandstone-type reservoirs relates to identifying and staying within the confines of the thick sequence of upper Morrow encountered in the areas of valley-fill sedimentation. An isopach from the top of the Morrow shale to the lower Morrow limestone is a critical map in predicting the occurrence and distribution of the Stockholm sandstone (fig. 5). In the Stockholm SW field, almost all of the Stockholm sandstone development is observed to be within a thick sequence defined by this isopach (fig. 7). The additional standard techniques of structural and isopach mapping also are very important.

The Johannes sandstone deposition, while generally parallel to, or coincident with, the thick sequences of upper Morrow containing Stockholm sandstones, is not as readily predicted by this isopach-mapping technique. The general lack of continuity of the

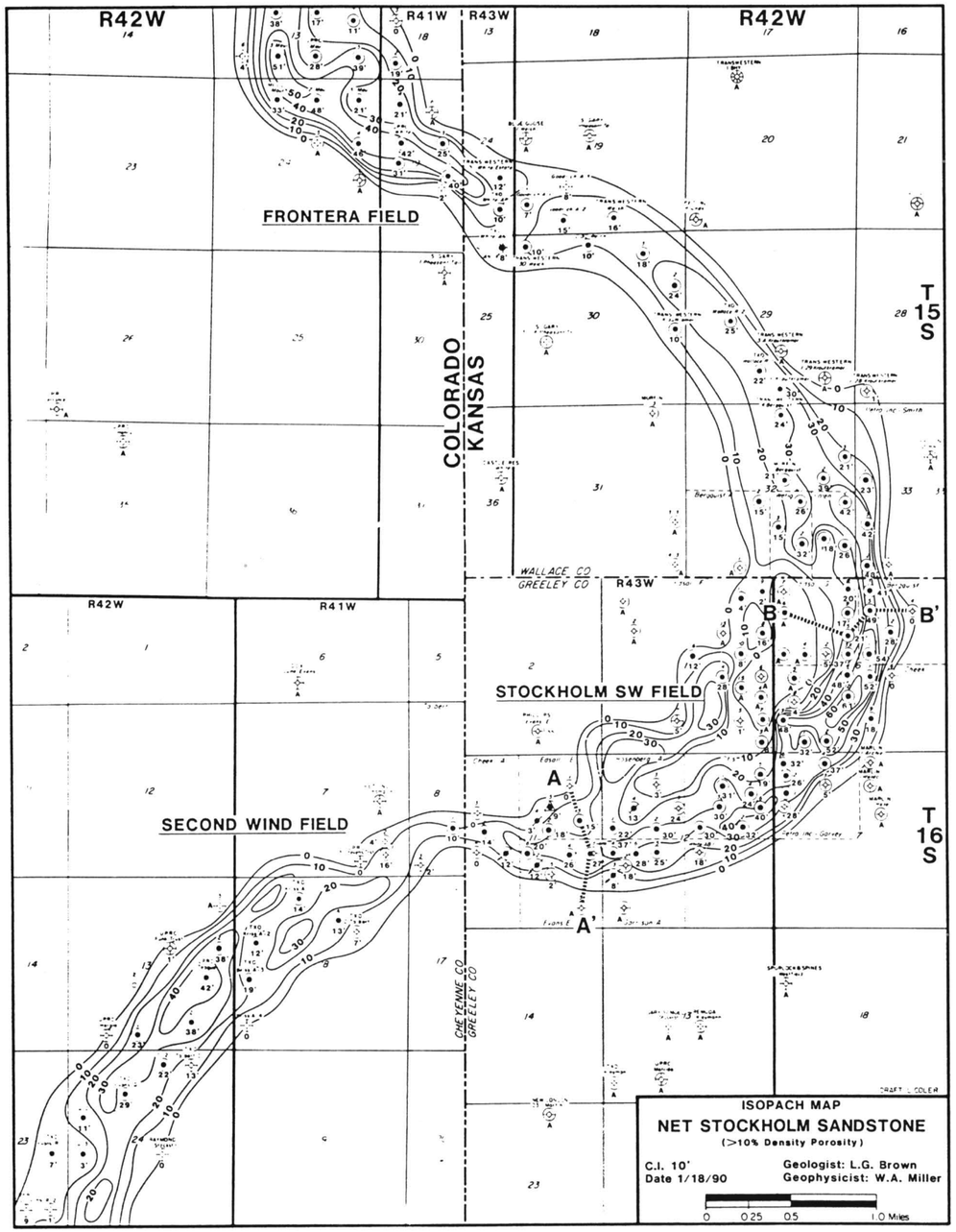

FIGURE 7—Isopach map, net Stockholm sandstone (density porosity greater than 10%).

Johannes sandstone reservoirs makes them a more difficult exploration target. The general exploration techniques employed for Johannes exploration involve detailed isopach and structural mapping.

Seismic Model

Though not used in the initial discovery of the Stockholm SW field, seismic methods have played an increasingly important role in the exploration for, and development of, the Morrow in the Stateline trend. The primary benefit of the use of seismic has been its ability to map the erosional valleys in which the Stockholm sandstone occurs. To illustrate this seismic signature, a seismic model generated from sonic log traces was constructed. Figure 8 shows an idealized sonic-log input model across the erosional valley system at Stockholm field. This input model was convolved with a zero-phase 10–15–70–80 Hz bandpass wavelet to generate the seismic-traces model response (fig. 9).

The primary contrasts in acoustic impedance that contribute the most to the seismic event are the change from carbonate to shale at the top of the Morrow, and the change from shale or sandstone to carbonate at the top of the lower Morrow limestone, or base of the upper Morrow. The Morrow shale is observed on the seismic model to be a left-deflecting trough while the top of the lower Morrow limestone is a right-deflecting peak. As the upper Morrow section thickens from less than 100 ft (30.5 m) on the flanks of the erosional valley to almost 150 ft (45.8 m) in the valley, the Morrow shale and limestone seismic reflectors diverge to the point where a "doublet" event forms over the thickest part of the Morrow channel. As the channel event begins to thin gradually on the flanks of the valley, this doublet event converges back to a single event.

The primary emphasis of mapping the valleys with seismic data has been the recognition of the "doublet" anomaly, or the actual time thickening of the Morrow section. The model illustrates one of the pitfalls in this interpretation of the "doublet" which is related to the nature of the lower Morrow limestone section. On the left portion of the model response (fig. 9), the peak at the lower Morrow limestone surface is a single event with little response immediately underneath. As the lower Morrow limestone occurs directly on top of the Mississippian carbonates, the net seismic effect is a massive combined carbonate section with the only reflecting interface being its top. The right-hand portion of the model shows a somewhat different response, and here the peak representing the top of the lower Morrow limestone is immediately followed by another peak event. This "peak-peak" response occurs where significant shale breaks develop either within the lower Morrow limestone section or at the Mississippian unconformity. Thus, the second peak creates a "doublet" appearance which in this case is not related to true thickening of the Morrow clastic section in a valley. One method of discriminating between the two signatures is to pay careful attention to the relative amplitudes of the top and bottom peaks comprising the "doublet." Experience has shown, and the model illustrates, that typically a true valley response will display more amplitude on the lower peak of the "doublet," while a "doublet" anomaly due to shale breaks below the top of the lower Morrow limestone often has more amplitude on the top peak of the "doublet." This analysis requires the data be as close to zero-phase as possible, and that all data used in the interpretation be phase-matched with a great deal of care.

A portion of actual seismic data across a Morrow channel is displayed at approximately the same scale as the model (fig. 10). There is very good agreement between the predicted model response and the actual response observed from the data.

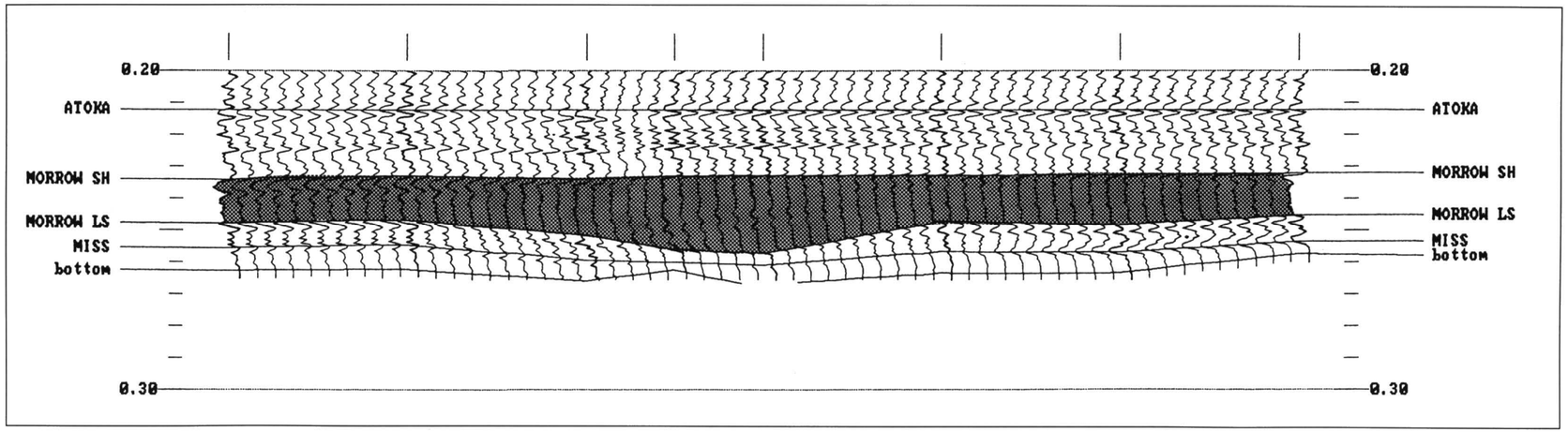

FIGURE 8—IDEALIZED MORROW CHANNEL SONIC LOG CROSS SECTION FOR INPUT INTO SEISMIC TRACE MODEL OF FIG. 9, FLATTENED ON THE MORROW SHALE. Only lower portion of section is shown to focus on the Morrow interval.

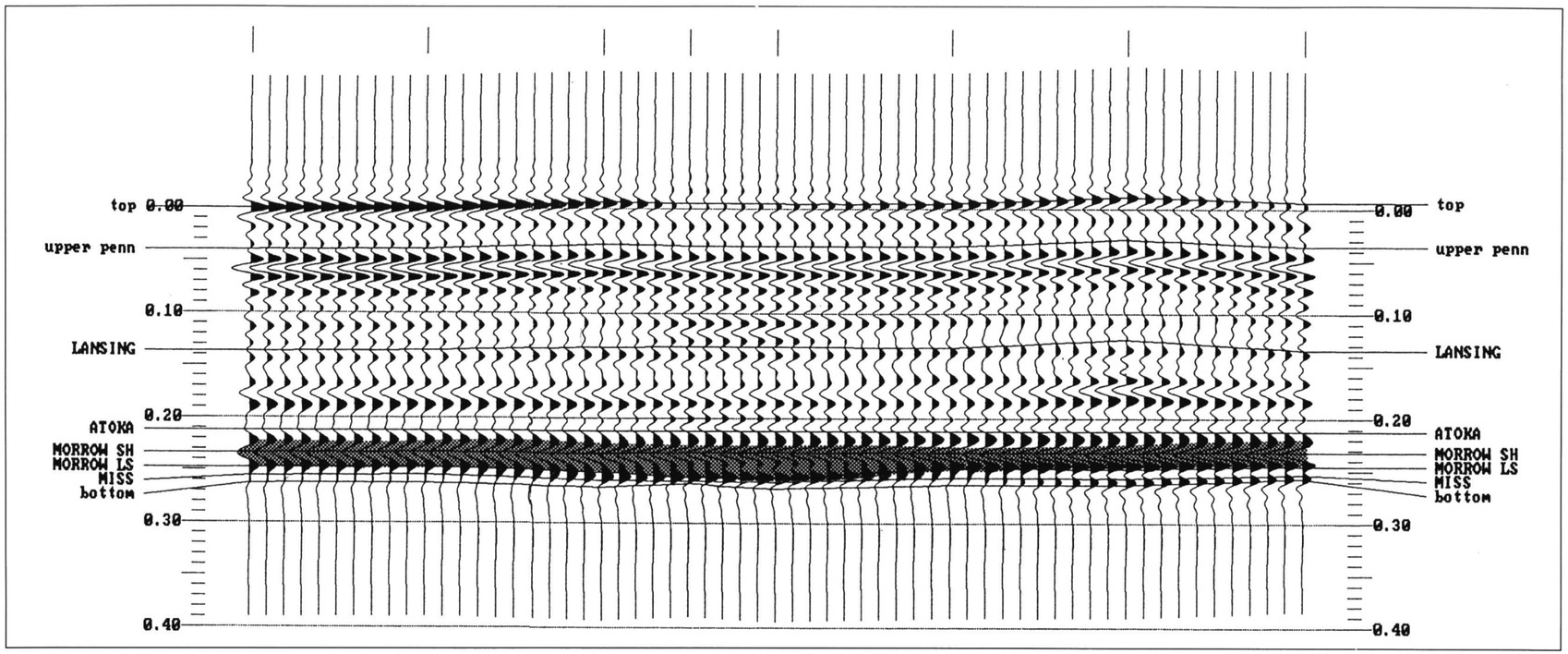

FIGURE 9—IDEALIZED MORROW CHANNEL SEISMIC TRACE MODEL GENERATED FROM THE INPUT LOG SECTION OF FIG. 8 BY CONVOLVING WITH A 10–15–70–80 HZ ZERO-PHASE WAVELET.

Seismic Data

Figure 11 is a portion of an east-west CDP-vibroseis seismic line through the Stockholm SW field in sec. 6, T. 16 S., R. 42 W., Greeley County, Kansas. The approximate location of the data in fig. 11 is indicated by cross section B–B′ on the Morrow isopach (fig 5). These 30-fold data were acquired with 120-channel recording using a group interval of 82.5 ft (25 m) and a source interval of 165 ft (50 m).

The deep incisement of the Stockholm erosional valley is apparent even at the display scale of these data. The three oil wells at the center of the section penetrated the Stockholm valley and produce from the Stockholm sandstone. The three oil wells just to the west produce from the Johannes sandstone on the flank of the main valley in a thinner upper Morrow clastic section.

A portion of the seismic data of fig. 11 was expanded to show the detailed seismic signature of the Stockholm erosional valley (fig. 12). A cross section of gamma-ray curves from the wells which tie these seismic data is shown to illustrate the change in thickness of the upper Morrow and its impact on the seismic response. As pointed out in the model discussion, the primary contrasts in acoustic impedance that contribute the most to the seismic event are the change from carbonate to shale at the top of the Morrow, and the change from shale or sandstone to carbonate at the top of the lower Morrow limestone, or base of the upper Morrow. The Morrow shale is observed on the seismic data to be a left-deflecting trough while the top of the lower Morrow limestone is a right-deflecting peak. As the upper Morrow section thickens from less than 100 ft (30.5 m) in the Edsall "G" No. 6 well to almost 150 ft (45.8 m) in the Bergquist No. 5 well, the Morrow shale and limestone seismic reflectors diverge to the point where a "doublet" event forms over the thickest part of the Morrow channel. As the channel event begins to thin gradually into the Bergquist No. 4 well, the doublet event converges back to a single event.

Synthetic seismogram traces generated from sonic and density logs run in the Bergquist No. 2 well are spliced into the seismic data of fig. 12 to show the tie with the subsurface data. Studies utilizing synthetic seismograms have shown that the generation of the "doublet" seismic event is primarily due to a tuning phenomenon as the Morrow shale to lower Morrow limestone interval thickens. As seen by the tie with the Edsall "G" No. 6 well, a Johannes sandstone lying in a thinner upper Morrow interval is, for all practical purposes, seismically transparent with this type of seismic data, which has a dominant frequency of about 65 Hz.

Seismic data have proved very effective in mapping the upper Morrow valleys in which Stockholm sandstones were deposited. The prediction of sandstone within these valleys, however, requires not only a knowledge of valley geometry but also an understanding of depositional environments. Development to the southwest of the Stockholm SW field in the Second Wind field was aided by the use of 3D seismic data, which can predict upper Morrow thickness changes as well as local structural changes with much greater precision than standard 2D seismic data.

Another geophysical tool that can be useful in the exploration for Morrow sandstones is magnetic data. Such data are most effective in mapping basement fault and compositional trends that may have had some indirect influence on later Morrow depositional trends.

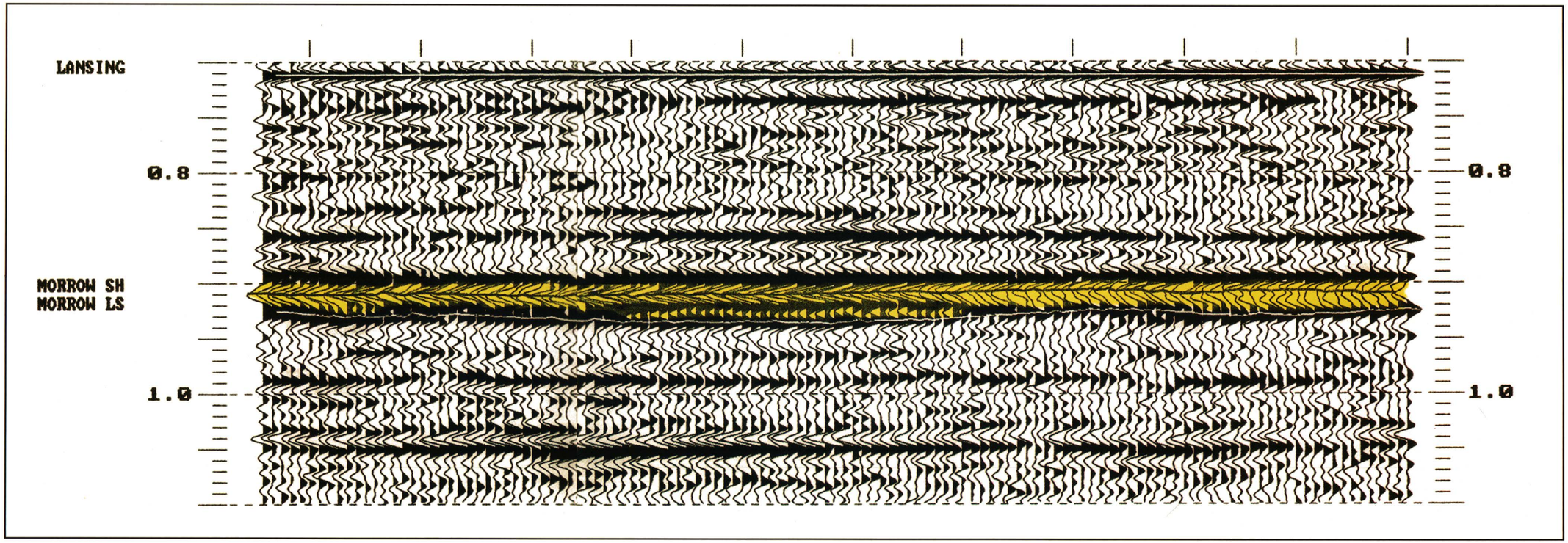

FIGURE 10—Actual seismic data example over a known Morrow channel, plotted to the same scale as the model in fig. 9 for comparison.

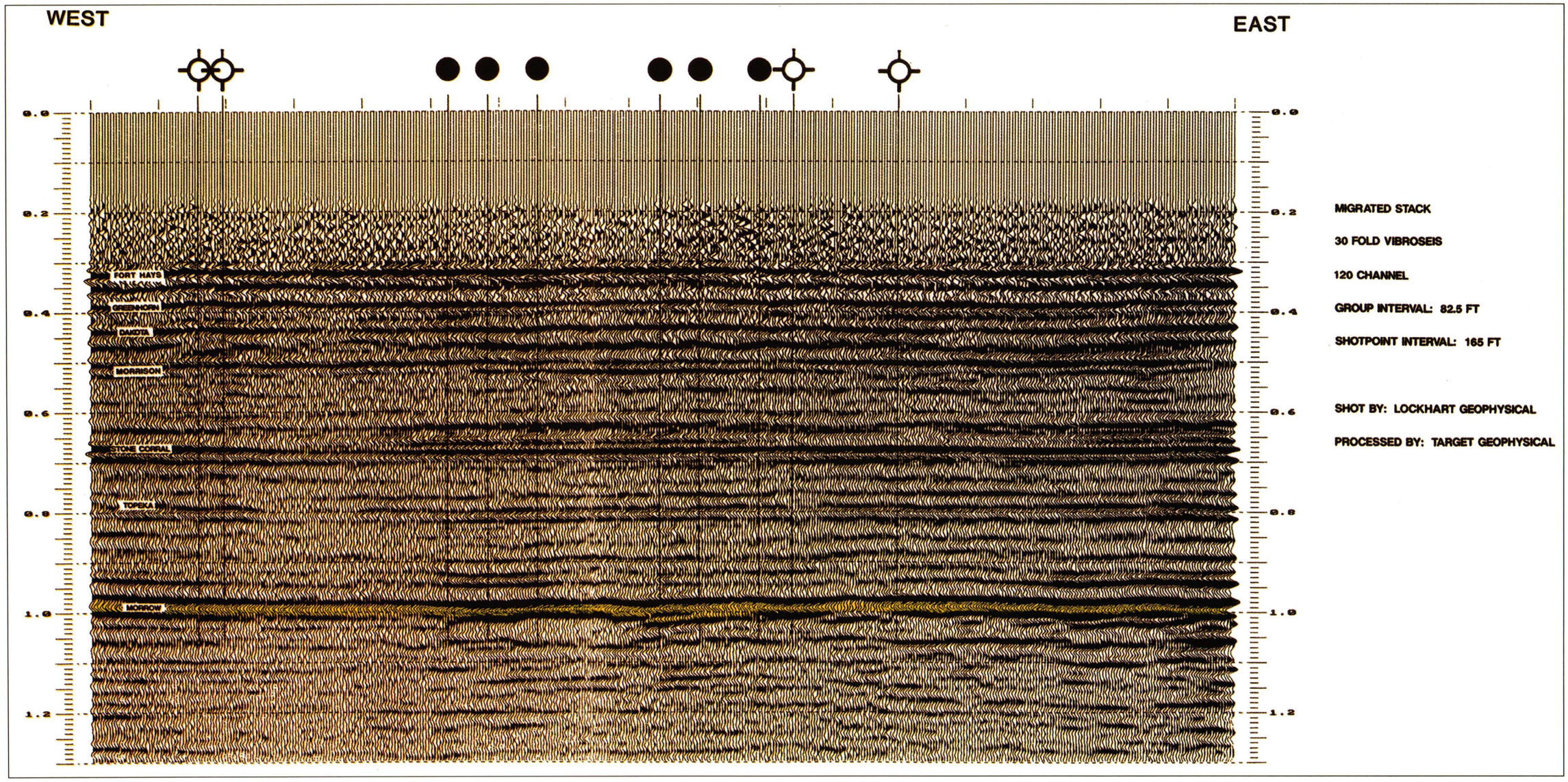

FIGURE 11—East-west seismic line across Stockholm SW field through the north half of sec. 6, T. 16 S., R. 42 W. and sec. 1, T. 16 S., R. 43 W. (Exact shotpoint locations not shown at owner's request.)

Conclusions

The discovery of Stockholm SW rekindled interest in the Morrow play of southeast Colorado and western Kansas. Few would have expected a productive trend with over 250 producing wells spanning greater than 30 mi (48 km) to exist in this previously dormant area. The true extent of the play is still not clear. However, the impact of the play on the oil and gas industry of the region is dramatic, and the potential the play holds has kept operators active in the trend. The development of the Stateline trend has resulted in a better understanding of the valley-fill model of sedimentation, as well as an advancement in the use of seismic stratigraphy and associated modern seismic technology in this area. The lessons learned throughout the course of this activity increase the likelihood that the search for other such plays will be equally as successful.

ACKNOWLEDGMENTS—This paper originally appeared under the same title and by the same authors in the Rocky Mountain Association of Geologists 1990 Guidebook, *Morrow Sandstones of Southeast Colorado and Adjacent Areas*. Although the paper has since been modified, many of the figures and much of the text are the same as previously published. The authors would like to express their appreciation to the Rocky Mountain Association of Geologists for allowing much of this paper to be republished.

The authors also would like to acknowledge individuals previously employed by TXO who provided invaluable assistance, particularly Larry Coler for drafting the figures and Larry Webster for coordinating the reduction of final figures. Doug Isern and Rick Olmsted of Transwestern Petroleum, Mark Germanerio and Ross Matthews of UPRC, Inc., and Dallas Donner of Mull Drilling Co., Inc, provided additional well data that made this paper complete. A final acknowledgment is due Loren E. Avis, formerly of TXO, who is responsible for the drilling of the Stockholm SW discovery well.

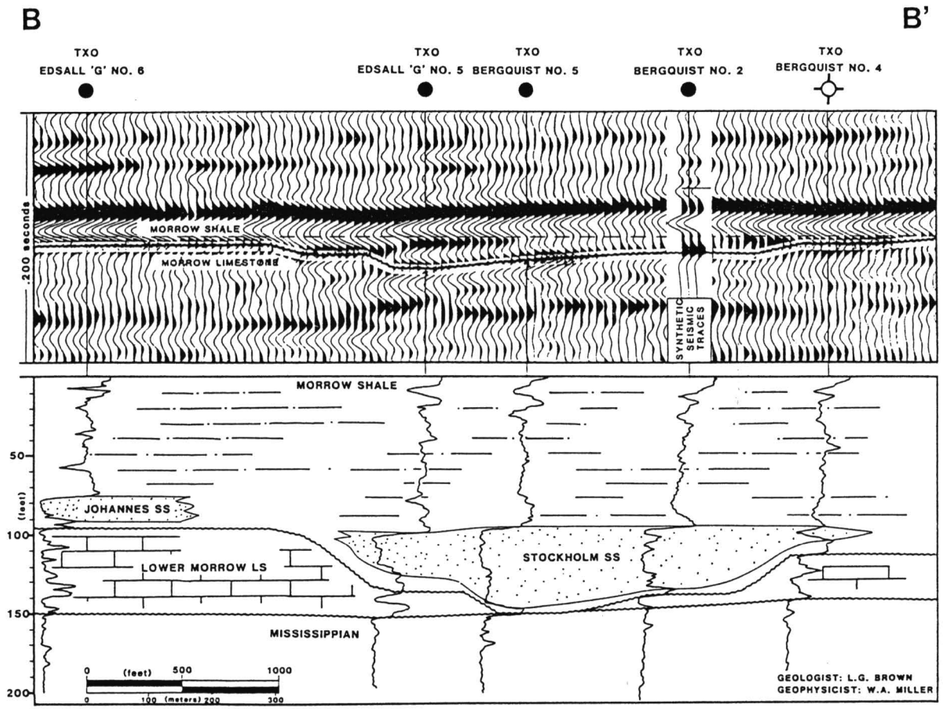

FIGURE 12—COMPOSITE STRATIGRAPHIC/SEISMIC CROSS SECTION B–B′. Note channel incisement and corresponding seismic anomaly.

References

Hurlbut, C. S., Jr., 1971, Dana's manual of mineralogy: John Wiley and Sons, New York, New York, 18th edition, 579 p.

Pettijohn, F. J., Potter, P. E., and Siever, R., 1972, Sand and sandstone: Springer–Verlag, New York, New York, 618 p.

Rader, K., 1987, Petrographic and subsurface analysis of Pennsylvanian Morrow sandstones of southwest Kansas: M.S. thesis, University of Colorado, Boulder, 106 p.; available from Kansas Geological Survey, Open-file Report 87–31

Stone, D. S., 1968, Wrench faulting and Rocky Mountain tectonics: The Mountain Geologist, v. 6, p.67–79

Swanson, D. C., 1979, Deltaic deposits in the Pennsylvanian Upper Morrow Formation of the Anadarko basin; *in*, Pennsylvanian Sandstones of the Midcontinent, N. J. Hyne, ed.: Tulsa Geological Society, Tulsa, Oklahoma, p. 115–168

Vail, P. R., Mitchum, R. M., and Thompson, S., 1977, Global cycles of relative changes of sea level; *in*, Seismic Stratigraphy—Application to Hydrocarbon Exploration, C. E. Payton, ed.: American Association of Petroleum Geologists, Tulsa, Oklahoma, p. 83–98

Yarger, H. L., Robertson, R. R., Martin, J., Ng, K., Sooby, R. L., and Wentland, R. L., 1981, Aeromagnetic map of Kansas: Kansas Geological Survey, Map Series M-16, 1 sheet

Exploration Case History, Coats South Area, Barber County, Kansas

Dennis E. Hedke[1], I. Wayne Woolsey[2], and L. A. Nicholson[3]
[1]Consultant, Wichita, KS 67202; [2]Woolsey Petroleum Corporation, Wichita, KS 67202; and
[3]Pickrell Drilling Co., Inc., Wichita, KS 67202

Abstract

The Coats South area is situated in north-central Barber County, Kansas, immediately east of the southern limit of the Pratt anticline. The geologic setting encompasses a variety of structural and stratigraphic traps. The case study discussed herein involves exploration targets in Mississippian- and Ordovician-aged carbonates and cherts. The trap for either target zone is stratigraphic. Recently (1991) acquired multifold Vibroseis data have been examined in an effort to characterize the reservoirs and the relatively complex structure and stratigraphy proximal to the Pratt anticline.

Significant topographic variation, highly variable materials in the weathered zone, and local areas of high data attenuation within the study area present special data-processing difficulties. These difficulties can be overcome by careful integration of known geologic constraints and iterative static solutions.

Seismic models of those geologic conditions relevant to hydrocarbon traps in the study area correlate well with processed seismic sections. The data utilized in this study are of sufficiently high frequency content that stratigraphic pinchouts and other thin-bed phenomena are clearly distinguishable on both conventional and enhanced trace-attribute plots. As a general rule, structure plays a minor role in the stratigraphic traps evaluated in this study.

Introduction

The Coats South study area is geographically situated in north-central Barber County, Kansas (fig. 1). As is evident from the production index map (fig. 2), numerous horizons with oil and gas potential have been exploited in the region. While the region is mature from an exploration standpoint, the region continues to yield significant discoveries. This paper will focus on various seismic indicators related primarily to stratigraphically entrapped Mississippian- and Ordovician-aged reservoirs. Other significant production is also yielded by various Pennsylvanian-aged reservoirs. These will not be discussed herein.

Production in the study area is controlled by structural, stratigraphic, and combination traps. Log cross sections and contour maps presented below demonstrate a variety of these controls. The purely stratigraphic traps are considerably more difficult to identify/predict in advance of drilling. Geologic indicators of such traps typically lack the level of detail necessary to yield either two-dimensional or three-dimensional control. Multifold seismic control, however, is capable of imaging these exploration targets and providing insight into reservoir development and reservoir quality definition.

Recent acquisition (1991) of detailed seismic coverage both perpendicular and parallel to the Pratt anticline has allowed for detailed reservoir-zone analysis and realistic structure mapping from an area of significant near-surface velocity contrast and gentle to moderate terrain. Some of these results are presented in this paper. Due to the proprietary nature of the data, specific profile location will be withheld in order to preserve confidentiality.

Subregional Geological Conditions

Portions of four townships comprising the Coats South study area (fig. 2) include some rather striking geological anomalies. Faulting on the east limb of the Pratt anticline, coupled with substantial stratigraphic zone variations present challenging interpretive problems, both from a modeling standpoint as well as subsurface correlation to seismic data.

An example of the abrupt subsurface structural change is indicated by contours on top of the Arbuckle (fig. 3). Note that the fault zone along the east limb of the Pratt anticline is offset laterally at numerous junctions. These offsets are indicated to be conjugate fracture zones related to the primary fracture set which tends locally to be more north-south in orientation. Note also that numerous structural closures, both on upthrown and downthrown blocks have yielded significant oil and gas accumulations (e.g., Coats field).

Significant reservoirs occur in primarily two key intervals in the study area: Mississippian and Ordovician Viola cherty porosity. The geologic histories of these

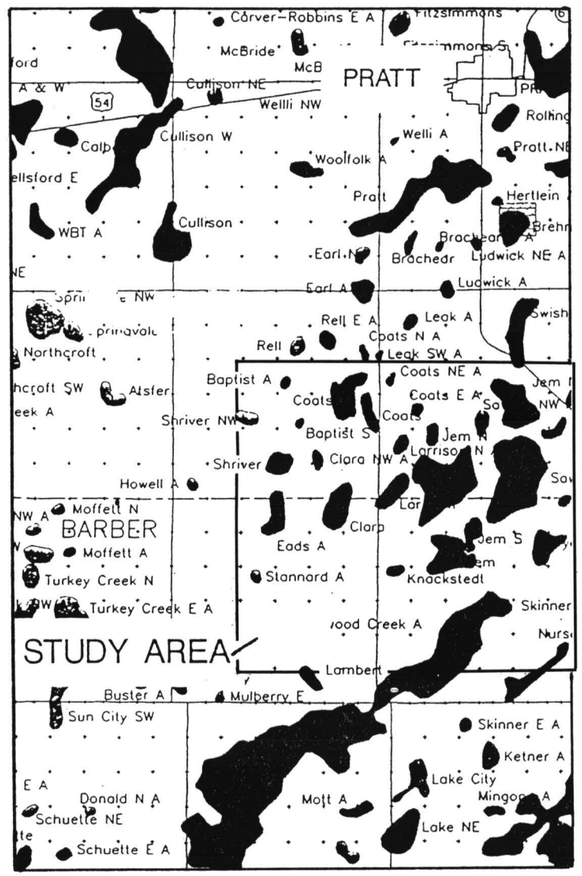

FIGURE 1—Regional location index, study area proximity to Pratt anticline, and regional geological features.

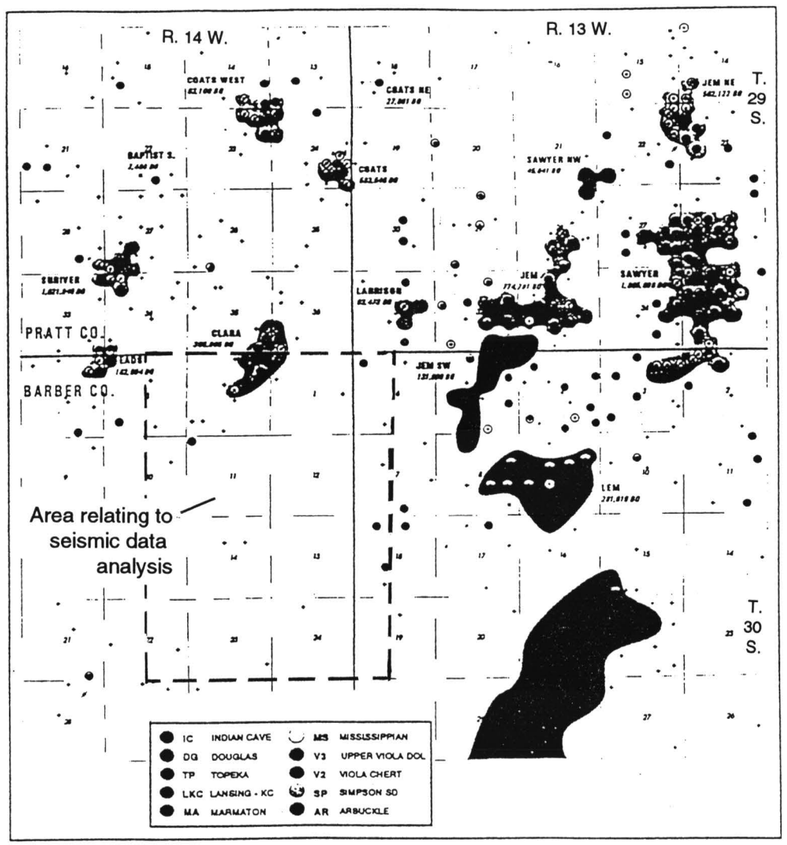

FIGURE 2—Production index map of portions of T. 29 and 30 S. and R. 13 and 14 W., Pratt and Barber counties, Kansas.

buildups is not completely understood. Clearly, however, some zones have developed secondary porosity. Complicated fluid migration and hydrodynamic or possible gas drives also play roles in final trap configurations and integrity. An indication of stratigraphic diversity over an interval encompassing Mississippian and Kinderhook sediments is evident in an isopach map of Marmaton–Viola (fig. 4). Similar maps (not shown here) can be generated to support exploratory development efforts for Viola targets. Log characteristics of stratigraphy from the Marmaton through the Arbuckle is shown on cross section B–B´ (fig. 5). This structural profile gives an idea of the level of complexity under consideration for seismic modeling. Vertical as well as lateral variation can be pronounced.

Seismic Modeling

Due to the structural and stratigraphic variation indicated by mapping and log cross sections, accurate seismic correlation is an essential ingredient to overall seismic-profile definition. Synthetic seismic signatures in one- and two-dimensions (1D and 2D) have been generated in support of the cases analyzed in this study. For 1D vertical control, sonic and density logs have been utilized from a well located at approximately NW NW NE sec. 14, T. 30 S., R. 14 W., to generate a synthetic seismogram (fig. 6). This downthrown-block well provides excellent detail of a particularly well developed Mississippian porosity zone; Viola and Simpson sections are also fairly developed in this well. At the time of this writing, this well was awaiting hookup to a natural gas pipeline, with the expectation of production from Mississippian chert. Other details are not available. Many upthrown-block wells have zero Mississippian section, though they may contain restricted Kinderhook and fully developed Ordovician sections.

A 2D synthetic seismic profile has also been generated utilizing the above well as a basis. This model is presented below where actual data can be viewed for direct comparison (see figs. 9 and 10).

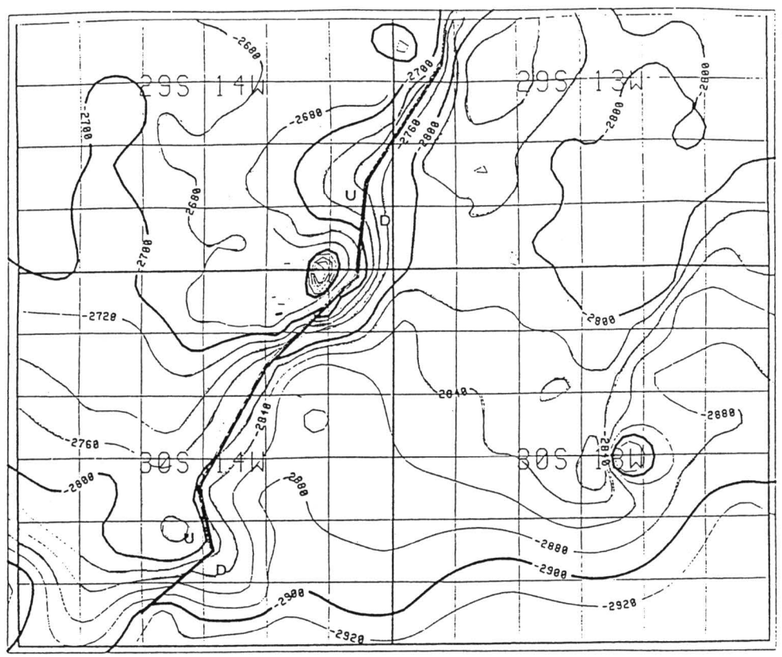

FIGURE 3—Structural configuration, top Arbuckle. Note vertical offset east of fault zone is approximately 150 ft (45 m).

Representative Seismic Profiles

Seismic data from the study area demonstrate the significant structural and stratigraphic variation indicated by log profiles presented earlier in this paper. The seismic profile chosen for display is oriented more or less perpendicular to the fault zone prevalent along the east limb of the Pratt anticline. Although the exact seismic profile location is proprietary, the well location shown near the center of the cross section is in close proximity to the profile; this is the well utilized in the synthetic modeling of the previous section.

Figure 7 is an unannotated "conventional" structural profile, covering the full stratigraphic section from surface to basement. Annotation for the profile (fig. 8) gives various formation boundaries and places the fault zone near station number 165. These profiles are displayed at a "typical" vertical scale of 10 inches per second (10 IPS). Horizontal scale is 15 traces per inch (15 TPI). Group interval is 82.5 ft (24.8 m), equating to a horizontal distance of about 1,200 ft/inch (930 m/cm). Vertical depth at 700 milliseconds (msec) is approximately 4,300 ft (1,290 m). This yields a vertical exaggeration of approximately 2× at 700 msec. Note that while the annotated profile shows "obvious" faulting, the unannotated profile may leave some room for interpretation. Also note that the total geological section over the Marmaton to Viola interval occurs over a relatively limited seismic interval. At a scale of 10 IPS, details related to these critical zones are barely visible.

The 2D seismic model referred to above is presented in fig. 9. In this display, vertical scale is 20 IPS, horizontal scale is relative, trace spacing is 6 TPI. The model has been generated to highlight particularly the thickness changes in Mississippian chert and the overall Viola. In the center of the model, Mississippian chert thickness is 50 ft and total Viola section is 64 ft (19 m). On the upthrown block, or model left, Mississippian chert is absent and total Viola is 50 ft (15 m). On the right end of the model, Mississippian chert thickness is 30 ft (9 m), Viola thickness is 110 ft (33 m). Variable interpolation rates have been applied from left to right to match the rate of horizontal geological change. The model has been generated with 5% noise added.

For comparison to actual data, the same data set utilized in figs. 7 and 8 has been redisplayed at a vertical scale of 20 IPS and a trace spacing of 40 TPI, with every third trace shown to compare model to actual data (fig. 9). Vertical exaggeration in this profile is approximately 5.4×. In contrast to the model, actual data have not been flattened at Heebner time. Note that while agreement between model and data is not perfect, good overall agreement is very much in evidence. Among other points of interest:

1. Frequencies and wavelet response immediately below the base Mississippian chert from station 165 to about station 230 are clearly anomalous. Drilling has confirmed oil- and gas-saturated chert, with thickness of 50 ft (15 m) in the vicinity of station 210. The actual well referred to was situated about 600 ft (180 m) out of the plane of this profile.
2. The right-most portion of actual data at Viola time shows a developed peak amplitude event at the top Viola. The model does show a developing amplitude response, but much weaker. Overall zone thickness comparison between model and data is very good.

The somewhat "choppy" appearance of the data is due to the third trace increment chosen in order to redisplay data at approximately the same relative horizontal scale as the model.

To provide an idea of overall data quality, an expanded scale profile of this same data set is shown in fig. 11. In this display, the trace attribute of instantaneous frequency displayed at a horizontal scale of 15 TPI (same as figs. 7 and 8) while vertical scale is 30 IPS, yielding a vertical exaggeration of approximately 6×. This profile shows very

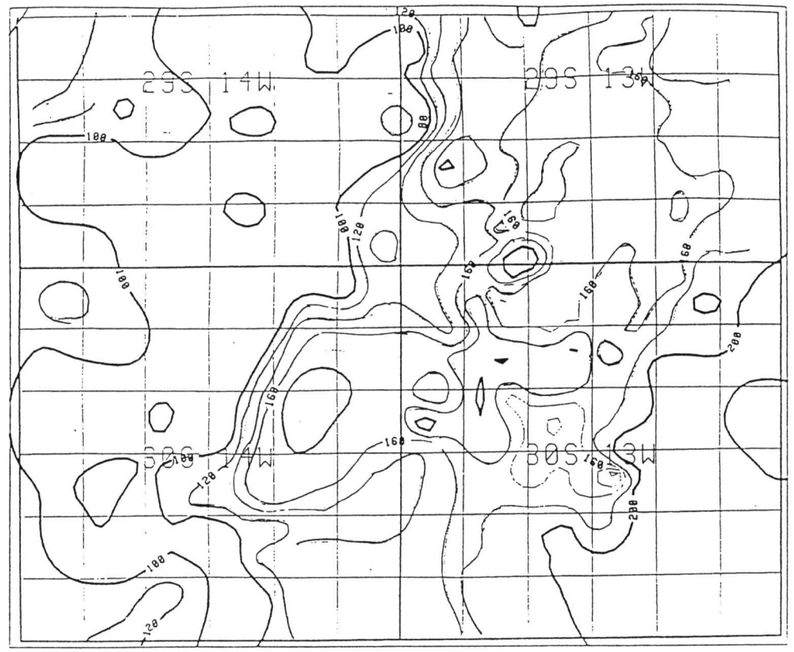

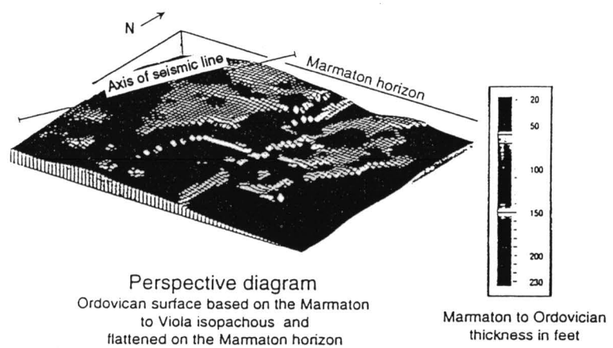

FIGURE 4—A) Isopach map of Marmaton–Viola. This interval emphasizes particularly the variation of Mississippian-aged sediment thickness. B) Perspective diagram of Ordovician surface at close of Marmaton time.

clearly both the structural and stratigraphic change occurring over the length of the profile. Structurally, the prominent Arbuckle event shows the full measure of displacement across the east-limb fault zone. Two-way time displacement is approximately 20 msec (0.020 sec); well control verifies structural-depth displacement at the top Arbuckle is greater than 150 ft (45 m). Although results are somewhat premature, an apparently productive zone in Mississippian chert has been encountered at the equivalent of station 210 in this profile. Note that a significant frequency change occurs between the Base Pennsylvanian and Base Mississippian chert from stations 197–212. Note also that a frequency anomaly occurs below the Base Mississippian chert, where between stations 200–230, frequencies consistently range from 36 to 48 Hz. Both left and right of this zone, frequencies are consistently above 50 Hz. This condition is weakly developed between stations 168–190. It is also apparent that frequencies in the Viola are significantly reduced between stations 173–230. These frequency distributions are significant in that velocity and frequency are directly related as follows:

$$v = f\lambda,$$

where v is velocity of the material, f is wave frequency, and λ is wavelength. Insofar as wavelength will remain relatively constant through a given time window, this relationship should yield relative velocity change within particular zones. Without going to a detailed model building and seismic trace inversion of amplitude to velocity, this display provides a quick look at potential velocity variation within any given zone.

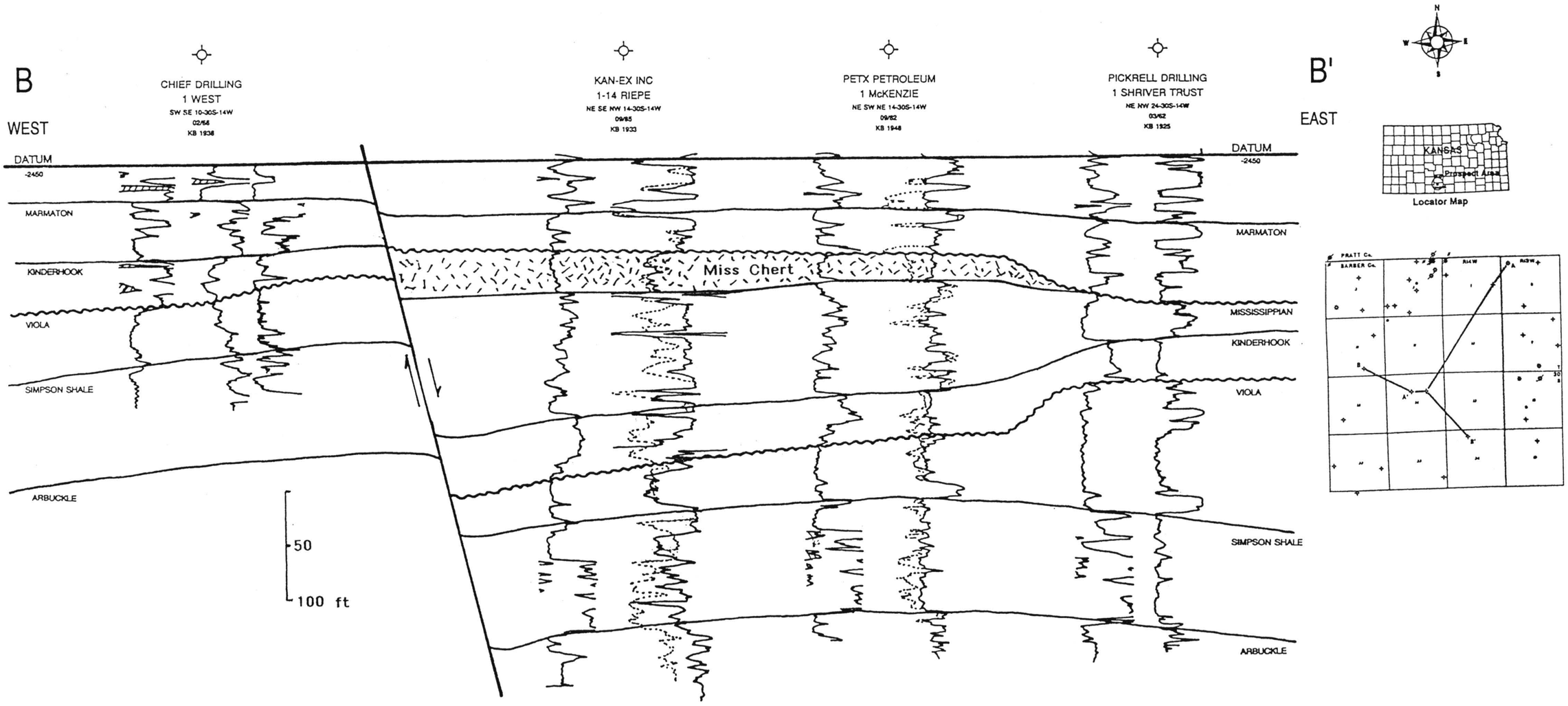

FIGURE 5—Structural cross section B–B´. Note variation of Mississippian-aged sediments as well as those of Ordovician Viola.

Summary/Conclusions

The datasets presented herein clearly illustrate the utility of seismic data in the Coats South study area. Multifold sampling, with particular objectives in the Mississippian- and Ordovician-aged sediments, has yielded accurate and detailed correlation. Higher input frequencies, coupled with processing geared toward true amplitude recovery, has assisted in refinement of stratigraphic zone characterization. As in all stratigraphic plays, signal quality must be maintained at the highest possible level. Three-dimensional (3D) sampling and processing may very well aid exploration for this type of play in the future.

In any case, it is also apparent that while conventional displays will continue to suggest wavelet character anomalies which have significant stratigraphic counterparts, carefully applied trace-attribute analysis will also play a continuing and expanding role in overall anomaly characterization. Beyond the tools demonstrated in this study, techniques related to wavelet inversion (amplitude -> velocity) as well as AVO, will almost certainly play increasingly more important roles in these types of stratigraphic plays.

Appendix

Acquisition and Processing Parameters

ACQUISITION (Lockhart Geophysical, Denver, CO) 1991

Source:	Vibroseis
Pilot:	20–128 Hz, 16 seconds × 12 sweeps
Sample rate:	2 msec
Source Array:	4 vibrators over 82.5 ft (24.8 m)
Source Interval:	165 ft (49.5 m)
Group Interval:	82.5 ft (24.8 m)
Spread:	Split
Near Offset:	412.5 ft (124 m)
Far Offset:	5,362.5 ft (1,608 m)
Group Array:	12 phones @ 7.5 ft
Instruments:	DFS V
Recording filters:	18–128 Hz
No. channels:	120 /240 (Swath surveys)
Nominal fold:	30

PROCESSING: (ECHO Geophysical Corporation, Denver, CO)

* Demux and gain recovery
* Geometry and trace edit
* Apply refraction statics
  Datum: + 1,800
  Vc: 7,000 ft/sec
* CDP gather
* Brute velocity analysis
* Final velocity analysis
* Auto surface consistent statics
* CDP trim statics
* Stack (30 fold)
* Spectral whitening
* F–X predictive filter
* Filter frequency: 15–20–90–105
* Trace equalization

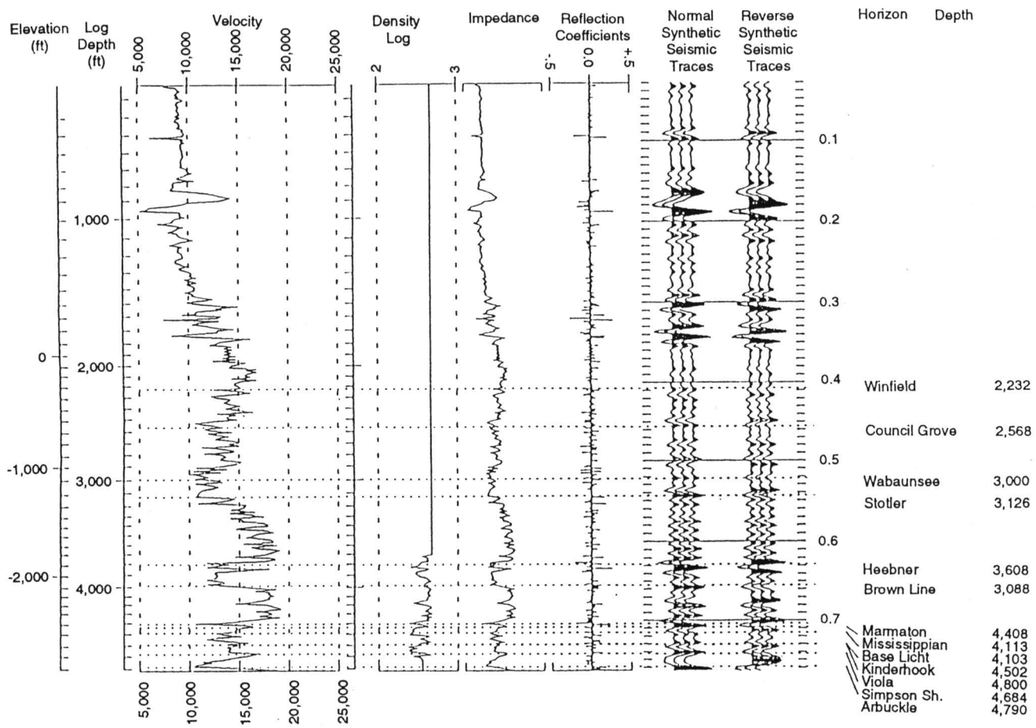

FIGURE 6—One-dimensional (1D) synthetic seismogram generated from Woolsey Petroleum Corporation—McKenzie # 1, NW NW NE sec. 14, T. 30 S., T. 14 W., Barber County, Kansas. Bandpass filter = 15–20 / 90–105. Vertical scale = 10 IPS. Winfield through Arbuckle annotated.

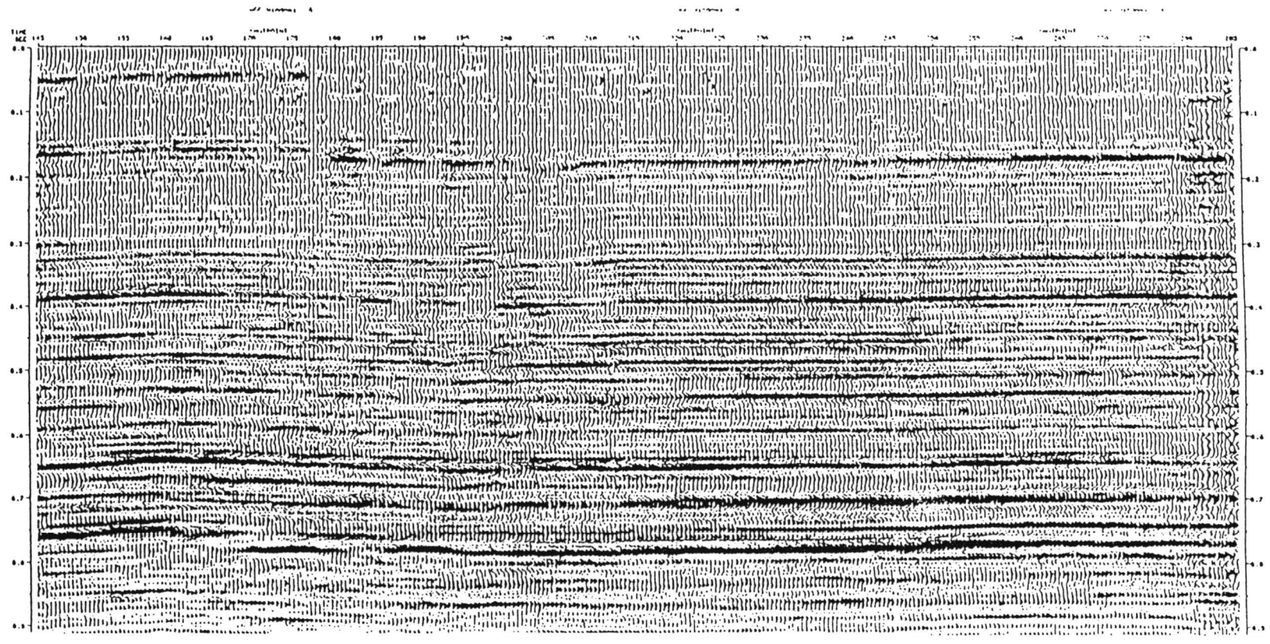

FIGURE 7—Conventional structural profile. Horizontal scale = 15 TPI; vertical scale = 10 IPS., V. E. = 2× at 700 msec.

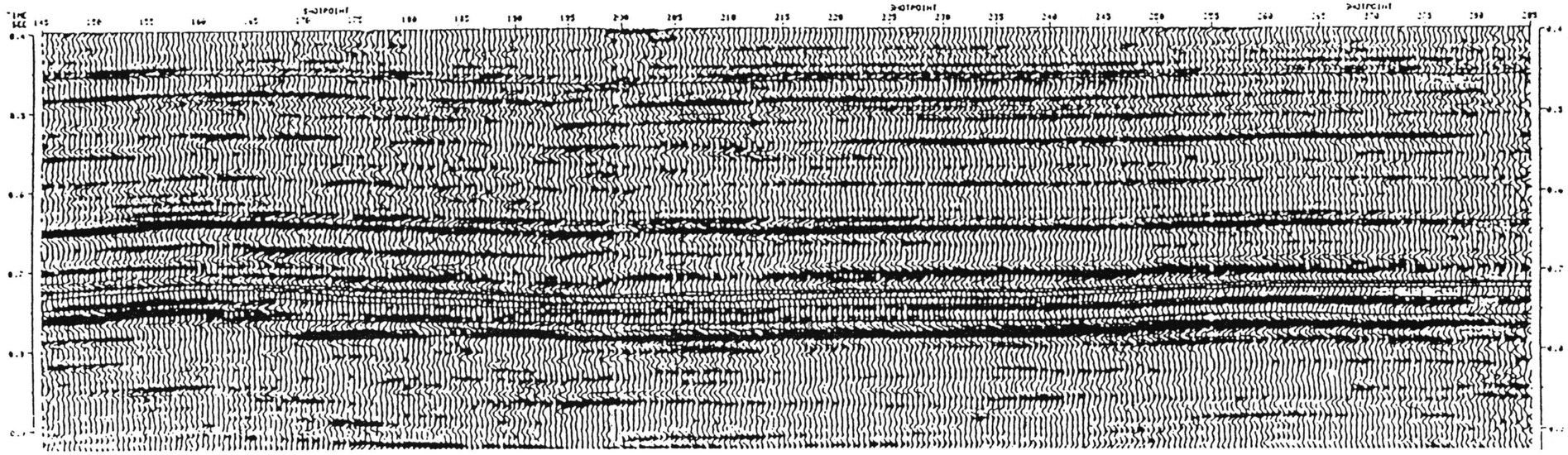

FIGURE 8—ANNOTATED SEISMIC PROFILE. Note that Marmaton–Viola interval (approximately 20 msec) contains considerable stratigraphic variation, most of which is not visible on this conventional profile. See text for detailed discussion.

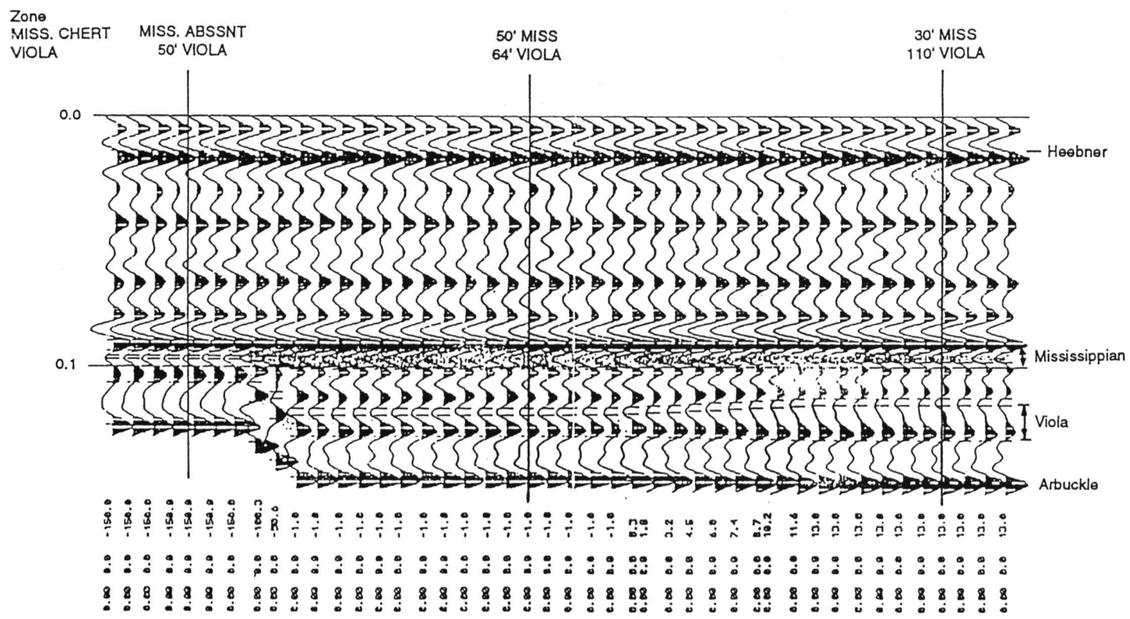

FIGURE 9—2D MODEL EMPHASIZING VARIATION IN MISSISSIPPIAN CHERT AND VIOLA. Horizontal scale is relative, vertical scale 20 IPS. Heebner–Arbuckle interval isolated. See related seismic profile fig. 10.

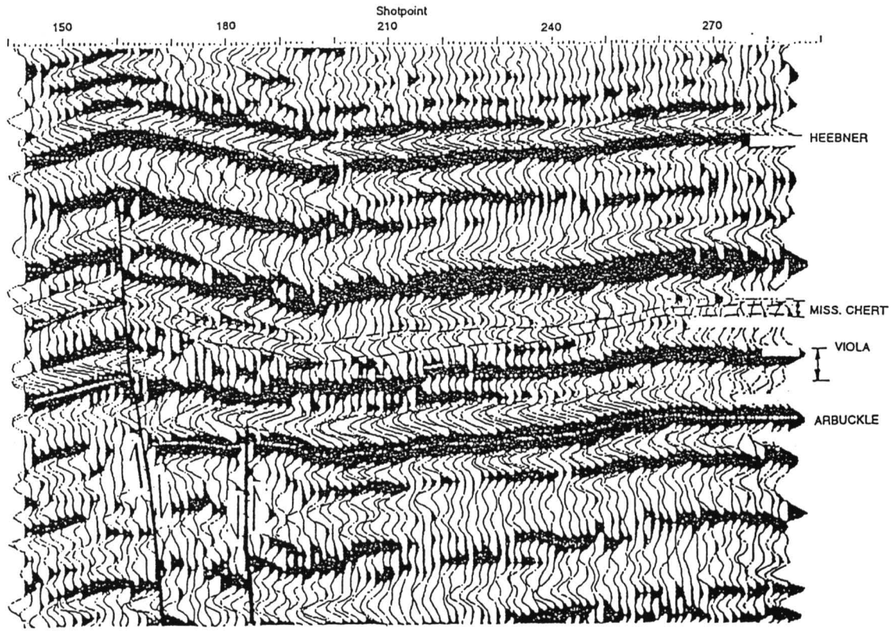

FIGURE 10—SAME PROFILE AS FIGS. 7 AND 8, REDISPLAYED AT 40 TPI AND 20 IPS TO MATCH MODEL OF FIG. 9. As compared to fig. 8, only every third trace is displayed. V. E. = 5.4×.

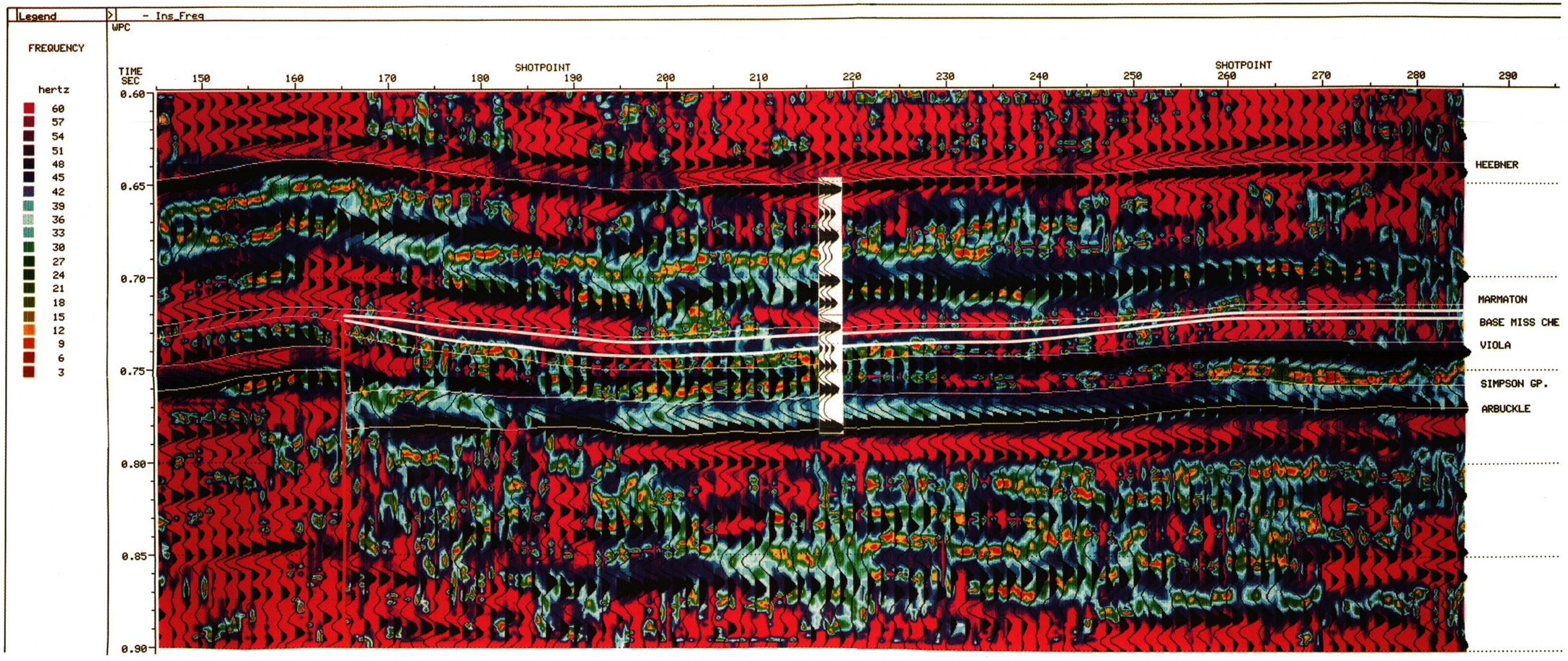

FIGURE 11—Instantaneous frequency redisplayed at 15 TPI and 30 IPS. V.E. = 6×. Note frequency anomalies in Mississippian chert and Viola intervals. See text for details.

Seismic Support Leading to Discovery and Development of Strahm South Field, Forest City Basin, Northeastern Kansas

Dennis E. Hedke
Consultant, Wichita, KS 67202

Abstract

For the past five or six decades, the Forest City basin has been subject to sporadic exploration activity. Prior to the advent of multifold seismic data acquisition, many significant fields (e.g., Davis Ranch in Wabaunsee County) were discovered by integrating subsurface well control with shallow core-hole data. In some cases (Strahm field, Nemaha County), spot correlation seismic data were utilized in conjunction with shallow surface/outcrop structure mapping.

At Strahm South field, east-central Nemaha County, Kansas, an initial subsurface lead was investigated by acquiring 6.25 mi (10.0 km) of nominal 12-fold CDP data in early 1984. This initial survey resulted in a discovery and was augmented by the phased acquisition of 11.4 mi (18.25 km) of "development" data. Pre-drilling seismic mapping indicated significant thinning over a key Lansing–Viola interval; this feature generally indicates deep subsurface structure, particularly at the Ordovician. The survey data also indicated critical west dip of more than 100 ft (30 m) at the top of the Viola and probable closure.

Drilling has confirmed this 100 ft (30 m) of dip and that the Strahm South field is an elongated, faulted, and closed feature. It is slightly over 1 mi (1.6 km) long, with a productive width apparently less than 1,300 ft (390 m). Estimated ultimate recovery from six Viola wells will likely exceed 275,000 bbls. Untested Hunton and Simpson pay remains behind pipe.

Although other geophysical and geochemical techniques can be of assistance prior to drilling untested structures in this area, multifold seismic results are especially encouraging. Both lateral and vertical resolution, particularly with modern recording geometries and processing, confirm good agreement with actual subsurface data. When measured against the cost of a typical dry hole in the area, the CDP surveys are also very cost effective if designed with appropriate constraint.

Introduction

Strahm South field is located in east-central Nemaha County, Kansas, slightly updip and west of the axis of the Forest City basin (figs. 1 and 2). The Forest City basin is asymmetric in that the western flank in proximity to the Nemaha Ridge is steeply dipping and faulted; elsewhere the basin is characterized by relatively gentle dips. The principal zones with production potential are the Silurian/Devonian-aged Hunton carbonates, Ordovician-aged Viola carbonates, and Simpson sandstones. Most, but not all, of the fields in the region are associated with faulting, generally of basement origin. Steeples (1982) illustrates the influence of the Humboldt fault zone throughout the flank of the Nemaha Ridge.

Some structures in the Forest City basin are of substantial areal extent. Davis Ranch (over 8 million bbls) has about 400 productive acres (16 hm^2), while John Creek (also over 8 million bbls) covers more than 1,400 acres (567 hm^2). Many smaller fields have also yielded fairly high reserves per unit area. Examples would be Mill Creek and Woodbury, each with less than 100 acres (40 hm^2) (fig. 3). Most structures with relief high enough to be picked up by shallow core drilling have been exploited long ago, though the technique still has merit on a smaller scale. The seismic method (spot correlation) is credited for the discovery of Strahm field (Elster, 1960). McClain field (1982) is the first discovery in the "new phase" to have shown the validity of CDP techniques in the area.

With respect to Strahm South field, nominal 12- and 24-fold data were acquired with 110-ft (34-m) groups, 220-ft (67-m) shots (Vibroseis), with 48- and 96-channel recording. (See also Appendix 1 for additional detail concerning acquisition and processing parameters.) The resolution provided by these surveys enabled the identification of faulting, the

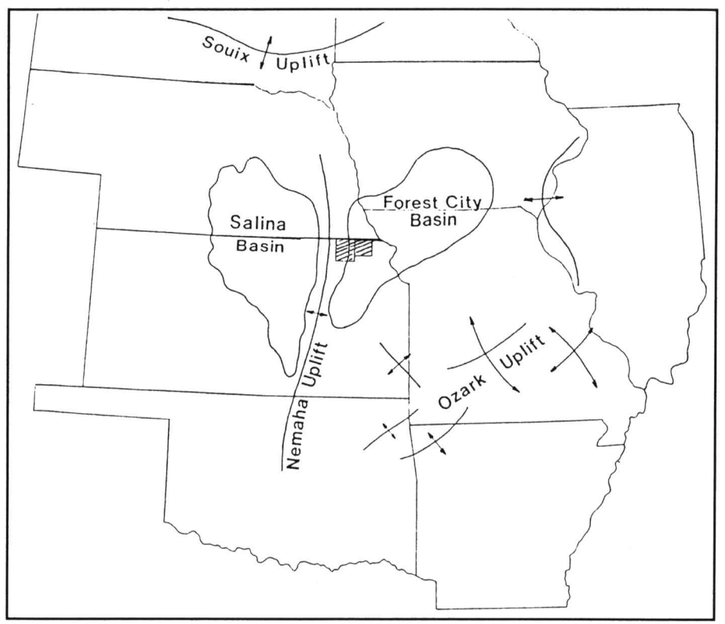

FIGURE 1—FOREST CITY BASIN AND REGIONAL TECTONIC FEATURES (after Cohee et al., 1962).

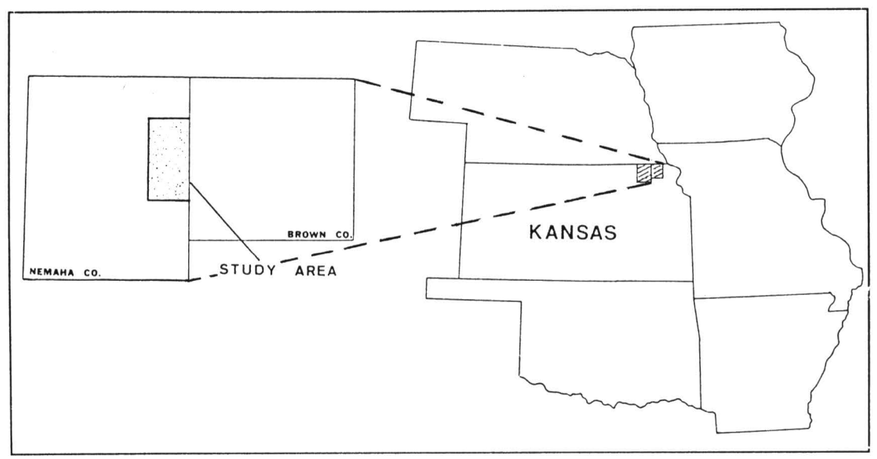

FIGURE 2—STUDY AREA INDEX MAP.

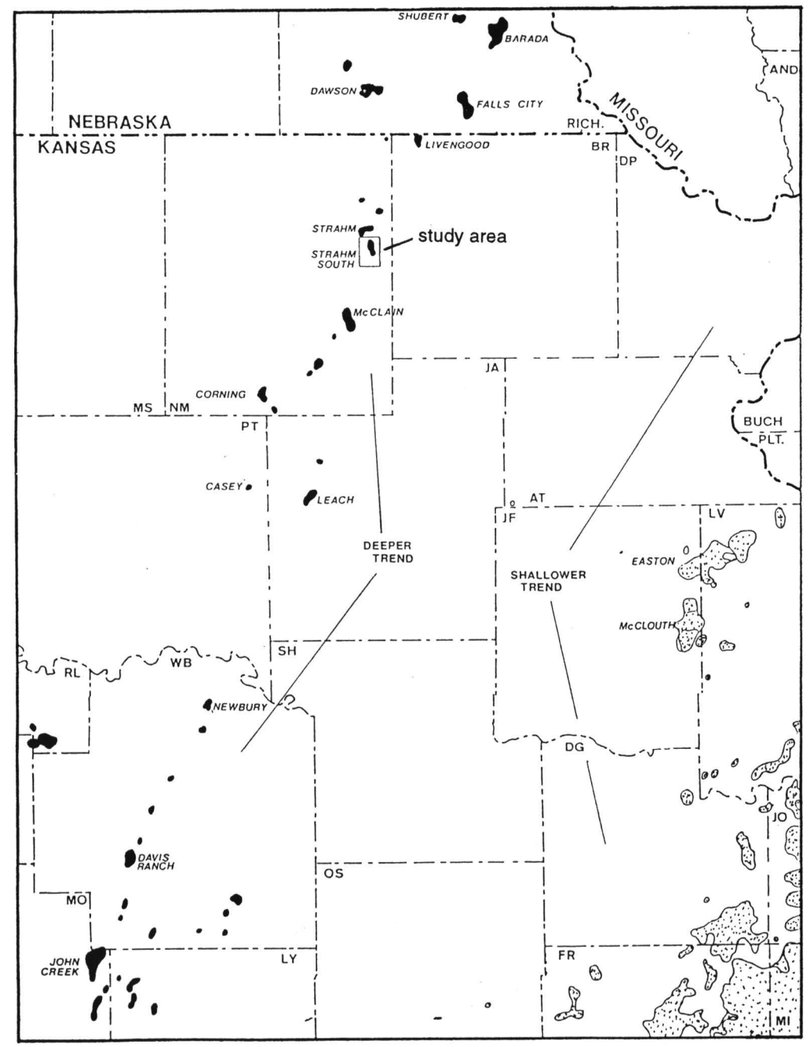

FIGURE 3—REGIONAL PRODUCTION TRENDS.

confirmation of structural dip and stratigraphic thinning, and generally limited the risk associated with exploration and exploitation of structures of limited areal extent.

The location of these initial surveys was based on regional mapping of numerous horizons and isopachs thought to be critical for entrapment and structural closure. This mapping allowed us to highlight an area downdip, but apparently on trend with Strahm field, a Hunton and Viola field discovered in 1948 by Carter Oil (Elster, 1960).

Geological/Geophysical Map Series

Regional geological mapping indicated anomalous conditions at a well which had weak but potentially significant shows from Hunton porosity: the Skelly–Hook #1, located NW SW SW sec. 11, T. 3 S., R. 14 E. Acquisition of approximately 6.25 line-mi of CDP data tied this well directly, and with velocity reference established at this point, allowed for an estimate of possible structural gain against the Ryan–Aberle #1, located in SW NW NW sec. 3, T. 3. S., R. 14 E.

Viola Time Structure and Lansing–Viola Isochron maps as drafted in 1984 are shown in figs. 5 and 6, respectively. These interpretations led to the drilling of the Teichgraeber–Brown Lierz "A" #1, SW SW SE sec. 3, T. 3 S., R. 14 E. The well encountered difficulties during an attempt to drill stem test (DST) the Viola. However, sample shows in the Viola and Simpson, coupled with significant structural gain relative to the Skelly–Hook #1, and thinning against all nearby wells warranted a production attempt. (The Lansing–Viola interval of 2,307 ft [703 m] encountered at the Lierz "A" #1 is the thinnest in all wells in the field area.) Upon completion, significantly oil-cut water was recovered from the Viola.

Subsequent to the drilling of the Lierz "A" #1, further analysis of the data indicated that it would be possible to gain structural advantage by moving north/northwest approximately 1/4 mi (1/2 km) from the Lierz "A" #1. At this new location, the Lierz "A" #2 encountered a 7-ft (2-m) structural gain, with Viola pay developed in a fractured and, in places, vuggy dolomite from about 3,555 ft to 3,565 ft (1,084 m to 1,087 m). Simpson sandstone at 3,775–3,780 ft (1,151–1,152 m) yielded a good show of free oil on DST but is much tighter than the Viola.

A core taken through the Viola pay zone registered porosity as high as 21% and permeability as high as 2,250 millidarcies. Average porosity was 16.2%, while average

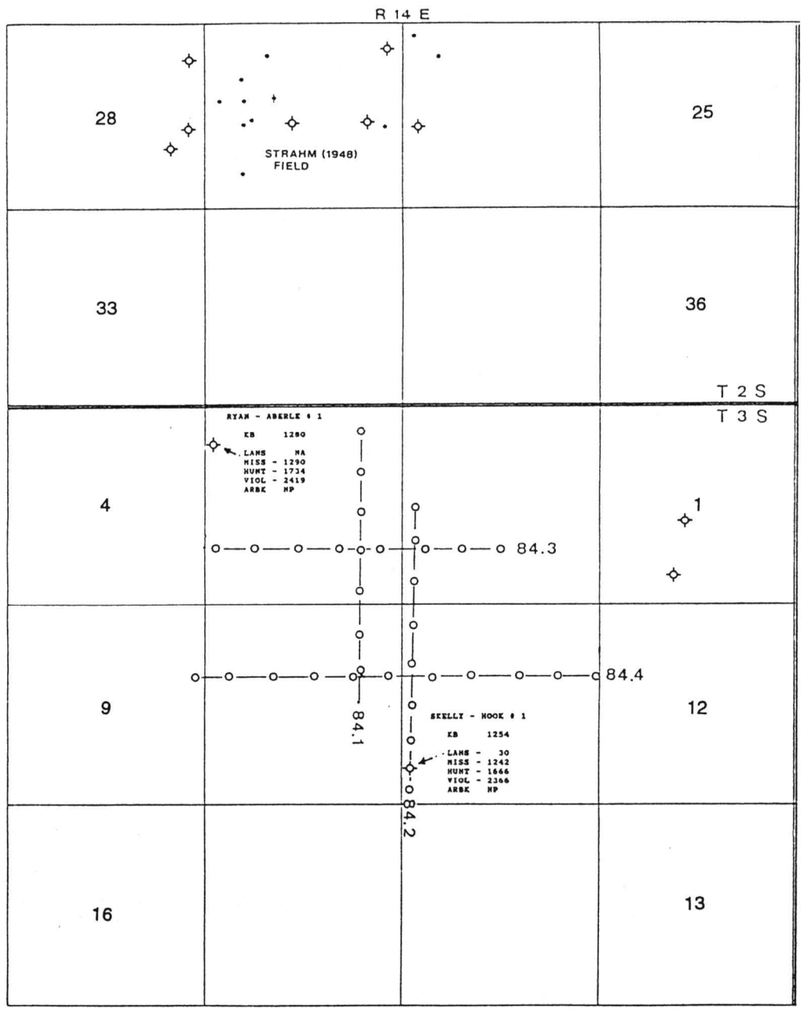

FIGURE 4—1984 CDP SURVEYS WITH WELL CONTROL.

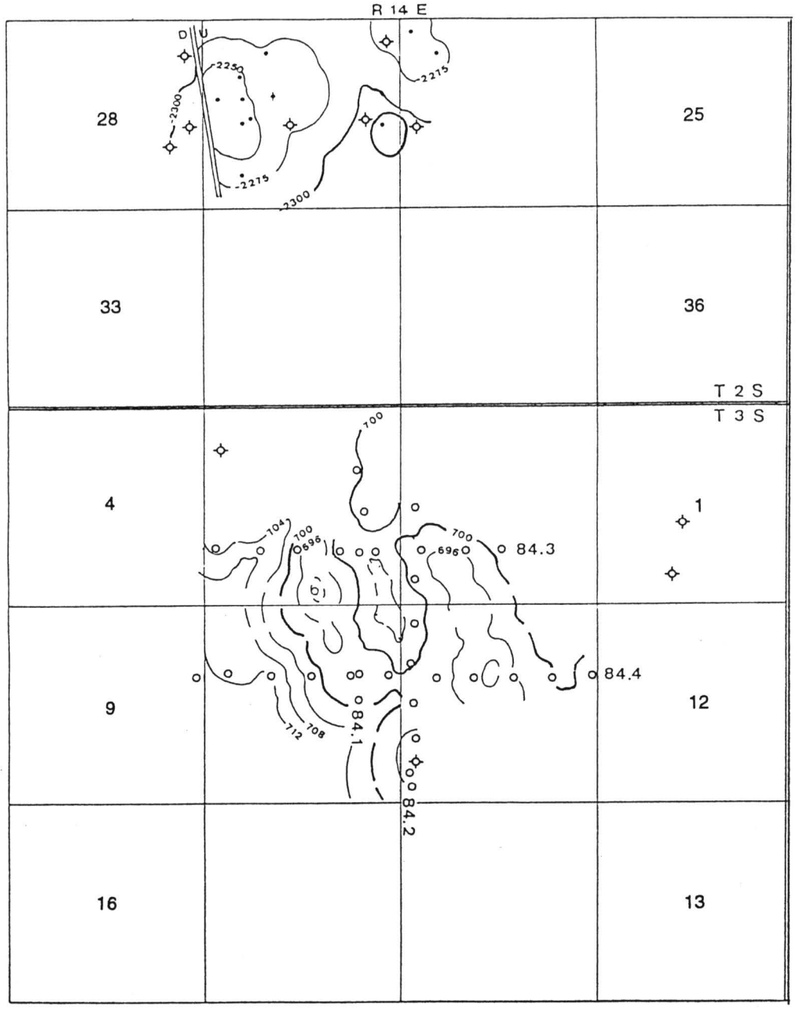

FIGURE 5—VIOLA TIME STRUCTURE, 1984 INTERPRETATION; contour interval = 0.004 sec.

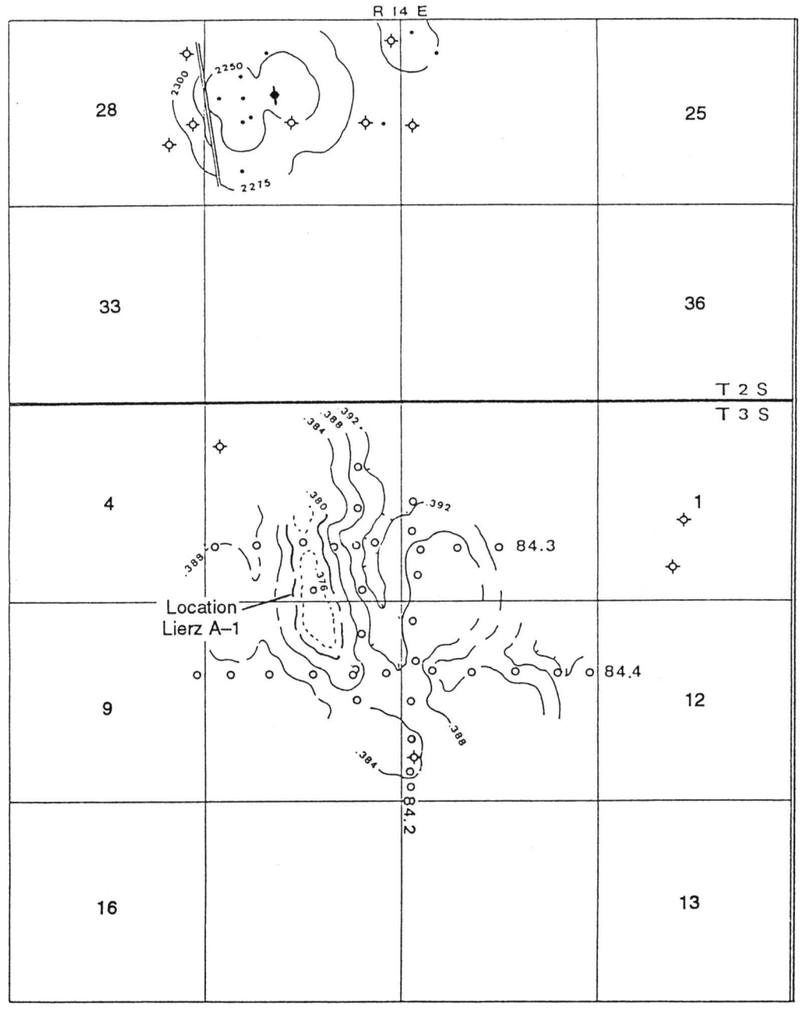

FIGURE 6—LANSING–VIOLA ISOCHRON/ISOPACH, 1984 INTERPRETATION; contour interval = 0.004 sec.

permeability was 523 millidarcies. DST chart extrapolation and calculations for the Viola indicated theoretical potential, with damage removed, of 985 BOPD. Extrapolated reservoir pressure was 1,334 psi.

Following this discovery, additional CDP surveys were conducted to assist both in development and the evaluation of extension exploratory ideas. This second phase (1985) is indicated on fig. 7. Results from these surveys led to the drilling of three additional successful wells and one dry hole.

A final phase of surveys was conducted in 1986 (fig. 8), bringing total survey mileage to 17.65 mi (28 km). Maps depicting the latest interpretation show Lansing–Viola Isochron (fig. 9) and Viola Structure (fig. 10). While the Viola Time Structure map (not shown) matches reasonably well with actual structure, the more diagnostic map is that of the Lansing–Viola isochron. Time-structure mapping is complicated by locally anomalous velocities in variable glacial till cover. Modern processing with refraction statics mitigates some of this distortion; however, better agreement between time and structure remains a significant processing challenge. Note that faulting is depicted as en echelon. Additionally, the east limb of the structure is likely faulted in the vicinity of the highest wells in the field. This portion of the structure would then be interpreted as a horst. This is a very reasonable interpretation and in agreement with Steeples (1982), wherein other similar features have been identified in the fairway of the "Humboldt fault zone."

Geological/Geophysical Cross Sections

Example seismic sections, which indicate both relative structure (dip line 84–3) and stratigraphic variation (strike line 86–4), are shown in figs. 12 and 13, respectively. These are structure-normal polarity sections; key reflections are annotated. Obvious structure below the indicated producing well on profile 84–3 confirms a good portion of the 80 ft (24 m) of relief known to exist between the Lierz #2 and the Ryan–Aberle #1 in NW sec. 3.

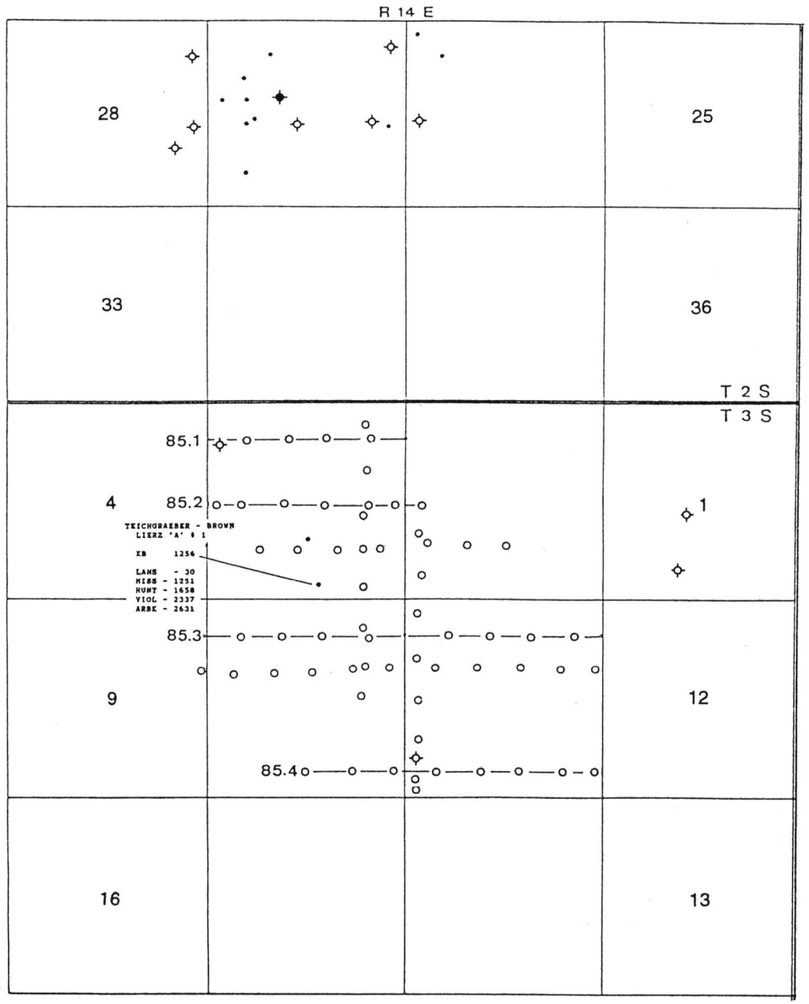

FIGURE 7—PHASE II CDP SURVEYS, 1985.

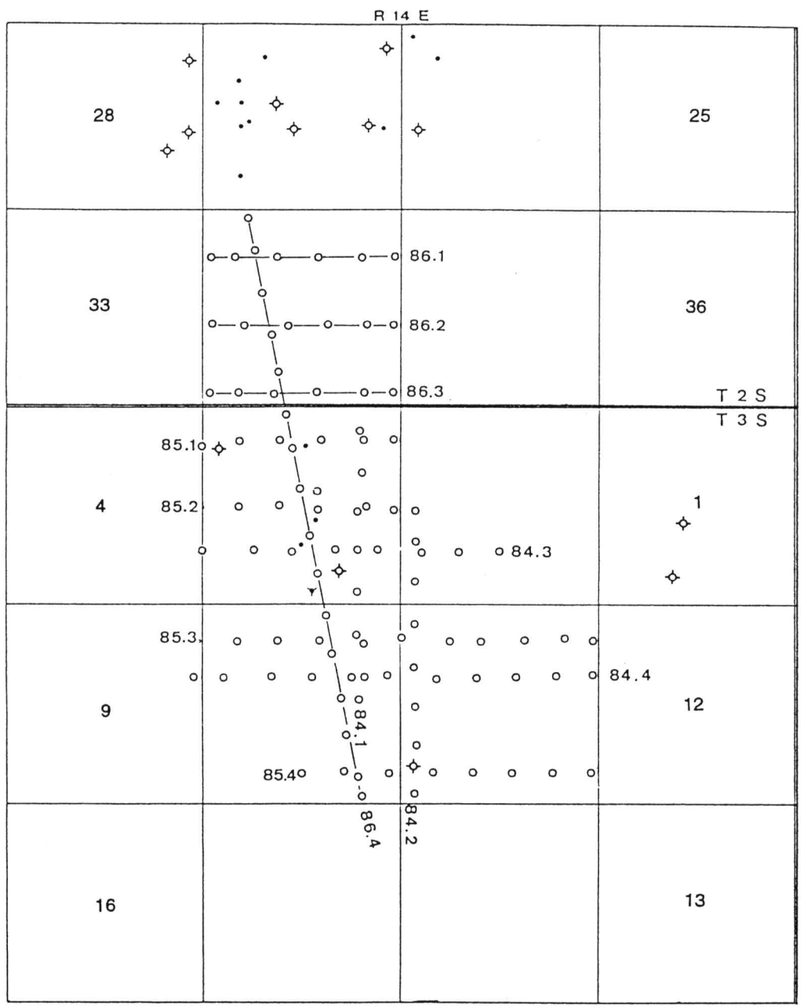

FIGURE 8—PHASE III CDP SURVEYS, 1986.

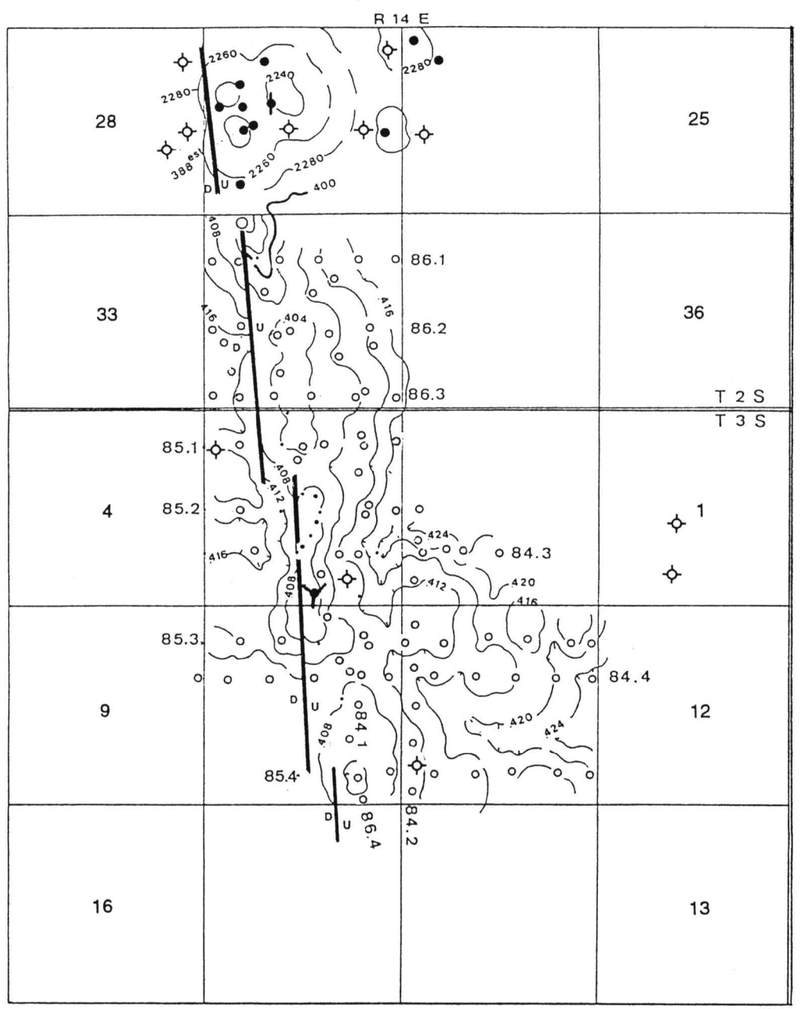

FIGURE 9—FINAL INTERPRETATION, LANSING–VIOLA ISOCHRON; contour interval = 0.004 sec.

While the good correlation to structure on dip lines is encouraging, one of the pitfalls of evaluating data in this area is illustrated by the strike-line interpretation. Compare fig. 14, based on a log cross section through many of the field wells, to profile 86–4 (fig. 12). Of special interest is the relationship of dry holes situated at positions 1 and 5 with respect to profile 86–4. It is possible that the time-structural relief at these locations may be partially an artifact of low-velocity surficial glacial drift deposits. Lateral variations in the thickness and velocity of these deposits can create false pullup, incorrectly suggesting higher structural position. These locations are in higher elevation positions and have more near-surface glacial material preserved.

Seismic correlation has been enhanced by the generation of numerous synthetic seismograms from field wells. The sample seismogram shown in fig. 14 was generated from sonic and density control from near-surface to granite basement at the dry hole located NE SW SE sec. 3, T. 3 S., R. 14 E. (Teichgraeber–Brown Priest "B" #1). In addition, a comparison of the synthetic seismic response between productive and nonproductive wells has been generated (fig. 15). In this profile, the integrated acoustic-impedance curve has been convolved with the same wavelet used in fig. 14; however, the interval has been limited to highlight the synthetic seismic response of the Viola. Note that the display is in depth rather than time. Datum for the display is the top Viola. These responses are very informative in what is indicated immediately below the top Viola. Note that in the productive well (Lierz #3), the amplitude response below the typical top Viola "peak" is very weak. The same zone in the transitional well (Priest "B" #1), which tested shows in Viola porosity, begins to develop a slight kick just above the top Simpson Group marker; the clear-cut dry hole (Wenger "A" #1) shows a strong trough developed followed by a well-developed peak at the top Simpson.

The validity of this theoretical response is substantiated by the signature of the Viola pay zone of fig. 11. As indicated earlier, this profile is a true dip profile and as such provides the better match to modeling. Nonetheless, the response of Viola porosity in fig. 12 also shows interesting correlations to the model response. In summary of this point, it is probable that significant porosity and oil saturation in this zone has yielded a seismic response characteristically different frrom nonproductive cases.

Additional data related to complex trace attributes, such as instantaneous phase and frequency, were utilized to assist in fault-zone definition and to attempt resolution of stratigraphic details. Reflection strength (decibels) further verified the theoretical relationship indicated above (fig. 16).

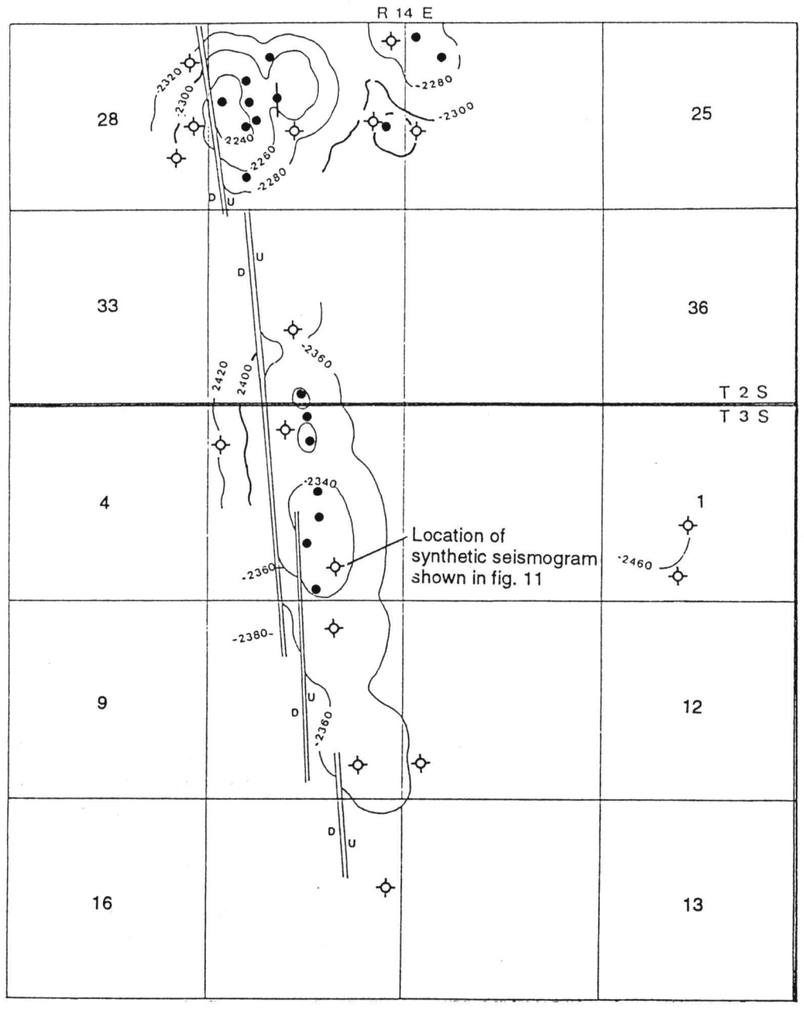

FIGURE 10—FINAL INTERPRETATION, VIOLA STRUCTURE; contour interval = 20 ft (6 m).

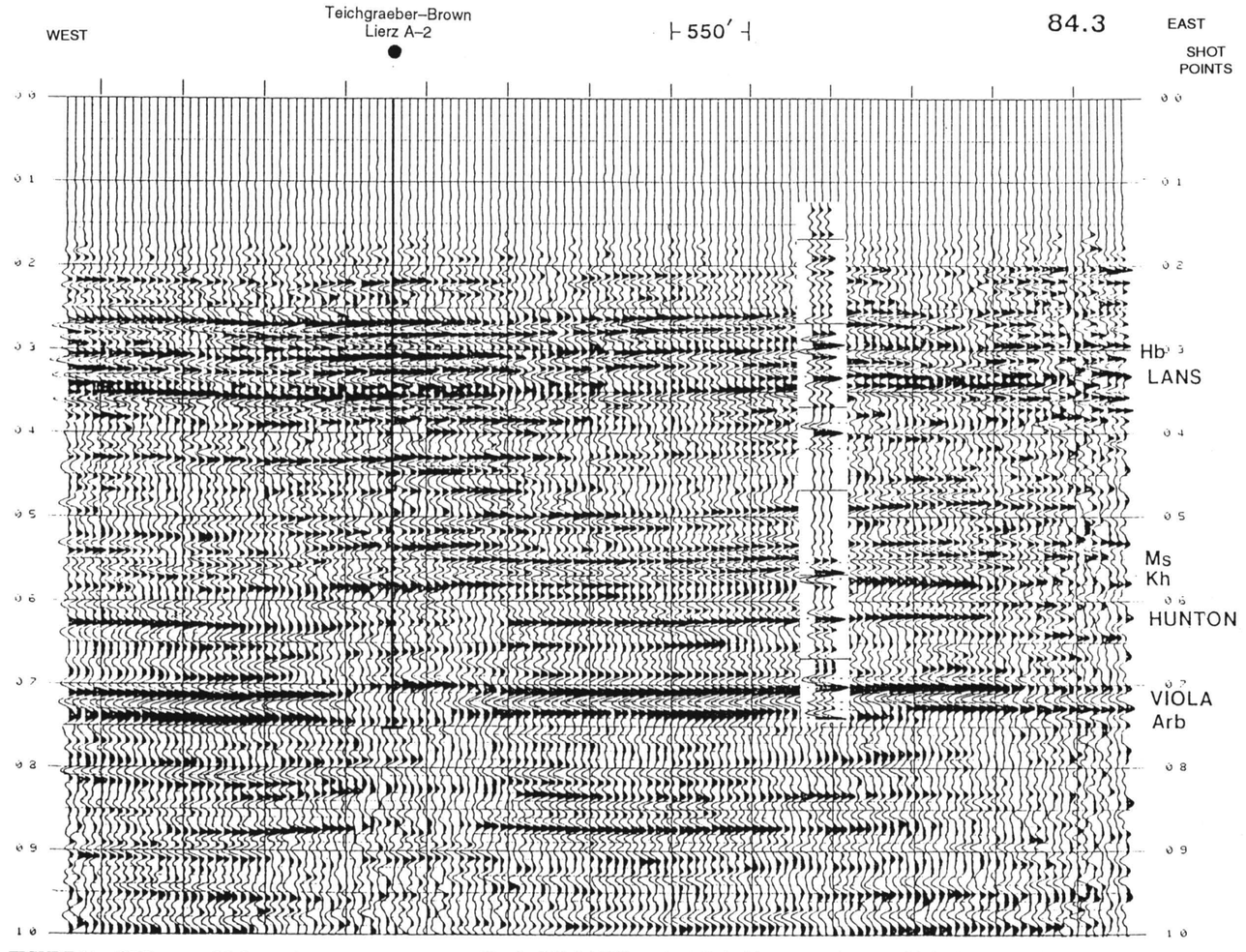

FIGURE 11—CDP PROFILE 84–3; STRUCTURE, NORMAL POLARITY. Nominal 12-fold Vibroseis; 110-ft (34-m) group interval, 20-ft (6-m) source interval.

Summary

While not a major accumulation (estimated ultimate recovery about 300,000 bbls), Strahm South has certainly proved commercial. It also confirms some of the relative complications related to exploration in this region. Among others, these include 1) the high probability of faulting associated with production; 2) relatively high relief, but narrow/small structures; and 3) surface overburden characteristically with glacial drift. Nonetheless, compelling reservoirs await further testing of ideas and technologies.

Though some might suggest that line spacings in this program represented "overkill," the fact is that these structures can and do change dramatically in any given direction. Future data-gathering alternatives including parallel offset (swath) surveys, or appropriately spaced 3D surveys, should yield highly accurate results in a framework utilizing scrutinized cost control.

ACKNOWLEDGMENTS—The author expresses sincere appreciation to R. K. Teichgraeber and W. Terrence Brown for permission to publish this paper.

References

Cohee, G. V., et al., 1962, Tectonic map of the United States: U.S. Geological Survey and American Association of Petroleum Geologists

Elster, T., 1960, Strahm field; *in*, Kansas Oil and Gas Fields, vol. III, Northeastern Kansas: Kansas Geological Society, p. 125–129

Steeples, D. W., 1982, Structure of the Salina–Forest City interbasin boundary from seismic studies: University of Missouri Rolla (UMR), Journal, no. 3, December, p. 55–81

Appendix

Acquisition and Processing Parameters

Acquisition:	48 and 96 channel
	12 and 24 fold
WESTERN	110-ft group interval
GEOPHYSICAL	220-ft source interval (Vibroseis)
&	120–20 Hz pilot
VIBRASONICS	12-sec sweeps, 10 sweeps/V.P.
	3 secs listening
Processing:	Demux-gain recovery
	Geometry-trace edits
ECHO	First break suppression, spectral enhancement
GEOPHYSICAL	Datum statics
	CDP gather
	Brute velocities, NMO
	Auto surface consistent statics
	Final velocity anaylsis
	Final NMO corrections
	Second pass auto surface consistent statics
	Auto CDP consistent statics
	Stack
	Filter: 10–15/80–90 Hz 0–2,000 msec
	Trace equalization

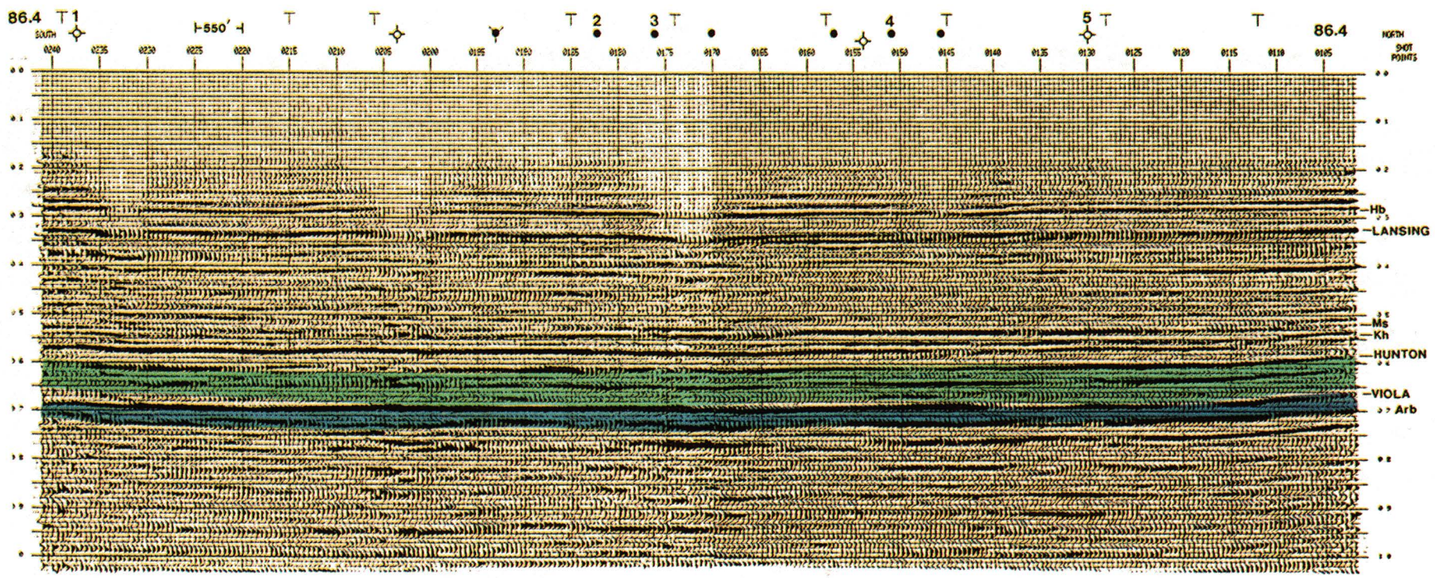

FIGURE 12—CDP PROFILE 86–4 (STRIKE LINE); STRUCTURE, NORMAL POLARITY. Numbers above wells refer to structural profile fig. 13.

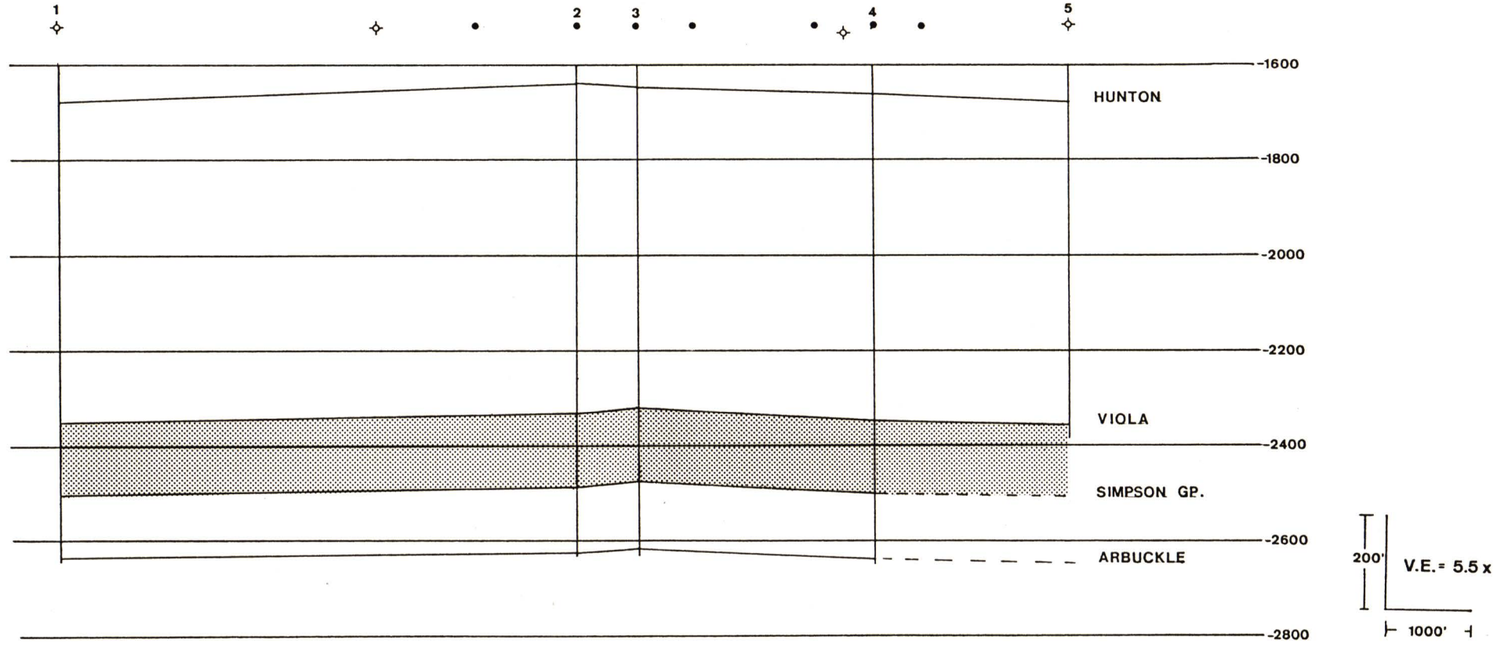

FIGURE 13—STRUCTURAL PROFILE FROM LOG DATA. Compare with CDP profile 86–4, fig. 12.

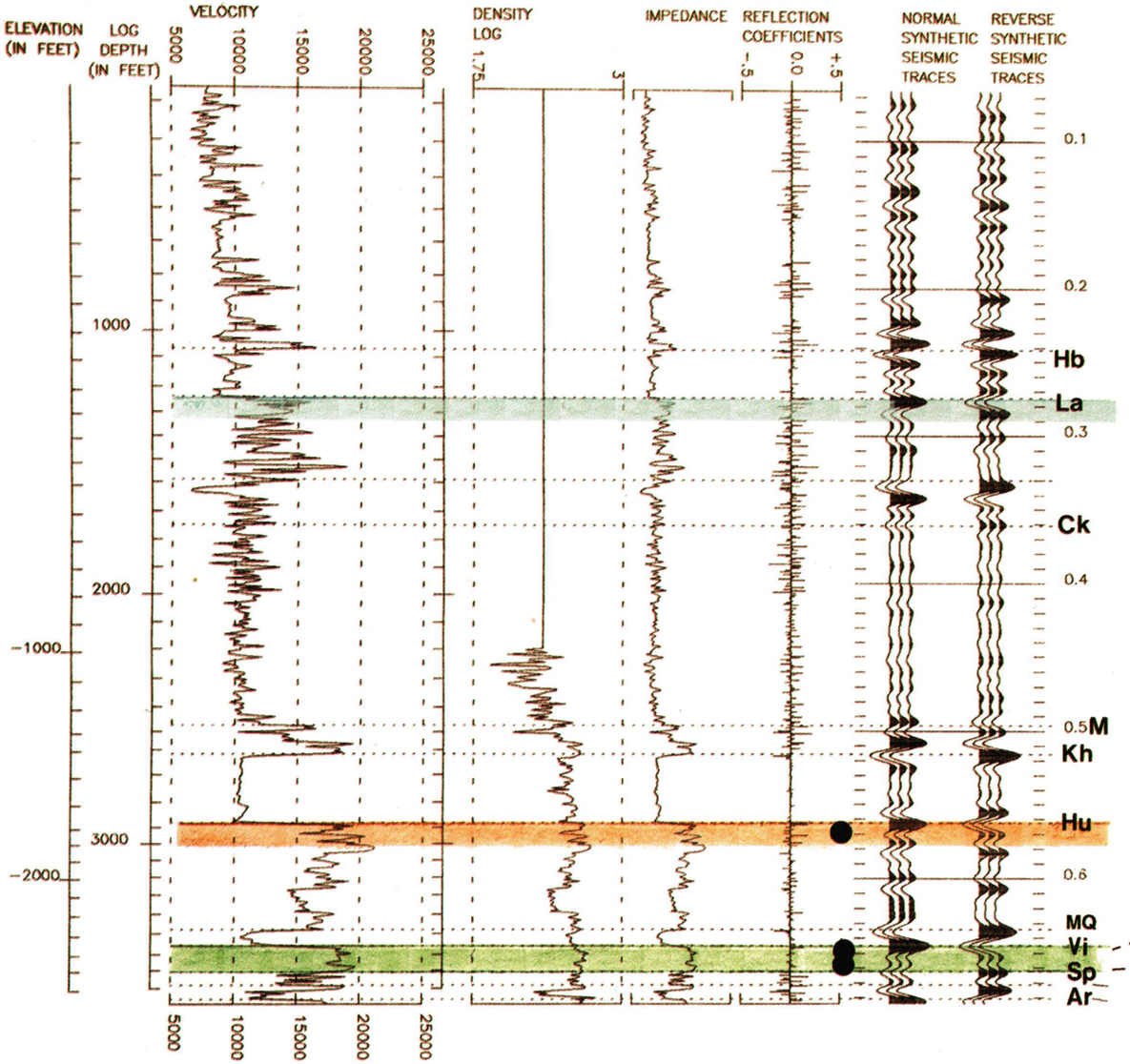

HORIZON	DEPTH	TIME	ELEVATION	DEPTH FROM SEISMIC DATUM	AVERAGE VELOCITY	ISOPACH	ISOCHRON	INTERVAL VELOCITY
HEEBNER	1071.0	0.241	142.00	1058.0	8754			
LANSING	1230.0	0.274	−17.00	1217.0	8869	159.0	0.0327	9716
BKC	1587.0	0.330	−374.00	1574.0	9538	357.0	0.0556	12838
CHEROKEE	1750.0	0.360	−537.00	1737.0	9628	163.0	0.0307	10603
MISS. LM.	2470.0	0.496	−1257.00	2457.0	9903	720.0	0.1354	10633
KINDERHOOK	2626.0	0.515	−1413.00	2613.0	10130	156.0	0.0196	15869
HUNTON	2874.0	0.562	−1661.00	2861.0	10169	248.0	0.0467	10604
MAQUOKETA	3486.0	0.634	−2273.00	3473.0	10955	612.0	0.0713	17143
VIOLA	3548.0	0.644	−2335.00	3535.0	10964	62.0	0.0107	11543
SIMPSON GP.	3710.0	0.662	−2497.00	3697.0	11162	162.0	0.0176	18393
st SAND	3781.0	0.671	−2568.00	3768.0	11223	71.0	0.0090	15703
ARBUCKLE	3849.0	0.680	−2636.00	3836.0	11268	68.0	0.0094	14435

FIGURE 14—SYNTHETIC SEISMOGRAM, TEICHGRAEBER–BROWN PRIEST "B" #1. Convolved with filter of 10–20/75–95 Hz, zero phase.

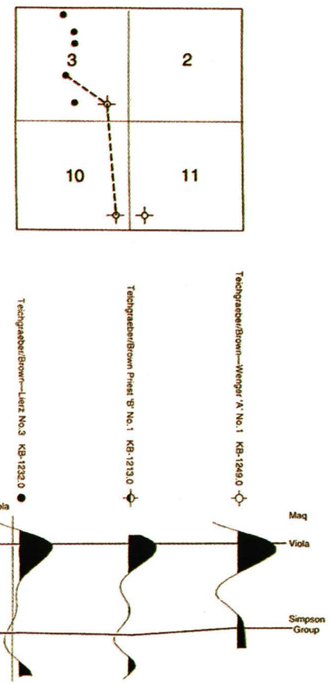

FIGURE 15—SYNTHETIC SEISMIC PROFILE ILLUSTRATING CONTRAST BETWEEN RESERVOIR/NONRESERVOIR ROCK AND FLUID MATERIAL.

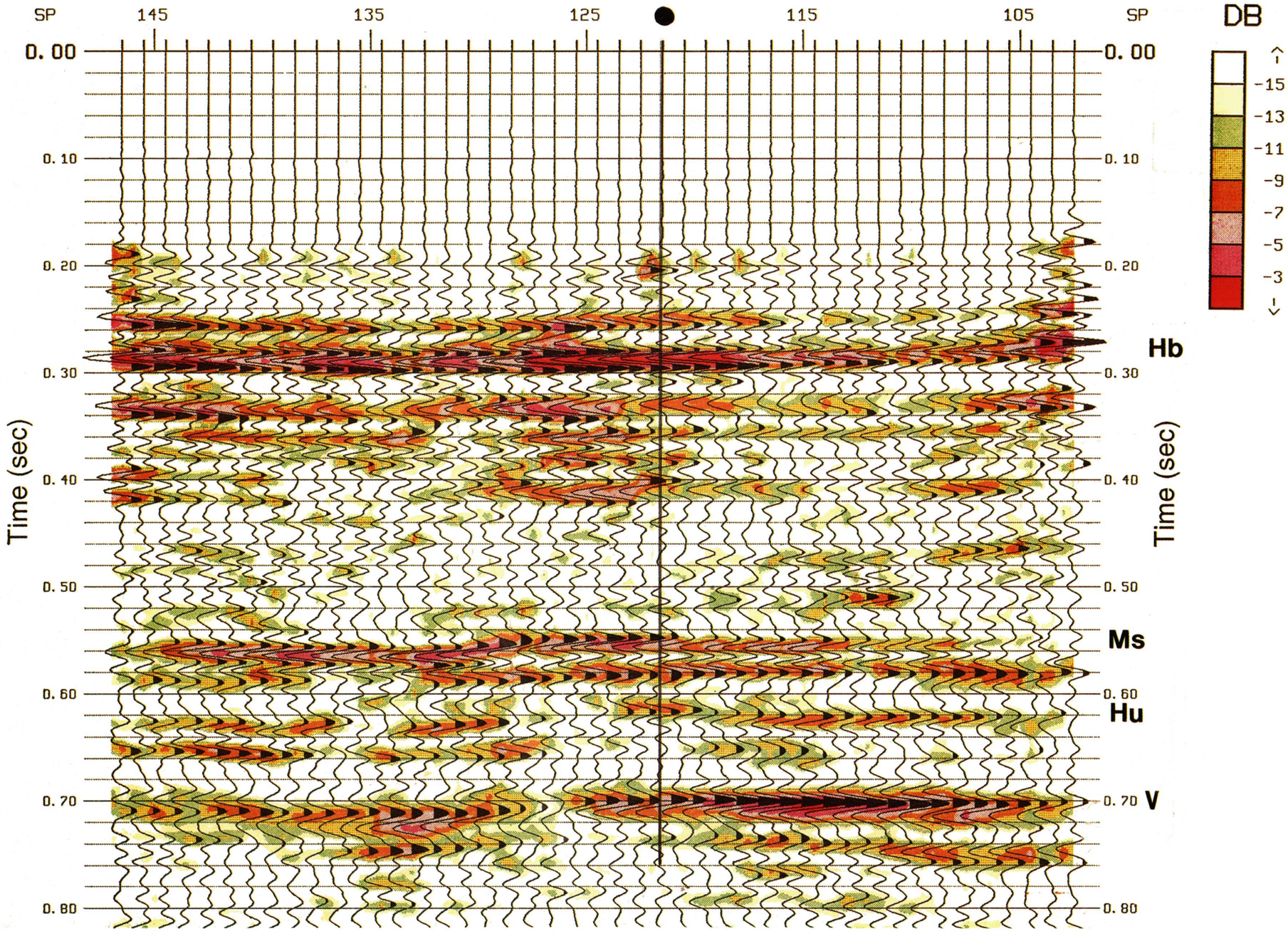

FIGURE 16—COMPLEX TRACE ATTRIBUTE OF REFLECTION STRENGTH.

Case History of Hampton Field (Arbuckle Group), Rush County, Kansas

Timothy R. Carr[1], John Hopkins[1], Neil L. Anderson[2], and Dennis E. Hedke[3]
[1]Kansas Geological Survey, University of Kansas, Lawrence, KS 66047;
[2]Department of Geology, University of Missouri–Rolla, Rolla, MO 65401; and
[3]Consultant, Wichita, KS 67202

Abstract

Hampton field, located in northwestern Rush County, Kansas (principally in secs. 5–8, T. 17 S., R. 19 W.), is a small Arbuckle field (1.12 MMBO) along the western flank of the Central Kansas uplift. The field is a classic example of an unconformity trap and reservoir related to development of "mature" karst features into a poorly organized hierarchy of closed depressions and erosional highs (e.g., fractures, sinks, steepheads, uvalas, and half-blind valleys). An understanding of the paleogeomorphology of the pre-Pennsylvanian exposure surface and its relationship to basement structure is critical to successful exploration and development. Seismic control provides evidence of pre-existing basement structure that influenced subsequent deposition and erosion. Structural relief and closure at the Arbuckle level across Hampton field can be recognized on the seismic data. The seismic data in conjunction with the well control are a valuable exploration and development tool. The seismic data provide insights into timing of tectonic movements, the influence of basement structure on subsequent deposition and erosional topography, and on differential compaction of post-Cherokee rocks across the pre-Pennsylvanian basement structure.

Introduction

Hampton field, a relatively small but significant Arbuckle field along the western flank of the Central Kansas uplift, is an example of a karsted fracture-controlled dolomite reservoir at the northern end of the Arbuckle–Ellenburger trend. Regionally, the Arbuckle–Ellenburger trend of the southern midcontinent is one of the most significant oil- and gas-producing horizons in the United States, stretching nearly a thousand miles from the Central Kansas uplift across Oklahoma and Texas to the Delaware basin of West Texas (Gatewood and Fay, 1992). In Kansas, Arbuckle reservoirs account for approximately 47% of the 16.3 billion barrels of original oil in place, and over 32% of the cumulative 5.9 billion barrels of the total oil produced (Watney and Paul, 1983; Newell et al., 1987; Carr, 1994). Reservoir development in the Arbuckle and equivalent units has been directly related to prolonged periods of subaerial exposure and karst development that initiated with the Middle Ordovician Sauk–Tippecanoe cratonic sequence boundary (Sloss, 1963). In areas such as the Central Kansas uplift, intermittent periods of subaerial exposure continued up through the Early Pennsylvanian (base of Absaroka Sequence, Sloss, 1963; Walters, 1946, 1958, 1991). During these episodes of widespread exposure, renewed karst development occurred. The result is a terrain characterized by the development of underground solution networks, disorganized surface drainage, and a surface topography characterized by a hierarchy of closed depressions resulting from solution and collapse (e.g., Walters, 1991).

Karst development in the Arbuckle section enhanced porosity and permeability, creating prolific petroleum wells and large reservoirs (Walters, 1958; Merriam, 1963; Adler, 1971; Ramondetta, 1990). Production is typically restricted to the top 25 ft of the Arbuckle (Adler, 1971). However, deeper low- to moderate-volume stratified production has been identified in a number of fields including El Dorado (Ramondetta, 1990) and Edwards (Mullins and Ireland, 1967). The presence of lower stratiform pay zones may be related to depositional stratification or stratified karst structures. The complete range of reservoir types in the Arbuckle has not been adequately characterized, and the Arbuckle should not be considered fully tested until Precambrian rocks are reached (Bloesch, 1964).

The major focus in this paper is the examination of available well and seismic data in the area of Hampton field using a karst model. Our goals are to develop an understanding of the effect of the paleogeomorphology of an erosional surface on petroleum production, the influence of basement controls on subsequent deposition and erosion, and the application of seismic data to imaging the erosional surface. The seismic profile incorporated in this paper crosses the southern flank of the Hampton field. The profile images what is believed to be a typical Arbuckle field along the southwestern margin of the Central Kansas uplift.

Field Description

Hampton field, located in northwest Rush County, Kansas (principally in secs. 5–8, T. 17 S., R. 19 W.), is one of numerous moderate to small Arbuckle fields (i.e., 1–5 MMBO) located along the southwestern flank of the Central Kansas uplift (fig. 1). The Central Kansas uplift, a northwest-trending complex of structural features, is the largest positive feature in Kansas. Post-Mississippian in age, the uplift was described by Merriam (1963) as "a maze of small anticlinal and synclinal structures, many of which are faulted." The crest of the uplift is recognizable by the superposition of Pennsylvanian sediments directly on Precambrian basement. The flanks exhibit truncated pre-Pennsylvanian strata overstepped by Pennsylvanian beds (Merriam, 1963).

In the 1960's, exploration moved off the crest of the Central Kansas uplift and away from the giant Arbuckle fields of Barton, Russell, and Ellis counties. Arbuckle production was discovered at Hampton field in March 1967 (Birmingham Bartlett #1 Littler "C," SE NW SE sec. 6, T. 17 S., R. 19 W.), and was followed the next year by discovery of oil in the overlying Pennsylvanian conglomerate (Rock Oil #1 Honska, NW NW NE sec. 8, T. 17 S., R. 19 W.). Reported initial production from the Arbuckle discovery well was 60 BOPD. Field production increased quickly to a peak in 1968 of over 400 BOPD from 17 wells (fig. 2). Production is from either the top few feet of the Arbuckle, or on the eastern extension of the field from the overlying Arbuckle "conglomerate" (figs. 3 and 4). The field, with the exception of a single well pool on the NW corner (Baldwin "B" lease, NW NW SW sec. 6), appears to have a common original oil-water contact at -1,745 ft subsea (-532 m) (fig. 4). Typical of the Arbuckle production, Hampton field has a strong bottom water drive. Average measured drilling depth to production is just over 3,800 ft (1,158 m). Hampton field covers approximately 600 acres (243 hm^2) and was developed on 40-acre (16-hm^2) spacing (fig. 3).

Reported cumulative production from Hampton is entirely oil, and through 1993 was 1.12 MMBO. Since the peak in 1968, field production has steadily decreased to a present rate of less than 25 BOPD (fig. 2, table 1). In 1992, only 10 wells located on two leases operated by Phillips Petroleum were actively producing. Average per well

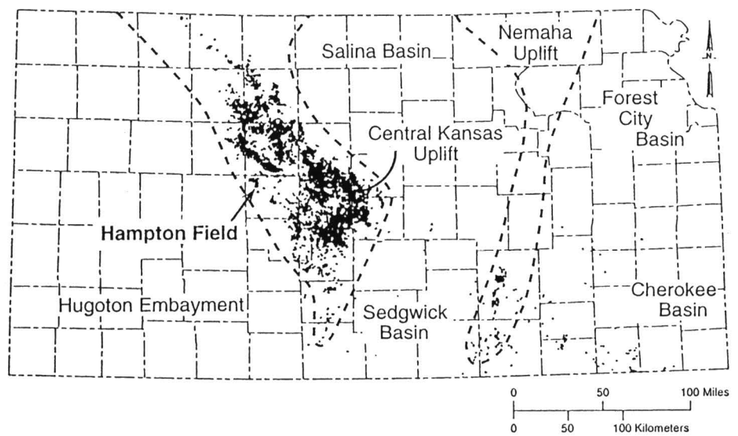

FIGURE 1—Map showing distribution of wells producing from the Arbuckle Group in Kansas in relation to the major structural features. The Hampton field is located in northwest Rush County.

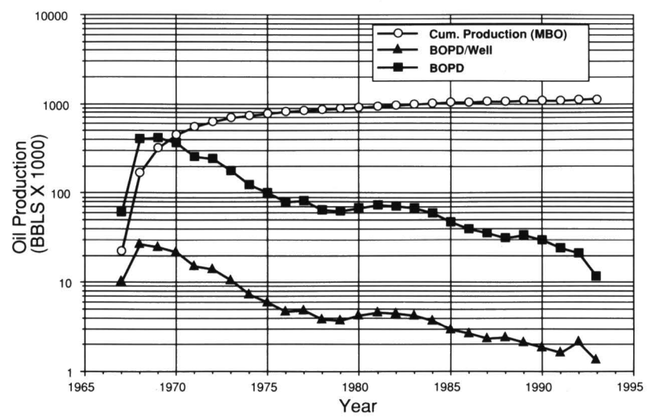

FIGURE 2—Annual production data from Hampton field from discovery in 1967 through 1992. Reported cumulative production from Hampton is entirely oil, and through 1993 was 1.12 MMBO.

TABLE 1—HAMPTON FIELD PRODUCTION BY LEASE.

Lease Name	Operator	Cumulative Production Through 1992	1992 Annual Production	Producing Wells
Baldwin "B"	Birmingham–Bartlett	44,792	0	1
Elmore "A"	Pintail Petroleum	155,146	0	2
Littler "C"	Phillips Petroleum	396,160	3,416	6
Moran	Phillips Petroleum	428,397	4,476	4
Honska	Oil Prod. Systems	94,894	0	3
House	Koch	310	0	1
Totals		1,119,699	7,892	17

cumulative recovery is over 60 MBO, and the best wells in the field have cumulative recoveries in excess of 100 MBO. Arbuckle wells on the crest of the Central Kansas uplift, although at a much tighter 10-acre (4-hm^2) spacing, have reported similar cumulative per well recoveries (Walters, 1991). Because of the heterogeneous nature of the fracture porosity and permeability in the Arbuckle and the absence of complete penetrations, Arbuckle fields such as Hampton have defied attempts by conventional methods to estimate original oil in place (OOIP). However, fields such as Hampton appear to be attractive economically because of the relatively shallow drilling depths and oil recoveries per surface acre ranging from 2,000 to 3,000 barrels.

Trap Description

Hampton field is interpreted as a stratigraphic trap formed by an erosional high on the top of the Arbuckle Group (i.e., a hill). The overlying Pennsylvanian Cherokee shales and silts provide vertical and lateral seals. Relief on the Arbuckle unconformity surface, defined by well control, is as much as 30 m (100 ft) over a distance of less than 0.5 km (1,600 ft). As contoured, relatively steep walls separate roughly flat-topped hills from irregular valleys and closed depressions. Hampton field is interpreted as an elongated roughly east-west erosional high that is surrounded by karst features such as sinks, steepheads, and half-blind valleys developed on top of the Arbuckle (fig. 5). Surface paleotopography as depicted on top of the Arbuckle is similar in morphology and scale to surface landforms described from other karst terrains (fig. 6). In particular, the abundance of closed depressions varying in size and arrangement mapped in the area resemble the compound sinks, blind and half-blind valleys, and generally disrupted surface-drainage pattern that are indicative of karst terrain (Jennings, 1985). The erosional surface developed on the Arbuckle in the Hampton area is interpreted as a poorly organized segmented surface drainage with reaches of both underground and surface flow (Jennings, 1985). Blind and half-blind valleys form as surface streams that gradually disappear underground (e.g., low separating the three fields in the Hampton area, fig. 5). In karst terrains stream emergence is often marked by a blind headwall or steephead (e.g., SW SW sec. 29, T. 16 S., R. 19 W., fig. 5). Headwalls are formed by headward retreat of the valley by stepping back of cliffs resulting from accelerated erosion at the base by a spring or rising (fig. 6; Jennings, 1985). As mapped, the morphology and scale of Arbuckle structure in the Hampton field area displays many of the features of "mature" karst development. Cherokee conglomerate production at Hampton field is concentrated in an area where the paleodrainage may have been underground, re-emerging immediately to the south of the field. Production in the conglomerate, which is composed of brecciated Arbuckle, may be related to collapse of this underground paleodrainage. A similar set of Arbuckle paleotopographic features (i.e., erosional highs with irregular outlines surrounded by closed depressions of various scales) are mapped at nearby Hampton Northeast and Roland Southeast fields (fig. 5). The morphology and scale of both the positive features and closed depressions in the Hampton field area strongly suggest genesis as surface landforms associated with karst.

The Pennsylvanian Cherokee shales and silts immediately overlie the Lower Ordovician Arbuckle Group in the Hampton field area. The Cherokee was deposited on the karsted pre-Pennsylvanian erosion surface along the flanks and over the crest of the Central Kansas uplift. Across the Central Kansas uplift, the Cherokee fills depressions and valleys in the underlying strata, and locally pinches out against paleotopographic highs (Walters et al., 1979). The Cherokee isopach in conjunction with the Arbuckle structural contour map show that the Cherokee thins from over 30 m (100 ft) in Arbuckle lows to less than a meter (2 ft) over highs (figs. 5 and 7). The Cherokee fills in much of the local Arbuckle relief, and isopachs between post-Cherokee markers (e.g., Marmaton to Lansing–Kansas City) show only a general regional thickening to the southwest off the Central Kansas uplift. On the basis of well tops, the Hampton field structure persists through the entire section, but diminishes significantly above the Cherokee. Local structural relief of over 100 ft (30 m) on the Arbuckle surface decreases to less than 5 m (15 ft) at the base of the Stone Corral Anhydrite. Local structural relief on higher markers (e.g., Heebner Shale and Stone Corral) is very subtle and is attributed to compaction over Arbuckle highs (fig. 4).

Inherited Precambrian structural grain appears to influence the position and axis of pre-Pennsylvanian karst features across the Central Kansas uplift. Many workers have recognized the relationship between the Precambrian basement structures and the distribution of overlying strata (e.g., Merriam, 1963). In addition to providing inherited structural relief, the Precambrian structural grain may provide zones of weakness for development of compound sinks (uvalas) and reaches of surface and subsurface drainage. The influence of inherited structural grains on modern karst development has been well documented (e.g., Jennings 1985).

Understanding of the paleogeomorphology of the Arbuckle weathering surface, the possible influence of Precambrian topography, and the relationship of karst landform development to pre-existing structure, are important components to hydrocarbon exploration and production. At El Dorado field in eastern Kansas, high rates of initial production in Arbuckle were reported to follow permeability trends similar to modern karst. These trends were related to inherited fracture systems (Ramondetta, 1990). East

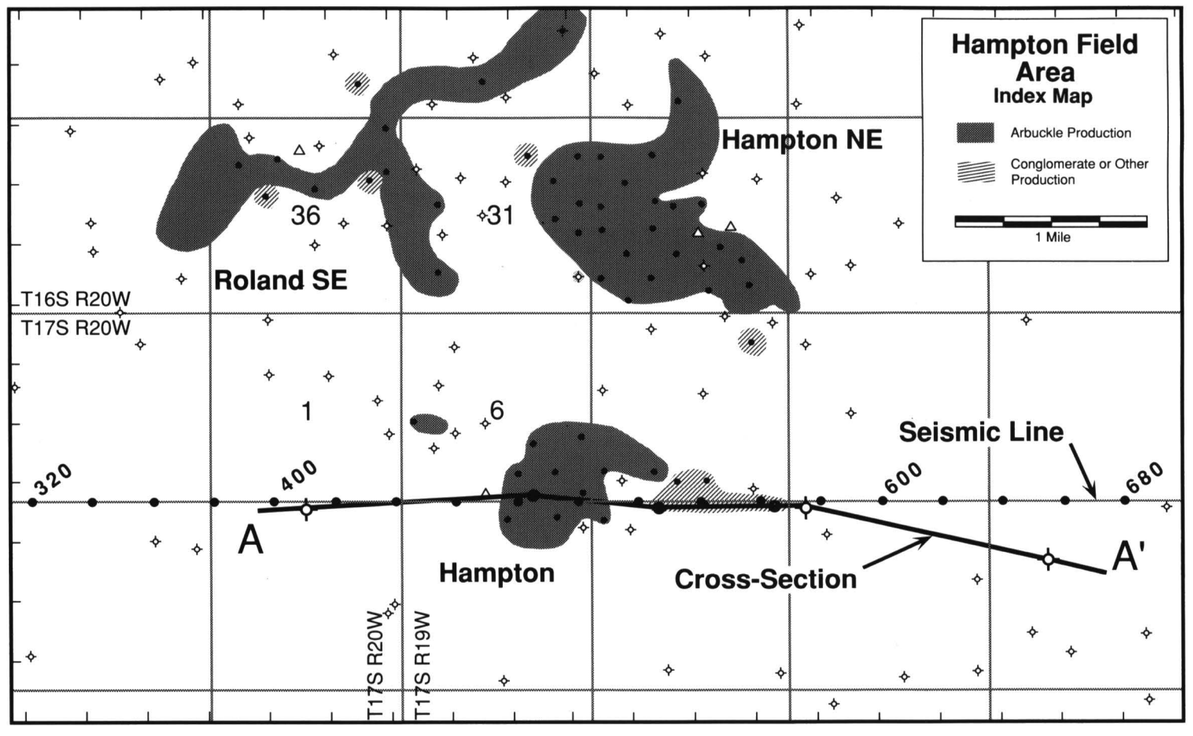

FIGURE 3—INDEX MAP OF HAMPTON FIELD AREA, SHOWING THE AREA OF OIL PRODUCTION FROM BOTH THE ARBUCKLE AND BASAL CHEROKEE CONGLOMERATE. Locations of the geologic cross section (fig. 4) and seismic section are shown (fig. 8).

of Hampton field, karst features, formed in the sedimentary rocks surrounding and covering buried Precambrian hills, were linked to the prolific oil production from the Arbuckle at Gorham, Kraft–Prusa, Beaver, and Bloomer fields in Barton and Russell counties (Walters, 1946, 1991). Solution features such as moatlike valleys and numerous small sinkholes and valleys formed by coalescing sinkholes (uvalas) surround many of these "buried hills" (Walters, 1946, 1991). These buried karst features were interpreted as forming in the Arbuckle carbonates in early Pennsylvanian when the entire area was above sea level and was undergoing weathering and erosion prior to deposition of Pennsylvanian sediments (Walters, 1991).

Seismic Data and Interpretation

The sample seismic line across Hampton field (figs. 8 and 9) crosses a closed structural high at the top of the Arbuckle Group (figs. 4 and 5). Closure at the top of the Arbuckle Group along the length of the seismic line is estimated (from geologic control only) to be on the order of 30 m (98 ft). At horizons above the Cherokee, structural relief is less than 10 m (32 ft) and decreases to less than 5 m (16 ft) at the Stone Corral. All horizons dip regionally to the west-southwest into the Hugoton embayment (fig. 1).

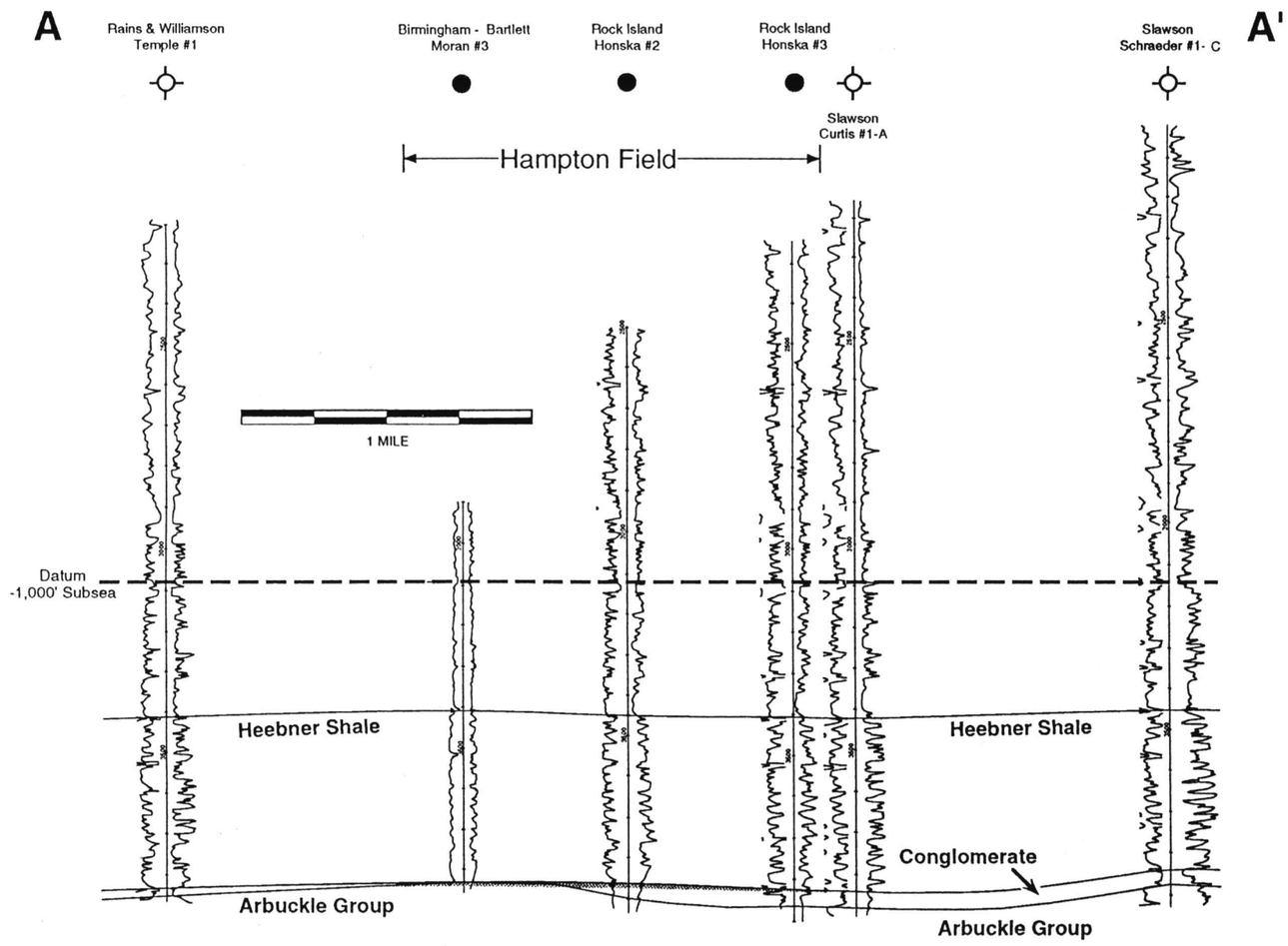

FIGURE 4—EAST-WEST STRUCTURAL CROSS SECTION ACROSS A PART OF HAMPTON FIELD (fig. 6). An original oil-water contact at approximately -1745-ft (-532-m) subsea is present in both the Arbuckle and Cherokee "conglomerate." Cherokee thins from over 30 m (100 ft) in Arbuckle lows to less than a meter (2 ft) over the highs, filling in much of the local Arbuckle relief (figs. 3 and 5). Structural relief on higher markers (e.g., Heebner Shale) is very subtle and is attributed to compaction. Section is roughly parallel to seismic profile (fig. 8).

The vibroseis-sourced seismic data (figs. 8 and 9) were acquired in 1988 by Lockhart Geophysical using a split-spread receiver array with a source interval of 165 ft (50 m), a group interval of 82.5 ft (25 m), and near and far offsets of 412.5 ft and 2,805 ft (126 m and 855 m), respectively. Twelve 12-sec, 14–150-Hz sweeps were summed at each source location. The notch filter was out. These data are interpreted to be zero-phase and reverse polarity.

As an aid to the interpretation of the example seismic line, two zero-phase, 52-Hz, Ricker-wavelet based, one-dimensional synthetic seismograms (normal and reverse polarity displays) were generated (figs. 10 and 11). The well in the SW NE NW sec. 6, T. 17 S., R. 19 W. (fig. 10), is about 0.8 km (0.3 mi) north of shotpoint 490; the corresponding synthetic seismogram ties the seismic line reasonably well (figs. 8 and 9). The well in the SE SE SE sec. 6, T. 17 S., R. 19 W. (fig. 11), is effectively on-line; the corresponding synthetic seismogram ties the seismic line at shotpoint 480 (fig. 8).

As is indicated on figs. 10 and 11, the synthetic seismograms utilize sonic-log data only; neither check shot nor density control is available for these wells. Throughout most of the subsurface geologic section, sediment density and acoustic velocity are directly proportional, and sonic-based synthetic seismograms are reasonable approximations to the seismic image of the subsurface. However, this generalized velocity/density relationship is not valid for salt-bearing strata. Rock salt has a relatively high acoustic velocity and an anomalously low density. As a consequence, the synthetic response to the relatively low-density Hutchinson Salt Member is somewhat misleading (fig. 10). In a relative sense, the top of the salt has a lower acoustic-impedance contrast than that indicated on the synthetic seismogram, and hence is a lower-amplitude reflection (relatively) on field seismic data; the base salt event in contrast is a better-defined, higher-amplitude reflection on actual seismic data.

With the exception of the Hutchinson Salt interval, the synthetic seismograms are presented as reasonable models of the processed vibroseis data (figs. 8, 9, 10, and 11). A number of significant geologic markers are identified on the synthetic seismograms; several of these generate prominent events. The Stone Corral, Topeka, Marmaton, and Arbuckle reflections, for example, are manifested as prominent troughs on the reverse-polarity synthetic display.

The seismic data were loaded into a computer workstation using Landmark interpretation software. Frequency analysis and spectral shaping of seismic data were performed to attenuate unwanted noise from a seismic section and to enhance resolution. Landmark's BCM2D system provides the opportunity to analyze and shape frequency spectra of post-stack data in an easy and efficient manner with almost instant feedback. Central difference operators were also applied to 'whiten' wavelet-frequency spectra. Application of frequency analysis, spectral shaping, and central difference operators to data dramatically improved vertical resolution (up to 4×), accentuating and resolving thin intervals that were represented as mere inflections in the original data. Variable-density fills and reflection-strength displays of the seismic data were generated (figs. 8 and 9). Prominent events have been correlated on these sections, and where possible these horizons are identified on the synthetic seismograms (figs. 7 and 8), and labelled on the geologic cross section (fig. 4).

The lowermost correlated reflection on the seismic section, the trough identified as the acoustic basement, is thought to originate at the top of the crystalline Precambrian surface (i.e., purple event in figs. 8 and 9). Due to a paucity of basement penetrations in the immediate study area, this seismic event cannot be directly time-tied to well-log control. The interpretation of basement is consistent in part with 1) Precambrian

structural trends in the region, 2) well-log control in the immediate surrounding area, 3) the patterns of time-structural relief exhibited by post-Precambrian events, and the observed "basement events" that terminate abruptly where the acoustic basement is interpreted as steeply dipping or faulted. The abrupt termination of basement reflections across the basement-involved faulting is evident in both the variable-density fill and reflection-strength displays (figs. 8 and 9). As interpreted, vertical offset of the basement across the fault is approximately 60 msec (approximately 100–150 m; 328–492 ft). In areas that the basement dips more gently, basement reflections show a pattern of erosional truncation associated with apparent depositional onlap of the overlying sedimentary package (e.g., area between shotpoints 300 and 480). The difference in reflection strength above and below the purple event was also used to discriminate between the Precambrian basement and the overlying Phanerozoic sedimentary sequence. A pattern interpreted as deposition onlap of a buried Precambrian positive feature has been imaged by the seismic data across the Hampton field area. Similar patterns of onlap of Precambrian positive features have been reported by well data from numerous areas of the Central Kansas uplift and are documented to form hydrocarbon traps (e.g., Walters, 1946, 1991; Miller, 1968).

The overlying Arbuckle event is represented as a trough on the synthetic seismograms (figs. 10 and 11), and can be directly time-tied to the seismic data (i.e., aqua event of figs. 8 and 9). The pattern of time-structural relief observed along this unconformable surface is consistent with 1) well-log control, 2) the observed thinning of the Stone Corral/Arbuckle time interval, and 3) the pattern of time-structural relief interpreted along the acoustic basement. Relief at the Arbuckle level can be attributed, in part, both to depositional thinning related to onlap of pre-existing Precambrian structure and to reactivation of pre-existing fault planes in post-Arbuckle to pre-Pennsylvanian time. Subsequent erosion of the Arbuckle related to karst development at the pre-Pennsylvanian exposure surface heavily modified the structural relief associated with both pre-existing depositional and structural patterns. In interwell areas on the geologic cross section of fig. 4, relief along the Arbuckle and shallower horizons is based on the interpretation of these seismic data.

Subsequent shallower events (e.g., Marmaton, Topeka, and Stone Corral) also appear to drape the basement structure (figs. 8 and 9). In a manner consistent with compaction-induced drape, the magnitude of this relief decreases at shallower levels. This apparent correlation does not preclude the possibility that a component of the structural relief observed at shallower levels could be due to the reactivation of basement faults; however, it does indicate that if this was the case, net vertical movement

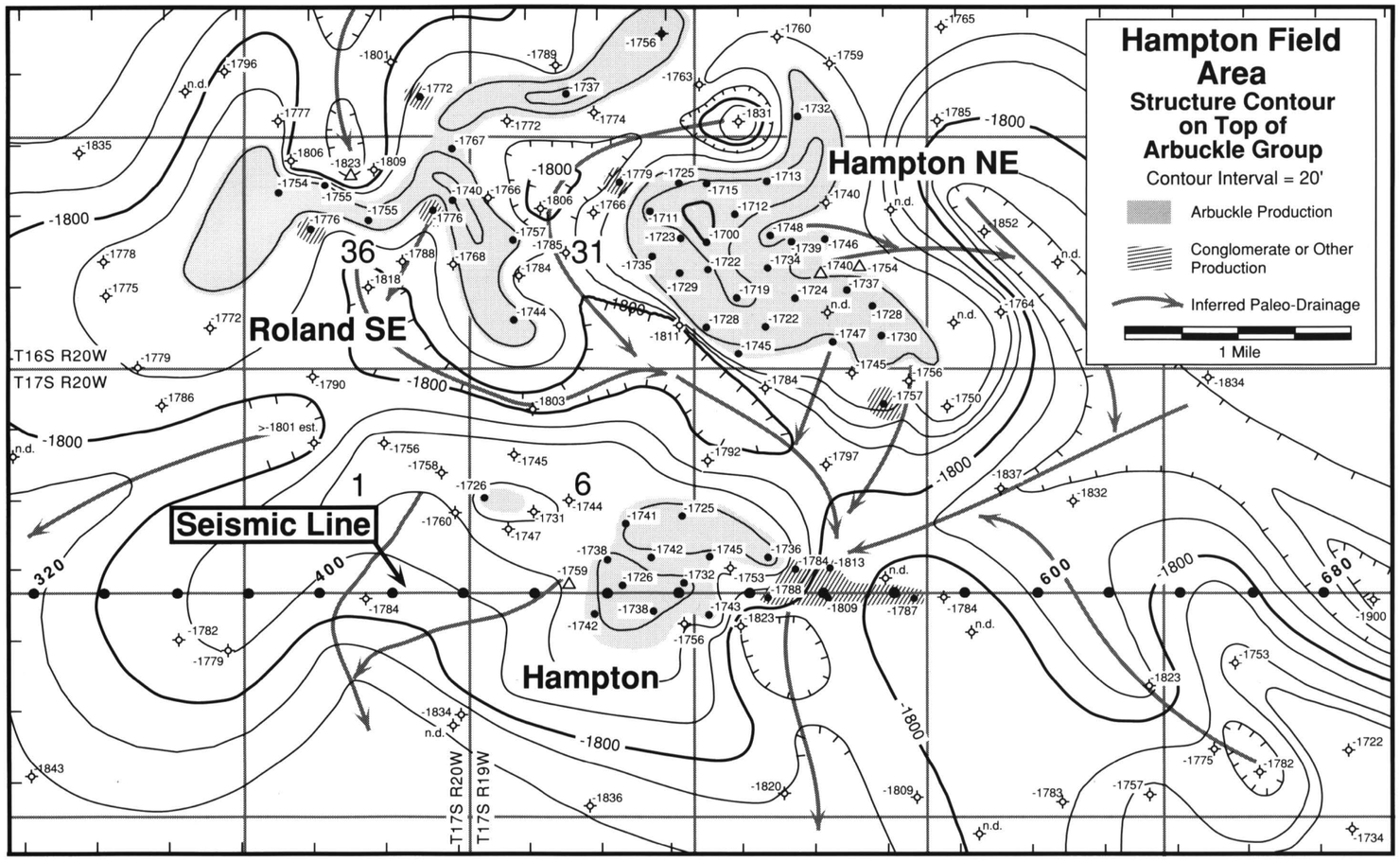

FIGURE 5—Structure contours on top of Arbuckle Group in the area of Hampton field. Oil production from the Arbuckle is confined to the tops of highs that are interpreted as erosional highs on a heavily karsted surface. Paleodrainage patterns are shown to be poorly organized and segmented as a connecting series of compound sinks, half-blind valleys, and steepheads. Cherokee conglomerate production at Hampton field is concentrated along an area where surface flow may have been underground and may be related to brecciation associated with cave collapse.

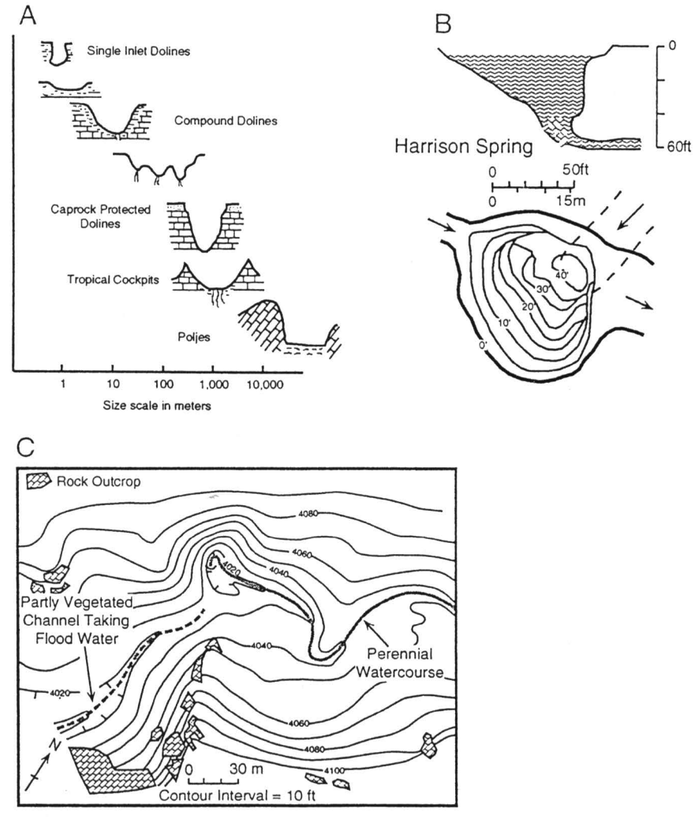

FIGURE 6—Selected surface landforms in modern karst regions: A) profile sketch illustrating scale and types of closed depression features; B) alluviated spring and rise pit; C) a half-blind valley. All figures modified from Jennings (1985).

was either relatively small (compared to pre-existing relief at the basement level) or that the sense of vertical movement was consistent with earlier faulting. Compelling evidence to attribute structure along the shallower horizons to compaction across crystalline basement (as opposed to post-depositional faulting) is the lateral continuity of reflections and the uniformity of such units as the Hutchinson Salt Member (figs. 8 and 9). Although the Hutchinson Salt drapes appreciably across basement highs, the time-thickness of this rock-salt unit is effectively uniform along the length of the seismic line. Additionally, there is no seismic evidence of salt dissolution. If structural relief at the Hutchinson level were primarily due to faulting, some localized salt dissolution would be expected (Anderson et al., this volume, p. 57–65; Anderson et al., this volume, p. 66–70).

Summary/Discussion

The seismic data across the Hampton field were used in conjunction with regional well control to provide insight into the geologic history and petroleum geology of the southwestern flank of the Central Kansas uplift. Paleotopographic relief at the level of the Arbuckle exposure surface appears to be a function of well-developed karst that was strongly influenced by pre-existing basement structure. The seismic data across Hampton image both the basement-involved faulting [approximately 100–150 m (328–492 ft) of vertical offset], and the effect of this basement relief on the subsequent depositional onlap of the Cambrian? and Ordovician sediments. Thinning of Cambrian–Ordovician sediments across the positive Precambrian feature at Hampton field appears to be of a magnitude of 75–100 m (248–330 ft) and is interpreted as a result of both depositional onlap and erosional truncation.

The Cherokee isopach, the Arbuckle structural map, and the seismic data show the effect of basement structure and erosional paleotopography on Cherokee sedimentation. The Cherokee was deposited, filling depressions and valleys in the underlying Arbuckle erosion surface. The Cherokee thins from over 30 m (100 ft) in Arbuckle lows to less than a meter (2 ft) over the highs (figs. 8 and 9). The seismic data across the Hampton area shows a well-developed onlap pattern of Cambrian and Arbuckle reflections on both sides of the basement high and are interpreted to represent up to 100 m (328 ft) of depositional relief (figs. 8 and 9). On the basis of well tops and the seismic data, structure persists but diminishes significantly up through the entire section. The local structural relief is over 30 m (100 ft) on the Arbuckle surface and decreases to less than 7 m (25 ft) at the Stone Corral Anhydrite. The structural and stratigraphic content of the seismic data appears to hold a high degree of integrity against the well data.

On the basis of the parallel nature of seismic reflections, absence of observed faults cutting well bores, and lack of significant local changes in post-Cherokee isopachs across Arbuckle highs, the structure after the pre-Pennsylvanian unconformity is interpreted as the result of differential compaction and drape across the pre-Cherokee structures. The pre-Desmoinesian to post-Mississippian development of the Central Kansas uplift and subsidiary features is probably related to the inherited and reactivated basement structure recognized on the seismic data (Merriam, 1963). Due to the absence of deep Arbuckle penetrations in the Hampton area, the degree of structural influence on the Arbuckle reservoir can not be determined from well control. However, based on seismic data, pre-existing basement structure appears to strongly influence the development of paleogeomorphic features observed on the Arbuckle erosional surface. Both Arbuckle structure and reservoir quality were significantly modified by karst at the pre-Pennsylvanian regional unconformity.

Karst terrains, such as that interpreted in the Hampton area, have poorly organized drainage systems separated from irregular shaped highs by relatively steep slopes. The highs are cut by re-entrants with steep head walls and sinks (dolines) at their heads. Arbuckle fields, such as Hampton and its neighboring fields, are examples of unconformity traps in which an understanding of paleogeomorphology and inherited basement structure are critical to successful exploration and development. The existence of extension opportunities has been demonstrated in the area such as the southwestern extension of Hampton Northeast (Littler "1," 1990 discovery), and the Roland Southeast field (1988 discovery). Examination of the structure map on top of the Arbuckle and comparison to cumulative production patterns indicates a number of additional infield and extension opportunities in the area. In addition stratigraphically lower intervals of the Arbuckle and Cambrian may be viable targets where they onlap the older Precambrian positive features.

ACKNOWLEDGMENTS—The seismic data were donated by Lockhart Geophysical. Their generosity is appreciated. Mr. James R. Daniels provided valuable feedback as to well locations and tops.

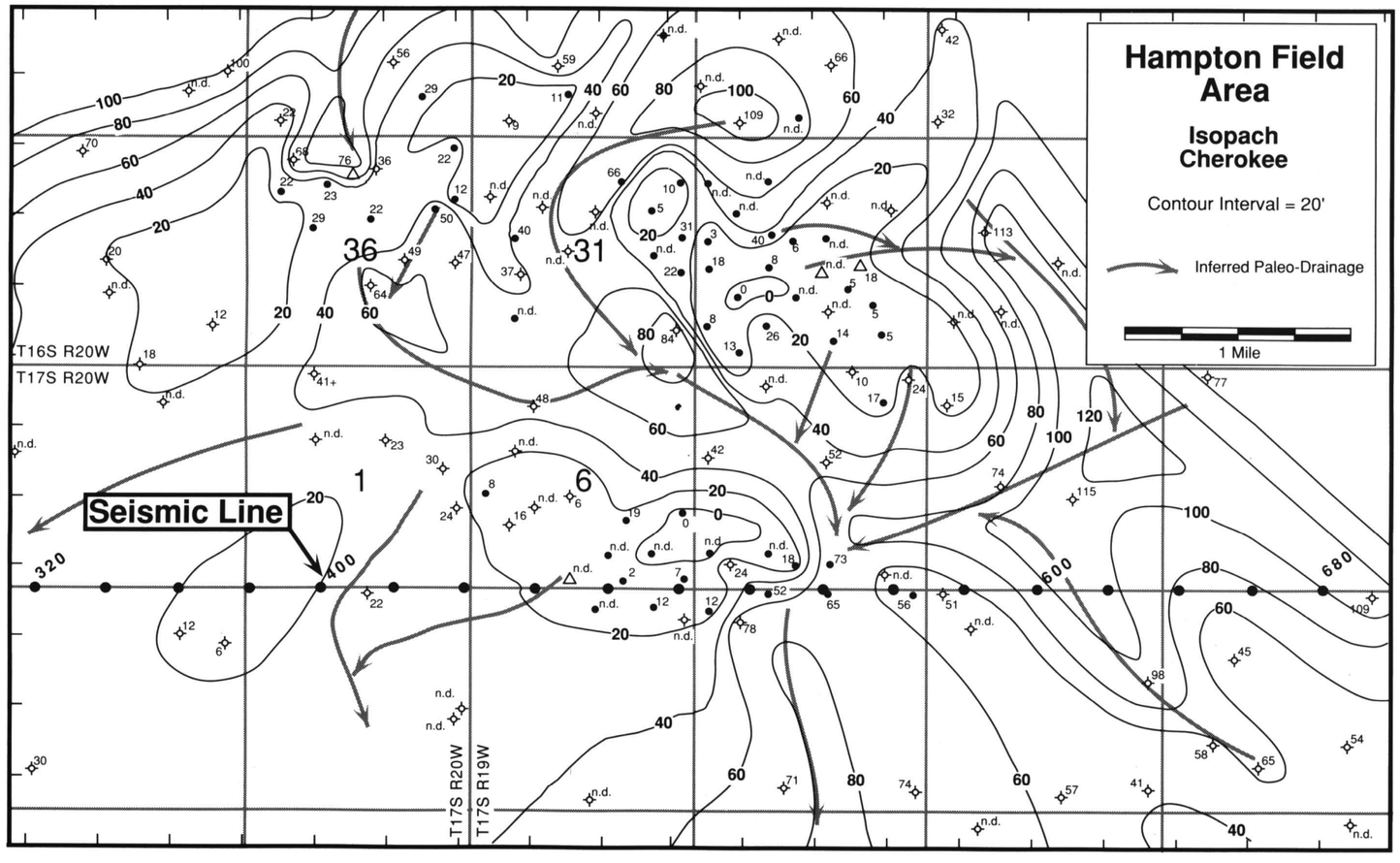

FIGURE 7—CHEROKEE ISOPACH IN THE AREA OF HAMPTON FIELD. The Cherokee fills in the Arbuckle paleotopograpy (figs. 3 and 5). Cherokee thins from over 30 m (100 ft) in Arbuckle lows to less than a meter (2 ft) over the highs.

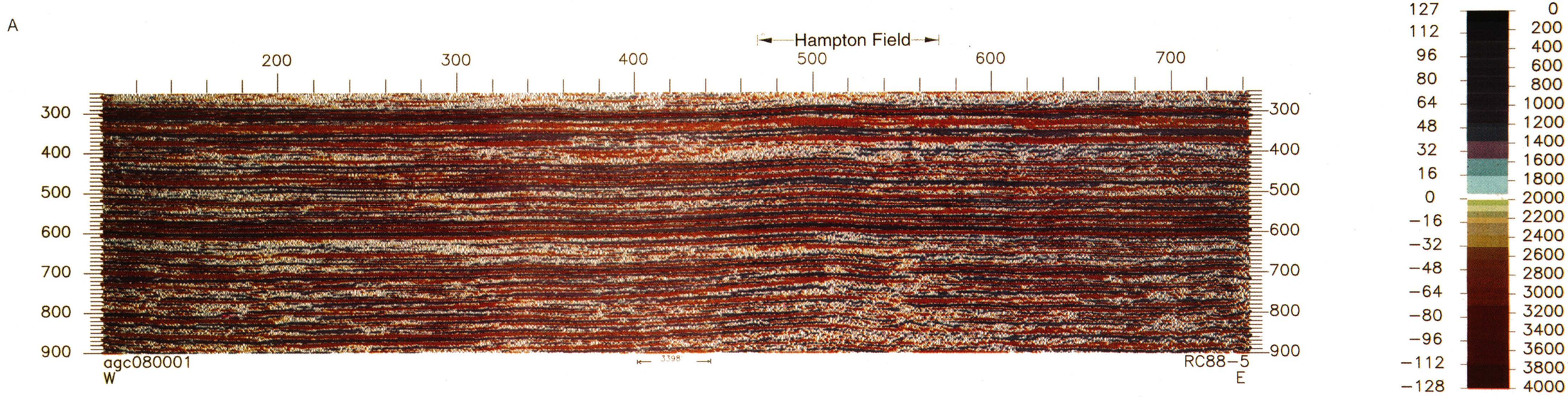

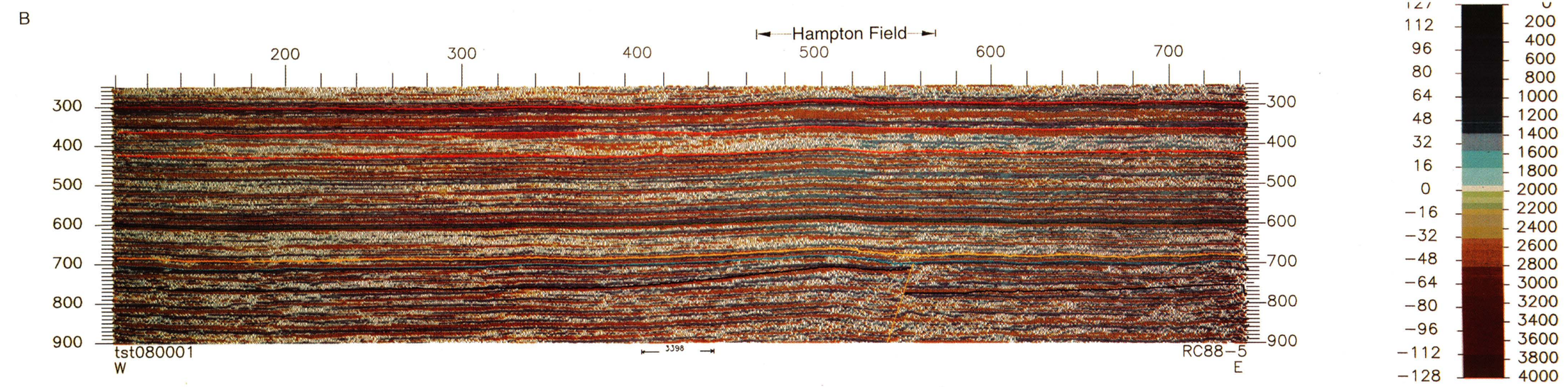

FIGURE 8A and 8B—UNINTERPRETED AND INTERPRETED, REVERSE-POLARITY, VIBROSEIS SEISMIC PROFILE ACROSS THE HAMPTON FIELD (fig. 3). These data are interpreted to show basement-involved faulting, depositional onlap of Cambrian and Arbuckle units, and compaction and were acquired by Lockhart Geophysical using a split-spread receiver array with a source interval of 165 ft (50 m), a group interval of 82.5 ft (25 m), and near and far offsets of 412.5 ft and 2,805 ft (126 m and 855 m), respectively. Twelve 12-sec, 14–150-Hz sweeps were summed at each source location. The notch filter was out. The interpreted horizons from the deep to shallow include top of interpreted basement (purple), top of Arbuckle Group (aqua), top of Marmaton Group (yellow), top of Topeka Limestone (green), base and top of Hutchinson Salt (orange), and top of Stone Corral Formation (red). Basement-involved faulting is highlighted in yellow.

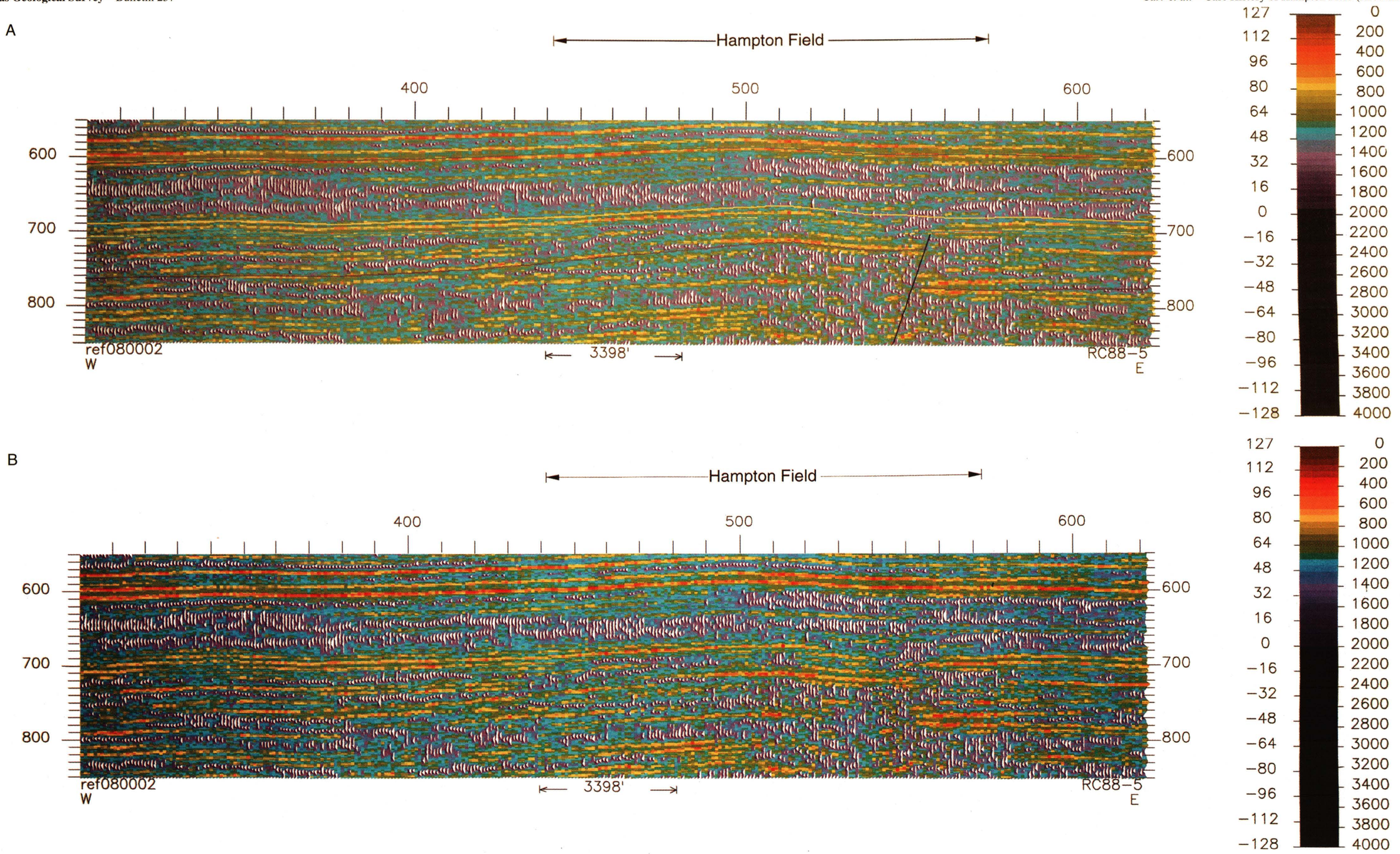

FIGURE 9A and 9B—UNINTERPRETED AND INTERPRETED REFLECTION-STRENGTH DISPLAY OF THE SAME SEISMIC DATA AS PRESENTED IN FIG. 8. The reflection-strength display highlights the difference in the interpreted Precambrian basement and the overlying Phanerozoic sedimentary sequence. The basement-involved fault is also highlighted in this display. Interpreted horizons are identical to fig. 8.

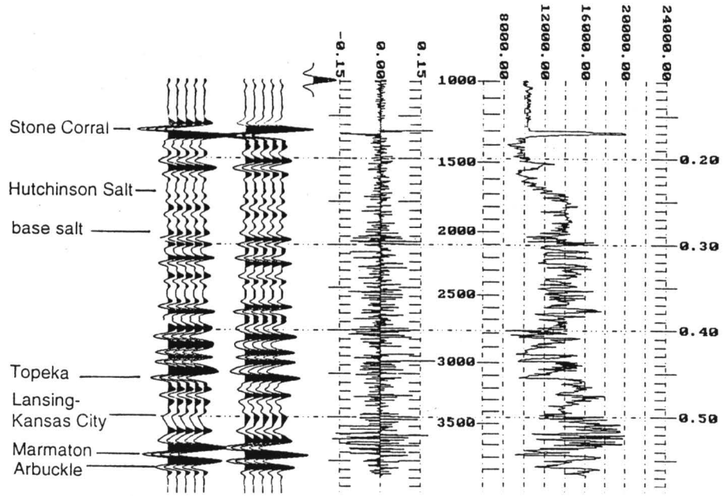

FIGURE 10—INTEGRATED SONIC LOG, ACOUSTIC-IMPEDANCE CURVE, AND 52-HZ, ZERO-PHASE, RICKER-WAVELET BASED SYNTHETIC SEISMOGRAMS FOR THE SW NE NW SEC. 6, T. 17 S., R. 19 W. WELL (fig. 3). The well is about 0.8 km north of trace 490; the corresponding normal-polarity synthetic seismogram ties the seismic line reasonably well at trace 1060 (figs. 8 and 9). These synthetic seismograms were generated using Geophysical Micro-Computer software.

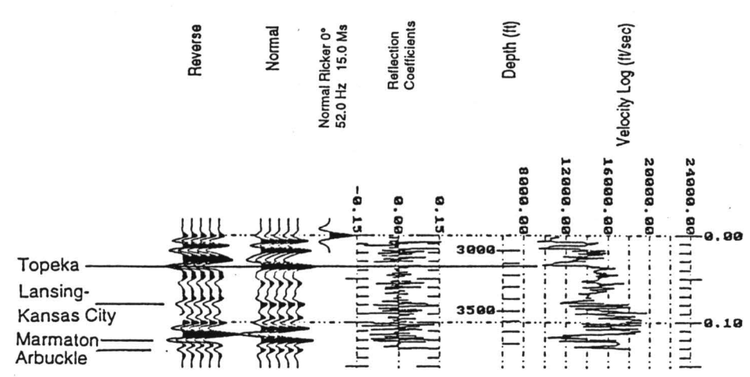

FIGURE 11—INTEGRATED SONIC LOG, ACOUSTIC-IMPEDANCE CURVE, AND 52-HZ, ZERO-PHASE, RICKER-WAVELET BASED SYNTHETIC SEISMOGRAMS FOR THE SE SE SE SEC. 6, T. 17 S., R. 19 W. WELL (fig. 3). The well is effectively on-line; the corresponding synthetic seismogram ties the seismic line at trace 980 (figs. 8 and 9). These synthetic seismograms were generated using Geophysical Micro-Computer software.

References

Adler, F. J., 1971, Future petroleum provinces of the midcontinent, region 7; *in,* Future Petroleum Provinces of the United States—Their Geology and Potential: American Association of Petroleum Geologists, Memoir 15, p. 985–1,120

Bloesch, E., 1964, Arbuckle production and prospects in northeastern Oklahoma: Tulsa Geological Society Digest, v. 32, p. 91–97

Carr, T. R., 1994, Kansas oil and gas production trends: Kansas Geological Society, Bulletin, v. 69, no. 8, p. 12–16

Gatewood, L. E., and Fay, R. O., 1992, Untapped potential from Mexico to Mississippi—Surprises of the Ellenburger–Arbuckle–Knox trend: Oil and Gas Journal, October 19, p. 93–96

Jennings, J. N., 1985, Karst geomorphology: Basil Blackwell, New York, 293 p.

Merriam, D. F., 1963, The geologic history of Kansas: Kansas Geological Survey, Bulletin 162, 317 p.

Miller, R. R., 1968, Geology of Otis–Albert field, Rush and Barton counties, Kansas; *in,* Natural Gases of North America, W. Beebe, ed.: American Association of Petroleum Geologists, Memoir 9, p. 1,588–1,615

Mullins, C. A., and Ireland, W. C., 1967, Additional Arbuckle reserves developed below original completion depth in stratified reservoir: Society of Petroleum Engineers of AIME, Paper No. SPE 1963

Newell, K. D., Watney, W. L., Cheng, S. W. L., and Brownrigg, R. L., 1987, Stratigraphic and spatial distribution of oil and gas production in Kansas: Kansas Geological Survey, Subsurface Geology Series 9, 86 p.

Ramondetta, P. J., 1990, El Dorado—an old field with potential: Oil and Gas Journal, March 26, p. 110–116

Sloss, L. L., 1963, Sequences in the cratonic interior of North America: Geological Society of America, Bulletin, v. 74, p. 93–114

Walters, R. F., 1946, Buried Precambrian hills in northeastern Barton County, central Kansas: American Association of Petroleum Geologists, Bulletin, v. 30, p. 660–710

_____, 1958, Differential entrapment of oil and gas in Arbuckle dolomite of central Kansas: American Association of Petroleum Geologists, Bulletin, v. 42, p. 2,133–2,173

_____, 1991, Gorham oil field, Russell County, Kansas: Kansas Geological Survey, Bulletin 228, 112 p.

Walters, R. F., Gutru, R. J., and James, A., III, 1979, Channel sandstone oil reservoirs of Pennsylvanian age in northwestern Ness County, Kansas; *in*, Pennsylvanian Sandstones of the Midcontinent, N. J. Hyne, ed.: Tulsa Geological Society, Special Publication No.1, p. 313–326

Watney, W. L., and Paul, S. E., 1983, Oil exploration and production in Kansas—present activity and future potential: Oil and Gas Journal, v. 81, p. 193–198

Case History of Walta Field (Simpson and Mississippian), Sumner County, Kansas

Timothy R. Carr[1], Neil L. Anderson[2], and Tim Pulliam[3]
[1]Kansas Geological Survey, Lawrence, KS 66047;
[2]Department of Geology, University of Missouri–Rolla, Rolla, MO 65401; and
[3]Consultant, Houston, TX

Abstract

Walta field (448 MBO) is a small field located in Sumner County, Kansas (principally in secs. 19 and 30, T. 33 S., R. 3 W., and sec. 25, T. 33 S., R. 4 W.). Cumulative production of 448 MBO is principally from a sandstone traditionally assigned to the uppermost Simpson Group (Middle Ordovician), but which may be Misener (Upper Devonian–Lower Mississippian), the basal transgressive sand below the Chattanooga Shale. Secondary production is from the Mississippian (Osagean) "chat" just beneath the sub-Pennsylvanian unconformity.

Production at the Mississippian level is structurally trapped, but deeper production at the Simpson/Misener level is stratigraphically trapped by either a pinchout of the "Simpson" sandstones reservoir as they onlap a pre-existing structure or by a truncation by pre-Chattanooga erosion. Primary structure at Walta field is related to Late Mississippian–Early Pennsylvanian tectonic movement that formed a series of westward-tilted fault blocks on a northeast-southwest-trending structural nose. This Late Mississippian–Early Pennsylvanian tectonic event is recognized throughout Kansas and formed a series of similar northeast-southwest-oriented structures throughout Sumner County and the Sedgwick basin of south-central Kansas. These structural elements appear to be the primary control on the distribution of Ordovician through Mississippian production in the vicinity of Walta field. Within Walta field, northwest-southeast cross-faults define separate pools at the Simpson–Misener reservoir interval, and provide additional extension and exploration opportunities.

Seismic data successfully image the northeast-southwest structural elements that are a critical component in both the Simpson–Misener and the Mississippian pools at Walta field. The seismic data provide insight into the stratigraphic geometries associated with the pinchout/truncation of the Simpson–Misener reservoir interval, and indicate the presence of pre-existing (pre-Chattanooga) structure. Integration of geophysical and geologic data provides an improved understanding of the depositional and tectonic events that led to the hydrocarbon accumulation at Walta field.

Introduction

Walta field is one of the numerous moderate to small fields (i.e., 0.2–5 MMBO) located throughout the part of the eastern Sedgwick basin that produce from either the Middle Ordovician Simpson or Upper Devonian–Lower Mississippian Misener sandstones and the Mississippian (Osagean) chat (figs. 1 and 2). The Sedgwick basin is a relatively broad southward-plunging embayment of the Anadarko basin of Oklahoma, and is bordered by the Central Kansas uplift and the Pratt anticline to the west, and by the Nemaha uplift to the east (fig. 1). Reported production from Walta field is primarily from a thin sandstone traditionally assigned to the uppermost Simpson Group (Middle Ordovician). Secondary, but important, production is also reported from the Mississippian (Osagean).

Mississippian (Osage) production is widespread in central and south-central Kansas and is typically at or near the top of the Mississippian section and just below the sub-Pennsylvanian unconformity. Mississippian production is reported from numerous small fields such as Walta in the Sedgwick basin (Newell et al., 1987). Solution weathering of the Mississippian limestones commonly produces a residual cherty, porous zone just beneath the unconformity called the "chat" (a modification of the word "chert;" Ver Wiebe, 1950). In general, reservoir characteristics of the chat zone (e.g., thickness, porosity, and permeability) are extremely variable. At Walta field the Mississippian reservoir displays characteristics of shallow weathering with chat grading to fresh chert in the top 3–4 m (10–15 ft) beneath the sub-Pennsylvanian unconformity.

The majority of the production reported from Walta field is from a thin sandstone traditionally assigned to the uppermost Simpson Group. Late Mississippian–Early Pennsylvanian tectonic movement removed the Simpson over much of the Central Kansas uplift, the Nemaha uplift, and northwestern Kansas. As a result, production from the Simpson Group is primarily limited to the Sedgwick basin and adjacent areas of south-central Kansas. Production trends are evident along the southern margin of the Central Kansas uplift and down the Pratt anticline where the Simpson Group subcrops beneath the sub-Pennsylvanian unconformity (Newell et al., 1987). The Simpson also produces beneath the sub-Pennsylvanian unconformity at the El Dorado field on the Nemaha uplift in Butler County (Jewett, 1954). The removal of the Simpson Group over much of the Central Kansas uplift, the Nemaha uplift, and northwestern Kansas is related to Late Mississippian–Early Pennsylvanian tectonic movement (Merriam, 1963). The absence of the Simpson in southeastern Kansas is due to pre-Devonian (pre-Chattanooga) erosion across the Chautauqua arch. Minor production in the Sedgwick basin comes from Simpson sandstones where they are truncated on the flanks of the Chautauqua arch. In Kansas, the Simpson Group is dominantly a sandstone-shale sequence with minor amounts of carbonate rock. The main reservoir rocks within the Simpson Group are light-gray, quartz-rich, friable sandstones sometimes called the St. Peter or Wilcox (Goebel, 1968).

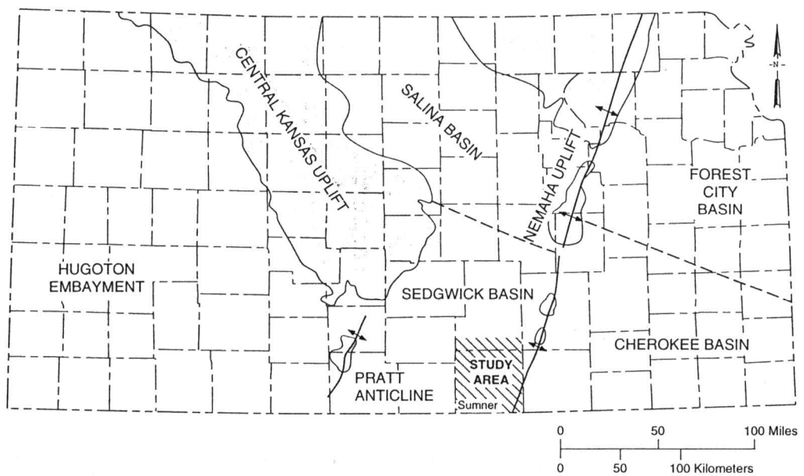

FIGURE 1—Map of Kansas showing the study area in relation to major structural features formed mainly in Late Mississippian and Early Pennsylvanian (after Merriam, 1963). Pattern indicates areas where Mississippian rocks are absent due to erosion on the sub-Pennsylvanian unconformity.

Simpson production is confined to the western flank of the faulted structural nose that forms the trap at the Walta field. The Simpson sandstone reservoir is not present or is very thin on the crest of the structure, being removed either by pre-Chattanooga erosion, or thinning by onlap onto a pre-existing high. If the onlap scenario is correct, the sandstone is probably a transgressive sand at the base of the Chattanooga Shale and should more appropriately be identified as Misener sandstone.

Misener sandstone is a thin, erratically developed transgressive sand at the base of the Chattanooga Shale. Misener sandstone reservoirs are scattered throughout the Sedgwick basin of south-central Kansas. In Kansas, the Chattanooga Shale is generally indentified by drillers as the Kinderhook Shale. The Misener sandstone can be up to

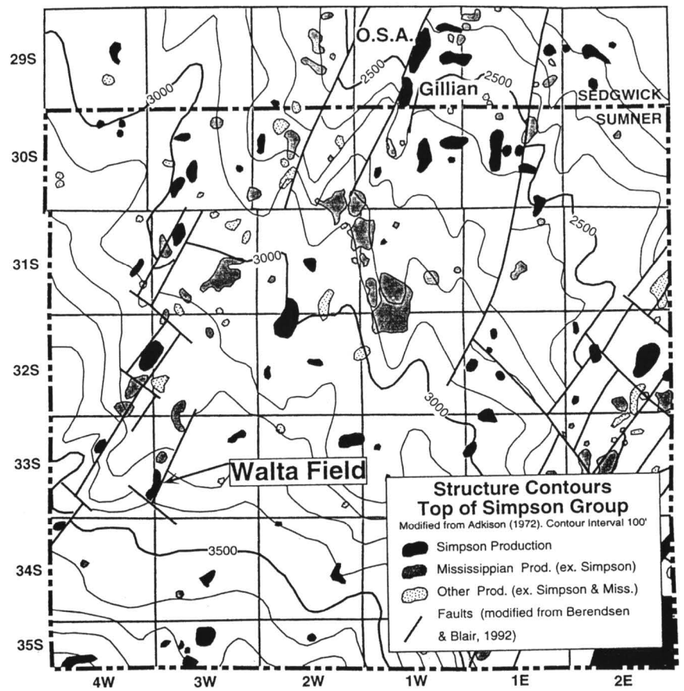

FIGURE 2—Structure contour map on top of Simpson Group in Sumner County and adjacent areas (modified from Adkison, 1972). Basement-involved faulting is modified from Berendsen and Blair (1992). Oil and gas fields that produce from the Simpson Group are highlighted. Structure contours. Field outlines and age of producing horizon from various sources.

several meters thick adjacent to the Central Kansas uplift, but elsewhere it is commonly represented by a slightly sandy zone at the base of the Chattanooga Shale. In areas along the eastern Sedgwick basin where Middle and Upper Ordovician shales and limestones have been removed by pre-Chattanooga erosion, the Misener can directly overlie the Simpson Group. Given that Misener sandstone was the result of reworking the exposed Simpson Group on the Chautauqua arch, it is difficult by lithologic criteria alone to distinguish the Misener from sandstones of the Simpson Group.

Distinguishing characteristics of the Misener were reported to be comparatively poor sorting, fairly abundant black phosphatic grains, and pyritic and siliceous cement (Adkison, 1972). Thirty miles (50 km) to the north at the O. S. A. field (T. 29 S., R. 1 W.), a thin sandstone reservoir in a similar stratigraphic position to the "Simpson" at Walta field was also assigned to the Simpson Group (Shawver, 1965a). This sandstone also thins by either erosion or onlap to the east across a faulted structural nose and forms a combination structural-stratigraphic trap. In addition, phosphatic grains ("specks") typical of Misener sandstone were reported to occur within this sandstone (Shawver, 1965a). The Simpson reservoir at the O. S. A. field may also be Misener and illustrates the difficulty in distinguishing the two in the absence of the overlying Ordovician shales and limestones. Further north at Valley Center field (T. 26 S., R. 1 W.), the overlying Viola Limestone is present, and the Misener sandstone can be recognized. Production at Valley Center field is reported from stratigraphic pinchout of the Misener sandstone along the flank of a structure. Structural traps are formed with both older and younger reservoirs on this anticline (Wright, 1960).

Based on present data, assignment of the sandstone-reservoir interval at Walta field to either the Misener or the Simpson is an open question. However, following tradition this reservoir interval at Walta will be simply referred to as "Simpson." In either case the "Simpson" sandstone at Walta field thins by either onlap or truncation onto a structure that existed prior to deposition of the Chattanooga (Kinderhook) Shale. Similar pre-Chattanooga structural influence is apparent in other "Simpson" pools in the eastern Sedgwick basin (e.g., O. S. A. field, Shawver, 1965a; and Gillian field, Shawver, 1965b).

Field Description

Walta field, located in Sumner County (principally in secs. 19 and 30, T. 33 S., R. 3 W., and sec. 25, T. 33 S., R. 4 W.), was discovered in 1959 by the Dorset #1 Walta (SE SE NE sec. 25, T. 33 S., R. 4 W.). Initial production was reported as 50 BOPD from the "Simpson." In 1961, oil was discovered in the Mississippian chat by the Dorset #3 Walta (SW NE SE sec. 25, T. 33 S., R. 4 W.). Annual production peaked in 1962 at over 135 BOPD from seven wells. Production declined steadily until the late 1970's (fig. 4). In the late 1970's, two wells, the Samson #3 Stewart (SW NW SW sec. 19, T. 33 S., R. 3 W.) and the Raymond #1 Stewart (NW NE SW sec. 19, T. 33 S., R. 3 W.), extended "Simpson" and Mississippian chat production in the Walta field to the north and resulted in a second peak in production (fig. 4). Production declined and has held steady at 3 BOPD from a single producing well from 1987 through 1993. Reported cumulative production through 1993 was 448 MBO (Beene, 1994).

The trap at Walta field is interpreted as being formed by a series of tilted fault blocks along a northeast-southwest-plunging anticlinal nose (fig. 3). The relatively steep eastern side of the structure is mapped as a northeast-southwest-trending fault. This fault is parallel and on line to other basement faults throughout the eastern Sedgwick basin (Berendsen and Blair, 1992). Similar tilted fault blocks have been noted at O. S. A. and Gillian fields (Shawver, 1965a), and may be a common trap component at other fields in the area (e.g., Fall Creek and Caldwell fields; Bass and Lukert, 1959). A structure contour map on top of the Simpson Group of Sumner County and adjacent areas (fig. 2) shows that oil and gas fields that produce from the Simpson Group and the Mississippian are associated with northeast-southwest structural trends that appear to be closely related to basement fault trends. The structure at Walta field, as based on subsurface mapping and depicted by a structural cross section (fig. 5), is attributed to Late Mississippian–Early Pennsylvanian tectonic movement. Structural relief decreases significantly above the sub-Pennsylvanian unconformity. The small amount of structural relief observed above the unconformity is attributed to depositional thinning and compaction over eroded and subdued paleotopography associated with the Late Mississippian–Early Pennsylvanian deformation and basal Pennsylvanian unconformity. This is consistent with previous interpretations of the tectonic and depositional history of Kansas (cf., Merriam, 1963). A series of northwest-southeast cross-faults define separate fault blocks and separate pools at the "Simpson" and possibly Mississippian levels at Walta field. The structural cross section shows one of the cross-faults between the #3 Stewart and #1 Stewart wells This fault has 30 ft (9 m) of vertical offset and defines separate "Simpson" pools (fig. 5). The cross-faulting in conjunction with the stratigraphic pinchout of the "Simpson" provide opportunities for additional extension and exploration activity in the vicinity of Walta field.

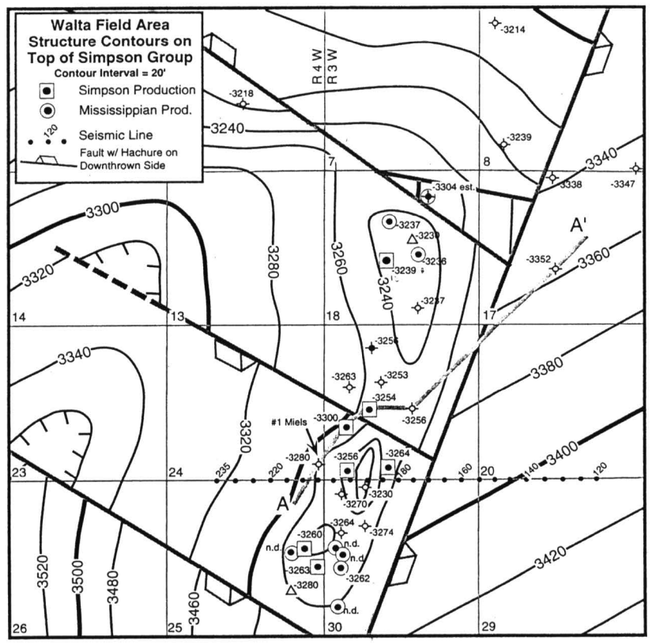

FIGURE 3—Structure contour map on top of Simpson Group of Walta field area, showing wells producing from both the "Simpson" and Mississippian chat. Locations of the geologic cross section (fig. 5) and seismic section (fig. 8) are shown.

Seismic Data and Interpretation

The example seismic profile for the Walta field (figs. 6 and 7) images the Late Mississippian–Early Pennsylvanian faulted anticline that provides the structural element of the "Simpson" and Mississippian hydrocarbon traps (figs. 3 and 5). This structural feature is characterized by up to 10 msec (66 ft, 20 m) of relative structural closure at the Simpson level. The Chattanooga Shale also shows up to 10 msec (66 ft, 20 m) of thinning and a pronounced lateral variation in its seismic image as it onlaps the high.

Data were acquired using a 24-fold air gun (75 cubic-inch chamber) and a 48-trace split-spread receiver array. Group and source interval was 82.5 ft (25 m). Near and far offsets were 82.5 ft (25 m) and 1,980 ft (603 m), respectively. Each group consisted of 12 inline Mark Products 30-Hz geophones. Three segments of six pops each were summed at each location. Sercel 338HR recording equipment was used with a recording sample rate of 2 msec. Low and high bandpass filters of 25 and 125 Hz were used, and the notch filter was out. Data are presumed to be zero-phase, and the displays are interpreted to be reverse polarity; therefore, increases in acoustic impedance correspond to troughs on the seismic data (figs. 6 and 7).

As an aid to the interpretation of the example seismic line, a suite of zero-phase, 52-Hz, Ricker-wavelet based, one-dimensional synthetic seismograms (both normal and reverse polarity displays) were generated for the #1 Meils well (E/2 SE SE sec. 24, T. 33 S., R. 4 W.; figs. 8, 9, and 10). The #1 Meils is effectively on-line, and the corresponding synthetic seismogram ties the seismic profile at trace 214. The synthetic seismogram and the seismic profile correlate reasonably well from the top of the Kansas City Group down to TD. The match is somewhat tenuous above the Kansas City Group. This is probably due to a combination of several closely spaced, thin low- and high-velocity layers, borehole cavitation (as indicated by the caliper log), and the use of a zero-phase Ricker wavelet in the construction of the synthetic seismogram.

The synthetic seismograms of fig. 8 were generated from the sonic log recorded at the #1 Meils well. On the reverse-polarity synthetic seismogram display, the tops of the

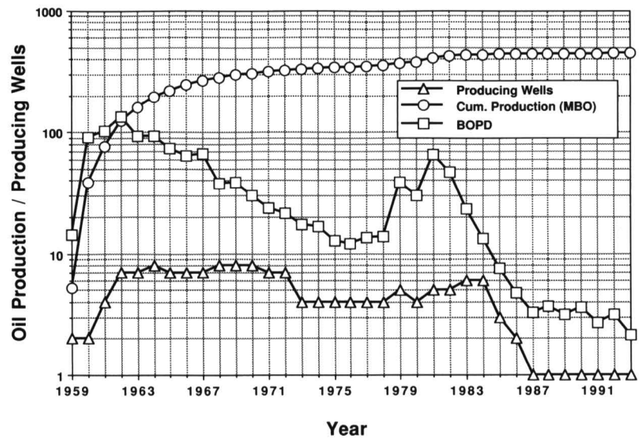

FIGURE 4—Annual production data from Walta field from 1966 through 1993. Cumlative production is from discovery in 1959 through 1993. Reported cumulative production from Walta is entirely oil, and through 1993 was 443 MBO. As of 1987, only a single well operated in the field. Data are from Kansas Geological Survey files and Beene (1994).

Mississippian subcrop and "Simpson" correspond to moderate-amplitude troughs. Conversely, the top of the Chattanooga is represented by a moderate-amplitude peak. The interval between the top of the Chattanooga and the top of the "Simpson" (Chattanooga/Simpson) interval is imaged as a doublet peak followed by a trough.

The synthetic seismograms of figs. 9 and 10 were generated for modified versions of the sonic log recorded at the #1 Meils well. More specifically, the Chattanooga/Simpson interval on the velocity log in fig. 9 was reduced (squeezed) by 10 ft (3 m) to simulate depositional thinning on-structure. In fig. 10, the Chattanooga/Simpson

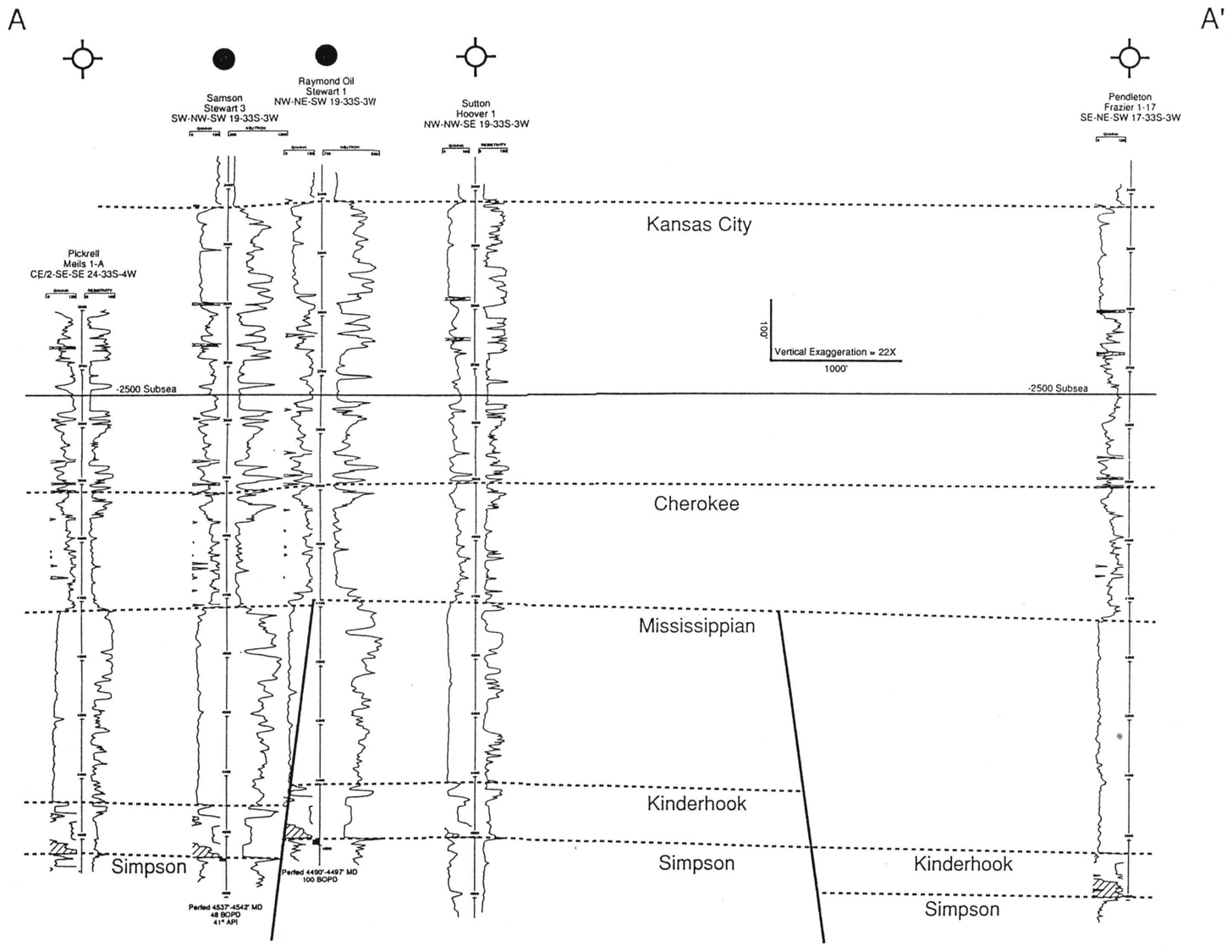

FIGURE 5—NORTHEAST-SOUTHWEST STRUCTURAL CROSS SECTION ACROSS A PART OF WALTA FIELD (see location on fig. 4). Structural relief at Simpson and Chattanooga levels decreases significantly in higher horizons. Faulting is interpreted to be related to Late Mississippian–Early Pennsylvanian tectonic movements. Erosion on the sub-Pennsylvanian unconformity has subdued relief at the unconformity. The fault between the #3 Stewart and #1 Stewart wells defines separate pools at the "Simpson" reservoir. This sandstone also pinches out up-structure toward the #1 Hoover well. Structural relief on higher markers (e.g., Kansas City) is very subtle, and is attributed to compaction across the eroded structural block.

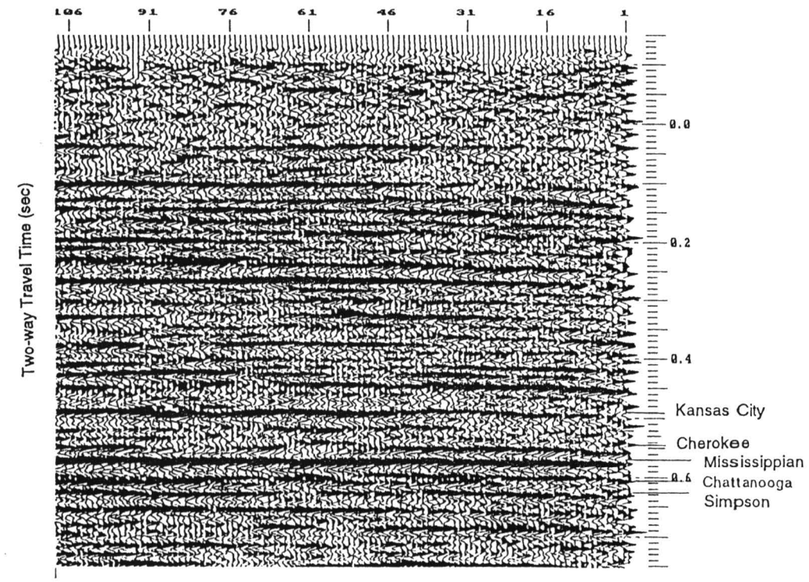

FIGURE 6—INTERPRETED, REVERSE-POLARITY DISPLAY OF THE EXAMPLE SEISMIC PROFILE ACROSS THE WALTA FIELD.

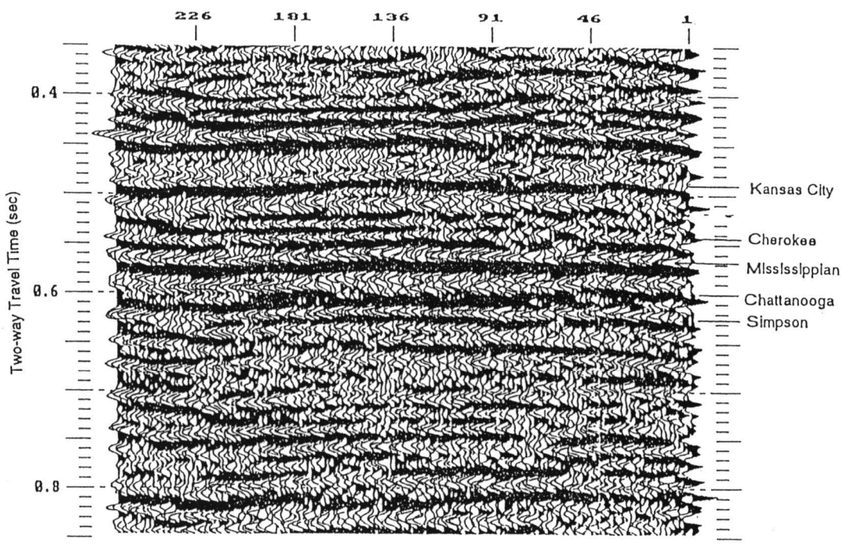

FIGURE 7—ENLARGED DISPLAY OF A PORTION OF THE EXAMPLE SEISMIC LINE (fig. 6).

interval on the velocity log in fig. 9 was increased (stretched) by 16 ft (5 m) to simulate depositional thickening off-structure. On the reverse-polarity displays of both synthetic seismograms, the tops of the Chattanooga and Simpson are represented by peaks and troughs of moderate amplitude, respectively. The significant difference is that the Chattanooga/Simpson interval on fig. 9 is imaged as a peak-trough sequence. On fig. 10, the Chattanooga/Simpson interval is imaged as a peak-trough-peak-trough sequence.

A reverse-polarity display of the field seismic data is presented in fig. 6. In fig. 7, a blowup of deeper reflections is shown in order to accentuate the seismic image of the subsurface at the pay-zone level. Several prominent events have been correlated on these sections; these horizons are identified on the synthetic seismograms (fig. 8), and labelled on the geologic cross section (fig. 5).

The lowest correlated reflection on the seismic profile is the trough identified as the Simpson. This horizon is characterized by up to 10 msec (66 ft, 20 m) of relative time-structural relief, being highest beneath the Walta field near the center of the profile. This pattern of time-structural relief is consistent with the thesis that the Misener or Simpson sandstones at the Walta field pinch out against the flanks of a positive structural feature at the Simpson level.

In contrast to the Simpson, the reflection associated with the top of the Chattanooga Shale is relatively flat across the Walta field, displaying less than 5 msec (33 ft, 10 m) of relief. This suggests that some of the structural relief at the Simpson level pre-dated the deposition of the Chattanooga Shale and Misener sandstone. This observation is also supported by the analysis of the seismic image of the Chattanooga–Simpson interval on the seismic profile (fig. 6). Off structure (east of trace 91 and west of trace 201), the Chattanooga–Simpson interval is generally represented by a peak-trough-peak-trough sequence. Across the crest of the structure (traces 123–147), this Chattanooga–Simpson interval is thinner and is represented by a peak-trough sequence. Elsewhere (on the flanks of the structure), the Chattanooga–Simpson interval is generally represented by a doublet peak-trough sequence of intermediate width. The change of character of the wavelets observed within the Chattanooga–Simpson interval on the seismic profile is similar to those observed on the suite of synthetic seismograms (figs. 8, 9, and 10). This observed similarity supports the interpretation that the Chattanooga–Simpson interval thins on-structure. The interpretation of the seismic data supports the concept that part of the structural relief at the "Simpson" pre-dates the major Late Mississippian–Early Pennsylvanian deformation and possibly influenced the deposition of the Misener and Chattanooga sequences.

The seismic reflection associated with the Mississippian strata subcropping the basal Pennsylvanian unconformity, like the Simpson reflection, is time-structurally higher (up to 5 msec; approximately 33 ft [10m]) across the Walta field than elsewhere on the seismic line. This pattern of relief could be the result of erosion at the Mississip-

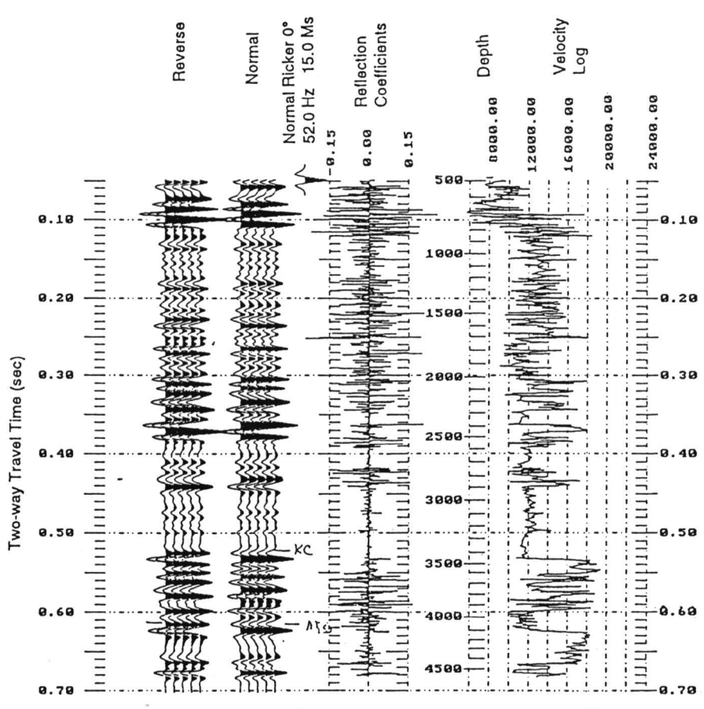

FIGURE 8—Integrated sonic log (ft/sec), acoustic-impedance curve, and 52-Hz, zero-phase, Ricker-wavelet based synthetic seismograms for the #1 Meils well (E/2 SE SE sec. 24, T. 33 S., R. 4 W.; see fig. 5). The #1 Meils is effectively on-line with the corresponding synthetic seismograms tying the seismic profile at trace 214. Horizon tops: Kansas City–3,448 ft (1,501 m); Cherokee–3,960 ft (1,207 m); Mississippian–4,112 ft (1,253 m); Chattanooga–4,456 ft (1,358 m); Misener–4,525 ft (1,379 m); Simpson–4,529 ft (1,380 m).

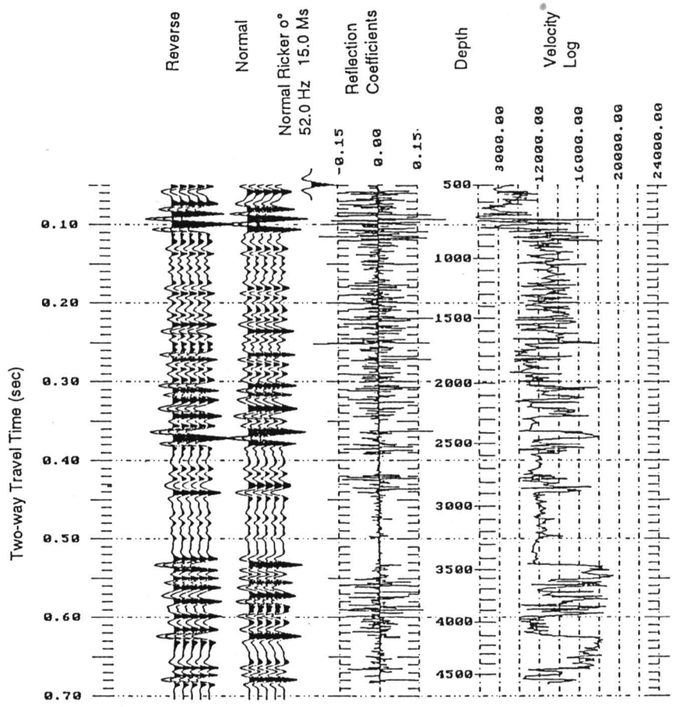

FIGURE 9—Modified synthetic seismograms for the #1 Meils well (E/2 SE SE sec. 24, T. 33 S., R. 4 W.; see fig. 5). The Chattanooga–Simpson interval in this model has been reduced (squeezed) by 10 ft (3 m) to simulate the depositional thinning of this interval over the crest of the structure. Horizon tops: Kansas City–3,448 ft (1,051 m); Cherokee–3,960 ft (1,207 m); Mississippian–4,112 ft (1,253 m); Chattanooga–4,456 ft (1,358 m); Misener–4,515 ft (1,376 m); Simpson–4,519 ft (1,377 m).

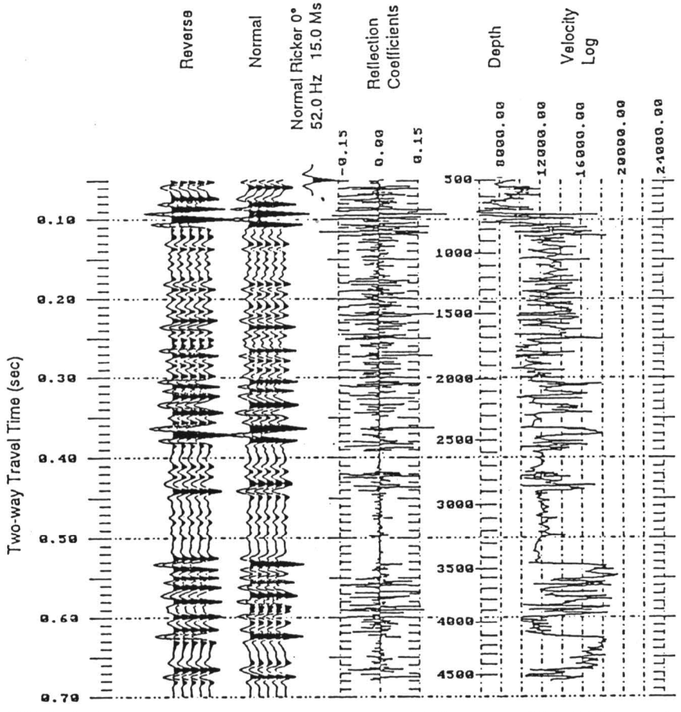

FIGURE 10—Modified synthetic seismograms for the #1 Meils well (E/2 SE SE sec. 24, T. 33 S., R. 4 W.; see fig. 5). The Chattanooga–Simpson interval in this model has been increased (stretched) by 16 ft (5 m) to simulate the depositional thickening of this interval on the flanks of the structure. Horizon tops: Kansas City–3,448 ft (1,051 m); Cherokee–3,960 ft (1,207 m); Mississippian–4,112 ft (1,253 m); Chattanooga–4,456 ft (1,358 m); Misener–4,542 ft (1,384 m); Simpson–4,546 ft (1,386 m).

pian subcrop level, compaction across the underlying Simpson structure, faulting as interpreted from the geologic data, a statics correction problem, or a combination of these processes or factors. The observation that less relief is observed at the Mississippian level than at the Simpson level supports the interpretation that some of the structure at the Simpson level pre-dates the deposition of the Misener sandstones.

Summary

Integration of geophysical and geological data provides an improved understanding of the depositional and tectonic events that led to the hydrocarbon accumulation at Walta field. Seismic data can successfully image the northeast-southwest structural elements that are a critical component in both the "Simpson" and the Mississippian pools in the eastern Sedgwick basin. The seismic data provide insight into stratigraphic geometries associated with the pinchout or truncation of the "Simpson" reservoir interval, and the presence of pre-existing (pre-Chattanooga) structure. The Walta field is a combination structural/stratigraphic trap at "Simpson" level. The "Simpson" sandstone is present only on the flanks of the structure, and either onlaps or is truncated by the unconformity at the base of the Chattanooga Shale. If the "Simpson" sandstones onlap the structure, they would more likely be related to the Chattanooga Shale and should be identified as Misener sandstone. In either case the "Simpson" sandstone at Walta field thins by either onlap or truncation onto a structure that existed prior to deposition of the Chattanooga Shale.

ACKNOWLEDGMENTS—Andre Steinle provided background information and contributed to the geologic interpretations. David Newell provided significant editorial feedback.

References

Adkison, W. L., 1972, Stratigraphy and structure of Middle and Upper Ordovician rocks in the Sedgwick basin and adjacent areas, south-central Kansas: U.S. Geological Survey, Professional Paper 702, 33 p.

Bass, B. L., and Lukert, L. H., 1959, Geophysical history of the Fall Creek pool, Sumner County, Kansas; *in,* Symposium on Geophysics in Kansas, W. W. Hambleton, ed.: Kansas Geological Survey, Bulletin 137, p. 287–295

Beene, D. L., 1994, Oil and gas production in Kansas: Kansas Geological Survey, Oil and Gas Production Dataset 92, 267 p.

Berendsen, P., and Blair, K., 1992, Midcontinent Rift System, Precambrian structure map: Kansas Geological Survey, Open-file Report 92–41A

Goebel, E. D., 1968, Ordovician System; *in,* The Stratigraphic Succession in Kansas, D. E. Zeller, ed.: Kansas Geological Survey, Bulletin 189, p. 14–15

Jewett, J. M., 1954, Oil and gas in eastern Kansas: Kansas Geological Survey, Bulletin 104, 39 p.

Merriam, D. F., 1963, The geologic history of Kansas: Kansas Geological Survey, Bulletin 162, 317 p.

Newell, K. D., Watney, W. L., Cheng, S. W. L., and Brownrigg, R. L., 1987, Stratigraphic and spatial distribution of oil and gas production in Kansas: Kansas Geological Survey, Subsurface Geology Series 9, 86 p.

Shawver, D. D., 1965a, O.S.A. field; *in,* Kansas Oil and Gas Fields, v.4: Kansas Geological Society, p. 175–183

_____, 1965b, Gillian field; *in,* Kansas Oil and Gas Fields, v.4: Kansas Geological Society, p. 78–87

Ver Wiebe, W. A., 1950, North American and Middle East oil fields: Edwards Brothers, Inc., Ann Arbor, Michigan, 259 p.

Wright, B. J., 1960, Valley Center field: Kansas Geological Survey, Kansas Oil Fields, v. 3, p. 149–156

Cherokee Sandstone Reservoir, Southeastern Kansas

Ralph W. Knapp[1], Neil L. Anderson[2] and John Youle[3]
[1]formerly with Kansas Geological Survey, Lawrence, KS 66047; [2]Department of Geology and Geophysics, University of Missouri–Rolla, Rolla, MO 65401; and
[3]Continental Exploration, Inc., Overland Park, KS 64081

Abstract

The oil reservoir encountered by the Timmons #1 well, Wilson County, Kansas, produces from a fluvial channel sandstone facies (point bar deposit) within the Cherokee Group known commonly as the "Bartlesville" Sandstone. Hydrocarbons are stratigraphically trapped, the porous sandstone facies effectively sealed within tight, dense shales. The reservoir is characteristic of many of the Pennsylvanian pools in southeastern Kansas in that the sandstone is both shallow (335 m; 1,105 ft) and thin (3 m; 10 ft). Its thinness makes it effectively transparent or invisible to conventional seismic data. High-resolution seismic data, however, use frequencies that are harmonic with the thickness of the sandstone, creating a tuning situation and effectively a bright-spot response of the horizon when sandstone is encountered. The interpretation is validated with the observation of drape over the channel and the polarity of the reflection.

Finally, the interpretation scheme was confirmed with the drilling of Timmons #3 directly north of Timmons #1 where a reflection character similar to that under Timmons #1 is seen on Line 2. Timmons #3 encountered porous sandstone of greater thickness than that under Timmons #1.

Introduction

Lower Middle Pennsylvanian sandstones of the Cherokee Group are estimated to have produced more than a billion barrels of oil in eastern Kansas over the past century. Traditionally, use of conventional CMP seismic methods has not been economically viable nor capable of detecting these sandstone lenses. However, using high-frequency CMP seismology, it is now possible to detect sandstone lenses as thin as 2 or 3 m (7–10 ft), encased in shales at depths of about 500 m (1,650 ft) or less.

General Geology

Pennsylvanian strata in the area of study (Wilson County, Kansas, fig. 1) accumulated in the Cherokee basin. This shallow foreland basin is the northen extension of the Arkoma basin. Although biostratigraphic control is poor, the basin probably began accumulating sediments during the Atokan Stage when the Arkoma basin rapidly subsided (Rascoe and Adler, 1983).

The entire Pennsylvanian section in the study area is about 450 m (1,485 ft) thick. Cyclic Missourian carbonate-dominated units, consisting of the classical Kansas cyclothem (Moore, 1936; Heckel, 1977) extend from the surface to about 18 m (59 ft) in depth. Below these rocks lie 75 m (248 ft) of carbonate- and shale-dominated cyclothems of the Marmaton Group (Desmoinesian). Below the Marmaton Group and above the basal Pennsylvanian unconformity surface lies about 150 m (495 ft) of siliciclastic mudrock-dominant cycles that comprise the Cherokee Group. Typically these cycles (3- to 15-m [10–50-ft] thick) consist of thin black or dark-gray marine shales and locally distributed thin limestones (less than 1 m [3.3 ft] thick) that grade upwards into coarsening-upward silty and sandy shales and locally thin sandstones. These coarsening-upward siliciclastic packages are interpreted to be the result of deltaic progradation into the marine realm. Delta plain underclays and coals cap most Cherokee cycles. Locally, Cherokee Group cycles may be partially or completely removed by incision and the resultant valleys may be filled with up to 75 m (248 ft) of sandstone. Sand-filled valleys, or shoestrings, may consist of several stacked, fining-upward successions (Staton, 1984; Brenner, 1989). Although early workers interpreted shoestring sandstones as marine barrier bars (Bass, 1936), recent workers have interpreted them to be deltaic distributary channels or upper delta-plain fluvial sands (Rich, 1923; Hulse, 1978; Staton, 1984; Walton et al., 1985; Jordan and Tillman, 1987).

The oil-productive sandstone in this investigation is referred to as upper "Bartlesville" (Bluejacket). It is confined within a valley that was incised up to 10 m (33 ft) into underlying noncyclic shales and localized coals. The lack of cyclicity in the underlying shales suggests that the upper "Bartlesville" valley may have incised into a slightly older valley, the upper part of which was filled with shale and minor coals. Insufficient control exists to map the lateral extents of the upper "Bartlesville" paleovalley; however, these valleys typically average about 400 m (1,320 ft) in width. Cores of the producing sandstone are not available and the genesis of the valley-fill sandstone is uncertain.

Sandstone in the Timmons #1 (fig. 1) is about 3 m (10 ft) thick (at 336–339 m; 1,104–1,114 ft) with an average porosity of 19.5%. The Timmons #2 well contains about 1.5 m (5 ft) of relatively tight sandstone (porosity, estimated from uncalibrated neutron logs, is about 9%). Although correlation of the sandstone between the two wells is tentative, they are probably genetically related (fig. 2).

Oil in the reservoir is stratigraphically trapped within a thin, shallow, and porous sandstone, probably of point-bar origin. The sandstone is encased in tight shales which effectively seal the reservoir and probably serve as the source. This is an excellent example of a stratigraphic trapping of hydrocarbons in a sandstone that can be resolved on high-resolution seismic data but cannot be seen on conventional-resolution data.

Subsurface Morphological Features

Figure 3 is a schematic diagram of the geological/morphological history of the shallow subsurface in the study area. In stage 1, a complete Pennsylvanian cyclothem has been deposited. These strata, from bottom to top, comprise a succession of nonmarine sandstone and shale, freshwater limestone, underclay and coal, and marine sandstone, limestone, and shale. In stage 2, fluvial sandstones representing the basal sediment of the overlying cyclothem are deposited in an incised channel. The channel sandstone is disconformable to the sediment of the underlying cyclothem. In stage 3, the cyclothem has gone through deep burial and subsequent uplift. It is once again proximal to the surface and is overlain by only a thin section of younger Pennsylvanian strata and a shallow veneer of Pleistocene sediment. Because of differential compaction, the pancake-layered stratigraphy of stages 1 and 2 has disappeared. The upper Pennsylvanian strata are now draped across the lensoid-shaped channel sandstone. Such drape is one of the keys, and a necessary condition, to identifying channel sandstones on seismic data.

Differential Compaction

As used here, the term *compaction* refers to net volume loss, whether physical or chemical, that a sediment undergoes in response to burial and loading. *Differential compaction* refers to the variable degrees to which different sediments with the same burial history will be compacted. The susceptibility of sediments to compaction is principally, although not exclusively, a function of lithology. The processes which contribute to the overall compaction of sediment include: 1) porosity loss due to the physical compression and deformation of strata and the expulsion of pore water (principally sandstone, shales, and clays); 2) pressure solution (principally carbonates); 3) dissolution (principally evaporites); 4) oxidation of organic matter (principally coals); 5) dehydration due to temperature (principally shales and clays); and 6) diagenetic chemical transformation (such as limestone/dolomite, gypsum/anhydrite, aragonite/calcite, and within clay minerals).

As suggested by fig. 3 and as seen on the seismic section (fig. 5), the channel sandstone is less compactable than the adjacent assemblage of interlayered shales,

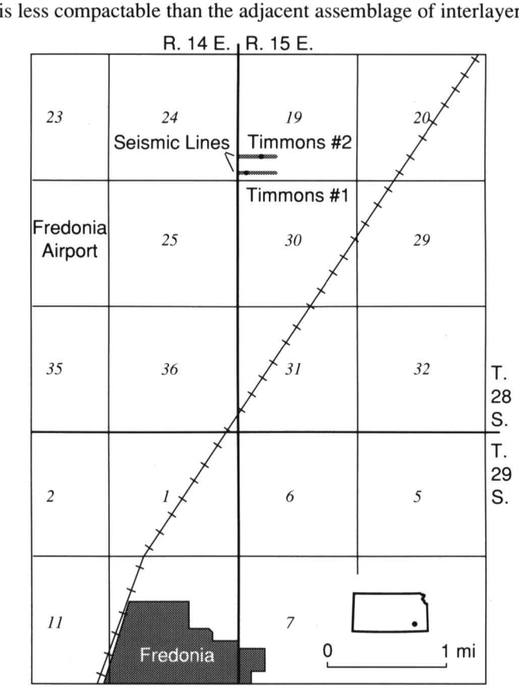

FIGURE 1—Map showing the locations of the example seismic lines and Timmons #1 and Timmons #2 wells.

sandstones, coals, clays, and limestones. The result is that post-channel Pennsylvanian strata are draped across the sandstone lense.

Seismic Tuning

Tuning occurs when the reflection from the base of a reflector constructively interferes with the reflection from the top of the reflector when there is a polarity reversal between the upper and lower reflections. In this situation, the travel path (two times the thickness of the layer) is half a wavelength, or the reflector thickness is one-fourth wavelength (fig. 4). Such thickness is termed *tuning thickness*. Knapp et al. (this volume, p.) show that the strongest reflections on a seismic section are not necessarily those with the largest reflection coefficient, but rather are those that are tuning. Tuning can nearly double the amplitude response, thus doubling the *apparent* reflection coefficient.

It is common practice to estimate the thickness of a reflector using tuning principles (Widess, 1972). In this manner, reflector thickness adjusts itself to the properties of the seismic data, and its thickness at that point is thereby derived. High-resolution methods, on the other hand, in effect adjust the seismic-data properties to the reflector. To create tuning of a thin reflector, a short wavelength (high-frequency) source function must be used. When the source function contains a wavelength that corresponds to that necessary for tuning of a thin sandstone lense, that lense will produce a strong reflection amplitude, i.e., a bright spot.

Further, Knapp (1990) shows that a particular thickness of cyclothem will tune to a particular frequency when that frequency is contained in the source function. This has two implications. First, data with a large bandwidth will be able to tune to more varieties of reflector thickness. This is the definition of high-resolution, a combination of high frequency (short wavelength) and broad bandwidth. Second, thickness of the pay zone can be estimated from the apparent frequency of the reflector.

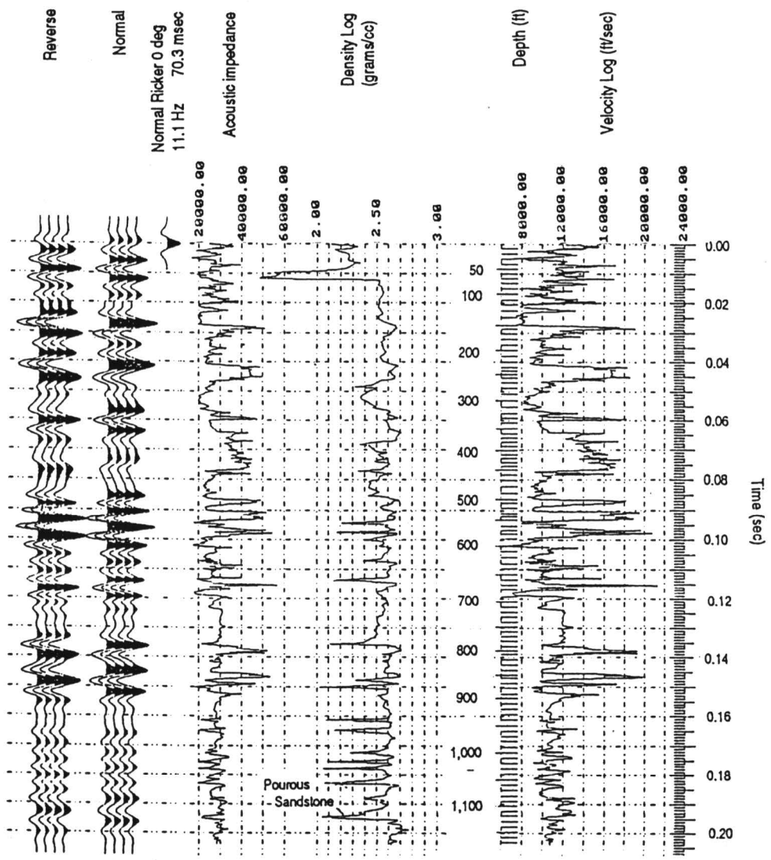

FIGURE 2—INTEGRATED VELOCITY LOG, DENSITY LOG, ACOUSTIC-IMPEDANCE CURVE, AND SYNTHETIC SEISMOGRAM FOR THE STROUD #5 WELL. This well encountered about 2.4 m (8 ft) of porous Cherokee sandstone at a depth of 341 m (1,119 ft). It is used as an illustrative example because of the availability of both density and sonic log control.

Seismic-data Acquisition

Twenty-four-fold CMP data (Mayne, 1962) were obtained along two west-east-oriented lines 470 m (1,551 ft) long (fig. 1). Line 1 passed through the Timmons #1 well where 3 m (18 ft) of reservoir sandstone were known to be. Line 2 passed through the Timmons #2 well where the sandstone was tight.

Group interval was 10 m (33 ft). Geophones were fixed in position and the source was shot through. The line used half-integer (5-m [16.5-ft] in-line offset) geometry (Knapp, 1985) and a lateral offset of 10 m (33 ft). The resulting near offset was 11 m. Due to cable restrictions only 36 channels could be recorded at a time, although the system had 48-channel capability. Geophones were Mark 23E models of 40-Hz natural frequency. Three bunched geophones were used per group. Data were recorded on two piggy-backed 24-channel model ES-2401 EG&G seismographs.

Seismic source was the "auger gun" (Miller et al., 1990) which screws into the ground, sealing the shot hole with the auger flighting. Air-blast is minimal and the energy coupling is maximized. The auger gun uses a blank 12-gauge shotgun shell, detonated at the bottom of 1-m (3.3-ft)-deep holes tamped with water.

Field records were 512 msec long with a sampling interval of 0.5 msec. To attenuate ground-roll noise, the records were low-cut filtered with a 70-Hz filter prior to digitization. Ground roll (and other noise) was further attenuated in processing (stacking) by use of the half-integer offset method (Knapp, 1985), stack-array principles (Morse and Hildebrandt, 1989), and correlation stack (Knapp, 1991a).

Special Aspects of Seismic Processing

Processing followed all normal procedures except that several special steps were performed to enhance quality of the results. To improve noise reduction of the data, two steps were followed:

First, stack-array processing was performed (Morse and Hildebrandt, 1989). The stack-array concept quantifies the attenuation of ground roll and other noises by CMP stacking. It assures that both the surface and subsurface are smoothly and evenly sampled in all possible sorting of the data: common shot (field files), common receiver, and common midpoint (CMP). It assures that the effective geophone array of the CMP gather is long and evenly sampled, which results in maximum possible rejection of ground-roll noise. Without stack-array processing and/or deliberate design of field arrays, the effective array of the CMP gather is a periodic square-wave function. The consequences of such an array are that it enhances particular frequencies of ground roll that are harmonic with the effective array. This enhancement is equal in magnitude to the enhancement of the reflection signal.

Second, a correlation-stack method (Knapp, 1991a) was used to perform CMP stacking. The correlation-stack routine used performs a residual normal moveout to enhance alignment of the reflection signal, and it weights the trace of each stack according to the correlation coefficient raised to a power n. In this case, $n = 4$. Both these function are time-variable. In short, the correlation stack performs a time-variable optimization of the reflection stack by time shifting and trace weighting.

Finally, post-stack spectral whitening (Knapp, 1991b) was performed to recover the losses of high frequencies due to source-function attenuation and the stacking process.

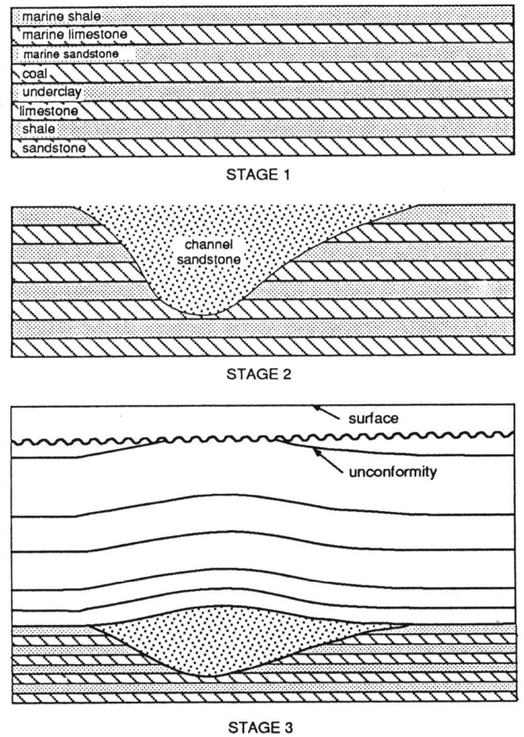

FIGURE 3—SCHEMATIC SHOWING THE SEQUENTIAL DEVELOPMENT OF A FLUVIAL CHANNEL SANDSTONE IN A TYPICAL CYCLOTHEM SEQUENCE.

This process is essential to the recovery of the full potential of the data. Resolution is proportional to frequency bandwidth, and this process enhances bandwidth by recovering the amplitudes of frequencies attenuated either by transmission through the earth or by unavoidable timing errors of the reflections prior to stacking during processing. Without spectral whitening, the data contain an unfulfilled resolution potential. The trick of spectral whitening is to recover the higher frequencies of the data without unnecessarily adding high-frequency noise. Thus, it is done experimentally with processor intervention and control.

Seismic Interpretation

To aid the interpretation of the seismic data (figs. 5 and 6), a suite of 1D synthetic seismograms were generated (figs. 7 and 4). The SP (sand present) synthetic and a synthetic seismic section were generated using the borehole density log for the Stroud #5. The SA (sand absent) synthetic A is a modified version of the SP synthetic created by replacing the porous sandstones by higher density shale. The SP synthetic C correlates satisfactorily with the seismic data of Line 1 (fig. 5) at the location of Timmons #1 (CMP 240). The SA synthetic A ties Line 2 (fig. 6) at the location of Timmons #2 (CMP 484), where the sand is absent.

Of particular interest on the synthetic seismic section is the signature of the channel sandstone (fig. 4). The channel sandstone is characterized by an anomalously high-amplitude trough-peak sequence which originates from the top and base of the upper and lower porous zones. This trough-peak sequence has a significantly lower amplitude on the SA synthetic, where the sandstone has been replaced by higher density shale. It is clear that, although interval velocity plays a roll in the reflection response, the reflection due to the sandstone is predominantly due to density, consistent with the lower density values of the porous sandstone compared to the tight surrounding shales. The magnitude of the reflection amplitude is enhanced by the fact that seismic-data wavelengths are harmonic with the two-way travel-time thickness of the channel, which causes tuning amplification.

The pattern of reflections on the seismic lines in the vicinities of the Timmons #1 (sandstone present) and Timmons #2 (sandstone absent) wells are similar in many respects to those on the SP and SA synthetic-seismic sections. Although comparison of the synthetic seismogram with the seismic data is consistent with the interpretation of the sandstone channel, an experienced interpreter knows that there can be coincidences between the two that are in fact unrelated and lead to mis-interpretation. (Such non-uniqueness is due to modeling and/or wavelet estimation errors, resolution limits of the wavelet, and/or inappropriate assumptions of the modeling process, e.g., omission of multiples).

An important aspect of the interpretation of the sandstone channel is the positive time-structural drape across it that is attributed to differential compaction between the channel sandstone and the surrounding regional facies (fig. 5, CMP 230 to CMP 260). The drape shown as indicative of the channel sandstone is not seen in the vicinity of the Timmons #2 well (CMP 484, fig. 6). This result is expected as the Timmons #2 well did not encounter any sandstone.

On Line 2, under CMP 445 (175 msec), one sees a signature similar to that under the Timmons #1 well on Line 1. One can even speculate that because the tuning frequency of this response is 100 Hz, that the sandstone is about 25% thicker under this location than at the Timmons #1 wellsite. Timmons #3 was drilled at this trace location, and this interpretation was confirmed. Oil production exceeded that of Timmons #1.

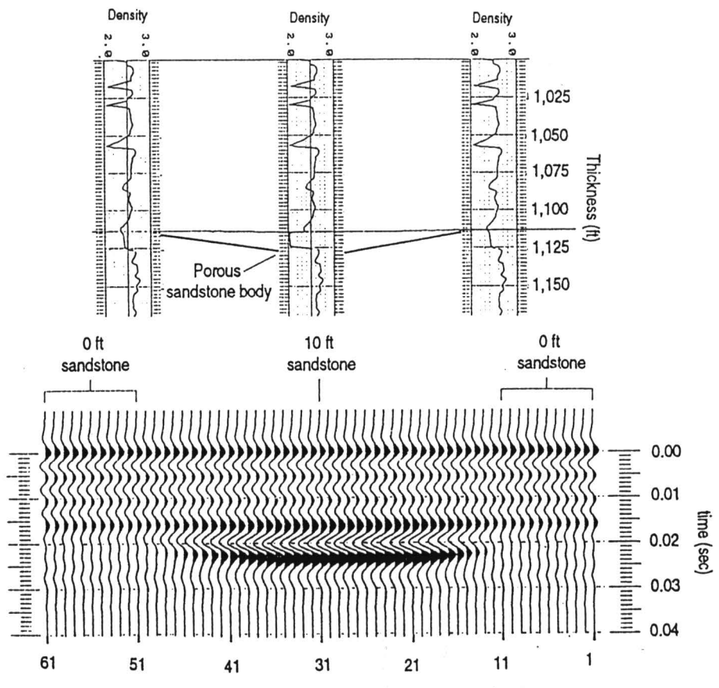

FIGURE 4—SYNTHETIC SEISMIC SECTION ILLUSTRATING THE SIGNATURE OF A 3-M (10-FT)-THICK CHANNEL SANDSTONE.

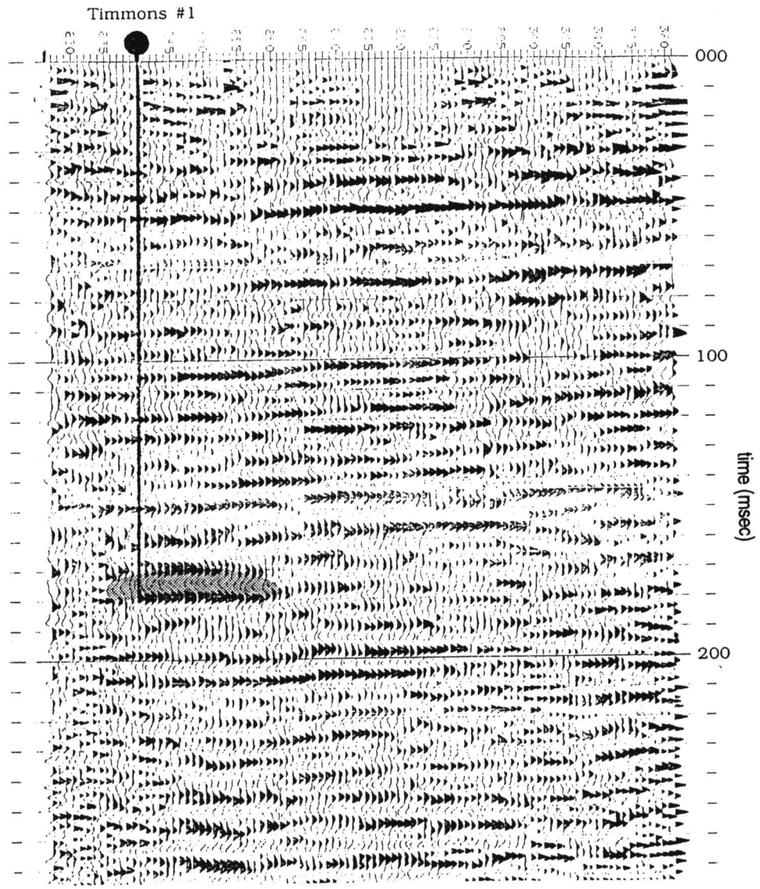

FIGURE 5—SEISMIC LINE 1. This seismic profile ties Timmons #1 well at trace 240.

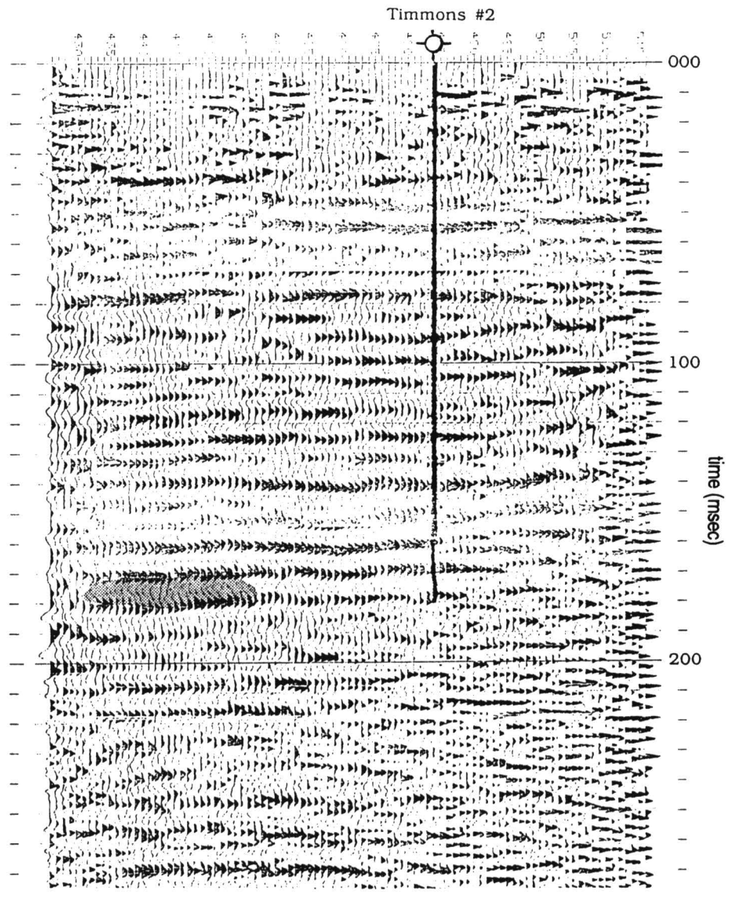

FIGURE 6—SEISMIC LINE 2. This seismic profile ties Timmons #2 at trace 484, and Timmons #3 at trace 440.

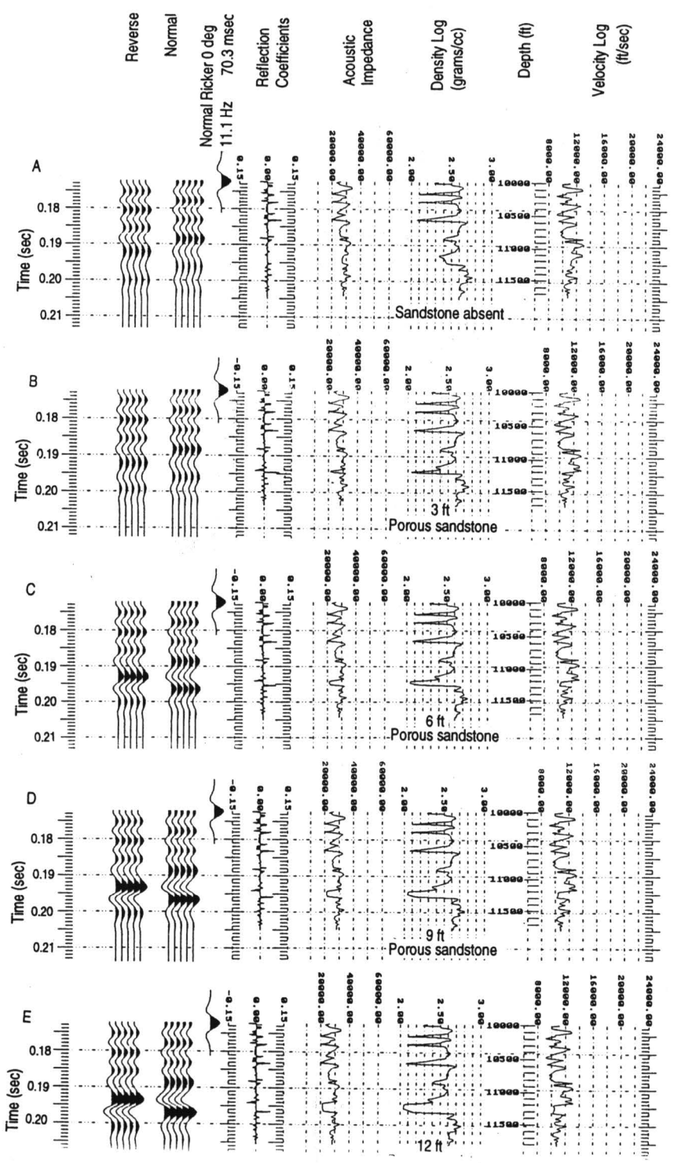

FIGURE 7—SUITE OF SYNTHETIC SEISMOGRAMS FOR THE STROUD #5 WELL. Seismogram A illustrated the situation where the porous sandstone has been removed from the section. In seismograms B through E, the thickness of the porous, low-density sandstone is increased from 0.9 m (3 ft) to 3.6 m (12 ft) in 0.9-m (3-ft) increments.

Summary

High-resolution seismic-reflection data were able to successfully map a thin, shallow channel sandstone. The channel sandstone was characterized by a high-amplitude trough-peak sequence that was sufficiently prominent to be called a bright spot. The trough-peak sequence is consistent with the fact that density of the sandstone is significantly less than the density of the adjacent shales. The bright spot is due largely to tuning amplification of signal considered to be high-resolution. The tuning frequency (125 Hz) is consistent with the thickness (3 m; 10 ft) of the channel sandstone with an interval velocity of about 1,500 m/sec (5,000 ft/sec).

Along with the amplitude anomaly of the seismic data, the data are characterized by draping of the surrounding strata over the bright-spot amplitude anomaly. This second line of evidence is also a necessary property of the data to derive the conclusion that the bright spot is a channel sandstone. The drilling of Timmons #3 confirmed the interpretation.

Thus, the channel sandstone is characterized by 1) a high-amplitude bright-spot density reflection, 2) negative polarity of the reflection (i.e., trough-peak sequence), and 3) draping of the overlying reflections over the lensoid-shaped sandstone.

References

Bass, N. W., 1936, Origin of the shoestring sands of Greenwood and Butler counties, Kansas: Kansas Geological Survey, Bulletin 23, 135 p.

Brenner, R. L., 1989, Stratigraphy, petrology, and paleogeography of the upper portion of the Cherokee Group (Middle Pennsylvanian), eastern Kansas and northeastern Oklahoma: Kansas Geological Survey, Geology Series 3, 70 p.

Heckel, P. W., 1977, Origin of phosphate black shale in Pennsylvanian cyclothems of midcontinent North America: American Association of Petroleum Geologists, Bulletin, v. 61, no. 7. p. 1,045–1,068

Hulse, W. J., 1978, A geologic study of the Sallyards field area, Greenwood County, Kansas: M.S. thesis, University of Kansas, 153 p.; also available as Kansas Geological Survey, Open-file Report 78–6

Jordan, D. W., and Tillman, R. W., 1987, Geologic facies analysis for enhanced oil recovery, Bartlesville sandstone, Greenwood County, Kansas; *in*, Reservoir Sedimentology, R. W. Tillman, and K. J. Weber, eds.: Society of Economic Paleontologists and Mineralogists, Special Publication, no. 40, p. 311–332

Knapp, R.W., 1985, Using half-integer source offset with split-spread CDP seismic data: The Leading Edge, v. 4, no. 10, p. 66–69

_____, 1990, Vertical resolution of thick beds, thin beds, and thin-bed cyclothems: Geophysics, v. 55, no. 9, p. 1,184–1,191

_____, 1991a, Correlation stack—seismic data processing technique: Kansas Geological Survey, Open-file Report 91–28, 10 p., 4 figs., 3 tables

_____, 1991b, Spectral whitening of seismic data: Kansas Geological Survey, Open-file Report 91–31, 13 p., 5 figs., 3 appendices

Mayne, W. H., 1962, Common reflection point horizontal data stacking: Geophysics, v. 27, no. 6, p. 927–938

Miller, R. D., Steeples, D. W., Grantham, R. L., Ali, M., Keiswetter, D. A., Anderson, J. M., Healey, J. M., Bennett, B. C., and Wirkar, F. T., 1990, Preliminary seismic tests to detect the presence of air in a semi-confined aquifer: Kansas Geological Survey, Open-file Report 90–16, 150 p.

Moore, R. C., 1936, Stratigraphic classification of the Pennsylvanian rocks of Kansas: U.S. Geological Survey, Bulletin 22, 256 p.

Morse, P. F., and Hildebrandt, G. F., 1989, Ground-roll suppression by the stack array: Geophysics, v. 54., no. 3, p. 290–301

Rascoe, B., and Adler, F. J., 1983, Permo-Carboniferous hydrocarbon accumulations, midcontinent, U.S.A. (abs.): Ninth International Congress Carboniferous Stratigraphic Geology: American Association of Petroleum Geologists, Bulletin, v. 67, no. 6. p. 979–1,001

Rich, J. L., 1923, Shoestring sands of eastern Kansas: American Association of Petroleum Geologists, Bulletin, v. 7, no. 2. p. 103–113

Staton, M. D., 1987, Stratigraphy and depositional environments of the Cherokee Group (Middle Pennsylvanian), central Cherokee basin, southeastern Kansas: M. S. thesis, The University of Kansas, 102 p.; also available as Kansas Geological Survey Open-file Report 87–24

Walton, A. W., Bouquet, D. J., Evenson, R. A., Rofheart, D. H., and Woody, M. D., 1985, Characterization of sandstone reservoirs in the Cherokee Group (Pennsylvanian, Desmoinesian) of southeastern Kansas, *in*, Reservoir Characterization, L. W. Lake and H. B. Carroll, eds.: Academic Press, Orlando, FL, p. 39–62

Widess, M. B., 1972, How thin is a thin bed?: Geophysics, v. 38, no. 6, p. 1,176–1,180

Index